



## Durham E-Theses

---

*Using sea-level and land motion data to develop an improved glacial isostatic adjustment model for the British Isles*

BRADLEY, SARAH, LOUISE

### How to cite:

---

BRADLEY, SARAH, LOUISE (2011) *Using sea-level and land motion data to develop an improved glacial isostatic adjustment model for the British Isles*, Durham theses, Durham University. Available at Durham E-Theses Online: <http://etheses.dur.ac.uk/600/>

### Use policy

---

The full-text may be used and/or reproduced, and given to third parties in any format or medium, without prior permission or charge, for personal research or study, educational, or not-for-profit purposes provided that:

- a full bibliographic reference is made to the original source
- a [link](#) is made to the metadata record in Durham E-Theses
- the full-text is not changed in any way

The full-text must not be sold in any format or medium without the formal permission of the copyright holders.

Please consult the [full Durham E-Theses policy](#) for further details.

---

Academic Support Office, Durham University, University Office, Old Elvet, Durham DH1 3HP  
e-mail: [e-theses.admin@dur.ac.uk](mailto:e-theses.admin@dur.ac.uk) Tel: +44 0191 334 6107  
<http://etheses.dur.ac.uk>

# **Using sea-level and land motion data to develop an improved glacial isostatic adjustment model for the British Isles**

**Sarah Louise Bradley**

**Department of Earth Sciences**

**Durham University**

A thesis submitted for the degree of  
*Doctor of Philosophy*

2011

## Abstract

The Glacial Isostatic Adjustment (GIA) of the British Isles is of interest due to the constraints that can be provided on key model parameters such as regional ice sheet history, viscoelastic earth structure and the global meltwater (eustatic) signal. Many past studies have used as their primary observable the high quality relative sea level (RSL) data from this region. However, as indicated in these studies, the data are notoriously difficult to fit due to the highly complex non-monotonic nature of the observed sea level change. In addition, the model predictions show a strong sensitivity to both regional ice and earth model parameters as well as the global meltwater history, resulting in a high degree of non-uniqueness when seeking an optimum model solution.

The principle aim of this thesis is to address this inherent non-uniqueness in the British Isles GIA problem and reduce the viable solution parameter space by considering additional datasets that display distinct sensitivities to local and global components of the GIA signal. This was achieved in a number of stages, using a combination of relative sea level data from both near and far-field sites, Continuous GPS data and the most recent geomorphological field constraints.

GPS observations of present day vertical crustal motion at sites across Great Britain are employed to provide an independent constraint on the choice of regional earth model parameters (viscoelastic earth structure). It was shown that the data are relatively insensitive to plausible variations in both the regional and global ice model history and as such, the data are used to identify an optimum range of earth model parameters for the region.

Using a set of previously un-modelled far-field sea level data from China and Malay-Thailand, a revised model of eustatic sea level change over the Holocene was developed. Constraining the eustatic component of sea level change is useful since it provides a direct measure of continental ice volume that can be compared to results from oxygen isotope methods. Additionally, inference of the eustatic signal over the mid-late Holocene, which was the primary focus of one aspect of this thesis can provide information on both: (i) the rate and timing of major ice melting at the end of the last deglaciation and (ii) the magnitude of melting during the late Holocene, which is an important baseline that can be compared to estimates of global sea-level rise in the 20<sup>th</sup> century. This new global ice model is characterised by an initial slowdown in the rate of eustatic sea level rise at 7 kyr BP, followed by a continuing rise, until 2 kyr BP, driven by continued melting from the Antarctic Ice sheet.

A new British-Irish Ice sheet model over the most recent glacial cycle was produced. This model was constrained to fit to most recent geomorphological field constraints and includes an extensive two-stage glaciation across the North Sea basin, with a greatly thickened and extended ice sheet within the Irish Sea, out along the NE Atlantic margin and across Ireland. During deglaciation, the Irish ice sheet now undergoes a very rapid thinning and retreat.

These results have been combined to produce a final new GIA model for the region, which has been constrained, for the first time, using an extended RSL database which includes observations from both Great Britain and Ireland. This new model captures reasonably well the regional trends in the observed sea level, with previous unresolved misfits relating to the timing and height of the Holocene highstand now largely removed.

## **Declaration**

**The copyright of this thesis rests with the author. No quotation from it should be published without the prior written consent and information derived from it should be acknowledged.**

**Sections of this thesis have been approved for publication.**

### **From Chapter 2:**

Shennan, I., Bradley, S., Milne, G., Brooks, A., Bassett, S., and Hamilton, S. (2006), Relative sea-level changes, glacial isostatic modelling and ice-sheet reconstructions from the British Isles since the Last Glacial Maximum, *Journal of Quaternary Science*, 21(6), 585-599.

Brooks, A. J., Bradley, S. L., Edwards, R. J., Milne, G. A., Horton, B., and Shennan, I. (2008), Postglacial relative sea-level observations from Ireland and their role in glacial rebound modelling, *Journal of Quaternary Science*, 23(2), 175-192.

### **From Chapter 3:**

Bradley, S. L., G. A. Milne, F. N. Teferle, R. M. Bingley, and E. J. Orliac (2009), Glacial isostatic adjustment of the British Isles: new constraints from GPS measurements of crustal motion, *Geophys J Int*, 178(1), 14-22.

### **From Chapter 5:**

Bradley, S. L., G. A. Milne, I. Shennan, and R. J. Edwards (2010), An improved glacial isostatic adjustment model for the British Isles, *Journal of Quaternary Science*, *accepted*.

**All work presented in this thesis is the author's original contribution.**

## Acknowledgements

There have been lots of people who have supported and helped me during the completion of this thesis, most of you know who you are, but I would like to thank some people especially below.

None of this work would have been possible without the willingness of my mam and dad to provide the financial support for this thesis – so big thanks there to start with, but this is just one tiny part of what they have done for me, supporting me through many emotional highs and lows and without them this end point would never have been reached.

An especially big thanks to Fabio!, who was been my 'guiding light of sunshine' and knows all that I owe to him.

My long suffering supervisor, Glenn who has guided me through 6 long years of this phd (and undergrad) to help make me into a much better and more rounded researcher than I would have been without him – I could not have asked for a better supervisor. He has taught me about 'academic ways', and provided guidance and the correct use of the English language!

All the members of staff in the department of Earth Science who have helped with my many questions, especially Karen and Janice for sorting out admin problems, and of course Gary and Dave who have answered many, no matter how obscure, IT related questions.

Thanks to my many friends in the department, some who have now left, Sophie, Chris G, Leanne, Matt, Pippa, Nicola, Jen, Jim, Ruth, Chris Mallow (thanks for all the endnote answers!), DR my boy!, we shared many happy fun moments together.

I am also indebted to other colleagues who have helped with various aspects of this project; Norman Teferle, (Univ. of Luxembourg) for advice on CGPS data, Ben Horton (Univ. of Pennsylvania), Y. Zong (Univ. of Hong Kong) and Robin Edwards (Trinity College, Dublin) for help with the many aspects of the sea-level work within this project; Tony Brooks who had to suffer many weeks of my ramblings when working with the Ireland Sea level data; and finally, Ian Shennan, who has helped me understand what is sea-level data and various aspects of the RSL work around the UK.

## Table of Contents

	Page
Abstract .....	ii
Declaration .....	iii
Acknowledgments .....	iv
Table of Contents .....	v
List of Figures .....	viii
Abbreviations used in text .....	xvii

### **Chapter 1: Introduction**

<b>1.1. <u>Introduction</u></b> .....	<b>1</b>
1.1.1. Background .....	1
1.1.2. GIA modelling – General .....	3
1.1.3. GIA Modelling application – British Isles .....	8
<b>1.2. <u>GIA Modelling and Theory</u></b> .....	<b>13</b>
1.2.1. Introduction .....	13
1.2.2. Theory .....	14
1.2.3. Input Ice Model .....	18
1.2.4. Input Earth Model .....	22
<b>1.3. <u>Observational Data</u></b> .....	<b>23</b>
1.3.1. Relative Sea Level Data .....	23
1.3.2. Continuous GPS Data .....	26
1.3.3. Geomorphological Data .....	27
<b>1.4. <u>Aims and Outline of Thesis</u></b> .....	<b>32</b>

### **Chapter 2: Developing an improved British-Irish Ice Sheet model**

<b>2.1. <u>Introduction</u></b> .....	<b>35</b>
<b>2.2. <u>Data</u></b> .....	<b>36</b>
2.2.1. Introduction .....	36
2.2.2. Geomorphological Data .....	37
2.2.2.1. Introduction .....	37
2.2.2.2. Chronology of Main Ice Sheet Advance and Retreat Phases .....	38
2.2.2.3. Constraints on Lateral and Vertical Extent .....	40
<b>2.2.3. Relative Sea Level Data</b> .....	<b>46</b>
2.2.3.1. Introduction .....	46
2.2.3.2. Data from Great Britain .....	48
2.2.3.3. Data from Ireland .....	52

<b>2.3. <u>Preliminary Data-Model Comparisons Using the Shennan et al. Model</u></b>	<b>55</b>
<b>2.4. <u>Modifications to the British-Irish Ice Sheet</u></b>	<b>59</b>
2.4.1. <u>Introduction</u>	59
2.4.2. <u>Modelling the Component for Great Britain</u>	61
2.4.3. <u>Modelling the Component for Ireland</u>	69
2.4.3.1. <u>Preliminary Modelling Comparison</u>	69
2.4.3.2. <u>Sensitivity Analysis of Changes to the Irish Ice Sheet History: Local Scale Ice Readvances</u>	73
2.4.3.3. <u>Sensitivity Analysis of Changes to the Irish Ice Sheet History: Improving the Fit to the Holocene Data</u>	77
2.4.3.4. <u>Sensitivity Analysis of Changes to the Irish Ice Sheet History: Improving the Fit during the Late Devensian Data</u>	80
2.4.4. <u>Combined Final Revised BIIS Model</u>	81
<b>2.5. <u>Discussion</u></b>	<b>89</b>
<b>2.6. <u>Conclusions</u></b>	<b>96</b>

### **Chapter 3: Glacial Isostatic Adjustment of the British Isles: new constraints from GPS measurements of crustal motion.**

3.1. <u>Introduction</u>	97
3.2. <u>CGPS Data</u>	99
3.3. <u>Modelling Results</u>	101
3.4. <u>Conclusions</u>	111

### **Chapter 4: Improving the Holocene melt history of the reference global ice model.**

4.1. <u>Introduction</u>	113
4.2. <u>Observations</u>	114
4.2.1. <u>China Sea-Level Data</u>	114
4.2.2. <u>Malay-Thailand Sea-Level Data</u>	117
4.3. <u>Preliminary Data-Model Comparisons</u>	119
4.3.1. <u>Introduction</u>	119
4.3.2. <u>China</u>	121
4.3.3. <u>Malay-Thailand</u>	123
4.3.4. <u>Summary</u>	124
4.4. <u>Towards an Improved Eustatic Model</u>	125
4.4.1. <u>Methodology</u>	125
4.4.2. <u>An Optimal Eustatic Model for China</u>	128

4.4.3. An Optimal Eustatic Model for Malay-Thailand. ....	134
4.4.4. Summary of New Eustatic Models. ....	139
4.4.5. An Optimum Model for Combined China and Malay-Thailand Data. ....	141
4.5. <u>Discussion</u> .....	154
4.6. <u>Conclusions</u> .....	164

## **Chapter 5: An improved glacial isostatic adjustment model for the British Isles**

5.1. <u>Introduction</u> .....	166
5.2. <u>Relative Sea-Level Data</u> .....	170
5.3. <u>Modelling</u> .....	176
5.3.1. Background to the GIA Model .....	176
5.3.2. Modifying the Eustatic Model .....	180
5.3.3. Determining the Optimal Earth Model Parameters .....	183
5.4. <u>Discussions and Conclusions</u> .....	190

## **Chapter 6: Summary and Future work**

6.1. <u>Introduction</u> .....	196
6.2. <u>Revised BIIS model and Modelling of the RSL Data</u> .....	197
6.3. <u>Modelling of CGPS Data</u> .....	202
6.4. <u>Modelling of the Far-Field RSL data</u> .....	205

## **Appendices**

<b>Appendix A:</b> Relative Sea Level data used within this thesis and corresponding references. ....	208
<b>Appendix B:</b> Predictions at all British Isles RSL data sites using the Shennan model. ....	221
<b>Appendix C:</b> Predictions at all Great Britain RSL data sites for the Northsea ice models (NS-Thick and NS-Thin) .....	232
<b>Appendix D:</b> Predictions at all Irish and a selection of Great Britain RSL data sites for the NS-Thick and Shennan models .....	241
<b>Appendix E:</b> Predictions at all Ireland and a selection of Great Britain RSL data sites using the three revised Irish Ice models (see Section 2.4.3.2-4). ....	245
<b>Appendix F:</b> Predictions at all British Isles RSL data sites for the Brooks et al. model. ....	249
<b>Appendix G:</b> Predictions at all British Isles RSL data sites for the Brooks et al and the final BIIS model .....	260

<b><u>References</u></b> .....	271
--------------------------------	-----

## List of Figures and Tables

### Chapter 1:

Fig. 1.1: Summary of Late Quaternary climatostrigraphic stages across Europe and the British Isles and approximate correlation with Marine Isotopes Stages (MIS). Timings of MIS are adapted from Bowen (1999) and correlation of glacial stages from Lowe and Walker (1997). Note that the diagram is not drawn to scale and the correlations are not completely resolved.....	1
Fig. 1.2: Predicted sea level at three sites using a GIA model: Site (A) Richmond Gulf, Canada, (B) Virginia, SE USA, and (C) Bonaparte Gulf, Australia. These sites were selected to illustrate the spatial and temporal variation in sea level during the most recent glacial-interglacial period. Frame (D) is modified from Clark <i>et al.</i> , (1978) and illustrates the six generalized zones of postglacial sea level change which will be discussed within the thesis. Site (A) is taken from Zone1, site (B) from Zone 2 and site (C) from Zone 6....	4
Fig. 1.3: Predictions of relative sea level at three selected sites across the British Isles using the Brooks <i>et al.</i> , (2008) ice model combined with an average earth model. More information regarding this model can be found within the following chapters of the thesis and the published reference. The total signal (solid black line) is separated into the signal due to non-local ice sheets (grey solid line) and the local British-Irish ice sheet (black dashed line).....	10
Fig. 1.4: Spatial plots of the ice extent of the starting ice model at the LGM (21 kyr BP) (A and B) and at present day (C and D) for the Northern and Southern Hemispheres. The global ice model is taken from Bassett <i>et al.</i> , (2005). The regional ice model, which includes the British and Irish Ice sheet, is taken from Shennan <i>et al.</i> , (2002).....	21
Fig. 1.5: Schematic representation of the variation with depth (km) of the viscosity structure of the input earth model. The viscosity value within the lithosphere is set to $10^{43}$ Pas. This value remains fixed throughout the thesis. The following three parameters: $LT$ , the lithosphere thickness, $\eta_{um}$ and $\eta_{lm}$ the upper and lower mantle viscosity are user defined inputs and are varied throughout this thesis.....	23
Fig. 1.6: Three proposed mechanisms for the formation of periglacial trimlines (adapted from Ballantyne, (2007)). (A) the ice-marginal (nunatak) hypothesis, in which the trimline marks the upper surface of the glacier at its maximum thickness, (B) the englacial hypothesis, where the trimline represents a thermal boundary between a lower warm based (erosive) ice and upper cold based (passive) ice within an ice sheet, (C) the readvance hypothesis, where the trimline forms due to the later readvance of a warm-based ice sheet..	29

### Chapter 2:

Fig. 2.1: Glaciation curve for the northern North Sea, which was used to constrain the timing of the growth and retreat phases for the BIIS and SIS. The diagram is adapted from Sejrup <i>et al.</i> , (1994) and is an illustrative profile extending between NE Scotland and Norway, where the shaded region represents periods of ice cover. The dates shown on the figure are $^{14}\text{C}$ radiocarbon ages, which were obtained from foraminifera samples taken from a range of core sites across the region. More information on the data analysis and location of the cores can be found within the text and in Sejrup <i>et al.</i> , (1994).....	39
---	----

Table 1: Range of ages and associated sources to infer initial timing of Mid-Devensian ice sheet build up. In cases where a range of values were published, only the maximum and minimum vales are shown to indicate the date range.....	41
Fig 2.2: Three dimensional reconstruction of ice surface altitude at the LGM. Note that the offshore margin is placed at the outermost morainal bank, close to the continental shelf edge. Taken from Ballantyne <i>et al.</i> , (2001).....	42
Fig. 2.3: Map showing the locations of the 80 data localities used in this study. The black triangles mark the locations of sites where primary and intercalated sea level index points have been obtained; the black circles mark sites where only intercalated sea level index points or other data points that provide a less precise constraint on sea level have been obtained. See Appendix A for a listing of all the data. Data and model predictions from sites labelled with white numbers in black boxes are shown in this chapter. Data and model predictions for all sites are shown in the Appendices.....	47
Fig. 2.4a: Comparison of predicted and observed sea level at eight locations across Great Britain (Results for all sites are shown in Appendix B). Symbols for the observed data are summarized in Appendix A and within the text. Predictions are shown for the Shennan ice model (shown in Fig. 2.5) for two earth models with different lithosphere thickness values: 71 km shown by solid red line and 96 km shown by the solid blue line; the upper and lower viscosity values are $5 \times 10^{20}$ Pa s and $4 \times 10^{22}$ Pa s, respectively.....	50
Fig. 2.4b: As 4a except for the eight chosen data localities across Ireland (Results for all sites across Ireland are shown in Appendix B).....	54
Fig. 2.5: Ice thickness maps of the British-Irish Ice sheet model presented in Shennan <i>et al.</i> , (2002) at the times (in kyr BP): (a) 32, (b) 25, (c) 21, (d) 20, (e) 19, (f) 18, (g) 17, (h) 16, (i) 13. Note the varying contour intervals: in frames a-g and heights between 0-150m the contour interval is 50m with annotation every 100m; for heights 150m and above the contour interval is 150m, with annotation every 300m.....	57
Fig. 2.6: Examining the affect of correcting the input ice model for underlying terrain at site 11, Arisaig. Predictions are shown for the Shennan model (solid lines) and Shennan-terrain corrected (dashed line) as described within the text using the two earth models with varying lithosphere thickness: 71km (grey line) and 96 km (black line) combined with an upper mantle viscosity of $5 \times 10^{20}$ Pa s and lower mantle viscosity of $4 \times 10^{22}$ Pa s.....	60
Fig. 2.7: Ice thickness maps of two British-Irish Ice sheet models generated from the Shennan model. The NS-Thick model at the times (in kyr BP): (a) 32, (b) 26, (c) 24, (g) 21; and the NS-Thin model at the times (in kyr BP): (d) 32, (e) 26, (f) 24, (h) 21. See main text for a description of these models. Note the varying contour intervals.....	63
Fig. 2.8: Comparisons of predicted and observed sea level at eight locations across Great Britain for the NS-Thick and NS-Thin ice models and the two reference earth models (see caption to Fig. 6). Predictions were generated using: the 71 km lithosphere earth model for the NS-Thick (solid red line) and NS-Thin (red-dashed line) models; the 96 km lithosphere earth model for the NS-Thick (blue solid line) and NS-Thin (blue dashed line). Additionally, predictions are shown using the 96 km lithosphere model for the Shennan model (solid black line) and the Shennan terrain-corrected model (grey line). Results are shown for all sites across Great Britain in Appendix C.....	65
Fig. 2.9: Ice Thickness maps of the NS-Thick BIIS model presented in Shennan <i>et al.</i> , (2006) for Ireland only at the times (in kyr BP): (a) 32, (b) 26, (c) 24, (d) 21, (e) 20, (f) 19, (g) 18, (h) 17, (i) 16. Note the varying contour intervals.....	71

Fig. 2.10: Comparison of predicted and observed sea levels at eight locations across Ireland. Predictions are shown using the 96 km lithosphere earth model (described in caption for Fig. 6) for the Shennan model (solid black line) and for the NS-Thick model (solid blue line). Results are also shown for the 71km lithosphere earth model for the NS-Thick model (solid red line). Results are shown for all sites across Ireland in Appendix D.....	72
Fig. 2.11: Comparison of predicted and observed sea levels at eight locations across Ireland. Predictions were generated for the NS-Thick (solid red line) and Model A (solid blue line) ice models using the 71 km lithosphere earth model. Results for all Ireland sites are shown in Appendix E.....	75
Fig. 2.12: Comparison of predicted and observed sea levels at eight locations across Ireland for three Irish ice models. Predictions were generated for the NS-Thick model (solid red line), Model B (solid blue line) and Model C (solid green line) using the 71 km lithosphere earth model. Results for all Ireland sites are shown in Appendix E.....	79
Fig. 2.13: Ice thickness maps for the revised British- Irish ice model presented in Brooks <i>et al.</i> , (2008) for Ireland only at the following times (in kyr BP) steps: (a) 24, (b) 21, (c) 20, (d) 19, (e) 18, (f) 17, (g) 16. Note the varying contour intervals.....	84
Fig. 2.14a: Comparison of predicted and observed sea level at eight locations across Great Britain. Predictions were generated for the original starting ice model (i.e. the Shennan model; solid red line) and the new revised ice model taken from Brooks <i>et al.</i> , (2008) (solid blue line) using the 71km lithosphere earth model. The dashed blue line is the prediction for the Brooks et al model but with a post modelling correction applied to create a continued rise in eustatic sea level of 5 m between 7-1 kyr BP.....	85
Fig. 2.14b: As 14a but for the eight chosen data localities across Ireland. Results for all Ireland and Great Britain sites are shown in Appendix F.....	86
Fig. 2.15: A revised glaciation curve for the main growth and retreat phases of the British-Irish Ice Sheet and Scandinavian Ice sheet across the Northsea, adapted from Sejrup <i>et al.</i> , (2009). Note NCIS is an abbreviation for Norwegian Channel Ice Stream and ages are given in calibrated <sup>14</sup> C.....	93

### Chapter 3:

Fig. 3.1: (a) Locations of CGPS sites considered in this analysis. (b) Contour map of absolute vertical rates over the UK region interpolated from CGPS data for data aligned to absolute gravity. The error bars show the uncertainty at each of the 16 data sites. (c) Horizontal velocity vectors estimated from the CGPS time series. (d) Same as (c) but with velocities from plate motion model removed. All uncertainties shown represent the 1 $\sigma$ range and are based on a post-processing scaling of the formal least squares values by a factor of 3 or more at most sites ( <i>see</i> Teferle <i>et al.</i> , (2008) for further information)	102
Table 2: Estimated crustal velocities (mm yr <sup>-1</sup> ) and locations of the CGPS sites considered in this study and shown on Fig. 3.1. The time series solutions are taken from Teferle <i>et al.</i> , (2008): table 5 for the horizontal velocities and table 9 for the AG-aligned vertical velocities. The following sites have been removed due to processing problems and data errors: ABER, ABYW, DUNK, HURN, LIVE, MORP, NPLD, NSTG – for the vertical velocity estimates, and ABER, ABYW, DUNK, HURN, LIVE, MORP, LOND, BLAK, COLC, NSTG, PMTG, OSHQ for horizontal velocity estimates. Note that a model of plate motion has been adopted to remove the tectonic signal from horizontal velocities (see Fig. 3.1 frames c & d and related discussion in text).....	103

Fig. 3.2: (a) Predictions of uplift rate on a 5 km by 5 km grid for the reference ice model and an Earth viscosity model that, when combined with the reference ice model, provides a good fit to the regional sea-level data base (Shennan *et al.*, (2006b)). This model adopts a 71km lithosphere thickness, and a upper and lower mantle viscosity of  $5 \cdot 10^{20}$  Pa s and  $1 \cdot 10^{22}$  Pa s respectively. The large positive uplift rates shown in the top right of the frame are associated with the deglaciation of the Fennoscandian component of the adopted ice model. (b) Same as (a) except that predicted velocity field sampled only at CGPS site locations. (c) Component of total predicted signal (a) associated with non-local ice sheet loading. (d) Component of total predicted signal (a) associated with local (British-Irish) ice sheet and ocean loading..... 106

Fig. 3.3:  $\chi^2$  values of data-model fit for a range of values for upper and lower mantle viscosity ( $v_{um}$  and  $v_{lm}$ , respectively) and lithospheric thicknesses of (a) 71 km, (b) 96 km and (c) 120 km. The black line and cross in each frame represent, respectively, the  $\chi^2$  value below which the quality of fit is equivalent at the 95% confidence level and the minimum value found..... 108

Fig. 3.4: Spatial plots of the contoured ice thickness for the reference ice model (Shennan *et al.*, (2006a)) and as described in section 2.4.2) and comparison ice model taken from Brooks *et al.*, (2008) and as described in section 2.4.3. Note the varying contour interval between each time slice..... 109

Fig. 3.5: Same as (b) in Fig. 3.3 except that an alternative ice loading history was adopted (see main text for details)..... 110

Fig. 3.6: Observed (triangles) and predicted (circles) uplift rates relative to Sheerness (site 18) for the sites located in Fig. 3.1a. The predictions are based on the best-fitting viscosity model with an assumed lithospheric thickness of 71 km (Fig. 3.3a). Error bars indicate  $1\sigma$  precision..... 111

## Chapter 4:

Fig. 4.1: Map showing location of 16 data sites used in this study. The sites in China are: BB – Bohai Bay, JP – Jingasu Province, YRD – Yangetese River Delta, FP – Fujian Province, HRD – Han River Delta, EG – East Guangdong, PRD – Pearl River Delta, WG – West Guangdong, HP – Hainan Province. The sites in Malay-Thailand are: Chao Phraya (CP), Prachaub (PA), Phuket (PH), East coast Thailand (ET), Keelang (KG), Strait of Malacca (MAL), and Tiomin Island (TI). The contours show relative sea level at 6 kyr BP predicted using the reference model. Black circles indicate the long/lat location of SLIP and red triangles shown average long/lat locations for each site used to calculate RSL at each locality..... 115

Fig. 4.2: Comparison of sea-level predictions generated for a range of earth models and the reference global ice model to the observations from China. Solid black circles mark each SLIP (complete RSL dataset summarised in Appendix A). Predictions generated using the reference model (as described in Section 4.3.1) is shown by the solid black lines. Variations in the input lithosphere thickness are shown by the dashed line: 71km (grey) and 120 km (black). The dotted line shows changes in the upper mantle viscosity from  $10^{20}$  Pa s (grey) to  $10^{21}$  Pa s (black). Changes in lower mantle viscosity are shown by the dot-dashed line:  $10^{21}$  Pa s (grey) and  $5 \cdot 10^{22}$  Pa s (black)..... 118

Fig. 4.3: Comparison of sea-level predictions generated for a range of earth models and the reference global ice model to the observations from Malay-Thailand. Solid black circles mark the location of each SLIP (complete RSL dataset summarised in Appendix A). The predictions generated using the reference model is shown by the solid black lines. Variations in the input lithosphere thickness are shown by the dashed line: 71km (grey) and 120 km (black). The dotted line shows changes in the upper mantle viscosity from $10^{20}$ Pa s (grey) to $10^{21}$ Pa s (black). Changes in lower mantle viscosity are shown by the dot-dashed line: $10^{21}$ Pa s (grey) and $5 \times 10^{22}$ Pa s (black).....	120
Fig. 4.4: Graphical representation of selected eustatic sea-level functions. Solid black line represents the input eustatic function ( $\Delta S_{est}^i(t)$ ) taken from the reference model (Basset <i>et al.</i> , (2005)). Three alternative melt scenarios are also illustrated: melt1 (light grey; solid line), melt2 (black; dotted line), and melt3a (dark grey; solid line) and melt3b (dark grey; dashed line) and are discussed in detail in 4.4.1. The height variation between the solid and dashed dark grey lines illustrates the range in highstand magnitude investigated for each of the three melt scenarios considered.....	121
Fig. 4.5: Flow chart to summarise the stages used in estimation of optimum earth model. See text for more details.....	126
Fig. 4.6: Contour plots of the $\chi^2$ misfit between predicted and observed sea levels for the China data set as a function of upper and lower mantle viscosity ( $\nu_{um}$ and $\nu_{lm}$ , respectively). Each frame gives the results for the four melt scenarios illustrated in Fig. 4.4: (a) melt1, (b) melt2, (c) melt3a, (d) melt3b. The black line represents the $\chi^2$ value below which the quality fit is equivalent at 95% confidence.....	129
Fig. 4.7: Contour plots of the $\chi^2$ misfit between predicted and observed sea levels for the China data set as a function of upper and lower mantle viscosities ( $\nu_{um}$ and $\nu_{lm}$ , respectively) and lithosphere thickness ( $L_l$ ) for the reference (a) and <i>EUSTI</i> (b) eustatic models.. Results in (a) and (b) are for a lithosphere thickness of 96 km. The solid black line represents the 95% confidence level and the cross indicates the min. $\chi^2$ misfit. Frame (c) shows $\chi^2$ values generated using the <i>EUSTI</i> ice model as a function of lithospheric thickness and upper mantle viscosity for a lower mantle viscosity of $2 \times 10^{21}$ Pa s.....	130
Fig. 4.8: As in Fig. 4.7 except that results are based on a subset of data points from the China data set believed to be the most reliable (see Section 4.3.2 for more detail).....	131
Fig. 4.9: Comparison of the predicted and observed sea-level change at each locality in China. Solid black circles mark each SLIP. The solid black line shows predictions for the reference ice-earth model. Predictions using the revised ice model ( <i>EUSTI</i> ) were generated for an optimum earth structure inferred from the $\chi^2$ results in Fig. 4.7 and 4.8: for the complete data set (dashed) with a lithosphere thickness of 96 km, upper mantle viscosity $1 \times 10^{20}$ Pa s and lower mantle viscosity $5 \times 10^{21}$ Pa s; reduced data set (dotted) with a lithosphere thickness 96 km, upper mantle viscosity $5 \times 10^{20}$ Pa s, lower mantle viscosity $2 \times 10^{21}$ Pa s. At locality HP, predictions based on the revised ice model are also for a location to the north of the island (dashed-dotted; see text for more information).....	133
Fig. 4.10: Contour plots of the $\chi^2$ misfit between predicted and observed sea levels for the Malay-Thailand data set as a function of upper and lower mantle viscosity ( $\nu_{um}$ and $\nu_{lm}$ , respectively). Each frame gives the results for the four melt scenarios illustrated in Fig. 4: (a) melt1, (b) melt2, (c) melt3a, (d) melt3b. The black line represents the $\chi^2$ value below which the quality fit is equivalent at 95% confidence. The blue region represents $\chi^2$ values greater than the maximum on the scale bar (80) up to 243.....	135

Fig. 4.11: Contour plots of the $\chi^2$ misfit between predicted and observed sea levels for the Malay-Thailand data set as a function of upper and lower mantle viscosities ( $v_{um}$ and $v_{lm}$ , respectively) and lithosphere thickness ( $L_t$ ) for the reference (a), <i>EUST2</i> (b) and <i>EUST1</i> (c) eustatic models. Results in (a), (b) and (c) are for a lithosphere thickness of 96km. The solid black line represents the 95% confidence level and the cross indicates the min. $\chi^2$ misfit. Frame (d) shows $\chi^2$ values generated using the <i>EUST1</i> ice model as a function of lithospheric thickness and upper mantle viscosity for a lower mantle viscosity of $2 \times 10^{21}$ Pa s. The blue colour represents $\chi^2$ values greater than the maximum on the scale bar (80) up to 193.....	137
Fig. 4.12: Comparison of predicted and observed sea levels at each of the seven localities in Malay-Thailand for three eustatic melt models. Solid black circles mark each SLIP. The solid black line represents prediction for the reference model, described in the text. Predictions for <i>EUST1</i> (dashed) and <i>EUST2</i> (solid grey) were generated for an earth model with a lithosphere thickness of 96km, upper mantle viscosity of $8 \times 10^{20}$ Pa s and lower mantle $5 \times 10^{21}$ Pa s. This model produced a good fit for both of the revised eustatic models (see Fig. 4.11).....	138
Fig. 4.13: Graphical representation of the eustatic sea level curve for three models: reference (solid black), <i>EUST1</i> (dashed) and <i>EUST2</i> (solid grey).....	140
Fig. 4.14: Flow diagram to outline the key steps in determining a eustatic model that provides a good fit to both the China and Malay-Thailand data sets.....	141
Fig. 4.15: Four of the melt models adopted to investigate the sensitivity of the data-model fit to the amount of melt partitioned before and after 7 kyr BP. The amount of melt prior to 7 kyr BP was systematically reduced to produce eustatic sea level at this time ranging from a depth of 4.7 m (dotted-dashed) to a depth of 8 m (dashed). The dotted and solid lines illustrate two intermediate models, with the red line highlighting the median model. All models are based on the timing of the ‘melt3’ model (Fig. 4.4) used to obtain <i>EUST1</i> and <i>EUST2</i> .....	142
Fig. 4.16: Contour plots of the $\chi^2$ misfit between predicted and observed sea level for the China data set as a function of upper and lower mantle viscosity ( $v_{um}$ and $v_{lm}$ respectively) for a lithosphere thickness of 96 km. The results are shown for four different melt models defined in terms of depth of eustatic sea level at 7 kyr BP (and described in greater detail within section 4.4.5): (a) 7.5 m, (b) 6.5 m, (c) 5.75 m and (d) 4.7 m. The black line represents the $\chi^2$ value below which the quality fit is equivalent at 95%. The black triangle marks the minimum $\chi^2$ misfit.....	144
Fig. 4.17: As in Fig 4.16 except that results are shown for the ‘reduced’ China data set.....	145
Fig. 4.18: As in Fig. 4.16 expect results are shown for the Malay-Thailand data set. The cross marks the location of the minimum $\chi^2$ misfit.....	146
Fig. 4.19: The $\chi^2$ misfit for the range of melt models considered for the China data (black) and Malay-Thailand data (grey). Results are shown for both the complete China data set (A) and the reduced data set (B). The solid horizontal line marks the location of the 95% confidence limit – models which result in values below this limit are statistically equivalent to 95% confidence. The melt models which satisfy this criterion for both data sets are indicated by the shaded region. Note that different earth models were used to generate predictions for each region (China and Malay-Thailand; see text for details).....	148

Fig. 4.20: Contour plots of the  $\chi^2$  misfit between predicted and observed sea level data for a range of upper and lower mantle viscosities ( $\nu_{um}$  and  $\nu_{lm}$ , respectively) and a lithosphere thickness of 96 km. The top two frames show results for the complete China data set for eustatic models *melt7m* (a) and *EUST3* (b). The lower frames show results for the Malay-Thailand data set for eustatic models *melt5.5m* (c) and *EUST3* (d). The black line represents the  $\chi^2$  value below which the quality fit is equivalent to a 95% confidence level. The triangle marks the location of the minimum  $\chi^2$  value..... 149

Fig. 4.21: Comparison of the predicted and observed sea levels at each of the nine localities in China. Solid black circles mark the individual SLIPs. The solid black line shows predictions for the reference ice-earth model. Predictions for *melt7m* (dashed black) and *EUST3* (solid grey) were generated for an optimum earth structure inferred from the  $\chi^2$  results presented in Fig. 4.20: lithosphere thickness 96 km, upper mantle viscosity  $5 \times 10^{19}$  Pa s, lower mantle viscosity  $1 \times 10^{21}$  Pa s..... 152

Fig. 4.22: Comparison of the predicted sea level and observations at each of the seven data regions in Malay-Thailand. Solid black circles mark the location of each SLIP. The solid line shows predictions for the starting ice-earth model. Predictions for *melt5.5m* (dashed-black) and *EUST3* (solid grey) were generated for an optimum earth structure inferred from the  $\chi^2$  analysis in Fig. 4.20 (frames c & d): lithosphere thickness 96 km, upper mantle viscosity  $2 \times 10^{20}$  Pa s, lower mantle viscosity  $8 \times 10^{21}$  Pa s..... 153

Fig. 4.23: Comparison of the optimum eustatic models inferred in this analysis for each data set (*melt7* – dashed black; *melt5.5* -dashed-dotted black; *EUST3* – solid black) to two published models: ICE-5G model (grey dotted; Peltier (2005)) and the model by Lambeck and Purcell, (2005) (solid grey; referred to as LP in main text)..... 154

Fig. 4.24: Contour map of relative sea-level at 4 kyr BP using the *EUST3* ice model and the reference earth model. Sites mentioned within the text are labelled as follows: FJ – Fiji Islands, CK – Cocos Keeling Islands, MU- Mauritius, and SI – Society Islands..... 160

Fig. 4.25: Map illustrating the location of the major plate boundaries and subduction zones across the study region: R.T – Ryukyu trench, M.T. – Manila trench, P.T. – Philippine trench. Red triangles mark the average longitude/latitude location of each data locality. Black circles highlight some recent earthquakes of magnitude 5 and greater. (Sourced from <http://neic.usgs.gov/neis/epic/epic.html>)..... 162

## Chapter 5:

Fig. 5.1: Predictions of relative sea level at three selected sites (17, 99 & 50; see Fig. 5.2) using the best-fitting ice and earth model from this analysis (see text for more information). The total signal (solid black line) is separated into the signal due to non-local ice (grey line) and the local British–Irish ice sheet (dotted black line). Note that the influence of ocean loading and GIA-induced perturbations in earth rotation associated with each of these two ice model components is included in the predictions..... 168

Fig. 5.2: Map showing the locations of the 80 data localities used in this study. The black triangles mark the locations of sites where primary and intercalated sea level index points have been obtained; the black circles mark sites with only intercalated sea level index points or other data points that provide a less precise constraint on sea level have been obtained. See Appendix A for a listing of all the data. Data and model predictions from sites labelled with white numbers in black boxes are shown in the main text. Data and model predictions for all sites are shown in Appendix G..... 171

Fig. 5.3: Observed sea level at nine locations across the study region. Symbols for the observed data are summarized within the text and Appendix A. Note the varying scale between each plot.....	173
Fig. 5.4: Ice thickness maps of the British-Irish Ice sheet model presented in Brooks <i>et al.</i> , (2008) and as described in Section 2.4.3 at the times: (a) 32 kyr BP, (b) 26 kyr BP, (c) 24 kyr BP, (d) 21 kyr BP, (e) 20 kyr BP, (f) 19 kyr BP, (g) 18 kyr BP, (h) 17 kyr BP, (i) 16 kyr BP, (j) 13 kyr BP. Note the varying contour intervals. Diagram (k) is a graphical representation of the two eustatic sea level models considered in this study: Bassett <i>et al.</i> , (2005) (grey line) and the revision to this model presented by Bradley <i>et al.</i> (2010) (and as referred to in Section 4.4.5 as the <i>EUST3</i> model)(black line).....	181
Fig. 5.5: Comparison of predicted and observed sea level at nine locations across the study region. Symbols for the observed data are summarized within the text and Appendix A. Predictions based on the optimum earth model inferred in Bradley <i>et al.</i> (2009) and as described in Chapter 3 - lithosphere thickness 71 km, upper mantle viscosity $0.5 \times 10^{21}$ Pa s, lower mantle viscosity $3 \times 10^{22}$ Pa s - are shown for the Brooks <i>et al.</i> /Bassett <i>et al.</i> ice model (dashed black line; see text for details) and the new ice model presented in this analysis (solid red line). The solid blue line is for the new ice model and an earth model that is identified from $\chi^2$ results presented in Fig. 5.8. This Earth model is identical to the one inferred in Bradley <i>et al.</i> (2009) except that the viscosity in the lower mantle is higher, at $6 \times 10^{22}$ Pa s. Note the varying scale for each plot. Predictions for all sites are shown in Appendix G.....	184
Fig. 5.6: Contour plots of the normalized $\chi^2$ misfit between predicted and observed sea level as a function of upper and lower mantle viscosity ( $v_{um}$ and $v_{lm}$ respectively) for a lithosphere thickness of 71km. The top two frames (a & b) show results for the Brooks <i>et al.</i> /Bassett <i>et al.</i> ice model (see text for details) and the lower two frames (c & d) show those for new ice model presented here. The results in frames (a) & (c) consider data from Great Britain data and those in frames (b) & (d) consider data from Ireland. The black line represents the $\chi^2$ value below which the quality fit is equivalent to 95 % confidence (194 in frame (a), 329 in frame (b), 106 in frame (c) and 272 in frame (d)). The triangle marks the location of the minimum $\chi^2$ value. The white line marks the region of optimum parameter values (95% confidence) inferred from the CGPS measurement of crustal motion (Bradley <i>et al.</i> , (2009) and as described in Chapter 3). Note that the darkest blue colour represents $\chi^2$ values greater than the maximum on the scale bar (400).....	187
Fig. 5.7: Contour plots of the normalized $\chi^2$ misfit between predicted and observed sea level as a function of upper and lower mantle viscosity ( $v_{um}$ and $v_{lm}$ respectively) for a lithosphere thickness of 71km for the new ice model. Frame (a) shows results for 'northern' data, (b) for 'central' data, and (c) for 'southern' data (see main text for more information).The triangle marks the location of the minimum $\chi^2$ value. The black line represents the $\chi^2$ value below which the quality fit is equivalent to 95 % confidence (96 in frame (a), 242 in frame (b) and 94 in frame (c)). Note that the darkest blue colour represents $\chi^2$ values greater than the maximum on the scale bar (400).....	188

Fig. 5.8: Contour plots of the normalized  $\chi^2$  misfit between predicted and observed sea level as a function of upper and lower mantle viscosity ( $v_{um}$  and  $v_{lm}$  respectively) for a lithosphere thickness of 71 km. Note that the range and density of viscosity values considered differs from those adopted in Figs 5.6 & 5.7 in order to better capture the region of best-fitting viscosity values. All results are based on the new ice model. Frame (a) shows results for all the data (from Great Britain and Ireland), while frame (b) shows the results using 'basal points' from Great Britain and primary index points from Ireland (see text). The triangle marks the location of the minimum  $\chi^2$  value. The black line represents the  $\chi^2$  value below which the quality fit is equivalent to 95 % confidence (111 in frame (a) and 130 in frame (b))..... 190

Fig. 5.9: Predictions of present-day sea-level change (a) and vertical land uplift (b) for the new ice model and its optimum earth model. The lower frames show the contribution to (a) from all ice sheets except the British-Irish Ice sheet (c) and from the British-Irish Ice sheet only (d). All predictions include the respective ocean loading and rotation component..... 192

## Abbreviations used in the thesis

### **Chapter 1:**

LIS	Laurentide Ice Sheet
SIS	Fennoscandian Ice Sheet
AIS	Antarctica Ice Sheet
WAIS	West Antarctic Ice Sheet
BIIS	British-Irish Ice Sheet
GIS	Greenland Ice Sheet
IIS	Irish Ice Sheet
LGM	Last Glacial Maximum
MIS	Marine Isotope Stage
GIA	Glacial Isostatic Adjustment
RSL	Relative Sea Level
CGPS	Continuous global positioning system
mwp	Meltwater Pulse
SLIP	Sea level index point
MSGGL	Mega scale glacial lineations

### **Chapter 2:**

NSB	North Sea Basin
IRD	Ice rafted debris
KPS	Killard Point Stadial
LLS	Loch Lomond Stadial
SIEM	South of Ireland end moraine
ISB	Irish Sea basin

### **Chapter 4:**

EAIS	East Antarctic Ice Sheet
APIS	Antarctic Peninsula Ice Sheet

# Chapter 1: Introduction

## 1.1. Introduction

### 1.1.1. Background

During the Late Pleistocene there have been repeated glacial-interglacial cycles where large land based ice sheets waxed and waned. At the end of the last interglacial (generally referred to as the Eemian across Europe and Ipswichian across the British Isles – see Fig. 1.1) around 116 kyr BP, the climate began to cool causing existing ice sheets (Greenland and Antarctica) to grow and previously melted ice sheets to grow again – for example, the Laurentide Ice Sheet (LIS) in North America and the Fennoscandian Ice Sheet (SIS) in Northern Europe. At this time, global mean sea level was at least 3 m above present (Stirling *et al.*, (1998)). This marked the start of a new glacial cycle, which culminated in the Last Glacial Maximum (LGM), defined as a global-scale maximum in ice volume between 26-21 kyr BP (Peltier and Fairbanks (2006), Yokoyama *et al.*, (2000)), when ice sheets had expanded to produce a global sea-level lowering of  $125 \pm 5$  m relative to present (Fleming *et al.*, (1998)).

Time (kyr) BP	Cold (Glacial)/ Temperate (Interglacial)	Marine Isotope Stage	Stage	
			NW Europe	British Isles
11.5	Interglacial	1	Holocene	
	Glacial	2	Late Weichselian =	Late Devensian
~ 30		3	Middle Weichselian	Middle Devensian
58		4	Early Weichselian	Early Devensian
70-80		5a	Early Weichselian	Devensian
		5b		
	5c			
	5d			
116	InterGlacial	5e	Eemian	Ipswichian

Fig. 1.1: Summary of Late Quaternary climatostratigraphic stages across Europe and the British Isles and approximate correlation with Marine Isotopes Stages (MIS). Timings of MIS are adapted from Bowen (1999) and correlation of glacial stages from Lowe and Walker (1997). Note that the diagram is not drawn to scale and the correlations are not completely resolved

Across Europe, during this most recent glacial cycle, there was a discontinuous and unsteady growth of the ice sheets, with significant fluctuations in volume. The classification and terminology adopted to define these glacial cycles varies notably within the literature and so will be clarified at this point. Marine geologists generally follow a timescale developed using the marine oxygen isotope record that is divided into a series of numbered stages, referred to as Marine Isotope Stages (MIS - see Fig. 1.1) which are derived from fluctuations in the oxygen isotope content of ocean water. In comparison, most field scientists follow a geological approach where litho- or bio-stratigraphic characteristics in the observed strata are used to develop a chronostratigraphic sequence, which is used to define a series of glacial/interglacial episodes. For example, the glacial stages of the British-Irish ice sheet (BIIS) are referred to using the term Devensian, whereas the corresponding stages of the SIS are referred to as Weichselian. For clarity within this thesis, the approximate correlation between the main climatostratigraphic stages and MIS units are summarised on Fig. 1.1 for Europe. It should be noted, however, that the exact age correlation is still not fully resolved and not all regional interstadials are marked. The Weichselian (NW Europe) or Devensian (British Isles) glacial period covers the interval from the end of MIS-5e to the start of the Holocene (MIS-1) around 11.5 kyr BP, and can be subdivided into three main glacial episodes as well as numerous shorter stadials not included in Fig. 1.1. For example, the Early Weichselian which spans the interval from ~ 116 - 70 kyr BP (MIS-5) can be further divided into a series of substages marking alternating warm interstadials (MIS-5c and MIS-5a) and colder stadials (MIS-5d and MIS-5a). The time interval considered in this thesis extends from the Ålesund interstadial (~ 33 kyr BP) to present day, and includes MIS-2 to MIS-1. This marked the end of the Mid Weichselian/Devensian and the onset of the most recent glaciation across NW Europe and the British Isles, referred to as Late Weichselian/Devensian episode.

The mass redistribution between land based ice sheets and oceans during the Late Pleistocene is sufficient to produce a significant deformation of the solid Earth and perturbation to the geopotential. Glacial Isostatic adjustment (GIA) is the study of this ice-earth interaction by comparing surface observations, such as sea level change with predictions generated using quantitative models. Through these comparisons, it is

possible to infer information on the rheological properties of the solid Earth, past and present ice sheet history and climate change. Some of these applications are outlined below.

### **1.1.2. Glacial Isostatic Adjustment Modelling - General**

Relative sea level (RSL) is one of the main data types used to constrain GIA model parameters. RSL is defined as height of the geoid (or time-averaged ocean surface) relative to the solid earth (or ocean floor). A vertical shift in either of these two surfaces will produce a change in RSL. Examination of the geological record has revealed that, during the late Quaternary, RSL changes have been spatially and temporally complex. The majority of the observed signal is due to the GIA processes.

GIA-induced sea-level changes have been studied from a variety of geographic regions to aid the understanding of the processes driving this variability and provide information relating to Pleistocene ice sheet history and earth viscosity structure. Clark *et al.*, (1978) summarised this global variation in post glacial sea level change into six separate geographical zones (see Fig 1.2D). For the purpose of this thesis, predicted sea level over the last 20 kyr BP is highlighted at 3 selected zones, two taken from within the near-field region (sites which were close to the major ice sheets) and one from far-field region (sites which are distant from the major glacial activity). These end member cases are shown not only to highlight the spatial variation but also to help illustrate the different GIA processes which drive this variability.

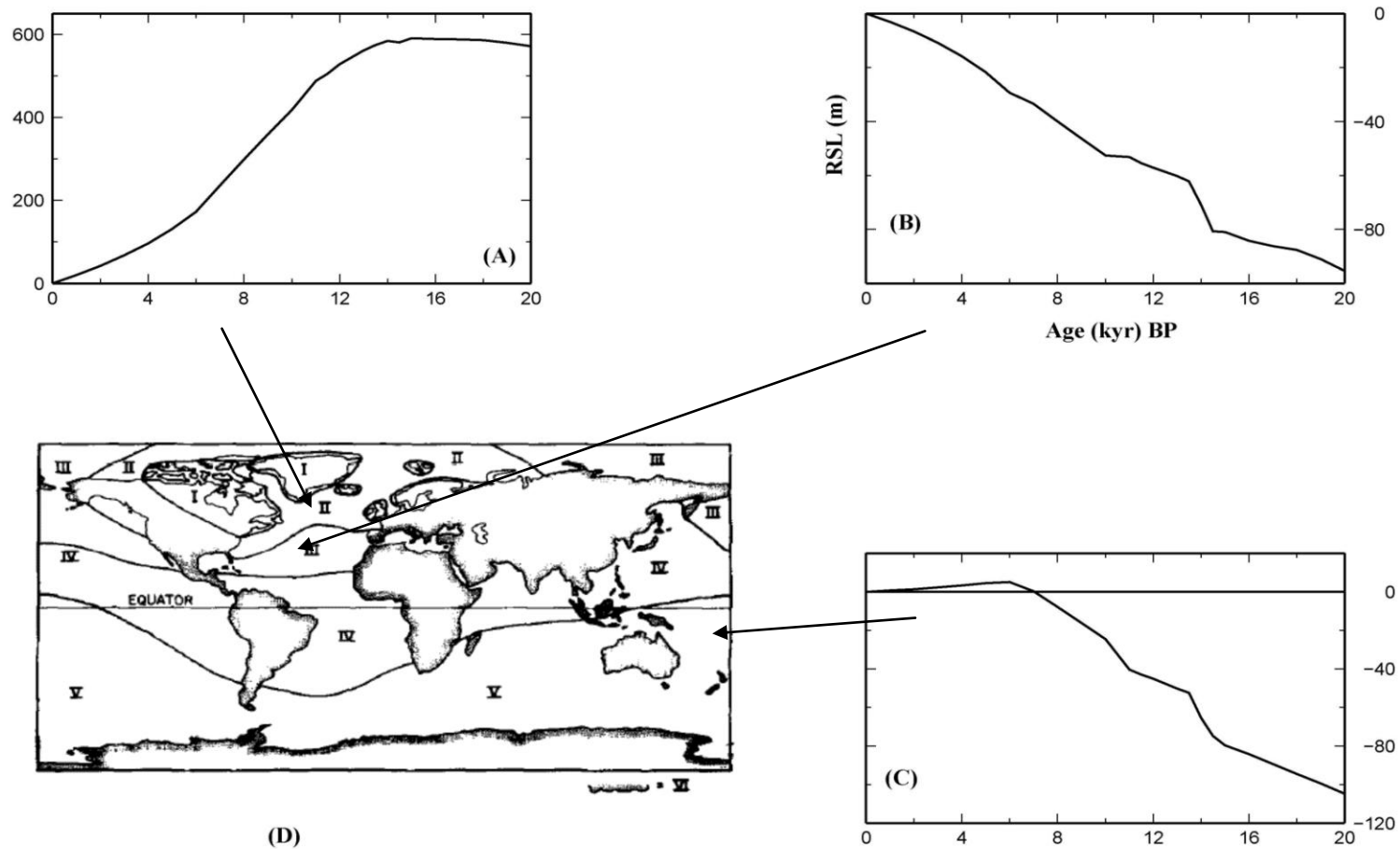


Fig. 1.2: Predicted sea level at three sites using a GIA model: Site (A) Richmond Gulf, Canada, (B) Virginia, SE USA, and (C) Bonaparte Gulf, Australia. These sites were selected to illustrate the spatial and temporal variation in sea level during the most recent glacial-interglacial period. Frame (D) is modified from Clark *et al.*, (1978) and illustrates the six generalized zones of postglacial sea level change which will be discussed within the thesis. Site (A) is taken from Zone 1, site (B) from Zone 2 and site (C) from Zone 6.

Site A (Fig. 1.2A; Zone 1 in Fig. 1.2D) and Site B (Fig. 1.2B; Zone 2 in Fig. 1.2D) illustrate the pattern of RSL change at sites within the near-field and intermediate-field respectively, where the signal is dominated by the isostatic response of the earth to the regional ice unloading. Site A, located at Richmond Gulf Canada, close to the centre of the LIS, is characterised by a monotonic sea level fall from ~ 600 m above present. This is driven by the unloading of the crust and rebound of the solid surface following the deglaciation of the LIS. This contrasts with the pattern at Site B (located along the NE Coast of USA), in Zone 2, which is characterised by a monotonic rise in sea level from ~ 100 m below present over the last 20 kyr, generally remaining below present over this period. Therefore in contrast to the far-field sites, no Holocene highstand is produced. This site was located close to the ice margins, where the collapse of the peripheral bulge and accompanying subsidence due to the movement of material back below the glaciated regions drives the associated rise. Past studies have used RSL data from these regions to constrain both the spatial and temporal history of Late Pleistocene ice cover and the rheological properties of the solid earth (Tushingham and Peltier (1992), Lambeck *et al.*, (1998), Kaufmann *et al.*, (2000), Simpson *et al.*, (2009), Mitrovica (1996), Quinlan and Beaumont (1981)). RSL changes in the British Isles and Ireland – the primary study area of this thesis – are significantly influenced by both crustal uplift and peripheral bulge subsidence.

In contrast, the sea level signal at sites within far-field regions (e.g. Zones 4-6 on Fig. 1.2D) are most sensitive to the rate and magnitude of meltwater input into oceans following deglaciation. The characteristic pattern of RSL at these sites varies between Zone 4, where sea level remains below present and no highstand develops, to sites within Zones 5 and 6 where sea level rises towards present to form a late Holocene highstand of varying amplitude, such as shown for Site C, Bonaparte Gulf, NE Australia (Fig. 1.2C). The main GIA processes which govern this spatial and temporal pattern are hydro-isostatic loading (continental levering) and ocean syphoning, as discussed in Mitrovica and Milne (2002). Clark *et al.*, (1978) also noted that the transition between these two contrasting regions will vary spatially and temporally with any adjustment to the Late Holocene pattern of melting. RSL data from these regions have been primarily used to constraint the pattern of melting from the global ice sheets (i.e. eustatic sea level) during

the last deglaciation, between LGM and present day, and also the rheological properties of the solid earth (Bassett *et al.*, (2005), Fleming *et al.*, (1998), Lambeck (2002), Nakada and Lambeck (1989), Nunn and Peltier (2001)). Eustatic sea level is defined as the spatially uniform change in sea level due to the mass exchange between the ice sheets and oceans and is important to constrain for a number of reasons. Firstly, it is used as a primary constraint for the total volume of continental ice – an important target for global ice model reconstructions. Also, this constraint is independent from marine  $\delta^{18}\text{O}$  records and so can be used to help calibrate these proxy data. Secondly, the rate and magnitude of meltwater influx at the end of the last deglaciation is used as a baseline for interpreting the rate of 20<sup>th</sup> century global mean sea level change.

At present there is still no general consensus on the rate and magnitude of eustatic sea level change during the last deglaciation, with only a limited number of studies (Fleming *et al.*, (1998)) using a global distribution of observations. This is partly due to the observed sea level at such far-field locations providing only an approximation of the eustatic sea level change, due to the interplay between GIA processes and also local-to-regional scale factors, such as tectonism (Milne and Mitrovica (2008)). This is exemplified by noted differences between the two most widely cited global models: ICE-5G (Peltier (2004)) and a model from the Australian National University Group (Lambeck and Purcell (2005)). For example, the former suggests that global melting ended at 4 kyr BP, compared to between 2-1 kyr BP in the latter. Examination of the eustatic sea level change over the Holocene is another factor which will be considered within this thesis.

Another more recent data type which is used to constrain models of GIA is the present-day 3D motion of the solid surface. Continuous global positioning system (CGPS) receivers monitor secular variations in the solid earth and provide a measure of the vertical and horizontal crustal motion. Unlike RSL data which is primarily taken from coastal sites, CGPS data has the advantage of spatial sampling from both coastal and inland areas. Over the last 10 years, there has been a marked improvement in the accuracy and precision of the estimated motion due to advances in the GPS satellites and receiver designs, processing techniques and reference frames; these advances have

enabled the data to be utilised in a greater range of GIA studies and locations. One of the most extensive and well studied CGPS network, in terms of both spatial coverage and quality of receiver monumentation, is the BIFROST network located across Sweden and Finland (Lidberg *et al.*, (2010)). Over the past decade the number and size of regional networks has been increasing (e.g. Sella *et al.*, (2007); Teferle *et al.*, (2009)). These data have been primarily used to infer information on the spatial and temporal history of past ice sheets and the rheological properties of the Earth (Argus and Peltier (2010), Milne *et al.*, (2001), Mitrovica *et al.*, (1994b), Sella *et al.*, (2007), Bevis *et al.*, (2009)). One aspect of this thesis is the consideration of CGPS data from Great Britain to constrain a model of GIA for this region.

Perturbations in Earth rotation are also sensitive to GIA processes resulting from changes in the ice extent over the Late Pleistocene and up to the present day (i.e. mass balance of the contemporary polar ice sheets). Other non-GIA processes which can affect the observed rotational signal include mantle convection and mountain building, but are not considered here. The perturbation in Earth rotation can be seen in two observable signals; a non-tidal acceleration in the rotation rate and a secular wander of the rotation pole relative to the surface geography (generally referred to a true polar wander (TPW)). The former has been found to be proportional to the change of degree-two zonal harmonic of the earths geopotential ( $J_2$ ) and can be observed using measurements from satellites (Nerem and Klosko (1996)) and in historical records (Mitrovica *et al.*, (2006)). As this measures a long-wavelength response of the earth, it has been shown to be primarily sensitive to the deeper earth structure, most specifically the viscosity of the lower mantle (Johnston and Lambeck (1999), Nakada and Okuno (2003), Mitrovica and Milne (1998)).

A number of earlier studies identified that the GIA-induced TPW signal is also strongly sensitive to the adopted rheological structure of the solid earth (Mitrovica and Milne (1998)). Comparisons of predictions to observations derived from historical and current space-geodetic measurements (Gross and Vondrak (1999), Mccarthy and Luzum (1996)) have been utilized to infer the rheological structure of the earth and limit the range of lower mantle viscosity (Johnston and Lambeck (1999), Mitrovica and Milne (1998)).

More recently changes in the observed rotational signal have been investigated to infer present day rates of melting from either the Antarctic ice sheets (AIS) or the Greenland ice sheet (GIS). For example, Mitrovica *et al.*, (2006) identified that to fit a range of observational datasets of both rotational signals (TPW and the rotation rate), required a  $0.3 \text{ mm yr}^{-1}$  eustatic sea level rise during the late Holocene and a  $0.8 \text{ mm yr}^{-1}$  rise during the 20th Century. Nakada and Okuno (2003) also compared GIA model predictions to both rotational datasets to infer a present day rise in eustatic sea level of  $1\text{-}1.5 \text{ mm yr}^{-1}$  due to the melting from the GIS and the Weddell Sea region of the West Antarctic ice sheet (WAIS).

This review has outlined some of the general applications of GIA modelling to a range of data sets. In the following sub-section, GIA modelling specific to the British Isles, the study region of this thesis, will be discussed. For clarity, the term 'British Isles' refers to Great Britain, Ireland and all adjacent smaller offshore islands around the coast of Scotland, including Shetland and the Isle of Man. Great Britain refers to all of England, Scotland, Wales and all smaller offshore islands around the coast of Scotland and the Isle of Man, whereas 'Ireland' refers to the geographic region, including both the political regions of Northern Ireland and the Republic of Ireland.

### **1.1.3. Glacial Isostatic Adjustment Modelling - British Isles.**

Over the past two decades there have been numerous GIA modelling studies for the British Isles: from the early work of Lambeck (Lambeck (1993a), Lambeck (1993b)), through the studies of Johnston and Lambeck (2000), Peltier *et al.*, (2002), to the most recent work by Shennan, Brooks and collaborators (Bradley *et al.*, (2009), Bradley *et al.*, (2010), Brooks *et al.*, (2008), Shennan *et al.*, (2006b)). These studies have led to constraints on various model components including the regional ice sheet history (Lambeck (1993a), Lambeck (1993b), Lambeck and Purcell (2001), Brooks *et al.*, (2008)), viscoelastic earth structure (Lambeck *et al.*, (1998)), and the global meltwater signal (Shennan (1999), Shennan *et al.*, (2002)). Not only do such models play an important role in understanding past sea level and climate change processes, but more recently have been adopted in predictions of future change through the influence of

vertical land motion on predictions of mean sea-level change (Lowe *et al.*, (2009)). Recent studies have demonstrated that GIA is the dominant contributor to long-term (century to millennial) vertical land motion in the UK region (e.g. Teferle *et al.*, (2009), Bradley *et al.*, (2009)).

The main surface observables which was used to constrain these GIA models was RSL data. Considering the six geographic zones of postglacial sea level change defined by Clark *et al.*, (1978) (see Fig. 1.2d), the study region falls approximately within Zone 1 for sites located close to the centre of ice loading (across the North and Central British Isles) and Zone 2, across the South of the British Isles. As with most modelling studies which used near-field RSL data there is an inherent non-uniqueness when constraining the choice of model parameters due to a distinct sensitivity to both the choice of regional ice and earth model. But unlike the other near-field RSL data sites, as shown in Fig. 1.2a and 1.2b, the sea level signal across the British Isles is more complex due to the regional glacio-isostatic sea level signal being of similar magnitude but opposite sign to that associated with the melting of non local ice sheets. As was discussed by Lambeck (1993b), this produces an RSL signal which is highly non-monotonic and equally sensitive to the choice of both local (such as the regional BIIS model) and non-local parameters (such as the global ice model).

The interplay between the local and non-local signals is illustrated for three sites on Fig. 1.3, where the total predicted sea-level is separated into the contribution due to the BIIS only and the contribution from all other ice sheets (abbreviated to non-local). (Note that adopted ice model and earth model is taken from Brooks *et al.*, (2008) with greater detail to be found in Chapter 2 and 5. The main aim of the figure is to illustrate the interplay between two key model inputs, the local and global ice model, rather than which GIA model is optimum to use for the region). The three sites shown were selected to highlight the north-south variation in the character of the RSL signal and that the relative contribution of local versus non-local processes is a function of location.

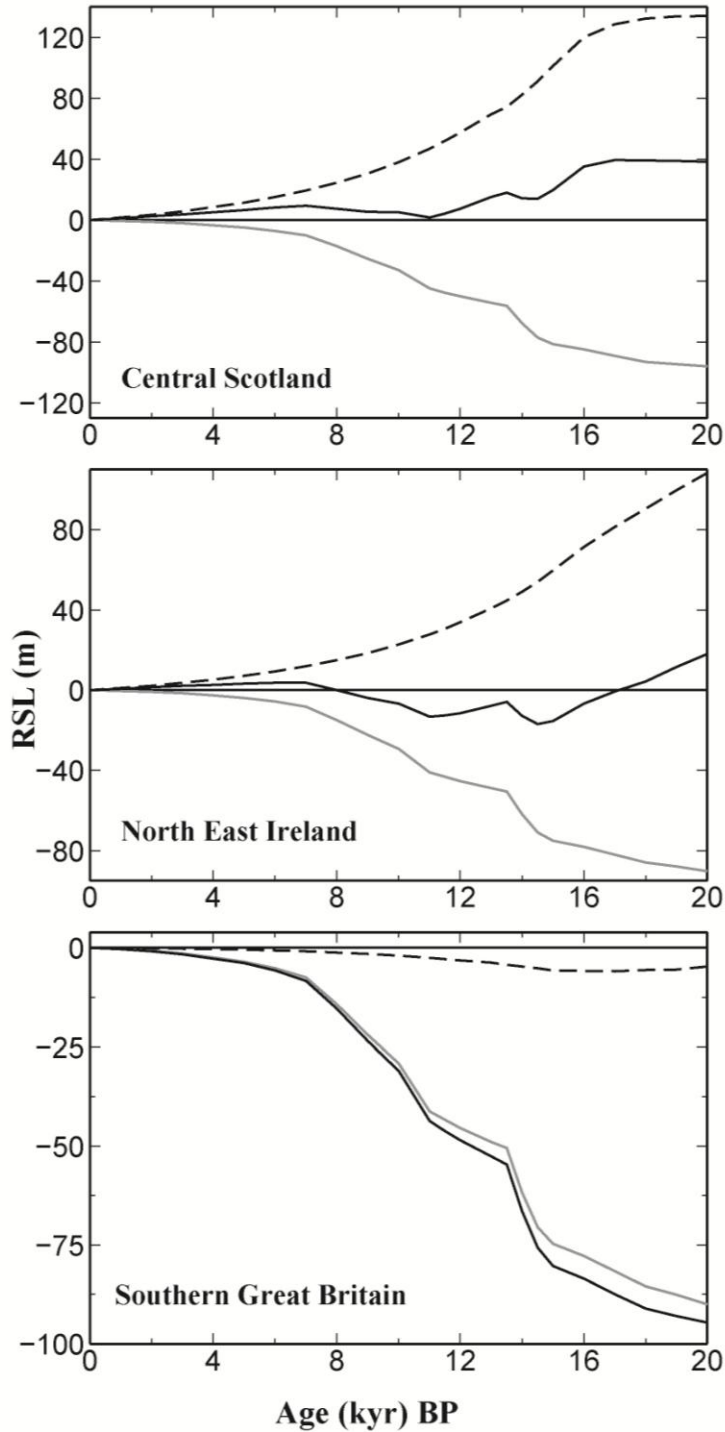


Fig. 1.3: Predictions of relative sea level at three selected sites across the British Isles using the Brooks *et al.*, (2008) ice model combined with an average earth model. More information regarding this model can be found within the following chapters of the thesis and the published reference. The total signal (solid black line) is separated into the signal due to non-local ice sheets (grey solid line) and the local British-Irish ice sheet (black dashed line).

The predictions shown at a site within Central Scotland are located close to the centre of the ice sheet and as such will experience the maximum rebound and RSL fall as the BIIS deglaciated. The BIIS-only signal produces a steady fall from 134 m towards present from the onset of deglaciation (~ 20 kyr BP) as the weight of the overlying ice sheet is removed and the solid earth rebounds. This signal is approximately equal in magnitude but opposite in sign to the RSL produced from the non-local ice sheets, where sea level at this site rises from 90 m at 20 kyr BP towards present day levels, with a gradual slowdown throughout the mid-to-late Holocene. The gradual rise of the predicted signal due to non-local ice is punctuated by a period of rapid sea-level rise at ~ 14 kyr BP, known as meltwater pulse 1A (mwp-1A). It is this event which produces the inflection evident in the total predicted sea-level signal at this time. The change from fall to rise at ~ 11 kyr BP is also due to an increase in the rate of global ice melt following the Younger Dryas cold period. This increased rate of melting, although not as high as that during mwp-1A, was sustained for several kyr until the early Holocene. In a past study (Shennan (1999)) it was highlighted that RSL data and surrounding field evidence from within isolation basins across NW Scotland could be used to constrain the possible magnitude and timings of these periods of increased global melting.

Across North East Ireland, the magnitude of the predicted BIIS signal is reduced due to the greater distance away from the centre of ice loading. The signal remains below present from the onset of deglaciation, only rising above present in the early Holocene when local hydro-isostasy and (global) ocean syphoning (Mitrovica and Milne (2002)) become dominant contributing processes to the signal. At the site situated in Southern Great Britain, the non-local signal dominates the total predicted signal, with the pattern similar to that displayed for Site B in Fig. 1.2. The magnitude of the BIIS signal has greatly reduced, with the minor rise from 14 kyr BP driven by the subsidence of the solid surface and collapse of the BIIS and SIS glacial forebulge.

The complexity of the British Isles RSL signal and the distinct sensitivity of predictions to both the local and non local processes results in the RSL data being notoriously difficult to fit and interpret in a rigorous manner. To accurately capture the pattern of the RSL signal requires a good constraint on both the regional ice sheet history, earth

rheology and the background melting history. As a consequence, past modelling studies differ not only in the fit to the RSL data but also in the optimum range of model parameters (see Milne *et al.*, (2006) and Shennan *et al.*, (2006a)). For example, early modelling studies of Lambeck *et al.*, (1996) and Shennan *et al.*, (2000) inferred that the optimum lithosphere thickness for the region was  $\sim 65$  km, compared to later work by Peltier *et al.*, (2002) who preferred a thicker lithosphere,  $\sim 90$ km. There have also been differences in the adopted spatial and temporal history for BIIS model, most specifically in the rate of ice build up prior to LGM and the maximum spatial extent. Peltier *et al.*, (2002) assumed that the BIIS was in equilibrium at the LGM, having maintained the same spatial extent throughout the Devensian up to the start of deglaciation. In contrast, Johnston and Lambeck (2000) stated the importance of the pre-LGM glacial period and proposed a BIIS model in which the British Isles was ice free prior to 27 kyr BP. Additionally, within this later model, a more extensive ice sheet was proposed with ice margins extending into the offshore regions and with ice across the entire of Irish mainland. It is noted that one key problem yet unresolved with capturing the RSL trend across the British Isles has been the overprediction in the height of the Holocene highstand (Shennan *et al.*, (2002)). This will be addressed within this study.

The above discussion indicates that to produce better constrained models of the GIA across the British Isles, additional datasets which offer a distinct parameter sensitivity to that of the RSL data must be considered. Milne *et al.*, (2006) first highlighted the use of CGPS data from across Great Britain as a useful complementary dataset with which to constrain the GIA processes across this region and reduce some of the inherent non-uniqueness described above. As the data monitor the motion associated with the local solid earth deformation, by calculating rates relative to a defined reference sites, it was shown that the sensitivity to the non-local GIA processes (such as global ice model) can be reduced. A primary aim of this thesis is to adopt as much data as possible to arrive at a better constrained GIA model for the British Isles (see Section 1.4).

## **1.2. GIA Modelling and Theory**

### **1.2.1. Introduction**

A GIA model is an isostatic computer model and has three key inputs: a model of the Late Pleistocene ice history (see Section 1.2.3 and Chapter 2), an earth model to reproduce the solid earth deformation resulting from the surface mass redistribution (see Section 1.2.4) and a model of sea level change to calculate the redistribution of ocean mass. The theory behind the latter was initially developed by Farrell and Clark (1976) in the form of an equation, known as the sea level equation, and will be referred to hereafter as ‘FC theory’. The first two inputs are user-defined and will be varied within this thesis. This type of model will be used throughout this thesis to generate predictions of RSL and present day land motion for a suite of earth models.

Early applications of the sea level equation by Clark *et al.*, (1978) enabled accurate predictions of sea level (as shown in Fig. 1.2D) for a defined input ice loading history and a non-rotating, spherically symmetric viscoelastic earth model. Over the past two decades there have been a number of advancements and extensions to the FC theory to address the two key assumptions: that the earth was non-rotating and that coastlines were fixed in time. The most recent version of the sea-level equation is adopted within this study, with further details found in Kendall *et al.*, (2005) and Mitrovica and Milne (2003). Revisions to the FC theory include: GIA-induced perturbations to the rotation vector (Milne and Mitrovica (1998b)); time-dependant shoreline migration (Milne and Mitrovica (1998a)) and an accurate treatment of sea level in regions of ablating marine-based ice (Milne *et al.*, (1999)).

In order to model observations of present-day vertical and horizontal deformation rates, the theory and approach described by Mitrovica *et al.*, (1994a), Mitrovica *et al.*, (1994b) is adopted. However, an extended version of this theory to include the influence of GIA-induced perturbations in Earth rotation (e.g. Mitrovica and Milne 2000) is used.

The complete theoretical background behind the most recent advances to the sea level equation and prediction of present day deformation rates are not evaluated within this thesis, but can be found in the above cited references. An overview of the key theoretical aspects of GIA modelling will be provided in the following sub-section (1.2.2), but it is noted that the equations do not represent the theory used within the thesis. This will be followed by a brief discussion on the ice and Earth model used as inputs in this thesis. More detail in this regard is provided in the appropriate chapters.

### 1.2.2. Theory

The redistribution of mass associated with the numerous past glacial cycles and associated change in sea level perturbs the system through a movement of mass both internally and externally (such as between the ice sheets and oceans). Assuming that climate-driven changes in surface mass flux stops, the system will tend towards a new configuration in which the total mass is in isostatic equilibrium. In moving towards this equilibrium, changes occur in the geopotential and height and horizontal position of the solid surface.

The theory applied to model the earth response to a change in surface load, or mass redistribution, is based upon the impulse response formalism (Peltier (1974)), where the response of a spherically symmetric, self gravitating, non-rotating viscoelastic earth to an arbitrary surface mass load can be calculated by the space-time convolution of a general load function  $L(\theta, \psi, t)$ , with an appropriate Green's function,  $G(\theta, \Psi, t)$  at co-latitude ( $\theta$ ) and longitude ( $\Psi$ ). This can be expressed as follows:

$$\phi(\theta, \Psi, t) = \int_{-\infty}^t \iint_{\Omega} L(\theta, \Psi, t) * G(\theta, \Psi, t) \partial\Omega \partial t \quad (1)$$

where  $\Omega$  is the spatial integration over unit sphere and  $*$  defines a spatial convolution.  $\phi(\theta, \Psi, t)$  is a general expression for the potential perturbation of the Earth system. As mentioned above, this can be considered in terms of three different components: a perturbation in both the radial and tangential displacement in the solid surface and a perturbation in the geopotential.

The impulse response formalism of Peltier (1974) is adopted to calculate the response of a viscoelastic (Maxwell) earth to an idealistic surface load that is point-like in both space and time. This response is represented through a series of viscoelastic surface load Love numbers which are coefficients of degree  $l$  in a Legendre polynomial expansion of the Green's functions for the radial,  $h_\lambda^L(t)$  and tangential  $l_\lambda^L(t)$  displacement fields and potential  $k_\lambda^L(t)$  perturbation and have the following form:

$$h_\lambda^L(t) = h_\lambda^{L,E} \delta(t) + \sum_{k=1}^K r_k^{\lambda,L} \exp(-s_k^\lambda t) \quad (2)$$

$$l_\lambda^L(t) = l_\lambda^{L,E} \delta(t) + \sum_{k=1}^K r_k^{\lambda,L} \exp(-s_k^\lambda t) \quad (3)$$

$$k_\lambda^L(t) = k_\lambda^{L,E} \delta(t) + \sum_{k=1}^K r_k^{\lambda,L} \exp(-s_k^\lambda t) \quad (4)$$

where  $t$  is time, the  $L$  superscript denotes that the Love numbers are associated with a surface mass loading,  $\delta(t)$  denotes the Dirac delta function. The first term on the right hand side represents the instantaneous elastic response to the applied load, the second term a non elastic response which is represented by a set of  $K$  modes of exponential decay. Each mode is defined by an inverse decay time ( $s_k^\lambda$ ) and an amplitude ( $r_k^{\lambda,L}$ ) which depends on the choice of adopted earth model. These Love numbers are used in the prediction of the surface observables outlined in section 1.1.2;  $h_\lambda^L(t)$  and  $l_\lambda^L(t)$  are used to predict radial (vertical) and horizontal displacement while both the  $k_\lambda^L(t)$  and  $h_\lambda^L(t)$  Love numbers are required to model sea-level change as outlined below.

These Love numbers are used to construct the impulse response Green Functions for the radial  $\Gamma^L(\gamma, t)$  and tangential  $\Upsilon^L(\gamma, t)$  displacement of the solid surface and geopotential perturbation on the undeformed surface  $Y^L(\gamma, t)$ ;

$$\Gamma^L(\gamma, t) = \frac{a}{M_e} \sum_{\lambda=0}^{\infty} h_\lambda^L P_\lambda(\cos \gamma) \quad (5)$$

$$T^L(\gamma, t) = \frac{a}{M_e} \sum_{\lambda=0}^{\infty} l_{\lambda}^L(t) \frac{\partial}{\partial \gamma} P_{\lambda}(\cos \gamma) \hat{\gamma} \quad (6)$$

$$Y^L(\gamma, t) = \frac{ag}{M_e} \sum_{\lambda=0}^{\infty} k_{\lambda}^L(t) P_{\lambda}(\cos \gamma) \quad (7)$$

where  $a$  and  $M_e$  are the mean radius and mass of the Earth respectively,  $g$  is the surface gravitational acceleration,  $\gamma$  represents the angular distance between the impulse load point and the observation point,  $\hat{\gamma}$  is a unit vector tangent to the surface in the direction of a great circle extending between the impulse load point and the observation point.

This thesis is mainly concerned with predictions of sea level change and present day radial displacement. To calculate these requires expressions for the radial displacement of the solid surface and perturbation to the geopotential (and later the geoid anomaly). As such, expressions which examine perturbations in the tangential displacement will not be evaluated further.

Substituting the relevant Green's function from (5) and (6) into the general equation (1) yields expressions for the perturbation to the radial displacement of the solid surface,

$R^L(\theta, \psi, t)$  and the geopotential at the undeformed surface,  $\Phi^L(\theta, \psi, t)$ ,

$$R^L(\theta, \psi, t) = \int_{-\infty}^t \iint_{\Omega} a^2 L(\theta', \psi', t') \Gamma^L(\gamma, t-t') \partial \Omega' \partial t' \quad (8)$$

$$\Phi^L(\theta, \psi, t) = \int_{-\infty}^t \iint_{\Omega} a^2 L(\theta', \psi', t') Y^L(\gamma, t-t') \partial \Omega' \partial t' \quad (9)$$

As was defined in section 1.1.2, sea level is the vertical height difference between the geoid (ocean surface) and the solid surface. A change in sea level  $S(\theta, \Psi, t)$  can therefore be defined simply as the difference between the perturbation in the geoid and the perturbation in the solid surface, as follows:

$$S(\theta, \Psi, t) = C(\theta, \Psi) [G^L(\theta, \Psi, t) - R^L(\theta, \Psi, t)] \quad (10)$$

where  $G^L(\theta, \Psi, t)$  and  $R^L(\theta, \psi, t)$  are the load induced perturbation in the geoid and solid surface respectively,  $C(\theta, \Psi)$  is the ocean function, defined to be unity over ocean and zero over land regions (Munk and Macdonald (1960))

An expression for the perturbation in the solid surface  $R^L(\theta, \psi, t)$  can be taken directly from equation (8). An expression for the perturbation in the geoid  $G^L(\theta, \Psi, t)$  can be evaluated using the expression in (9) as follows,

$$G^L(\theta, \Psi, t) = \frac{\Phi^L(\theta, \Psi, t)}{g} + \Delta\Phi(t) \quad (11)$$

The first term right hand side of equation (11) represents a spatially variable shift in the geoid, where the perturbation in the geopotential (9) is normalized by  $g$ , the surface gravitational acceleration. As the geoid is defined as an equipotential surface of the earth's gravity field, any perturbation in the geoid (or ocean surface) height must also reflect a perturbation in the earth gravity field. The second term on the right hand side  $\Delta\Phi(t)$  is the spatially uniform shift in the geoid, which is to account for the conservation of mass between the ice sheet and oceans, where the change in the volume of the region bounded by the geoid and the ocean floor must be consistent with the volume of ice lost or gained. It is defined as follows

$$\Delta\Phi(t) = \frac{-1}{\rho_w} \int_0^t \frac{M_I(t)}{A_o(t)} - \frac{1}{A_o} \int_p \left\langle \frac{\Phi^L(\theta, \Psi, t)}{g} - R^L(\theta, \Psi, t) \right\rangle \partial t \quad (12)$$

where  $M_I(t)$  is the rate of change of mass in grounded ice since the onset of loading,  $\rho_w$  is the density of the water,  $A_o$  is the surface area of oceans basins.

The first term on the right hand side can be used to calculate the eustatic sea level  $\Delta S_{est}(t)$  or a globally uniform height shift in the ocean surface that would occur in the absence of gravitational effects and earth deformation due to mass input from continental ice reservoirs (Farrell and Clark (1976)).

$$\Delta S_{est}(t) = -\frac{\rho_{ice}}{\rho_w} \int_0^t \left( \frac{V_{ice}(t)}{A_o(t)} \right) \partial t \quad (13)$$

where  $p_{ice}$  is the density of ice,  $V_{ice}$  is the rate of change in grounded ice volume between time  $t$  and  $t=0$ . This relationship will be used later within this thesis, within Chapter 4 which focuses on constraining a model of global ice volume changes.

The general expression for the sea level given in (10) can now be re written using the above expressions as follows,

$$S(\theta, \Psi, t) = C(\theta, \Psi) \left[ \int_{-\infty}^t \iint_{\Omega} a^2 L(\theta', \Psi', t') \left\{ \frac{Y^L(\gamma, t-t')}{g} - \Gamma^L(\gamma, t-t') \right\} \partial \Omega' \partial t' + \Delta \Phi(t) \right] \quad (14)$$

This equation is referred to as the sea level equation, from Farrell and Clark, 1976.

The general load function,  $L(\theta, \psi, t)$  represents a model of the spatial-temporal variation in ice-ocean mass. It can be defined as follows:

$$L(\theta, \psi, t) = p_{ice} I(\theta, \Psi, t) + p_w S(\theta, \Psi, t) \quad (14)$$

$I(\theta, \Psi, t)$  defines the space-time variation of ice thickness of the input ice model, and as was mentioned above is one of the main user defined inputs into a GIA model, as will be described below.

### 1.2.3. Input Ice model

There are a range of different types of models which can be used to reproduce the evolution of an ice sheet over a glacial cycle. The main types can be defined as: geomorphologically-driven models (such as Greenwood and Clark (2009b)), 3D numerical thermomechanical models (such as Hubbard (1999), Hubbard *et al.*, (2009), Boulton and Hagdorn (2006)) and isostatic load models (such as Peltier (2004), Lambeck *et al.*, (2010), Brooks *et al.*, (2008)). Geomorphologically-models are qualitative (i.e data-derived) reconstructions, which incorporate information from the mapped geomorphological landform record (i.e Greenwood and Clark (2009a)) and the inferred

paleo-ice flow record. These models provide information on past the changes in the centres of ice mass, ice divides or ice flow geometries throughout a glacial cycle. 3D numerical thermomechanical ice sheet models are developed using physics of ice-flow and mass balance (Boulton and Hagdorn (2006)), forced by prescribed climate conditions to simulate the 3D geometry of an ice sheet and additional physical characteristics (i.e basal temperature or ice velocity) as a function of time. These paleo-climate forcings include records taken from ice cores (such as the North Greenland Ice Core project) and models of global eustatic sea level (Fairbanks (1989))

The type of ice model used within this thesis is a 3D isostatic load model, where the surface of the earth is divided into an equally spaced longitude/latitude grid with a spacing of  $\sim 0.7^\circ \times 0.7^\circ$  (77km) (and so greater spatial resolution is achieved at high latitudes). The model is separated into a series of 40 loading increments, at a resolution of 7000 yrs between 116 kyr and 25 kyr and at  $\sim 1000$  yr intervals between the LGM and the present day (with an increased time resolution of 500 yr during periods of rapid change). The ice model is not a glaciologically realistic model, hence there is no treatment of surface mass balance or ice flow geometries, as within the two types of model described above, but is assumed to follow a simplistic parabolic shape. At each time interval for each grid point across the earth surface, the thickness and spatial extent of ice is defined. To constrain these values, geomorphological data (see Section 1.3.3 and 2.2.2) on the spatial and vertical extent of an ice sheet are used. For example (see Fig. 1.4A) at 21 kyr BP, the defined ice thickness can range from 0 m within the Pacific Ocean to  $\sim 4000$  m across Antarctica.

The starting ice model used within this thesis is a composite of two published models: a global ice model taken from Bassett *et al.*, (2005) and a higher resolution regional BIIS model taken from Shennan *et al.*, (2002). The global ice model developed by Bassett *et al.*, (2005) (which will be referred to throughout the study as the Bassett et al. model) includes the Northern Hemisphere ice sheets of North America (Laurentian, Innuitian and Cordilleran), Greenland, Eurasia (Barents Kara and Fennoscandia), and the Southern Hemisphere ice sheets of West and East Antarctica and the smaller Patagonian ice fields. The spatial extent of the ice in these regions, as incorporated in the model, is illustrated

on Fig. 1.4 for the LGM (~ 21 kyr BP) and the present day. In the Bassett et al. study, their starting model - the ICE3G ice history model (Tushingham and Peltier (1991)) – was altered to produce an optimum fit to a suite of far-field RSL data from Barbados, Huon Peninsula, Sunda Shelf, Bonaparte Gulf and Tahiti between LGM and 10 kyr BP. Two main modifications were made to the ICE3G model: a pre –LGM glaciation phase was introduced to create a new glaciation period which extended over 100 kyr BP; secondly, the glacial histories of the LIS and AIS were altered to achieve an optimum fit to the far-field sea level data, with the introduction of a rapid rise in eustatic sea level of ~ 22 m, associated with mwp-1A. One key finding of this study was that a far better fit was achieved to the RSL data when a dominant contribution to mwp-1A is sourced from the AIS, rather than the North American ice sheets.

Comparing Fig. 1.4B & D highlights the significant reduction in the size and volume of global ice cover within the Northern Hemisphere between the LGM and the present day. At the LGM, large ice sheets covered most of North America, Greenland and across NW Eurasia and the high Arctic. During this final glacial period, these major ice sheets retreated, with the deglaciation of North America largely complete by ~ 7 kyr BP and Eurasia by ~ 8 kyr BP. The only remaining significant ice sheet in the Northern Hemisphere at present is the Greenland ice sheet. Across the Southern Hemisphere at the LGM (Fig. 1.4A), glaciation was limited to the southern tip of South America with the growth of the Patagonian Ice sheet and the larger, more extensive AIS, across the whole of Antarctica. Within the Bassett et al. model the Patagonian ice sheet has completely deglaciated by 14 kyr BP, with the final deglaciation phase of the AIS ending at 8 kyr BP, by which time the ice sheet had thinned by over 1700 m and retreated inland.

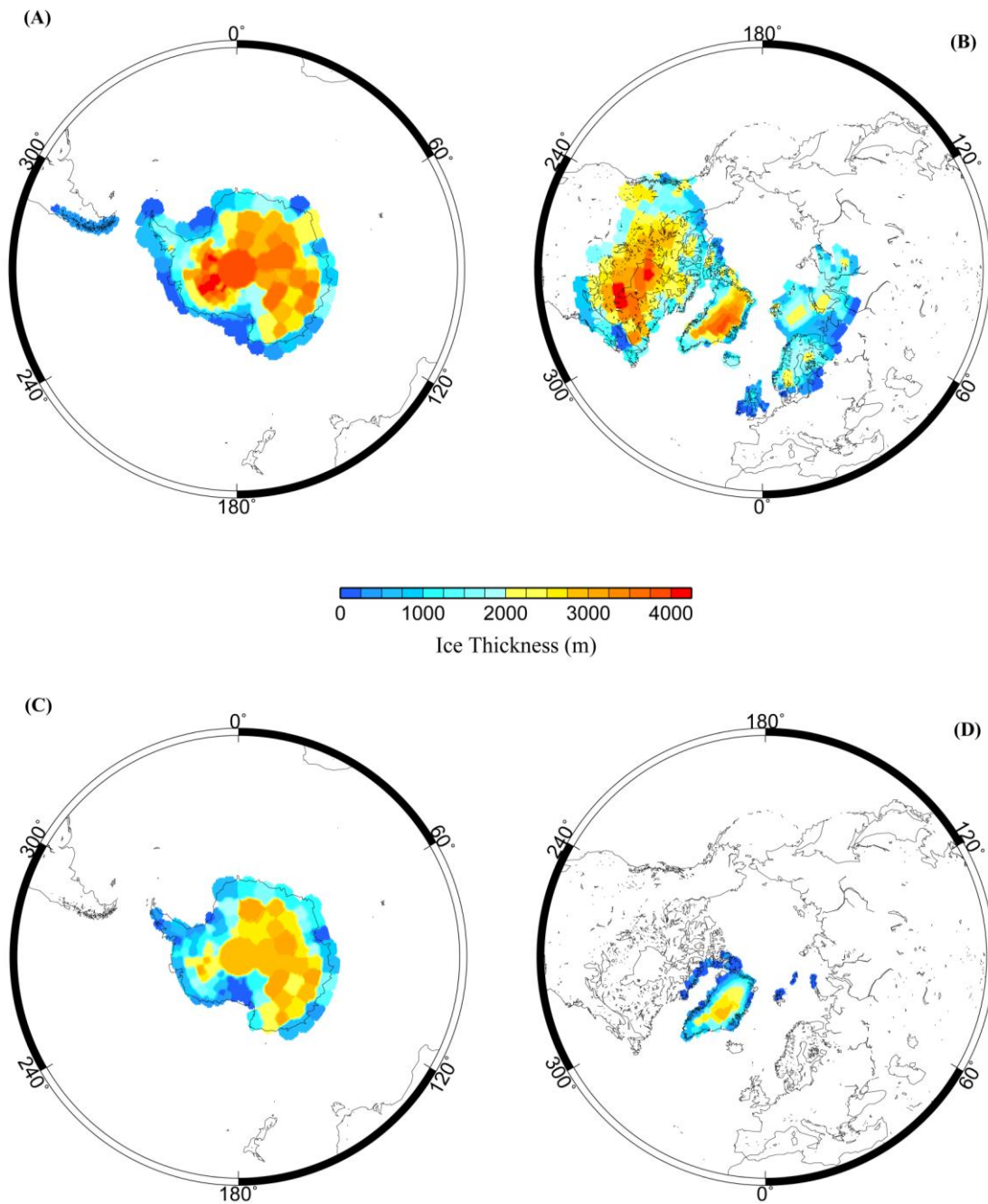


Fig. 1.4: Spatial plots of the ice extent of the starting ice model at the LGM (21 kyr BP) (A and B) and at present day (C and D) for the Northern and Southern Hemispheres. The global ice model is taken from Bassett *et al.*, (2005). The regional ice model, which includes the British and Irish Ice sheet, is taken from Shennan *et al.*, (2002).

Also shown on Fig. 1.4B is the extent at the LGM of the BIIS. This regional ice model was developed to fit a suite of RSL data from sites across the Great Britain and to be

consistent with the current geomorphological constraints on the BIIS spatial and temporal history. A more detailed description of this ice model can be found later within this thesis (Section 2.3).

#### **1.2.4. Input Earth model**

The Earth model adopted within this thesis is a spherically symmetric, self gravitating viscoelastic (Maxwell) body. The input model has five parameters which are defined with depth: density, P and S wave velocity, gravity and viscosity. The first four of these are taken from seismic constraints (Dziewonski and Anderson (1981)) and depth parameterised at resolution of 10km within the crust, 25km within the mantle, 70 km in the outer core and 38 km in the inner core. The viscosity structure is parameterised at a cruder resolution than the above parameters into 5 main layers, as summarised on Fig. 1.5: an upper layer of high viscosity ( $10^{43}$  Pa s) to simulate the elastic lithosphere (which includes the crust), an upper mantle which extends from the base of the lithosphere to the 670 km seismic discontinuity and a lower mantle which extends from this depth to the core-mantle boundary, and two lower regions which represent the outer and inner core. The lithosphere thickness and upper and lower mantle viscosity values are free parameters within the modelling. All other earth model parameters remain unchanged throughout the thesis. A range of values for these three input parameters will be examined based on the spread of possible values inferred in recent GIA studies (e.g. Forte and Mitrovica (1996), Milne *et al.*, (2001), Nakada and Lambeck (1989), Davis *et al.*, (1999), Kaufmann and Lambeck (2002)). The maximum and minimum values for upper and lower mantle viscosity will be  $0.08-5 \times 10^{21}$  Pa s and  $1-50 \times 10^{21}$  Pa s, respectively, for lithosphere thicknesses of 71, 96 or 120 km.

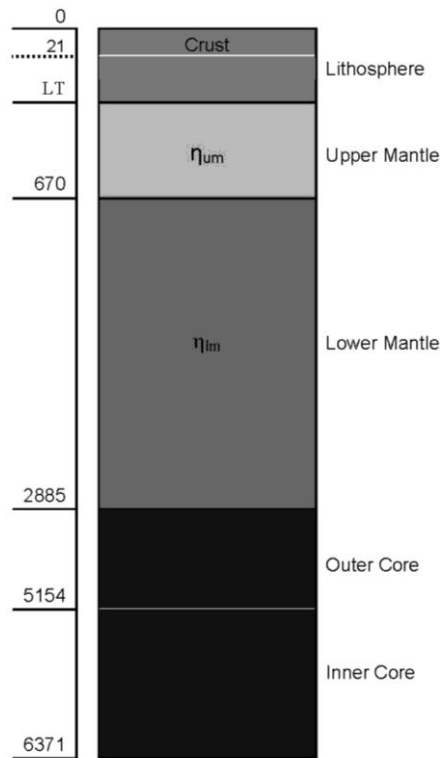


Fig. 1.5: Schematic representation of the variation with depth (km) of the viscosity structure of the input earth model. The viscosity value within the lithosphere is set to  $10^{43}$  Pas. This value remains fixed throughout the thesis. The following three parameters:  $LT$ , the lithosphere thickness,  $\eta_{um}$  and  $\eta_{lm}$  the upper and lower mantle viscosity are user defined inputs and are varied throughout this thesis.

### 1.3. Observational Data

#### 1.3.1. Relative sea level data

Over 30 yrs of research, coordinated through the International Geological Correlation Programmes (IGCP), has produced a well defined methodology for developing records of relative sea level change from geomorphological features (such as raised shorelines, beach deposits) or sedimentary environments and their associated fauna and flora (Van De Plassche (1986), Shennan (1982) and Tooley (1982)). This methodology is based around the development of sea level index points (SLIPs) which rests on the principle that “variations between terrestrial and marine sedimentation reflects changes in the balance between land and ocean levels moderated by local scale processes such as rate of

sedimentation” (Van De Plassche (1986)). For a fossil sea level indicator to be defined as a SLIP it must be possible to establish the following four attributes: location (longitude and latitude), age (defined in calendar years), altitude (relative to a levelling datum) and its vertical relationship to a contemporaneous tide level (termed the indicative meaning).

Based on the ability of a sea level indicator to fulfil these four requirements, samples can be separated into four classes. The highest quality sea level indicators are Primary SLIPs, which possess information on all four attributes. They are the most useful for constraining predictions of RSL generated by GIA models as they provide a direct measure of past RSL with clear defined height uncertainty. In the Ireland RSL database (Brooks and Edwards (2006)) a second subset was introduced, which will be referred to as secondary SLIP. These are derived from dated sea level indicators but where one or more of the key attributes is unquantified or associated with a significant uncertainty. This may be due to limited accompanying microfossil analysis, poor chronological control or where material was sourced from archaeological evidence.

When it is not possible to define a quantitative relationship between the field evidence and the contemporaneous tidal regime for the dated sea-level indicator it is classified as a limiting date. These samples can only be used to indicate whether sea level occupied a position above or below a certain altitude and are derived from material such as freshwater peats or in situ tree stumps.

The majority of sea level indicators from around the British Isles are taken from low energy coastal environments, such as salt marshes, or isolation basins. An isolation basin is defined as a ‘naturally enclosed rock basin that was once below sea level but has subsequently been raised above it and hence become isolated from the sea (Lloyd and Evans (2002)). This isolation procedure is recorded in the litho- and biostratigraphy by a transition from marine to terrestrial deposits and in a change in the microfossil assemblages preserved within the basin sediments. The microfossils are sensitive to changes in the salinity within the basin and as such, provide a record of the change from brackish to freshwater depositional environment. The age of the sample is derived by dating the contact between the marine and terrestrial deposits and associated microfossils,

with the altitude and indicative meaning defined by the height of the lowest part of the rock sill which separates the basin from the open sea (Edwards (2006)).

SLIP records from other low energy coastal environments, such as salt marshes are also derived from the transitions recorded in lithostratigraphic records between terrestrial and marine sediments, with supporting microfossil evidence (such as pollen or diatoms). The most common sequence found in such records around the British Isles is alternating horizons of freshwater peats, organic rich sediments and marine clastic sediments. The age and altitude of sea level indicator is derived from the contact between these contrasting stratigraphic sequences, with microfossil analyses often used to corroborate and further quantify the indicative meaning.

When modelling sea level data it is important to quantify the magnitude and possible sources of the uncertainty associated with determining the altitude and indicative meaning. Altitude errors may arise during sampling, such as associated with levelling to the datum, or measurement of lithostratigraphic contacts, or in establishing the indicative meaning. A standardized vertical error calculation as described in Shennan (1986) or Horton *et al.*, (2000) can account for all quantifiable vertical errors, including problems with field levelling, present tide heights and interpretation of the indicative meaning. This calculation has been applied throughout the RSL database used in this thesis.

An unquantifiable factor which may affect the reliability of a SLIP is post-depositional compaction (or consolidation), which acts to lower the reconstructed altitude of the sample. There is no widely accepted approach to quantify or account for the affect of this process (Shennan and Horton (2002)). Most studies aim to minimise its impact on the quality of the SLIP by concentrating on sediment samples that have undergone minimal or no compaction. For example, in isolation basin reconstructions, since the altitude of the sample is defined from the height of the sill which is commonly bedrock, these SLIPs are not affected by compaction. Samples taken from thin basal peats or the base of basal peats which are deposited over a hard substrate are also not as significantly affected by sediment compaction, in contrast to samples derived from thick intercalated clay, silt and peat sequences.

Another possible source of error is the assumption, when estimating the indicative meaning, that there have been no significant changes in the local tidal range since sample deposition. In reality, many regions will have experienced some change in tidal range which may produce changes in the reference water level through time. These will be greatest within macro-tidal regions such as estuaries or regions with pronounced changes in coastal geometry. One method to account for this is to correct the affected sites using estimates of these changes from a paleo-tidal model (Shennan and Horton (2002)).

### **1.3.2. Continuous GPS data**

Over the last ~ 10 years, the CGPS network across the British Isles has steadily expanded to now include over 130 receivers (*see www.bigf.ac.uk*). The majority of these were not deployed with the aim of monitoring the secular motion of the solid earth; most were established as a network real-time system that did not require a stable site that monitors the solid earth motion and as such can be located on unstable buildings. As such, the number of receivers which provide an accurate measure of the 3D crustal motion at a precision of  $\text{sub mm yr}^{-1}$  is significantly less than the total number of receivers. A number of criteria were considered when choosing which CGPS sites to use within this thesis.

First, sites with less than 4 years of consistent and uninterrupted recorded data and whose station-specific monumentation was considered to be unstable or unsuitable were removed (see Teferle *et al.*, (2009) for a complete discussion of these issues). Second, the time series and crustal velocities at each site were compared using two different processing techniques (Teferle *et al.*, (2009)): (a) the IESSG's (Institute of Engineering Surveying and Space Geodesy, Nottingham) GPS analysis software version 2.4 which produced a series of daily double-difference regional network solutions and (b) a series of daily precise point positioning globally transformed solutions generated using Bernese GPS software version 5.0 (Dach *et al.*, (2007)). In both cases crustal velocities (vertical and horizontal) at each site were obtained from a model-fit using maximum-likelihood estimation (Williams *et al.*, (2004)), which has been shown to accurately take into account uncertainties and systematic offsets in the processed signal arising from, for

example, white and coloured noise, unmitigated tropospheric delays or bias in the satellite orbits. Sites where difference in the vertical and horizontal velocities obtained using these two processing techniques was greater than  $1 \text{ mm yr}^{-1}$ , and the calculated time series displayed anomalous trends, were rejected. Also if the calculated site velocities were inconsistent with the rates from surrounding stations, the anomalous sites were removed. When all of these criteria were applied, the total number of suitable sites reduced to 16 for vertical motion and 21 for horizontal motion.

When processing the CCPS data to produce an estimation of the vertical crustal motion, a systematic bias can also be introduced due to uncertainties in the adopted terrestrial reference frame, which in this study was ITRF2000 (Altamimi *et al.*, (2002)). A simple procedure to address this and also improve the accuracy of the vertical velocity estimates, as shown by Teferle *et al.*, (2006), is to calibrate the CGPS derived velocities with those estimated from measurements of absolute gravity (AG). AG-derived estimates of vertical velocity were taken from two sites; Lerwick in Scotland and Newlyn in SW England. By calculating the difference between the CGPS and AG derived estimates of vertical velocities at these two stations (rates summarised in Teferle *et al.*, (2009)) and subtracting this offset from the CGPS-vertical velocity at each station, AG-aligned CGPS estimates of vertical velocity can be generated. More information is provided in Chapter 3.

### **1.3.3. Geomorphological Data**

When developing an ice model for any given region there are key elements that need to be constrained: the timings of the main advance and retreat phases as well as the lateral and vertical extent through time. Geomorphological field evidence can provide constraints on the vertical and lateral extent of the past ice sheets, and a combination of radiocarbon and cosmogenic dating of such features can be used to constrain the associated chronological history.

In the following section a brief overview of the main landforms and associated dating techniques mentioned within this thesis will be given. It is noted that a complete description of all glacial landforms and related dating techniques is beyond the scope of

this thesis. The reader is referred to the following papers for more information: Evans and Benn (2007), Colgan (2007), Mickelson and Winguth (2007).

There are two main dating techniques mentioned within this thesis: Accelerator Mass Spectrometry (AMS) radiocarbon and cosmogenic nuclide surface exposure dating. The former method is most commonly applied in the dating of RSL data but also routinely used to date landform features such as glacial moraines. This method is limited to deposits which contain organic material, and to the last 50 kyr BP due to the practical limitations of the technique.

Cosmogenic nuclides, such as  $^{26}\text{Al}$ ,  $^{36}\text{Cl}$  or  $^{10}\text{Be}$  are produced in surface rocks by the action of cosmic radiation. The length of time that a rock surface has been exposed can therefore be determined by calculating the concentration of such nuclides within a sample of the rock surface. Other natural processes can affect the concentration of the cosmogenic nuclides in the rock sample, such as erosion, weathering and as such will act to produce older exposure ages. As most glacial surfaces will have experienced some level of post-exposure erosion, locating a sample from a fresh surface is complicated. As there is no reliable estimation of erosion rates for rock surface across the British Isles, a range of rates are usually considered, between 0- 3 mm kyr<sup>-1</sup> taken from studies in other similar glaciated regions (Ballantyne (2010), Bowen *et al.*, (2002)). This dating technique is commonly used to produce surface exposure ages at older, pre-LGM times.

The main geomorphological feature which is used to constrain the vertical extent (i.e. the thickness) of the BIIS is periglacial trimlines, which are defined as “the upper level to which glacial erosion has removed or ‘trimmed’ a pre-existing cover of pre-glacial or periglacial (frost-weathered) regolith on the flanks of nunataks or other mountain surface” (Ballantyne (2007)). This marks a weathering limit or horizon which separates an upper zone of more advanced rock breakdown (generally due to frost action) from a lower zone which is characterised by glacial erosion and more limited post-deglaciation rock weathering.

There are a range of theories proposed to account for the development of trimlines, which have been recently reviewed in Ballantyne (2007). Three of the main theories which have been considered within mapping studies across the British Isles are summarised below and illustrated on Fig. 1.6.

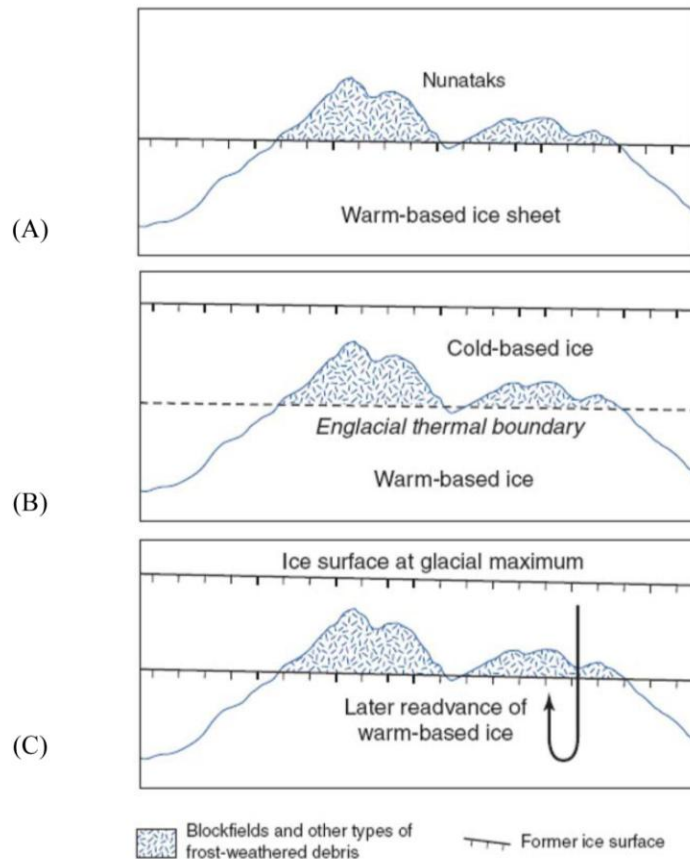


Fig. 1.6: Three proposed mechanisms for the formation of periglacial trimlines (adapted from Ballantyne, (2007)). (A) the ice-marginal (nunatak) hypothesis, in which the trimline marks the upper surface of the glacier at its maximum thickness, (B) the englacial hypothesis, where the trimline represents a thermal boundary between a lower warm based (erosive) ice and upper cold based (passive) ice within an ice sheet, (C) the readvance hypothesis, where the trimline forms due to the later readvance of a warm-based ice sheet.

The most widely applied theory to explain the formation of trimlines, and adopted in the early mapping studies across the British Isles can be referred to as the ice-marginal hypothesis (Fig. 1.6A), where the trimline marks the upper limit of a warm-based

(erosive) ice sheet with ice free nunataks above the ice limit. In this theory, the trimline is used to define the maximum vertical thickness of the ice sheet. A second theory (Fig. 1.6B), referred to as the englacial hypothesis, proposes that the trimline represents a thermal boundary between a lower horizon of warm based ice and an upper region of passive, cold based ice within an ice sheet. In this theory the highest summits were overridden by the regional ice sheet and the trimline can only be used to infer the minimum thickness of the lower warm based horizon. The final theory, shown on Fig. 1.6C, is where the trimline is produced due to the later readvance of a warm based ice sheet and as such will delimit the maximum thickness of this later glacial episode and not the vertical height at LGM. The main method applied to distinguish between hypothesis one and three is dating (either radiocarbon or surface exposure) the blockfields and frost-weathered debris on the exposed higher ground.

There are a range of techniques which can be applied to identify an horizon as a 'periglacial trimline', most of which relate to the identifying different degrees of rock and soil weathering between the two zones. Some of these include: a Schmidt hammer device which records the percentage of rebound from a rock surface. This is related to the elastic properties of the rock which will be affected by the amount of weathering that the surface has experienced. Generally, samples taken from a more weathered or 'rough' rock surface will produce lower rebound values, such as above a trimline. Other techniques include the distribution of dilation (open) joints which are generally deeper and more open above a trimline; or clay mineral analysis within soil samples. Ballantyne *et al.*, (1998) found that gibbsite is preferentially represented in soil samples taken from above a trimline or rock surface which have escaped glacial erosion.

Once a feature has been identified as a trimline, assigning a method of formation between hypothesis one and hypothesis two is more problematic. Interpretation of a trimline as forming due to the ice-marginal hypothesis is only valid if three main lines of evidence can be satisfied; (1) lack of erratics or glacially transported boulders above the trimline, (2) application of cosmogenic nuclide dating, generally using  $^{26}\text{Al}/^{10}\text{Be}$  to test for uninterrupted exposure of the rock surface above the trimline, indicated by pre-LGM exposure ages. (3) Consistency with other geomorphological evidence, such as decline in

the altitude of trimlines along former flowlines and glaciological constraints (such as reconstructed ice surface altitudes). Any one of these lines of evidence does not on its own provide unequivocal support of hypothesis one over hypothesis two. For example, it was initially proposed that a sharp contact between the lower ice scoured and upper frost-weathered terrain was indicative of an ice-marginal origin, but it has now been shown that sharp boundaries can develop at englacial trimlines (Ballantyne (2007)).

Ballantyne (2010) proposed four lines of interpretation to support an englacial rather than ice-marginal hypothesis for the trimlines across the British Isles. First, the presence of local sourced erratics within the blockfield debris above the trimline and preservation of the higher summits under a cold-based ice sheet. Second, maps of the ice surface altitude were interpolated based on an assumed ice thickness taken from the trimline evidence following hypothesis one (ice-marginal). These ice heights were found to be inconsistent with the spatial limits inferred from other evidence in the surrounding region, mostly relating to the offshore extent, implying a thicker ice sheet was required. Finally, numerical modelling of the BIIS using a glaciological model (Boulton and Hagdorn (2006)) has shown it is difficult to produce an ice model which complies with the thickness defined using the ice-marginal hypothesis. Additionally, optimum basal melting temperatures from these reconstructions were consistent with the development of englacial trimlines.

Reinterpretation of trimlines across the British Isles as having formed as englacial rather than ice-marginal boundaries will have important implications for the future modelling of the BIIS as discussed later in this thesis.

Unlike constraining the vertical extent of an ice sheet, there are numerous possible geomorphic landforms which are used to constrain the spatial extent, including moraines, outwash plains, eskers, many of which have been identified and summarised for the British Isles in, for example, Clark *et al.*, (2004), Evans *et al.*, (2005). The complete range of data used to constrain the BIIS in this thesis will be outlined in Section 2.2.2, with some of the main landforms that are most commonly adopted for this task defined below.

A moraine is one of the most commonly used landforms to constrain the early LGM ice limits across the British Isles and is defined as an ice marginal accumulation of sediment with a topographic expression defining a distinct landform. There are many different types of moraines, including lateral moraines which form along the edge of a glacier, end (or terminal) moraines, which define the maximum lateral extent that ice margin reached onshore or submarine morainal banks which can be used to constrain the offshore extent of an ice sheet. The two main offshore landforms which are mentioned in the development of the BIIS model are mega-scale glacial lineations (MSGSL) and trough mouth fans. MSGSL's are longitudinally aligned topographic ridge-groove corrugations, up to 100km long and tens metres high (Clark (1993) and represent the signature of fast-flowing ice within a grounded ice sheet. Due to the larger size of these landforms, they are most often identified on satellite images, or using 2D and 3D swath-bathymetry and marine seismic data. Trough mouth fans are large accumulations of subglacial sediment, which are deposited by debris flow processes from ice streams, during periods of shelf edge glaciations. Examination of the various sediment packages within the fans can be used to infer the history of ice-sheet advance and retreat across the continental shelf.

#### **1.4. Aims and Outline of Thesis**

The principal focus of the work presented in this thesis is to develop a revised GIA model for the British Isles by using independent datasets to reduce the ambiguity and sensitivity to both the local and global model input parameters. This will be achieved in a number of stages using a combination of relative sea level data from both near and far-field sites, as outlined in Section 2.2.3 and 4.2, CGPS data as described in Section 3.2 and the most recent geomorphological field constraints outlined in Section 2.2.2 and within Chapter 5.

The first step is to create a revised spatial and temporal history for the BIIS which is consistent with the most recent geomorphological data from the British Isles and the NorthSea (Section 2.2.2) and takes into account the underlying terrain. The model will be developed in two stages; first a regional model for the complete BIIS will be developed which will be calibrated against an extended RSL database from across Great Britain.

Second, the Irish Ice Sheet (IIS) component of the BIIS will be examined in more detail, an aspect of the GIA model for the British Isles which has largely been overlooked in past modelling studies. A revised IIS will be produced which addresses specific issues relating to the history of the IIS, and examines the sensitivity of RSL predictions to transient and small scale changes in the ice sheet. This model will be calibrated against a new, previously un-modelled RSL database from Ireland. A final BIIS model will be produced which combines the regional model with the revised IIS. This model will be adopted within later chapters in the thesis (Chapters 3 and 5).

In Chapter 3, a new CGPS dataset from across Great Britain will be employed to provide an independent constraint on the choice of regional earth model parameters (shallow viscoelastic structure). This is one of the key inputs into a GIA model which, as discussed above, has significantly varied within past studies. It will be shown that the CGPS data are relatively insensitive to uncertainties in the choice of both global and regional ice model. Predictions of vertical crustal motion for a suite of earth models will be examined to identify an optimal range of earth model parameters, which will be adopted within Chapter 5.

Another key input into GIA models and to which the GIA of the British Isles is distinctly sensitive is the adopted model of eustatic sea level change (or the melt history of the global ice model). In Chapter 4, I will address this issue by using a previously un-modelled far-field RSL dataset, from across China and the Malay-Thailand region to develop a revised model of eustatic sea level change over the Holocene. This work will extend an earlier published global ice model (Bassett *et al.*, (2005)), which was tuned to fit a suite of far-field data from LGM to 10 kyr BP. The model remains unconstrained over the Holocene, a time period, as mentioned above, where misfits to the RSL data across Great Britain are still unresolved. This will be achieved by examining a range of eustatic melt scenarios investigating both the pattern and rate of global melting over the last 10 kyr BP for a suite of earth models. The final optimum model of eustatic sea level change or global ice model will be adopted in Chapter 5.

In Chapter 5, the results of each of the previous chapters will be combined to produce the final revised GIA model. The revised regional ice model from Chapter 2 will be combined with the new global ice model from Chapter 4 to produce a final BIIS model. For the first time, predictions will be compared to a complete RSL database containing data from both Ireland and Great Britain for a complete suite of earth models. The range of earth models will be compared to the limits for the regional shallow viscoelastic structure constrained from the CGPS data considered in Chapter 3.

## Chapter 2: Developing an improved British-Irish Ice Sheet model

### 2.1. Introduction

Over the past decade there have been numerous GIA modelling studies for the British Isles: from the early work of Lambeck (1993a), Lambeck (1993b) to the more recent studies of Johnston and Lambeck (2000), Peltier *et al.*, (2002). In these studies a loading history model for the British-Irish Ice sheet (BIIS) was developed. While the results produced a reasonable fit to the observed RSL data, there are a number of differences between some of the analyses including the choice of input parameters - most specifically the BIIS - and the size of the available RSL database.

One noted similarity between all the proposed BIIS models (Shennan *et al.*, (2002), Johnston and Lambeck (2000)) has been the use of trimline data to constrain the thickness of the input ice model. As was pointed out by Milne *et al.*, (2006) this neglects to take into account the considerable underlying terrain across Central Scotland, which will lead to a significant overestimation in the defined ice thickness.

Only the most recent studies of Peltier *et al.*, (2002) and Shennan *et al.*, (2002) had available the extended RSL database, with data from 55 locations and a total of 943 SLIP but did not include any SLIP data from across Ireland. Some of the earlier modelling work such as Johnston and Lambeck (2000) did include data from across Ireland but there was a much smaller number of SLIP's, only 441 available.

It is evident from examining these past studies, that the changes to the BIIS reconstructions over the past few decades reflect both the constraints from new geomorphological evidence and the choice of key model input parameters (as outlined in Chapter 1). For example, the early model of Lambeck (1993a) proposed an advance of the BIIS across the North Sea to join with the SIS, which was later rejected by Lambeck (1993b) due to new evidence that suggested the LGM ice sheet terminated close to the coastal margins. Peltier *et al.* 2002 assumed that the BIIS was in equilibrium at the LGM, with the same spatial extent maintained throughout the Devensian up to the start of

deglaciation. In contrast, Johnston and Lambeck (2000) stated the importance of the pre-LGM glacial period and proposed a BIIS model in which the British Isles was ice free prior to 27 kyr BP. Additionally, within this later model, a more extensive ice sheet was proposed, compared to Peltier *et al.* 2002, with ice margins extending onto offshore regions and with ice across the entire of Irish mainland.

The main aim of this chapter is to revise an earlier published regional BIIS model (Shennan *et al.*, (2002)) to take into account a large amount of new geomorphological and chronological constraints which provide a much improved picture of the spatial and temporal history of the ice sheet during the Devensian. Also, as was mentioned above, the thickness of the input ice model needs to be adjusted to take into account the underlying terrain. This revised model is also tested by comparing predictions of RSL to observations from both Ireland and Great Britain. In this chapter, these two databases are considered separately, due to the availability of the new Ireland RSL data at the time of the model development. A more extensive comparison, for the entire combined RSL database and a large suite of earth models, is performed in Chapter 5.

The key steps followed to produce a new BIIS model are reflected in the structure of this chapter. In Section 2.2, the geomorphological and sea level data used to constrain the model are described. A revised model is generated in Section 2.3 that complies with the new geomorphological constraints and accounts for underlying terrain; this is done for the component over Great Britain (2.3.2.2) and Ireland (2.3.2.3) separately and the results from these sections are combined (2.3.3) into a new model for the BIIS that is used to generate predictions to compare to the RSL database. The results are then discussed in Section 2.4 and conclusions drawn in Section 2.5

## **2.2. Data**

### **2.2.1. Introduction**

When developing an ice model for any given region there are key elements that need to be constrained: the timings of the main advance and retreat phases as well as the lateral

and vertical extent through time. Examining geomorphological field evidence, such as moraines and trimlines can provide constraints on the vertical and lateral extent of the past ice sheet, and a combination of radiocarbon and cosmogenic dating of such features can be used to define the chronological pattern of the glacial history. New geomorphological evidence from recent studies focussing across and around the British Isles will be outlined below.

The accuracy of a given ice model can also be tested by comparing modelled GIA output, such as predictions of RSL, present-day vertical land motion and palaeo-shoreline positions, to the respective observations. The main observables utilised in this chapter to gauge the accuracy of the ice sheet reconstruction will be sea level data. The sea level database is composed of SLIPs and limiting data from 80 locations around Great Britain and Ireland, as described in detail below.

## **2.2.2. Geomorphological Data**

### **2.2.2.1. Introduction**

Despite a wealth of field evidence and modelling studies examining the pattern of Mid-Late Devensian glacial history of the BIIS, a number of contentious issues relating to the reconstruction of the ice sheet have been debated over the years, most specifically to the possible coalescence of the BIIS with the SIS across the North Sea basin (NSB) and whether northeast Scotland (Caithness and Orkney) remained ice free. Early models, such as Sissons (1967) proposed that the ice sheet across Scotland terminated near the continental shelf edge along the west coast and was confluent with the SIS across the NSB. Later studies rejected this expanded model, preferring instead an independent BIIS with ice margins restricted to the coastal regions and peripheral ice-free regions across NE Scotland and along the north and west coast of Ireland (Anderson (1981), Bowen *et al.*, (1986), Lambeck (1993b)).

As an increasing amount of new evidence from across the British Isles and NSB now supports the earlier view of a larger, more laterally extensive BIIS (e.g Carr *et al.*, (2000),

Sejrup *et al.*, (1994), Sejrup *et al.*, (2000)). These new data, used to constrain the revised ice model (Section 2.4) are outlined below.

#### **2.2.2.2. Chronology of main ice sheet advance and retreat phases**

The timings of the main growth and retreat phases to be used for the revised ice model are taken from the Sejrup *et al.*, (1994) glaciation curve (Fig. 2.1), which was developed from a series of AMS-dated material from boreholes and gravity cores from a range of sites across the NSB. The radiocarbon dating of carbonate fossils found within till and sub-till sediments across the region suggest periods of marine sedimentation, and as such, ice free conditions. During the Mid-Late Devensian a two stage-glaciation across the NSB is proposed with an initial coalescence between the BIIS and SIS marking the end of the Ålesund interstadial, ~ 33 kyr BP. This advance was interrupted by a rapid retreat ~ 26 kyr BP and opening of an ice-free corridor across the central NSB. A second readvance of the two ice sheets commences ~ 24 kyr BP, but with the central NSB remaining ice free.

The timing of the initial ice build up, after 33 kyr BP, correlates with the end of a period of restricted or ice free conditions across the British Isles, defined as the Tolsta interstadial (Whittington and Hall (2002)), which spanned 37- 31 kyr BP. A range of dates have been published to support this period of reduced ice cover, with a selection summarised in Table 1. Most of the studies are concentrated across in Scotland and are based upon the radiocarbon dating of organic deposits. Jacobi *et al.*, (2009) reviewed the dating of Woolly Rhinoceros bones at a range of sites across the British Isles. Based upon these dates it is implied that the Woolly Rhinoceros became extinct after 34 kyr BP, suggesting ice free or limited ice cover up to this time.

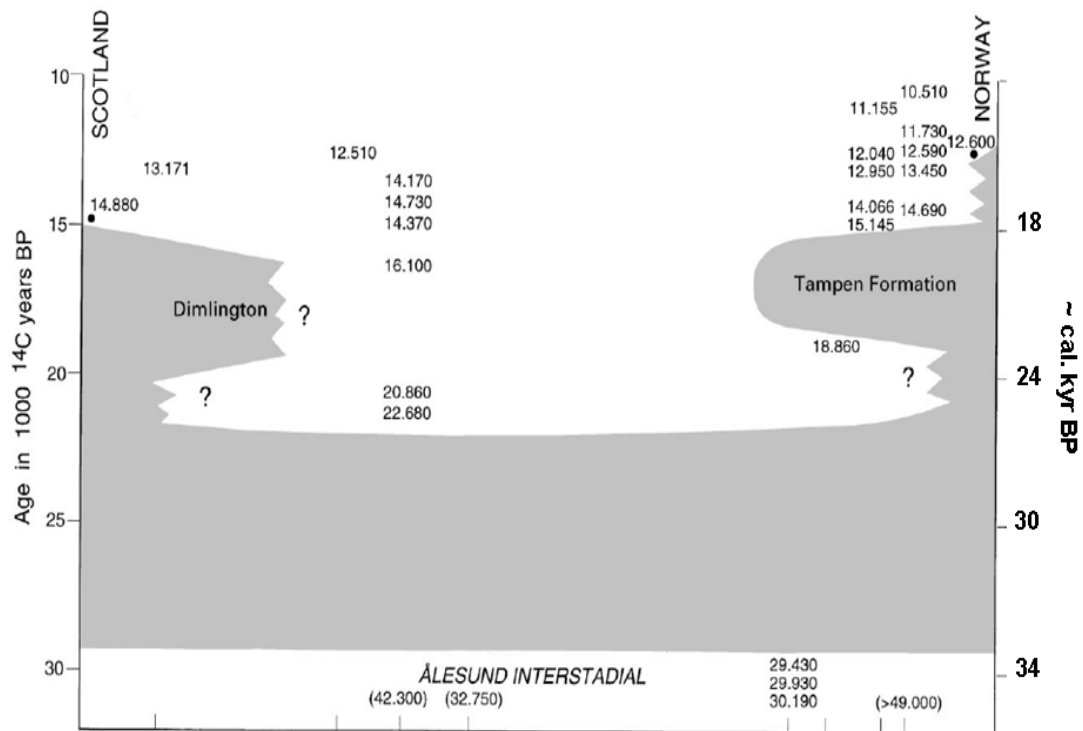


Fig. 2.1: Glaciation curve for the northern North Sea, which was used to constrain the timing of the growth and retreat phases for the BIIS and SIS. The diagram is adapted from Sejrup *et al.*, (1994) and is an illustrative profile extending between NE Scotland and Norway, where the shaded region represents periods of ice cover. The dates shown on the figure are  $^{14}\text{C}$  radiocarbon ages, which were obtained from foraminifera samples taken from a range of core sites across the region. More information on the data analysis and location of the cores can be found within the text and in Sejrup *et al.*, (1994).

The number of dates to constrain the Mid Devensian or pre-LGM history of the BIIS is limited, partly due to later re-growth of the ice sheet across the same regions. A few studies are discussed below.

The earlier advance (32-27 kyr BP) of the BIIS across the NSB is partly corroborated by a range of  $^{36}\text{Cl}$  cosmogenic dates published by Bowen *et al.*, (2002). Within this study, however, it is argued that the advance was initiated as early as 37.5 kyr BP with a widespread retreat by 25.1 kyr BP, which conflicts with the extensive range of dates used to identify the Mid-Devensian interstadial (see Table 1). The study does highlight though that the BIIS was more variable in extent prior to LGM than previously considered.

Another study into ice rafted debris (IRD) within the Barra Fan, northwest Scotland by Knutz *et al.*, (2001) suggested a grounded ice sheet was present across the shelf from ~ 30 kyr BP, indicated by the change from hemipelagic to glaciomarine environment within core samples. This period of glacial activity across the shelf lasted until ~ 21 kyr BP, when ice margin retreat from the shelf edge began, indicated by an increase in fine clastic sediments within the examined core material.

The chronology of deglaciation in the starting model (Shennan *et al.*, (2002)) will not be altered; the major phase of ice retreat was completed by 15 kyr BP. During this regional deglaciation, a localised readvance across Ireland, generally referred to as the Killard Point Stadial (KPS) is included within the model at ~ 18 kyr BP (McCabe and Clark (2003), McCabe *et al.*, (2005), Brooks (2007)). A later second readvance during the Younger Dryas or Loch Lomond Stadial (LLS) has been dated to have occurred between 12.5- 11.5 kyr BP (Benn (1997), Lowe *et al.*, (1999)) and as such is included in the starting model as a 1 kyr event initiated at 13 kyr BP.

### **2.2.2.3. Constraints on lateral and vertical extent**

As recent work and the glaciation curve in Fig. 2.1 indicates, the BIIS was more laterally extensive than represented in a number of previous models, including the starting model (Bowen *et al.*, (2002), Bowen *et al.*, (1986), Lambeck (1993b), Sutherland (1984)). For example, the work of Ballantyne, (2001) (Fig. 2.2) is compatible with an ice margin extending almost to the continental shelf edge off Western Scotland. Additional studies of offshore records around the coastline of the British Isles also support the occurrence of a relatively extensive ice sheet. An overview of these records is outlined below, in terms of constraints on vertical extent (or ice height) and lateral extent.

Locality	Material dated	Radiocarbon Age <sup>14</sup> C kyr BP	Calibrated Age (kyr BP)	Reference
Sourlie, West Scotland	Organic Sediments	33,270 ±370	38.7±0.4	Bos <i>et al.</i> , (2004)
		29000 ±430	34.4±0.5	
Tolsta Head, Outer Hebrides	Organic Sediments	26150±280	31.3±0.3	Whittington and Hall, (2002)
		31500±600	37.1±0.6	
Bishopbriggs, W Central Scotland	Woolly rhinoceros Bones	31,140 ±170	36.5±0.2	Jacobi <i>et al.</i> , (2009)
		32,250 ±700	32.3±0.7	
Goats Hole, Swansea	Woolly rhinoceros Bones	32,870 ±200	38.3±0.2	Jacobi <i>et al.</i> , (2009)
Torquay, Devon	Woolly rhinoceros Bones	36,040 ±330	41.3±0.3	Jacobi <i>et al.</i> , (2009)
Balglass, Scotland	Organic Sand	30 080±200	35.5±0.2	Brown <i>et al.</i> , (2007)
		34 480 ±340	39.8±0.4	
Derryvree, Ireland	Organic sediments	30500±1100	35.88±1.1	Colhorn <i>et al.</i> , (1972)

Table 1: Range of ages and associated sources to infer initial timing of Mid-Devensian ice sheet build up. In cases where a range of values were published, only the maximum and minimum vales are shown to indicate the date range.

Carr *et al.*, (2000), Carr *et al.*, (2006) examined seismic, sedimentological and micromorphological data at a number of borehole sites across the NSB to infer three Weichselian glacial episodes, two during the Mid Devensian when the BIIS and SIS were confluent, and extended out to the continental shelf edge. The lateral extent of these ice margins was delimited by the occurrence of subglacial till units across the area. Subsequent to this, there is less extensive readvance of the two ice sheets, with an ice-free corridor developing across the NSB. The eastern limit of the BIIS is marked by the location of the Wee Bankie and Bosies Bank moraines.

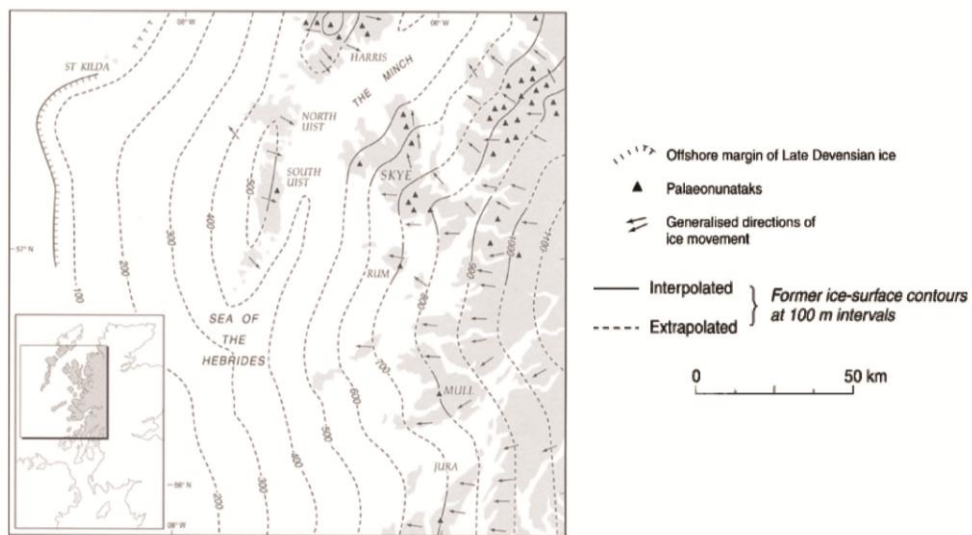


Fig. 2.2: Three dimensional reconstruction of ice surface altitude at the LGM. Note that the offshore margin is placed at the outermost morainal bank, close to the continental shelf edge. Taken from Ballantyne *et al.*, (2001).

Numerous studies examining the behaviour of BIIS around the coasts of Scotland support the view of an earlier more laterally extensive advance of the ice sheet beyond the limits of the Wee Bankie and Bosies Bank moraines out across the NSB (Evans *et al.*, (2005), Hall *et al.*, (2003), Merritt *et al.*, (2003)). Across the Firth of Tay, eastern Scotland, flow patterns of ice streams, recorded within terrestrial and marine subglacial bedforms, suggest that the BIIS either terminated to the east of the Wee Bank moraine or was confluent with the SIS during the Mid Devensian (Golledge and Stoker (2006), Bradwell *et al.*, (2008)). It is widely believed that an ice stream originating within the Moray Firth

was deflected northwards due to the presence of a grounded ice sheet within the NSB (Hall and Whittington (1989), Merritt *et al.*, (2003), Sissons (1967), Sutherland (1984)).

Submarine morainal banks (e.g. St. Kilda) and MSGL mapped across the Minch and Hebridean shelf off the west coast of Scotland, provide evidence for the extension of a grounded ice sheet out to the shelf edge, with sediment eroded from the mainland deposited in large trough mouth fans (Barra and Sula Sgeir) along the shelf edge (Clark *et al.*, (2004), Evans *et al.*, (2005), Stoker and Bradwell (2005), Stoker *et al.*, (1993)).

The main geomorphological features used to constrain the vertical extent (or thickness) of the BIIS are periglacial trimlines (see section 1.3.3. for further information). Extensive mapping of the trimlines across north-west Scotland (Ballantyne (1997), Ballantyne *et al.*, (1998)), Outer Hebrides (Ballantyne and Hallam (2001)) and the highlands (Ballantyne (1999), Ballantyne and Mccarroll (1997)) has led to the production of 3D reconstructions of the maximum ice surface elevation (Fig. 2.2). These limits indicate that the highest summits across Wester Ross (900 -1100 m) were over run by ice at the LGM. Also the ice reached over 600 m and 700 m across Skye and North Uist, respectively.

As is shown on Fig. 2.2, it is possible to extrapolate from the ice surface heights, assuming an approximate parabolic ice sheet profile, beyond the mapped limits and into the offshore regions, to infer the lateral extent of the ice sheet. Although no account is taken for additional factors such as seabed topography, these limits indicate that the ice sheet extended beyond the coastal margin and out to the continental shelf around the northwest coast of Scotland (Ballantyne (1999), Ballantyne and Hallam (2001), Ballantyne *et al.*, (1998)).

It should be noted that there is a relative paucity of similar studies to constrain the ice surface height across other areas of Great Britain and Ireland. Lamb and Ballantyne (1998) inferred a maximum ice sheet altitude over the southwest Lake District of between 800-870 m. Mccarroll and Ballantyne (2000) conducted a similar study across Snowdonia, North Wales to infer that the ice reached up to 850 m across the central massifs. Glasser and Smith (1999) inferred from modelling that an ice sheet between 250

– 500 m thick was required to produce meltwater channels mapped across the Mid Cheshire Ridge, northwest England.

These trimline limits across Scotland were adopted as the main constraint for the maximum ice surface elevation and as such the defined maximum thickness of the BIIS within the starting model and have not been altered with this study. It is also worth noting that deglaciation pattern of the British component of the BIIS was also not altered from that adopted within the starting model, taken from Shennan *et al.*, (2002), and was constrained within the starting model by limits taken from Bowen *et al.*, (1986). (It is noted that since the development of the starting and final ice model within this Chapter, reinterpretation of the trimline evidence across Scotland (Ballantyne (2010)) now suggests these feature may not mark the maximum ice surface elevation (see section 2.4). As this information was not available at the time of the model development, it is not considered but is suggested for future work)

Since the development of the starting model, there has been an increase in information on the lateral extent (Ballantyne *et al.*, (2006), Hiemstra *et al.*, (2006), O' Cofaigh and Evans (2001)) and thickness (Ballantyne *et al.*, (2006), Rae *et al.*, (2004)) of the IIS. Also, new AMS radiocarbon dates have been published that constrain the timing of the deglaciation (McCabe *et al.*, (2005)). A full review of this information was published within Brooks (2007). In the remainder of this section, only a few key points are discussed that will be used when conducting RSL sensitivity tests of the IIS later in this chapter.

At the LGM, field evidence suggests that Ireland was covered by a laterally extensive ice sheet which extended out onto the adjacent continental shelf (Clark and Meehan (2001), McCabe and Clark (2003), McCabe *et al.*, (2005)). Constraints on the vertical thickness of the LGM ice sheet are limited. Across County Kerry, southwest Ireland, Rae *et al.*, (2004)) constrained the ice surface height across the area to lie between 440-600 m. Ballantyne *et al.*, (2006) suggested that the Wicklow Mountains, east Ireland, were covered by a thick ice sheet, with only summits over 725 m remaining ice free at the LGM. To the south, it is now believed that ice extended beyond the traditional South of Ireland End moraine (SIEM), with a thicker more expansive ice sheet within the Irish Sea

basin (ISB) (Ballantyne *et al.*, (2006), Hegarty (2004), Hiemstra *et al.*, (2006), O' Cofaigh and Evans (2001), Scourse and Furze (2001)). Recent studies suggest that the Irish Sea glacier underwent a rapid, short lived advance into the Celtic Sea and down to the Isles of Scilly (Hiemstra *et al.*, (2006), O' Cofaigh and Evans (2001), Scourse and Furze (2001)). At the time of development of the revised ice model for the IIS, as discussed later in this chapter, there were no published dates to constrain the timing of this advance. Therefore, it was introduced into the model as a short lived, 1 kyr event at ~ 24 kyr BP, when the ice sheet was at its maximum extent. Subsequently, Cofaigh and Evans (2007) have published dates taken from marine shells to constrain the advance of the Irish Sea ice stream to between 25 and 23.9 kyr BP.

Unlike the steady retreat of the BIIS across Scotland during deglaciation, which is adopted, the IIS is believed to have retreated rapidly, with the Irish Midlands being ice free and the ice margin located close to, or on the Isle of Man by 19 kyr BP (Brooks *et al.*, (2008)). This retreat is interrupted by the KPS readvance where ice extended across most of the country, extending as far south as the Shannon estuary (McCabe and Clark (2003)). It is noted that during the deglaciation of the BIIS, this steady retreat pattern is now implied to be an oversimplification, with a regional-scale readvance of the retreating ice margin across Scotland, defined the Wester Ross Readvance occurring between 13.5 and 14.0 kyr BP (Ballantyne *et al.*, (2009)). As the pattern of the deglaciation was adopted from Shennan *et al.*, (2002) these were not added to the model and additionally, the modelling processes is not sensitive to these smaller scale episodes (see section 2.4.3.2.1).

During the LLS, a major ice field up to 700m thick (Thorp (1986)) grew across the west highlands of Scotland, extending from Loch Lomond in the south to Wester Ross in the north. Smaller ice fields developed within mountain corries in some Scottish islands (e.g. Skye and Mull), across the Lake District, Ireland and Wales. The overall extent of the ice cover is well established through extensive mapping of geomorphological features such as trimline data, lateral or frontal moraines (Ballantyne (2002), Benn (1997), Benn and Ballantyne (2005), Thorp (1986)) and using a high resolution numerical ice model (Golledge and Hubbard (2005), Hubbard (1999)).

### 2.2.3. Relative Sea-Level Data

#### 2.2.3.1. Introduction

The accuracy of the BIIS model revised to comply with the geomorphological data outlined above can be tested further using RSL data. This is done in Section 2.3. In this section the RSL data used later in this chapter and also in Chapter 5 will be reviewed. Two databases of sea-level reconstructions from across Great Britain and Ireland will be outlined. The total database consists of 80 localities, 59 across Great Britain and 21 across Ireland, as shown on Fig. 2.3. The data at each site have been separated based upon the criteria outlined below, and as summarised in Appendix A.

The range of data types within each RSL database has been outlined in greater detail in past studies (e.g. Brooks *et al.*, (2008), Shennan *et al.*, (2006), Shennan and Horton (2002), Brooks and Edwards, 2006), therefore only a brief summary is given here. For a data point to be classified as a SLIP, information regarding the following is required: location (longitude and latitude), the age (defined in calibrated radiocarbon years), altitude and the indicative meaning. These data points are the most useful for constraining model predictions as they provide a direct measure of past relative sea-level with a clearly defined height uncertainty. At sites across Ireland, a data sample is classified as a secondary SLIP when the indicative meaning was less well quantified (Brooks *et al.*, (2008)). When it is not possible to define the direct relationship of the sea-level data point to contemporaneous tidal regime it was classified as a limiting date, either a primary point where the source environment could be defined (such as from a freshwater peat) or a secondary point if the environment of formation was unclear or contested.

The Great Britain dataset is composed of a total of 1107 primary SLIPS and 194 limiting data. This compares to the significantly smaller dataset for Ireland, which contains only 61 primary SLIPS, 15 secondary SLIPS and 161 limiting data (including primary and secondary). It is important to note that the majority of the data, from both Great Britain and Ireland, are from the southern coasts of both regions.

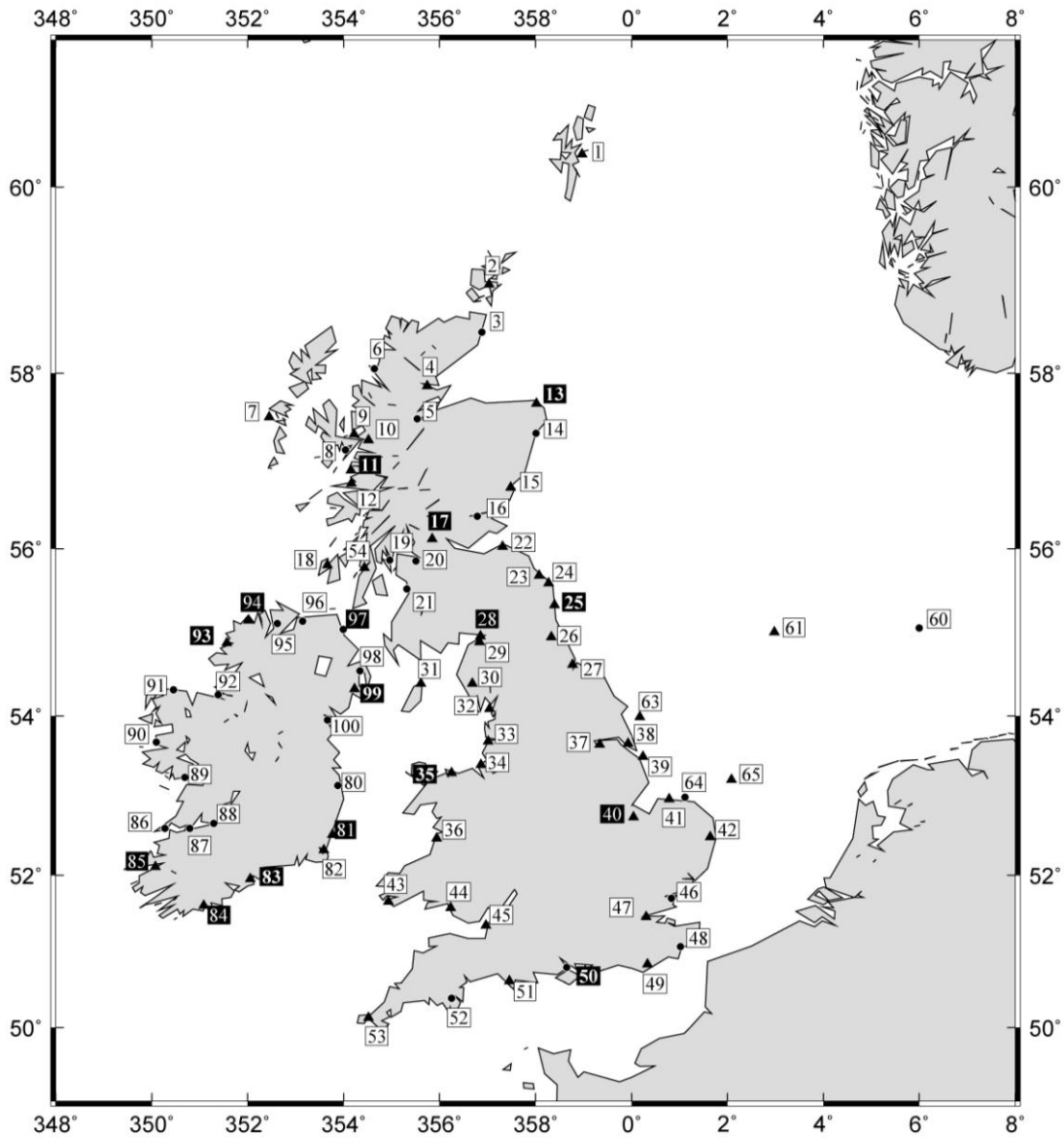


Fig. 2.3: Map showing the locations of the 80 data localities used in this study. The black triangles mark the locations of sites where primary and intercalated sea level index points have been obtained; the black circles mark sites where only intercalated sea level index points or other data points that provide a less precise constraint on sea level have been obtained. See Appendix A for a listing of all the data. Data and model predictions from sites labeled with white numbers in black boxes are shown in this chapter. Data and model predictions for all sites are shown in the Appendices

When using primary SLIPs, it is important to also consider the additional local scale processes within the coastal system that may affect the reliability of the data point, such as compaction or consolidation. It is generally considered that SLIP samples taken from basal peats (i.e. peat layer deposited on top of bedrock) provide the most accurate measure of sea-level change, as they are deposited over a hard substrate and as such, are not affected by sediment consolidation. Intercalated SLIPs, on the other hand, from host material that lies within a sequence of clay and peat deposits, may have been compacted or consolidated. Consequently, the palaeo sea-level marker could have been displaced lower over time. Within the Great Britain database, the 1107 primary SLIPs were further divided based upon these criteria into two smaller subsets; those which are taken from either basal peat layers or a sediment horizon that was considered to be unaffected by consolidation or compaction (referred to as basal points within Appendix A) and those classed as either an intercalated SLIP or from a sample which may provide a less precise constraint on the observed sea-level (referred to in Appendix A as Intercalated points).

An additional factor to consider is long term variations in tidal regime, which may result in variations of the reference water level through time (Uehara *et al.*, (2006)) and therefore influence the indicative meaning of a given SLIP. At present, palaeo-tidal corrections have only been applied to five localities within the database (as indicated in Appendix A), but other sites where changes in tidal regime go unresolved and may be important when using the sea-level data are sites 28, 29, 32, 45, and 47.

#### **2.2.3.2. Data from Great Britain**

Fig. 2.4a shows reconstructed sea-level change at a subset of eight localities from across Great Britain, which were chosen to illustrate the variation in the character of the sea-level signal across the study region and the range of available sea-level data types, as described above, within the database. Note that the complete data set is shown Appendix B.

Site 13, located on the eastern coast of Scotland is the most northern site displayed in Fig. 2.4a. The sea-level record at this locality, composed of a mixture of primary and

intercalated SLIPs, typifies the characteristic trend of data from the NE coast and highland regions of Scotland, with a rise from below present, -10 m at ~ 9.5 kyr, to form a small highstand of amplitude ~ 1m at ~ 5.5 kyr BP. Sites 11 and 17 display the typical record of sites situated close to the centre of an ice sheet, with sea-level elevated above present, during and following the deglaciation period. The signal recorded in these northerly data is sensitive to both local and global processes (see Section 1.1.3 and Chapter 5). Site 11, situated on the NW coast of Scotland, contains the longest and most complete record, with over 16 kyr of data composed entirely of primary SLIPs.

The sea level record is characterised by a fall from 34 m at ~ 16 kyr BP, with noted data gaps over the observed timings of meltwater pulses 1A and 1B, reaching a minimum of 3 m at ~ 10 kyr BP. Following this, sea-level rises gradually towards a late Holocene highstand of magnitude ~ 6.5 m between 6 -7.5 kyr BP, before falling towards present day level. Although the data record at site 17, is shorter than at site 11 and composed of a mixture of both primary and intercalated SLIPs, the observed trend over the majority of the Holocene is similar, with sea-level rising to produce the highest Holocene highstand in the entire study area of 11.5 m at 7.5 kyr BP. This site is inferred to be very near to the area of maximum ice thickness, and as such, should record the maximum uplift following the deglaciation of the BIIS.

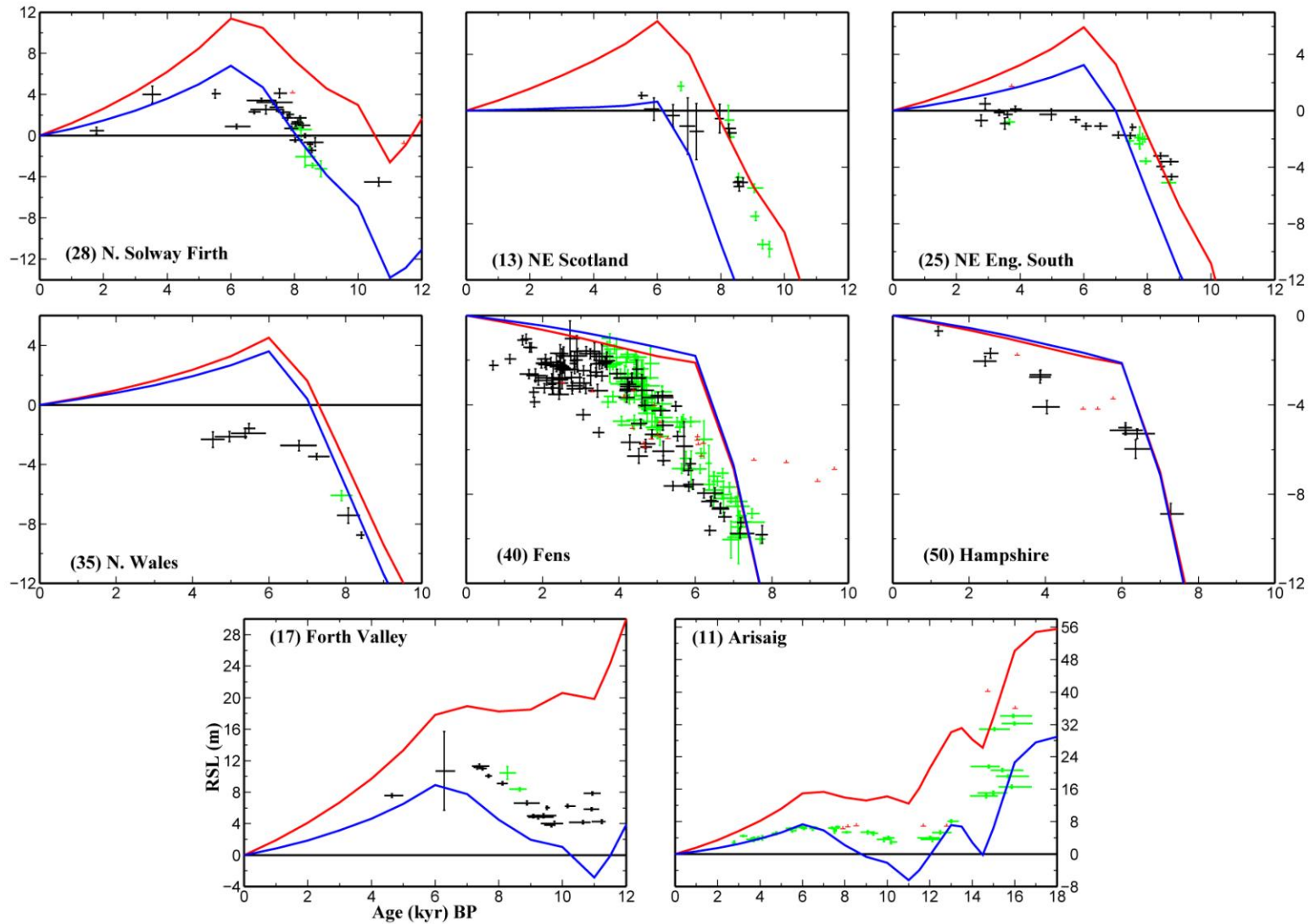


Fig. 2.4a: Comparison of predicted and observed sea level at eight locations across Great Britain (Results for all sites are shown in Appendix B). Symbols for the observed data are summarized in Appendix A and within the text. Predictions are shown for the Shennan *ice* model (shown in Fig. 2.5) for two earth models with different lithosphere thickness values: 71 km shown by solid red line and 96 km shown by the solid blue line; the upper and lower viscosity values are  $5 \times 10^{20}$  Pa s and  $4 \times 10^{22}$  Pa s, respectively

Sites 28, 35, and 25 typify the pattern of sea level change across the central region of Great Britain (NE and NW England) where there is a transition from sites with a small (site 28) or minor (site 25) Holocene highstand, to sites where RSL is below present throughout the late Holocene (site 35). The geographical location of this region of transition between sites where Holocene sea level was above present to those where it was not is inferred to fall between sites 25 and 27, along the east coast and sites 33 and 35 on the west coast. This region is often defined as the Holocene hingline, or region of zero sea-level change and will be referred to in this chapter as the zero-isobase. This is not to be confused with the location of the zero-isobase referring to present day rate of sea-level change, which is described within later Chapters.) This is a key feature with which to validate the model predictions and within past studies was a region which exhibited consistent discrepancies between predictions and observations (Brooks *et al.*, (2008), Shennan *et al.*, (2006), Shennan and Horton (2002)). This gradual north-south reduction in the height of the Holocene highstand and associated location of the zero isobase is more apparent when examining data at all sites (see Appendix B).

Not only is there the noted N-S reduction in the height of the highstand, there is also a pronounced W-E trend across this central region, with notably higher sea-level at sites along the west coast of Great Britain compared to latitudinally sites along the east coast. This variation can be seen by comparing two sites such as 25 and 28, situated along the NE and NW coast of England. At 28, sea-level rises from -4m below present at 9 kyr BP to form a highstand of ~ 4m between 6-4 kyr BP before falling towards present day level. In contrast, at 25, sea-level again rises from ~ -5m at 9 kyr BP, but forms only a minor (~ 0.5m), if any, highstand at 3kyr BP. As mentioned above, the observed record at 28 may be affected by variations in tidal regime through time, which would alter the height of the observed highstand. However, this would not account for the total ~ 4 m difference.

At site 35, the record is much shorter, with a rise from -9m at 8.5 kyr BP to - 2.5m at 4.5 kyr BP. Although there is a noted lack of SLIPs at this site and 25 with which to constrain the variation of sea-level during the mid-late Holocene, it is possible to infer the occurrence of a relatively minor highstand from the field evidence. At site 25, field evidence indicates that sea-level did not rise above 0.5m over the last 3 kyr and so a

steady fall towards present day levels can be inferred. At site 35, there is again no evidence that sea level rose significantly above present day level over the last 5 kyr.

Sites 40 and 50 located along the southern coast of Great Britain, illustrate the typical pattern of relative sea-level change at sites furthest from the main centre of ice loading in Scotland. The characteristic sea level trend at both of these sites is similar, with a gradual rise over the last 7 kyr BP towards present day sea levels. There is no record of sea level reaching above present day levels or abrupt changes in the rate of sea-level rise. Site 40 not only consists of by far the greatest number of SLIPs (194) but is one of the few sites where the data, using modelled estimates taken from Shennan and Horton (2002), have been corrected for changes in tidal range over the late Holocene. This resulted in a shift of ~ 2 m in the observed sea level during the mid-holocene.

### **2.2.3.3. Data from Ireland**

Fig. 2.4b shows reconstructed sea-level change at a subset of eight localities from across Ireland, which were chosen to illustrate the variation in the character of the sea-level signal across this region and the range of available sea-level data types, as described above, within the database. Note that the complete data set is shown in Appendix B.

As mentioned above, the greatest concentration of primary SLIPs (2/3 in total) within the Irish database is found at sites along the southern coast (Sites 81 and 85) and these are concentrated on the last 6 kyr BP. These sites (a selection of which are shown on Fig. 2.4b) display the typical pattern of sites distal from the major centre of ice loading (as described above for sites 40 and 50), with a gradual rise over the past 7 kyr BP towards present day levels.

Across the central region of Ireland, and similar to that observed for central Great Britain, there is a marked transition from sites with no or a minor highstand (such as 90 and 92, on the west coast and 80, on the east coast) to the pronounced highstand along the Northern coast, as seen at sites 96 and 100. The location of the zero isobase is inferred to fall between sites 93 and 94 along the west coast and close to site 80 on the east coast.

Additionally, there is an evident east to west trend in the height of the highstand, where sites along the NW coast (such as 93 and 94) have a lower Holocene sea-level maximum (<1m) compared to NE coast where sea-level is inferred to rise to over 3m (from the maximum/minimum limits of the limiting data). This is most evident when comparing two sites from the west coast such as site 92, where there is a lack of field evidence for sea level being elevated above present during the Holocene, and site 100 on the east coast, where using only the minimum height of the primary limiting data as a guide, sea level rose to at least 4m at ~ 6 kyr BP.

Sites 93 and 94, located on the west coast of Ireland, were previously highlighted as being important sites for constraining the predicted sea level over the Holocene and location of the zero isobase (Brooks *et al.*, (2008)). Although there is a lack of data over the last 3 kyr BP from 94, the general trend between the two sites and this coastal area is very similar. Sea level rises from -2 m below present at ~ 5 kyr BP and reaches present day level at ~ 3 kyr BP, with evidence for only a minor (< 1 m), if any, highstand over the last 2 kyr BP.

Even though along the NE coast of Ireland there is a noted paucity of primary SLIPs, (only two at site 99), limiting data when combined with additional field evidence (such as raised shorelines) can be used to provide a useful constraint on the general pattern of sea-level change. This is especially useful in areas such as Ireland where there are a restricted number of SLIPs both in space and time. A major feature of the observed trend at sites along this coastline, compared to the NW coast, is the evidence for sea levels significantly elevated above present during the late Devensian. The height of the elevated sea-level over this period is constrained from numerous studies investigating abundant raised shorelines around the coastline and a range of limiting data. For example, at sites 96 and 98 around the timing of the LGM, raised shorelines have been found between 25 and 30 m (Brooks *et al.*, (2008) and references therein). Producing these elevated sea levels in past studies has been a problem. It is noted that the dating of raised shorelines can be problematic and the heights inferred from these data are only taken as a guide for the possible height of sea level over this period.

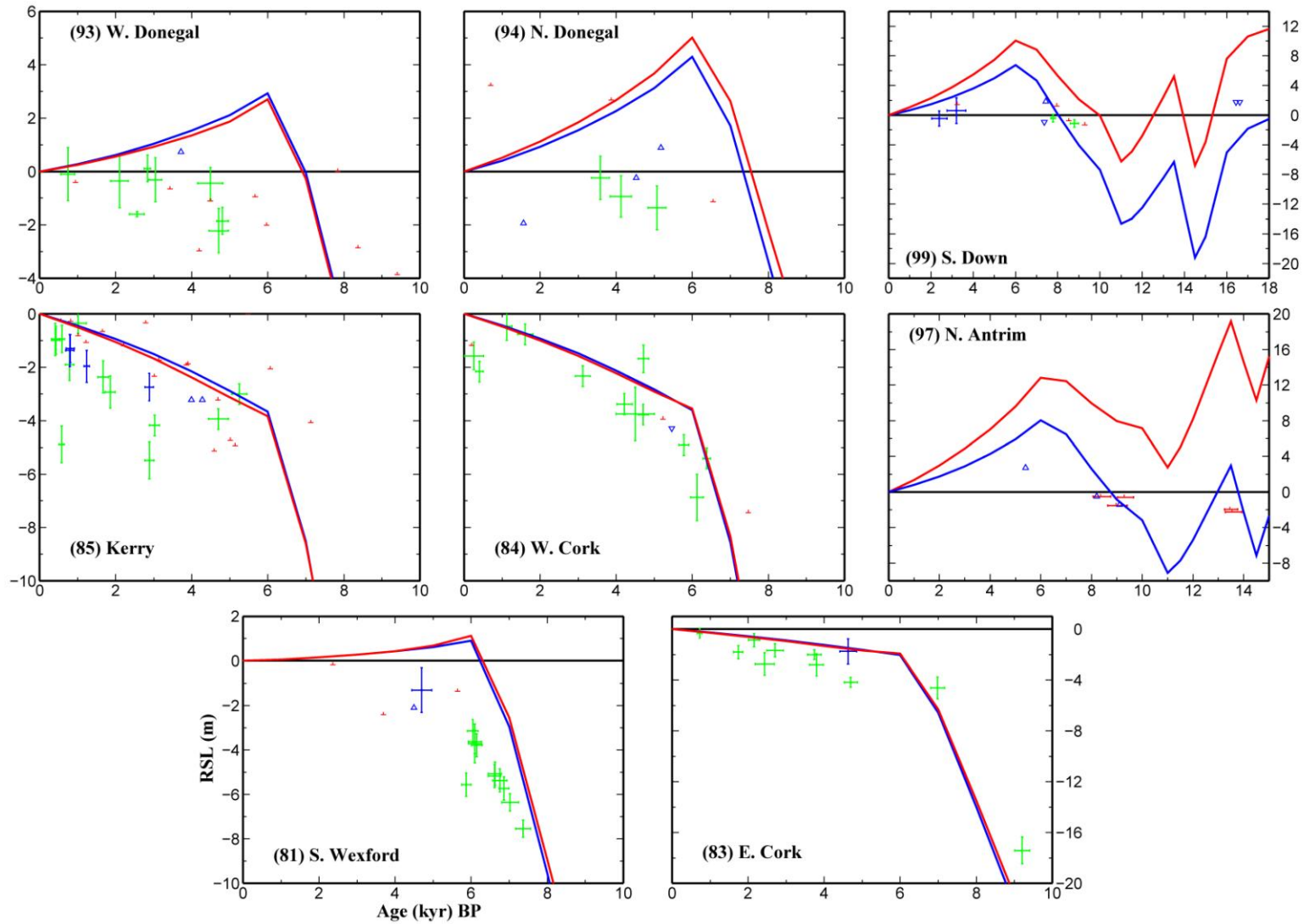


Fig. 2.4b: As 2.4a except for the eight chosen data localities across Ireland (Results for all sites across Ireland are shown in Appendix B).

The two sites illustrated on Fig. 2.4b from this coastline were chosen to illustrate this trend. At site 99, the limiting data at ~ 16 kyr BP suggest that sea-level was falling from a minimum of 2 m. Following this fall, sea level rises from an unconstrained lowstand, initially reaching present day levels at ~ 8 kyr BP. The trend is unconstrained, but possibly elevated above present between ~ 8 – 4 kyr BP, to be followed by a fall towards present day level constrained by the secondary SLIPs at ~ 2 kyr BP. At site 97, the limiting data at ~ 14 kyr BP constrain the minimum height of the lowstand to 2 m and are useful to distinguish between various model predictions over this period of large and rapid changes.

### **2.3. Preliminary Data-Model Comparisons Using the Shennan et al. BIIS Model**

The three key input parameters within a GIA model have been explained in greater detail in Chapter 1 and so are only summarised here; a model of the late Pleistocene ice history, which will be considered in terms of a regional (British-Irish) component and a global model; an Earth model to reproduce the solid earth deformation resulting from surface mass redistribution (between ice sheets and oceans) and a model of sea-level change to calculate the redistribution of ocean mass (e.g Kendall *et al.*, (2005), Mitrovica and Milne, (2003) and as outlined in section 1.2.1).

The regional BIIS model was taken from Shennan *et al.*, (2002), with key time slices illustrating the evolution the model shown on Fig. 2.5, note that the maps display ice thickness, not ice elevation. Between 32- 21 kyr BP, the lateral extent and thickness of the ice model remains the same, this was done to ensure that the ice sheet reached (or was close to) isostatic equilibrium by the LGM. The maximum thickness of the ice sheet across Scotland, centred over the west, is 1193 m; this is constrained by the trimline limits as outlined in Section 2.2.2.3. Across NE Ireland ice reaches up to 680 m with an independent ice cap over SW Ireland (Kerry) up to 128 m. The ice margins are restricted to the coastal regions with ice expanding within the Irish Sea (to thicknesses of ~ 100m) but with Pembrokeshire in Wales and Wexford in Ireland remaining ice free. Also, a lobe of ice extends down the eastern coast of England. As deglaciation commences at 20 kyr, the ice sheet gradually thins and retreats, with complete ice retreat by 15 kyr BP. During

the Younger Dryas event, ~ 13 kyr BP, there is small scale ice growth across the highlands of Scotland, with ice modelled up to 716m based on trimlines and field evidence, as described in Section 2.2.2.

This regional model was combined with the global ice model, Bassett *et al.* (as defined in Section 1.2.3). This model was tuned to fit a suite of far-field data spanning the LGM to 10 kyr BP. The combination of these two components will be referred to in the following as the ‘Shennan model’. Using the Shennan model, predictions were generated at the 16 localities indicated on Fig. 2.4a and 2.4b (see Fig. 2.3 for map of locations) using two reference earth models with the same upper and lower mantle viscosity of  $5 \times 10^{20}$  Pa s and  $4 \times 10^{22}$  Pa s, respectively, and two different lithosphere thickness values of 71 km and 96 km.

In the following section, these earth models will be referred to as the 71 km and 96 km models and, when combined with the Shennan ice model, as Shennan-71 and Shennan-96, note the complete set of predictions at all sites is shown in Appendix B).

The choice of lower mantle viscosity values was taken from the Bassett *et al.*, (2005) study as this produced the optimum fit to the far-field data set used in the development of the model. The upper mantle viscosity value was chosen as an average value between the ranges used in earlier studies (Peltier *et al.*, (2002), Shennan *et al.*, (2000)). Two values of lithosphere thickness are investigated to incorporate the spread of possible values that have been used in previous studies; a thicker model (96 km) to be consistent with that favoured by Peltier *et al.*, (2002) and a thinner model (71 km) to be closer to that favoured by Lambeck *et al.*, (1996) and Shennan *et al.*, (2000).

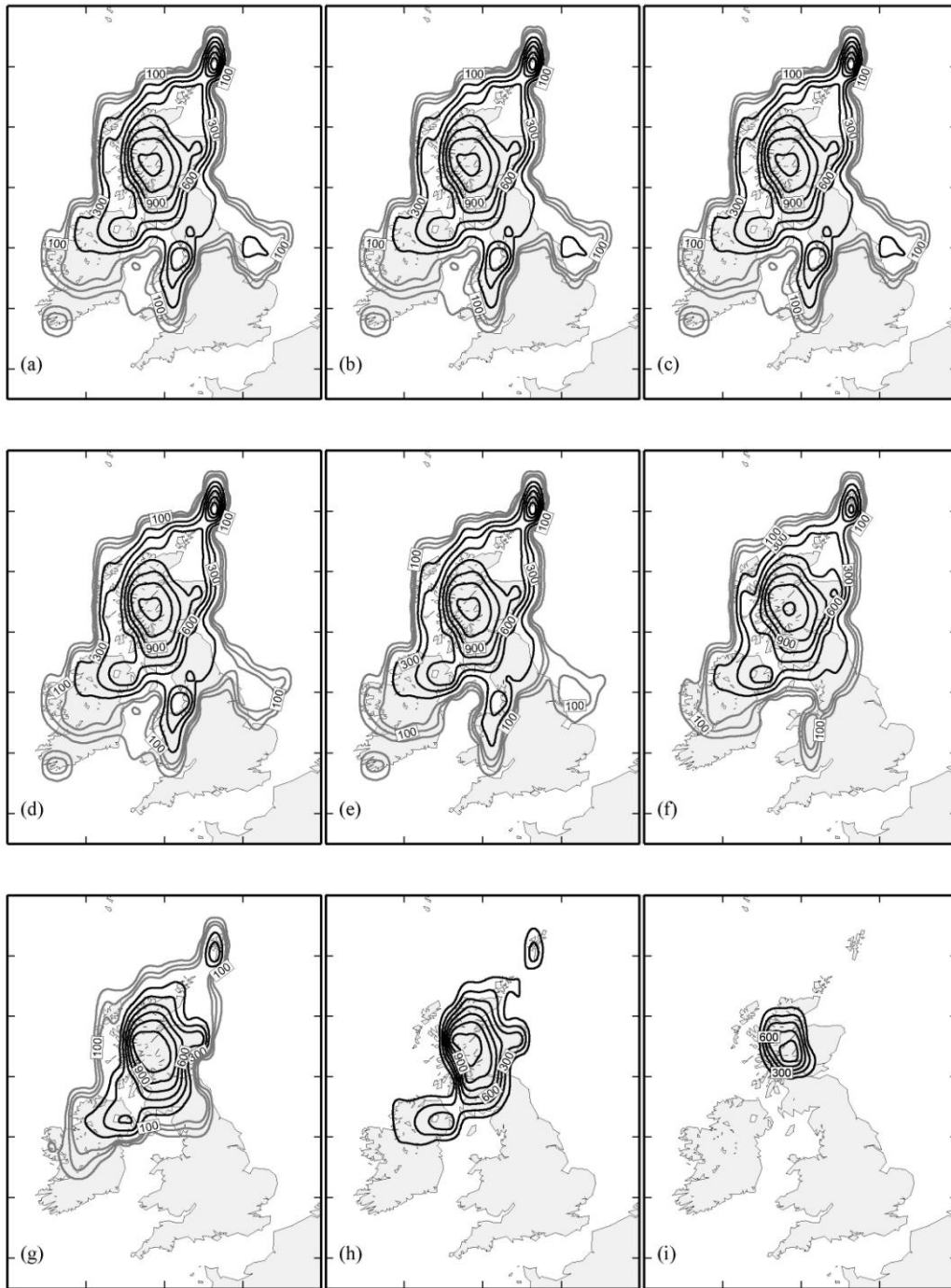


Fig. 2.5: Ice thickness maps of the British-Irish Ice Sheet model presented in Shennan *et al.* (2002) at the times (in kyr BP): (a) 32, (b) 25, (c) 21, (d) 20, (e) 19, (f) 18, (g) 17, (h) 16, (i) 13. Note the varying contour intervals: in frames a-g and heights between 0-150m the contour interval is 50m with annotation every 100m; for heights 150m and above the contour interval is 150m, with annotation every 300m.

Of the two models shown, the Shennan-96 model produces a consistently better fit to the observed data at most sites. At sites across Scotland and northern regions, located close to the centre of the ice loading, the predictions display the characteristic non-monotonic pattern of RSL (such as seen at sites 11, 17, 97, or 99) where, following deglaciation, predicted RSL falls from significantly elevated levels. This fall is punctuated by two inflections or periods of rapid sea-level rise, ~ 14 kyr BP and 11 kyr BP, followed by a steady rise towards a pronounced mid-Holocene highstand before falling towards present sea levels. At these sites, the Shennan-96 model captures the trend in the data more consistently over the mid-late Holocene. The Shennan-71 model does produce a closer fit to some of the older, late Devensian data due to the higher predicted RSL around, for example, the NE coast of Ireland (such as sites 98, 99, 100) and at site 11 across Scotland.

Neither model adequately replicates the RSL pattern, during these periods of rapid change as inferred in the SLIP data (such as sites 11 or 17); with an underprediction using the Shennan-96 model and an overprediction using the Shennan-71. Also, note that, although the Shennan-96 model generally captures the trend better at the Scottish and Central sites, it results in sea levels that are too low during the Late Devensian.

At sites across the central region of Great Britain and Ireland, located close to the ice margin, there is a transition in the predictions from sites where sea level rises over the late Holocene from below present to produce either a noted highstand (such as at sites 94, 97, or 25) or no highstand at all (such as at site 43). At these sites the difference between the two models is smaller than at the northern sites, with the difference in the predicted height of the highstand between 4-1 m. Generally, the Shennan-96 predicts a smaller highstand and so produces a closer fit to the SLIPs. However, both models produce a pronounced overprediction in the height of RSL over the late Holocene. This is discussed in the remainder of this section.

As a result of this overprediction, neither model reproduces the north-south/west-east variation in the height of the Holocene highstand. This results in the location of the zero isobase being displaced too far south across both Great Britain and Ireland. Across

Ireland this transition falls between sites 91 and 92, along the west coast and 81 and 82, along the east coast. Across Great Britain the transition falls between sites 27 and 37, on the east coast and between 36 and 43, along the west coast. This overprediction is most evident at sites such as 94 and 35, where both models predict RSL up to 4m higher than the observed SLIPs.

At the distal sites situated along the southern coastlines, such as sites 40, 50 or 83 there is little variation between either models, with both producing the characteristic steady rise towards present from the onset of deglaciation. It is noted though, that the apparent sharp slowdown in the rate of rise at ~ 6 kyr BP is not shown within the SLIPs. Also, the predictions tend to sit slightly above the SLIPs, as seen at sites 40 and 48, partly due to the previously mentioned inflection.

## **2.4 Modifications to the British Isles Ice Sheet Model**

### **2.4.1. Introduction**

Although a reasonable fit was produced at the majority of the RSL data sites using the Shennan ice model, there are some major inconsistencies with the adopted regional component of this model which need to be addressed: Firstly to correctly adjust the ice model to account for the underlying terrain and secondly to revise the regional ice model to comply with new geomorphological constraints (as outlined in Section 2.2.2).

With regard to the first point, the thickness of the adopted ice sheet is constrained using trimline data, which was taken to mark the maximum surface elevation the ice sheet reached (as outlined in Section 1.1.3 and 2.2.2.3), assuming that ice grew over a flat terrain at sea-level. But in regions of high terrain, such as across Scotland, this will lead to an overestimation in the defined thickness of the ice sheet within the model and as such, the corresponding loading signal.

This is highlighted for one selected site in Scotland: site 11, (Fig. 2.6), where the predicted RSL is shown for the Shennan-96 and Shennan-71 models, and a 'terrain-

corrected' version of each of these models (referred to as Shennan96-terrain and Shennan71-terrain).

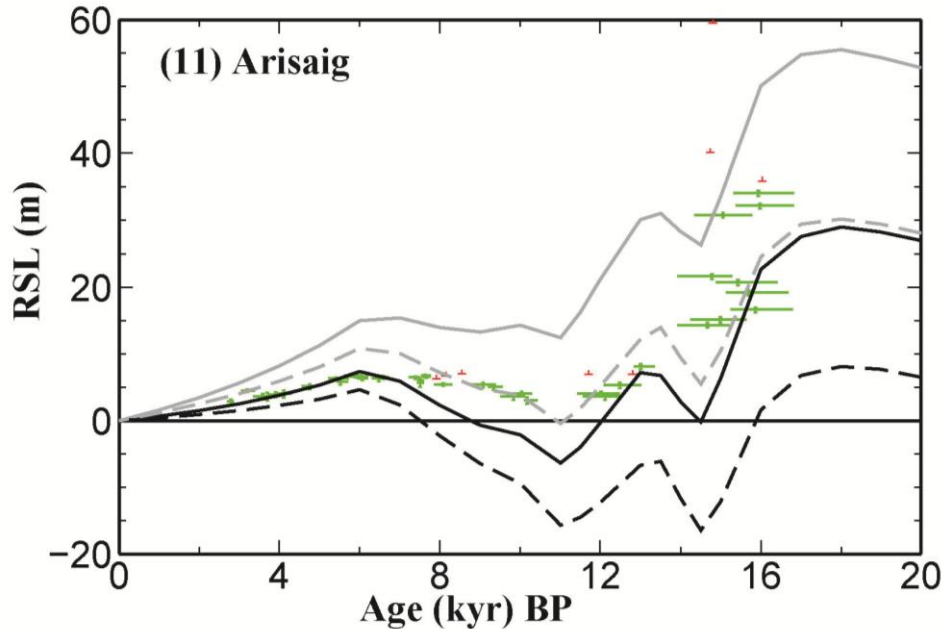


Fig. 2.6: Examining the affect of correcting the input ice model for underlying terrain at site 11, Arisaig. Predictions are shown for the Shennan model (solid lines) and Shennan-terrain corrected (dashed line) as described within the text using the two earth models with varying lithosphere thickness: 71km (grey line) and 96 km (black line) combined with an upper mantle viscosity of  $5 \cdot 10^{20}$  Pa s and lower mantle viscosity of  $4 \cdot 10^{22}$  Pa s.

Correcting the thickness of the ice sheet for underlying terrain leads to a thinning of over 400 m at the LGM, and a general lowering in the predicted RSL throughout the last 20 kyr BP. The greatest impact is during the main stage of deglaciation (20-16 kyr BP), where sea-level is lowered by over 20 m, which results in the optimum fit to the RSL data now produced using an earth model with a 71 km lithosphere thickness. This comparison highlights the trade-off that can be produced between lithosphere and ice model thickness, (comparing the solid-black and dashed-grey lines on Fig. 2.6) where an equally good fit to the RSL data is achieved with either a thick ice model and lithosphere (Shennan-96) or with a thinner ice model and lithosphere (Shennan71-terrain). The affect of revising the ice model for underlying terrain upon the RSL predictions will be variable across the data sites, with the greatest impact across the Scottish Highlands.

The second major aspect of the Shennan model to be addressed is to ensure that the spatial and temporal patterns of the main glacial and deglacial phases comply with the new geomorphological evidence as outlined in section 2.2.2. This will be addressed in three stages: First a revised regional BIIS model will be produced that addresses the ‘terrain correction’ issue and complies with the regional geomorphological data (Section 2.3.2.2). This model will be compared initially to the Great Britain RSL data only. The results of this work have been published in Shennan *et al.*, (2006). The second stage will involve examining only the IIS component of the revised regional BIIS model. The aim is to address specific issues relating to the history of the IIS and the Ireland RSL data, which have largely been neglected in past GIA modelling studies of the British Isles (Section 2.3.2.3). A key aspect of stage two will involve examining the sensitivity of the RSL predictions to relatively transient and small scale changes in the ice sheet. The main conclusions from this work have been published in Brooks *et al.*, (2008). Finally, in the third stage, the regional BIIS and local IIS models will be combined and compared to the complete British Isles RSL database (Section 2.3.3), with a more extensive comparison in Chapter 5.

#### **2.4.2. Modelling the component for Great Britain**

The Shennan model was revised in two steps in the following section to address the aspects outlined above. Firstly, the ice model was corrected for underlying terrain, which results in a thinner ice sheet within the onshore regions. Secondly, the spatial and temporal patterns of BIIS evolution over the last glaciation were revised to comply with the above described geomorphological evidence (Section 2.2.2). Key time slices from this new ice model, referred to in the following section as the North Sea (NS) models, are shown on Fig. 2.7. The major changes applied to the Shennan model to arrive at these models are outlined below.

When the NS models were developed, there was little information to constrain the vertical height of the ice sheet across the NSB; therefore, some basic assumptions were followed to define the thickness of ice across this area. Firstly, it was assumed that as the

ice sheet grew outwards either across the British Isles or Scandinavia, the maximum surface elevation in the NSB could not exceed that within onshore regions. Secondly, to adjust the ice sheet for underlying terrain, as has been applied in the onshore regions, the thickness of the ice sheet was increased to account for the deepening of the seabed across the NSB. These assumptions lead to the possibility of two models with different thicknesses in these offshore regions. A thicker model, which will be referred to as NS-Thick (as shown in Fig. 2.7 a, b, c and g), where the maximum thickness of the ice sheet as it expanded into the offshore regions was maintained further both across the NSB and the western coastal regions. The thickness across the Central NSB, in the approximate zone of confluence between the BIIS and SIS, is between 800-750 m, and reaches up to 650-500 m at the margin near to the Hebridean shelf. In the second model, which will be referred to as NS-Thin (as shown in Fig. 2.7, d, e, f and h), the ice sheet was assumed to thin more rapidly once expanding into the offshore regions, reaching only 600-500 m across the Central NSB and between 480-360 m around the western Highlands.

The following revisions to the timings of glacial and deglacial phases were applied to both the NS-Thin and NS-Thick models.

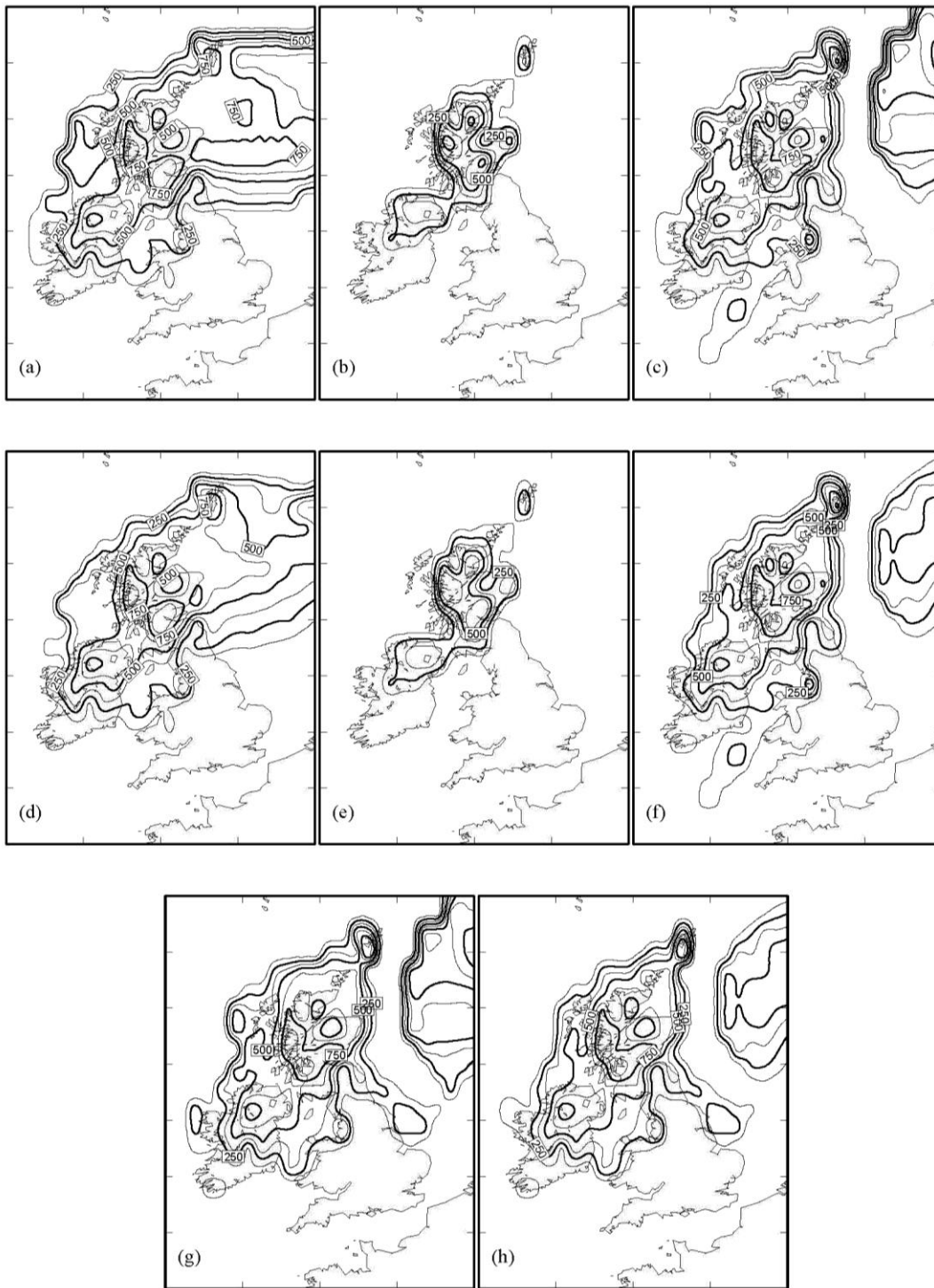


Fig. 2.7: Ice thickness maps of two British-Irish Ice sheet models generated from the Shennan model. The NS-Thick model at the times (in kyr BP): (a) 32, (b) 26, (c) 24, (g) 21; and the NS-Thin model at the times (in kyr BP): (d) 32, (e) 26, (f) 24, (h) 21. See main text for a description of these models. Note the varying contour intervals

The pattern of the late Devensian growth and retreat has been revised to fit with the timings suggested by Sejrup *et al.*, (1994) (as summarised in Fig. 2.1), which defines a two-stage glaciation pattern during this period across the NSB. It is worth noting, for comparison, that the Shennan model had only one main glacial phase, extending throughout the Mid-Late Devensian). An initial early growth phase begins after 33 kyr BP, with the BIIS extending across the Central and Northern NSB to coalesce with the SIS between 32-27 kyr BP (shown on Fig. 2.7, a and d). Following a rapid retreat between 26-25 kyr BP (shown in Fig. 2.7, b and e), there is a second readvance starting at 24 kyr BP (shown in Fig. 2.7, c and f), where the SIS advances across the Central and Northern NSB but does not coalesce with the BIIS. Instead an ice free corridor remains between the two ice sheets, extending approximately north-south across the Northern NSB to Central NSB. During both these advance phases, the spatial limits of the ice sheet have been extended to reach the continental shelf edge. The ice sheet has been thickened, reaching up to 250 m within the ISB, and 650 m and 220 m along the coasts of NW Scotland and Ireland respectively. Additionally, the model now includes two short-lived ice streams, one at 24 kyr BP (see Fig. 2.7, c and f), extending down to the Isles of Scilly and one at ~ 21.5 kyr, extending down the east coast of Great Britain (see Fig. 2.7, g and h). The pattern of deglaciation remains unchanged from the Shennan model, apart from the previous mentioned correction for underlying topography, and so these time steps are not shown on Fig. 2.7.

Predictions were generated using the NS-Thick and NS-Thin models at the eight sites across Great Britain (Fig. 2.8), using the same two reference earth models as defined above (Note the predictions are shown at all sites in Appendix C). The combination of the two ice models with each of these earth models will be referred to as NS-Thick71, NS-Thin71 and NS-Thick96, NS-Thin96 (abbreviated to NS-71 and NS-96). Additionally, the predictions are shown for the Shennan-96, which produced the optimum fit to the RSL data and the Shennan96-terrain model (as described above)

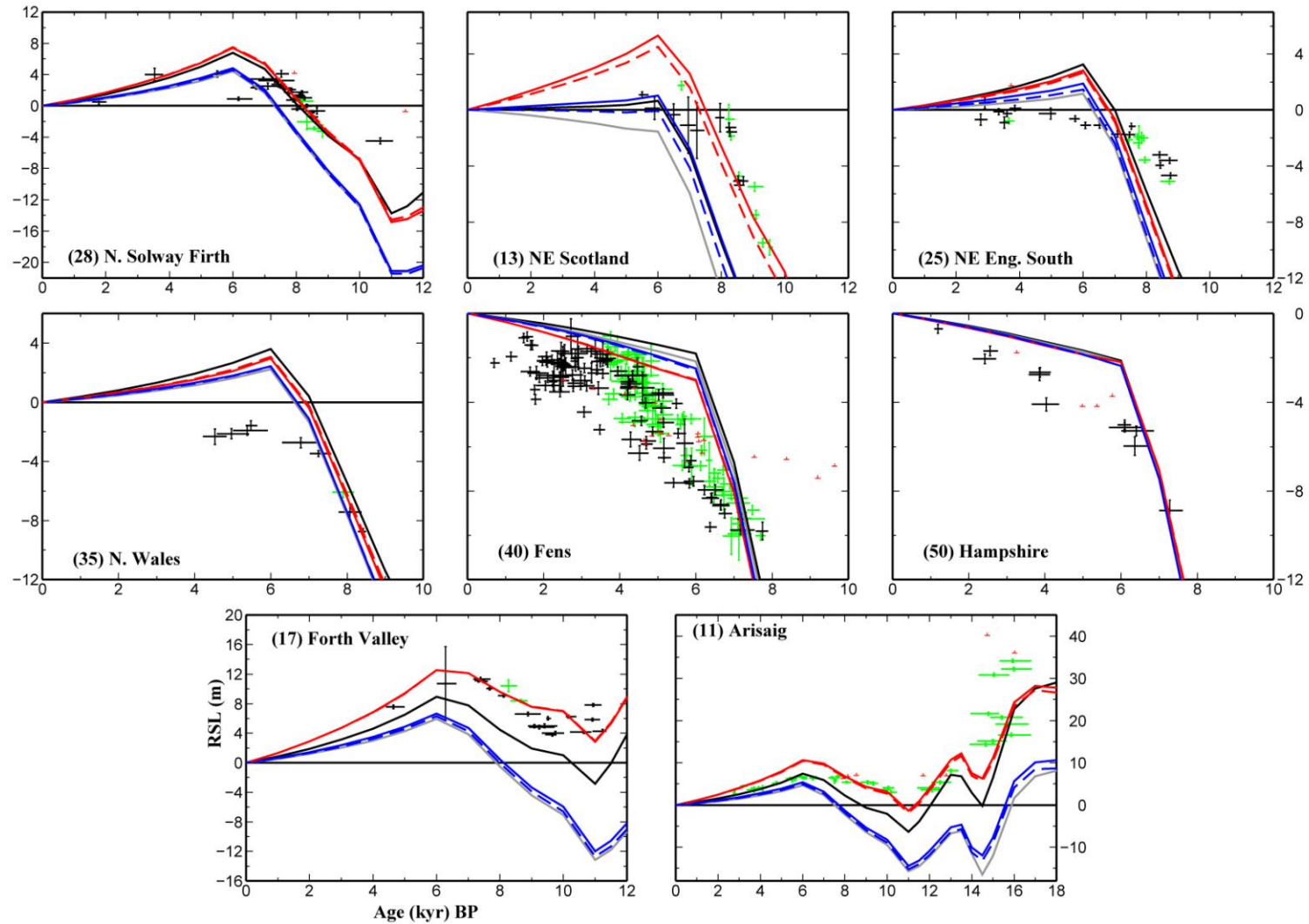


Fig. 2.8: Comparisons of predicted and observed sea level at eight locations across Great Britain for the NS-Thick and NS-Thin ice models and the two reference earth models (see caption to Fig. 2.6). Predictions were generated using: the 71 km lithosphere earth model for the NS-Thick (solid red line) and NS-Thin (red-dashed line) models; the 96 km lithosphere earth model for the NS-Thick (blue solid line) and NS-Thin (blue dashed line). Additionally, predictions are shown using the 96 km lithosphere model for the Shennan model (solid black line) and the Shennan terrain-corrected model (grey line). Results are shown for all sites across Great Britain in Appendix C.

Comparing the results for the Shennan model to the NS models (96km or 71km), it is evident that the greatest difference is at sites located near to the centre of the ice sheet across Scotland, where the predictions based on the terrain-corrected models are displaced to substantially lower RSL values compared to the Shennan model (compare the solid black line to blue lines on Fig. 2.8). For example, at sites 17 and 11, the predictions are reduced by ~20 -25 m over the deglacial period (20 -15 kyr BP) and ~2 m in the mid Holocene. This difference is primarily due to the correction of the ice model for underlying terrain, as described above and is highlighted by comparing the NS-96 model predictions on Fig. 2.8 to the Shennan96-terrain model (compare blue lines to grey line). There are some noted exceptions to this noted sensitivity across the Scottish sites. Along the NE coast of Scotland, such as site 13 (sites 14 or 15, as shown in Appendix C) there is little change in the predictions between the Shennan and NS models. The reduction in the predictions due to the correction for underlying terrain, which is evident at most other sites across the Scotland, has been offset at these sites by the influence of the increased ice load across the NSB. At a selection of sites along the eastern coastline of Great Britain, such as site 40, (also sites 37 and 38 shown in Appendix C), the NS models generate a shift in the depth of the RSL over the last 8 kyr BP (between 2-1 m) compared to the Shennan model and, correspondingly, produces a closer fit to the SLIP data at these sites

Of the two lithosphere thickness models investigated, the NS-71 models now produce the optimum fit to the majority of data sites, although there is some spatial variability in the quality of fits for these models, as highlighted below. This contrasts with the Shennan model, where the optimum fit was generated using the 96 km lithosphere model.

The significantly higher predicted RSL generated using the NS-71 models at most of the Scottish sites, such as sites 11, or 17 (also sites 54, 18, and 21, in Appendix C), captures the trend in the older SLIP data. Despite this, the new model does not resolve the underprediction prior to 16 kyr BP, as can be seen at site 11 or the size of the fall-rise-fall sequence during the periods of rapid change (~ 14 kyr BP)

At sites across the Central region of Great Britain, differentiating between the NS-96/NS-71 models is more complex. Both models still produce an overprediction in the height of the Holocene highstand, between 2-5 m, which is most pronounced along the NE and NW coasts of England (sites such as 23, 24, 30 and 35). Although the NS-96 model generates a slightly lower highstand compared to the NS-71 at these central sites, and hence a better fit to the SLIP data, it significantly underpredicts at sites across Scotland. It is for this reason that the NS-71 model is still the preferred model to use for the complete Great Britain dataset.

The misfit in the location of the RSL zero isobase still remains, as there has only been a minor reduction in the height of the Holocene highstand compared to the Shennan model (between 2-1 m). It has moved little on the west coast of England, still falling between sites 36 and 43, but on the east coast of England this transition now occurs very close to site 27.

At most of the distal sites there is, again, little or no difference in the predictions using either the NS-96 or 71 models. Sites 40 and 50 on Fig. 2.8, illustrate the typical pattern at these sites: a steady rise towards present but with sharp slowdown at ~ 6 kyr BP, which is not seen in the SLIPs.

Comparing the predictions using the NS-Thick(96 or 71) and Thin(96 or 71) models (dashed and solid lines on Fig. 2.8, respectively) the maximum impact of extending and thickening the ice sheet, both across the NSB and around the west coast of the British Isles, is over the deglacial period (20-15 kyr BP). There is an obvious lack of SLIP data at most sites over this time period with which to differentiate between the two models. Over the last 12 kyr BP, where the majority of the SLIPs are concentrated, the differences are either negligible (e.g. at southern sites such as 50) or between 1- 0.5 m (such as site 23) and generally lie within the spread of the SLIP data.

There are a few sites along the western and eastern margins of Scotland where the differences in thickness between the two NS models have a greater impact on the RSL prediction, but there are still a limited number of SLIP data points with which to

differentiate between the models. For example, at site 7, situated close to the western shelf margin, there is an offset of between 6-2 m over the deglacial period (20-15 kyr BP), reducing to less than 0.5 m over the last 8 kyr BP where there are only two SLIPs. Along the east coast of Scotland (sites such as 13 on Fig. 2.8 and the following sites in Appendix C: 15, 3, 2, and 1), differences between the two NS models again have the most significant impact on predictions prior to 12 kyr BP. For example, at 13, between 20-15 kyr BP there is a difference of 7- 3 m between the two models, but < 1.5 m over the last 10 kyr BP where most of the SLIP data occur. Clearly, new RSL data or new geomorphological constraints dating to this earlier period from sites in NE Scotland (e.g. sites 7 or 13) would provide useful information that could help to discriminate between these two ice models.

There are only two sites where the difference in ice thickness between the NS-Thick and NS-Thin models has a visible impact on the predictions, at a time when SLIP data is available. At site 11, with the oldest RSL data record, using the NS-Thick model slightly reduces the amount of underprediction at ~ 16 kyr BP (by about 1 m) although a noted misfit of ~ 10 m remains. At site 1, there was also an underprediction using the Shennan model (96 or 71) between 8-6 kyr BP, where there is a cluster of SLIP data. The NS Thick model (96 or 71) produces a 1.5 m higher RSL around this time, reducing the underprediction and generating a closer fit to the RSL data.

Despite the relative insensitivity of the RSL to changes in thickness of the ice across the NSB and coastal region (NS-Thick vs NS-Thin models), a choice must be made between which of the two should be adopted within the rest of the study. At sites where there are differences between predictions (such as site 1 or 11) the NS-Thick model performed better. Also, as the general view regarding the behaviour of the BIIS is of an ice sheet that was more expansive and thicker than previously assumed (see section 2.2.2 and 2.4), using the thicker model is the most appropriate choice. However, the reader should note that this choice was made on only a few data sites and so this aspect of the model may require adjustment in the future as more data become available.

To summarise, a revised ice model has now been created which is more consistent with the new geomorphological data and accounts for the underlying terrain. An optimum fit to the complete Great Britain RSL database is produced with the NS-Thick model combined with a 71 km thick lithosphere model. While some of the earlier identified misfits from the Shennan model (Section 2.3.1) have been reduced, there remain a number of issues, the most notable of which are summarised here. There is an underprediction in the amount of sea-level fall across the northern sites following the end of glaciation (15-16 kyr BP). During the two periods of rapid change at ~ 14 kyr and 11 kyr BP, also most evident at the northern sites, the NS model has not resolved the overprediction in the magnitude of this change. This is to be expected, as these inflections (as was discussed in the Introduction section), are primarily due to accelerations in the rate of melting, driven by the global ice model, which has not been altered at this stage in the modelling. The height of the Holocene highstand has been reduced using the NS-Thick71 model, but an overprediction of between 2-5 m still remains and the Holocene zero isobase is still displaced to far to the south along the NE and NW coastline of England. At the distal sites, the sharp slowdown in the rate of rise at 6 kyr BP, which is not seen in the SLIP data, still remains. Again, this is related more to the global ice model which will be considered in Chapter 4.

### **2.4.3. Modelling the component for Ireland**

#### **2.4.3.1. Preliminary modelling comparison**

In past BIIS GIA modelling studies there has been a noted lack of work which has examined both or either Irish RSL data or the IIS, with two noted exceptions (Lambeck (1996), Lambeck and Purcell (2001)). This section aims to address this by examining the spatial and temporal history of the IIS in greater detail, which is motivated by new geomorphological data to constrain the IIS history. Additionally, the new and more extensive RSL database for Ireland needs to be examined, with key misfits specific to this region and model sensitivities to be explored.

Initially, predictions using the revised regional NS-Thick model (highlighted just for Ireland on Fig. 2.9) will be examined at the Irish data sites to identify the ability of the model to capture the general trends within the data set. Only the NS-Thick model was adopted within this section as this model produced the optimum fit to the Great Britain data and the new field evidence implies that the IIS was thicker within the offshore region, most specifically along the western margin. Results are shown on Fig. 2.10 for NS-Thick model and the two earth models considered for the Great Britain analysis. Eight representative sites are shown in Fig. 2.10, but the complete set of predictions at all data sites are shown in Appendix D.

When examining the fit of the predictions to the Holocene and Late Devensian RSL data in Fig. 2.10 (and at all sites in Appendix D), it is apparent that the NS-Thick71 model produces the optimum fit and so this Earth model (71 km lithosphere) will be used most frequently in the following ice model sensitivity tests.

The model captures reasonably well the trend in the sea level data along the south (such as site 83) and south west coast (85), where there is little variation between the NS-Thick71 and NS-Thick96 predictions. But at sites across Northern Ireland, which are more sensitive to changes in the ice and earth model, there are a number of misfits associated with both NS-Thick71 and NS-Thick96. The first problem, as highlighted with the Shennan-96 model, is recreating the inferred height of sea level during the late Devensian, around the LGM, along the NE coastline (as can be seen at sites 97 or 99). Adopting the NS-Thick71 model does increase the predicted RSL over this time compared to the Shennan-96 model (or the NS-Thick96), but there is still an underprediction compared to the constraints given by the limiting data and raised shoreline evidence from across this region. This evidence suggests that along this coastline, sea level reached over 20 m compared to the modelled sea level of ~ 10 m.

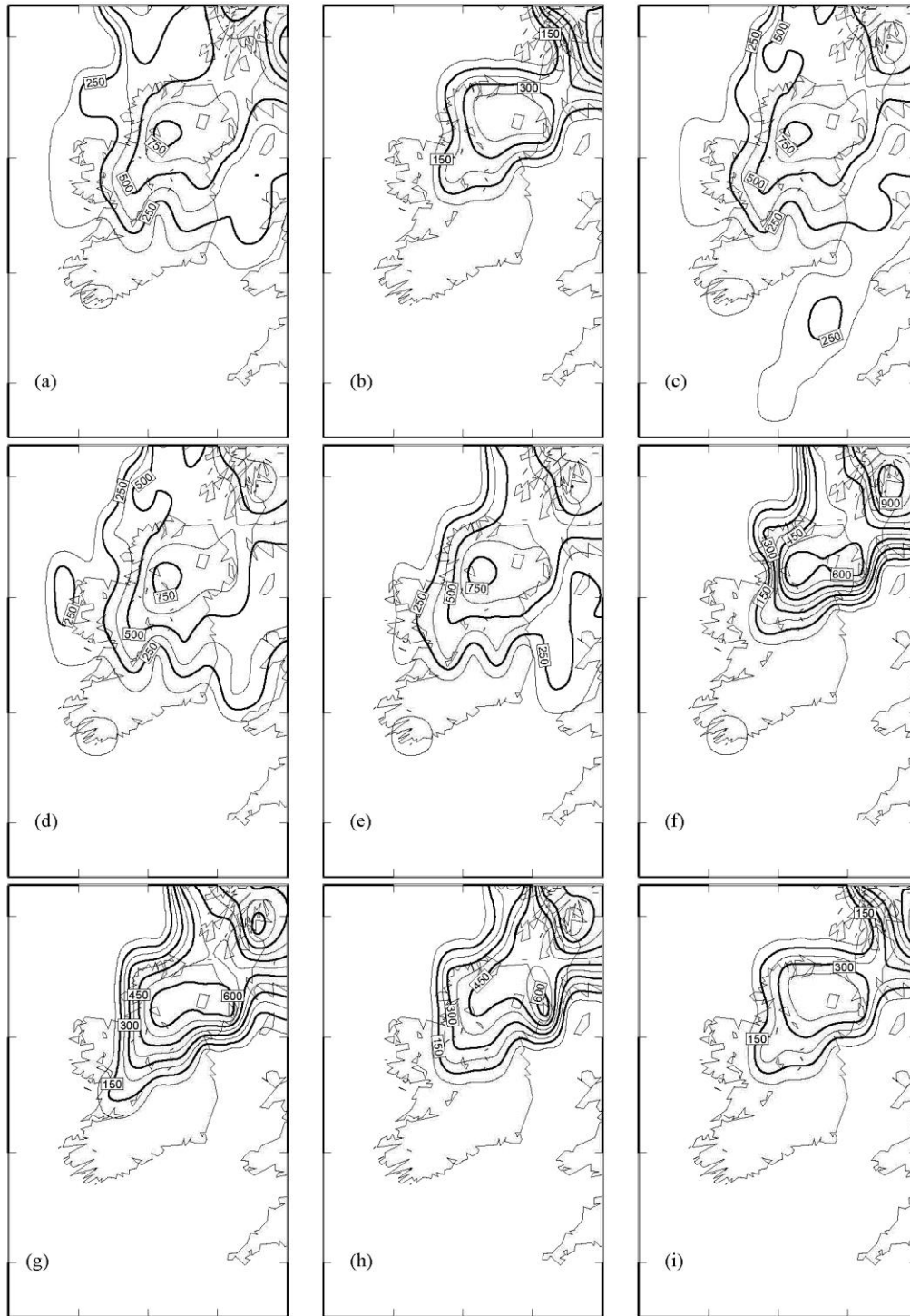


Fig. 2.9: Ice thickness maps of the NS-Thick BIIS model presented in Shennan *et al.*, (2006) for Ireland only at the times (in kyr BP): (a) 32, (b) 26, (c) 24, (d) 21, (e) 20, (f) 19, (g) 18, (h) 17, (i) 16. Note the varying contour interval.

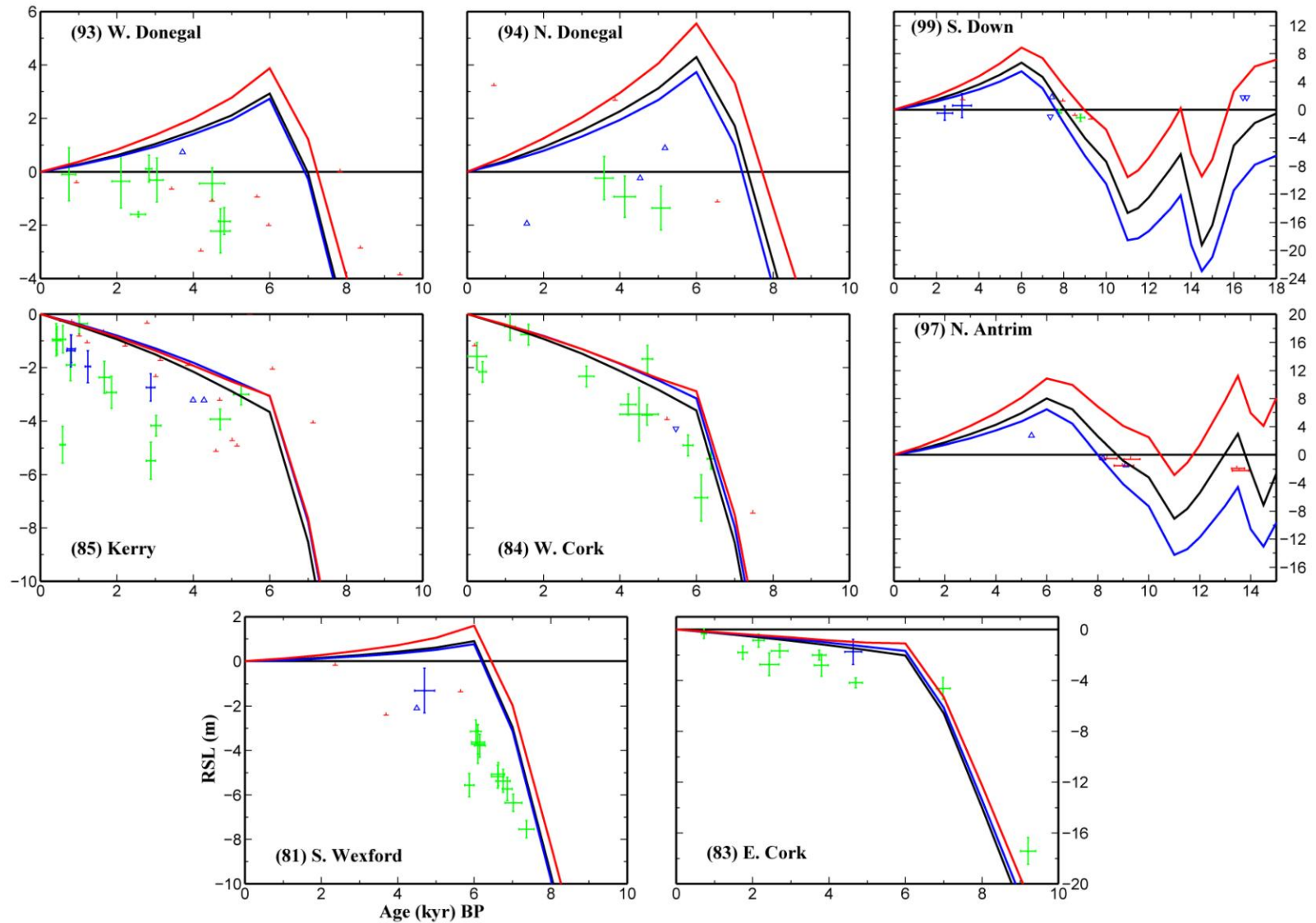


Fig. 2.10: Comparison of predicted and observed sea levels at eight locations across Ireland. Predictions are shown using the 96 km lithosphere earth model (described in caption for Fig. 2.6) for the Shennan model (solid black line) and for the NS-Thick model (solid blue line). Results are also shown for the 71km lithosphere earth model for the NS-Thick model (solid red line). Results are shown for all sites across Ireland in Appendix D

Adopting the NS-Thick71 model does not resolve the earlier described discrepancy in capturing the north-south/west-east variation in the height of the Holocene highstand and location of the zero isobase. The height of the Holocene highstand has been increased along the Northern coastline compared to the Shennan-96 model, with an overprediction now of between 4-6 m. This is highlighted at site 93, where at ~ 5 kyr BP the data constrain sea level to ~ -2 m, compared to the model RSL of 2.7 m. The misfit in the location of the zero isobase along the west coast has not changed, with the predicted location still falling between sites 91 and 92. However, this isobase is now displaced further south along the east coast to lie between sites 82 and 83. Using the NS-Thick96 model would generate a lower highstand, by 3-4 m along the west coast (such as site 97) and 1-1.5 m along the east coast (such as sites 92 or 93) compared to the NS-Thick71 model. However, using the NS-Thick96 model would significantly underpredict the height of RSL along the NE coastline.

This issue of reducing the height of RSL during the Holocene while maintaining the elevated RSL during the Late Devensian is a problem also highlighted with the Great Britain data. This issue, for the case of Ireland, will be addressed further in the following section by revising the spatial extent and timing of the glacial and deglaciation phase of the IIS.

#### **2.4.3.2. Sensitivity analysis to changes to the Irish ice sheet history: Local Scale Ice Readvances.**

The ability of GIA ice models to capture local scale ice movements (or ice loading events) has been questioned by past researchers (McCabe (1997)). Furthermore, the IIS component typically used within GIA models has been criticised as not being an accurate geographical reconstruction of the ice sheet, with small scale advance-retreat phases and the location of ice margins significantly at odds with the field evidence.

To investigate this, two ice models are developed that include small scale adjustments in the spatial and temporal history of the IIS to determine the extent to which these impact regional and local scale RSL predictions. This sensitivity test will shed light on the ability

of RSL data to constrain local small scale and transient changes in the ice model. Two scenarios will be considered: (1) an ice model where deglaciation across Ireland is complete by 19 kyr BP, removing the later KPS readvance (which will be referred to as Model A), and (2) a model where the ice stream down to the Isles of Scilly at 24 kyr BP (as shown in Fig. 2.9c) is not included.

Predictions using Model A are compared to the NS-Thick71 model on Fig. 2.11 (shown in Appendix E for all Ireland sites and a selection of sites across Great Britain). At sites along the south and SW coast of Ireland (such as 83 or 86) and NW coast of England (selected sites in Appendix E such as 33 or 36), the impact of the removal of the KPS readvance is minimal (less than 1-1.5 m), over the late Holocene where the majority of the SLIP data are concentrated. This highlights that these sites distal to the main centre of ice loading, along the southern coast, are relatively insensitive to changes in the deglaciation pattern of the IIS. At sites around Northern Ireland (such as site 94, 95, or 99) and selected Great Britain sites (54, 18, or 31 shown in Appendix E), which were closer to the centre of ice loading, the impact of this change is more pronounced. Between 18-15 kyr BP RSL predictions for Model A are reduced by 18-15 m compared to the NS-Thick71 model, increasing the already noted underprediction. The complete removal of the ice sheet at 19 kyr BP which introduces a very rapid deglaciation, produces the sharp fall in RSL from this time onwards, as can be seen at 97 (and site 100, in Appendix D). In contrast, the height of the Holocene highstand along the northern coastline has been significantly reduced, by ~ 2.5m, as can be seen at 94 or 31. Adopting Model A does produce a closer fit to the RSL data over this period compared to the NS-Thick71 model but an overprediction remains, with the zero isobase still situated too far south along the NW coastline (falling between 91 and 92). This result emphasises the more pronounced sensitivity of sites across North Ireland sites to changes in the deglacial pattern of the IIS.

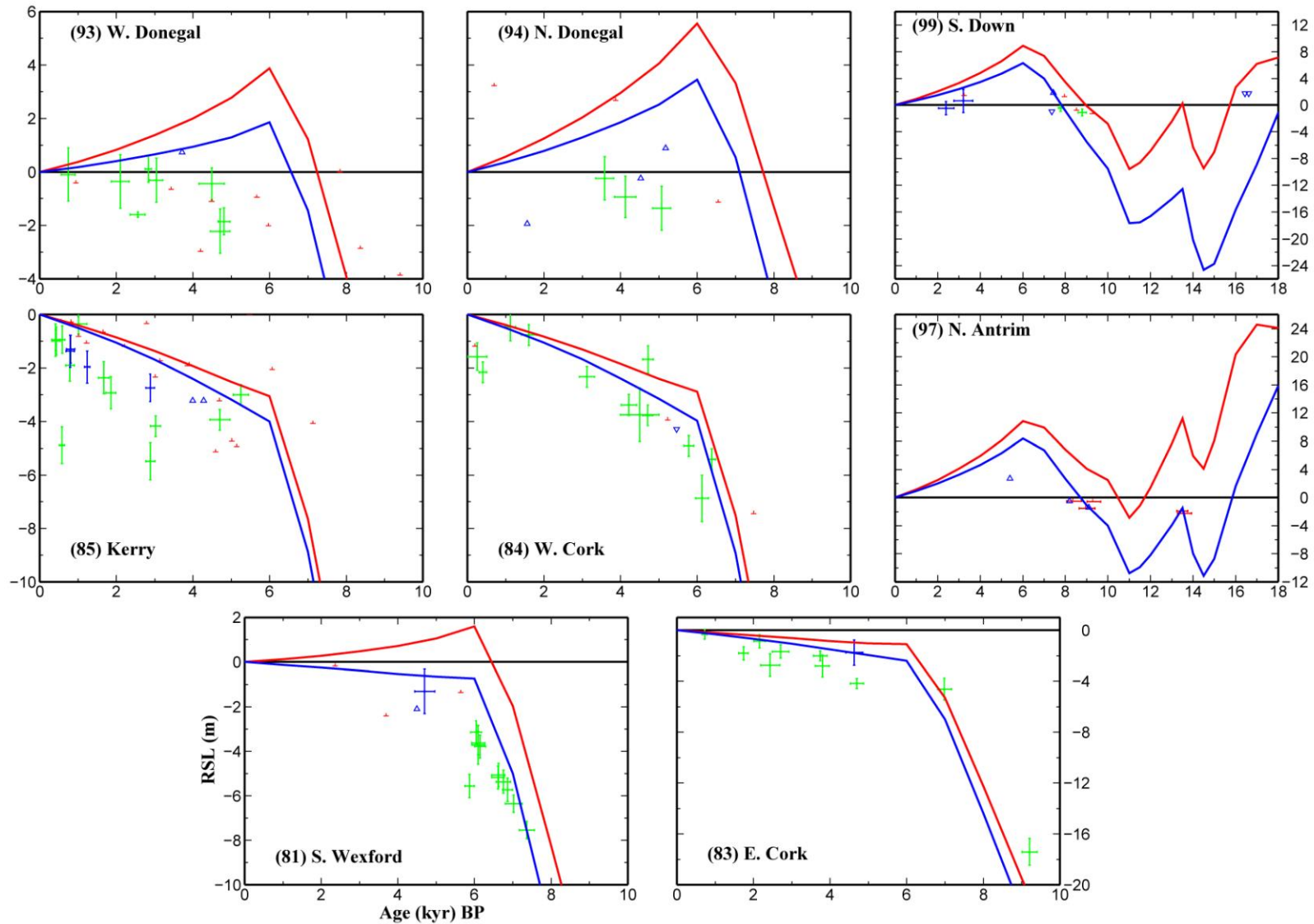


Fig. 2.11: Comparison of predicted and observed sea levels at eight locations across Ireland. Predictions were generated for the NS-Thick (solid red line) and Model A (solid blue line) ice models using the 71 km lithosphere earth model. Results for all Ireland sites are shown in Appendix E

The second scenario, in which the ice stream flowing down to the Isles of Scilly was removed, had no discernable impact on the RSL predictions at any of the data sites (and so the results are not shown).

As briefly stated above, the IIS model used within this study is not intended to be an accurate reproduction of the spatial and temporal history of the ice sheet at scales of 10's of km and less. Many small advances, localised ice lobes or meltwater channels which form during the glacial and deglacial phases and are recorded in the field evidence (e.g. see Clark *et al.*, (2004), Evans *et al.*, (2005)) would have no effect on the RSL predictions and so do not need to be built into the ice model. This insensitivity is illustrated by the results for models with and without an Isles of Scilly ice stream. This contrasts with the impact of the more substantial loading event of the KPS advance, both in terms of spatial extent and duration; in this case RSL predictions at sites near or under the ice were significantly affected.

The insensitivity of the predictions to small-scale loading changes arises from the mechanical properties of the lithosphere, which includes the crust and shallow upper mantle. The lithosphere is defined as a mechanically strong layer that can behave as an elastic material over time scales considerably longer than those under investigation here. Surface loads of relatively small spatial scale (10's of km) are supported by the lithosphere and so the resultant stresses will not be transmitted to produce significant flow in the mantle, thus producing minimal impact on the RSL predictions.

The above sensitivity analysis has indicated that one possible method of removing the overprediction of RSL in the late Holocene, at sites across NE Ireland and NW Great Britain, is to introduce a very rapid retreat and thinning during the deglacial period. On the other hand, this will significantly impact on the ability of the model to recreate the Late Devensian sea-level data, around the Northern coastline and sites across Great Britain. These issues will be considered in the following sections.

### **2.4.3.3. Sensitivity analysis to changes to the Irish ice sheet history: Improving the fit to the Holocene data**

Revisions to the spatial and temporal history of the IIS will be examined within this section with the aim of reducing the overprediction from both the NS-Thick71 and Shennan-71 models during the late Holocene at sites around North Ireland and Great Britain. It is noted that within the remainder of this section the 71 km earth model will be combined with all revised ice models.

It is useful to first discuss the processes which could act to generate the Holocene highstand across these near-field sites. The height of Holocene sea levels is controlled by the interaction between local isostatic processes (dominated by ice unloading), which produces a fall in sea level, and non-local processes such as the melting of non-local ice and increase in ocean basin volume through isostatic deflection of the ocean floor (ocean syphoning – see Mitrovica and Milne (2002).). If the local crustal loading signal and the syphoning signal (which also drives a sea-level fall) exceed the global melt signal, the Holocene sea level is elevated above present. Conversely, Holocene sea levels remain below present. A reduction in the height of Holocene sea levels could be achieved by adjusting a model parameter to either increase the rate of sea-level rise through melting (for example the global ice model) or decrease the rate of fall through local and global isostatic processes.

In this section, the second option is considered; specifically, the spatial extent and thickness of the IIS will be revised in order to reduce the size of the crustal loading signal. This could be achieved by reducing the thickness and lateral extent of the IIS during the glacial period (24-21 kyr BP). However, this would also have a considerable impact on the predictions during the Late Devensian, which are already too low. Alternatively, altering the pattern of deglaciation by adjusting the timing for the onset of ice sheet retreat (hence reducing the length of the glacial phase and loading period) or introducing a rapid retreat and thinning, would also achieve a similar result.

To examine this, the NS-Thick model was altered in two ways; firstly, an earlier deglaciation was induced, now starting at 22 kyr BP (as suggested in McCabe *et al.*, (2005)) and secondly, during the deglacial period, a thinner IIS is adopted, approximately half of the NS-Thick, while maintaining the same spatial extent. This model will be referred to as Model B, with predictions compared to the NS-Thick71 model on Fig. 2.12 (Note the complete set of predictions at all sites across Ireland and a selection of sites across Great Britain is shown in Appendix E). As to be expected, the impact of Model B on the RSL predictions is similar to that produced using Model A, as both models recreated a restricted IIS during the deglacial phase. Once again, at distal sites along the southern coastline, (such as 83 to 90), the differences in RSL predictions using Model B compared to NS-Thick71 is minimal. Generally, the depth of predicted sea level over the last 10 kyr is reduced by < 1 m, which does produce a minor improvement in the fit to the observed sea level data, as can be seen at 84.

However, along the Northern coastline, the difference between Model B and NS-Thick71 is more pronounced, with a reduction in predicted sea level throughout the glacial period, by up to 20m during the Late Devensian (20-15 kyr BP) and up to 5m over the Holocene. The reduction in the Holocene highstand along the NW coastline (by ~ 2m), results in a far better fit to the SLIP (such as at sites 93 and 94) and resolves some of the mismatch in the location of the Holocene zero isobase: now falling between sites 81 and 82, along the SE coast and displaced closer to sites 91 along the NW coast. Additionally, the revised deglacial history in Model B reduces the size of the misfit during the Holocene, at the selected sites from Great Britain along the NW coast of England and Scotland (as can be in Appendix E for sites such as 33 and 36). This is exemplified at sites 31, where the reduction by ~ 2m during the last 9 kyr generates a closer fit to the SLIP record, but a 4 m misfit still remains.

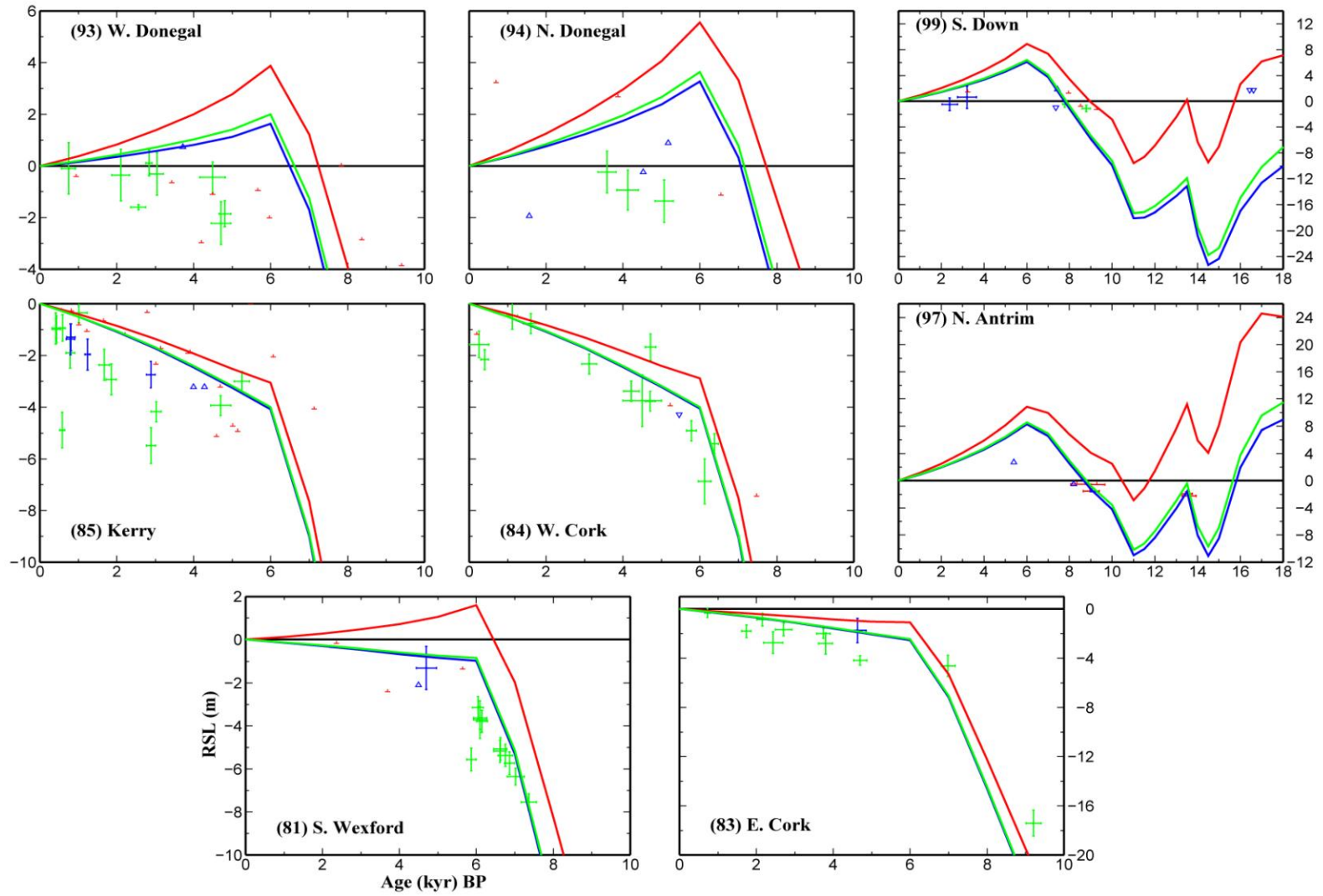


Fig. 2.12: Comparison of predicted and observed sea levels at eight locations across Ireland for three Irish ice models. Predictions were generated for the NS-Thick model (solid red line), Model B (solid blue line) and Model C (solid green line) using the 71 km lithosphere earth model. Results for all Ireland sites are shown in Appendix E

As expected, altering the deglacial phase has not improved the ability of the model to capture the RSL trend during the Late Devensian, with the fit of the RSL predictions to the data worse than using the NS-Thick71 model. This is most evident at sites along the NE coast of Ireland (such as at sites 95 and 97) and NW Scotland (such as sites 18 and 54 shown in Appendix E). Introducing an earlier and very rapid thinning produces a sharp fall in predicted sea-level, which further displaces sea level below present by between 11 and 20 m. For example, at 100, at ~ 20 kyr BP, Model B predicts sea level at -10 m whereas the limiting data suggest sea level was at present levels, if not higher.

To summarise, the misfit over the Holocene can be reduced by introducing an earlier and more rapid thinning of the IIS during deglaciation. However, this change does not reproduce well the higher sea-levels around the NE coast between 20-15 kyr BP. This issue will be examined further in the following section.

#### **2.4.3.4. Sensitivity analysis to changes to the Irish ice sheet history: Improving the fit to Late Devensian data**

As discussed above, the key aim is to recreate the relatively high sea levels during the Late Devensian around the NE coastline of Ireland while producing lower sea levels during the Holocene. Using the NS-Thick model, predicted sea levels across this region are around ~ 10 m or more lower than observational constraints, which suggest heights of over 20 m. The discrepancy is greater with Model B.

One method of generating higher sea levels during this period is through an increase in the ice volume (and as such the crustal loading signal); either by extending the duration of the glacial phase, increasing the thickness and spatial extent of the IIS, or adopting a slower retreat during deglaciation. As the latter would impact significantly on the predicted Holocene sea level (as was seen in the above section), a revised model will be created where the final glacial phase is adjusted. However, it must be noted that introducing a considerable thickening of the ice sheet across the onshore regions of north Ireland would have a direct impact on the Holocene predictions across this region. Therefore, initial revision to the NS-Thick model will be concentrated within the offshore

regions and south Ireland. Model B will be adopted to generate an improved fit (compared to NS-Thick) over the Holocene. Additionally the first glacial period (32-25 kyr BP) from the NS-Thick model remains unchanged. During the final glacial phase (24-22 kyr BP), the IIS is thickened and extended into the offshore regions along the NW coast of Ireland and within the North ISB, to now reach up to 650m . The southern limit for the IIS has so far been taken as the SIEM, as can be seen in Fig. 2.7h and 2.9c, which separated the main ice sheet from a smaller ice dome across SW Ireland. The SIEM was assumed to be an end moraine and marked the LGM limit of the IIS. As was alluded to in section 2.2.2.3, it can also be interpreted as having formed during a retreat phase. To take this into account, the revised IIS has been extended across the entire Irish mainland down to the coastline. This model will be referred to as Model C with predictions shown on Fig. 2.12 (Note the complete set of predictions at all sites across Ireland and selected sites across Great Britain is shown in Appendix E).

Comparing the predictions using Model B and C on Fig. 2.12, there is minimal difference over the last 10 kyr, with an increase in the height of the highstand at most sites of < 0.5 m. Despite increasing the thickness of the ice sheet between Model B and C (by ~ 300 m), the increase in sea level over the late Devensian around the NE coast of Ireland and NW Scotland is only ~ 5 m, at most. See, for example, sites 97 and 95, where predictions still lie below the limiting data and those produced using the NS-Thick model. This suggests that the increase in the loading signal within Model C is still not sufficient to offset the reduction in the crustal loading signal due to the earlier onset of deglaciation (22 kyr BP compared to 21 kyr BP) and the more rapid retreat and thinning during the earlier phase of deglaciation. This implies that further revisions to the IIS during this earlier glacial phase are required, such as altering the earlier onset of deglaciation introduced in Model B and/or increasing the ice volume, to recreate the higher sea levels inferred from the field evidence (such as O’Cofaigh and Evans (2007)).

#### **2.4.4. Combined final revised BIIS model**

In the above sections, the spatial and temporal history of the IIS was modified with the aim of reducing key misfits of predicted sea level using the NS-Thick71 model to the

Irish sea-level data. It was demonstrated that introducing a rapid thinning and retreat during the deglacial phase can reduce, but not remove entirely, the overprediction along the northern coastline throughout the late Holocene. The underprediction during the late Devensian across this region remains, despite a thickening and extension of the IIS within the offshore region and ISB.

To address these remaining problems a final BIIS is produced, which is a combination of the regional BIIS (taken from the NS-Thick Model) and a revised IIS model. The main advance and retreat phases are summarised as follows, with key time slices illustrated on Fig. 2.13 for Ireland. During the Mid-Late Devensian, the first glacial advance (32-27 kyr BP) and later retreat (26-25 kyr BP) in the model is unaltered from NS-Thick model as described in section 2.3.2.2 (see Fig. 2.7 a and b). During the second glacial phase (24-21 kyr BP) the Great Britain component is taken from the NS-Thick model (see Fig. 2.7c and g), but with the start of deglaciation at 21 kyr BP, rather than 22 kyr BP as used in the above IIS modifications. This Great Britain component was combined with a final revised IIS, which incorporates some of the revisions discussed above. Following on from Model C, the IIS model has been extended and thickened further out into the offshore region along the NW coast and across southern Ireland. The maximum thickness is increased across the central regions (Wicklow Mountains) and the entire ISB to over 600 m to comply with the trimline evidence (Ballantyne *et al.*, (2006), Rae *et al.*, (2004)). These time slices are illustrated in Fig. 2.13a and b. During the deglacial period, the Great Britain component (unaltered from that used in NS-Thick model) is combined with an IIS model similar to Model B, where the ice sheet thins and retreats rapidly. The maximum thickness is reduced, now reaching only 400 m across NE Ireland following the KPS readvance, compared to 650 m with the NS-Thick model (compare Fig. 2.9g to Fig. 2.13e).

This model will be referred to in the following sections and chapters as the Brooks *et al.* model and is published in Brooks *et al.*, (2008). Predictions using this model are compared to the starting model (i.e. the Shennan ice model), using the 71 km earth model on Fig. 2.14a for the eight selected Great Britain sites and Fig. 2.14b for the eight Ireland sites. Predictions for the complete data set are shown in Appendix F.

When comparing the fit of the Brooks et al. model to the Shennan model, it may not be apparent that there has been a significant improvement in resolving the original misfits or in the ability of the model to capture the regional trends in the SLIP data. However, it must be reiterated, as was noted in section 2.1 and in the above discussions, the main aim of this chapter is to adjust the Shennan model to produce a revised regional ice model which is both compatible with the new geomorphological evidence (as outlined in section 2.2.2), and correctly accounts for the underlying terrain when defining the maximum thickness of the ice sheet. In this regard, the two ice models are significantly different, with the Brooks et al. model being the more up-to-date and accurate of the two.

In the above sections, a more in-depth study of IIS was conducted to address specific issues regarding the fit of the RSL predictions to the Irish data. This will be concluded by examining the impact of the Brooks et al. model in capturing the SLIP trends at the Irish sites.

The thickening of the IIS within the Brooks et al. model (from that used in Model C) has gone some way to resolve the earlier identified problem of increasing the height of sea level during the Late Devensian, while maintaining a lower sea level during the Holocene around the northern coastline of Ireland. At sites along the southern coastline of Ireland (82 to 87), the removal of the SIEM constraint and thickening across southern Ireland has impacted slightly on the predictions during the last 10 kyr. The height of sea-level has increased by  $< 0.7$  m, which does not significantly influence the ability of the model to capture the late Holocene trend. Along the NW coast, the minor increase in the predicted amplitude of the Holocene highstand of less than 0.5 m (such as at site 93), also does not significantly alter the geographic location of the zero-isobase or misfit to the SLIP data. A noted exception is site 81 (compare Fig. 2.14b to Fig. 2.12), where the thickening of the ice across this region and within the ISB has elevated predicted RSL and increased the misfit to the SLIP data.

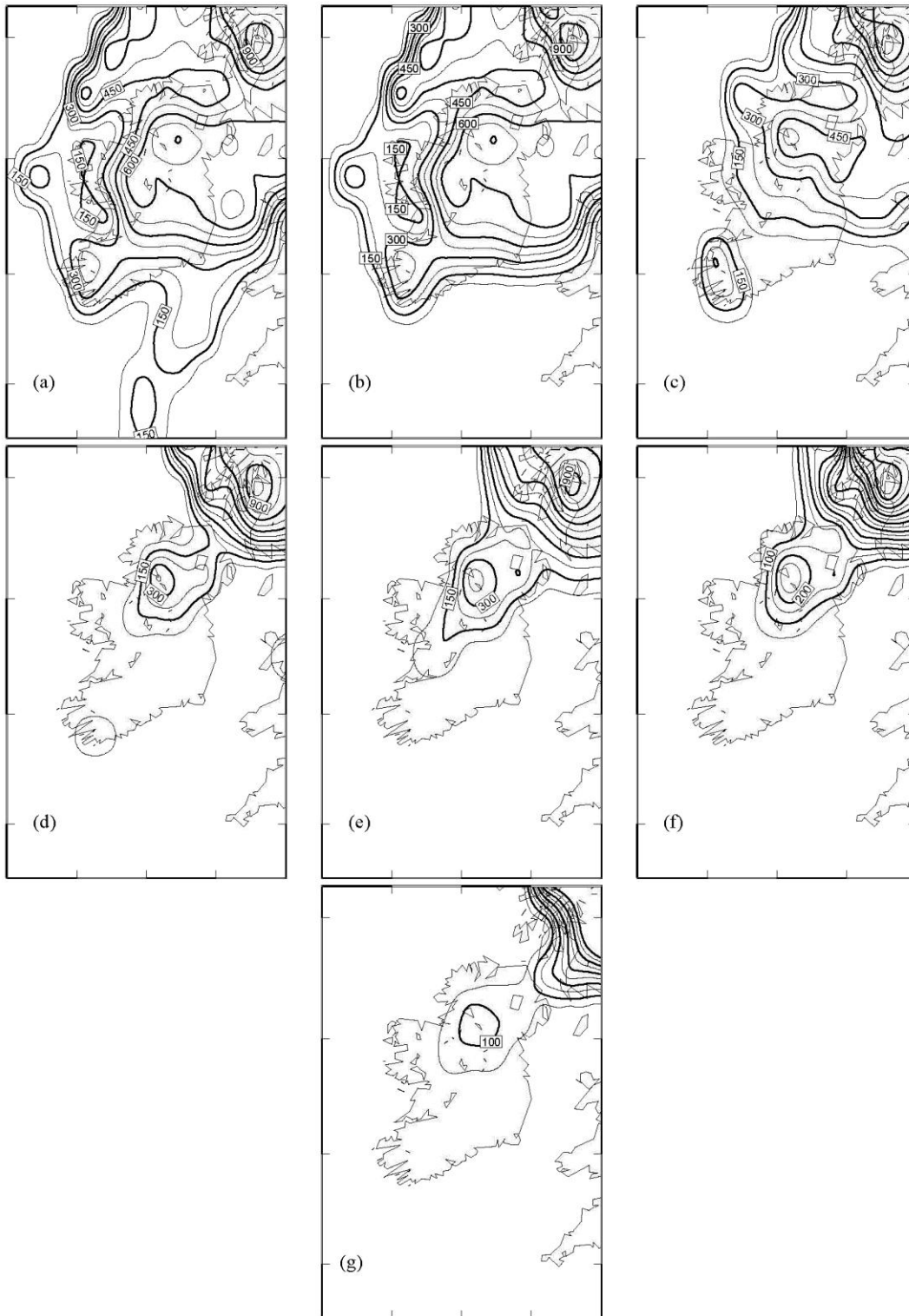


Fig. 2.13: Ice thickness maps for the revised British- Irish ice model presented in Brooks *et al.*, (2008) for Ireland only at the following times (in kyr BP) steps: (a) 24, (b) 21, (c) 20, (d) 19, (e) 18, (f) 17, (g) 16. Note the varying contour intervals

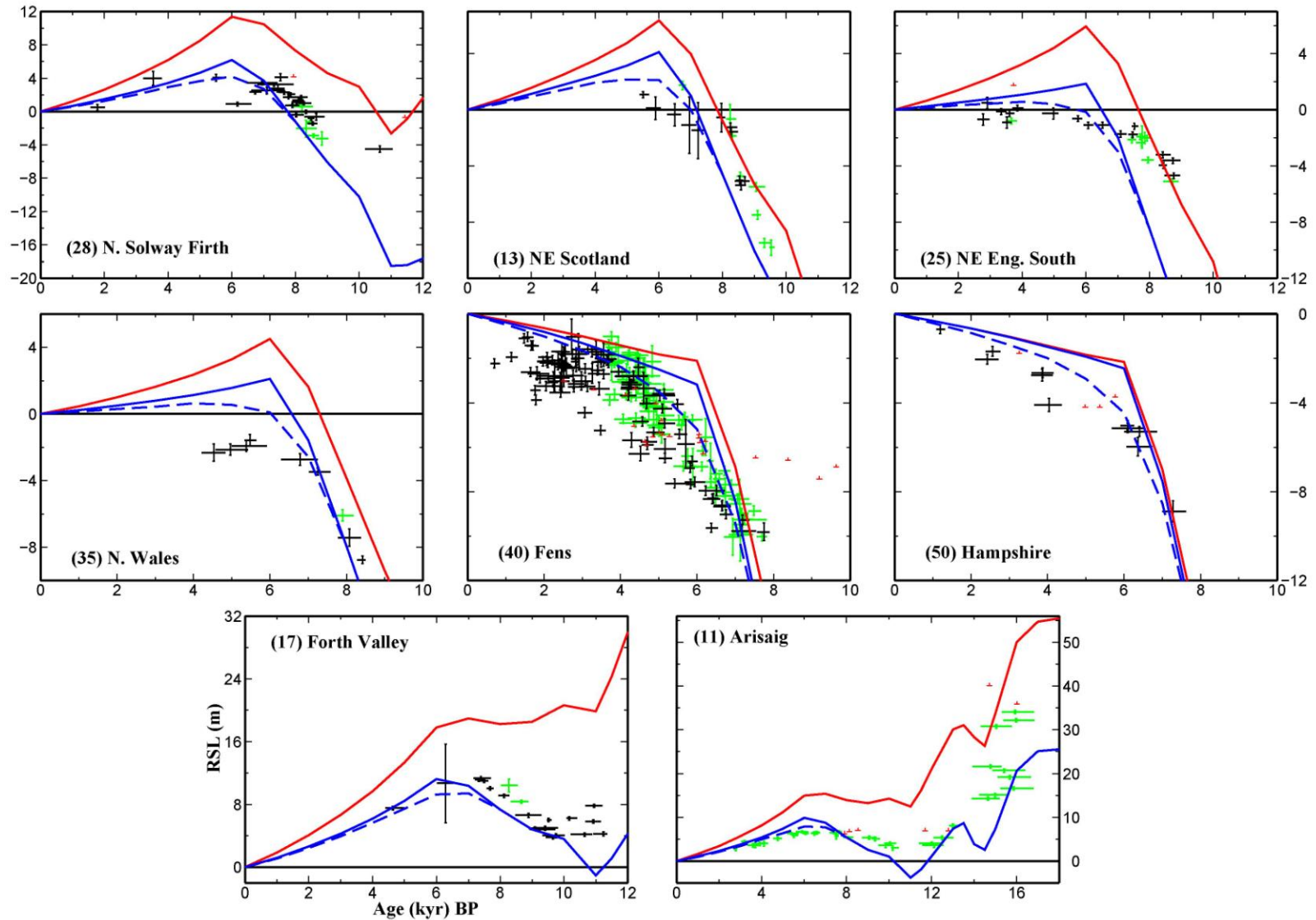


Fig. 2.14a: Comparison of predicted and observed sea level at eight locations across Great Britain. Predictions were generated for the original starting ice model (i.e. the Shennan model; solid red line) and the new revised ice model taken from Brooks *et al.*, (2008) (solid blue line) using the 71km lithosphere earth model. The dashed blue line is the prediction for the Brooks *et al* model but with a post modeling correction applied to create a continued rise in eustatic sea level of 5 m between 7-1 kyr BP.

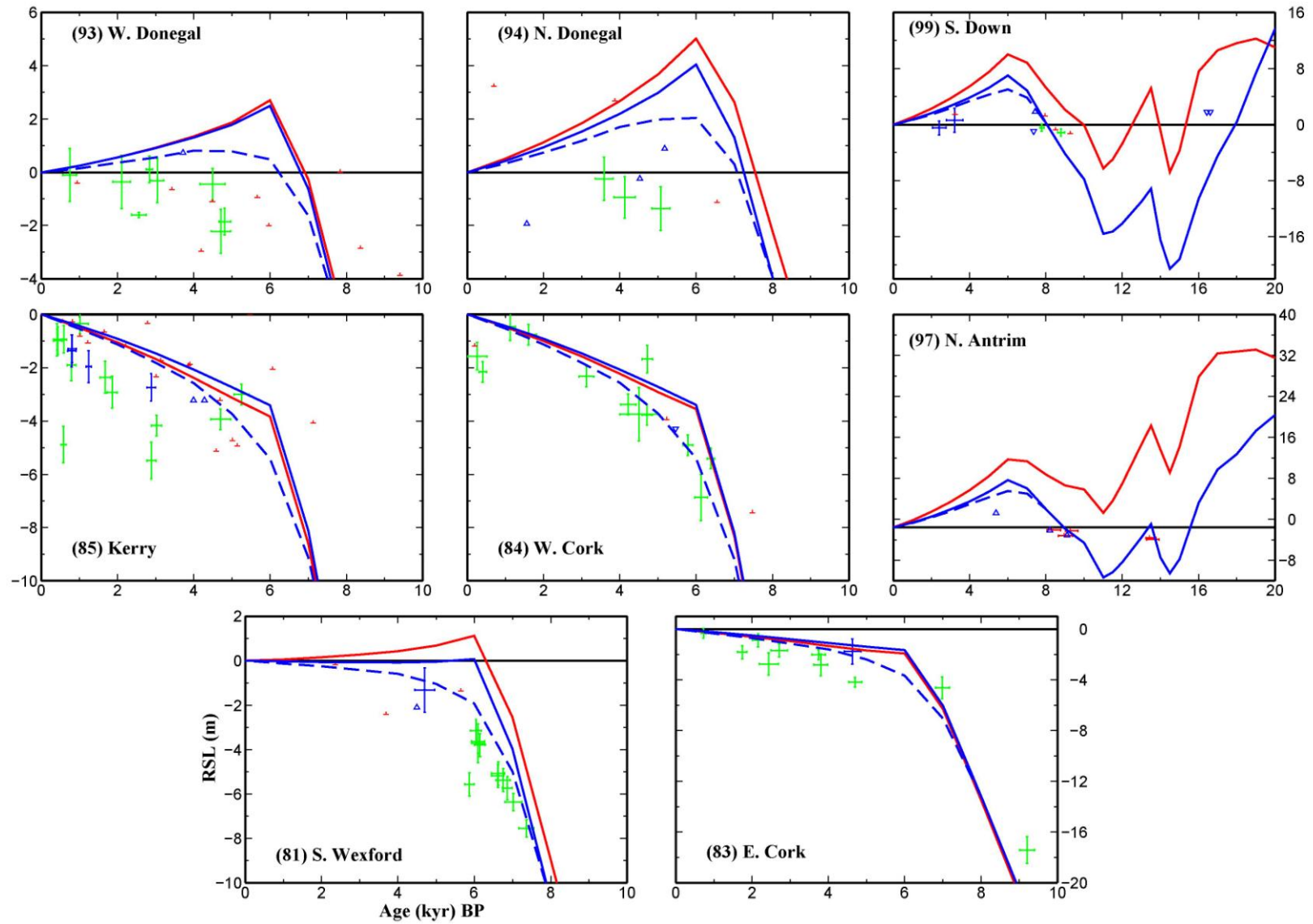


Fig. 2.14b: As 2.14a but for the eight chosen data localities across Ireland. Results for all Ireland and Great Britain sites are shown in Appendix F.

The most pronounced improvement of the Brooks et al. model is at sites along the NE coast such as sites 100 or 97, where the predicted height of sea-level during the Late Devensian has been increased by between 11 m and 5 m respectively (compared to Model C). This goes some way to satisfy the mismatch to the limits inferred from the shoreline evidence and limiting data that sea level reached up to 25-30 m during this period. It is noted though that an underprediction of ~ 15 m still goes unresolved.

Examining the predicted sea level using the Brooks et al. model at all British Isles sites it is apparent that the results are generally lower than using Shennan-71, which is to be expected given the considerable reduction in the thickness of the ice sheet between the two ice models. This reduction is most pronounced across the northern and central sites (for example sites 17 or 25, across Great Britain and site 97, across Ireland), where the height of predicted sea level during the late Devensian has been reduced by ~ 20m and over the Holocene by 5m. The impact of this revision was described in greater detail in Section 2.3.2.1., when altering the thickness of the ice sheet to take into account the underlying terrain.

The Brooks et al. model captures the pattern of sea level on a regional scale reasonably well, as can be seen in Fig. 2.14a and 2.14b, but there are a number of consistent misfits to highlight. Firstly an underprediction in the magnitude of sea level fall during the late Devensian (between 20-15 kyr BP), as can be seen at sites 11 or 99. As was highlighted for the Irish sites, this could not be resolved through reasonable changes to the local IIS model. Possible solutions to address this misfit will be discussed below, specifically in light of new geomorphological evidence. Secondly, the late Holocene highstand remains too high, by up to 4 m (for example at sites 93, 11 and 25) which leads to the location of the Holocene zero isobase being displaced too far south: falling between sites 26 and 27 and close to site 36, along the NE and NW England coasts, respectively, and close to sites 81 and 91, along the east and west coasts of Ireland. Finally, at southern sites, the late Holocene rise towards present is characterised by a sharp change in rate at ~ 6 kyr BP, which is not consistent with the smooth trend inferred from the SLIP data, as is highlighted at sites 40 or 50.

It has been highlighted in section 2.4.3.3. that reasonable adjustments to the spatial and temporal history of the IIS could not reconcile the misfit of predictions to the late Holocene SLIP data. As was discussed within this chapter (and in Section 1.1.3) the height of the highstand is also sensitive to the pattern of melting during the Holocene, which is governed by the non-local ice model. In the current global ice model, adopted from Bassett *et al.* 2005, the rise in eustatic sea level due to the melting of the global ice sheet reduces in magnitude abruptly at 6 kyr BP, with melting complete by 5 kyr BP - hence the timing of the highstand at central and northern sites. If the melting of the global ice model was to continue into the late Holocene, this would lower the height of the Holocene highstand.

To investigate the impact of such a change on resolving the data-model misfit over the Holocene, predictions were generated by applying a post modelling correction to the predictions from the Brooks et al. model to replicate a gradual 5 m rise in eustatic sea level between 7 – 1 kyr BP. Results are shown for selected sites on Fig. 2.14a and 2.14b by the dashed blue lines.

As expected, the revised pattern of Holocene melting impacts predictions at all sites, not only by lowering the height of sea level during the Holocene but also by altering the style of RSL rise over the last 7 kyr BP, which could not be achieved through revision to the local IIS. Introducing a gradual rise in eustatic sea level to 1 kyr BP produces a smoother trend to the RSL predictions more characteristic of that shown in the SLIP data, especially at the southern sites (such as at 40 or 50). The overprediction during the Holocene has been reduced at most sites by between 2-3 m, removing the misfit at 81 and improving the fit at most other sites (as can be seen at 11 or 35).

These results indicate that adopting a revised global ice model, in which melting from the global ice sheets is continued into the late Holocene is an important step to take to reduce some of the remaining misfits. This step will be the focus of Chapter four, in which previously un-modelled far-field sea level data from China and Malay-Thai Peninsula are utilised to constrain a revised global ice model for the Holocene.

## 2.5. Discussion

A new BIIS model has been developed within this chapter that is based on the model published in Shennan *et al.*, (2002). The revised model is compatible with recently published geomorphological data and includes an extensive two-stage glaciation across the NS, thickening across Ireland and out onto the western continental shelf, and a rapid thinning and retreat of the IIS component during deglaciation. Additionally, the thickness of the ice model has been adjusted to correctly account for the underlying terrain. Using a small number of earth models, RSL predictions have been generated to perform some preliminary sensitivity tests with the new ice model for both Great Britain and Ireland. The new ice model will be utilised further within Chapters 3 and 5.

Since the development of this model and publication in Brooks *et al.*, (2008), Shennan *et al.*, (2006) there has been a wealth of new information published regarding the history of the BIIS and SIS. Some key papers include reviews of the spatial extent (Chiverrell and Thomas (2010), Finlayson *et al.*, (2010), Lambeck *et al.*, (2010), O' Cofaigh *et al.*, (2010b), O' Cofaigh *et al.*, (2010a), Sejrup *et al.*, (2009)) and cosmogenic dates used to constrain the timing of glacial/deglacial phases (Ballantyne (2010), Phillips *et al.*, (2008), Telfer *et al.*, (2009)). New offshore geophysical data (Bradwell *et al.*, (2008), Graham *et al.*, (2007), Graham *et al.*, (2009), Graham *et al.*, (2010)) as well as updated and expanded IRD records (Hibbert *et al.*, (2010), Scourse *et al.*, (2009)) can both be used to constrain of the behaviour of the BIIS at earlier, pre-LGM times and also within offshore regions, when/where there are little or no SLIP data to constrain the model. Other new developments include numerical (Hubbard *et al.*, (2009), Boulton (2010)) and geomorphological-driven models (Evans *et al.*, (2009), Greenwood and Clark (2009b)) which also aim to replicate the evolution of the BIIS through the last glacial cycle. In general, the information published in these very recent studies supports a greatly extended BIIS during the last glacial period and so is compatible with the Brooks *et al.* model.

Identification of offshore geomorphological features, such as MSGL and moraines on single beam bathymetric data (Bradwell *et al.*, (2008)) and 3D/2D marine seismic data

from across the Central and Northern NSB (Graham *et al.*, (2007), Graham *et al.*, (2009)) support an extensive grounded ice sheet across the NSB, forming due to the convergence of the BIIS and SIS. Following a period of large-scale reorganisation when the two ice sheets separated, a marine embayment opened across the Witch Ground Basin, identified by overprinted moraines and seismic stratigraphy.

Accumulating onshore records, developed from geomorphological mapping and lithostratigraphic data, also support a more laterally extensive, dynamic ice sheet around West-Central Scotland (Finlayson *et al.*, (2010)). Golledge *et al.*, (2008) suggested that the expanse of an independent ice sheet across Shetland during an early glacial period was prevented due to the confluence of the BIIS and SIS across the NSB. Greenwood and Clark (2009b) developed a model of the IIS evolution over the last glacial cycle using a new geomorphological data set of glacial landforms (such as glacial lineations, meltwater channels and moraines (Greenwood and Clark (2009a))). Although the highly dynamic and mobile nature of the IIS suggested by these data (e.g. changes in the location of ice divides and flow geometries) are not replicated well in the Brooks *et al.* model, the overall inferred glacial history is of an IIS which extended offshore and across the entire mainland. It was found that the decay of the IIS was twice as fast as during the advance phase, which adds some support to the revised behaviour of the IIS introduced in new model.

In the Brooks *et al.* model, following the timings outlined in section 2.2.2.2, the initial build up of ice is rapid, expanding to the extensive, widespread glaciation across the onshore and offshore regions between 32-27 kyr BP (as shown in Fig. 2.7a). From the reviews of Ballantyne (2010), Telfer *et al.*, (2009), and Sejrup *et al.*, (2009) it is apparent how few available dates there are to constrain this early glacial advance of the ice sheet, thus highlighting some of the conflicting views on the behaviour and timings of the growth of the ice sheet over this period (as outlined below). One new set of AMS radiocarbon dates published recently by Graham *et al.*, (2010) suggest that an active grounded ice sheet and extensive glaciation across the Witch Ground Basin, Central NSB developed after 30.8  $^{14}\text{C}$  kyr BP (36.1 kyr BP) and prior to 16.2  $^{14}\text{C}$  (19.2 kyr BP), when marine conditions developed, thus supporting the timings used in the new model.

Sejrup *et al.*, (2009) refined the chronology of advance and retreat phases across the NSB such that the Mid Devensian growth of the BIIS and SIS across the NS occurred later, and followed a more gradual build up phase (compare Fig.2.1 to Fig. 2.15). (Note that, this revision was not based on new dates to constrain the timing of ice extent changes.) Following an early (~ 39-29 ka) restricted period of onshore glaciation, ice expanded gradually across the NS, leading to the coalescence of the BIIS and SIS for a shorter period, between 29-25 kyr BP only. At 25 kyr BP, in agreement with the earlier interpretation (Fig. 2.1), the more recent interpretation shows the ice sheets had separated due to the opening of the marine embayment across the NSB (as discussed above).

This revised chronology for the NSB is supported by a recent GIA modelling study for the SIS, in which Lambeck *et al.*, (2010) review information constraining the timings and pattern of glaciation between MIS4 and MIS2 and stated that the results from the NS and Norwegian coasts were not completely consistent. The growth of the SIS across the NSB, constrained to data from coastal regions around Denmark and Norway, was initiated from ~30 kyr BP when ice advanced from within the Norwegian trench and out onto the continental shelf to join with the BIIS by 28 kyr BP. This was followed by a brief retreat period 26.5 kyr BP, with a later, more restricted growth of the SIS along the NS coastal margin. Although the timings of these glacial episodes do not completely correlate with the new BIIS model developed here, it does provide some validity to the two-stage glaciation across the NS region, with an earlier more extensive glacial phase. A complete review and correlation of the behaviour of the BIIS and SIS during the various interstadials/stadials is beyond the scope of this study. As the two ice sheets were independent during last glacial period, the growth and retreat phases do not necessarily have to correlate. However, there should be a level of consistency between the observed and modelled timing of coalescence across the NSB.

Hubbard *et al.*, (2009) published a 3D numerical (thermomechanical) model of the growth and retreat of the BIIS at various times slices between 38 and 10 kyr BP forced by climate change inferred from the North Greenland Ice Core project (NGRIP). Their model output shows that glaciation is limited to Central Scotland up until ~ 32 kyr BP,

when ice begins to advance and expand offshore, reaching onto the adjacent shelf areas around Scotland, Ireland and the NSB by 29 kyr BP. It is noted that during this phase the ice sheet extent is more restricted compared to the Brooks et al. model and that inferred by Sejrup *et al.*, (2009) (Fig. 2.15). Following a short-lived retreat, a more substantial advance begins at 27 kyr BP, to produce an extensive glaciation, similar to that depicted in the Brooks et al. model between 23-19 kyr BP. Although the timings and spatial extent of the growth/retreat phase are not entirely consistent with the new glaciation curve (Fig. 2.15) or the Brooks et al. model, the results do support a two-stage glaciation of the BIIS during the Late Devensian, separated by a rapid short-lived retreat.

IRD records taken from around the coast of the British Isles can provide an additional record of the timings of glacial activity of the adjacent land based ice sheets (this is particularly useful at earlier periods when sea level records are limited). Peaks in the recorded flux can be directly related to episodes of either ice sheet advance or decay depending on a range of factors, including the presence of a marine margin, rate of iceberg calving or debris content of icebergs (Hibbert *et al.*, (2010)). Therefore, although the record can be used to infer the presence of an ice sheet with an active calving margin on the continental shelf, it is insensitive to the presence of a small ice sheet with no calving margin, during either an initiation phase or late in the deglaciation (Scourse *et al.*, (2009)). This needs to be considered when interpreting records and looking for past glacial episodes within the IRD records as not all records from along the Atlantic margin fully support the two-stage glaciation proposed by some authors and as incorporated in the Brooks et al. model.

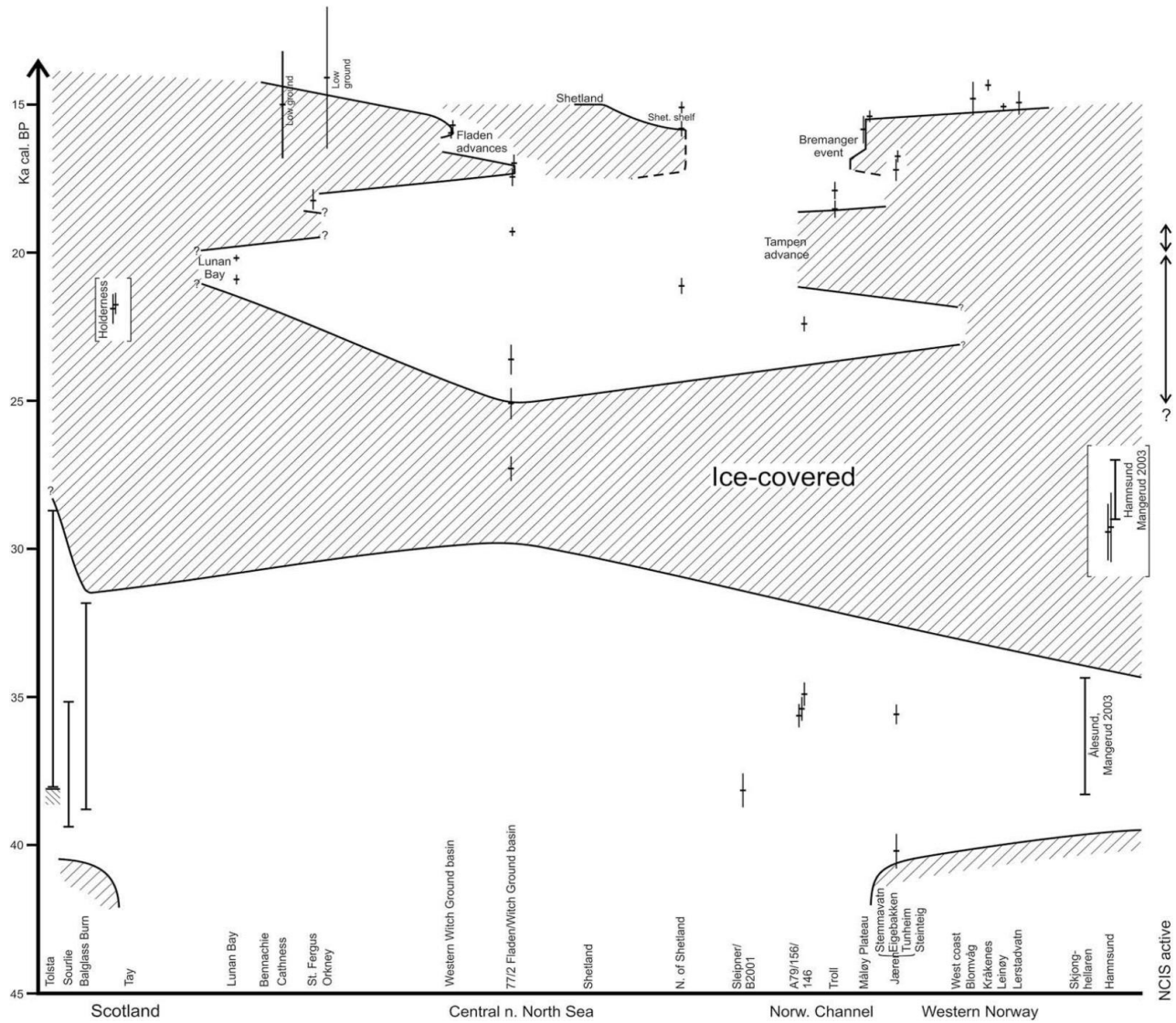


Fig. 2.15: A revised glaciation curve for the main growth and retreat phases of the British-Irish Ice Sheet and Scandinavian Ice sheet across the North Sea, adapted from Sejrup *et al.*, (2009). Note NCIS is an abbreviation for Norwegian Channel Ice Stream and ages are given in calibrated  $^{14}\text{C}$ .

Hibbert *et al.*, (2010) published a new record from the Barra-Donegal fan, NW Scotland, that shows a near continuous flux of IRD between MIS3-MIS2, which was taken to indicate a prolonged period of glacial activity on the continental shelf. A noted peak at 27 kyr BP was thought to result from either “expansion of the BIIS to the shelf margin or destabilisation of an existing marine margin” (page 477), the latter of which is consistent with the Brooks *et al.* model. Continuing high IRD values into MIS2 were also associated with (re)advance of the BIIS onto the continental shelf. In contrast, a review of IRD-records from three locations along the NE Atlantic margin by Scourse *et al.*, (2009) inferred multiple advance and retreat phases during this period. Major growth of the ice sheet onto the continental shelf did not occur until after 29 kyr BP, with the maximum extent reached by 24 kyr BP. A rapid retreat at ~ 23 kyr BP is followed by a second, more restricted readvance between 22-16 kyr BP. This inferred pattern of early growth onto the shelf along the NE Atlantic margin followed by a later more extensive episode is supported by the modelling results from Hubbard *et al.*, 2009.

One main point to conclude from the above information is that during the Mid-Late Devensian, the BIIS was a dynamic ice sheet, which extended beyond the coastal margins inferred in the Shennan model. Evidence from the NS records and modelling of ice sheets imply that, during this early phase, the BIIS expanded from a restricted onshore extent, across the NSB to join with the SIS. In contrast, IRD records from NE Atlantic margin suggest a more restricted extent during this early period, with the maximum expanse after 24 kyr BP, which would contradict the timing for the growth across the NSB. The exact timings of these advance phases need to be examined further, but one point that can be concluded is that the initial glacial phase in the Brooks *et al.* model (32-27 kyr BP) most likely started later and was shorter (~ 30-27 kyr BP), with a gradual expansion to the extended limits (see Fig. 2.15).

Preliminary calculations (not shown) to investigate the sensitivity of sea level predictions to revisions in the timing and spatial extent of the BIIS during this early glacial event were conducted. During this first glacial phase the BIIS was altered to create a gradual advance from a small ice sheet centred across Scotland extending into the offshore regions to reach the maximum limits later, (29 -27 kyr BP). The impact of these changes

on the RSL predictions was found to be relatively small (<5m) and occurs before or during LGM times. Given the lack of pre-LGM RSL data, the most direct means of improving the accuracy of the ice history during this earlier period lies with obtaining more dates from offshore morphological features and additional IRD records.

Since the development of the Brooks et al. model, reinterpretation of trimline evidence from across Scotland and Ireland (Ballantyne *et al.*, (2009), Ballantyne and Hall (2008), Ballantyne *et al.*, (2008)) has some important implications for the definition of the model ice thickness in these areas (see section 1.3.3. for further information on trimlines). In earlier studies (as outlined in section 2.2.2.3), these horizons were thought to mark the upper limit of glacial erosion from a warm-based ice sheet, and, as such, delimit the maximum altitude of the BIIS surface. New studies, summarised in Ballantyne (2010), suggest these horizons may have formed as englacial thermal boundaries, between a lower, warm based 'erosive' ice and an upper, cold based 'non-erosive' ice. This implies that the trimline evidence now marks the minimum altitude that the ice sheet reached. It was concluded in Ballantyne, 2010 that the reinterpretation is not conclusive but some key points cited to support it are: (1) reconstructed ice surface altitudes (such as illustrated in Fig. 2.2) will require a thicker ice sheet than inferred using the old interpretation to reach the extended offshore limits onto the continental shelf (Ballantyne *et al.*, (2008)); (2) Examination of tors and blockfields across the Caithness mountains imply the area was over run by a cold-based ice sheet (Ballantyne and Hall (2008)); (3) in a numerical model of the BIIS by Boulton and Hagdorn (2006), it was shown that the optimum basal melting temperature from the reconstructions were consistent with the development of englacial trimlines.

This alternative interpretation of the trimline observations has important implications for the defined thickness of the ice model and may provide a possible solution to address the underprediction of RSL during the Late Devensian. In earlier studies, no attempt was made to alter the thickness of the BIIS during the glacial phase as this was limited by the constraints from the trimline evidence. If, instead, the BIIS was thicker during the glacial advances, most specifically between 24- 21 kyr BP, this would in turn lead to an increase in the predicted RSL (as was seen for the IIS - see section 2.4.3.4). It is hoped that future

work will be conducted to rigorously determine which interpretation is accurate so that models of the BIIS can use this information in an unambiguous manner. At this time, the Brooks et al. model will remain based on the original interpretation (i.e., trimlines define the maximum ice surface altitude).

## **2.6. Conclusions**

A new BIIS model has been developed using recently published geomorphological data and an extended RSL database with sites from across Great Britain and Ireland. Additionally, the thickness of the input ice model was adjusted to account for the underlying terrain. The model is characterised by a two stage glaciation across the NSB with an initial coalescence of the BIIS and SIS between 32-27 kyr BP, followed by a short lived retreat between 26-25 kyr BP. Following this retreat, the BIIS readvances out across the NSB, and is greatly thickened and extended within the ISB and along the NE Atlantic margin, with a short lived ice stream down to the Isles of Scilly. In this final glacial phase, the BIIS and SIS do not join. Deglaciation begins at 21 kyr BP, with a rapid thinning and retreat of the IIS, with complete ice retreat by 15 kyr BP.

This model will be adopted within Chapter 3, in which CGPS data will be examined to provide an independent constraints on the choice of earth model parameters (shallow viscoelastic structure) and in Chapter 5, where additional constraints on the earth model (from Chapter 3) and the global ice model (from Chapter 4) will be combined to arrive at a final GIA model for the British Isles.

## **Chapter 3: Glacial Isostatic Adjustment of the British Isles: new constraints from GPS measurements of crustal motion**

### **3.1. Introduction**

The on-going viscous response of the solid Earth to the melting of the last great ice sheets is currently a significant contributor to intraplate deformation around the globe, particularly in previously glaciated regions such as Canada and NW Europe. In these regions, this geodynamic process, more formally known as glacial isostatic adjustment (GIA), dominates the solid Earth deformation field (e.g. Johansson *et al.*, (2002), Sella *et al.*, (2007)). A number of studies have considered the GIA of these previously glaciated (so-called ‘near-field’) regions through the measurement and interpretation of relative sea-level observations (e.g. Tushingham and Peltier (1991), Davis *et al.*, (1999), Lambeck (1993a), Lambeck *et al.*, (1998), Mitrovica (1996)) and, more recently, space geodetic data (e.g. Milne *et al.*, (2001), Tamisiea *et al.*, (2007)). Studies such as these have provided important constraints on both past ice extent and Earth viscosity structure.

There is a long history of sea-level observation in the British Isles (e.g. Selby and Smith (2007), Shennan *et al.*, (1995), Sissons (1966), Sissons and Brooks (1971), Tooley (1982), Tooley (1974)) and this has led to the development of a high-quality and extensive regional data base (Shennan *et al.*, (2006b)). This data base has been employed to determine empirical estimates of GIA-induced land motion (Dawson *et al.*, (2002), Fretwell *et al.*, (2004), Smith *et al.*, (2000)) as well as constrain parameters in geophysical models of the GIA process (Lambeck (1993a), Lambeck (1993b), Milne *et al.*, (2006), Peltier *et al.*, (2002), Shennan *et al.*, (2006a), Shennan *et al.*, (2000)) While there has been a dramatic advance in the development of GIA models for the British Isles since the early 1990s, there remain significant differences in key parameters inferred by different groups and the model fits to the ever-expanding data base have been poor in certain areas (e.g. Shennan *et al.*, (2006a)). These discrepancies reflect the constant emergence of new geomorphological constraints on ice sheet extent and thickness as well as the high-degree of non-uniqueness inherent to modelling near-field GIA (Shennan *et al.*, (2006a), see Chapter 1 and 2). This non-uniqueness is particularly acute for the

British Isles given the relatively small size of the local ice sheet which results in the local isostatic component of the sea-level signal being of similar magnitude to that associated with the melt water (eustatic) contribution from non-local ice sheets (e.g. Lambeck (1993b)).

The application of the global positioning system (GPS) to monitor secular variations of the solid Earth has provided a new data set that can be applied to the GIA problem. The main advantages of GPS measurements over those of past sea-level changes is that a direct measurement of present-day vertical and horizontal crustal motion is recorded at each site and spatial sampling is not limited to coastal areas.

Results obtained from a regional GPS network in Fennoscandia demonstrated that continuous GPS (CGPS) was able to resolve both vertical and horizontal crustal motion at sub-mm yr<sup>-1</sup> precision (Johansson *et al.*, (2002), Lidberg *et al.*, (2007)). Subsequent modelling studies have demonstrated that the Fennoscandian CGPS data provide useful constraints on GIA models that complement those imposed by the RSL observations and thereby reduce the level of non-uniqueness in inferring model parameters (Milne *et al.*, (2001), Milne *et al.*, (2004)).

A CGPS network was first established across Great Britain in the late 1990s and there are currently around 130 receivers in operation (*see www.bigf.ac.uk*). The position time series for a subset of these receivers are now long enough to constrain 3-D crustal motion at the sub-mm yr<sup>-1</sup> level (Milne *et al.*, (2006), Teferle *et al.*, (2006)). A primary aim of this study is to examine the CGPS-derived 3D velocity field for Great Britain and to quantify the component of the motion associated with GIA. In addition, we aim to determine if the CGPS data will be useful in reducing the non-uniqueness of the British Isles GIA problem outlined above. Note that this study extends that of Milne *et al.*, (2006) by: (1) considering a GPS solution based on longer time series and improved processing techniques; (2) adopting a recently improved British-Irish ice model that is consistent with a subset of the regional RSL data base as well as a variety of new geomorphological information on ice extent (Shennan *et al.*, (2006a)); and (3) by performing a much more complete Earth model parameter study (243 models compared

to 7 in Milne *et al.*, (2006)). In Section 3.2 we briefly introduce the CGPS data employed in this study and we present our modelling results in Section 3.3

### **3.2. CGPS data**

The majority of CGPS stations in Great Britain were not deployed to monitor secular motions of the solid Earth and so most of the 130 sites now in operation are not suitable for this purpose. A companion paper (Teferle *et al.*, (2009)), 44 of the 130 sites were initially considered after rejecting real-time kinematic (RTK) sites with time series less than 4 years in duration (non-RTK sites were not subjected to this criterion). This number was reduced to 24 after checking for consistency of results between two different processing strategies (sites were rejected when the discrepancy was greater than  $1 \text{ mm yr}^{-1}$ ). For this analysis, we begin with these 24 stations and reduce the number further by applying the 4 year time series criterion to all sites and removing stations at which: (i) the observed velocity is clearly not consistent with surrounding stations and therefore suspect, (ii) the data quality is poor, or (iii) monumentation is unsuitable. After applying these criteria, the number of sites considered was reduced to 16 sites for vertical motion and 21 sites for horizontal motion (Fig. 3.1a, Table 2). Despite this reduction in the number of sites, there remains an adequate spatial sampling of crustal motion across Great Britain.

The CGPS data were processed using the Precise Point Processing (PPP) strategy (Teferle *et al.*, (2009), Teferle *et al.*, (2007)) implemented in the Bernese GPS software (version 5.0, Astronomical Institute of the Uni. of Bern, Bern, Switzerland) (Dach *et al.*, (2007)), to produce time series of daily position estimates from which the site velocities were obtained from a model-fit using maximum likelihood estimation (e.g. Williams (2008), Williams (2003)). Although all velocity errors are given to  $1\sigma$ , these are of considerably larger magnitude, due to the proper handling of non-random errors in the time series during the model-fit, than those that would be obtained assuming random errors only (Teferle *et al.*, (2009)). When processing the CGPS data to produce an estimate of vertical crustal motion, a systematic bias can be introduced due, largely, to uncertainty in the adopted terrestrial reference frame (see Teferle *et al.*, (2009) for greater detail and figures of all position time series). To address this issue and attempt to improve

the accuracy of the data, measurements of absolute gravity have been used to calibrate the CGPS-derived vertical rates (e.g. Teferle *et al.*, (2006)). Comparison of CGPS-derived vertical crustal motion to that inferred from absolute gravity measurements at Lerwick and Newlyn indicates that the CGPS rates are biased too high by around  $0.5 \text{ mm yr}^{-1}$  (Teferle *et al.*, (2009)). This result is somewhat tentative, however, given the small number of gravity measurements available in this region.

In the following section, we estimate model parameters using site-differenced rates for two reasons: (i) it removes, to a large extent, uncertainty associated with the reference frame and (ii) it isolates the signal associated with the BIIS (see next section). We chose to calculate motion relative to Sheerness (18 in Fig. 3.1a), as this site offers one of the longest observation periods (since March 1997) and the time series data are of high quality (Teferle *et al.*, (2009)). Since we model relative rates, the difference between the absolute gravity aligned and non-aligned versions of the CGPS vertical motion data is of no consequence.

Figure 3.1b illustrates the pattern of absolute vertical motion for the aligned CGPS data (with associated error) across Great Britain. Note that the non-aligned data produce the same pattern but with an increase in rates of  $0.56 \text{ mm yr}^{-1}$  at each site. The pattern, which comprises a region of maximum uplift centred over eastern Scotland and a zone of subsidence throughout most of England, is clearly correlated with the thickness extent of the most recent British-Irish ice sheet (BIIS) (e.g. Shennan *et al.*, (2006a) and references therein). The maximum uplift velocity is  $1.07 \pm 0.35 \text{ mm yr}^{-1}$  at EDIN (site number 5) and the maximum subsidence velocity is  $1.2 \pm 0.40 \text{ mm yr}^{-1}$  at LOWE (site number 13). The pattern of vertical motion estimated from the AG-aligned CGPS time series is broadly consistent with estimates of land motion obtained from late Holocene RSL observations (Shennan and Horton (2002), Teferle *et al.*, (2009)).

The horizontal velocity field (Fig. 3.1c) is characterised by motion directed towards the NE, with a magnitude of  $\sim 15 \text{ mm yr}^{-1}$ , and an average error of  $0.29 \text{ mm yr}^{-1}$ . This signal is dominated by motion of the Eurasian plate relative to the chosen reference frame. So, for each CGPS site, a modelled value of plate motion, estimated from the published ITRF2000 data set, was subtracted from the observed data to try and isolate a regional

intraplate deformation pattern. The resulting velocity field (Fig. 3.1d) shows poor spatial coherence and the scatter in the rates is near the level of data precision.

The horizontal velocity field due to GIA predicted for this region is dominated by the deglaciation of the Laurentide ice sheet that covered most of North America at the last glacial maximum (e.g Milne *et al.*, (2006)). The predicted signal is of magnitude 1-2 mm yr<sup>-1</sup> directed predominantly NW (e.g. see Fig. 6 of Milne *et al.*, (2006)). The isostatic component of horizontal motion associated with the BIIS – which has a radial geometry centred on western Scotland with a magnitude of ~0.1 mm yr<sup>-1</sup> adds a minor perturbation to the Laurentide signal. We considered spatially differencing horizontal rates relative to a chosen reference station in order to isolate the BIIS signal. However, in contrast to a previous study (Milne *et al.*, (2006)), a correlation between the predicted and observed strain field was not apparent. We conclude, therefore, that the current level of precision is not able to resolve a coherent pattern of horizontal motion associated with GIA. For this reason, the horizontal data will not be used in the remainder of this study. We will revisit the application of horizontal data in the future, when we would hope for a better correlation through the use of longer time series and a re-processing of the CGPS data, carried out using new and improved GPS satellite orbit and clock products (Steigenberger *et al.*, (2006)).

### **3.3. Modelling Results**

The GIA model adopted in this study has three key inputs – a model of the Late Pleistocene ice history, an Earth model to reproduce the solid earth deformation resulting from surface mass redistribution (between ice sheets and oceans), and a model of sea-level change to calculate the redistribution of ocean mass (e.g Farrell and Clark (1976)).

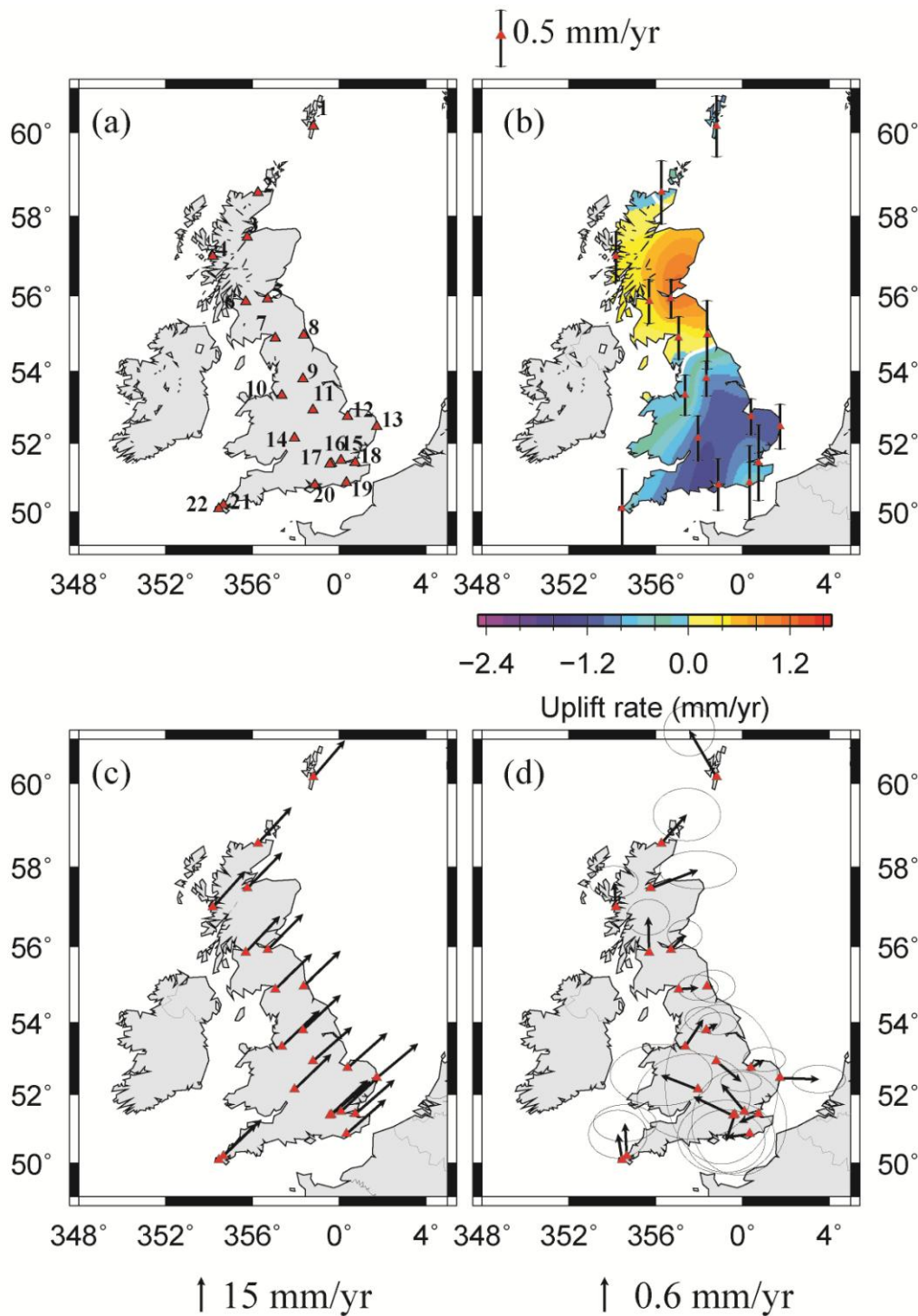


Fig. 3.1: (a) Locations of CGPS sites considered in this analysis. (b) Contour map of absolute vertical rates over the UK region interpolated from CGPS data for data aligned to absolute gravity. The error bars show the uncertainty at each of the 16 data sites. (c) Horizontal velocity vectors estimated from the CGPS time series. (d) Same as (c) but with velocities from plate motion model removed. All uncertainties shown represent the  $1\sigma$  range and are based on a post-processing scaling of the formal least squares values by a factor of 3 or more at most sites (see Teferle *et al.*, (2009) for further information).

NUMBER	NAME	Longitude	Latitude	East	Error	North	Error	Vertical	Error
1	LERW	358.82	60.14	13.65	0.18	15.94	0.18	-0.65	0.54
2	THUR	356.27	58.58	14.53	0.24	15.72	0.19	-0.13	0.56
3	INVE	355.78	57.49	15.18	0.27	15.55	0.13	/	/
4	MALG	354.17	57.01	14.13	0.17	15.70	0.11	0.39	0.44
5	EDIN	356.71	55.92	15.34	0.12	15.47	0.10	1.07	0.35
6	GLAS	355.70	55.85	14.89	0.15	15.84	0.13	0.45	0.39
7	CARL	357.06	54.90	15.86	0.14	15.22	0.09	0.12	0.38
8	NEWC	358.38	54.98	15.89	0.16	15.15	0.11	0.37	0.61
9	LEED	358.34	53.80	16.35	0.14	15.27	0.08	-0.82	0.31
10	DARE	357.36	53.34	16.41	0.13	15.66	0.09	-0.09	0.36
11	IESG	358.81	52.94	16.96	0.14	14.78	0.07	/	/
12	KING	0.40	52.75	17.16	0.15	15.22	0.09	-1.07	0.32
13	LOWE	1.75	52.47	17.96	0.19	14.99	0.10	-1.17	0.40
14	PERS	357.96	52.15	15.97	0.36	15.42	0.22	-1.11	0.40
15	BARK	0.10	51.52	16.85	0.40	15.56	0.57	/	/
16	NPLD	359.66	51.42	17.03	0.27	14.65	0.22	/	/
17	SUNB	359.58	51.40	16.49	0.40	15.44	0.30	/	/
18	SHEE	0.74	51.45	17.07	0.34	14.91	0.37	-0.77	0.67
19	HERS	0.34	50.87	17.09	0.35	15.02	0.26	-0.43	0.65
20	PMTG	358.89	50.80	/	/	/	/	-1.15	0.46
21	CAMB	354.67	50.22	16.51	0.22	15.83	0.13	/	/
22	NEWL	354.46	50.10	16.45	0.21	15.71	0.17	-0.43	0.70

Table 2: Estimated crustal velocities ( $\text{mm yr}^{-1}$ ) and locations of the CGPS sites considered in this study and shown on Fig. 3.1. The time series solutions are taken from Teferle *et al.*, 2008: table 5 for the horizontal velocities and table 9 for the AG-aligned vertical velocities. The following sites have been removed due to processing problems and data errors: ABER, ABYW, DUNK, HURN, LIVE, MORP, NPLD, NSTG – for the vertical velocity estimates, and ABER, ABYW, DUNK, HURN, LIVE, MORP, LOND, BLAK, COLC, NSTG, PMTG, OSHQ for horizontal velocity estimates. Note that a model of plate motion has been adopted to remove the tectonic signal from horizontal velocities (see Fig. 3.1 frames c & d and related discussion in text).

We adopt a recently developed ice model for the UK and North Sea that was constrained using both RSL and geomorphological data (see section 2.4.3, ‘NS-Thick model’ and Shennan *et al.*, (2006a)). This regional model is patched into a global model of ice extent that provides an optimal fit to equatorial sea-level records (Bassett *et al.*, (2005)). The

Earth model is a spherically symmetric, self-gravitating Maxwell body, with the elastic and density structure taken from a seismic model (Dziewonski and Anderson (1981)) with a depth resolution of 10 km within the crust and 25 km in the mantle. The viscous structure within the mantle is more crudely parameterized into three layers: a high viscosity ( $10^{43}$  Pa s) outer shell to simulate an elastic lithosphere, an upper mantle region of uniform viscosity extending from beneath the model lithosphere to the 660 km seismic discontinuity, and a lower mantle region extending from this depth to the Core-Mantle boundary. The thickness of the lithosphere and the viscosity within the upper and lower mantle are free parameters in the modelling. The initial reference earth models used is taken from 'Shennan *et al.*, (2006a), with a lithosphere thickness of 71km, and an upper mantle and lower mantle viscosity of  $5 \times 10^{20}$  Pa s and  $1 \times 10^{22}$  Pa s respectively. This model provided a good fit to the regional sea-level database.

The sea-level model we adopt solves the generalised sea-level equation (Kendall *et al.*, (2005), Mitrovica and Milne (2003)) and includes the influence of GIA-perturbations to Earth rotation (e.g. Milne and Mitrovica (1998)). The algorithm we adopt to calculate present-day crustal motion in response to a specified ice and ocean loading history is based on the spectral technique described by Mitrovica *et al.*, (1994) and extended to incorporate the signal associated with GIA perturbations in Earth rotation (Mitrovica *et al.*, (2001)).

The predicted uplift pattern (Fig. 3.2a) is that of an ellipse, oriented approximately SSW-NNE, covering most of Scotland and a part of Ireland. The centre of uplift is located in central western Scotland with a magnitude of  $\sim 0.6$  mm yr<sup>-1</sup>. The majority of England is subsiding with rates exceeding  $\sim 1$  mm yr<sup>-1</sup> in places. While there is a broad similarity between predictions and observations (compare Fig. 3.1b and Fig. 3.2a), there are significant differences. Part of the difference is due to the contrasting spatial sampling of the two patterns in Figs 3.1b and 3.2a and so, to permit a more direct comparison, we show in Fig. 3.2b the pattern predicted when sampled at CGPS site locations only. On comparing Figs 3.1b and 3.2b, the most obvious difference is that the observed region of uplift is located further to the east and is of larger magnitude. Given the current precision and distribution of the data sites, it is not clear if this difference in geometry is necessarily

a flaw in the adopted ice-earth model, which has the largest impact on this aspect of the prediction.

As the primary aim of this study is to employ the CGPS data from Great Britain to constrain parameters associated with the deformation driven by the local BIIS model, it is necessary to identify the contribution to the signal from non-local ice sheet loading in order to try and isolate the observed signal due to the BIIS and ocean loading only. The total predicted signal (Fig. 3.2a) was decomposed into two separate signals: that due to the non-local ice sheets only (Fig. 3.2c) and that due to the BIIS and ocean load only (Fig. 3.2d, note that the ocean loading is the sea-level change driven by all ice sheets). As expected, the signal due to the non-local ice sheets (predominantly the Fennoscandian ice sheet) is that of long wavelength subsidence of magnitude  $>1 \text{ mm yr}^{-1}$  over the study area. The most straightforward way to isolate the signal associated with the BIIS and ocean load is to consider relative vertical rates. As described above, we chose to calculate motion relative to Sheerness (18 in Fig. 3.1a). The predicted rates relative to Sheerness associated with the non-local ice sheets (Fig. 3.2c) do not exceed  $-0.3 \text{ mm yr}^{-1}$  and so this component of the signal is effectively removed by considering relative rather than absolute rates.

We performed a forward modelling analysis using the relative vertical data. The analysis considered values of upper and lower mantle viscosity in the range  $0.08\text{-}5 \times 10^{21} \text{ Pa s}$  and  $1\text{-}50 \times 10^{21} \text{ Pa s}$ , respectively, for assumed lithospheric thicknesses of 71, 96 or 120 km. The results for this suite of calculations are shown in Fig. 3.3. The solid black line in each frame indicates the  $\chi^2$  value below which all earth viscosity models fit the data to within the 95 % confidence level. There are a number of points to conclude from Fig. 3.3. First, there is a relatively mild trade-off between values of lithospheric thickness and upper mantle viscosity. As the lithosphere is thickened (going from frame a – c) the region of ‘best fit’ viscosity space migrates towards higher values of upper mantle viscosity. That is, an equally good fit can be achieved by raising or lowering the lithospheric thickness as long as the upper mantle viscosity is also raised or lowered to compensate. This parameter trade-off has been demonstrated in previous studies (e.g. Lambeck *et al.*, (1996), Milne *et al.*, (2004)).

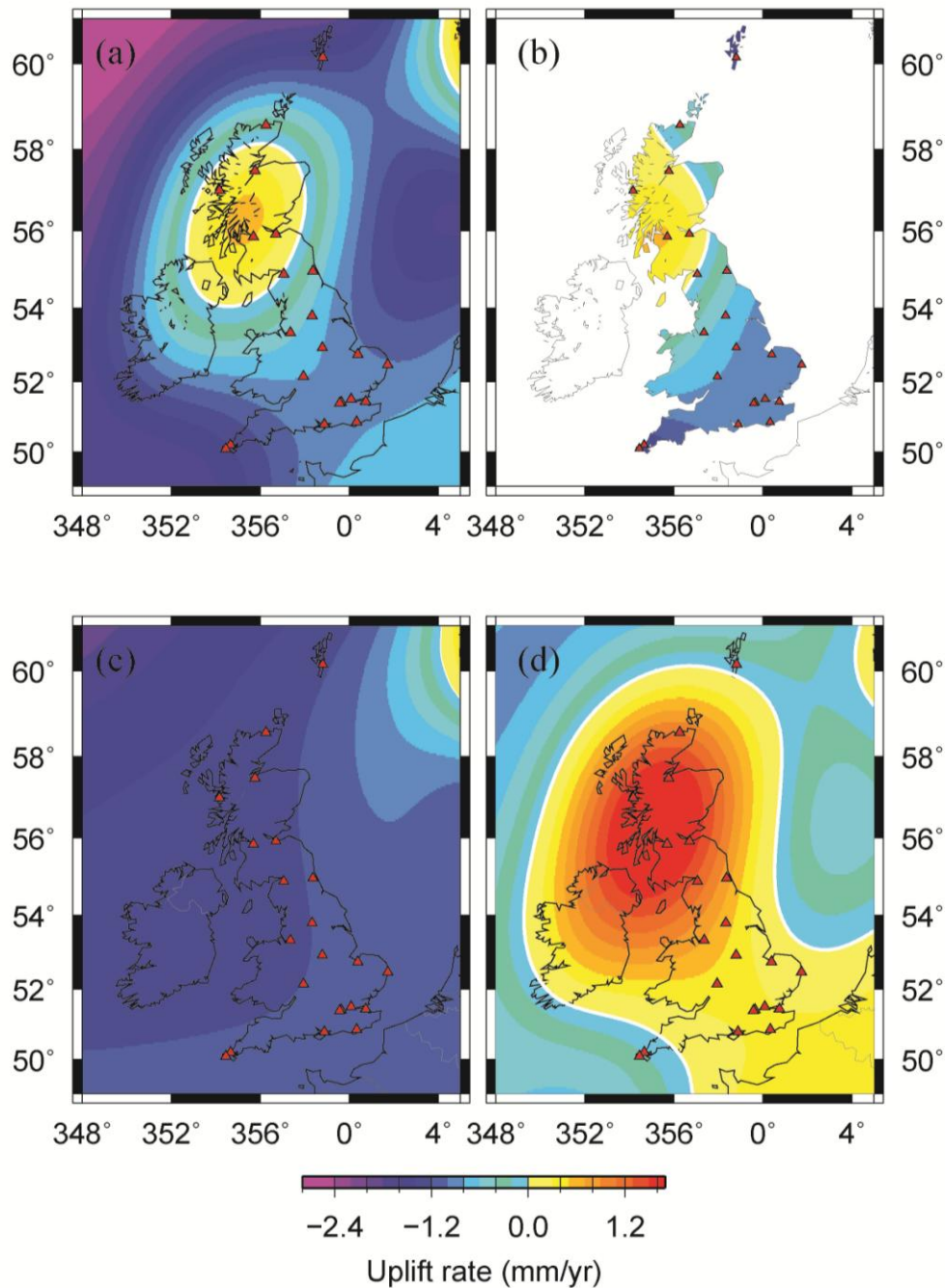


Fig. 3.2: (a) Predictions of uplift rate on a 5 km by 5 km grid for the reference ice model and an Earth viscosity model that, when combined with the reference ice model, provides a good fit to the regional sea-level data base (Shennan *et al.*, (2006a)). This model adopts a 71km lithosphere thickness, and a upper and lower mantle viscosity of  $5 \cdot 10^{20}$  Pa s and  $1 \cdot 10^{22}$  Pa s respectively. The large positive uplift rates shown in the top right of the frame are associated with the deglaciation of the Fennoscandian component of the adopted ice model. (b) Same as (a) except that predicted velocity field sampled only at CGPS site locations. (c) Component of total predicted signal (a) associated with non-local ice sheet loading. (d) Component of total predicted signal (a) associated with local (British-Irish) ice sheet and ocean loading.

Second, the data rule out upper mantle viscosity values outside the (approximate) range  $0.3-2 \times 10^{21}$  Pa s (for the range of lithospheric thicknesses considered). Viscosity values less than the lower bound of this range permit the uplift to proceed too rapidly following the end of the main phase of deglaciation (~15 kyr BP) which results in predicted uplift rates that are dramatically lower than those observed. A similar constraint on upper mantle viscosity was reached using the vertical CGPS rates from Fennoscandia (e.g. Milne *et al.*, (2004)). Finally, the data do not provide a useful constraint on lower mantle viscosity or lithospheric thickness. The former is evident in the result that an equally good fit (to within 95% confidence) can be achieved for all values of lower mantle viscosity considered. This reflects the fact that the deformation field sampled by the relative rates does not extend significantly into the lower mantle. A similar result is evident for lithospheric thickness: the quality of fit is equally good to within the specified confidence limit for the range considered.

The range of viscosity models preferred by the CGPS data from Great Britain is compatible with those inferred using relative sea-level data from this region (Brooks *et al.*, (2008), Lambeck *et al.*, (1996), Shennan *et al.*, (2006a)). We note, however, that the sea-level data display a clear preference for a relatively thin lithosphere (e.g. Lambeck *et al.*, (1996)) and so a joint inversion of sea-level and CGPS data will likely provide a better constraint on Earth viscosity structure.

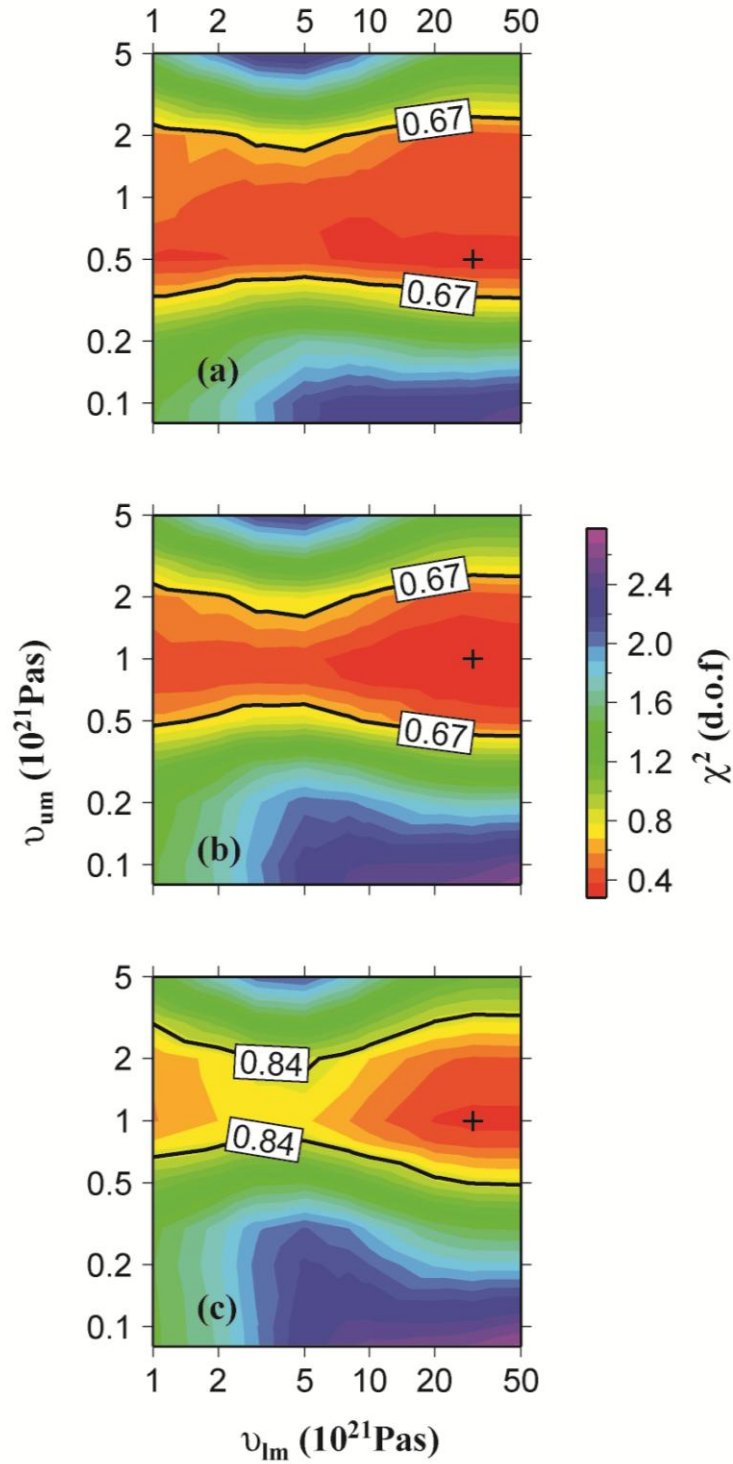


Fig. 3.3:  $\chi^2$  values of data-model fit for a range of values for upper and lower mantle viscosity ( $v_{um}$  and  $v_{lm}$ , respectively) and lithospheric thicknesses of (a) 71 km, (b) 96 km and (c) 120 km. The black line and cross in each frame represent, respectively, the  $\chi^2$  value below which the quality of fit is equivalent at the 95% confidence level and the minimum value found

The above viscosity inference will depend, to some extent, on the adopted local ice sheet history. The greater this dependence, the more sensitive (and therefore less robust) the viscosity inference will be to errors in the ice model. We explored this issue by generating predictions for the Earth models considered in Fig. 3.3 and a significantly altered ice model that is still compatible with current field constraints. Given recent discussion on the extent and thickness of ice in Ireland and the Irish Sea (Ballantyne *et al.*, (2006), Hiemstra *et al.*, (2006), Roberts *et al.*, (2007)), we considered a model that is significantly thickened and extended within the Irish Sea Basin and out to the continental shelf, with a more rapid deglaciation after 21 kyrs (see section 2.4.3 and Brooks *et al.*, (2008)). Spatial plots of ice thickness for the two ice models are shown on Fig. 3.4 for key time steps.

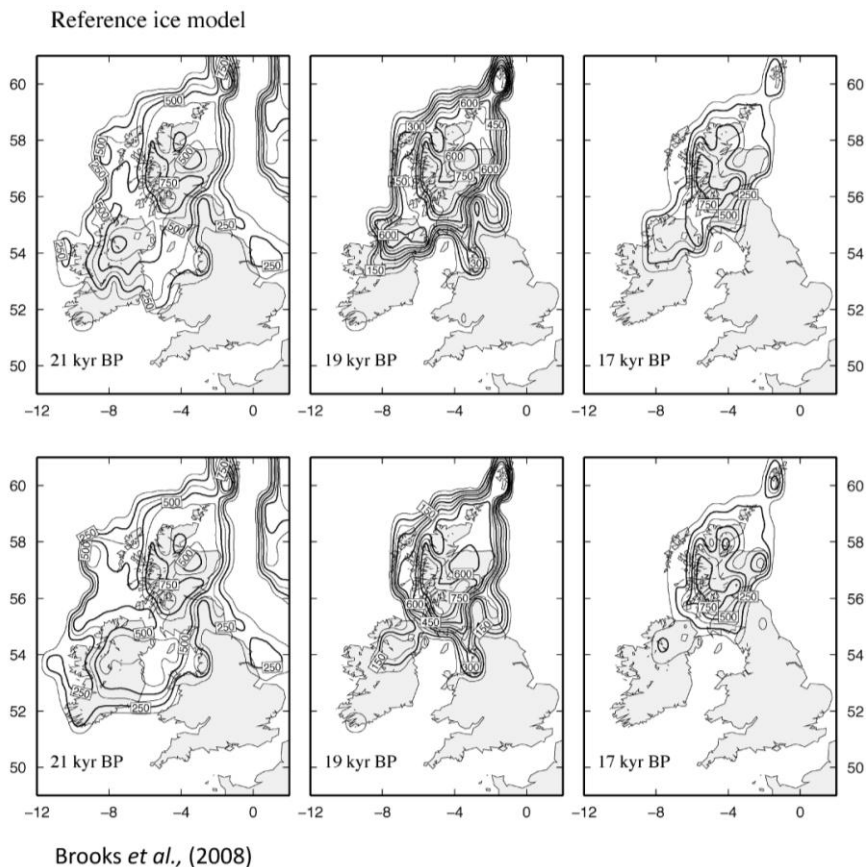


Fig. 3.4: Spatial plots of the contoured ice thickness for the reference ice model (Shennan *et al.*, (2006a)) and as described in section 2.4.2) and comparison ice model taken from Brooks *et al.*, (2008) and as described in section 2.4.3. Note the varying contour interval between each time slice.

The  $\chi^2$  plot for this model, assuming a lithospheric thickness of 96 km, is shown in Fig. 3.5. Comparison between Figs. 3.3b and 3.5 shows that the results are insensitive to the changes made to the ice model and so we conclude that the viscosity inference based on the CGPS data is insensitive to plausible variations in the ice history. This insensitivity was also evident for the other values of lithospheric thickness considered. This result is most likely related to the fact that the region has been free of extensive ice cover since  $\sim 15$  cal kyr BP.

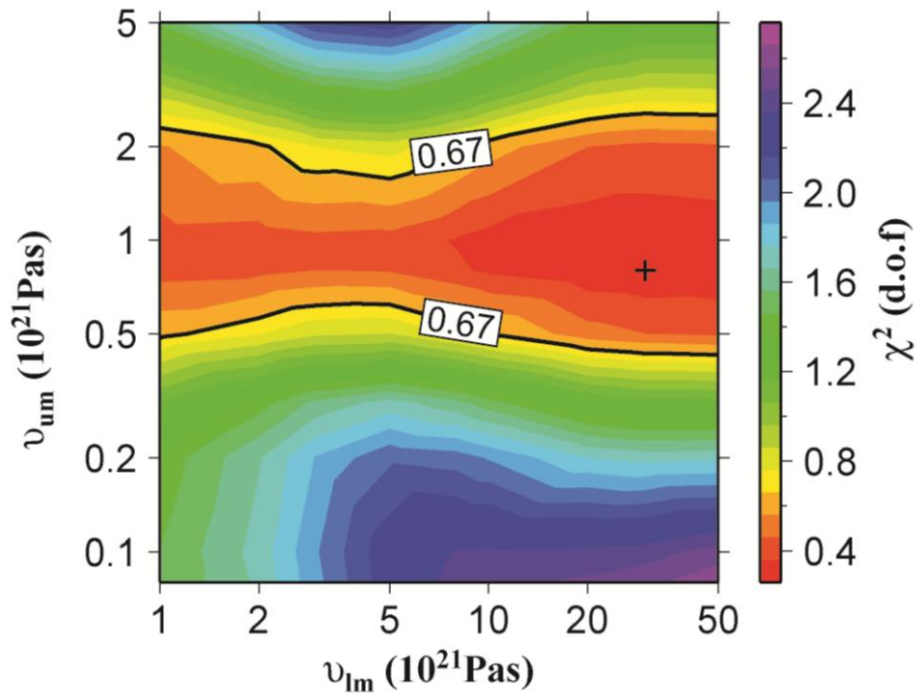


Fig. 3.5: Same as (b) in Fig. 3.3 except that an alternative ice loading history was adopted (see main text for details).

Adopting an optimum earth model from Fig. 3.3a (we chose a thin lithosphere to be consistent with constraints from sea-level data), we present in Fig. 3.6 a comparison between predicted and observed relative vertical rates at each site. Inspection of Fig. 3.6 shows that the predictions agree with the observations at all sites to within the estimated  $1\text{-}\sigma$  uncertainty.

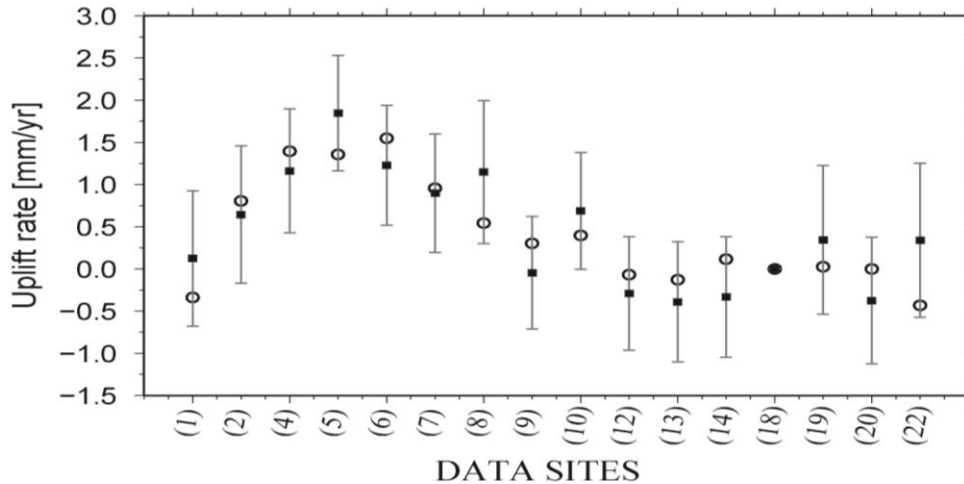


Fig. 3.6: Observed (triangles) and predicted (circles) uplift rates relative to Sheerness (site 18) for the sites located in Fig. 3.1a. The predictions are based on the best-fitting viscosity model with an assumed lithospheric thickness of 71 km (Fig. 3.3a). Error bars indicate  $1\sigma$  precision

### 3.4. Conclusions

We considered CGPS-derived estimates of crustal velocities within Great Britain to constrain a model of GIA for the British Isles. Only the vertical component of the motion was employed to constrain model parameters since a coherent pattern of horizontal motion was not evident once a model of plate motion was removed. The observed vertical signal is strongly correlated with predictions based on a recent GIA model constructed to fit geomorphological constraints of ice extent as well as a subset of the extensive regional sea-level data base (Shennan *et al.*, (2006a)). A detailed forward modelling search, using this ice model and observations of relative vertical motion, was performed to locate optimum parameters in a three layer Earth viscosity model. The results of this analysis indicate that the (relative) vertical CGPS rates are able to place a useful constraint on the average value of viscosity within the upper mantle but are not able to constrain effectively the lithospheric thickness or lower mantle viscosity. Furthermore, parameter trade-off between lithospheric thickness and upper mantle viscosity indicates that a unique constraint on upper mantle viscosity is not possible without the consideration of additional data (e.g. sea-level). A viscosity inference based on an alternative and plausible ice model demonstrate that the data are relatively insensitive to possible errors

in the adopted ice loading model. We conclude, therefore, that the CGPS data provide an important constraint on the Earth component of the GIA model and so will aid in reducing the non-uniqueness inherent to the British Isles GIA problem when combined with the sea-level and geomorphological data.

## **Chapter 4: Improving the Holocene melt history of the reference global ice model**

### **4.1. Introduction**

There have been a number of previous studies of far-field sea-level data that estimated the rate and magnitude of Holocene melting. For example, Nunn and Peltier (2001) compared predictions generated using the ICE-4G model to a suite of data from Fiji, and inferred a eustatic model with an initial decrease in the rate of global melting ~ 8 kyr BP, followed by a steady rise of 4m between 7 -4 kyr BP and no melt subsequent to 4 kyr BP. In a number of studies by Lambeck and colleagues using a range of data from around the coastline of Australia (e.g. Lambeck (2002), Lambeck and Nakada (1990) ), a markedly different conclusion was drawn about the pattern of Holocene melting. From the most recent study in 2002, a 5m rise between 7- 2kyr BP was inferred, with melting ending at 2kyr BP. Fleming *et al.*, (1998), one of a small number of studies that considered a global distribution of observations, concluded on a eustatic change consistent with that of Lambeck and colleagues, with a 3-5m rise in eustatic sea- level between 7-2 kyr BP. At present there is no general consensus on the rate and magnitude of eustatic sea-level change throughout the Holocene. In contrast, it is widely agreed that the main source of meltwater during the mid-to-late Holocene was the AIS and mountain glaciers. Evidence to support this can be found in a number of studies (e.g. Sugden *et al.*, (2006)).

In this chapter, the primary aim is to improve the adopted reference global ice model by revising the Holocene melt history to fit previously unmodelled data from the coastlines of China and the Malay-Thai Peninsula. As stated above, the reference global ice model was not calibrated to fit observations during the Holocene. Considering the six zones of postglacial sea-level changes as defined by Clark *et al.*, (1978), the study region lies within ‘zone VI’, where a band of offshore sea-level rise and on shore sea-level fall encompasses the major shorelines of the continental regions. This generates a characteristic sea level signal which rises throughout the early Holocene, reaching a maximum elevation above present day sea-level, followed by a subsequent fall towards the present. The timing and magnitude of the mid-Holocene highstand is affected by the

history of global ice melting during this period as well as the complex coastal geometries in some of these locations through the ocean loading process.

The key steps followed to achieve the above aim are as follows: (1) sea-level predictions from the reference ice model and a small suite of Earth models were compared to each of the two data sets to identify key misfits; these misfits were then used to develop a range of melt scenarios; (2) an optimum history of Holocene melting was identified for each region from the range of defined melt scenarios and a large suite of Earth models; (3) in order to create a combined model which fitted both data sets, the spatial and temporal pattern of deglaciation was adjusted and a final revised eustatic sea-level model generated. This is compared to other published eustatic models in Section 4.5.

## **4.2. Observations**

### **4.2.1. China sea-level data**

Sea level data were obtained from around the coastline of China, extending from Bohai Bay in the North, to HP Province in the South (see Fig. 4.1). Along the 2900 km coastline, the morphology and depositional environment is varied, from the chenier and deltaic plains in the north, to the fault controlled rocky headlands and small coastal plains in the central and southern regions. Additional information regarding these can be found in Zong (2004) and Wang and Vanstrydonck (1997).

The coastal region is situated at the eastern edge of the Eurasian plate and therefore adjacent to a subduction zone. Despite the close proximity of some sea-level sites to an active plate boundary, the vertical tectonic motion is estimated to be relatively minor and so all site locations are classed as ‘geologically stable’ (Zong (2004)). As a consequence, no corrections for vertical tectonic motion were applied to the data in this analysis.

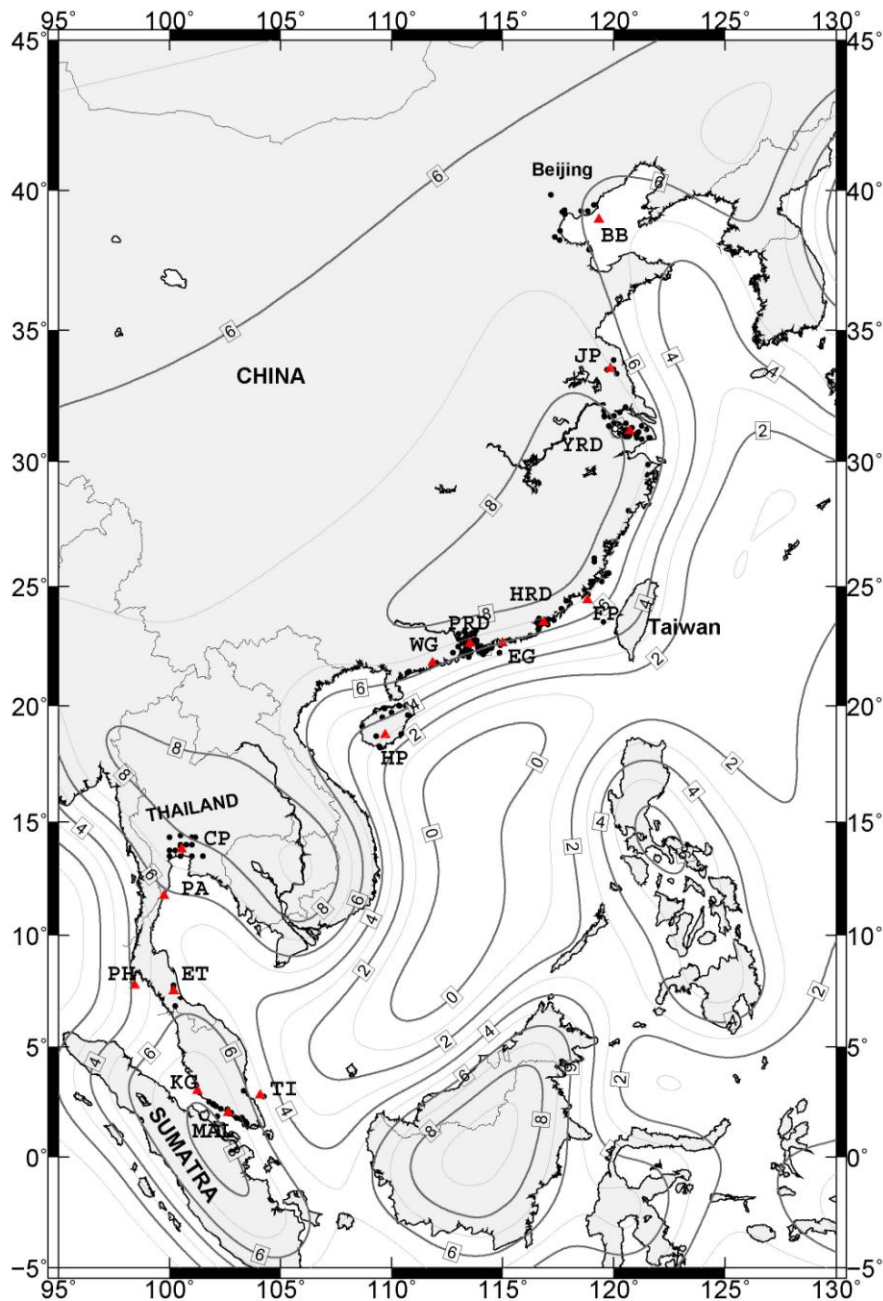


Fig. 4.1: Map showing location of 16 data sites used in this study. The sites in China are: BB – Bohai Bay, JP - Jingasu Province, YRD – Yangetese River Delta, FP – Fujian Province, HRD – Han River Delta, EG – East Guangdong, PRD – Pearl River Delta, WG – West Guangdong, HP – Hainan Province. The sites in Malay-Thailand are: Chao Phraya (CP), Prachaub (PA), Phuket (PH), East coast Thailand (ET), Keelang (KG), Strait of Malacca (MAL), and Tiomin Island (TI). The contours show relative sea level at 6 kyr BP predicted using the reference model. Black circles indicate the long/lat location of SLIP and red triangles shown average long/lat locations for each site used to calculate RSL at each locality.

The database comprises a range of sea-level indicators, including oyster reefs, beachrocks and organic silts. Each indicator has its own set of limitations which are reflected in the height error bars of each SLIP. These limitations and their assessment are outlined in Zong (2004). For example, deltaic areas can be problematic for sea-level studies due to long term subsidence and sediment consolidation affecting the quality of the data. At the YRD site, the SLIPs for the study were taken from the edge of the delta plain, into the lowlands region, which is considered geologically stable. This was not possible for the HRD, and the effect of subsidence upon the recorded sea-level recorded will be noted when comparing predictions to the data.

The data were grouped into nine geographical regions (Fig. 4.1), based upon the spatial clustering of the indicators considered in each coastal sector. Within each of the nine localities, a spatial mean is computed to define a co-ordinate at which to generate a predicted RSL curve for that locality. When combining the data from a given locality to produce a sea level curve, it is important to ensure that the distribution of the data is such that the influence of spatial gradients in RSL, as contoured on Fig. 4.1 using the starting model (see next section), is minimal and within observational uncertainty. This is the case for all sites except HP; this issue will be returned to in Section 4.3.2. In addition, a reduced selection of the data sites will be modelled separately, including BB, JP, EG and WG (to be referred to as the '*reduced data set*'). These sites were chosen on the basis of reliability and quality of the data, with the aim of removing localised effects due to site stability such as subsidence within the deltaic sites (HRD, YRD), localised uplift due to the plate margin (FP), or poor quality data.

When comparing the nine RSL curves shown in Fig. 4.2, some spatial variability is evident. In northern (BB, JP, YRD) and southern sites (WG, HP), sea level rises from around -20m at 9 Kyr BP, with a marked slowdown between 7-7.5 kyr, as it approaches present day levels. There is little evidence for sea levels above present day values. As an example, HP (which is the most stable of all the nine localities) displays a consistent sea level trend close to  $0 \text{ mm yr}^{-1}$  over the last 6.5 Kyr BP. In contrast, the central sites (FP, HRD, EG, PRD) exhibit a gradual slowdown in the rate of sea-level rise, approaching present day level later, between 5-6 Kyr BP. Furthermore, a small highstand of 1-1.5 m

can be identified at some of the central sites. As discussed below, some of this spatial variability is associated with isostatic processes while some is more likely of tectonic origin.

#### **4.2.2. Malay-Thailand Sea-level data**

Horton *et al.*, (2005) compiled a database of SLIPs from the Malay-Thai peninsula, extending from Chao Phraya (CP) in northern Thailand to Tiomin Island (TI) in the south (Fig. 4.1). The study region lies within the 'Sundaland Platform' and is surrounded by active plate boundaries, indicated by frequent earthquakes and volcanic activity. Despite this, the region is defined as 'geologically stable', undergoing very slow crustal movement at a rate of less than  $0.1 \text{ mm yr}^{-1}$  (Tjia (1996)). Therefore no corrections were applied for vertical tectonic motion.

Previously published sea-level studies have inferred sea-level changes from a variety of indicators including corals, shoreline features or fossilised mangrove swamp and paleo-environments. There was a noted lack of consistency between the studies in corrections applied (such as method used to reduce observations to mean sea-level, or tidal corrections applied) or age estimation methods adopted when interpreting the data. These limitations were addressed and are outlined, along with the revised data set in Horton *et al.*, (2005). The 75 SLIPs were separated into seven separate regions (Fig. 4.1) and are displayed on Fig. 4.3.

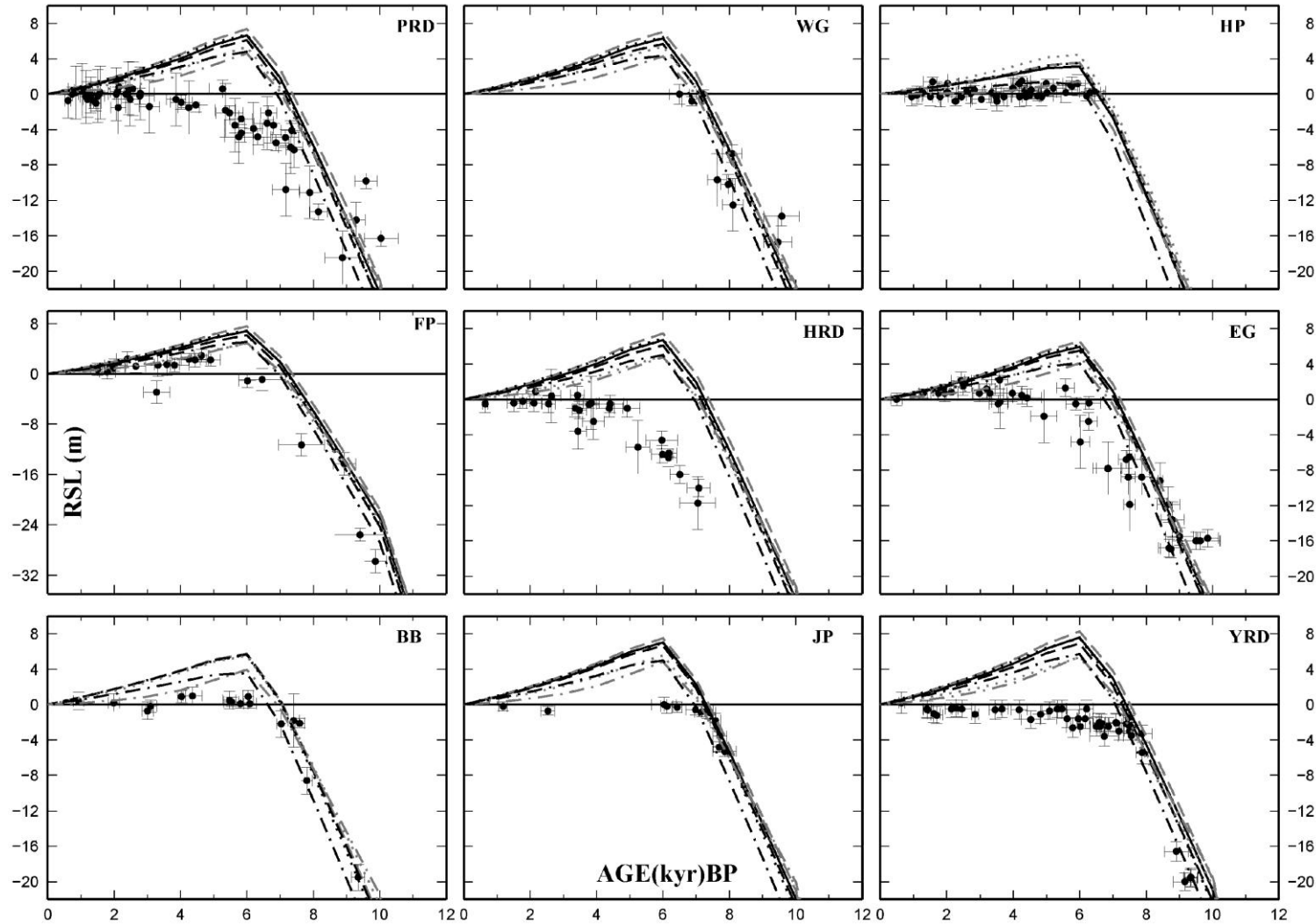


Fig. 4.2: Comparison of sea-level predictions generated for a range of earth models and the reference global ice model to the observations from China. Solid black circles mark each SLIP (complete RSL dataset summarised in Appendix A). Predictions generated using the reference model (as described in Section 4.3.1) is shown by the solid black lines. Variations in the input lithosphere thickness are shown by the dashed line: 71km (grey) and 120 km (black). The dotted line shows changes in the upper mantle viscosity from  $10^{20}$  Pa s (grey) to  $10^{21}$  Pa s (black). Changes in lower mantle viscosity are shown by the dot-dashed line:  $10^{21}$  Pa s (grey) and  $5 \times 10^{22}$  Pa s (black).

It is apparent that the Malay-Thailand dataset is less complete compared to the China data, with gaps between 6-3 kyr BP at most sites. This causes problems when constraining the overall sea-level trend across the region and when resolving an optimal Holocene melt history. This is especially noticeable at sites CP and ET, where there are significant gaps in the data coverage. In general, the data are consistent with a marked slowdown between 7-8 kyr BP, with sea-level rising steadily to form a highstand of ~ 2- 4m between 6-4 kyr. This is followed by a steady fall, reaching present day levels by ~1 kyr. There is some spatial variability in the observed highstand height, with a maximum sea level of ~ 4m at sites within the Strait of Malacca (KG+MAL) on the western coast and site CP, compared to ~1.5m at the central sites. This can be explained by the influence of hydro-isostasy across the region, which will be discussed in greater detail below.

### **4.3. Preliminary Data-Model Comparisons**

#### **4.3.1. Introduction**

The starting ice model, and hence ice-volume equivalent sea level change  $\Delta S_{esl}^i(t)$  (as defined in Chapter 1) is Bassett *et al.*, (2005). This model was tuned to fit a suite of far-field data prior to 10 kyr BP and hence is unconstrained from 10 kyr to present. The equivalent sea level curve during the Holocene is shown on Fig. 4.4. It is characterised by a relatively rapid rise in the early Holocene up to 6 kyr BP, associated with the final stages of global melting. Major melting ceased at 6 kyr BP, with a small amount melting (0.5 m) between 6-5 kyr. There is no further melting.

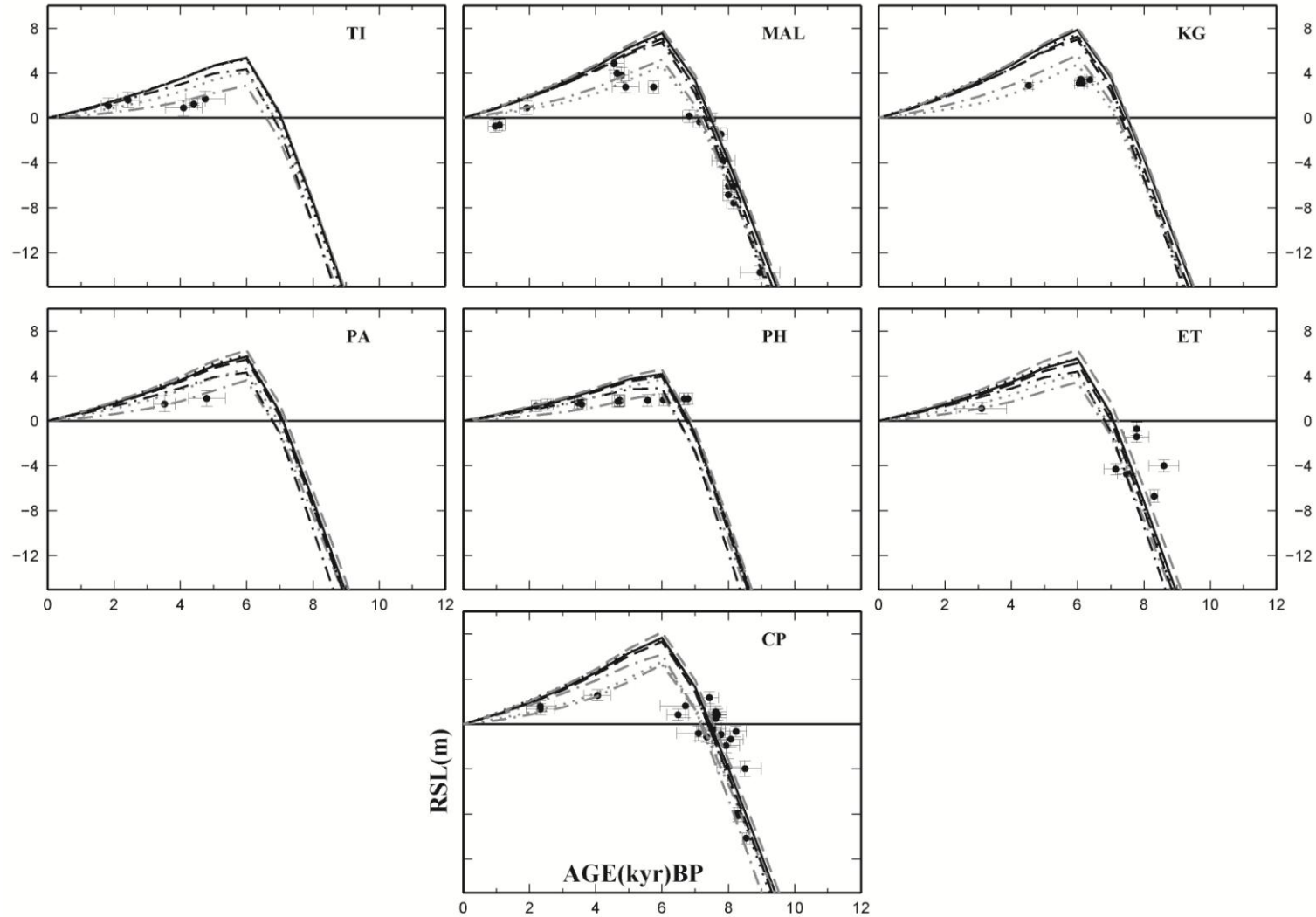


Fig. 4.3: Comparison of sea-level predictions generated for a range of earth models and the reference global ice model to the observations from Malay-Thailand. Solid black circles mark the location of each SLIP (complete RSL dataset summarised in Appendix A). The predictions generated using the reference model is shown by the solid black lines. Variations in the input lithosphere thickness are shown by the dashed line: 71km (grey) and 120 km (black). The dotted line shows changes in the upper mantle viscosity from  $10^{20}$  Pa s (grey) to  $10^{21}$  Pa s (black). Changes in lower mantle viscosity are shown by the dot-dashed line:  $10^{21}$  Pa s (grey) and  $5 \times 10^{22}$  Pa s (black).

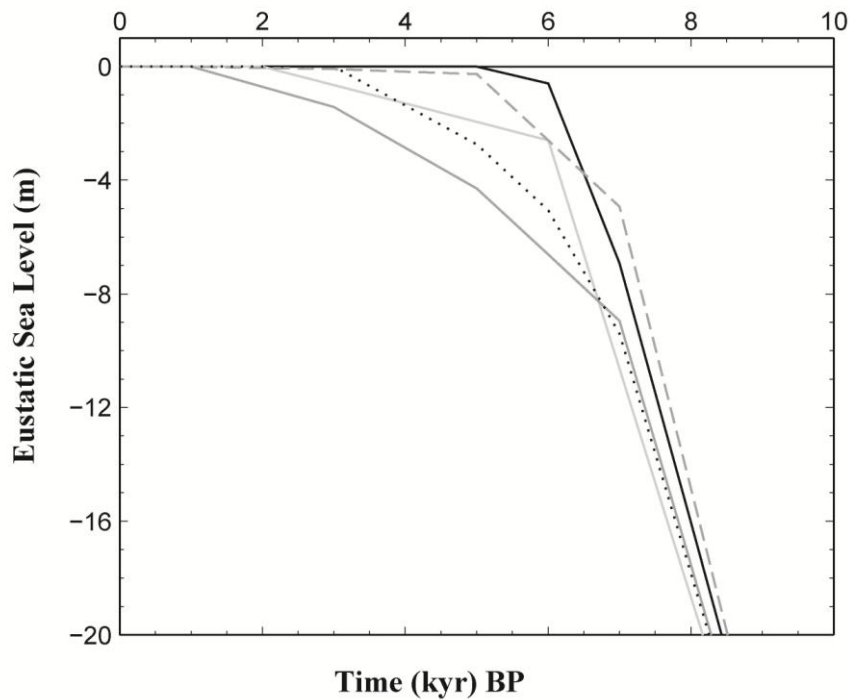


Fig. 4.4: Graphical representation of selected eustatic sea-level functions. Solid black line represents the input eustatic function ( $\Delta S_{est}^i(t)$ ) taken from the reference model (Basset *et al.*, (2005)). Three alternative melt scenarios are also illustrated: melt1 (light grey; solid line), melt2 (black; dotted line), and melt3a (dark grey; solid line) and melt3b (dark grey; dashed line) and are discussed in detail in 4.4.1. The height variation between the solid and dashed dark grey lines illustrates the range in highstand magnitude investigated for each of the three melt scenarios considered.

The starting ice model was combined with an earth model (which is described in greater detail in chapter 1) characterised by a 96 km lithosphere, upper and lower mantle viscosity of  $5 \times 10^{20}$  Pa s and  $10^{22}$  Pa s respectively, which is broadly compatible with a number of recent GIA studies e.g. Forte and Mitrovica (1996), Milne *et al.*, (2001), Nakada and Lambeck (1989). This ice-earth model combination (hereafter referred to as the reference model) will be adopted in the following sections.

#### 4.3.2. China

Using the reference model, sea level predictions were generated at each of the nine localities discussed above and compared to the suite of SLIP (Fig. 4.2). The predicted

sea level across the study region (solid black line) displays the same general form with a slow steady rise up to a maximum highstand of 6-7m at 6 kyr BP - which marks the end of the main stage of melting within the reference ice model - followed by a subsequent steady fall towards zero. This fall is caused by two isostatic processes: hydro-isostasy and syphoning (e.g. Clark *et al.*, (1978) Mitrovica and Milne (2002)). There is little spatial variation in the height of the highstand between the nine sites, with the amplitude at most sites falling between 6 - 7.5 m. This spatial variation is driven by hydro-isostasy (see Fig. 4.1).

Inspection of the fit of the predictions to the data indicates that at most locations the misfit is generally large: the maximum height attained is too high, by up to 7 m at YRD, and the significant highstand predicted is not evident in the data. The data generally rule out sea level across the region reaching values greater than 1.5 m. Furthermore, the variation in the timing of the marked slowdown in the rate of sea-level rise evident in the central and Southern sites is not captured by the model.

The model adequately captures the timing at which sea level first reaches present day levels, between 7-8 kyr BP at the Northern and Southern sites. For example, at JP the model captures the cluster of SLIPs around 7.5 kyr. For the central sites, this is not the case. For example, at the HRD, the data suggest a gradual slowdown in global melting, with present day sea level attained around 5-6 kyr BP. The discrepancy is consistent at all central sites and may be related local tectonism or sediment compaction within the deltaic sites (as mentioned above).

Previous investigations into the spatial and temporal variability of sea level at far-field locations (e.g. Lambeck and Nakada (1990)) have identified the main processes affecting the pattern of sea level: hydro-isostatic loading (continental levering), ocean syphoning and/or local tectonism. The origin of spatial variations within the study region will not be investigated in great detail, only briefly mentioned to examine marked differences. Comparing the predicted sea level (at 6 kyr BP) along the China coastline (contoured on Fig. 4.1), there is no notable difference between the Northern and Central sites, suggesting it is not hydro-isostasy that is driving the observed variability, but rather site-specific processes (e.g, sediment compaction, displacing the data to lower values, as mentioned at HRD) or tectonism, due to active plate margin, such as at FP.

It should be noted that there is a significant spatial gradient in the predicted isostatic signal across some of the data localities. The HP shows the greatest variability, with a range of up to 2 m (Fig. 4.1), which is not evident in the observations, however. It is important to note that this limitation in forward model (spatial averaging of data locations) will not impact the parameter estimation carried out below as the exact longitude and latitude position of each data point will be used. This procedure is only adopted here for the sake of visual comparison between data and observations over the Holocene.

### **4.3.3. Malay-Thailand**

Fig. 4.3 illustrates the predicted sea level generated using the reference Earth and ice model at the seven localities in Malay-Thailand (Fig. 4.1). The general predicted trend (solid black line) is similar to that of China, with maximum sea-level reached at 6 kyr, followed by a steady fall towards zero. Compared to the predictions for the Chinese sites, there is an increased spatial variability in the resultant highstand (up to 4 m; see Fig. 4.1), which is also evident in the observations. This suggests that hydro-isostasy dominates the observed spatial variability in this region. This process results in sea-level gradients that are parallel to the coastline (Fig. 4.1) with amplified sea-level fall (due to land uplift) increasing inland. As a consequence, the highest sea levels are found at sites closer to the larger landmasses, where this process is well established. For example at Keelang (KG), sea level reaches a height of 8m compared to Phuket (PH) where it reaches only 4.3m.

Comparison of the starting model to the data indicates that, at most sites, there is a significant misfit between ~ 7- 2 kyr BP, with an overprediction of up to 4m. The timing of the initial slowdown and approach/reaching of present day sea-level between 7-8 kyr, is captured well by the model. For instance, at both MAL and CP, the predictions lie within error limits of the cluster of SLIPs ~ 7 kyr BP. Despite this, when constraining the timing and maximum sea-level (or highstand) reached at each site, the above noted gaps in the data between 6-3 kyr, are a major limitation. At sites where there is data (such as PH or KG) it does not coincide with the timing of maximum sea-level predicted by the starting model.

The low rate of sea level change between 5-2 kyr BP at TI and PH is not captured by the model, or inferred at any of the other sites. As it is suggested that on a larger scale over this time period, the rate of global sea-level rise is falling, it would be hard to reconcile this pattern with regional scale sea-level processes. This infers that the observed trend is related to local scale processes affecting the change in sea level. For example, defining the indicative meaning for coral data, as used at Phuket PH, can be a limitation when correcting the sea-level data, which may affect the SLIPs. Additionally, underestimating the changes in tidal range can affect the altitude correction for each SLIP.

#### 4.3.4. Summary

Despite the differences in the site-specific patterns of observed sea-level between China and the Malay-Thailand Peninsula, some of the main misfits to the starting model are notably consistent: (1) an overprediction in the height of the maximum sea level (or highstand) attained; (2) timing of the highstand; (3) temporal variation of sea-level from time of the highstand to present. This suggests that a modification to the input eustatic function and hence the global rate of melting would result in an improved data-model fit.

Before doing this, however, it is important to determine if the data-model misfits can be accounted for by changing earth model parameters. It is well established that the character of a highstand at far-field sites is sensitive to both the chosen input earth structure and the rate and magnitude of melt water flux into the oceans. For example, Nakada and Lambeck (1989) noted that simple modifications to the viscosity structure could resolve some of the misfits between predicted and observed sea-level around Australia. They also discuss in some detail the sensitivity of far-field sea level data to changes in earth structure and eustatic history (ice model). This leads to some degree of non-uniqueness when inferring these quantities (see next section).

A suite of earth models was defined based on the spread of parameters inferred in a range of GIA sea level studies (Davis *et al.*, (1999), Kaufmann and Lambeck (2002)). The maximum and minimum values are: 71, 120 km for lithosphere thickness,  $0.1-1 \times 10^{21}$  Pa s for upper mantle viscosity, and  $1-50 \times 10^{21}$  Pa s for lower mantle viscosity.

Predictions for these earth models and the starting ice model are shown on Fig. 4.2 (for China data) and Fig. 4.3 (for Malay-Thailand data).

It is apparent from Figs. 4.2 and 4.3 that the majority of the data-model misfits cannot be resolved with relatively large changes to the earth model parameters. Lithosphere thickness changes made little difference to the predicted sea-level with variations in highstand height generally less than a 1m. Adopting a weaker upper or lower mantle viscosity reduced the height of the highstand by up to 3m around the Malay-Thailand Peninsula and 2m around China, but this still did not resolve the significant misfit between 7-5 kyr BP. The rate of slowdown was also slightly modified by reducing the upper and lower mantle viscosity, which is evident for both data regions where the predicted sea-level broadens. For some of the Malay-Thailand sites, (PA, KG and TI) adopting a weak lower mantle removed the misfits, with predictions lying within the error limits of the observed data. This is quite an extreme value for lower mantle viscosity and it does not improve the fit at all sites across the region (such as CP) or the China sites.

In summary, adjustments to the adopted earth model parameters primarily control the amplitude of the predicted highstand, reducing the noted overprediction at all sites, with the shape and timing of predicted sea-level remaining relatively unaltered. Therefore, changes in the adopted earth model parameters can not resolve the noted misfits in the timing of sea level across the region. For this reason, it is apparent that adjustments to the input ice history (eustatic sea level) are required to resolve the noted misfits to the data..

#### **4.4. Towards an Improved Eustatic Model**

##### **4.4.1. Methodology**

Outlined below is the procedure followed to estimate a revised eustatic Holocene melt history (summarised also as a flowchart in Fig. 4.5). In all revised models, the total global eustatic sea-level change between LGM and present was not altered from that defined in the starting model; only the timing and contribution of the two main ice sheets, (LIS and AIS) over the last 10 kyr. This ensures that the high-quality fit of the

ice model to far-field data between the LGM and the late glacial Bassett *et al.*, (2005) is preserved.

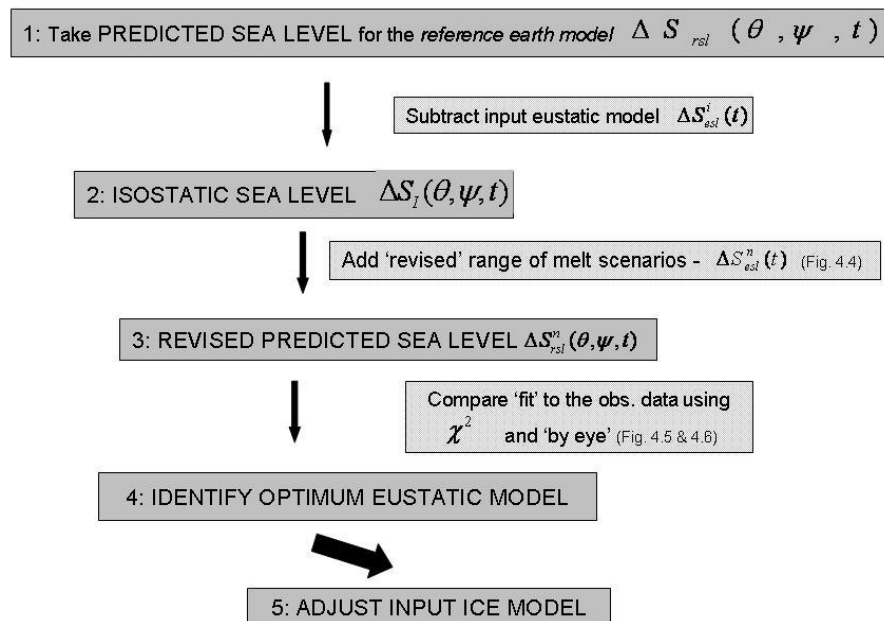


Fig. 4.5: Flow chart to summarise the stages used in estimation of optimum earth model. See text for more details

As shown in 4.3.4, the data-model misfits cannot be accounted for by varying earth model parameters. Therefore, the first step is to develop a first iteration melt scenario that reduces the misfits to the data described above. In this process, the reference earth model was adopted as the predictions using this model lie, approximately, within the middle of the models considered above (see Figs 4.2 & 4.3). When a first iteration melt scenario is found for each data set - China (Section 4.4.2) and Malay-Thailand (Section 4.4.3), these are then combined in a final step that considers variations in both earth and ice model parameters to arrive at a final model that provides an optimum fit at all sites (Section 4.4.5).

This first step in developing the first iteration melt scenario for each data set is to subtract the input eustatic function,  $\Delta S_{est}^i(t)$ , using the relationship defined in (1) (and outlined in greater detail in chapter 1) from the sea-level predictions at each SLIP location.

$$\Delta S_I(\theta, \psi, t) = \Delta S_{rsl}(\theta, \psi, t) - \Delta S_{est}^i(t) \quad (1)$$

A set of ~ 300 eustatic melt scenarios based on the subset shown in Fig. 4.4 were added to the residual  $\Delta S_I(\theta, \psi, t)$  to produce a revised set of sea level predictions. The  $\chi^2$  misfit was calculated between the observed data and the revised predictions to identify an optimum first-iterate melt scenario.

The melt scenarios considered were adjusted systematically in three ways to address the key misfits identified between the observed data and the input model. Two of these relate to the timing of changes during the Holocene, specifically: (1) the initial timing and nature (rate) of melt slowdown in the early to mid Holocene and (2) the timing and nature (rate) of melt shutdown in the late Holocene. Three models are shown in Fig. 4.4 to outline the implementation of these changes (*melt1*, *melt2* and *melt3*). These three models consider a reasonable range of temporal evolution in ice melting during the Holocene.

First, timing of the initial melt slowdown was addressed, changing from 6 kyr (*melt1*) to 7 kyr (*melt2* and *melt3a/3b*). Next, the period during which melt slowdown occurred was investigated, progressing from the ‘abrupt’ slowdown (*melt1*) to the two-staged slowdown illustrated models *melt2*, *melt3a/3b*. Three different timings for the end of global melting are illustrated in the three models: 3 kyr (*melt2*); 2 kyr (*melt1*); 1 kyr (*melt3a/3b*). Finally, the nature of the end of melting was investigated by considering a ‘uniform’ slowdown (*melt2*) and a ‘staged’ slowdown (*melt3a/3b*). Representing the end of global melting as a gradual slowdown in the rate of ice sheet deglaciation was considered a more realistic replication of ice sheet behaviour. The third aspect of the eustatic function that was varied is the distribution of melt between the early, mid and late Holocene, with the aim of adjusting the resultant height of the predicted highstand. For each of the three temporal scenarios illustrated in Fig. 4.4, the amount of Holocene melt distributed prior to and after 7 kyr BP was varied. For example, the difference between *melt3a* and *melt3b* in Fig. 4.4 illustrates the range explored in varying this aspect of that particular melt model. Clearly, the distribution of melt magnitude has an impact on the height of the predicted highstand: the greater the amount of melt added to the global oceans prior to the start of the initial melt slowdown, the higher the resultant highstand (as less melt is then available

from the time of the highstand to the present day to counter balance syphoning and continental levering).

Note that the procedure outlined above does not take into account the ocean loading signal associated with the difference between the original eustatic function and that of the revised scenarios considered. In the case of the China data analysis (next section), the difference between these two functions is large (~ 5.5 m at 6 kyr BP) and so the ocean loading signal is considerable. Therefore, it was necessary to adjust the input ice model so that this ocean-loading signal would be accounted for in the prediction. At each time step between 10-0 kyr BP, the thickness of either the LIS or AIS was adjusted until the resulting eustatic function matched the melt scenario that produced the best fit to the data.

#### 4.4.2. An optimal eustatic model for China

The  $\chi^2$  misfit for the melt scenarios in Fig. 4.4 are displayed in Fig. 4.6 for a range of Earth viscosity models. While these results are only a small subset of the eustatic models considered, they illustrate the sensitivity of the data-model fit to the three aspects of the eustatic function varied in this analysis (as detailed above).

It is evident through examining Fig. 4.6 that the data are sensitive to alterations in the rate and timing of the initial slowdown in melting. Progressing from the sharp, rapid reduction at 6 kyr in the *melt1* model (Fig. 4.6a), to the gradual and earlier staged reduction in the *melt2* and *melt3a* models (Fig. 4.6b and 4.6c) reduces the  $\chi^2$  misfit. This pattern of slowdown is more compatible with the observed trend. Introducing a reduction in the rate of melting towards present, (changing from *melt2* to *melt3a* models in Fig. 4.4) further reduced the  $\chi^2$  misfit (compare (b) and (c) in Fig. 4.6). Although the data do not effectively constrain when global melting ended, continued addition of melt water to the oceans from 3 kyr to 1 kyr is more consistent with observations on the evolution of the AIS during the late Holocene (e.g. Sugden *et al.*, (2006)). It is also apparent that there is little variation in the region of optimum earth structure (comparing (a) (b) and (c)) for three of the melt models investigated.

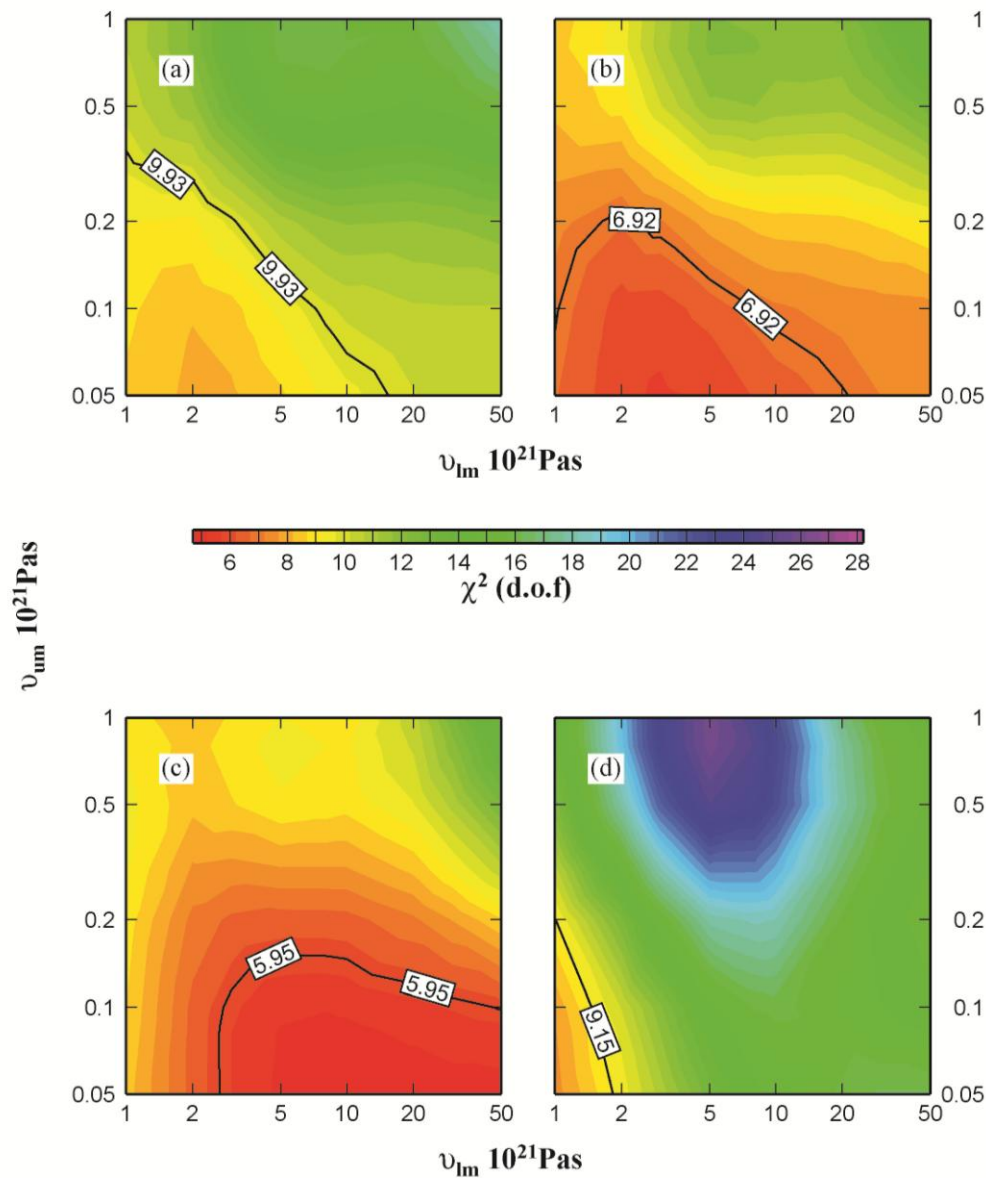


Fig. 4.6: Contour plots of the  $\chi^2$  misfit between predicted and observed sea levels for the China data set as a function of upper and lower mantle viscosity ( $v_{um}$  and  $v_{lm}$ , respectively). Each frame gives the results for the four melt scenarios illustrated in Fig. 4.4: (a) melt1, (b) melt2, (c) melt3a, (d) melt3b. The black line represents the  $\chi^2$  value below which the quality fit is equivalent at 95% confidence.

The data-model fit is also significantly affected by varying the distribution of Holocene melt. On comparing the results in Fig. 4.6 c & d (melt3a & melt3b), it is evident that a better fit is achieved for the majority of Earth models considered when the amount of melting in the mid-to-late Holocene is increased significantly compared to the starting eustatic model. This is compatible with the fact that the data show no evidence of a clear, well-defined highstand across the region. In addition, comparing

the results for these two melt models, there is a shift in the optimum earth model parameters. This parameter trade-off will be discussed further in 4.4.5.

Considering the chi-squared results for the entire suite of melt scenarios considered, an optimum first-iteration melt scenario is similar to model 3a in Fig. 4.4. As the pattern of melting in the optimum model is markedly different to that in the reference model, the ice model was altered to simulate this revised pattern, as outlined in 4.4.1. This model will be hereafter referred to as EUST1.

The  $\chi^2$  results for the starting model and EUST1 for all sites and reduced data set are displayed on Figs. 4.7 and 4.8, respectively.

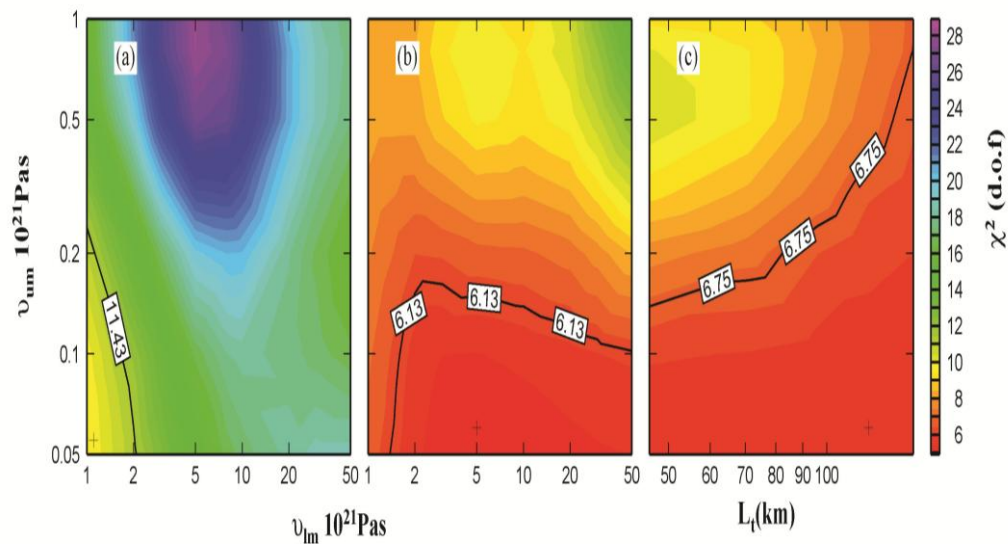


Fig. 4.7: Contour plots of the  $\chi^2$  misfit between predicted and observed sea levels for the China data set as a function of upper and lower mantle viscosities ( $v_{um}$  and  $v_{lm}$ , respectively) and lithosphere thickness ( $L_l$ ) for the reference (a) and *EUST1* (b) eustatic models. Results in (a) and (b) are for a lithosphere thickness of 96km. The solid black line represents the 95% confidence level and the cross indicates the min.  $\chi^2$  misfit. Frame (c) shows  $\chi^2$  values generated using the *EUST1* ice model as a function of lithospheric thickness and upper mantle viscosity for a lower mantle viscosity of  $2 \times 10^{21}$  Pa s.

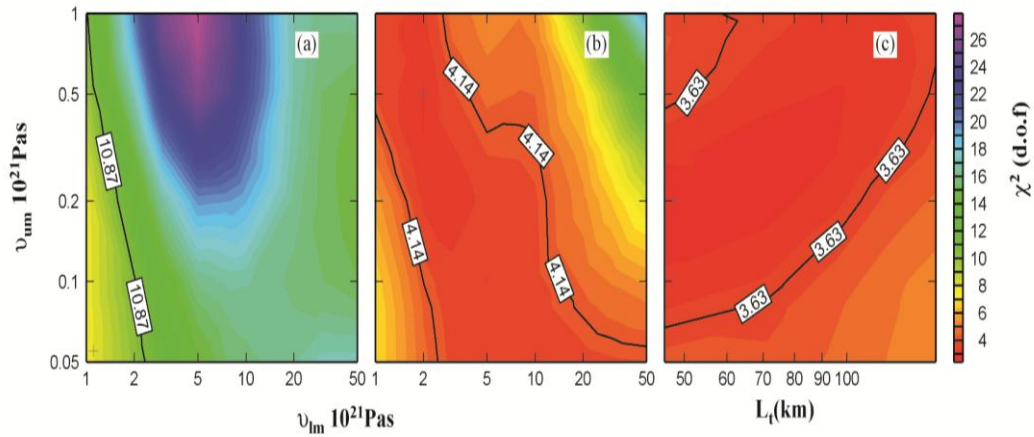


Fig. 4.8: As in Fig. 4.7 except that results are based on a subset of data points from the China data set believed to be the most reliable (see Section 4.3.2 for more detail).

It is apparent that the starting model (Fig. 4.7a, 4.8a) only produces a reasonable fit, within the 95% confidence, to the data for a small subset of viscosity models with low values of upper and lower mantle viscosity. Correcting the input ice model dramatically improves the fit to the data and influences the optimum earth model parameters (Fig. 4.7b, 4.8b, 4.7c and 4.8c). For the complete data set, the data rule out values of upper mantle viscosity greater than  $\sim 0.15 \times 10^{21}$  Pa s (at the 95% confidence level). The data are less sensitive to variations in lower mantle viscosity and lithospheric thickness and so do not provide useful constraints on these parameters. The reduced data set shows a different sensitivity to the earth model parameters: there is a more pronounced trade-off between upper and lower mantle viscosity; specifically, the region of optimum fit migrates to larger values of  $v_{um}$  for a progressively weaker lower mantle (Fig. 4.8b). In contrast to the complete data set, the reduced data set is not able to constrain  $v_{um}$  to lie within a subset of the range of values explored.

Based on the results in Figs. 4.7 & 4.8, two earth models were adopted to partner the revised (EUST1) ice model. One based on the fit to the complete data set: upper and lower mantle viscosities of  $1 \times 10^{20}$  and  $5 \times 10^{21}$  Pa s, respectively; and the other based on the fit to the reduced data set: upper and lower mantle viscosities of  $5 \times 10^{20}$  and  $2 \times 10^{21}$  Pa s, respectively. For both data sets an average lithosphere thickness of

96 km was chosen. Predictions based on these two ice-earth model combinations are compared to the observations in Fig. 4.9. The predictions are characterised by a steady rise in sea-level towards a marked slowdown beginning at 7 kyr BP, followed by a staged slowdown (at 5 and 3 kyr BP) towards present day levels.

It is evident from Fig. 4.9 that the predictions based on the EUST1 model are a significant improvement compared to those for the starting model. As expected, the large highstand is removed and the predictions track the observed data more closely during the mid-Holocene. Furthermore, the revised model predicts the spatial variation in the time at which present day sea-level is reached: progressively earlier in the northern sites than central, which is consistent with the observations. For example, at BB the staged slowdown in the revised model reaches present day sea-level ~ 7 kyr, compared to 5 kyr BP at HRD.

There remain some significant data-model misfits even with the revised ice model. At HRD the predictions closely match the observed trend from 5 kyr – present, but still over shoot the earlier data. This discrepancy is consistent with active compaction and/or subsidence at this locality in the mid-to-late Holocene. At HP, the predictions are too low between 6-4 kyr BP with present day sea-level reached too late in the model (3 kyr).

As previously described, there was a noted spatial variation in the predicted RSL across HP of approximately 2m (see contours on Fig. 4.1) which is not evident within the observed data. On Fig. 4.9 predictions are shown (using earth model for complete data set; dashed-dotted line) for an additional location in the north of the island to highlight the overall reduction in this spatial variability (to less than 0.5 m) when the revised ice model is employed. This is a consequence of partitioning more ocean loading into the mid-to-late Holocene compared to the starting model, thus decreasing the continental levering signal across the Island in the mid-Holocene.

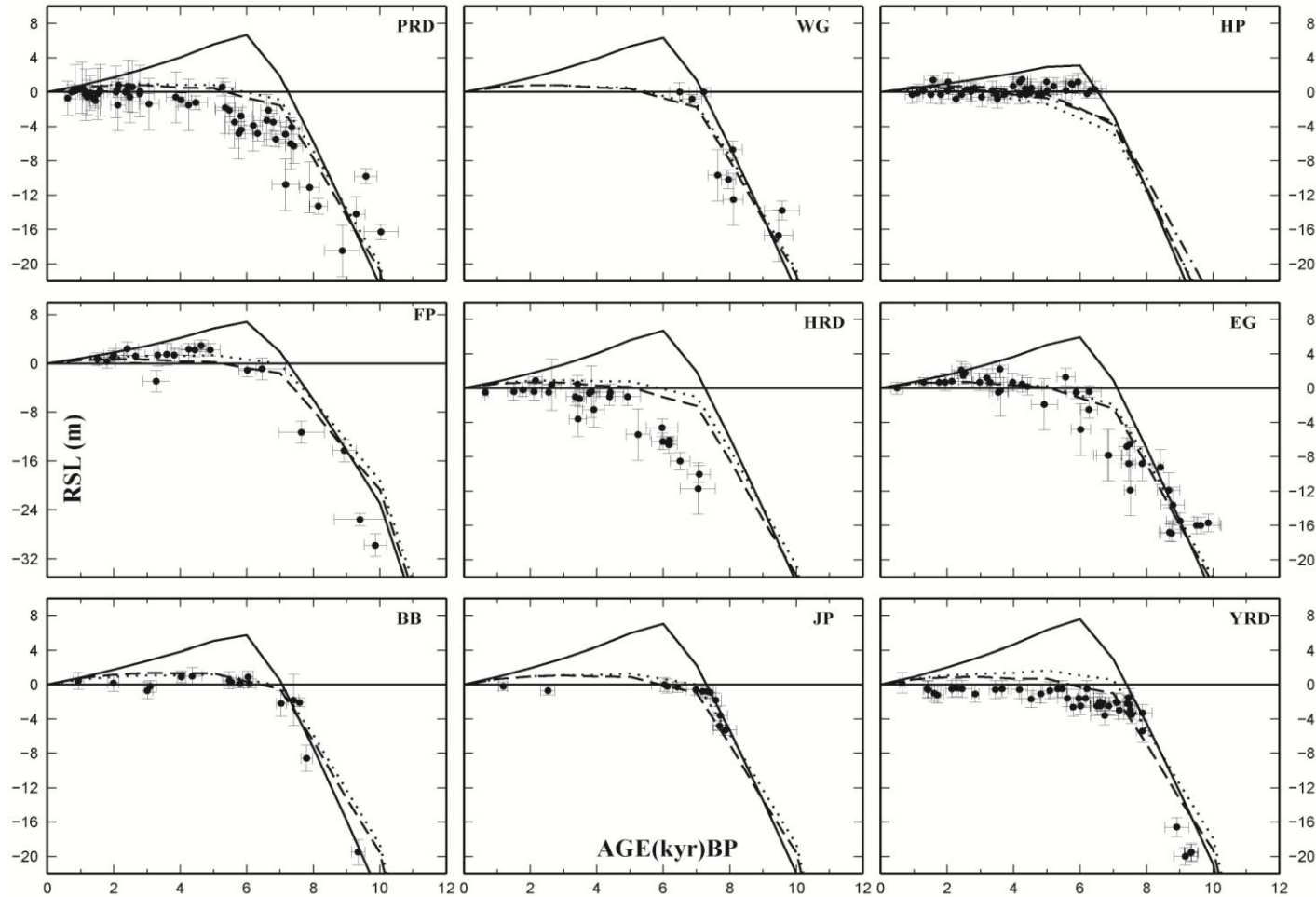


Fig. 4.9: Comparison of the predicted and observed sea-level change at each locality in China. Solid black circles mark each SLIP. The solid black line shows predictions for the reference ice-earth model. Predictions using the revised ice model (*EUSTI*) were generated for an optimum earth structure inferred from the  $\chi^2$  results in Fig. 4.7 and 4.8: for the complete data set (dashed) with a lithosphere thickness of 96 km, upper mantle viscosity  $1 \cdot 10^{20}$  Pa s and lower mantle viscosity  $5 \cdot 10^{21}$  Pa s; reduced data set (dotted) with a lithosphere thickness 96 km, upper mantle viscosity  $5 \cdot 10^{20}$  Pa s, lower mantle viscosity  $2 \cdot 10^{21}$  Pa s. At locality HP, predictions based on the revised ice model are also for a location to the north of the island (dashed-dotted; see text for more information).

### 4.4.3. An optimal eustatic model for Malay-Thailand

The method outlined above was repeated for the Malay-Thailand data set to identify an optimum Holocene melt history. The  $\chi^2$  results for the four example melt models in Fig. 4.4 are displayed in Fig. 4.10. The EUST1 model, which provided an optimum fit to the China data, will also be compared to the Malay-Thailand data set. As mentioned previously, the Malay-Thailand data set contains fewer SLIPs compared to the China data set with a relatively small number of data during the mid-Holocene (7-4 kyr BP). The resulting eustatic function will therefore be less well constrained, particularly during this period.

From Fig. 4.10, similar conclusions can be made regarding the sensitivity of the Malay-Thailand data to revisions in the eustatic melt as for the China data set. While both data sets prefer the timing of the melt3a model, where following an initial slowdown around 7 kyr BP there is a gradual decrease in melt rate until cessation at 1 kyr BP, they differ in the preferred rate of melt partitioned before and after 7 kyr BP. Specifically, comparing Fig. 4.10c- 4.10d, the Malay-Thailand data prefer a greater amount of melt to be placed prior to 7 kyr BP and so the optimal eustatic history is closer to that of the melt3b model (rather than the melt3a model preferred by the China data). This is not surprising given that the Malay-Thailand data display a clear highstand of up to 4 m during the mid-Holocene. Based on the ~300 melt models considered, an optimum melt scenario for the Malay-Thailand data set was identified and will be referred to as EUST2 (which is close in form to the melt3b model in Fig. 4.4).

As the alterations in the timing and rate of eustatic sea level rise were not as significant between *EUST2* and *EUST1* in comparison to *EUST1* and the reference model (see Fig. 4.13), it was not necessary to alter the ice model to account for the residual ocean loading signal (see discussion in Section 4.4.1). Note that the isostatic component of the predictions ( $\Delta S_I(\theta, \phi, t)$ ) in eqn (1) was calculated using the *EUST1* ice model rather than the starting model.

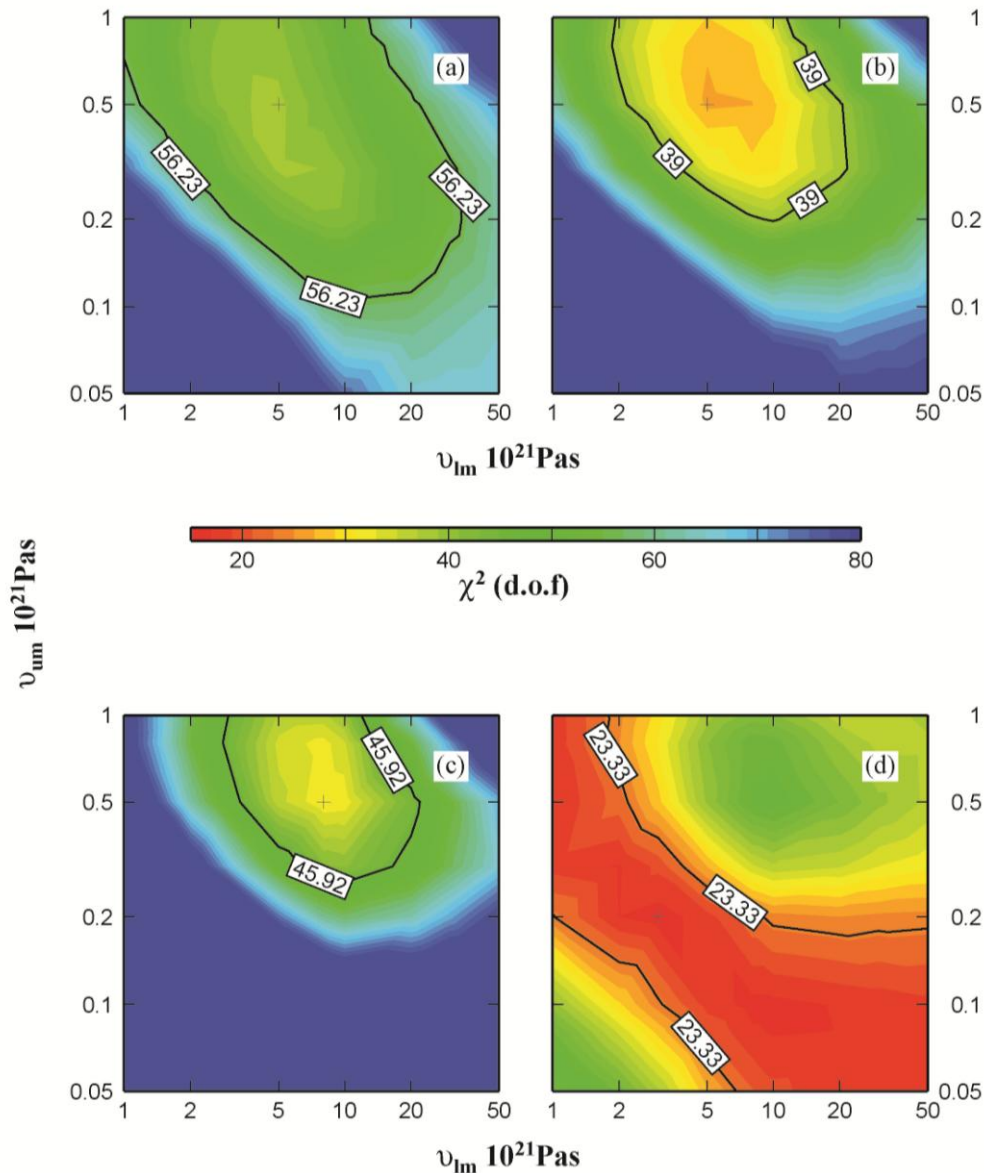


Fig. 4.10: Contour plots of the  $\chi^2$  misfit between predicted and observed sea levels for the Malay-Thailand data set as a function of upper and lower mantle viscosity ( $\nu_{um}$  and  $\nu_{lm}$ , respectively). Each frame gives the results for the four melt scenarios illustrated in Fig. 4: (a) melt1, (b) melt2, (c) melt3a, (d) melt3b. The black line represents the  $\chi^2$  value below which the quality fit is equivalent at 95% confidence. The blue region represents  $\chi^2$  values greater than the maximum on the scale bar (80) up to 243.

Inspection of Fig. 4.11 demonstrates, in a similar fashion to Fig. 4.6, that the quality of fit is sensitive to both earth model parameters and the adopted eustatic model. For the first iterate eustatic model (*EUST2*; Fig. 4.11b), the optimum set of earth model parameters (within 95% confidence limit) does not place useful constraints on either lower mantle viscosity or lithospheric thickness. This model does, however, rule out

upper mantle viscosity values less than  $\sim 2 \times 10^{20}$  Pa s. Note that this inference lies outside the 95% confidence zone as inferred from the China data (complete data set; Fig. 4.7b), suggesting that there are significant lateral variations in upper mantle structure between the two regions.

Sea-level predictions using *EUST1* and *EUST2* are compared to the observed data (Fig. 4.12) for an earth model which fitted within the 95% confidence range of both eustatic models, so that the fit could be compared without the bias of adopting two different earth models. *EUST1* and *EUST2* produce a broadly similar pattern of sea-level change across the data region and remove the over prediction in the maximum height of sea-level generated with the starting model. The *EUST2* model shows a slowdown in the rate of melting at 7 kyr, reaching a sea-level maximum at 5 kyr followed by a steady fall towards present day levels. The two revised models bound the data at all sites, (apart from site PH), with *EUST2* producing a closer match at most sites. Adopting the *EUST2* model increases the highest predicted sea level by  $\sim 2$ m due to the greater amount of melt added to the ocean prior to 7 kyr. This also results in present day sea levels being reached earlier than for the *EUST1* model by up to 2 kyr. *EUST1* does capture the trend reasonably well at some sites, such as Chao Phraya (CP) but generally under predicts the observed Holocene sea levels in this region.

Predictions based on *EUST1* and *EUST2* diverge the most between 7-4 kyr BP, when there is relatively poor data control. At sites KG and MAL, where there is data during this period, only the *EUST2* model predictions fall within the error limits of the data. Phuket (PH) also includes data during this period; however, neither model closely reproduces the trend observed between 7-5 kyr BP. The predicted sea levels show a steady rise compared to a minor but steady fall inferred from the observations. This difference is attributed to problems with the data, as described in Section 4.3.3.

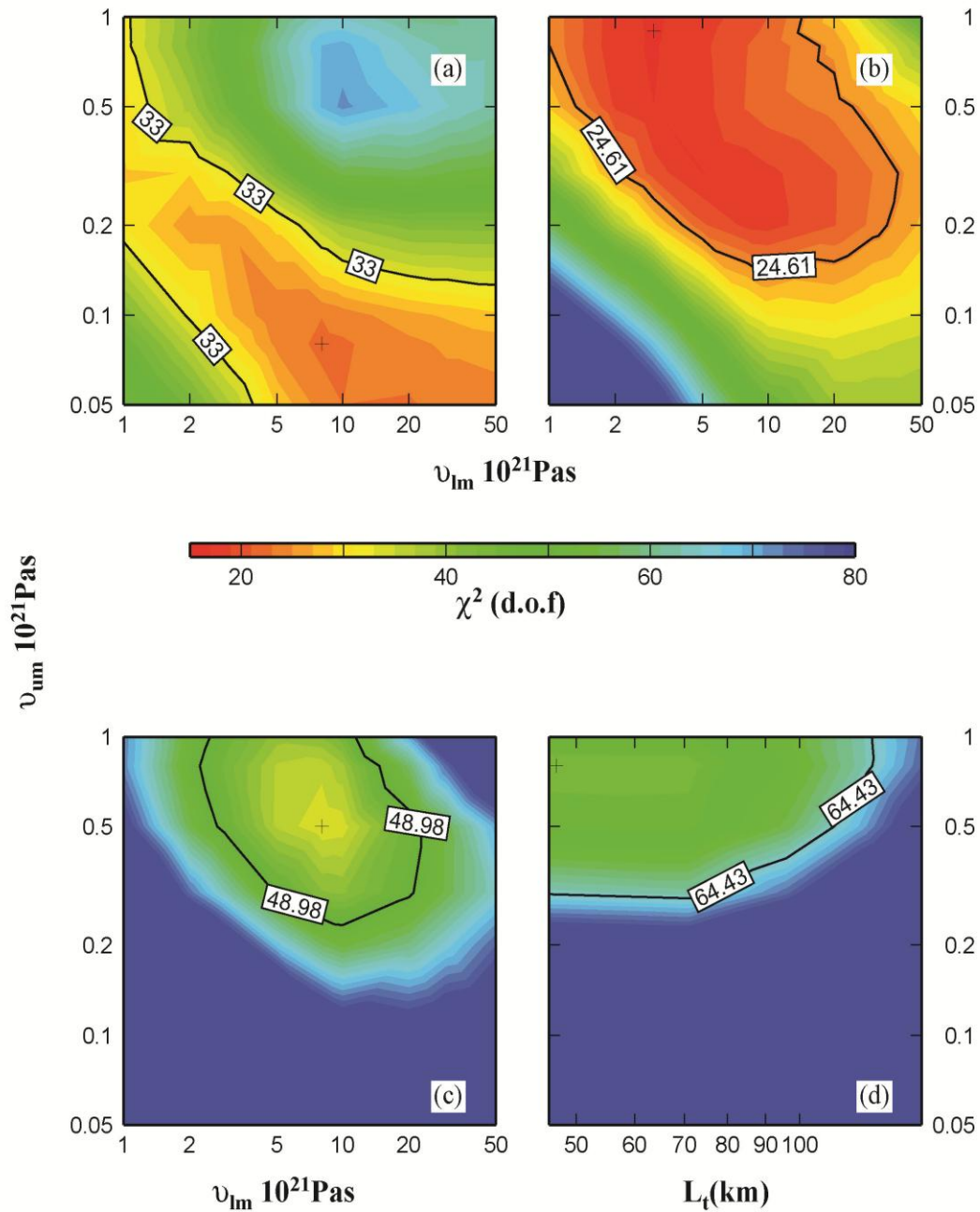


Fig. 4.11: Contour plots of the  $\chi^2$  misfit between predicted and observed sea levels for the Malay-Thailand data set as a function of upper and lower mantle viscosities ( $v_{um}$  and  $v_{lm}$ , respectively) and lithosphere thickness ( $L_t$ ) for the reference (a), *EUST2* (b) and *EUST1* (c) eustatic models. Results in (a), (b) and (c) are for a lithosphere thickness of 96km. The solid black line represents the 95% confidence level and the cross indicates the min.  $\chi^2$  misfit. Frame (d) shows  $\chi^2$  values generated using the *EUST1* ice model as a function of lithospheric thickness and upper mantle viscosity for a lower mantle viscosity of  $2 \times 10^{21}$  Pa s. The blue colour represents  $\chi^2$  values greater than the maximum on the scale bar (80) up to 193

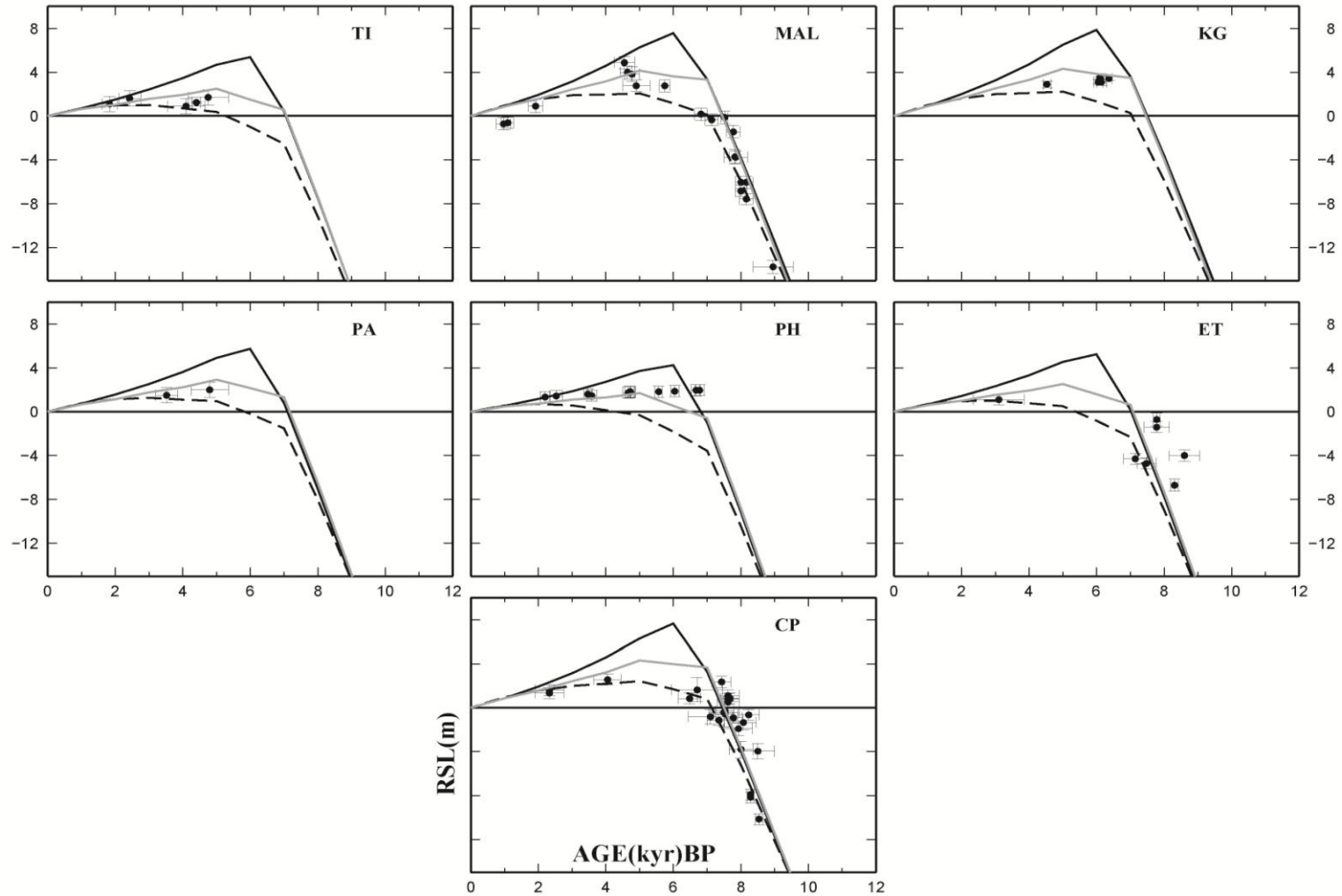


Fig. 4.12: Comparison of predicted and observed sea levels at each of the seven localities in Malay-Thailand for three eustatic melt models. Solid black circles mark each SLIP. The solid black line represents prediction for the reference model, described in the text. Predictions for *EUST1* (dashed) and *EUST2* (solid grey) were generated for an earth model with a lithosphere thickness of 96km, upper mantle viscosity of  $8 \cdot 10^{20}$  Pa s and lower mantle  $5 \cdot 10^{21}$  Pa s. This model produced a good fit for both of the revised eustatic models (see Fig. 4.11).

#### 4.4.4. Summary of new eustatic models:

Two first iterate melt scenarios (*EUST1* and *EUST2*; Fig. 4.13) were created to provide a good fit to the China (*EUST1*) and Malay-Thailand (*EUST2*) data sets and addressed the three key misfits outlined above: (1) amplitude of the Holocene highstand, (2) timing of the highstand, (3) sea-level trend following the highstand. The two models were developed independently of each other, to produce an optimum fit to either the China or Malay-Thailand datasets.

The overall style of the eustatic melting history is similar between the two revised models and is summarised by the following changes from the starting model: (1) the timing of the initiation of the slowdown in global melting was made earlier, from 6 kyr to 7 kyr BP, (2) a staged slowdown (highlighted on Fig. 4.13) in global melting with melt rate reductions at 7, 5, 3 & 1 kyr (melting is ceased at 1 kyr BP). The average rate of melting over the last 5 kyr BP in *EUST2* is half of that in *EUST1*. As described above, the main difference between *EUST1* and *EUST2* is the partitioning of melt prior to and following 7 kyr BP, which influences the development (magnitude) of a highstand across each region. In *EUST2* an extra 2.5m of melt is added to the oceans prior to the slowdown at 7 kyr, compared to *EUST1*. As the style of melting and total eustatic sea-level rise is the same in both scenarios, this in turn reduces the contribution from *EUST2* in the final 5 kyr to 1.9m less than *EUST1*. Finally, the rate of melting over the last 3 kyr is  $1.2 \text{ mm yr}^{-1}$  for *EUST1*, approximately twice the rate of *EUST2*. This highlights a distinct sensitivity between the two data sets to the amount of melt added to the oceans following the 7 kyr slowdown. It is noted that at 7 kyr BP, the amount of total eustatic sea-level change between *EUST2* and the starting model is the same (see Fig. 4.13).

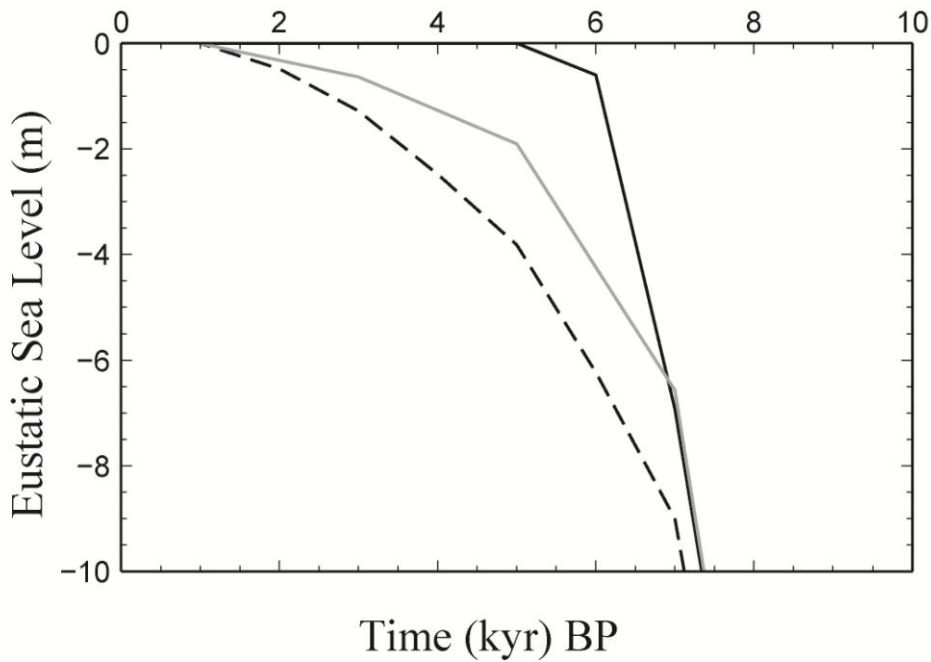


Fig. 4.13: Graphical representation of the eustatic sea level curve for three models: reference (solid black), *EUST1* (dashed) and *EUST2* (solid grey).

Distinctly different constraints are provided on the optimum earth structure for each region. Both are relatively insensitive to variations in the lower mantle viscosity but prefer markedly different upper mantle values. For China the best fit is achieved with a weak upper mantle, less than  $2 \times 10^{20}$  Pa s (for the complete data set), compared to Malay-Thailand data, where a stronger mantle, greater than  $2 \times 10^{20}$  Pa s is preferred. The ranges of inferred values using these data are broadly compatible to those identified from sea-level studies around Australia and other far-field locations (Lambeck (2002)).

Using the two eustatic models tuned to fit each data set, it is not possible to define an optimum earth structure for the entire region (south East Asia). This is not surprising given the tectonic complexity and geographic size of the study region. It is likely that the proximity of some sites to subduction zones will have an impact on the subsurface rheology (e.g. James *et al.*, (2000)). It is logical, therefore, to adopt distinct Earth models for each data set. In contrast, the eustatic history must be the same at all locations by definition. Therefore, in the next section, we identify a single melt model that provides an optimum fit to the combined data set under the condition that

different Earth parameters can be adopted for each region (China and Malay-Thailand).

#### 4.4.5. An optimum model for combined China and Malay-Thailand data

In the above section, the misfits to the data were reduced by revising the pattern and timing of Holocene melt to produce a eustatic model which fitted each data set. In this section, the aim is to create a combined eustatic model optimised to fit both data sets. The adopted stages are summarised in a flowchart on Fig. 4.14.

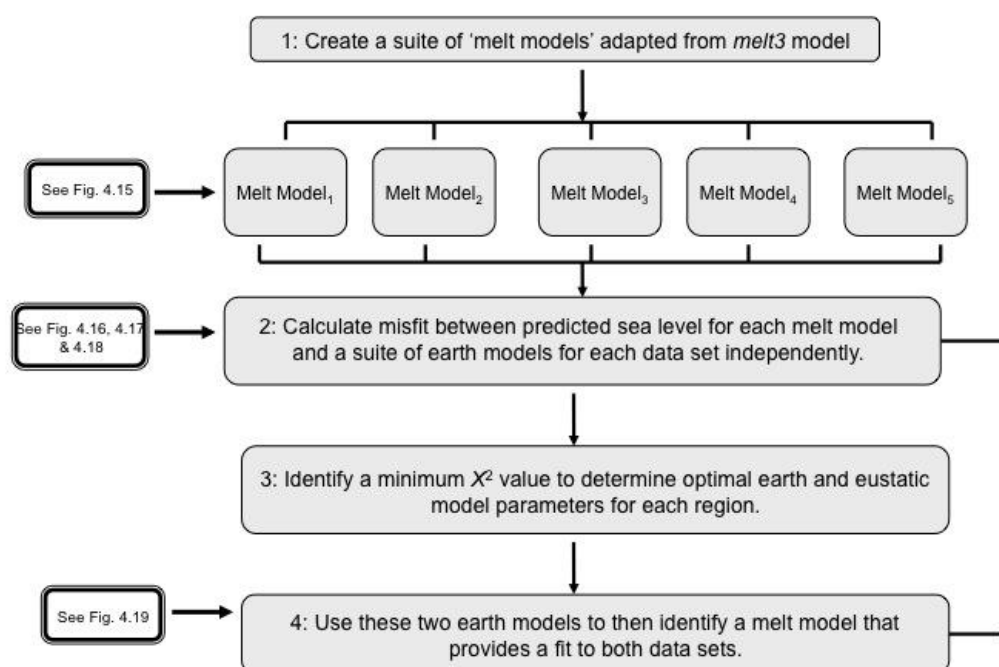


Fig. 4.14: Flow diagram to outline the key steps in determining a eustatic model that provides a good fit to both the China and Malay-Thailand data sets

Firstly using the 'melt3' model (the model that provided the best fit to both data sets) as a template, a number of melt models were defined by varying the amount of melt partitioned prior to and following 7 kyr BP. Four examples are shown in Fig. 4.15. This partitioning is reflected in the value of eustatic sea level at 7 kyr BP (the greater the melt added prior to this time the shallower eustatic sea level will be). The depth of

eustatic sea level at 7 kyr was incremented from a maximum of 8m (Fig. 4.15 dashed line) to a minimum of 4.7m (Fig. 4.15 dotted dashed). The models will be referred to in the following discussion in terms of the depth of eustatic sea level at 7 kyr. (e.g. a model with a eustatic sea level at 7 kyr of 8m will be referred to as the ‘8 m’ model).

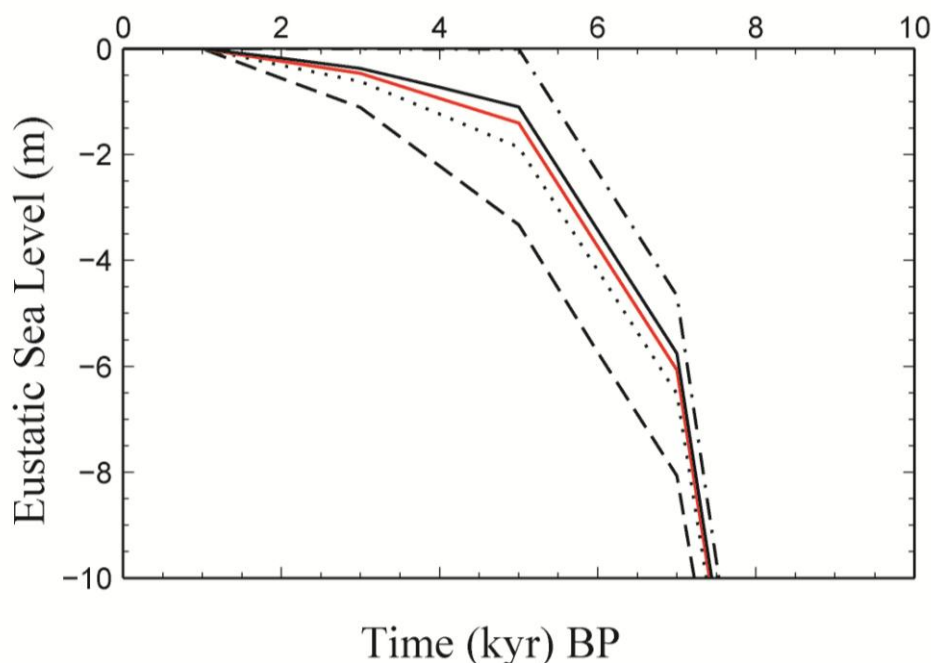


Fig. 4.15: Four of the melt models adopted to investigate the sensitivity of the data-model fit to the amount of melt partitioned before and after 7 kyr BP. The amount of melt prior to 7 kyr BP was systematically reduced to produce eustatic sea level at this time ranging from a depth of 4.7 m (dotted-dashed) to a depth of 8 m (dashed). The dotted and solid lines illustrate two intermediate models, with the red line highlighting the median model. All models are based on the timing of the ‘melt3’ model (Fig. 4.4) used to obtain *EUST1* and *EUST2*.

Secondly, the dependence of the predicted sea level to changes in both the eustatic sea level (specifically the adopted melt model) and earth structure was investigated, with the aim of identifying (1) the best fit earth model parameters, (2) a sub-set of earth models that provide a fit to the data (within the 95% confidence) for the range of earth models considered.

Following the method outlined in section, 4.4.1: a revised set of predictions were generated for each of the melt models and a suite of earth models (as described above), for the China (complete and reduced) and Malay-Thailand data sets. The

corresponding  $\chi^2$  misfits are shown in Figs. 4.16, 4.17 and 4.18 are shown for a subset of four melt models.

There are a number of points to conclude from these figures. Firstly, it is apparent that the fit to the China data (reduced and complete) as a function of earth model parameters is less sensitive to changes in melt model compared to the Malay-Thailand data (see Fig. 4.16 and Fig. 4.17). Specifically, there is little change from the 6.5 m melt model onwards in terms of the location of the 95% confidence region. Generally the data prefer a weak upper mantle viscosity (as indicated by the position of the triangle) and rule out lower mantle values greater than  $2 \times 10^{21}$  Pa s. Comparing the progression in the value of the  $\chi^2$  minimum with each melt model, it is again evident that the data prefer a eustatic melt pattern with less melt prior to 7 kyr BP. (Fig. 4.16a to 4.16c)

For the Malay-Thailand data, the change in the value of the  $\chi^2$  minimum for each melt model is the reverse of that for the China data, with the data preferring a greater amount of melt prior to 7 kyr (Fig. 4.18a to Fig. 4.18c). As stated above, the set of optimum earth model parameters is more sensitive to the choice of eustatic model in this case. For melt models with relatively little melt prior to 7 kyr BP (8-6m models, see Fig. 4.18a and 4.18b), which have a higher  $\chi^2$  misfit, the data rule out upper mantle viscosities less than  $1.5 \times 10^{21}$  Pa s. Progressing to models with a greater amount of melt after 7 kyr, the optimum region of earth parameter values remains relatively stable (see Fig. 4.18c and Fig. 4.18d). For these melt models, earth models that have weak upper and lower mantle viscosity values are ruled out (note that these are the models which fit the China data set).

From the above investigations, an earth model/melt model combination was chosen for each region which produced both a minimum  $\chi^2$  value and fitted within the 95% confidence earth model parameter range for most of the melt models considered. The earth model parameters were as follows: (1) lithosphere thickness of 96 km for both data sets; (2) upper and lower mantle viscosities of  $8 \times 10^{19}$  Pa s and  $1 \times 10^{21}$  Pa s, for China and  $2 \times 10^{20}$  Pa s and  $5 \times 10^{21}$  Pa s for Malay-Thailand, respectively.

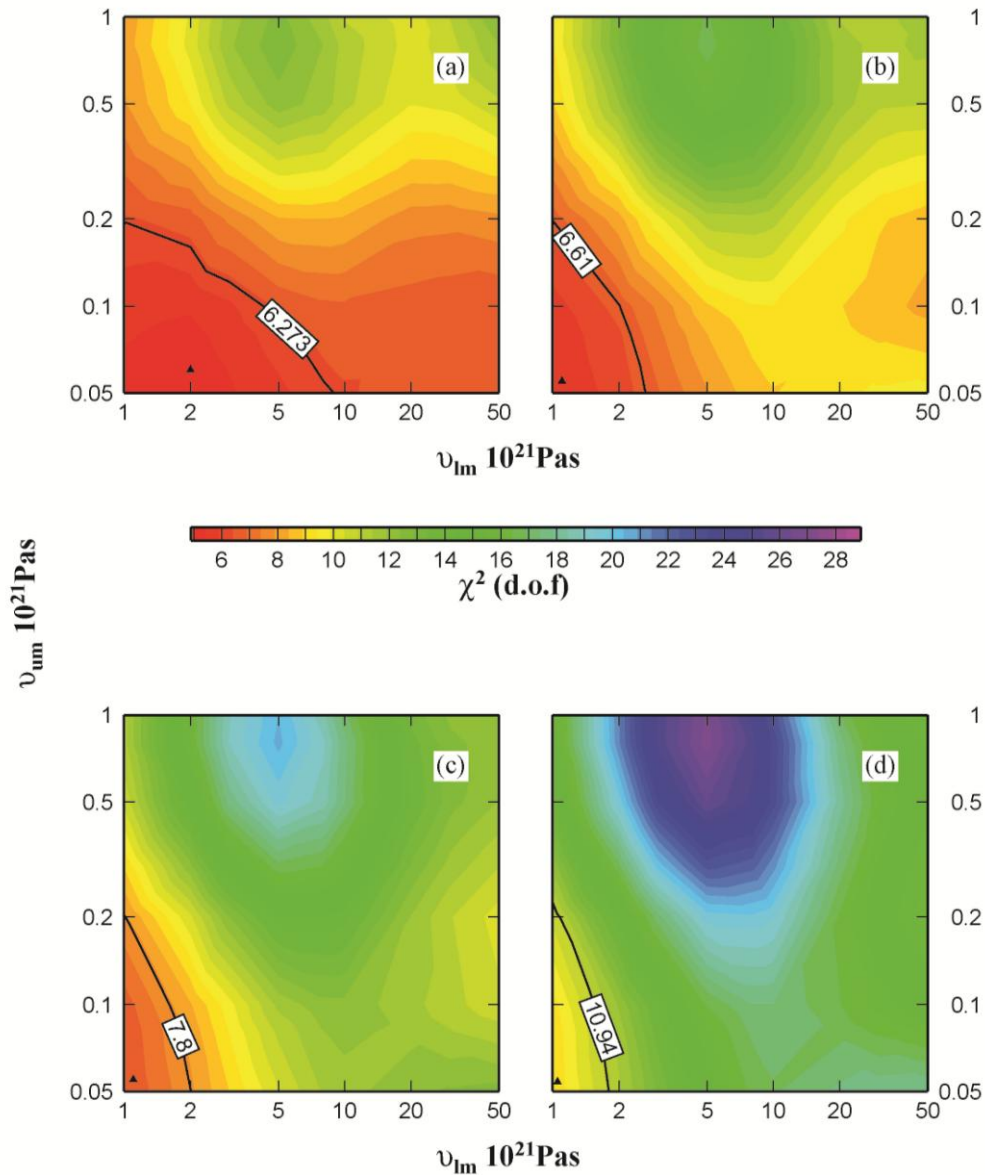


Fig. 4.16: Contour plots of the  $\chi^2$  misfit between predicted and observed sea level for the China data set as a function of upper and lower mantle viscosity ( $\nu_{um}$  and  $\nu_{lm}$  respectively) for a lithosphere thickness of 96 km. The results are shown for four different melt models defined in terms of depth of eustatic sea level at 7 kyr BP (and described in greater detail within section 4.4.5): (a) 7.5 m, (b) 6.5 m, (c) 5.75 m and (d) 4.7 m. The black line represents the  $\chi^2$  value below which the quality fit is equivalent at 95%. The black triangle marks the minimum  $\chi^2$  misfit

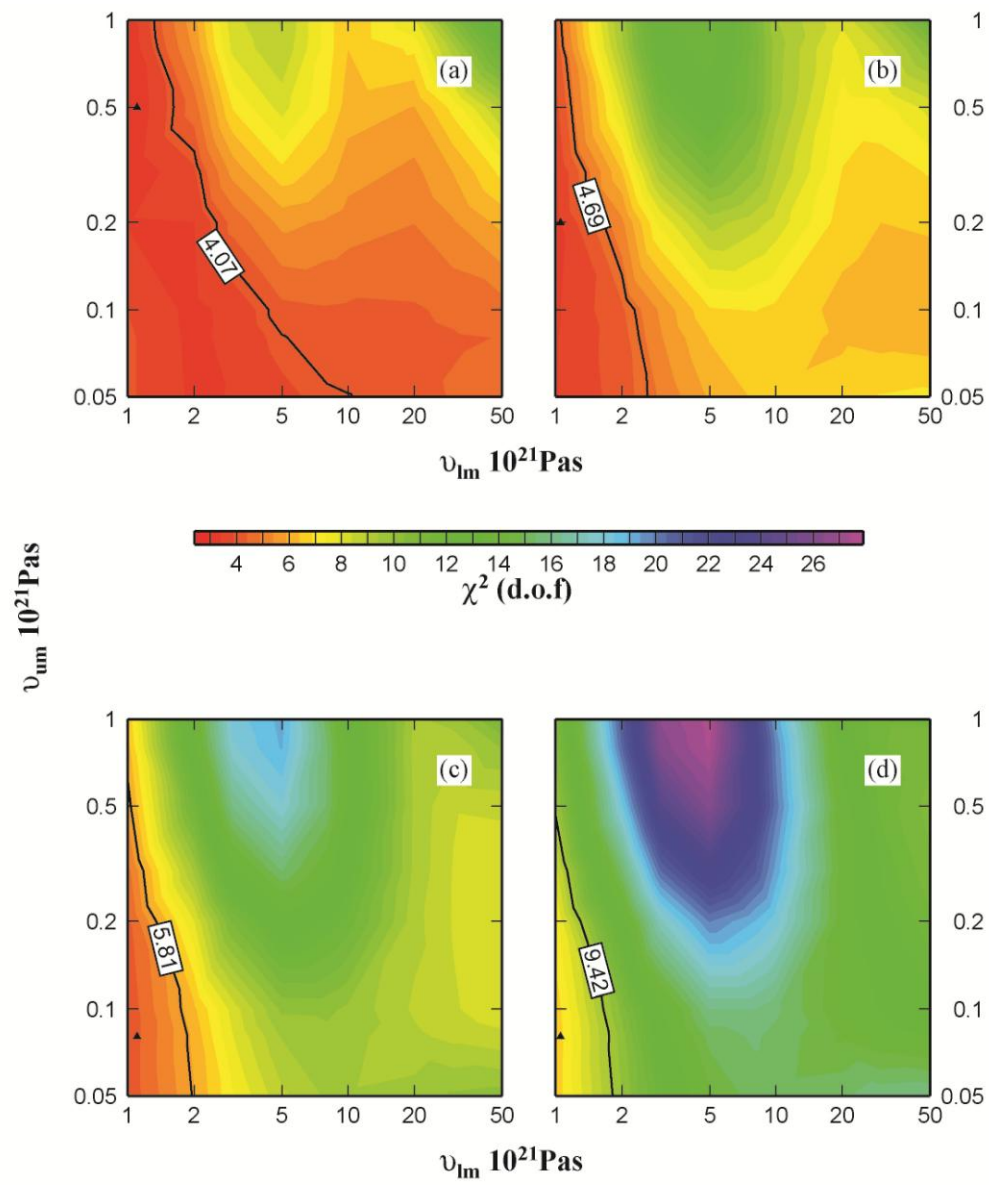


Fig. 4.17: As in Fig 4.16 except that results are shown for the 'reduced' China data set

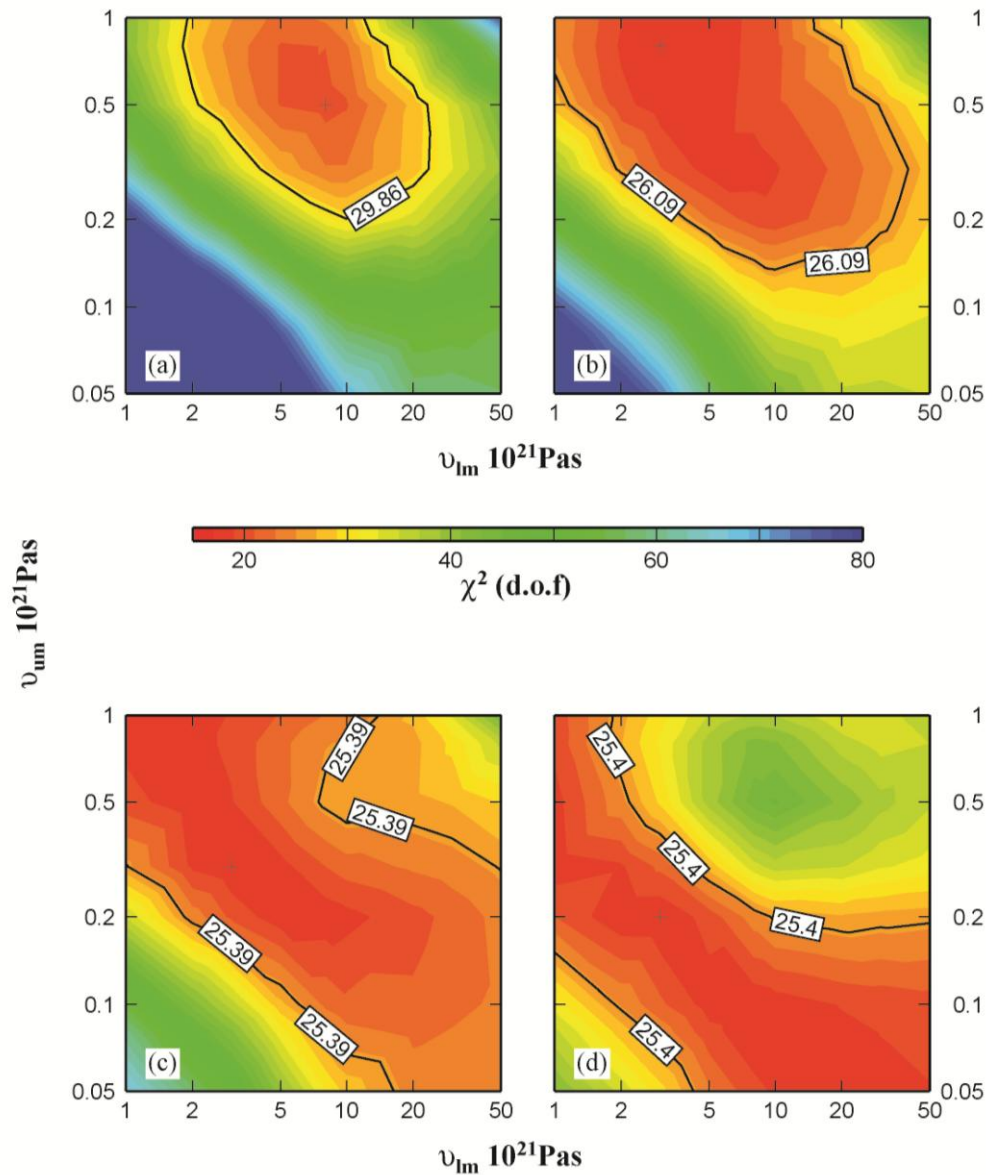


Fig. 4.18: As in Fig. 4.16 expected results are shown for the Malay-Thailand data set. The cross marks the location of the minimum  $\chi^2$  misfit.

The melt models chosen were the 7 m and 6.5 m for the complete and reduced China data set and 5.5 m for Malay-Thailand. Note that these optimum melt models are different to those inferred earlier based on the reference earth model (*EUST1* and *EUST2*). In these models, eustatic sea level at 7 kyr BP was 9 m (*EUST1*) and 6.6 m (*EUST2*). This is entirely due to the different earth model parameters used and so highlights the importance of examining the trade off between the chosen earth model parameters and eustatic melt history.

Using these combinations of melt model and earth model to define a minimum  $\chi^2$  value, a 95% confidence interval was estimated (using  $F$ -test tables) for each data set. Melt models were then determined which produced a  $\chi^2$  value (calculated for each region-specific earth model) within this 95% confidence interval. The results for each region were then compared to identify a range of possible models that fit each data set within the defined confidence limit (see Fig. 4.19).

An optimum fit (minimum  $\chi^2$ ) is produced for the Malay-Thailand data with melt model '5.5m' compared to '7m' for the complete and '6.5m' for the reduced China data set. The noted difference in the 'optimum' melt model chosen for each data set was to be expected based on the conclusions made in the above sections: the China data set prefers a lower amount of melt prior to 7 kyr and hence the lower eustatic sea-level. It is evident from Fig. 4.19, that the range of melt models which will fit both data sets is constrained by the upper limit from the Malay-Thailand data and the lower limit from the China data set. This limits the range of possible models, highlighted by the shaded region on Fig. 4.19, to between 5.7 m and 6.6 m. If the reduced China data set information is adopted this range is increased to 5.3-6.6 m. A median model was adopted from within this range, with a eustatic sea-level of depth 6m at 7 kyr (represented by the red line in Fig. 4.15)

Following the method described in Section 4.4.2, the *EUST1* ice model was altered to generate this revised melting pattern, and will be referred to as *EUST3*. Revised sea-level predictions were generated for each data set using *EUST3* and the  $\chi^2$  misfit recalculated. The  $\chi^2$  misfit for the optimum (*melt7m* and *melt5.5m*) and combined (*EUST3*) eustatic models for each data set are shown in Fig. 4.20.

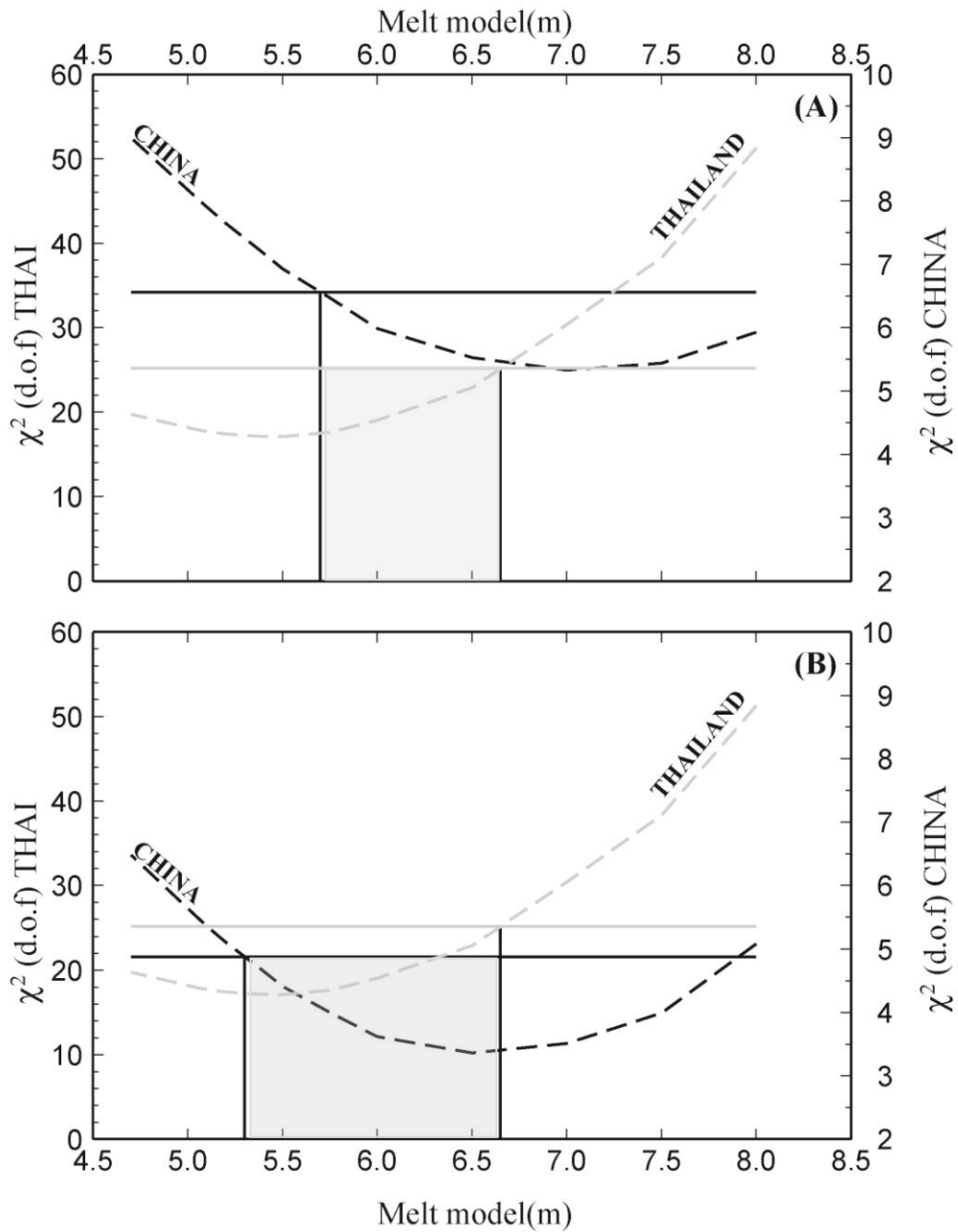


Fig. 4.19: The  $\chi^2$  misfit for the range of melt models considered for the China data (black) and Malay-Thailand data (grey). Results are shown for both the complete China data set (A) and the reduced data set (B). The solid horizontal line marks the location of the 95% confidence limit – models which result in values below this limit are statistically equivalent to 95% confidence. The melt models which satisfy this criterion for both data sets are indicated by the shaded region. Note that different earth models were used to generate predictions for each region (China and Malay-Thailand; see text for details).

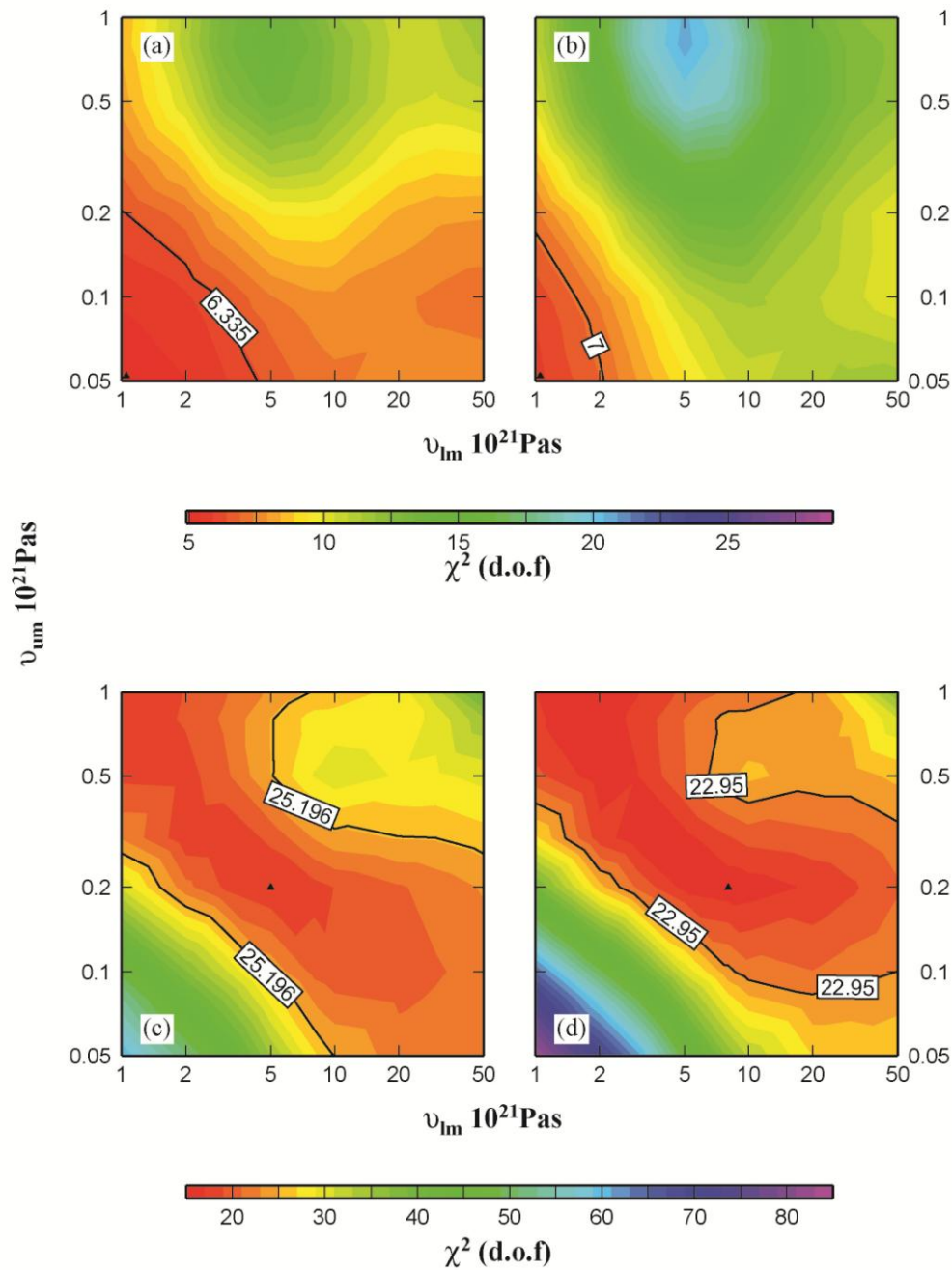


Fig. 4.20: Contour plots of the  $\chi^2$  misfit between predicted and observed sea level data for a range of upper and lower mantle viscosities ( $\nu_{um}$  and  $\nu_{lm}$ , respectively) and a lithosphere thickness of 96 km. The top two frames show results for the complete China data set for eustatic models *melt7m* (a) and *EUST3* (b). The lower frames show results for the Malay-Thailand data set for eustatic models *melt5.5m* (c) and *EUST3* (d). The black line represents the  $\chi^2$  value below which the quality fit is equivalent to a 95% confidence level. The triangle marks the location of the minimum  $\chi^2$  value.

For the China data, there is a slight increase in the  $\chi^2$  minimum between the *EUST3* and *melt7m* models, although both models are a significant improvement from the reference model (see earlier Figs). It is evident that the *EUST3* model provides a tighter bound on the possible earth structure parameters, compared to *melt7m*, ruling out upper and lower mantle viscosities greater than  $1.5 \times 10^{20}$  Pa s and  $2 \times 10^{21}$  Pa s, respectively. The best fit model parameters chosen to fit within the 95% confidence level for both eustatic models are an upper mantle and lower mantle viscosity of  $5 \times 10^{19}$  Pa s and  $1 \times 10^{21}$  Pa s respectively

For the Malay-Thailand data, both revised models are an improvement on the fit achieved using the reference model, with *EUST3* model providing the lower  $\chi^2$  value. Similar constraints on the preferred earth model are inferred from both models, with the optimum region migrating to progressively weaker upper mantle viscosities for each lower mantle viscosity. There is a minor shift with *EUST3*, where upper mantle viscosities less than  $0.8 \times 10^{20}$  Pa s are ruled out. Generally the lower  $\chi^2$  misfit occurs with a combination of an average upper mantle and weak lower mantle, and, hence, the best fit parameters which fit both *melt5.5m* and *EUST3* are an upper and lower mantle viscosity of  $2 \times 10^{20}$  Pa s and  $8 \times 10^{21}$  Pa s respectively.

It is not possible to define an earth model which will fit within the 95% confidence level for both data sets. Possible reasons for this will be discussed in the following section.

Sea-level predictions were generated at each site (Figs. 4.21 and 4.22) for the *EUST3* model and compared to the results for the *melt7m* (China data) and *melt5.5m* (Malay-Thailand data) models. The earth models defined above were adopted in each region.

From Fig. 4.21, both revised eustatic models (*EUST3* and *melt7m*) displays a broadly similar trend in sea-level across the region, with a gradual rise towards present day levels, slightly earlier with *EUST3* (~7 kyr BP compared to ~5 kyr BP) to produce a minor highstand at 5 kyr BP. At most sites there is little difference between the two models from 5 kyr BP onwards. The most noted misfit is between 7-5 kyr BP at HRD where the rate of rise towards present day levels is too fast. As mentioned previously, these SLIPs may be affected by subsidence within the delta and so will sit below the predicted levels. At FP and EG, localised uplift may account for the slightly elevated

levels of SLIPs between 4 kyr and present, which were estimated in a recent study (Pedoja *et al.*, (2008)) to be  $0.18 \text{ mm yr}^{-1}$  and  $0.13 \text{ mm yr}^{-1}$  or a displacement of 0.7 m and 0.52 m, respectively, over the past 4 kyr. Note that at two sites, the *EUST3* predictions produce an improved fit compared to *EUST1* (see earlier Figs.) and *melt7m*: at HP the predicted sea level is close to the present day level from 6.5 kyr onwards; at WG, the cluster of SLI points around 7 kyr BP are captured well. These two sites are considered to be the most tectonically stable (Zong (2004)).

The *EUST3* and *EUST2* models predict very similar patterns across the Malay-Thailand region (Fig. 4.22), with a gradual rise towards present day sea-level at 7.5 kyr, rising to a maximum sea level at ~5 kyr of between 1.5-4 m, followed by a gradual fall towards present. The greatest difference in the predicted sea level between the two models is ~1 m between 7-5 kyr BP. The most marked improvement from the reference model is at sites CP and MAL, where *EUST3* captures both the timing of slowdown and the gradual fall towards present from 5 kyr onwards. This predicted fall is also captured at sites PA, KG and TI, which supports the need for continued melting throughout the late Holocene. There are a few SLIPs which *EUST3* fails to capture: (1) the previously mentioned uniform trend at Phuket (PH); (2) the cluster of points at sites MAL and ET at 5 kyr and 8 kyr, respectively, which display large vertical scatter. Clearly, it is not feasible to create a sea-level prediction which could capture these trends and, as such, this misfit is not considered important.

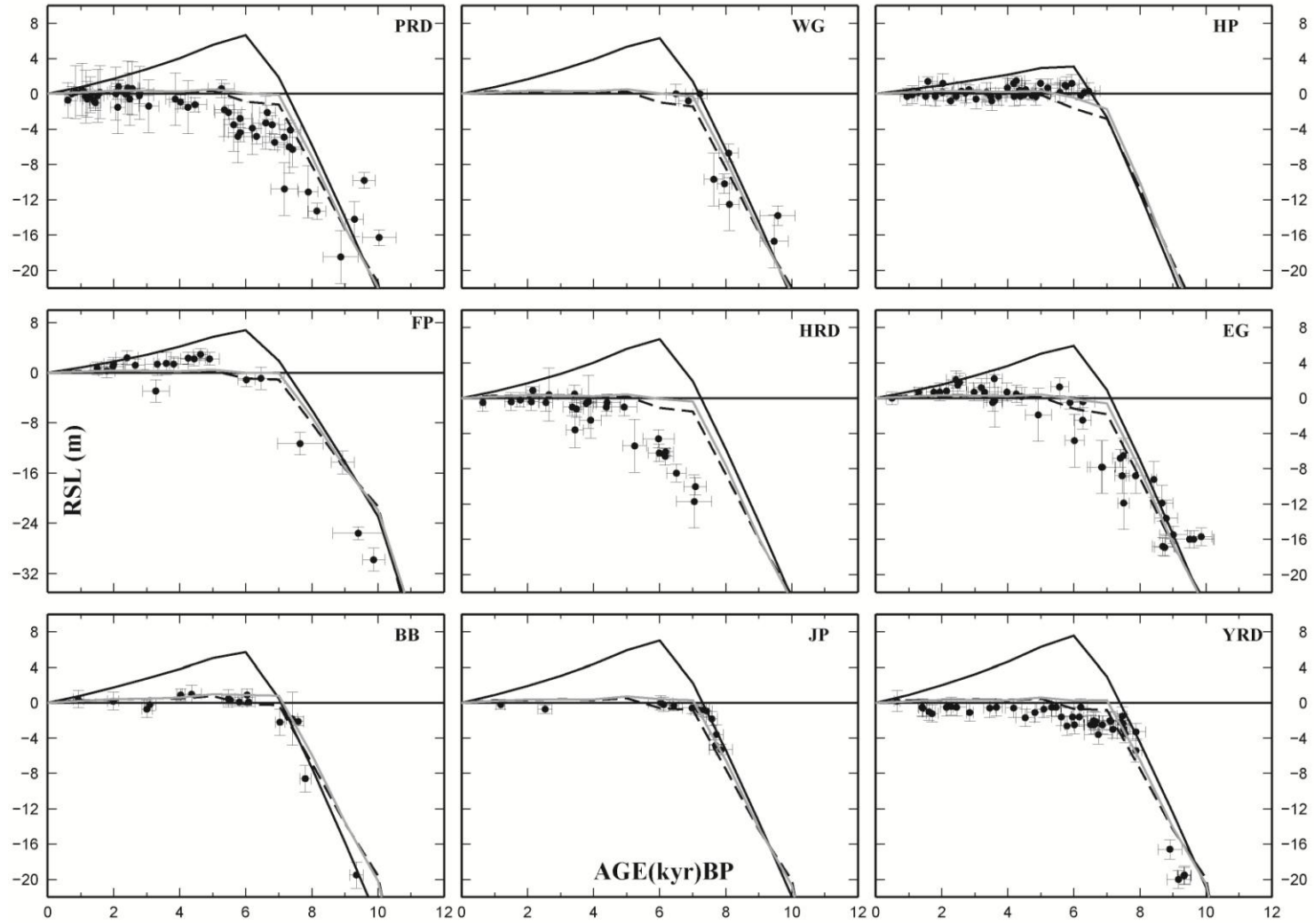


Fig. 4.21: Comparison of the predicted and observed sea levels at each of the nine localities in China. Solid black circles mark the individual SLIPs. The solid black line shows predictions for the reference ice-earth model. Predictions for *melt7m* (dashed black) and *EUST3* (solid grey) were generated for an optimum earth structure inferred from the  $\chi^2$  results presented in Fig. 4.20: lithosphere thickness 96 km, upper mantle viscosity  $5 \times 10^{19}$  Pa s, lower mantle viscosity  $1 \times 10^{21}$  Pa s

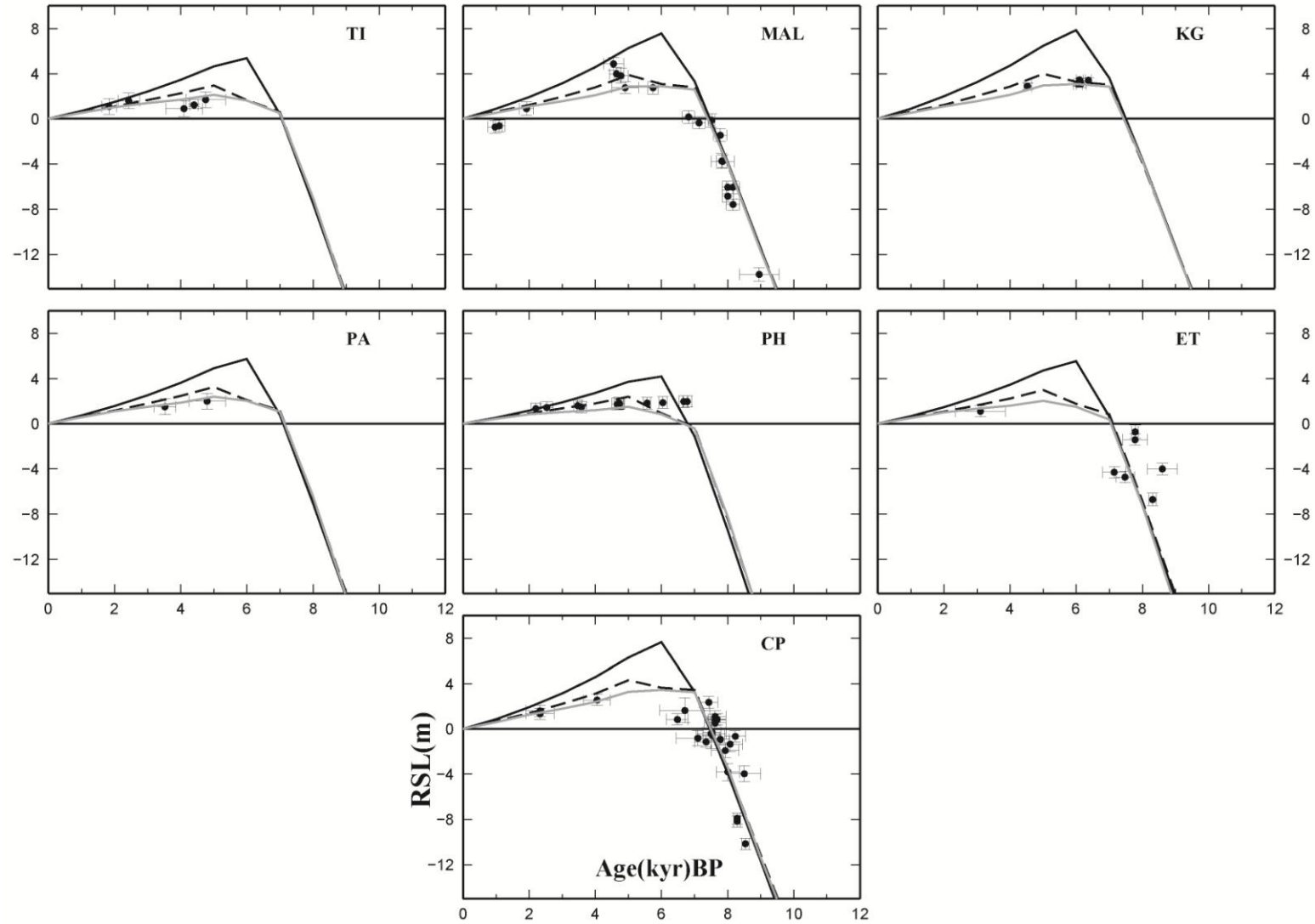


Fig. 4.22: Comparison of the predicted sea level and observations at each of the seven data regions in Malay-Thailand. Solid black circles mark the location of each SLIP. The solid line shows predictions for the starting ice-earth model. Predictions for *melt5.5m* (dashed-black) and *EUST3* (solid grey) were generated for an optimum earth structure inferred from the  $\chi^2$  analysis in Fig. 4.20 (frames c & d): lithosphere thickness 96 km, upper mantle viscosity  $2 \times 10^{20}$  Pa s, lower mantle viscosity  $8 \times 10^{21}$  Pa s

#### 4.5. Discussion

Three new Holocene eustatic models have been developed from the above investigation (shown on Fig. 23); (1) *melt7m* which was optimised to fit only the China data set, (2) *melt5.5m* which was optimised to fit only the Malay-Thailand data. (Both of these models are non-ice corrected) (3) *EUST3* a model produced to fit both the China and Malay-Thailand data using earth models optimised for each region. From Fig. 4.23 the three revised models display a similar pattern and timing of eustatic sea level change, with a notable reduction in the rate of melting over the late Holocene, from maximum of  $0.6 \text{ mm yr}^{-1}$  (*melt7m*) to  $0.21 \text{ mm yr}^{-1}$  (*melt5.5m*). As to be expected *EUST3* forms an intermediate model between these two optimised models.

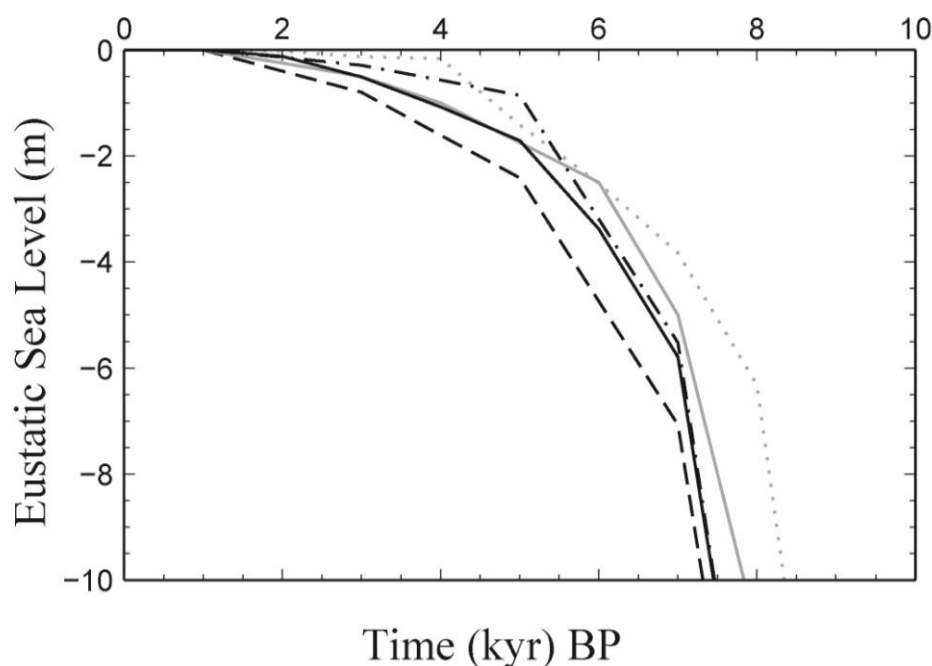


Fig. 4.23: Comparison of the optimum eustatic models inferred in this analysis for each data set (*melt7* – dashed black; *melt5.5* -dashed-dotted black; *EUST3* – solid black) to two published models: ICE-5G model (grey dotted; Peltier 2005) and the model by Lambeck and Purcell (2005) (solid grey; referred to as LP in main text).

Additionally on Fig. 4.23 these three revised models are compared to the two most widely cited global eustatic melt models: (1) *ICE-5G* (Peltier (2004)), (2) a model from the Australian National University group – in this case a recent model published

by Lambeck and Purcell (2005), which will be referred to as *LP* in the following discussion.

The pattern of Holocene global eustatic sea level in the *ICE-5G* model is characterised by a rapid rise to 8 kyr BP, when there is a marked slowdown in the rate of melting. Following a secondary minor slowdown at 7 kyr, there is a continued steady rise until melting ceases at 4 kyr BP. This is the most recent version in a series of models which have been progressively updated to incorporate new information regarding the spatial and temporal history of the major ice sheets, the earth viscosity structure and revisions to the sea-level theory (Peltier (2004), Peltier (1996)). It has been adopted in a wide range of sea-level studies (Peltier (2002)), including the British Isles (Shennan *et al.*, (2002)) and North America (Tarasov and Peltier (2004)) as well as applications in geodetic studies, such as GPS and satellite gravity.

Two key differences between the *ICE-5G* model and the other models shown in Fig. 4.23 is the timing of the initial slowdown in global melting (8 versus 7 kyr BP) and the timing of cessation of global melting (4 versus 2-1 kyr BP). The early timing of the initial slowdown in global melting in *ICE-5G* contradicts the data from both China and Malay-Thailand. For example, at the northern sites in the China data set (BB, JP and YRD), where the slowdown is the earliest of all the data considered in this study, few data points support an initial slowdown prior to 7.5 kyr BP.

Evidence in support of a cessation in global melting at 4 kyr in the *ICE-5G* model is mainly cited from two far-field studies: Nunn and Peltier (2001) and Rostami *et al.*, (2000). In the former, corals microatolls from the Fiji Islands were examined to infer an average sea-level trend for the region. Present day levels were reached initially around 6 kyr BP, with a continued rise in sea-level to a maximum of 1.35-1.5m around 4 kyr BP. As the model produced a reasonable fit to the data, it was argued that no revisions were necessary (and so no need for further melting after 4 kyr). In the latter study, data of varied quality from the east coast of South America was compared to the model and, again, it was argued that no revisions were required. There is wide and abundant scatter in the data, with the model under-predicting the data at a number of sites. Although the sea-level predictions generated a reasonably close match to both of these data sets, there is certainly scope to fit a model with continued melting into the late Holocene given the observational uncertainty.

Cessation of melting at other times prior to present was not considered within the study.

Not all comparisons of the *ICE-5G* model predictions to far-field data have been favourable. For example, in a review of paleoshoreline data from Pacific Islands (Dickinson (2001)), it was noted that predictions using the *ICE4G* model (which has the same Holocene eustatic history as the *ICE-5G* model) over-predicted the height of the highstand measured at Society Islands and French Polynesia by up to 1.6m. Although the model is widely adopted, it does not produce a reasonable fit at all sites, indicating there is room for revision.

The *LP* eustatic sea-level model has been developed by modelling an extensive RSL database from around the coast of Australia (Lambeck and Nakada (1990), Lambeck (2002)) and the Mediterranean (Lambeck and Purcell (2005)). It has been applied in a wide range of global studies (Fleming and Lambeck (2004) Lambeck (1993), Lambeck (1997), Yokoyama *et al.*, (2006), Yu *et al.*, (2007)) highlighting its ability to reproduce the observed sea-level pattern at a wide range of locations. A similar model was obtained in a study that considered a wider global data set (Fleming *et al.*, (1998)) including Africa, Barbados and Malaysia. Earlier studies (e.g. Nakada and Lambeck (1989)) used spatial differences in observed sea-level highstands to separate model sensitivity to earth and ice melt parameters – thus reducing parameter trade-off and arriving at a more robust solution. This is a notably different method as was used in the development of *ICE-5G*. Although a recent study has demonstrated that the resolving power of differential highstands to constrain mantle viscosity is relatively poor (Kendall and Mitrovica (2007)), the utility of the method in reducing parameter trade-off is sound.

The results of the earlier studies (e.g. Nakada and Lambeck (1989)) have been refined in the past few decades (e.g. Lambeck (2002), Lambeck and Purcell (2005)) to arrive at the model shown in Fig. 4.23. The model is characterised by a steady rise in eustatic sea-level until a staged slowdown in the rate of melting at 7 and 6 kyr BP. From 5 kyr onwards eustatic sea level rises steadily at an average rate of  $0.63 \text{ mm yr}^{-1}$  until 1 kyr BP, which is similar to the rates and timings of *EUST3* ( $0.68 \text{ mm yr}^{-1}$ ) and *melt5.5m* ( $0.64 \text{ mm yr}^{-1}$ ). Although the chronology of melting is similar in *melt7m*, the amount of eustatic sea level rise is markedly greater than in the *LP* model.

In the LP model, the source for the continued melting into the late Holocene was attributed to the AIS and mountain glaciers. For the three eustatic models developed here, the overall total global eustatic sea level rise over the past 10 kyr was fixed and the deglaciation of the LIS completed by 5 kyr. To recreate this continued rise in eustatic sea level until 1 kyr, the AIS deglaciation history was altered and it is therefore important to compare evidence in support of this late Holocene deglaciation of the AIS.

The AIS can be divided into three main ice regions, which underwent highly variable and desynchronised retreat patterns - detailed in a number of recent studies (Anderson *et al.*, (2002), Bentley (1999), Ingolfsson *et al.*, (1998), Sugden *et al.*, (2006)). These areas are: marine based West AIS (WAIS) (including glaciers feeding the Weddell Sea, Central and Eastern Ross Sea), land based East AIS (EAIS) and the Antarctic Peninsula ice sheet (APIS).

As the main period of deglaciation of the APIS and EAIS ended by 7 kyr BP (Bentley *et al.*, (2006), Ingolfsson *et al.*, (1998), Mackintosh *et al.*, (2007), Sugden *et al.*, (2006)), it is unlikely that these ice regions contributed significantly to the late Holocene eustatic sea level rise. For instance, the main documented activity between 5-2 ka for the APIS is local ice rafting from small ice shelves with the Prince Gustav Channel (Pudsey and Evans (2001)), with estimations of the total contribution to eustatic sea-level rise less than 1.7m (Evans *et al.*, (2005)), while the EAIS was undergoing localised advances and retreats (Anderson *et al.*, (2002), Bentley (1999), Ingolfsson *et al.*, (1998)). Therefore, this leaves the WAIS as the most likely source for continued melting into the late Holocene.

A full study of the extensive range of geomorphological onshore and offshore features supporting a late Holocene deglaciation of the WAIS is beyond the scope of this study, but the most recent evidence is summarised in Sugden *et al.*, (2006). Three regions of the ice sheet are thought to have contributed to eustatic sea level during the mid-to-late Holocene: (1) Marie Byrd Land mountains, which fed outlet glaciers, such as Pine Island Bay glacier draining into the Amundsen Sea; (2) Ross Ice Shelf and Ross Sea; (3) Weddell Sea and Ellsworth Mountain. The reader is referred to the above article for more information.

Cosmogenic dating ( $^{10}\text{Be}$ ) of exposed peaks (glacially eroded boulders) within the Ford mountain ranges, Marie Byrd Land, has been used to infer thinning and retreat of the ice sheet by over 700m, continuing until at  $\sim 2.4$  kyr BP, with a reduction of 30-40km in the grounding line extent over the last 3500 yrs (Stone *et al.*, (2003)). This region of activity shows similar timing and pattern to a number of outlet glaciers, the Pine Island, Pope and Smith, whose thinning rates were estimated at between  $23 \pm 2$  mm yr $^{-1}$  (over 14.5 kyr) and  $38 \pm 3$  mm yr $^{-1}$  (4.7 yrs) respectively. (Johnson et al, 2008) There was no record of ceasing in thinning or recession but with activity continuing till present day

The Ross Sea and Ross Ice Shelf are fed by glaciers draining from both the EAIS and WAIS. The contribution from glaciers draining the EAIS ended between 8.3-6.5 kyr BP (Bentley (1999), Hall *et al.*, (2004), Ingolfsson *et al.*, (1998)), which contrasts markedly with the noted continued thinning and retreat from the WAIS regions. In one recent model of the AIS, it is suggested that after 6 kyr BP (end of the retreat of the EAIS) and stabilisation of surrounding environmental forcing, the WAIS developed its own internally controlled dynamics, which aided this continued retreat throughout the Holocene (Huybrechts (2002)). Some studies (Conway *et al.*, (1999), Pollard and Deconto (2009)) suggested that the grounding line (which marks the boundary between the ice shelf and the ice sheet) retreated across the Ross Ice Shelf, throughout the Holocene, reaching Roosevelt Island by 3.2 kyr BP and from there retreated towards its present day position. Although other studies have suggested a more complex pattern for retreat (e.g. Anderson *et al.*, (2002)) most evidence supports continued thinning and retreat.

The above studies highlight some of the observational evidence in support of continued melting from the AIS. Ivins and James (2005) published a revised AIS ice load model (IJ05), which was constrained by new published information on the glacial history and data of the present-day mass balance, and supports the view that the WAIS contributed to global eustatic sea-level rise until present day. Between 11.5-7.6 kyr BP, the eustatic sea-level rise resulting from this AIS deglaciation was estimated at 1.75 mm yr $^{-1}$ , with a marked order of magnitude reduction after 3.2 kyr BP (0.23 mm yr $^{-1}$ ). This rate is comparable to the rate estimated from *EUST3* between 10-7 kyr, at 1.6 mm yr $^{-1}$ , with a similar order of magnitude reduction after 3 kyr observed in the

model ( $0.36 \text{ mm yr}^{-1}$ ). Although note that the rate for the earlier period includes a contribution from other ice sheets.

Another widely used method to infer ice sheet deglaciation patterns is glaciological ice sheet models. Huybrechts (2002) published a 3D glaciological (thermomechanical) model which reproduced the growth and retreat of the AIS throughout the last glacial cycle forced by realistic climatic and environmental factors. Under these conditions it was found that the WAIS continued to melt throughout the late Holocene, with a total contribution to eustatic sea level of  $\sim 4.3 \text{ m}$  over the last 4 kyr.

The three new eustatic models are characterised by a specific chronology of Holocene eustatic sea-level change. Predictions based on the *EUST3* model show a distinct slowdown around 7 kyr BP and a marked highstand reached 7 -5 kyr BP at most sites. In the following, other far-field sea-level data and additional datasets from the study region are examined to determine if they are consistent with the new *EUST3* model.

Dickinson (2001) reviewed a range of paleoshoreline data from sites across the Pacific Ocean to infer that the maximum sea-level reached between 5-4 kyr BP ranged from between 2.8-3.1m on Marianna Islands to 2m on Fiji. A reconstruction of the average sea-level trend from the Western Indian Ocean (volcanic islands including Mauritius, Comoros, Reunion, Seychelles, Madagascar) by Camoin *et al.*, (2004) and Central and Eastern Indian Ocean (Woodroffe (2005)), found little evidence for Holocene sea levels lying above present day levels. The variation in predicted sea-level using *EUST3* across the Pacific and Indian Ocean over the last 7 kyr is broadly consistent with these data constraints. Fig. 4.24 illustrates one example time slice, at 4 kyr BP, where sea level has risen to over 1.25 m across Pacific Ocean, and generally remains below 0 m within the Indian Ocean. Following this, sea level was found to rise slightly within the Indian Ocean, but remained less than 0.25 m (within the limits of the observational data).

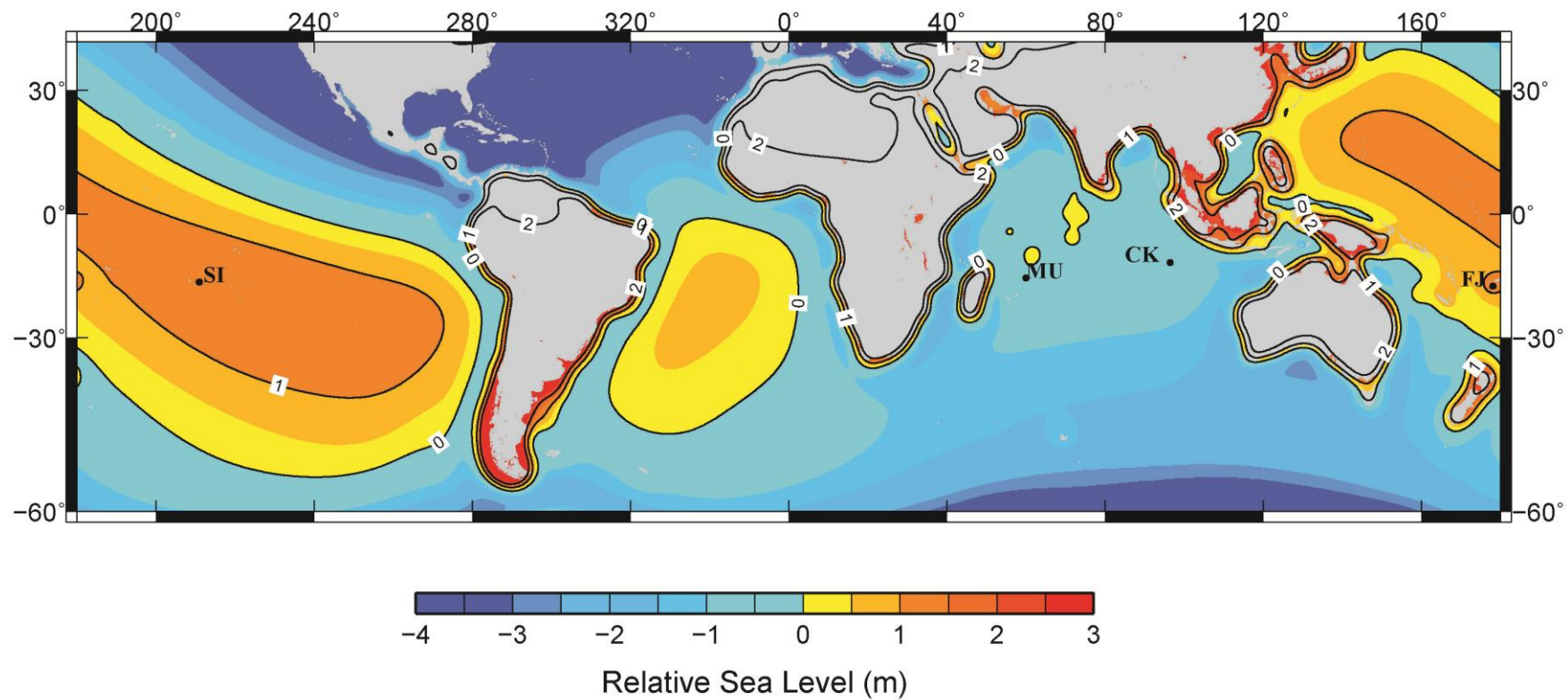


Fig. 4.24: Contour map of relative sea-level at 4 kyr BP using the *EUST3* ice model and the reference earth model. Sites mentioned within the text are labelled as follows: FJ – Fiji Islands, CK – Cocos Keeling Islands, MU- Mauritius, and SI – Society Islands.

The chronological pattern of melt slowdown in *EUST3* is supported by additional studies from across the study region. Yu *et al.*, (2002) investigated the growth of corals at Leizhou Peninsula, South China Sea (close to the WG data locality) and estimated the timing of slowdown in sea-level rise between 7.2-6.7 kyr BP. Radiocarbon dating of plant matter and shells from sites around Hong Kong were combined with additional sedimentological and paleontological evidence to infer that sea level initially reached present day levels between 8-6 kyr BP (Yim (1999)). Bird *et al.*, (2007) radiocarbon dated samples from mangrove swamps to produce a new sea-level curve for Singapore, covering the period 9.5-6.5 kyr BP. The data set covers a time period and data location (southern edge of the Strait of Malacca, between sites MAL and TI) where as previously mentioned there is a lack of data. In this reconstruction, present day sea level is reached initially at ~ 7 kyr following a staged rise and remained constant between 7.7-7.3 kyr BP. Predictions using *EUST3* from the nearby sites correlate well with the observed trend. However, the noted inflection interpreted from these data is not recreated by *EUST3*.

Both study sites are located within the Eurasian plate and close to active subduction zones, illustrated on Fig. 4.25. Along the eastern coast of China the Pacific plate and Philippine sub-plate subducts below the Eurasian plate. The Sunda arc bounds the lower limit of the study region, where the Indo-Australian Plate subducts below the Eurasia plate, close to the Malay-Thailand data sites. Despite the similar tectonic setting of the two study areas, the region around the coast of China appears a more geodynamically complex zone than across the Malay Peninsula. This may account for the notably different optimum earth structure inferred below China, compared to Malay-Thailand, of a very weak upper and lower mantle viscosity

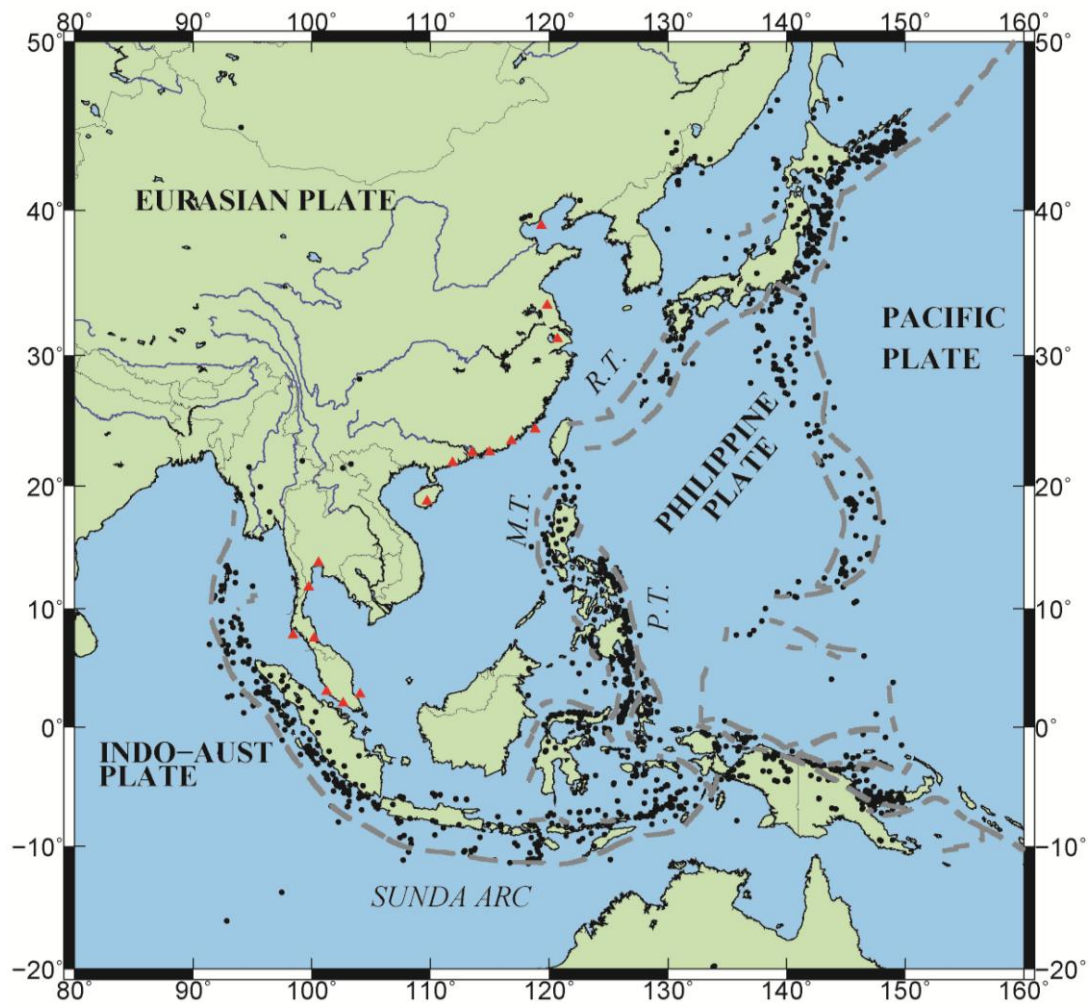


Fig. 4.25: Map illustrating the location of the major plate boundaries and subduction zones across the study region: R.T – Ryukyu trench, M.T. – Manila trench, P.T. – Philippine trench. Red triangles mark the average longitude/latitude location of each data locality. Black circles highlight some recent earthquakes of magnitude 5 and greater. (Sourced from <http://neic.usgs.gov/neis/epic/epic.html> )

Subduction zones define dynamic plate margins where cold oceanic lithosphere subducts into the hot, weaker oceanic mantle. Consequently, the complex geodynamic processes active at such margins affects the surrounding mantle viscosity. There are a range of methods used to estimate the mantle viscosity within these regions. For example, Hirth and Kohlstedt (2003) used flow law parameters for olivine to estimate a mantle wedge viscosity of  $\sim 10^{18}$  Pa s; with the viscosity of the adjacent upper mantle between  $10^{18}$  -  $10^{22}$  Pa s, depending on the choice of strain rate (deformation mechanism). Numerical models of subduction zones generally adopt a background upper mantle viscosity between  $10^{20}$ - $10^{21}$  Pa s (Billen and Hirth (2005), Winder and Peacock (2001)), and have highlighted the development of weaker, lower viscosity regions with the mantle wedge, surrounding the subducting slab and extending into the back-arc region (Billen (2008), Currie and Hyndman (2006)). This reduction in viscosity has been associated with the addition of water and partial melt from the subducting slab and associated small scale convection (Billen (2008), Currie and Hyndman (2006)). Estimates of viscosity within these regions range between less than  $10^{18}$  -  $10^{19}$  Pa s. In a recent GIA study near the Cascadia subduction zone in the north east Pacific (James *et al.*, (2009)) found that to fit the sea-level observations a weak upper mantle viscosity was required, with optimum values constrained to lie between  $5 \times 10^{18}$  to  $5 \times 10^{19}$  Pa s. The upper limit is close to the value inferred above for the China region.

The Sunda arc - the closest active subduction zone to the Malay Peninsula - is defined as a classic convergent margin (Kopp *et al.*, (2002)) and has been analysed to infer many of the general characteristics of such active plate margins. Many studies analysing the upper mantle and crustal structure using seismic data have identified the lithospheric slab penetrating to depths greater than 1000 km (Widiyantoro and Vanderhilst (1997), Widiyantoro and Vanderhilst (1996), Puspito and Shimazaki (1995)). Although the subducting slab of the Philippine plate has been imaged using seismic tomography along the northern coast of China (Lebedev and Nolet (2003)), additional seismic anomalies were found within the upper mantle structure, creating a more complicated shallow earth structure than that associated with the Sunda Arc below the Malay Peninsula. For instance, seismic imaging of the active orogeny around Taiwan due to the interaction of the Ryukyu and Osaka trench have highlighted low velocities (high temperatures and therefore low viscosity values) within the crust and upper mantle. Recent tomography studies have imaged the Pacific slab below China

and suggest that it flattens or deflects near the mantle transition zone, without penetrating into the lower mantle (Ai *et al.*, (2008)). A weak, ductile lower crustal layer, with an estimated viscosity of  $\sim 10^{18}$  Pa s (Clark *et al.*, (2005)), has been identified below the Tibetan Plateau and mainland China and is thought to continue offshore below the China Sea. In addition, seismic images of the crust and upper mantle below the North China Craton, produced by inverting teleseismic data, have suggested a thinner lithosphere below the eastern edge of the craton (close to the coast) and that the continued subduction across the region generates asthenospheric upwellings into the upper mantle (Tian *et al.*, (2009)). The most pronounced feature supporting a weaker region within upper earth structure was imaged below the south-east coast and Hainan Island, extending from the surface to depths of up to 900km (Lebedev and Nolet (2003), Lei *et al.*, (2009)) and is generally referred to as the Hainan Plume.

In a recent review which summarised the most recent constraints on the mantle below China (Zang *et al.*, (2008)), a degree of partial melt at a depth of 410 km was identified and attributed to high conductivity and low viscosity values ( $1.2 \times 10^{18}$  Pa s and  $3.6 \times 10^{19}$  Pa s), estimated for the lower crust and upper mantle, respectively. Using seismic data, basin geometry and subsidence modelling, Clift *et al.*, (2002) concluded that the continental slope of the South China Sea is underlain by a low viscosity layer, between  $10^{18}$ - $10^{19}$  Pa s.

The above constraints give support to the low viscosities inferred from the China data. They also highlight that the earth structure below China (and, to a lesser extent, Malay-Thailand) has significant lateral structure and so the application of a 1-D earth model is limited.

#### **4.6. Conclusions**

Using two previously un-modelled data sets from China and Malay-Thailand, a revised model of late Holocene eustatic sea-level was developed (*EUST3*). This model is characterised by: (1) an initial slowdown in the rate of eustatic sea level rise at 7 kyr, (2) subsequent decelerations at 5 and 3 kyr, (3) a steady rise between 3 kyr and 1 kyr at an average rate of  $0.36 \text{ mm yr}^{-1}$ . It is suggested, based on a variety of evidence,

that the most likely source for the continuing rise in eustatic sea-level in the late Holocene is the WAIS.

The model was compared to two previously published models, *ICE-5G* and *LP*, and found to be more consistent with the overall characterises of *LP*, where eustatic sea level rises steadily until a staged slowdown in the rate of melting at 7 and 6 kyr BP. From 5 kyr onwards eustatic sea level rises steadily at an average rate of  $0.63 \text{ mm yr}^{-1}$  until 1 kyr BP, which compares to an average rate of  $0.68 \text{ mm yr}^{-1}$  in *EUST3*.

Examining the  $\chi^2$  misfit between the observed and predicted sea level for each data set identified a distinctly different optimum earth viscosity structure. Both data sets were relatively insensitive to variations in lower mantle viscosity but prefer markedly different upper mantle values. For China the best fit is achieved with a weak upper mantle, less than  $2 \times 10^{20} \text{ Pa s}$  (for the complete data set), compared to Malay-Thailand data, where a stronger mantle, greater than  $2 \times 10^{20} \text{ Pa s}$  is preferred. It is thought that this difference is related to distinct lateral variations with the upper earth structure below China, associated with the nearby active subduction zones and the Hainan Plume.

## **Chapter 5: An improved Glacial-Isostatic Adjustment model for the British Isles**

### **5.1. Introduction**

Many past studies have investigated the glacial isostatic adjustment (GIA) across the British Isles by modelling the comprehensive relative sea-level (RSL) database for this region (e.g. Johnston and Lambeck (2000), Lambeck *et al.*, (1996), Peltier *et al.*, (2002)). These studies have led to constraints on various model components including the regional ice sheet history, viscoelastic earth structure, and the global meltwater signal. The GIA sea-level models that have been developed through comparison to the British Isles RSL database play an important role in our understanding of past and present sea-level changes as well as our ability to predict future changes through the influence of vertical land motion on predictions of mean sea-level change (e.g. Lowe *et al.*, (2009)). Recent studies have demonstrated that GIA is the dominant contributor to long-term (century to millennial) vertical land motion in the UK region (e.g. Teferle *et al.*, (2009); Bradley *et al.*, (2009) ).

Despite significant improvements in the GIA models for the region, there remain significant differences in the quality of model fits to the expanding RSL database (Shennan *et al.*, (2006)). In addition, earth model parameters inferred in different studies are not consistent (e.g. Milne *et al.*, (2006)). These discrepancies are due to differences in model configuration and the complex non-monotonic form of RSL change in northern parts of Great Britain. Although the BIIS was small compared to the other major ice sheets during the last major glaciation, it still produced a substantial local isostatic signal which is recorded in elevated shorelines (Smith *et al.*, (2006)) and past sea-level records (Brooks *et al.*, (2008), Shennan *et al.*, (2006)). Nevertheless, it is the relatively small size of the BIIS which results in a complex sea-level history because the local isostatic-driven sea-level fall is similar in magnitude to the rise associated with the melting of non-local ice sheets. As discussed in previous articles (e.g Lambeck (1993a), Lambeck (1993b)), it is the change in the dominance of the signals associated with these processes that results

in the complexity of the observed RSL changes and the sensitivity of the predictions to both local and non-local model parameters.

The interplay between local and non-local signals is illustrated for three sites in Fig. 5.1, where the total predicted sea level is separated into the contribution due to the BIIS only and the contribution from all other ice sheets (abbreviated to non-local). The three sites shown were selected to highlight the north-south variation in the character of the RSL signal. From Fig. 5.1 it is evident that there is little spatial variation in the non-local ice signal (grey curve), compared to the progressive decrease in the magnitude of the BIIS signal (dotted curve) with increasing distance away from the centre of ice loading (compare site 17, Forth Valley to site 50, Hampshire). This results in the total predicted relative sea-level signal at localities across Scotland being equally sensitive to the BIIS and non-local ice sheet signal (as seen at site 17, Forth Valley), compared to the southern sites (such as site 50, Hampshire) where the non-local signal is the dominant contribution. Note that a Holocene RSL highstand is only predicted at sites where the local signal contributes to a fall in RSL that is larger than the rise due to non-local processes (e.g. Lambeck (1993a)).

The complexity of the British Isles RSL signal and the sensitivity of the predictions to local and non-local ice and earth parameters means that it is difficult to fit the data (particularly from Scotland) and to obtain a robust solution due to the trade-off between parameters. Achieving a high quality and well-constrained solution requires the consideration of data that provide information that is complementary to that obtained from the RSL data. For example, field information can be used to constrain the lateral and vertical extent of the BIIS preceding, during, and following the last glacial maximum (LGM); also, far-field RSL data can be used to constraint the melt history of the non-local ice sheets. The accuracy of this complementary information is a crucial component for addressing the British Isles GIA problem.

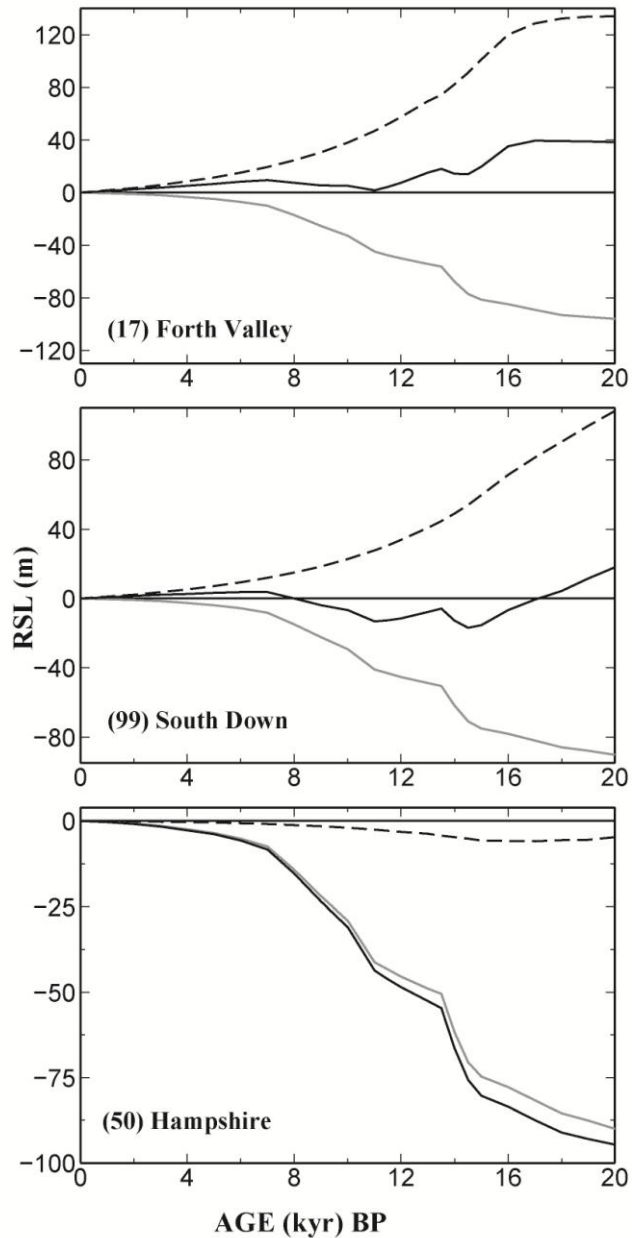


Fig. 5.1: Predictions of relative sea level at three selected sites (17, 99 & 50; see Fig. 5.2) using the best-fitting ice and earth model from this analysis (see text for more information). The total signal (solid black line) is separated into the signal due to non-local ice (grey line) and the local British–Irish ice sheet (dotted black line). Note that the influence of ocean loading and GIA-induced perturbations in earth rotation associated with each of these two ice model components is included in the predictions.

A primary contribution of this study is the comprehensive nature of the complementary constraints applied to supplement the information provided by the British Isles RSL data. Regarding the local BIIS model, the recent reconstruction described in Shennan *et al.*, (2006) and Brooks *et al.*, (2008) is adopted. The development of this model is outlined in much greater detail in Chapter 2, with the final model adopted described in Section 2.4.3. This reconstruction is an update of an earlier model to include a number of recent field observations on the extent of the ice sheet and also takes into account the underlying topography (Milne *et al.*, (2006)). The eustatic model, or melt history of the non-local ice sheets, is the combination of results from two recent studies: the eustatic model of Bassett *et al.*, (2005) for the period LGM to the end of the Lateglacial and the extension of this model (referred to as *EUST3* model in Section 4.4.5 and Bradley *et al.*, (2010)) to constrain the melt volume during the Holocene (see Section 5.3.1 for more details). The background to the development of this model is given in greater detail in Chapter 4. Constraints on local earth viscosity structure obtained from Global Positioning System (GPS) observations of vertical land motion are also considered to provide an independent control on this model component (see Bradley *et al.*, (2009) and Chapter 3). As demonstrated in this previous study, the GPS data are relatively insensitive to uncertainties in the local ice model and so provide a robust constraint on local earth viscosity structure. This constraint is adhered to in seeking a fit to the RSL data in the Section 5.3.3.

A second important aspect of this study is the consideration of RSL data from Great Britain and Ireland, which is outlined in Chapter 2, Section 2.2.3. Indeed, this is the first GIA modelling study that considers the entirety of RSL data from both islands. The data from Ireland are taken from the recent compilation by Brooks and Edwards (2006) that were used in the modelling study of Brooks *et al.*, (2008). Given the proximity of these two islands, and the fact that the ice sheets originating on each interacted with each other, it is perfectly logical to combine these two RSL data sets and seek a solution that is compatible with both.

In essence, this study brings together elements from a number of recent papers on GIA in Great Britain and Ireland (Bradley *et al.*, (2009), Brooks *et al.*, (2008), Milne *et al.*,

(2006), Shennan *et al.*, (2006)) and combines the final results from each of the preceding Chapters: A revised BIIS model and updated global ice model, *EUST3* from Sections 2.4.3 and 4.4.5 respectively and incorporates the constraints on the optimum local earth structure from Section 3.3. The best-fitting model presented below can be considered as the culmination of these previous efforts in terms of seeking a GIA model that is compatible with a variety of observations from Great Britain and Ireland.

## **5.2. Relative sea-level data**

The sea-level data employed in this study were reconstructed from field evidence that was interpreted using geological models and radiocarbon age models. These reconstructions comprise a database of 80 sites, including those from Shennan *et al.*, (2006) for England, Scotland and Wales, and Brooks and Edwards (2006) for Ireland (Figure 5.2 and Appendix A). In total, there are 1169 primary sea-level index points (SLIPs), separated into 414 primary and 755 intercalated. Additionally, there are 15 secondary SLIPs and 355 limiting data (primary and secondary), these terms are defined in the following two paragraphs. Significantly, there are fewer data points across Ireland compared to Great Britain, and the majority of the latter are from south and east England.

The criteria used to define the data classifications mentioned above has been described in past studies (Brooks *et al.*, (2008), Shennan *et al.*, (2006), Shennan and Horton (2002)), therefore only a brief summary is given here. For a data point to be a SLIP, information regarding the following is required: location (longitude and latitude), age (defined in calibrated radiocarbon years), present elevation, and the indicative meaning. The indicative meaning of a given dated marker defines its vertical relationship to a chosen contemporaneous tide level. Most index points have a reference water level at or close to mean high water of spring tides. These data points are the most useful for constraining model predictions as they provide quantitative estimates of past relative sea-level with clearly defined height and age ranges. At sites across Ireland, a data sample was classified as a secondary SLIP when the indicative meaning was less well quantified (Brooks and Edwards (2006)). When it is not possible to define a quantitative relationship between the field evidence and the contemporaneous tidal regime, the sea-level information obtained is classified as a limiting date. A limiting date is defined as either a

primary point when the source environment can be defined (such as from a freshwater peat and therefore a maximum constraint on relative sea level) or a secondary point if the environment of formation is unclear or contested.

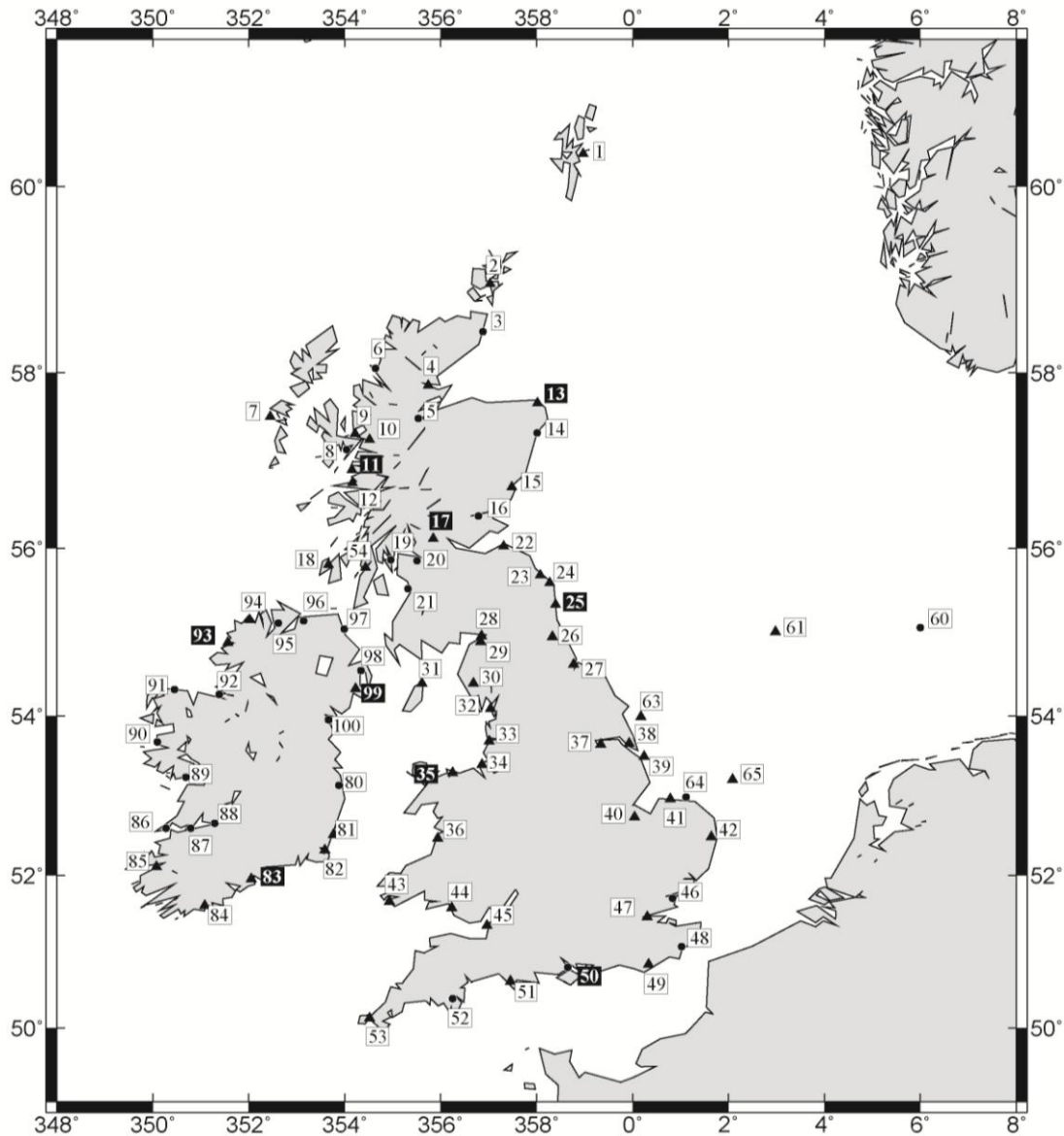


Fig. 5.2: Map showing the locations of the 80 data localities used in this study. The black triangles mark the locations of sites where primary and intercalated sea level index points have been obtained; the black circles mark sites with only intercalated sea level index points or other data points that provide a less precise constraint on sea level have been obtained. See Appendix A for a listing of all the data. Data and model predictions from sites labelled with white numbers in black boxes are shown in the main text. Data and model predictions for all sites are shown in Appendix G.

When using SLIPs it is important to consider the additional local scale processes within the coastal system that may affect the reliability of the data point, such as compaction or consolidation. SLIP samples taken from thin basal peats or the base of basal peats shown to have formed under a tidal influence (referred to in the database as primary SLIPs) provide the most accurate measure of sea-level change, as they are deposited over a hard substrate and as such, are not affected by sediment consolidation. Intercalated SLIPs, on the other hand, form within clay, silt and peat sequences, which may have been compacted or consolidated, and as such, may result in the palaeo sea-level marker being displaced lower over time. Within the Great Britain database, the 1107 primary SLIPs were further divided based upon these criteria into two smaller subsets; those which are taken from either basal peat layers or a sediment horizon that was considered to be unaffected by consolidation or compaction (referred to as basal points within Appendix A) and those classed as either an intercalated SLIP or from a sample which may provide a less precise constraint on the observed sea-level (referred to in Appendix A as intercalated points). The first subset, basal points, will be examined separately later within this study.

An additional factor to consider is long term variations in tidal regime, which may result in variations in the estimation of the indicative meaning, due to changes in the reference water level through time (Shennan *et al.*, (2003), Shennan and Horton (2002), Uehara *et al.*, (2006)). At present, palaeo-tidal corrections have only been applied to five localities within the database (as indicated in Appendix A), but other sites where changes in tidal regime maybe important include areas with presently large tidal ranges, such as sites 28, North Solway; 29, South Solway; 32, Morecambe Bay; 45, Bristol Channel and 47, Thames.

Fig. 5.3 shows reconstructed sea-level change at a subset of nine localities which were chosen to illustrate the variation in the character of the sea-level signal across the study region and the range of available sea-level data types, as described above, within the database. Note that the complete data set is shown in the Appendix G.

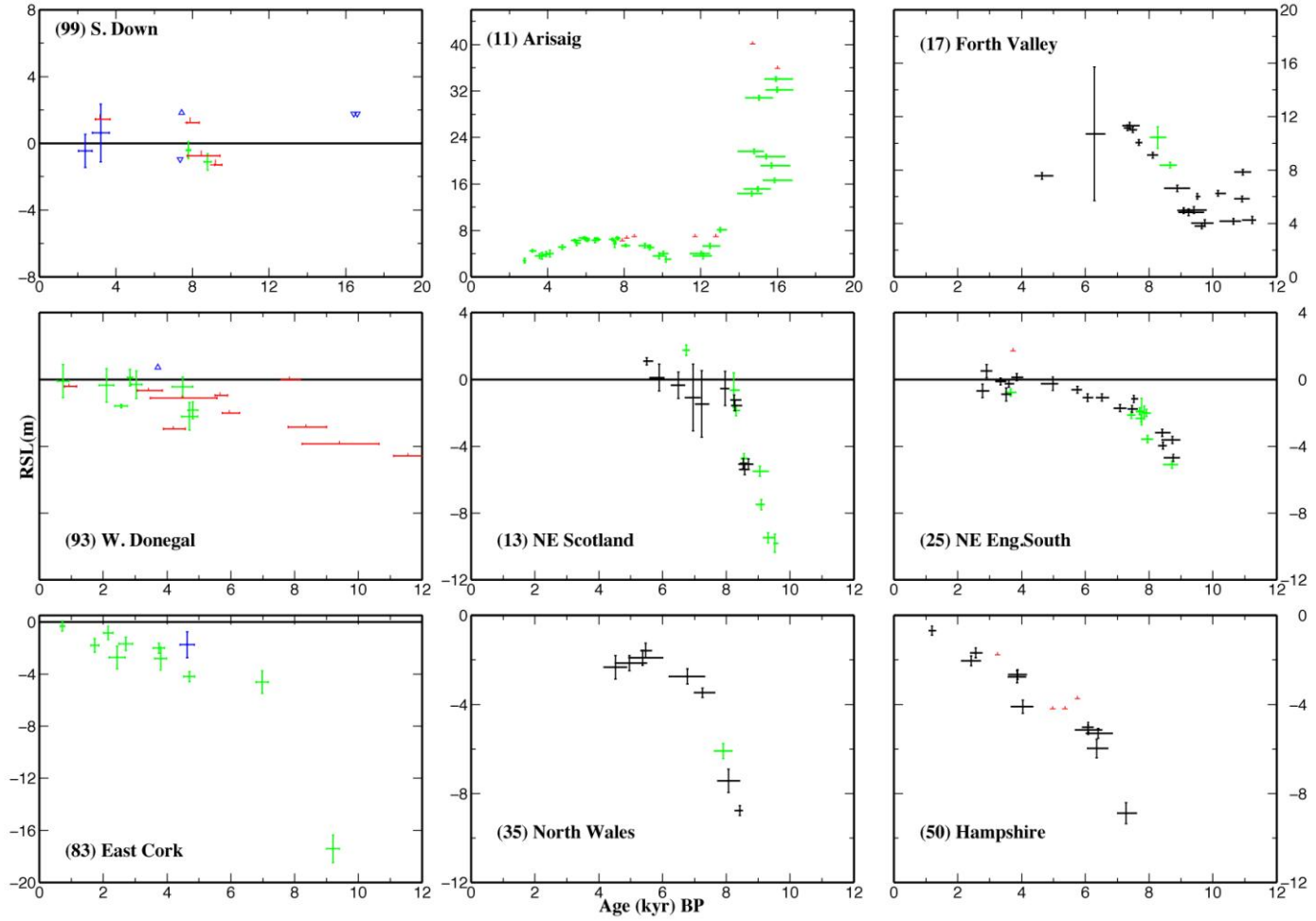


Fig. 5.3: Observed sea level at nine locations across the study region. Symbols for the observed data are summarized within the text and Appendix A. Note the varying scale between each plot

Site 13, N.E. Scotland, located on the eastern coast of Scotland is the most northern site displayed in Fig. 5.3. This sea-level record, composed of a mixture of primary and intercalated SLIPs, typifies the characteristic trend of data from the NE coast and highland regions of Scotland, with a rise from below present, -10 m at ~ 9.5 kyr, to form a small highstand of amplitude ~ 1m at ~ 5.5 kyr BP. Sites 11, Arisaig and 17, Forth Valley display the typical record of sites situated close to the centre of ice sheet, with sea level elevated above present, during and following the deglaciation period. As discussed above, the signal recorded in these northerly data is sensitive to both local and global processes. Site 11, Arisaig situated on the NW coast of Scotland, contains the longest and most complete record, with over 16 kyr of data composed entirely of primary SLIPs. The sea level record is characterised by a fall from 34 m at ~ 16 kyr BP, with noted data gaps over the observed timings of meltwater pulse 1A at 14 kyr BP and between 12 - 11 kyr BP, reaching a minimum of 3 m at ~ 10 kyr BP. Following this, sea-level rises gradually towards a late Holocene highstand of magnitude ~ 6.5 m between 6 -7.5 kyr BP, before falling towards present day levels. Although the data record at site 17, Forth Valley is shorter than at site 11, Arisaig and composed of a mixture of both primary and intercalated SLIP, the observed trend over the majority of the Holocene is similar, with sea-level rising to produce the highest Holocene highstand in the entire study area of 11.5 m at 7.5 kyr BP. This site is inferred to be very near to the area of maximum ice thickness, and as such, should record the maximum uplift following the deglaciation of the BIIS.

Even though there is a noted paucity of primary index points along the NE coast of Ireland (only two at site 99, South Down), limiting data and secondary SLIPs, when combined with additional field evidence such as raised shorelines, can be used to provide a useful constraint on the general pattern of sea-level change over the late Devensian.

(The term Late Devensian refers to the time interval extending from the Ålesund interstadial, ~ 33 kyr BP, to the start of the Holocene, ~ 11.5 kyr BP). This is especially useful in areas such as Ireland where there are a restricted number of SLIPs both in space and time. A major feature observed at sites along this coastline, compared to the NW, is the evidence for sea-level significantly elevated above present over the late Devensian, where raised beaches have been found up to 25-30 m above present (Brooks *et al.*, (2008)). Producing these elevated sea levels in past studies has been a noted problem.

Site 99, South Down displays the typical pattern of sea-level change from around this region. At 16 kyr BP, constrained from the limiting data, sea-level falls a minimum of + 2m to produce an unconstrained lowstand, before rising again to initially reach present day levels at ~ 8 kyr BP. The subsequent changes are poorly constrained, but it is likely that sea level rose above present between ~ 8 – 4 kyr BP to be followed by a fall towards present day level as indicated by the secondary SLIPs at ~ 2 kyr BP.

Sites 25, N.E. England South; 35, North Wales; 93, West Donegal and 99, South Down typify the pattern of sea level change across the central region of the British Isles (NE and NW England and Northern Ireland) where there is a transition from sites with a small or minor Holocene highstand (sites 25, N.E. England South; 99, South Down and 93, West Donegal) to sites where RSL is below present throughout the late Holocene (site 35, North Wales). The location of this transition (often referred to as the zero isobase) is inferred to fall between sites 25, N.E. England South and 27, Tees along the NE coast and 33, Lancashire and 35, North Wales along the NW coast of England and close to sites 93, West Donegal and 80, Dublin along the NW and NE coasts of Ireland. Data from these sites exhibited consistent discrepancies compared to predictions in past studies (Brooks *et al.*, (2008), Shennan *et al.*, (2006), Shennan and Horton (2002)). Not only is there a noted N-S reduction in the height of the observed sea-level over the Holocene, there is also a pronounced W-E trend across this central region, with notably higher sea levels at sites along the west coast of Great Britain and east coast of Ireland, compared to sites along the opposite coasts.

For example, along the east coast of Ireland (such as sites 93, West Donegal and 94, North Donegal) there is evidence for only a very minor (less than 1 m), if any, highstand over the late Holocene. This compares to the west coast (such as sites 97, North Antrim and 99, South Down), where the limiting data suggest that sea level was elevated above present by at least 2m. This gradual reduction in the height of the Holocene highstand is more apparent when examining the complete data set (see Appendix G) and is a key feature with which to validate the model predictions.

At site 25, N.E. England South, located on the east coast of Great Britain, the data are composed of primary and intercalated SLIPs extending from 9 kyr BP. The data indicate

that sea level rose from -5 m to form a minor highstand of 0.5m at ~ 3 kyr BP. Although there are a noted lack of SLIPs at this site and site 35, North Wales, with which to constrain the variation of sea level during the mid-to-late Holocene, it is possible to infer the occurrence of only a minor highstand from the field evidence. At site 25, N.E. England South, field evidence indicates that sea level did not rise above 0.5 m during the past 3 kyr and so a steady fall towards present day levels can be inferred. At site 35, North Wales, there is again no evidence that sea level rose significantly above present day level over the last 5 kyr BP. Despite the shorter record at site 93, West Donegal, on the west coast of Ireland, the observed trend is similar to that implied at sites 25, N.E. England South and 35, North Wales, with a small rise in sea-level over the last 5 kyr BP from - 3 m to produce a minor highstand of about 1 m between 2-1 kyr BP, before falling towards present day levels.

Sites 83, East Cork and 50, Hampshire located along the southern coast of Ireland and Great Britain, respectively, illustrate the typical pattern of relative sea level change at sites furthest removed from the main centre of ice loading in Scotland. The characteristic sea level trend at both these sites is similar, with a gradual rise over the last 7 kyr BP towards present day levels and no evidence of sea levels reaching above present day values.

### **5.3. Modelling**

#### **5.3.1. Background to the GIA model**

The GIA model adopted in this study has three key inputs - a model of the late Pleistocene ice history; an Earth model to reproduce the solid earth deformation resulting from surface mass redistribution (between ice sheets and oceans) and a model of sea-level change to calculate the redistribution of ocean mass (Farrell and Clark (1976)).

The sea-level model solves the generalized sea-level equation (Kendall *et al.*, (2005), Mitrović and Milne (2003)) and includes the most recent advances in GIA sea-level modelling: time-varying shoreline migration, an accurate treatment of sea-level change in

regions of ablating marine-based ice and the influence of GIA perturbations to the Earth's rotation vector (Milne and Mitrovica (1998), Mitrovica *et al.*, (2001)).

The Earth model is a spherically symmetric, self-gravitating Maxwell body. The elastic and density structure are taken from a seismic model (Dziewonski and Anderson (1981)), with a depth resolution of 10 km within the crust and 25 km in the mantle. The viscous structure is more crudely parameterized into three layers: a high viscosity ( $10^{43}$  Pa s) outer shell to simulate an elastic lithosphere, an upper mantle region of uniform viscosity extending from beneath the model lithosphere to the 670 km seismic discontinuity, and a lower mantle region extending from this depth to the Core-Mantle boundary. The thickness of the lithosphere and the viscosity within the upper and lower mantle are free parameters in the modelling.

As has been discussed in previous work (Shennan *et al.*, (2006)) the optimum earth model adopted for the British Isles has varied within past GIA studies, most notably between the choice of parameters for the shallow viscous structure. To provide an additional, independent constraint on the choice of viscosity values in this study, the range of optimal earth model viscosity parameters inferred from a study of present-day vertical crustal motion around Great Britain (see Bradley *et al.*, (2009)) and as described in Chapter 3 is also considered. The starting Earth model used here is the optimal model this chapter as discussed in Section 3.3: lithosphere thickness of 71km, upper mantle viscosity of  $5 \times 10^{20}$  Pa s, lower mantle viscosity of  $3 \times 10^{22}$  Pa s.

As mentioned briefly above, the pattern of relative sea-level change across the British Isles is also sensitive to the adopted regional (BIIS) and global (non-local) ice model, which is evident by examining the contribution from these signals at three sites across the study region (Fig. 5.1). Site 17, Forth Valley, is situated below the estimated region of thickest ice at the LGM and, as such, will experience the maximum rebound and relative sea-level fall as the BIIS deglaciated. The BIIS signal produces a steady fall from 134 m towards present from the onset of deglaciation (~ 20 kyr) as the weight of the overlying ice sheet is removed and the solid earth rebounds. This signal is approximately equal in magnitude but opposite in sign to the relative sea-level signal produced from the non-local ice sheets (grey line), where sea level rises from - 90 m at 20 kyr BP towards

present day levels, with a gradual slowdown throughout the mid-to-late Holocene. The gradual rise of the predicted signal due to non-local ice is punctuated by a period of rapid sea-level rise at ~ 14 kyr BP, known as meltwater pulse 1A (mwp-1A) (Bard *et al.*, (1996), Bard *et al.*, (1990), Clark *et al.*, (2002), Fairbanks (1989), Hanebuth *et al.*, (2000)). It is this event which produces the inflection evident in the total predicted sea-level signal at this time. The change from fall to rise at ~ 11 kyr BP is also due to an increase in the rate of global ice melt following the Younger Dryas cold period (Bard *et al.*, (1996), Bard *et al.*, (2010)). This increased rate of melting, although not as high as that during mwp-1A, was sustained for several kyr until the early Holocene. Note that a secondary control on the shape of the predicted RSL curves in Scotland is the exponential decrease in the rate of land uplift following the removal of the ice load (~ 15 kyr BP). However, the relatively abrupt changes noted above are controlled primarily by the influence of meltwater addition from the non-local ice sheets.

As the distance from the major centre of ice loading across Scotland is increased, the contribution of the BIIS (dotted line) to the total predicted sea-level signal is reduced, with little change in the magnitude of the far-field signal. This can be seen at site 99, South Down, which is situated on the NE coast of Ireland. This reduction in the BIIS signal results in the total predicted signal remaining below present from the onset of deglaciation, rising above present only in the early Holocene when local hydro-isostasy and (global) ocean syphoning (Mitrovica and Milne (2002)) dominate the signal. At site 50 situated along the southern coast of Britain, the non-local signal dominates the total predicted sea-level change (compare the dotted curve to the grey curve). At this site, the magnitude of the relative sea-level change due to the BIIS has significantly reduced compared to sites 99, South Down and 17, Forth Valley, with a steady rise from about -8 m at 14 kyr BP, reaching close to present day levels by 5 kyr BP. This sea-level rise is driven by subsidence of the solid surface due to the collapse of the BIIS glacial forebulge.

The results shown in Fig. 5.1 demonstrate that RSL data across the British Isles vary in their sensitivity to the history of the BIIS. Clearly, RSL data from more northerly locations will provide the strongest constraints on the local ice history. As a consequence of this range in sensitivity, the ice model adopted in this analysis will be described explicitly in terms of the regional and non-local component.

The starting BIIS component of the model was taken from Section 2.4.3 (as published in Brooks *et al.*, (2008)) and will be referred to as the Brooks *et al.* model. Key time slices illustrating the evolution of this regional ice sheet model are shown on Fig. 5.4. Note that the maps illustrate the thickness of the ice sheet, as opposed to the ice surface elevation, which has been corrected for underlying topography (see Shennan *et al.*, (2006)). The chronology of the main advance and retreat phases are based upon the results of Sejrup *et al.*, (1994), Sejrup *et al.*, (2005)), with a coalescence of the BIIS and the Fennoscandian ice sheet across the North Sea between 32- 27 kyr BP. Following a short retreat phase, the BIIS rapidly expands around the timing of the LGM, with extended and thickened ice on the continental shelf and within the Irish Sea basin. Deglaciation in the model begins at 21 kyr BP, with a rapid thinning and retreat of the Irish Ice sheet at 19 kyr BP, followed by a later readvance across northern Ireland to simulate the ‘Killard point stadial’, with complete ice retreat by 15 kyr BP. During the Younger Dryas event, ~ 13 kyr BP, there is small scale ice growth across the highlands of Scotland. The model also includes two short lived ice streams, one extending down to the Isles of Scilly at 24 kyr BP and one extending down the east coast of Great Britain at 21.5 kyr BP. For more discussion of this model see published material in Brooks *et al.*, (2008) and Shennan *et al.*, (2006) and the model development in Section 2.4.

To generate RSL predictions for the British Isles, the BIIS model must be partnered with a global (non-local) ice model. In the Brooks and Edwards (2006)) and Shennan *et al.*, (2006)) studies, the model from Bassett *et al.*, (2005) (hereafter referred to as the Bassett *et al.* model) was used for this purpose (note that the UK component of the Bassett *et al.* model was removed). The Bassett *et al.* model was tuned to fit a suite of far-field data from the LGM to 10 kyr BP (and so is unconstrained during the Holocene); the primary aim of their study was to constrain the volume partitioning of global ice loss during mwp-1A. Their results demonstrated that far-field sea-level data are better fit when a dominant contribution to mwp-1A is sourced from the Antarctic ice sheet, as opposed to the North American ice sheets. The Holocene component of eustatic sea level predicted from the Bassett *et al.* model since 7.5 kyr BP is illustrated on Fig. 5.4k. It is characterised by a relatively rapid rise in the early Holocene with major melting ceasing at 6 kyr and a small

amount melting (0.5 m) between 6-5 kyr BP. There is no further melting from 5 kyr BP to present.

Using the Brooks *et al.*/Bassett *et al.* ice models (the British Isles component of the Bassett *et al.* model was removed) and the starting earth model defined above, RSL predictions were generated at the nine localities shown on Fig. 5.5. (Predictions at all sites are shown in Appendix G) Although the model produces a reasonable fit at most sites, there are a number of consistent misfits on a regional scale: (a) an underprediction in the magnitude of the late Devensian sea-level fall, which is especially evident at sites 11, Arisaig and 100, Dundalk; (b) a late Holocene highstand which is generally too high (as seen at sites 35, North Wales and 93, West Donegal) and too late (as seen at sites 11, Arisaig; 17, Forth Valley and 25, N.E. England South); (c) a late Holocene rise towards present day levels which is characterised by a sharp change in the rate of sea-level rise ~ 6 kyr BP which is not consistent with the smooth trend inferred from all southern sites (such as site 50, Hampshire).

### **5.3.2. Modifying the eustatic model**

Brooks *et al.*, (2008) and Shennan *et al.*, (2006) both highlighted that many of the above misfits to the RSL data during the late Holocene, most notably the height of the Holocene highstand, were a result of the rapid termination of melting during the mid Holocene (see Fig. 5.4k). In these studies it was concluded that one method of resolving this issue was to continue global ice melting through the late Holocene. This was achieved by applying a post-modelling correction to reproduce ~ 5 m of eustatic sea-level rise distributed between 7 kyr and 2 kyr BP. Applying this correction is a reasonable method to improve the model fits. However, it will lead to a source of error as the loading signal associated with the additional 5 m of eustatic sea-level is not taken into account. Ideally, the ice model would be altered to implement this revision to the eustatic component.

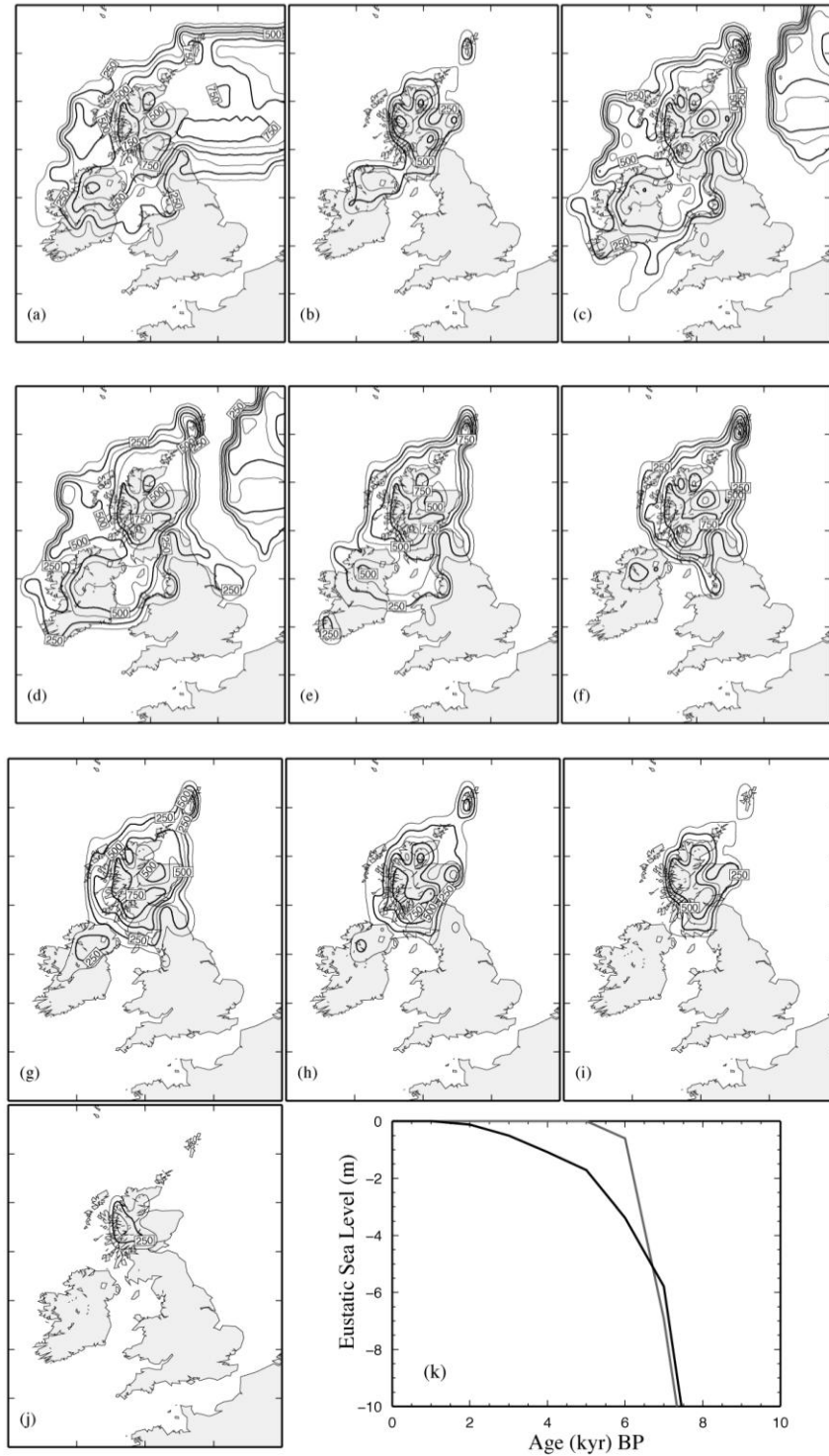


Fig. 5.4: Ice thickness maps of the British-Irish Ice sheet model presented in Brooks *et al.*, (2008) and as described in Section 2.4.3 at the times: (a) 32 kyr BP, (b) 26 kyr BP, (c) 24 kyr BP, (d) 21 kyr BP, (e) 20 kyr BP, (f) 19 kyr BP, (g) 18 kyr BP, (h) 17 kyr BP, (i) 16 kyr BP, (j) 13 kyr BP. Note the varying contour intervals. Diagram (k) is a graphical representation of the two eustatic sea level models considered in this study: Bassett *et al.*, (2005) (grey line) and the revision to this model presented by Bradley *et al.* (2010) (and as referred to in Section 4.4.5 as the *EUST3* model)(black line).

This is the procedure applied here: the original Bassett *et al.* model is replaced by an improved non-local model, referred to as *EUST3* in Section 4.5. The new model is a revision of the Bassett *et al.* model for the Holocene period only (not constrained in the original analysis) to fit a suite of far-field data from China and Malay-Thailand (Bradley *et al.*, (2010)) as described in Chapter 4. The eustatic sea level change generated by this model is shown on Fig. 5.4k: following an initial slowdown at 7 kyr BP, sea-level rises steadily towards present, with melting ending by 1 kyr BP. This pattern of Holocene eustatic sea level change is compatible with another, independently constructed model (e.g. Lambeck and Purcell (2005)). The combination of the *EUST3* global model (Bradley *et al.*, (2010)) (with the British Isles component removed) and the Brooks *et al.* BIIS regional model will be referred to as the new ice model.

Comparing the predictions using the new ice model to the Brooks *et al.*/Bassett *et al.* model, it is apparent that the key misfits over the late Holocene have been greatly reduced (see Fig. 5.5). Specifically, the over-predicted Holocene highstand is reduced at a number of sites: NW Coast of Ireland (site 93, West Donegal and site 94, North Donegal shown in the Appendix G); Northern England (e.g. sites 35, North Wales and 25, N.E. England South); and the following sites in the Appendix G: 24, N.E. England Central; 31, Isle of Man and 34, Mersey. In addition, the location of the zero isobase is more consistent with the general pattern inferred from the sea-level and shoreline data. At more southerly sites, such as site 50, Hampshire; 40, Fens and 48, Kent (latter two shown in Appendix G), the new ice model predicts a smooth rise in sea level during the mid-to-late Holocene which is more consistent with the general character of the data. Additionally, there has been a slight increase in the magnitude of the Late Devensian fall at the most Northern sites, as is apparent at sites 11, Arisaig; 12, Kentra and 54, Knapdale.

Despite this improvement, there remain some misfits to be addressed. The model still underpredicts the amount of sea-level fall across the Northern sites following the end of glaciation (15-16 kyr BP) such as at site 11, Arisaig. As described above, the global ice model results in two periods when RSL changes from a fall to a rise at more northern sites (due to accelerations in the rate of melting at ~ 14 and ~ 11 kyr BP). At the time of these two accelerations, the predictions generally lie below the data or at a time with no SLIPS (e.g. see sites 11, Arisaig and 54, Knapdale). As discussed above, the RSL

oscillation at ~ 14 kyr BP is due to the occurrence of meltwater pulse 1A in the non-local ice model. Although there are no SLIPs at this time, the data following this event (dated at 12-13 kyr BP) come from isolation basins, with marine sedimentation prior to the age of the SLIP, indicating no RSL fall-rise-fall sequence. Therefore, the modelled oscillations, as shown at sites 11, Arisaig and 54, Knapdale are too large.

Between 8-10 kyr BP there is an apparent spatial variation in the ability of the model to capture the observed trend in the data. At sites situated along the Northern and NE coast (e.g. sites 25, N.E. England South; 11, Arisaig; 21, Ayr and 16, Tay Valley) the predicted sea-level values fall either below the SLIPs or there are gaps in the data and therefore no constraint. This is not seen at more distal and central sites (e.g. sites 47, Thames; 45, Bristol Channel and 31, Isle of Man) where the predicted sea-level change captures the observed trend and lies within error limits of the SLIPs.

### 5.3.3. Determining optimal earth model parameters

The possibility of improving the fit further by varying the Earth model viscosity structure will now be considered. A forward modelling analysis was conducted for a suite of earth models and the  $\chi^2$  misfit calculated; this is defined as:

$$\chi^2 = \frac{1}{(N-1)} \sum_{i=1}^N \left( \frac{(SL_i^p - SL_i^{obs})}{\sigma_i} \right)^2$$

where  $SL_i^p$  and  $SL_i^{obs}$  are the predicted and observed sea-level, respectively, defined at a given location and time  $i$ ;  $\sigma_i$  is the error on the observed sea-level point and N is the total number of data points.

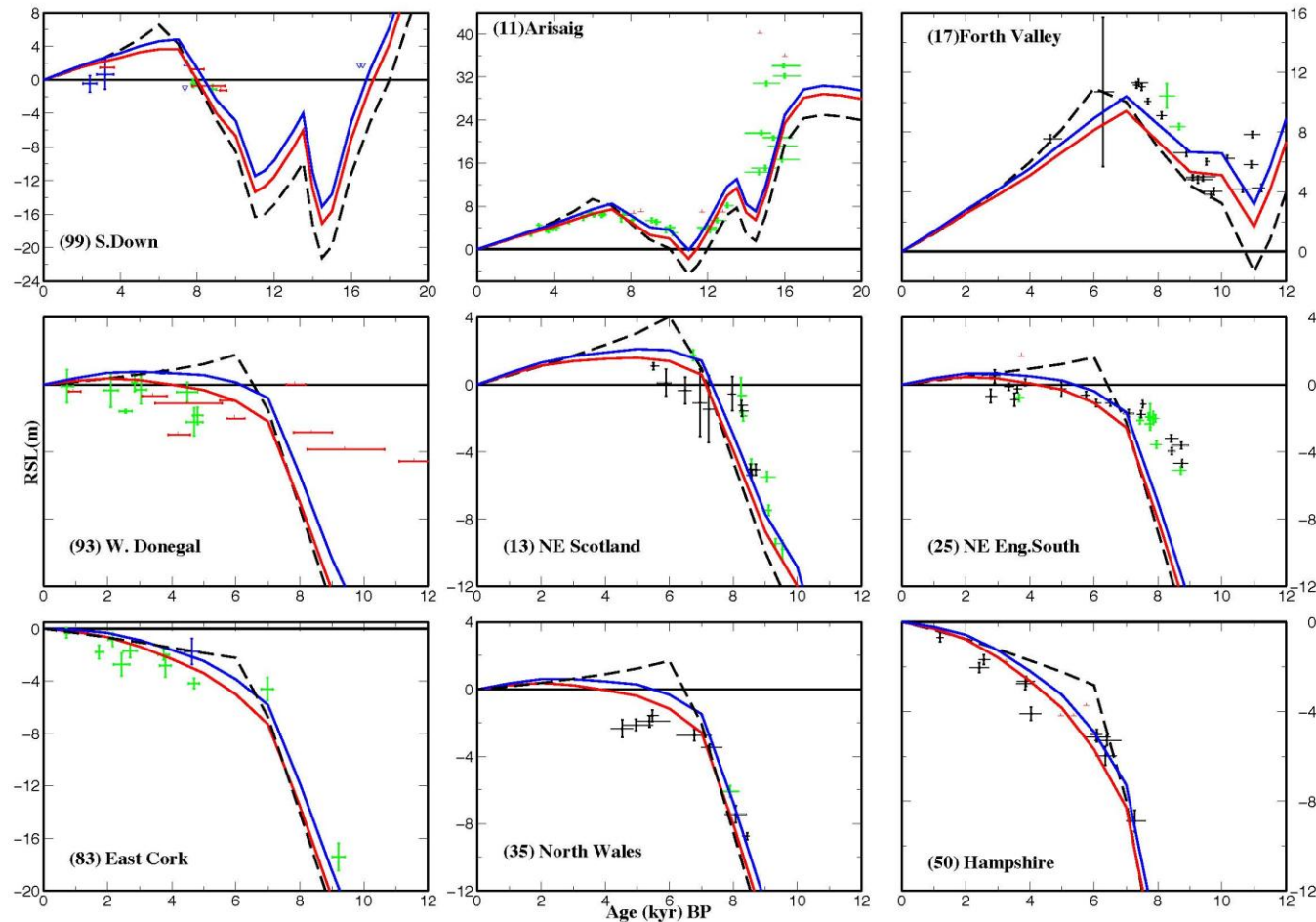


Fig. 5.5: Comparison of predicted and observed sea level at nine locations across the study region. Symbols for the observed data are summarized within the text and Appendix A. Predictions based on the optimum earth model inferred in Bradley *et al.* (2009) and as described in Chapter 3 - lithosphere thickness 71 km, upper mantle viscosity  $0.5 \times 10^{21}$  Pa s, lower mantle viscosity  $3 \times 10^{22}$  Pa s - are shown for the Brooks *et al.*/Bassett *et al.* ice model (dashed black line; see text for details) and the new ice model presented in this analysis (solid red line). The solid blue line is for the new ice model and an earth model that is identified from  $\chi^2$  results presented in Fig. 5.8. This Earth model is identical to the one inferred in Bradley *et al.* (2009) except that the viscosity in the lower mantle is higher, at  $6 \times 10^{22}$  Pa s. Note the varying scale for each plot. Predictions for all sites are shown in Appendix G

The suite of earth models considered spans the spread of parameters inferred in a range of GIA sea level studies (e.g. Davis *et al.*, (1999), Forte and Mitrovica (1996), Kaufmann and Lambeck (2002)). The minimum and maximum values for each earth model parameter are: 71, 120 km for lithosphere thickness,  $0.1-5 \times 10^{21}$  Pa s for upper mantle viscosity, and  $1-50 \times 10^{21}$  Pa s for lower mantle viscosity. Adopting a thicker lithosphere (96 km or 120 km) resulted in a significant increase in the minimum  $\chi^2$  value (greater than 99% confidence) compared to that for the 71 km model. Therefore, results in the following sections will only be shown for a lithosphere thickness of 71 km. As mentioned before, the results will also be compared to the range of feasible earth models inferred in a recent analysis of GPS crustal motion data from across Great Britain (see Chapter 3 and Bradley *et al.*, (2009)).

Results are shown in Fig. 5.6 for both ice models considered - the Brooks *et al.*/Bassett *et al.* model and the new model - as well as for the entirety of data from Great Britain (including all basal and intercalated sea level index points as listed in Appendix A) and Ireland separately. When the two data sets were combined, due to the greater number of SLIPs across Great Britain (1107) compared to Ireland (61), the Great Britain data set dominated the results to produce  $\chi^2$  values which were very similar to those shown in Fig. 5.6a and 5.6c. Therefore, the results for the two data sets are shown separately to determine the optimum viscosity values for each region.

There are a number of key points to conclude from the  $\chi^2$  results in Fig. 5.6. Firstly, the minimum  $\chi^2$  misfit (and thus optimum earth model parameters) falls within the range of best-fitting earth models inferred in the above mentioned study (Bradley *et al.*, (2009) and Section 3.3) of present-day vertical land motion in Great Britain. When comparing the results for the two different ice models, there is a clear reduction in the  $\chi^2$  values for the better fitting viscosity model; however, there is only a minor change in the optimum earth model parameters, with a slight shift in the optimum range of lower mantle viscosities to higher values. A similar result was found by Lambeck *et al.*, (1996), who showed that the adopted late Holocene global melt history reduced the variance between predicted and observed sea level but did not alter the earth-model parameters at which the variance minimum occurred. For the new ice model, the Irish data prefer a lower mantle viscosity greater than  $1 \times 10^{22}$  Pa s,

for an upper mantle viscosity between  $0.3\text{-}5 \times 10^{21}$  Pa s. This broad range of plausible parameter values contrasts to the very limited range permitted by the Great Britain data (see the 95% confidence boundary in Fig. 5.6c).

While the optimum models for each of the two data sets considered in Fig. 5.6 are not incompatible, the Great Britain data produce a remarkably tight constraint on plausible viscosity models (to within 95% confidence). To investigate this further, the complete Great Britain dataset was separated into three geographic regions: (1) ‘northern data’ which includes all sites that were covered throughout the last glaciation and whose relative sea-level signal would contain a significant contribution due to the local ice loading. This set included sites 1-23, 28, 29 and 31; (2) ‘central data’ which includes sites 24-27, 30, 32-35, where the influence of the local ice loading is reduced; (3) ‘southern data’ which includes all sites with little or no evidence of a highstand and whose relative sea-level signal would be dominated by non-local ice sheet changes. This includes sites 36-65 across Great Britain. It is noted that the majority of SLIPs in this subset are limited to the late Holocene.

The  $\chi^2$  misfit functions for these three subsets of the Great Britain data are shown on Fig. 5.7. It is apparent when comparing Fig. 5.7a to Fig. 5.6c that it is the northern data sites, which result in the limited range of plausible earth models inferred for the complete Great Britain data set. There is a marked shift in the geometry of the  $\chi^2$  surface when these northern sites are removed (compare Fig. 5.7a to 5.7b & 5.7c). The central and southern sites are compatible with a wider range of upper mantle viscosity values compared to the northern data. Indeed, sub-dividing the data further demonstrates that the pre-Holocene data from northwest Scotland are responsible for the remarkably tight constraint on upper mantle viscosity evident in Fig. 5.7a.

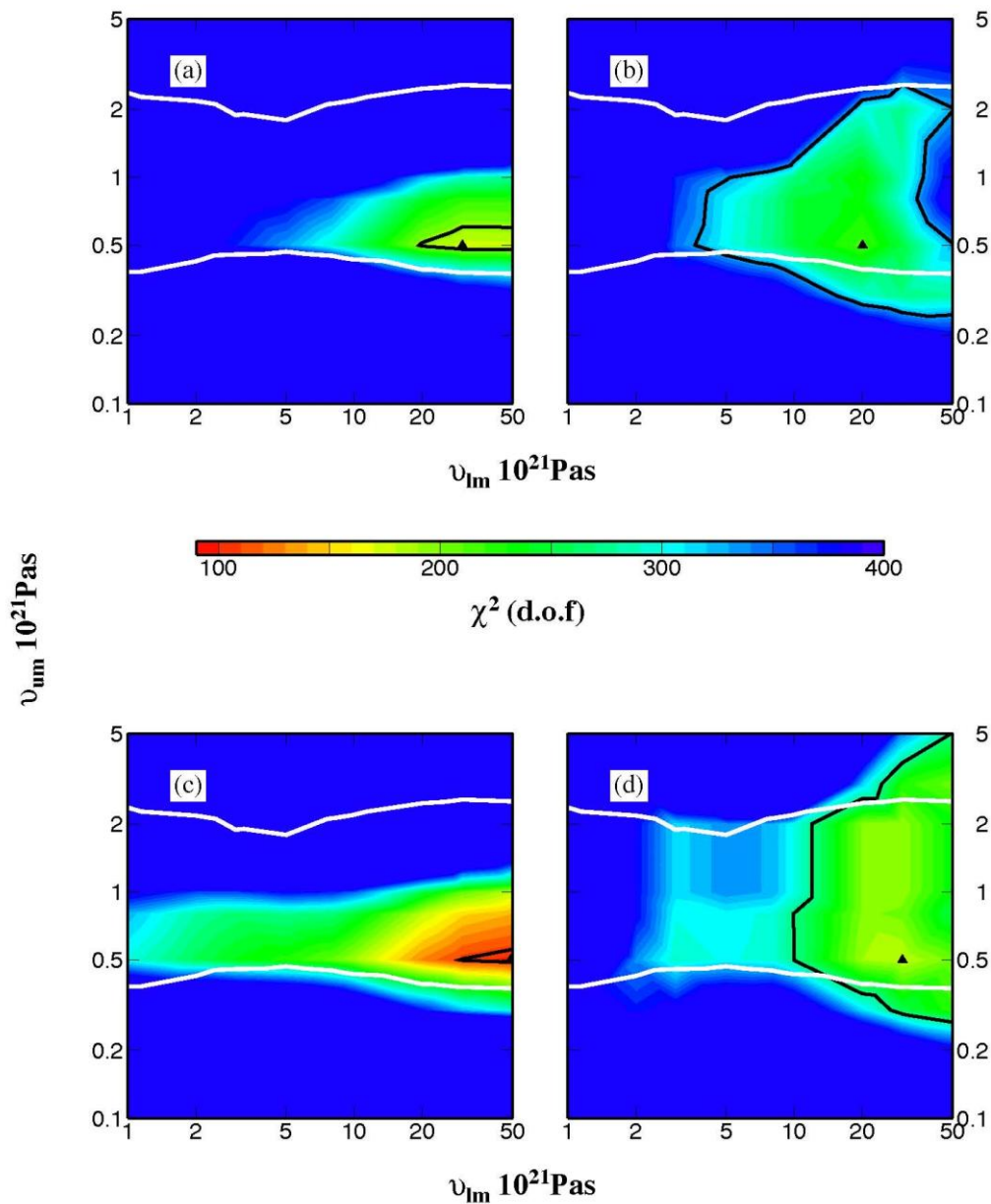


Fig. 5.6: Contour plots of the normalized  $\chi^2$  misfit between predicted and observed sea level as a function of upper and lower mantle viscosity ( $\nu_{um}$  and  $\nu_{lm}$  respectively) for a lithosphere thickness of 71km. The top two frames (a & b) show results for the Brooks *et al.*/Bassett *et al.* ice model (see text for details) and the lower two frames (c & d) show those for new ice model presented here. The results in frames (a) & (c) consider data from Great Britain data and those in frames (b) & (d) consider data from Ireland. The black line represents the  $\chi^2$  value below which the quality fit is equivalent to 95 % confidence (194 in frame (a), 329 in frame (b), 106 in frame (c) and 272 in frame (d)). The triangle marks the location of the minimum  $\chi^2$  value. The white line marks the region of optimum parameter values (95% confidence) inferred from the CGPS measurement of crustal motion (Bradley *et al.*, (2009) and as described in Chapter 3). Note that the darkest blue colour represents  $\chi^2$  values greater than the maximum on the scale bar (400).

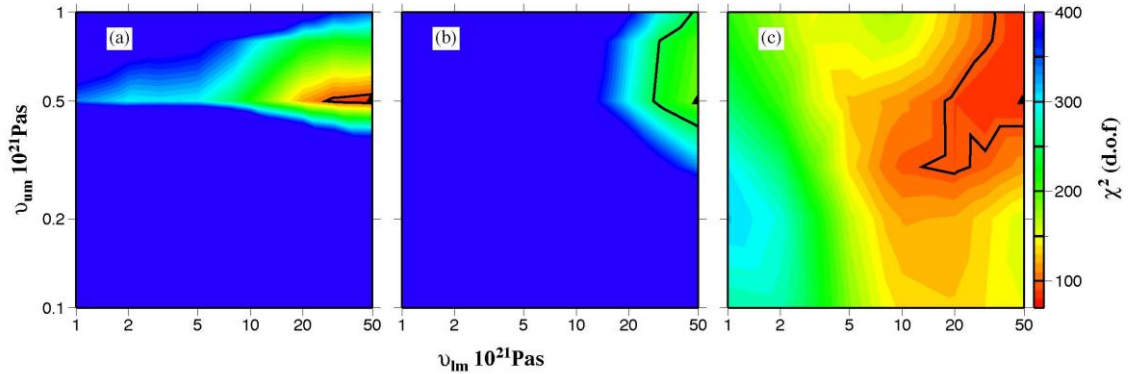


Fig. 5.7: Contour plots of the normalized  $\chi^2$  misfit between predicted and observed sea level as a function of upper and lower mantle viscosity ( $v_{um}$  and  $v_{lm}$  respectively) for a lithosphere thickness of 71km for the new ice model. Frame (a) shows results for 'northern' data, (b) for 'central' data, and (c) for 'southern' data (see main text for more information). The triangle marks the location of the minimum  $\chi^2$  value. The black line represents the  $\chi^2$  value below which the quality fit is equivalent to 95 % confidence (96 in frame (a), 242 in frame (b) and 94 in frame (c)). Note that the darkest blue colour represents  $\chi^2$  values greater than the maximum on the scale bar (400).

The variation in the range of optimum earth models with data region can be attributed to two factors. Firstly, with increasing distance away from the centre of ice loading, the relative sea-level signal includes an increasingly larger contribution from non-local processes (Fig. 5.1), such as the influence of peripheral bulge dynamics associated with Fennoscandian GIA. In addition, the influence of eustasy and syphoning will also become more significant. Peripheral bulge dynamics and syphoning are mostly sensitive to viscosity structure in the deep upper mantle and lower mantle (Mitrovica and Milne 2002). Therefore, the southern data (Fig. 5.7c), which are influenced more strongly by these processes, do not result in a tight constraint on upper mantle viscosity. This contrasts to the northern data, which exhibit a stronger sensitivity to changes in the value of upper mantle viscosity adopted. Secondly, the SLIPs within the southern Great Britain and/or Ireland datasets are concentrated over the late Holocene (two-thirds of the Primary SLIPs within the Ireland dataset are from the last 5000 yrs only). Given the relatively early demise of the BIIS (by  $\sim 15$  kyr BP), the contribution of land motion due to this ice sheet is small by the late Holocene. Also, the amplitude of the signal during the late Holocene

is relatively small and so the data can be fit with a larger number of viscosity models (compared to those from the glacial period or early Holocene).

This variation in sensitivity to earth model parameters with location emphasises the advantage of integrating the full range of the Great Britain and Ireland data to constrain both earth model and ice model parameters. The northerly sites provide the best controls on earth model structure beneath the study region while the southern sites provide better constraints on non-local earth model structure and the background (non-local) ice model.

As the optimum viscosity models for the Great Britain RSL data are constrained to such a small region of the viscosity space considered (Fig. 5.6c), these results have been extended to include values of lower mantle viscosity up to  $1 \times 10^{23}$  Pa s and a denser sampling of upper mantle viscosity in the range  $3\text{--}8 \times 10^{20}$  Pa s (at  $1 \times 10^{20}$  Pa s resolution). Fig. 5.8a shows the  $\chi^2$  values for this extended and better resolved viscosity space for the complete data set (Great Britain and Ireland). The  $\chi^2$  minimum is captured at viscosity values of  $5 \times 10^{20}$  Pa s and  $6 \times 10^{22}$  Pa s in the upper and lower mantle, respectively. Note that the 95% confidence limits on upper mantle viscosity are relatively tight compared to those for lower mantle viscosity.

Fig. 5.8b shows the results when only SLIP data from the Great Britain database defined as 'basal points' (as listed in Appendix A and defined above) and Primary SLIP data from Ireland were used. This was to examine the affect of removing any data points which may be affected by local processes, such as compaction. The results in Fig. 5.8b indicate that if there are data significantly influenced by compaction in the data base, they do not impact the inference of Earth viscosity structure. A similar exercise was carried out to examine the possible influence of changes in palaeo-tidal range on the data, the effect of which has been highlighted in many studies (Hinton (1995), Gehrels *et al.*, (1995), Shennan *et al.*, (2003)). The results (not shown) indicate that this signal, which is not accounted for in the data used here, does not significantly impact the inferred earth viscosity model.

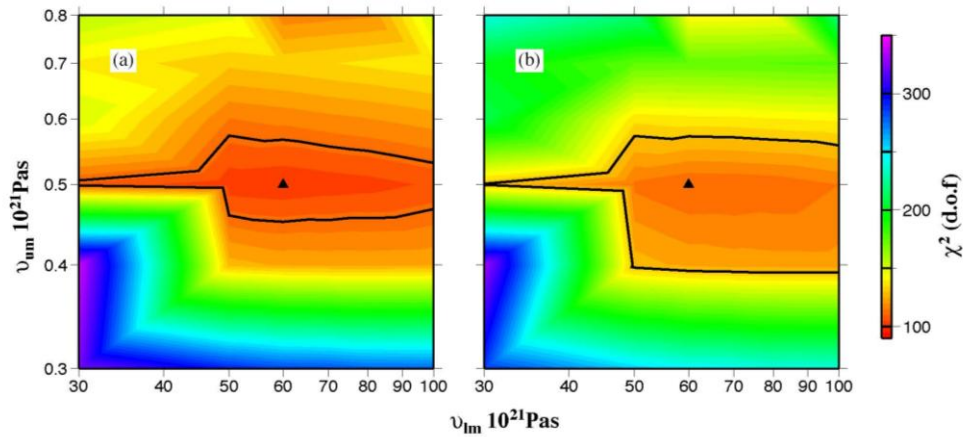


Fig. 5.8: Contour plots of the normalized  $\chi^2$  misfit between predicted and observed sea level as a function of upper and lower mantle viscosity ( $\nu_{\text{um}}$  and  $\nu_{\text{lm}}$  respectively) for a lithosphere thickness of 71 km. Note that the range and density of viscosity values considered differs from those adopted in Figs 5.6 & 5.7 in order to better capture the region of best-fitting viscosity values. All results are based on the new ice model. Frame (a) shows results for all the data (from Great Britain and Ireland), while frame (b) shows the results using 'basal points' from Great Britain and primary index points from Ireland (see text). The triangle marks the location of the minimum  $\chi^2$  value. The black line represents the  $\chi^2$  value below which the quality fit is equivalent to 95 % confidence (111 in frame (a) and 130 in frame (b)).

#### 5.4. Discussion and Conclusions

From the above forward modelling analysis, within the 95% confidence limits, the  $\chi^2$  misfit minimum was obtained for two earth models with the same lithosphere thickness and upper mantle viscosity (71 km and  $5 \times 10^{20}$  Pa s, respectively) but varying lower mantle viscosity: either  $3 \times 10^{22}$  Pa s (the starting model) or  $6 \times 10^{22}$  Pa s. At most sites an equally good fit is achieved adopting either model, with the higher viscosity model producing a consistently higher sea level, up to 1m (see Fig. 5.5).

Despite the similarity in the predictions, there are a number of key sites where the data lie closer to predictions generated with the weaker lower mantle viscosity model ( $3 \times 10^{22}$  Pa s) due to the reduced height of Holocene highstand. For example at sites along the West coast of Ireland (93, West Donegal and 94, North Donegal) and Great

Britain (31, Isle of Man; 34, Mersey and 35, North Wales) the stronger lower mantle viscosity model ( $6 \times 10^{22}$  Pa s) generates a highstand outside the limits of the SLIP data. Additionally, from the analysis of GPS data (see Bradley *et al.*, (2009) and Section 3.3), which provides a constraint on the earth model that is only weakly influence by uncertainties in the ice model; an optimum fit was also produced using the weaker lower mantle viscosity. Therefore, the following optimum earth model parameters were adopted: lithosphere thickness of 71km and upper and lower mantle viscosity values of  $5 \times 10^{20}$  Pa s and  $3 \times 10^{22}$  Pa s, respectively. These model parameters are similar to those inferred from past relative sea level studies for the British Isles (e.g. Lambeck *et al.*, (1998), Shennan *et al.*, (2000)), in which the lower mantle viscosity was found to be greater than  $1 \times 10^{22}$  Pa s and the upper mantle viscosity  $\sim 4 \times 10^{20}$  Pa s.

Using this optimum earth model and the new ice model, maps of the spatial patterns of present day relative sea-level change and vertical land motion across the British Isles can be produced (Fig. 5.9). These maps are useful as they provide a baseline for studies investigating sea-level hazard associated with future climate change (Lowe *et al.*, (2009)). To better understand the origin of present day sea-level change due to GIA across the British Isles, the total signal (Fig. 5.9a) is decomposed into the signal due to non-local ice sheets (Fig. 5.9c) and the signal due to the BIIS only (Fig. 5.9d). The non-local ice sheets produce a long-wavelength sea level rise across the region, varying between  $0.8 \text{ mm yr}^{-1}$  across Scotland to  $0.6 \text{ mm yr}^{-1}$  across southern England. This contrasts with the concentric pattern of sea level fall due to the BIIS only, with a maximum rate of  $1.7 \text{ mm yr}^{-1}$  centred over central Scotland. The total present-day relative sea-level signal replicates this concentric pattern of sea level fall, but of reduced spatial magnitude due to the influence of the non-local ice sheets.

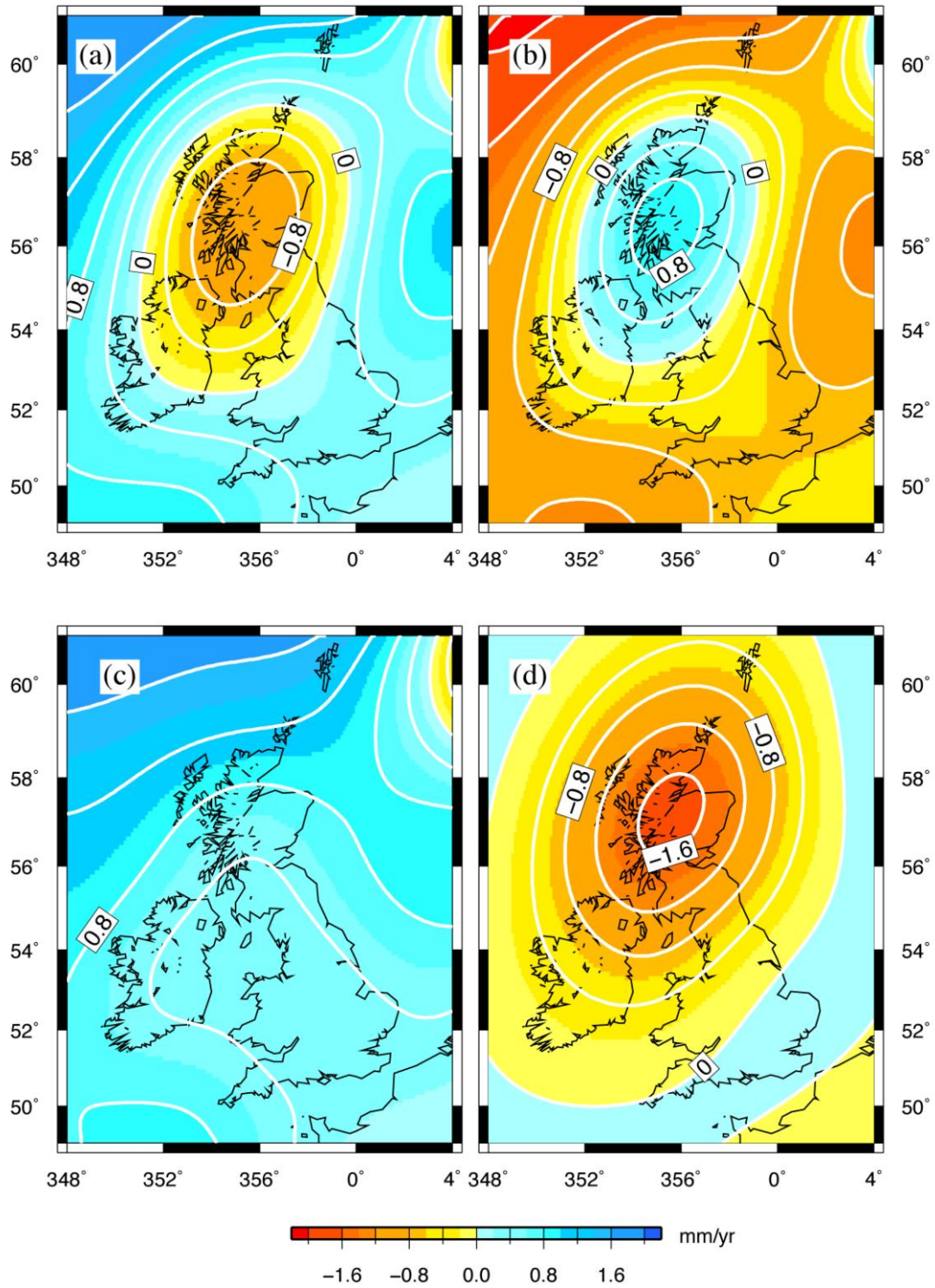


Fig. 5.9: Predictions of present-day sea-level change (a) and vertical land uplift (b) for the new ice model and its optimum earth model. The lower frames show the contribution to (a) from all ice sheets except the British-Irish Ice sheet (c) and from the British-Irish Ice sheet only (d). All predictions include the respective ocean loading and rotation component.

Comparing Fig. 5.9a to Fig. 5.9b, the spatial pattern of present day sea level and vertical land motion are very similar in magnitude, but as to be expected, of opposite sign. The region of maximum uplift ( $0.95 \text{ mm yr}^{-1}$ ) and present day sea level fall ( $-1.1 \text{ mm yr}^{-1}$ ) are both centred over western Scotland, which is near the region of maximum ice thickness at the LGM. The predicted maximum uplift rate is compatible with that obtained from GPS data ( $1.1 \pm 0.3 \text{ mm yr}^{-1}$ ; Teferle *et al.*, (2009)). Note, however, that the location of the GPS-inferred maximum is located in the east of Scotland (Edinburgh). In contrast, the location of our maximum predicted uplift rate is compatible with that inferred directly from the RSL data (Gehrels (2010); Shennan and Horton, (2002)) but the magnitude is less by  $0.65 \text{ mm yr}^{-1}$ . However, the rate obtained from the RSL data is based on a single date (Gehrels (2010)) and so the significance of this difference in amplitude requires further investigation. An interesting point to note when comparing frames a & b in Fig. 5.9 is the location of the zone of zero sea-level change, or zero isobase in frame (a). This does not coincide with the zero uplift contour in Fig. 5.9b. This is largely due to ocean syphoning, which contributes a present-day global sea-surface fall of  $\sim 0.3 \text{ mm yr}^{-1}$  and so is a component of the GIA-induced sea-level change but not vertical land motion.

On comparing the dashed and solid lines in Fig. 5.5, it is evident that there remain a number of local scale misfits between predicted and observed sea-level changes, most notably at northern sites around the timing of mwp-IA (around 14 kyr BP). As mentioned above, the predicted magnitude of the sea-level oscillation (fall-rise-fall) associated with this event is too large, as there is no isolation basin at any site recording an oscillation. The fit can be improved in a number of ways, for example: (1) changing the timing and amplitude of local ice loss as well as the earth viscosity model to steepen the land uplift component, (2) change the volume partitioning of the meltwater source. With regard to the latter, the amplitude of the rise associated with mwp-IA will be particularly sensitive to changes in the melt volume contribution from the Fennoscandian ice sheet. Other remaining misfits include an underprediction in amplitude of Late Devensian sea-level fall at some northern sites (e.g. 11, Arisaig and 100, Dundalk). It is hoped that with future revisions to the regional ice model to incorporate revised interpretations of trimline data (Ballantyne (2010)), this misfit might be resolved. It is possible that some of the remaining data-model misfit relates

to the influence of lateral variations in earth properties. Lateral structure has been shown to play a significant role in the GIA of Fennoscandia (e.g. Whitehouse *et al.*, (2006)) and so an important aim for future studies is to determine the significance of this structure for interpreting observations of both RSL and present-day land motion in the British Isles.

As mentioned above, the main advance and retreat phases of the regional ice model were taken from Sejrup *et al.*, (2005)), who suggested ice growth across the North Sea from 32 kyr BP. Recent studies (Scourse *et al.*, (2009), Sejrup *et al.*, (2009)) now suggest that this early phase of ice sheet growth across the North Sea was later, around 29 kyr BP. There still remain relatively few onshore dates with which to constrain the timing of this pre-LGM glaciation, with most published dates suggesting that Scotland remained ice free till after 35 kyr BP (Bos *et al.*, (2004), Brown *et al.*, (2007), Jacobi *et al.*, (2009)). Preliminary calculations (not shown here) to investigate the sensitivity of the sea-level predictions to the timing of this early event indicate that the largest impact is relatively small (< 5 m) and occurs before and during LGM times. Given that there is a lack of pre LGM RSL data of this age, the most direct means of improving the accuracy of the ice history for this time period is by dating morphological features.

In summary, a new GIA model for the British Isles is presented which brings together a number of elements from previous work and earlier Chapter of this thesis to address the inherent non-uniqueness in the model parameter inference procedure for this region. We adopted a regional ice sheet reconstruction that was based on some of the most recent field constraints from both Great Britain and Ireland (Brooks *et al.*, 2008; Shennan *et al.*, 2006 and as outlined in Chapter 2). This regional ice model was combined with a new global ice model which is the combination of results from two recent studies: one which focused on best-fitting a suite of far-field sea-level data for the LGM to late Glacial period (Bassett *et al.*, (2005)) and a second which extended this model by calibrating to Holocene sea-level data from China and the Malay-Thai Peninsula (see Chapter 4, Section 4.5 and Bradley *et al.*, (2010)). Incorporating this new global ice model resulted in a reduction in the magnitude of predicted Holocene highstands and, therefore, significantly improved data-model fits at a number of sites

compared to previous studies (Brooks *et al.*, (2008), Shennan *et al.*, (2006)). The new, hybrid, ice model was employed in a detailed forward modelling analysis to infer earth model viscosity structure using, for the first time, RSL data from both Great Britain and Ireland. This combined data set results in a small set of optimal viscosity models in which the upper mantle viscosity is tightly constrained. The set of optimal earth models is compatible with that inferred using observations of present-day vertical land motion (see Sections 3.3, 3.4 and Bradley *et al.*, (2009)).

The optimum ice-earth model pair resulting from this study represents a significant improvement compared to the earlier analyses of Shennan *et al.* (2006) and Brooks *et al.* (2008). However, there remain data-model misfits at a number of sites which reflect limitations in the GIA model (e.g. consideration of only 1D earth structure) as well as possible inaccuracies in the data linked to sediment compaction and the influence of changes in tidal range. Studies are already underway to address some of these issues.

## Chapter 6: Summary and Future work

### 6.1. Introduction

Many past studies have investigated the GIA across British Isles by primarily modelling RSL data to provide constraints on various model components including the regional ice sheet history, viscoelastic earth structure and the global meltwater signal. But as with many GIA modelling studies using near-field RSL data, the inference procedure is non-unique. This is particularly true for the British Isles data due to the comparable magnitude between the local isostatic signal and the global eustatic signal. As a result, the data are sensitive to both the choice of regional ice and earth model parameters and the global ice model. This sensitivity, along with the highly non-monotonic pattern of RSL change across the region has led to significant differences in the quality of the fit to the RSL data and between the choice of parameter values inferred in past studies.

The main aim of the research presented in this thesis was to address the GIA of the British Isles using a methodology intended to reduce this ambiguity by adopting additional datasets that have different sensitivities to the key model parameters; specifically CGPS data from across the Great Britain and suite of far-field RSL data. In Chapter 3, for the first time, CGPS data of vertical land motion was shown to provide a robust constraint on the regional earth structure, relatively independent to the choice of input regional or global ice model. Holocene far-field RSL data, (Chapter 4) have been used to extend a previously published global ice model (Bassett *et al.*, (2005)) by improving the melt history during this period. A new spatial and temporal history for the BIIS (Chapter 2) during the Late Devensian has been developed which is compatible with the most recent (at the time of publication) geomorphological evidence. These results have been combined to produce a final revised GIA model for the British Isles which has been constrained, for the first time, using an extended RSL database comprising data from across both Great Britain and Ireland.

Given that extensive discussion and summaries are provided at the end of Chapters 2-5, the main aim of this chapter is to present the main findings and wider implications of the research with respect to the aims set out in Chapter 1, Section 1.4. In addition, possible

avenues for future research are suggested that either address issues outstanding from this work or expand upon the results obtained.

## **6.2. Revised BIIS model and modelling of the RSL data**

A new BIIS model has been developed (Chapter 2) which is consistent the most recent geomorphological evidence from across the British Isles and North Sea and whose ice thickness has been corrected to take into account underlying topography. The glacial history of the BIIS prior to LGM has been considerably altered to include an extensive two-stage glaciation across the NSB. The ice sheet is greatly thickened and extended within the Irish Sea, out along the NE Atlantic margin and across Ireland. During deglaciation, the IIS now undergoes a rapid thinning and retreat, with complete ice removal across the British Isles by 15 kyr BP. A short lived ice stream advance down to the Isles of Scilly is also now included.

The primary conclusion from the modelling to develop an improved IIS model was the need for a thick, spatially extensive ice sheet during the final glacial phase, which underwent a rapid retreat and thinning after 21 kyr BP and throughout the deglacial phase. This model is substantially different to an earlier proposed model for the IIS and highlights the importance of combining a realistic IIS component within GIA models for the British Isles.

In the Brooks et al. model, the BIIS build up is rapid during the first glacial episode, with ice expanding across the NSB to coalesces with the SIS and out onto the continental shelf in ~ 1 kyr, reaching maximum extent by 32 kyr BP. Since the development of this model, some new evidence now questions the nature of this first glacial episode, implying it may have been a more gradual growth, expanding over 1000s yr and/or reaching maximum glacial extent later, after 30 kyr BP. Preliminary sensitivity tests have shown that the impact of this earlier glacial phase on the RSL predictions is small and occurs prior to or during LGM times. Also, accurately altering this earlier phase of the BIIS history is limited due to the relatively few available dates which constrain the spatial and temporal history. The Mid-Late Devensian behaviour of the BIIS is an aspect that requires further

research in the future, but such a study depends on an increase in older, pre 30 kyr BP records. Possible records to target include dating of offshore geomorphological landforms or additional IRD records.

A second issue which arose during the development of the Brooks et al. model is the interpretation of trimline evidence used as the main constraint for the maximum surface elevation of the ice sheet, and as such the input ice thickness. This alternative interpretation has implications for the defined maximum thickness of the BIIS in future modelling work. Introducing a thicker ice sheet, which exceeds the maximum earlier altitude of 1100 m may provide a possible solution to address the underprediction of RSL during the Late Devensian (as discussed below) and would also be more consistent with ice model reconstructions generated using glaciological models (e.g. Boulton (2010), Hubbard *et al.*, (2009))

The new British Isles GIA model presented in Chapter 5 was calibrated using an RSL database which, for the first time, included data from across both Great Britain and Ireland. This new model captures reasonably well the regional trends in the RSL data at most of the 80 localities. By combining the regional Brooks et al. model (Chapter 2) with the new global eustatic model (Chapter 4), the previous identified misfit in the timing and height of the Holocene highstand and the form of sea level rise across Southern sites has largely been resolved.

A key issue which has not been resolved is the underprediction in the sea level amplitude during the Late Devensian, which is most apparent across the Scottish Sites and around the North West coast of Ireland. In Chapter 2, the spatial and temporal history of the IIS was examined in greater detail to try and resolve this misfit for a selection of the Irish and Great Britain RSL data sites. It was concluded that it was not possible to recreate the higher predicted RSL during the Late Devensian while maintaining the fit to data during the Holocene through reasonable adjustments to the local ice sheet history. Note that, this sensitivity analysis did not consider increasing the thickness of the Great Britain component of the BIIS as, at the time of the model development; this was constraint by the trimline data.

One method of generating higher RSL during the Late Devensian is to increase the thickness of the BIIS, which would incorporate the revised interpretation of the trimline data, as mentioned above. Using a 3D numerical (thermo-mechanical) ice model, which is forced by realistic climatic and environmental factors (*Hubbard et al., (2009)*), a model of the spatial and temporal history of the BIIS during the last glacial cycle was developed which suggests a thicker ice sheet than the trimline evidence indicates (when interpreted as an ice surface constraint). Preliminary calculations (*G. A. Milne, personal communication*) using the model output of *Hubbard et al., (2009)* to predict RSL across the British Isles have shown that a reasonable fit to the RSL data can be achieved and the underprediction during the Late Devensian is largely removed. To rigorously investigate resolving this remaining misfit and reinterpretation of the BIIS thickness will also require older sea level data (either SLIP or limiting data) with which to calibrate any revised model outputs. In the current database there is only 64 SLIP older than 10 kyr BP and it is hoped in the future this can be increased.

A second issue which has not been addressed and only briefly mentioned within this thesis is the use of predicted and observed RSL data from sites across Scotland to constrain the magnitude and source of mwp-1A. The source distribution, magnitude and causal mechanism associated with this global ~20 m rise in eustatic sea level is still not fully resolved and is widely debated in the general science community. Yet it is important to understand these factors not only to better understand the behaviour of the climate system and ice sheets during periods of rapid climate change but also for the numerous feedback mechanisms. For example, the large flux of freshwater into the oceans during meltwater pulses would have most likely impacted the pattern of ocean circulation (e.g. *Weaver et al., (2003)*). *Milne et al., (2006)* highlighted the sensitivity of RSL predictions to changes in the adopted dominant source ice sheet for mwp-1A, with a 2 m higher sea level predicted with a AIS source compared to using a Northern hemisphere (LIS) source. But using this sensitivity to resolve some of the debate about the source of mwp-1A is only possible if there is a sufficient amount of suitable observed RSL data with which to test the differences between the possible scenarios. In the current RSL database there are only 4 sites (8, 9, 11 and 54) with records (SLIPs and associated field evidence) which

extend around the timing of mwp-1A and so could be used to constrain the magnitude and source of this event. The Brooks et al. model predicts a RSL oscillation (fall-rise-fall) at these sites ranging between 5.9 - 6.6 m. Despite no SLIPs and noted gaps in the records at these sites during this period, field observations of changes in the microfossils and sedimentation do not record a RSL fall-rise-fall of this magnitude, as is apparent by the noted misfits to the RSL predictions (see Chapter 2 and Chapter 5). Shennan (1999) constrained the maximum size of mwp-1A that could be fit within the limits from the observations of sea level change at site 11, to no larger than 1-2 m, which is notably smaller than that predicted using the Brooks et al. model.

Capturing the trend in sea-level during this period could be improved by altering a number of components of the input model which affect the size of this oscillation. For example, the rate of modelled meltwater flux over this period could be too large, which in the Bassett et al. model is  $22 \text{ mm yr}^{-1}$ . Alternatively the rate of regional uplift in the Brooks et al. model could be too low. Another factor which affects the size of this RSL oscillation is the contribution of the SIS to the meltwater pulse. Most past modelling studies have examined the sensitivity of RSL predictions to changes in the contribution from either the AIS or LIS, with little consideration to the possible contribution from the SIS over this period. Within this thesis, no sensitivity analysis was conducted to examine the affect of the SIS on RSL predictions, either as a possible avenue to address the misfit over the timing and amplitude of mwp-1A or the underprediction during the Late Devensian. It is noted that the SIS within the Bassett et al. model is largely unchanged from the version published in ICE3G (Tushingham and Peltier (1991)), which has been proceeded by newer, more up to date models of the spatial and temporal history of the ice sheet (e.g. Lambeck *et al.*, (2010)). It is considered that prior to using the RSL record around the British Isles to constrain the magnitude or source of mwp-1A, the BIIS model should be combined with a more up to data SIS model and a more comprehensive examination of the affect of the SIS upon modelling predictions conducted.

An extensive forwarding modelling analysis was conducted to examine the sensitivity of RSL predictions to changes in the modelled viscoelastic earth structure. This work highlighted the distinct spatial sensitivity of the British Isles RSL data in constraining the

choice of input model parameters. It was found that data taken from northern sites (predominately located across Scotland and Northern England) exhibited a stronger sensitivity to the choice of earth model parameters and provided the best constraint on the optimum range of regional viscoelastic earth model parameters. In contrast, data from sites across Southern Great Britain and Ireland are more strongly influenced by the non-local earth and ice model parameters. This is important to bear in mind for future projects which aim to target new areas for data collection to better constrain regional model parameters: an increase in older records from across Scotland and Northern England would be more useful in this regard.

SLIPs were one of the main data types used to constrain the new GIA model presented in this thesis. It is important to ensure that when using such data, any local scale processes not related to GIA that may affect the reliability and quality of the data samples have been fully considered. To address the issue of SLIP reliability, the results in Chapter 5 were generated for different subsets of SLIPs which were considered to be of the highest quality and accuracy. Within these smaller subsets, all points were removed which may have been affected by post-depositional compaction or consolidation (such as intercalated samples), or by changes in the paleo-tidal regime over the Holocene. Using these smaller subsets of data had little or no impact on the inference of regional earth viscosity structure.

The affect of changes in the paleo-tidal regime on the RSL data was only briefly addressed within this thesis. Post-modelling corrections have so far only been applied at a few sites across Southern Britain and only for during the Holocene. Early modelling work into changes in paleo-tidal ranges across the NW European shelf and post LGM have highlighted that along the NW coast of Scotland and Ireland, tidal currents were considerably larger prior to 10 kyr BP, by up to 8 m (Scourse *et al.*, (2010), Uehara *et al.*, (2006)). RSL data from along this coast have been shown to provide the best constraint on earth model parameters and also the source and magnitude of mwp-1A. Additionally, these are some of the main regions where misfits between the predictions and the observations go unresolved. Therefore, an important avenue for future study is a careful

examination of the influence of changes in tidal range on the interpretation of SLIPs at sites across this region (such as 11 and 54).

### **6.3. Modelling of CGPS data**

A principal aim of this thesis was to determine if a new CGPS dataset of present-day vertical and horizontal crustal motions could be useful in reducing the non-uniqueness of the British Isles GIA problem by providing an independent constraint on the range of earth model parameters.

To isolate the deformation signal driven by the BIIS only and effectively remove the influence of other ice sheets, relative rates were calculated for both the vertical and horizontal motions. It was concluded that adopting this method did not produce a coherent pattern in the observed horizontal motion, and as such this motion component was not used within the modelling analysis. This was not due to limitations with the approach of calculating relative rates, but the small magnitude of the horizontal deformation signal due to the BIIS only (See Fig. 3.1 b and c) compared to the much larger and dominant contribution from the tectonic motion of the Eurasian plate and the deglaciation of the LIS and SIS. The current accuracy of the absolute observed horizontal motion ( $0.29 \text{ mm yr}^{-1}$ ) is larger than the maximum size of the predicted regional BIIS signal ( $0.1 \text{ mm yr}^{-1}$ ). The precision of the horizontal rates will improve as time series lengthen and analysis techniques are improved. It will certainly be worth revisiting the horizontal data once the level of precision is high enough to resolve a signal of amplitude  $\sim 0.1 \text{ mm yr}^{-1}$ .

Although there was a broad agreement in the spatial pattern of absolute predicted and observed vertical signal, a difference in the location of the centre of uplift between the two signals which was raised briefly in Chapter 3. The predicted centre of uplift is located across western Scotland whereas the observed is located across eastern Scotland. It was suggested that this difference could be due a number of factors such as the precision of the observed signal, the limited distribution of data sites (only 16 in the current study) or a flaw in the adopted ice-earth model. Since the publication of the data

used in this study, a revised set of vertical motions at the same 16 sites has been developed. This updated dataset, which will be published soon, was generated using the new ITRF2005 reference frame, an updated atmospheric modelling technique and a newer reference frame network (*F. N. Teferle, personal communication*). In this new dataset, the centre of uplift is now situated across western Scotland, which is more consistent with both the spatial pattern of predicted vertical motion and the inferred location of centre of the BIIS. This implies that the earlier difference in the geometry was due to limitations in the observed data rather than problems with the choice of model parameters.

From the forward modelling analysis in Chapter 3, it was concluded that the relative vertical rates can be used to limit the possible range of viscosities for the upper mantle but are not able to constrain effectively the lithosphere thickness or lower mantle viscosity. The lack of sensitivity to the deeper earth structure is to be expected as the deformation field sampled by the data does not extend significantly into the lower mantle. A 71 km lithosphere thickness was chosen as the optimum value despite the same minimum  $\chi^2$  misfit achieved for both the 71 km and 96 km values. This thinner lithosphere value is consistent not only with constraints from forward modelling of the RSL data but with estimates of the lithosphere thickness across the region inferred from seismic data (as outlined below).

Another main conclusion from this thesis is that the range of viscosities constrained using the relative vertical rates were insensitive to changes in the regional ice history. The two ice models compared (NS-Thick and Brooks et al.) may be considered insufficiently different to have fully examined the sensitivity to changes in the regional ice history; with the main difference between the two models being the revised deglaciation history for the IIS and the thickness and spatial extent along the western continental margin (see Chapter 2, Section 2.4.3). In earlier preliminary work conducted as part of the forward modelling analysis (not shown), the range of optimum earth models was considered for a significantly different BIIS: the Shennan model (see Chapter 2), which has a significantly different spatial and temporal history compared to both the Brooks et al. and the NS-Thick model. Using this model as an input to the GIA model had a minimal impact on the

range of inferred optimum viscosity values. These results were not presented as this model is now considered implausible; however, as part of the sensitivity analysis, they add further weight to the conclusion that the data are relatively insensitive to regional scale changes in the adopted BIIS model.

A limitation of the CGPS analysis is the relatively small number of data sites (only 16 across Great Britain) and lack of data from sites across Ireland. Since the publication of the CGPS dataset modelled in Chapter 3, as mentioned above, a newer version has been developed with vertical rates from 46 stations including sites from across Northern Ireland (*F. N. Teferle personal communication*). It is still not possible to determine rates from sites across the Republic of Ireland due to the relatively short time series of these CGPS stations. Due to the improved processing techniques applied to these 46 stations, the accuracy of the vertical rates has improved, with an average  $0.34 \text{ mm yr}^{-1}$ , compared to  $0.47 \text{ mm yr}^{-1}$  for the dataset presented in Chapter 3. The aim is to extend this revised processing technique to include the horizontal rates in the near future. When the complete dataset becomes available, it is hoped that future research will consider the implication of a more precise and spatially extensive data set on the inference of earth model parameters.

All sensitivity analysis conducted within this thesis were based upon the assumption of a simplified 1-D (depth dependant) viscosity structure. Recent work has shown that lateral variations in earth viscosity structure, whether heterogeneities in lithosphere thickness or mantle viscosity structure, can directly impact the prediction of 3D crustal velocities and RSL predictions (e.g. Kaufmann *et al.*, (2000), Wu (2006), Wu *et al.*, (2005)) A range of investigations using seismic data (including tomography and wide angle reflection data) have proposed that Great Britain, specifically Scotland and central Ireland is underlain by a 'hot, low density region within the upper mantle, possible originating from the Icelandic plume' (Bott and Bott (2004), Arrowsmith *et al.*, (2005), Wawerzinek *et al.*, (2008)). Clegg and England (2003) mapped the depth to the Moho across Great Britain and suggested a pronounced thinning below Scotland compared to Southern Britain. No work has been conducted to examine the possible impact of such structure upon predictions of

either the 3D velocities or RSL predictions across the British Isles, so this is most certainly a target for future research.

The influence of lateral earth structure may be particularly important for modelling the RSL data given the distinct spatial sensitivity of the RSL predictions to the choice of earth model parameters. It was demonstrated in Chapter 5 that data from northern sites exhibited a stronger sensitivity to the choice of earth viscosity structure compared to data from southern sites. It is also noted that the most significant and yet unresolved data-model misfit exists at northern sites.

#### **6.4. Modelling of far-field RSL data**

One of the original aims of this thesis, and a key input to the final BIIS GIA model, was the development of a new global ice model, *EUST3* (Bradley *et al.*, (2010b) and as described in Section 4.4.5), which extended the published ice model of Bassett *et al.*, (2005), which was unconstrained over the last 10 kyr, using a set of un-modelled far-field RSL data from China and Malay-Thailand.

The *EUST3* model was optimised to fit both datasets and is characterised by an initial slowdown in the rate of eustatic sea level rise at 7 kyr BP, associated with the final deglaciation of the LIS, followed by a continued rise in eustatic sea level till 1 kyr BP. The pattern of eustatic sea level rise between 5 and 1 kyr BP is driven by continued melting from the AIS, at an average rate of  $0.68 \text{ mm yr}^{-1}$ , slowing to  $0.36 \text{ mm yr}^{-1}$  after 3 kyr BP.

As discussed in greater detail in Chapter 4, there is a large amount of evidence to support the continued melting of the AIS during the late Holocene (over the last 5 kyr), with the WAIS being the most likely source for the continued rise. However, it is important to note that, during the development of *EUST3*, no direct comparison was made between the revised pattern for the Holocene deglaciation history of the ice sheet and models of AIS deglaciation constrained using near-field evidence, such as RSL data or geomorphological observations. As far-field RSL data are generally only sensitive to the

total volume of the input global ice model, rather than the specific spatial and temporal history of the ice sheet configuration, this was not of key importance for this thesis. However, it is hoped that future research may compare the new Holocene deglacial pattern in *EUST3* with an AIS model which is consistent with near-field observations.

As was recently addressed in Milne and Mitrovica (2008), modelling eustatic sea level using far-field RSL records is not a straightforward procedure where observations of sea level change from a few or limited sites can be used as a direct indication of the global change in ice volume. This is emphasised by the differences between the two Holocene melt models that were developed in Chapter 4 when optimised to fit only the data from China or Malay-Thailand. Although the chronology and style of the melting between the two models was similar; with both preferring a staged slowdown beginning at 7 kyr BP and continued melting till 1 kyr BP; the average rate at which melt was added to the oceans during the last 5 kyr is markedly greater ( $0.96 \text{ mm yr}^{-1}$ ) for the China model compared to the Malay-Thailand model ( $0.63 \text{ mm yr}^{-1}$ ).

Since the development of *EUST3*, the model has subsequently been compared to other far-field RSL data, including those from Sumatra, the Caribbean and along the Spain-Portugal coastline (Leorri *et al.*, (2010), Peros and Milne (2010)). Although these modelling studies were not as extensive as the analyses carried out as part of this research, the predicted RSL at these additional sites was compatible with the observed data. It would be useful in future work to further compare the model to other far-field RSL datasets.

An important result from the forward modelling analysis in Chapter 4 is the distinctly different optimum earth viscosity structure identified for each region. It was not possible to define a single earth model that produced a high quality fit for the complete study area. The China data preferred weak values of upper and lower mantle viscosity, ruling out values greater than  $1.5 \times 10^{20} \text{ Pa s}$  and  $2 \times 10^{21} \text{ Pa s}$ , respectively. In contrast, the Malay-Thailand data prefer larger values, generally ruling out upper mantle values that are less than  $2 \times 10^{20} \text{ Pa s}$ . Although both studies regions are located within the Eurasian plate and close to active subduction zones, these results imply a more geodynamically complex

shallow earth structure below China, related to a weak upper mantle region associated with the subduction zone and the influence of the Hainan Plume. Only recently has the influence of active subducting margins on RSL predictions using GIA models been explored (James *et al.*, (2009)). One avenue of future research is to examine the impact of inferred lateral structure across China on RSL predictions using either a complete 3D earth model or a model with distinct weak layer within the upper mantle. Such a study may provide additional information on the possible range of viscosity values associated with regions of active subduction.

**Appendix A: Relative Sea Level data used within this thesis and corresponding references**

	Site Name.	Latitude	Longitude	Primary Sea-Level Index Points		
				Basal	Intercalated	Limiting
				Points	Points	Data
				+	+	↓
1	Shetland	60.34	-1.03	4		
2	Orkney	58.97	-2.97	3	3	9
3	Wick	58.45	-3.12		11	3
4	Dornoch Firth	57.86	-4.26	1	6	
5	Moray Firth	57.49	-4.46		9	
6	Coigach	58.05	-5.36		7	1
7	Hebrides	57.51	-7.55	1	1	1
8	Skye	57.14	-5.96		7	1
9	Applecross	57.32	-5.78	7		
10	Kintail	57.25	-5.48	16		
11	Arisaig	56.91	-5.85	39		8
12	Kentra	56.76	-5.84	14		2
13	NE Scotland	57.66	-1.98	8	11	5
14	Aberdeen	57.33	-1.99		4	
15	Montrose	56.71	-2.52	1	6	
16	Tay Valley	56.38	-3.21		36	
17	Forth Valley	56.12	-4.15	2	19	
18	Islay	55.81	-6.34	10		
19	Ardyne	55.87	-5.04		6	
20	Clyde	55.86	-4.49		5	
21	Ayr	55.53	-4.68		10	
22	SE Scotland	56.03	-2.69	1	2	
23	NE England North	55.69	-1.92	5	7	5
24	NE England Central	55.60	-1.73	1	7	2
25	NE England South	55.34	-1.60	9	17	1
26	Tyne	54.96	-1.67	1		
27	Tees	54.63	-1.23	9	21	
28	North Solway Firth	54.97	-3.15	6	24	2
29	South Solway Firth	54.90	-3.17	6	8	1
30	Cumbria	54.40	-3.32	1	5	
31	Isle of Man	54.40	-4.39	1	11	2
32	Morecambe Bay	54.09	-2.96	7	21	3
33	Lancashire	53.69	-2.99	4	38	1
34	Mersey	53.40	-3.14	3	12	
35	North Wales	53.30	-3.75	1	8	
36	Mid Wales	52.47	-4.06	7	7	3
37	Humber (Inn. Estuary)*	53.65	-0.66	11	20	30
38	Humber (Outer Estuary)*	53.66	-0.07	12	22	8
39	Lincolnshire Marshes *	53.50	0.24	12	18	3
40	Fens *	52.74	0.04	84	110	28
41	Norfolk *	52.97	0.79	5	26	18
42	East Anglia	52.49	1.64	10	15	5
43	Pembrokeshire	51.66	-5.07	1		

44	Glamorgan	51.58	-3.77	2	3	3	
45	Bristol Channel	51.35	-3.03	15	55		
46	Essex	51.70	0.83		11	1	
47	Thames	51.46	0.31	13	37	24	
48	Kent	51.07	1.02		71		
49	Sussex	50.84	0.33	1	10	3	
50	Hampshire	50.80	-1.35		11	4	
51	Dorset	50.62	-2.54	1	3		
52	Devon	50.39	-3.75		6	2	
53	Cornwall	50.13	-5.48	4	3		
54	Knapdale	55.78	-5.56	10		7	
60	German Bight	55.07	6.00		3		
61	Dogger Bank	55.02	2.98	1			
63	Offshore Yorkshire	53.99	0.17	1		1	
64	Offshore North Norfolk	52.99	1.11		1	1	
65	Offshore N.E. Norfolk	53.21	2.08	1	1	6	
<b>Site No.</b>	<b>Site Name.</b>	<b>Latitude</b>	<b>Longitude</b>	<b>Primary</b>	<b>Secondary</b>	<b>Limiting Data</b>	
				<b>Index Point</b>	<b>Index points</b>	<b>Primary</b>	<b>Secondary</b>
						 (max);  (min)	 (max);  (min)
80	Dublin	53.14	-6.12		1	3	3
81	South Wexford	52.52	-6.23	11	1	3	1
82	North Wexford	52.32	-6.41	1			
83	East Cork	51.95	-7.94	10	1		
84	West Cork	51.61	-8.91	13		3	1
85	Kerry	52.11	-9.92	13	4	20	2
86	South Clare	52.60	-9.72		1	4	
87	Middle Shannon	52.60	-9.21		3		
88	Inner Shannon	52.66	-8.71			15	8
89	Galway	53.24	-9.31			1	
90	Connemara	53.68	-9.90			10	
91	North Mayo	54.32	-9.54				8
92	Sligo	54.26	-8.61			1	
93	West Donegal	54.89	-8.43	8		10	1
94	North Donegal	55.16	-7.98	3		3	3
95	Lough Swilly	55.12	-7.38				7
96	Derry	55.15	-6.85			4	6
97	North Antrim	55.05	-6.01			5	3
98	North Down	54.55	-5.66			10	5
99	South Down	54.33	-5.77	2	2	4	4
100	Dundalk	53.95	-6.34			4	12

A1: Number of sea-level index points and data type at each site (see Fig. 2.3) used within Chapter 2 and 5. The graphical symbol used for each data type is shown in the third row. Sites 1-65 are located across the Great Britain and sites 80-100 are located in Ireland. Note that predictions and data at all sites are shown in Appendix B-G. The asterisk indicates sites where corrections for changes in tidal regimes have been applied.

Site reference	Site Name	Latitude	Longitude	Primary Sea level Index Points
				•
BB	Bohai Bay	38.98	119.33	23
JP	Jiangsu Province	33.55	119.84	13
YRD	Yangtze river delta	31.18	120.71	43
FP	Fujian Province	24.43	118.81	30
HRD	Han River delta	23.52	116.84	25
EG	East Guangdong	22.64	114.98	36
PRD	Pearl River Delta	22.63	113.53	55
WG	West Guangdong	21.81	111.84	9
HP	Hainan Province	18.77	109.71	39
CP	Chao Phraya	13.80	100.55	24
PA	Prachaub	11.75	99.75	2
PH	Phuket	8.53	98.42	11
ET	East Coast of Thailand	8.75	100.18	7
KG	Keelang	3.00	101.25	6
TI	Tiomin Island	2.80	104.07	5
MAL	Strait of Malacca	2.01	102.64	20

A2: Number of sea-level index points at each site (see Fig. 4.1) within the far-field RSL dataset used within Chapter 4. Sites BB, JP, YRD, FP, HRD, EG, PRD, WG and HP are located in China. Sites CP, PA, PH, ET, KG, MAL and TI are located across Malay-Thailand.

A3: References for all the British Isles RSL data, summarized for the Great Britain and Ireland dataset.

Site No.	Site Name.	Reference(s)
1	Shetland	Hoppe, 1965
2	Orkney	De La Vega and Smith, 1996
3	Wick	Dawson and Smith, 1997
4	Dornoch Firth	Smith <i>et al.</i> , 1992
5	Moray Firth	Firth and Haggart, 1989; Haggart, 1987
6	Coigach	Shennan <i>et al.</i> , 2000c
7	Hebrides	Ritchie, 1985
8	Skye	Selby <i>et al.</i> , 2000
9	Applecross	Shennan <i>et al.</i> , 2000c
10	Kintail	Shennan <i>et al.</i> , 2000c
11	Arisaig	Shennan <i>et al.</i> , 1993; 1994; 1995b; Shennan <i>et al.</i> , 1999; Shennan <i>et al.</i> , 2000c
12	Kentra	Shennan <i>et al.</i> , 1995a; Shennan <i>et al.</i> , 1996; Shennan <i>et al.</i> , 2000c
13	NE Scotland	Smith <i>et al.</i> , 1982
14	Aberdeen	Smith <i>et al.</i> , 1983
15	Montrose	Smith and Cullingford, 1985
16	Tay Valley	Smith <i>et al.</i> , 1985a; Smith <i>et al.</i> , 1985b
17	Forth Valley	Robinson, 1993
18	Islay	Dawson <i>et al.</i> , 1998
19	Ardyne	Peacock <i>et al.</i> , 1978
20	Clyde	Haggart, 1988
21	Ayr	Donner, 1970; Jardine, 1975; 1982
22	SE Scotland	Robinson, 1982
23	NE England North	Shennan <i>et al.</i> , 2000a
24	NE England Central	Plater and Shennan, 1992; Shennan <i>et al.</i> , 2000a
25	NE England South	Plater and Shennan, 1992; Shennan <i>et al.</i> , 2000a
26	Tyne	Shennan <i>et al.</i> , 2000a
27	Tees	Gaunt and Tooley, 1974; Plater and Poolton, 1992; Tooley, 1978b; c
28	North Solway Firth	Jardine, 1975; 1982; Lloyd <i>et al.</i> , 1999
29	South Solway Firth	Huddart <i>et al.</i> , 1977; Lloyd <i>et al.</i> , 1999; Tooley, 1978c
30	Cumbria	Huddart <i>et al.</i> , 1977; Tooley, 1978c
31	Isle of Man	Tooley, 1977
32	Morecambe Bay	Birks, 1982; Tooley, 1974; 1978c; Zong and Tooley, 1996; Zong, 1997
33	Lancashire	Huddart, 1992; Tooley, 1978a; c; 1985
34	Mersey	Bedlington, 1993; Cowell and Innes, 1994; Tooley, 1974; 1978a; c
35	North Wales	Bedlington, 1993; Kidson and Heyworth, 1982; Tooley, 1978c
36	Mid Wales	Heyworth and Kidson, 1982

37	Humber (Inn. Estuary)*	Andrews <i>et al.</i> , 2000; Gaunt and Tooley, 1974; Long <i>et al.</i> , 1998; Metcalfe <i>et al.</i> , 2000; Millett and Mcgrail, 1987; Smith, 1958; Van de Noort and Ellis, 1995; 1997; 1998
38	Humber (Outer Estuary)*	Andrews <i>et al.</i> , 2000; Gaunt and Tooley, 1974; Long <i>et al.</i> , 1998; Metcalfe <i>et al.</i> , 2000; Rees <i>et al.</i> , 2000; Van de Noort and Ellis, 1995
39	Lincolnshire Marshes *	Horton <i>et al.</i> , 2000; Waller, 1994
40	Fens *	Brew <i>et al.</i> , 2000; Shennan, 1986a; b; Waller, 1994
41	Norfolk *	Andrews <i>et al.</i> , 2000; Funnell and Pearson, 1989
42	East Anglia	Brew <i>et al.</i> , 1992; Coles and Funnell, 1981
43	Pembrokeshire	Heyworth and Kidson, 1982
44	Glamorgan	Heyworth and Kidson, 1982
45	Bristol Channel	Heyworth and Kidson, 1982
46	Essex	Devoy, 1982; Greensmith and Tucker, 1980; Wilkinson and Murphy, 1986
47	Thames	Devoy, 1982; Devoy, 1979
48	Kent	Long, 1992; Long and Innes, 1993; 1995; Tooley and Switsur, 1988
49	Sussex	Devoy, 1982; Jennings and Smyth, 1987
50	Hampshire	Long and Tooley, 1995
51	Dorset	Devoy, 1982
52	Devon	Devoy, 1982
53	Cornwall	Healy, 1995
54	Knapdale	Sutherland, 1981
60	German Bight	Ludwig <i>et al.</i> , 1981
61	Dogger Bank	Shennan <i>et al.</i> , 2000b
63	Offshore Yorkshire	Shennan <i>et al.</i> , 2000b
64	Offshore North Norfolk	Shennan <i>et al.</i> , 2000b
65	Offshore N.E. Norfolk	Shennan <i>et al.</i> , 2000b
Site No.	Site Name.	Reference(s)
80	Dublin	Mitchell, 1976
81	South Wexford	Carter and Orford, 1982; Dresser, 1980; Maloney, 1985; Mitchell, 1977; Orford and Carter, 1982; Sinnott, 1999
82	North Wexford	Sinnott, 1999
83	East Cork	Carter <i>et al.</i> , 1989; Mitchell, 1976; 1977; Sinnott, 1999
84	West Cork	Buzer, 1980; Sinnott, 1999; Stillman, 1968
85	Kerry	Carter <i>et al.</i> , 1989
86	South Clare	Devoy <i>et al.</i> , 1996; O'Sullivan, 2001; Pearson, 1979
87	Middle Shannon	O'Sullivan, 2001
88	Inner Shannon	O'Sullivan, 2001
89	Galway	Mitchell, 1976
90	Connemara	Devoy <i>et al.</i> , 1996; Jessen, 1949
91	North Mayo	McCabe <i>et al.</i> , 1986; McCabe <i>et al.</i> , 2005
92	Sligo	Burenhult, 1980

93	West Donegal	Carter, 1982; Gaulin et al., 1983; Gehrels, 2004; Harmon, 2006; Pearson, 1979; Shaw, 1985; Shaw and Carter, 1994; Smith and Pilcher, 1973; Telford, 1978
94	North Donegal	Shaw, 1985; Shaw and Carter, 1994
95	Lough Swilly	Colhoun et al., 1973; McCabe and Clark, 2003; Shaw and Carter, 1994
96	Derry	Woodman (unpuba); Bazley (unpuba); Battarbee et al., 1982; Carter and Wilson, 1980; Pearson, 1979
97	North Antrim	Mitchell and Stephens, 1974; Prior et al., 1981; Smith et al., 1974
98	North Down	Harkness and Wilson, 1979; Kelley et al., 2006; Manning et al., 1970; McCabe and Clark, 1998; Morrison et al., 1965; Morrison and Stephens, 1961; Pearson and Pilcher, 1975; Smith et al., 1974; Stephens and Collins, 1960
99	South Down	Carter, 1982; Dresser et al., 1973; Harmon, 2006; Hubbs et al., 1965; McCabe and Clark, 1998; Singh and Smith, 1973
100	Dundalk	Jessen, 1949; McCabe and Haynes, 1996; McCabe and Clark, 1998; McCabe et al., 2005; Mitchell, 1971; Penney, 1983; Clark et al. (submittedb)
		a cited in Carter, 1982 bcited in McCabe et al., 2005

### References for Great Britain Data:

Andrews, J., G. Samways, P. F. Dennis, and B. A. Maher (2000), Origin, abundance and storage of organic carbon and sulphur in the Holocene Humber Estuary: emphasising human impact on storage changes, in *Holocene land-ocean interaction and environmental change around the North Sea*, edited by I. Shennan and J. E. Andrews, pp. 145-170, Geological Society, Special Publications, 166.

Bedlington, D. J. (1993), Holocene sea-level changes and crustal movements in North Wales and Wirral, Thesis thesis, University of Durham, Durham City.

Birks, H. J. B. (1982), Mid-flandrian forest history of Roudsea Wood National Nature Reserve, Cumbria, *New Phytologist*, 90, 339-354.

Brew, D. S., B. M. Funnell, and A. Kreiser (1992), Sedimentary environments and Holocene evolution of the Lower Blyth Estuary, Suffolk (England), and a comparison with other East Anglian coastal sequences, *Proceedings of the Geologists' Association*, 103, 57-74.

Brew, D. S., T. Holt, K. Pye, and R. Newsham (2000), Holocene stratigraphy, sediments and palaeocoastlines of the Fenland embayment, eastern England, in *Holocene land-ocean interaction and environmental change around the North Sea*, edited by I. Shennan and J. E. Andrews, pp. 253-273, Geological Society, Special Publications, 166, London.

Coles, B. P. L., and B. M. Funnell (1981), Holocene palaeoenvironments of Broadland, England, *International Association of Sedimentologists*, 5, 123-131.

Cowell, R. W., and J. B. Innes (1994), The Wetlands of Mersyde. Northwest Westlands Survey 1.

Dawson, S., and D. E. Smith (1997), Holocene relative sea-level changes on the margin of a glacio-isostatically uplifted area: an example from northern Caithness, Scotland, *The Holocene*, 7, 59-77.

Dawson, S., A. G. Dawson, and K. J. Edwards (1998), Rapid Holocene relative sea-level changes in Gruinart, Isle of Islay, Scottish Inner Hebrides, *Holocene*, 8(2), 183-195.

De La Vega, A. C., and D. E. Smith (1996), Holocene relative sea-level and coastal changes in Scapa Bay, Orkney, in *The Quaternary of Orkney Field Guide*, edited by A. M. Hall, pp. 69-83, Quaternary Research Association, London.

- Devoy, R. J. (1982), Analysis of the geological evidence for Holocene sea-level movements in southeast England, *Proceedings of the Geologists' Association*, 93, 65-90.
- Devoy, R. J. N. (1979), Flandrian sea level changes and vegetational history of the lower Thames estuary, *Phil. Trans. R. Soc. Lond. B*, 285, 355-410.
- Donner, J. J. (1970), Land/sea level changes in Scotland, in *Studies in the vegetational history of the British Isles*, edited by D. Walker and R. G. West, pp. 23-39, Cambridge University Press, Cambridge.
- Firth, C. R., and A. Haggart (1989), Loch Lomond Stadial and Flandrian Shorelines in the Inner Moray Firth Area, Scotland, *JQS*, 4(1), 37-50.
- Funnell, B. M., and I. Pearson (1989), Holocene sedimentation on the north Norfolk barrier coast in relation to relative sea-level change, *JQS*, 4, 25-36.
- Gaunt, G. D., and M. J. Tooley (1974), Evidence for Flandrian sea-level changes in the Humber estuary and adjacent areas, *Bulletin of the Institute of Geological Sciences*, 48, 25-41.
- Greensmith, J. T., and E. V. Tucker (1980), Evidence for differential subsidence on the Essex coast, *Proceedings of the Geologists' Association*, 91, 169-175.
- Haggart, B. A. (1987), Relative sea-level changes at a site in the Beaulieu Firth area, Scotland, in *Sea-Level Changes*, edited by M. J. Tooley and I. Shennan, pp. 67-108, Blackwell, Oxford.
- Haggart, B. A. (1988), A review of radiocarbon dates on peat and wood from Holocene coastal sedimentary sequences in Scotland, *Scottish Journal of Geology*, 24, 125-144.
- Healy, M. G. (1995), The lithostratigraphy and biostratigraphy of a holocene coastal sediment sequence in Marazion Marsh, west Cornwall, U.K. with reference to relative sea-level movements, *Marine Geology*, 124, 237-252.
- Heyworth, A., and C. Kidson (1982), Sea-level changes in southwest England and Wales, *Proceedings of the Geologists' Association*, 93, 91-111.
- Hoppe, G. (1965), Submarine peat in the Shetland Islands, *Geografiska Annaler*, 47, 195-203.
- Horton, B. P., R. J. Edwards, and J. M. Lloyd (2000), Implications of a microfossil based transfer function in Holocene sea-level studies., in *Holocene Land-ocean interaction and environmental change around the North Sea.*, edited by I. Shennan and J. Andrews, pp. 41-54, Geological Society, London.
- Huddart, D., M. J. Tooley, and P. A. Carter (1977), The coasts of north-west England, in *The Quaternary History of the Irish Sea*, edited by C. Kidson and M. J. Tooley, pp. 119-154, Seel House Press, Liverpool.
- Huddart, D. (1992), Coastal environmental changes and morphostratigraphy in southwest Lancashire, England, *Proceedings of the Geologists' Association*, 103, 217-236.
- Jardine, W. G. (1975), Chronology of Holocene marine transgression and regression in south-western Scotland, *Boreas*, 4, 173-196.
- Jardine, W. G. (1982), Sea-level changes in Scotland during the last 18000 years, *Proceedings of the Geologists' Association*, 93, 25-42.
- Jennings, S., and C. Smyth (1987), Coastal sedimentation in East Essex during the Holocene, *Prog. Oceanog*, 18, 205-241.
- Kidson, C., and A. Heyworth (1982), Sea-level changes in southwest England and Wales, *Proceedings of the Geologists' Association*, 93, 91-112.
- Lloyd, J. M., I. Shennan, J. R. Kirby, and M. M. Rutherford (1999), Holocene relative sea-level changes in the inner Solway Firth, *Quat. Int.*, 60, 83-105.
- Long, A. J. (1992), Coastal responses to changes in sea-level in the East Kent Fens and southeast England, *Proceedings of the Geologists' Association*, 103, 187-199.
- Long, A. J., and J. B. Innes (1993), Holocene Sea-Level Changes and Coastal Sedimentation in Romney Marsh, Southeast England, UK, *Proceedings of the Geologists' Association*, 104, 223-237.
- Long, A. J., and J. B. Innes (1995), The back-barrier and barrier depositional history of Romney Marsh, Walland Marsh and Dungeness, Kent, England, *JQS*, 10, 267-283.

Long, A. J., and M. J. Tooley (1995), Holocene sea-level and crustal movements in Hampshire and southeast England, United Kingdom, *Journal of Coastal Research*, 17, 299-310.

Long, A. J., J. B. Innes, J. R. Kirby, J. M. Lloyd, M. M. Rutherford, I. Shennan, and M. J. Tooley (1998), Holocene sea-level change and coastal evolution in the Humber estuary, eastern England: an assessment of rapid coastal change, *The Holocene*, 8(2), 229-247.

Ludwig, G., H. Muller, and H. Streif (1981), New dates on Holocene sea-level changes in the German Bight, *Spec. Publs int. Ass. Sediment.*, 5, 211-219.

Metcalf, S. E., S. Ellis, B. P. Horton, J. B. Innes, J. McArthur, A. Mitlehner, A. Parkes, J. S. Pethick, J. Rees, J. Ridgway, M. M. Rutherford, I. Shennan, and M. J. Tooley (2000), The Holocene evolution of the Humber Estuary: reconstructing change in a dynamic environment, in *Holocene land-ocean interaction and environmental change around the North Sea*, edited by I. Shennan and J. Andrews, pp. 97-118, Geological Society, Special Publications, 166, London.

Millett, M., and S. Mcgrail (1987), The archaeology of the Hasholme logboat, *Archaeol. J.*, 144, 69-155.

Peacock, J. D., D. K. Graham, and I. P. Wilkinson (1978), Late-Glacial and post-Glacial marine environments at Ardyne, Scotland, and their significance in the interpretation of the history of the Clyde sea area, *Report of the Institute of Geological Sciences*, 78/17, 1-25.

Plater, A. J., and N. R. J. Poolton (1992), Interpretation of Holocene sea level tendency and intertidal sedimentation in the Tees Estuary using sediment luminescence techniques: a viability study, *Sedimentology*, 39, 1-15.

Plater, A. J., and I. Shennan (1992), Evidence of Holocene sea-level change from the Northumberland coast, eastern England, *Proceedings of the Geologists' Association*, 103, 201-216.

Rees, J., J. Ridgway, S. Ellis, R. O'B Knox, R. Newsham, and A. Parkes (2000), Holocene sediment storage in the Humber estuary, in *Holocene land-ocean interaction and environmental change around the North Sea*, edited by I. Shennan and J. E. Andrews, pp. 119-144, Geological Society, Special Publications, 166.

Ritchie, W. (1985), Inter-tidal and sub-tidal organic deposits and sea level changes in the Uists, Outer Hebrides, *Scottish Journal of Geology*, 21, 161-176.

Robinson, M. (1982), Diatom analysis of Early Flandrian lagoon sediments from East Lothian, Scotland, *Journal of Biogeography*, 9, 207-221.

Robinson, M. (1993), Microfossil analyses and radiocarbon dating of depositional sequences related to Holocene sea-level change in the Forth valley, Scotland, *Transactions of the Royal Society of Edinburgh*, 84, 1-60.

Selby, K. A., D. E. Smith, A. G. Dawson, and T. M. Mighall (2000), Late Devensian and Holocene relative sea-level and environmental changes from an isolation basin in southern Skye, *Scottish Journal of Geology*, 36, 73-86.

Shennan, I. (1986a), Flandrian sea-level changes in the Fenland I. The geographical setting and evidence of relative sea-level changes, *JQS*, 1, 119-154.

Shennan, I. (1986b), Flandrian sea-level changes in the Fenland II. Tendencies of sea-level movement, altitudinal changes and local and regional factors, *JQS*, 1, 155-179.

Shennan, I., J. B. Innes, A. J. Long, and Y. Zong (1993), Late Devensian and Holocene relative sea-level changes at Rumach, near Arisaig, northwest Scotland, *Norsk Geologisk Tidsskrift*, 73, 161-174.

Shennan, I., J. B. Innes, A. J. Long, and Y. Zong (1994), Late Devensian and Holocene relative sea-level changes at Loch nan Eala, near Arisaig, northwest Scotland, *JQS*, 9, 261-283.

Shennan, I., J. B. Innes, A. J. Long, and Y. Zong (1995a), Holocene relative sea level changes and coastal vegetation history at Kentra Moss, Argyll, Northwest Scotland, *JQS*, 9, 261-283.

Shennan, I., J. B. Innes, A. J. Long, and Y. Zong (1995b), Late Devensian and Holocene relative sea-level changes in northwestern Scotland: new data to test existing models, *Quat. Int.*, 26, 97-123.

- Shennan, I., F. M. L. Green, J. B. Innes, J. M. Lloyd, M. M. Rutherford, and K. Walker (1996), Evaluation of rapid relative sea-level changes in north-west Scotland during the last Glacial-Interglacial transition: evidence from Ardtoe and other isolation basins, *Journal of Coastal Research*, 12, 862-874.
- Shennan, I., M. J. Tooley, F. M. L. Green, J. B. Innes, K. Kennington, J. M. Lloyd, and M. M. Rutherford (1999), Sea level, climate change and coastal evolution in Morar, northwest Scotland, *Geologie en Mijnbouw*, 77, 247-262.
- Shennan, I., B. P. Horton, J. B. Innes, W. R. Gehrels, J. M. Lloyd, J. J. McArthur, and M. M. Rutherford (2000a), Late Quaternary sea-level changes, crustal movements and coastal evolution in Northumberland, UK, *JQS*, 15, 215-237.
- Shennan, I., K. Lambeck, R. Flather, B. P. Horton, J. J. McArthur, J. B. Innes, J. M. Lloyd, M. M. Rutherford, and R. Wingfield (2000b), Modelling western North Sea palaeogeographies and tidal changes during the Holocene, in *Holocene land-ocean interaction and environmental change around the North Sea*, edited by I. Shennan and J. Andrews, pp. 299-319, Geological Society, Special Publications, 166, London.
- Shennan, I., K. Lambeck, B. Horton, J. Innes, J. Lloyd, J. McArthur, T. Purcell, and M. Rutherford (2000c), Late Devensian and Holocene records of relative sea-level changes in northwest Scotland and their implications for glacio-hydro-isostatic modelling, *Quaternary Science Reviews*, 19(11), 1103-1135.
- Smith, A. G. (1958), Post-Glacial deposits in south Yorkshire and north Lincolnshire, *New Phytologist*, 57, 19-49.
- Smith, D., E. C. Firth, R. S. Turbayne, C. and C. Brooks, L (1992), Relative sea-level changes and shoreline displacements in the Dornock Firth area, Scotland, *Proceedings of the Geologists' Association*, 103, 237-257.
- Smith, D. E., R. A. Cullingford, and W. P. Seymour (1982), Flandrian relative sea-level changes in the Philorth valley, north-east Scotland, *Transactions of the Institute of British Geographers*, 7, 321-336.
- Smith, D. E., R. A. Cullingford, and C. L. Brooks (1983), Flandrian relative sea level changes in the Ythan Valley, Northeast Scotland, *Earth Surface Processes and Landforms*, 8, 423-438.
- Smith, D. E., and R. A. Cullingford (1985), Flandrian relative sea-level changes in the Montrose Basin area, *Scottish Geographical Magazine*, 101, 91-105.
- Smith, D. E., R. A. Cullingford, and B. A. Haggart (1985a), A major coastal flood during the Holocene in eastern Scotland, *Eiszeitalter und Gegenwart*, 35, 109-118.
- Smith, D. E., A. G. Dawson, R. A. Cullingford, and D. D. Harkness (1985b), The stratigraphy of Flandrian relative sea-level at a site in Tayside, Scotland, *Earth Surface Processes and Landforms*, 10, 17-25.
- Sutherland, D. G. (1981), The raised shorelines and deglaciation of the Loch Long/Loch Fyne area, western Scotland, Thesis thesis, University of Edinburgh, Edinburgh.
- Tooley, M. J. (1974), Sea-level changes during the last 9000 years in northwest England, *The Geographical Journal*, 140, 18-42.
- Tooley, M. J. (1977), *The Isle of Man, Lancashire Coast and Lake District. Field Guide A4. X INQUA Congress*, 60 pp., Geo. Abstracts Ltd., Norwich.
- Tooley, M. J. (1978a), Interpretation of Holocene sea-level changes, *Geologiska Foreningens i Stockholm Forhandlingar*, 100, 203-212.
- Tooley, M. J. (1978b), The history of Hartlepool Bay, *International Journal of Nautical Archaeology and Underwater Exploration*, 7, 71-75.
- Tooley, M. J. (1978c), *Sea-level changes in north-west England during the Flandrian Stage*, 232 pp., Clarendon Press, Oxford.
- Tooley, M. J. (1985), Sea-level changes and coastal morphology in North-West England, in *The Geomorphology of North-West England*, edited by R. H. Johnson, pp. 94-121, Manchester University Press, Manchester.

- Tooley, M. J., and V. R. Switsur (1988), Water level changes and sedimentation during the Flandrian age in the Romney Marsh area, in *Romney Marsh evolution, occupation, reclamation*, edited by J. Eddison and C. P. Green, pp. 53-71, Oxford Committee for Archaeology, Monograph No. 24, Oxford.
- Van de Noort, R., and S. Ellis (1995), *Wetland heritage of Holderness*, Humber Wetlands Project, University of Hull, Hull.
- Van de Noort, R., and S. Ellis (1997), *Wetland heritage of the Humberhead Levels*, Humber Wetlands Project, University of Hull, Hull.
- Van de Noort, R., and S. Ellis (1998), *Wetland Heritage of the Ancholme and Lower Trent Valleys*, Centre for Wetland Archaeology, University of Hull, Hull.
- Waller, M. (1994), *The Fenland Project, Number 9: Flandrian Environmental Change in Fenland, East Anglia*, East Anglian Archaeology Report No. 70, Fenland Project Committee, Cambridgeshire County Council, Cambridge.
- Wilkinson, T. J., and P. Murphy (1986), *The Hullbridge Basin Survey, 1985*, Interim Report No. 6 ed., Essex County Council.
- Zong, Y., and M. Tooley (1996), Holocene sea-level changes and crustal movements in Morecambe Bay, northwest England, *JQS*, 11, 43-58.
- Zong, Y. (1997), Mid and late-Holocene sea-level changes in Roudsea Marsh, Northwest England: a diatom biostratigraphical investigation, *The Holocene*, 7(3), 311-323.

### References for Ireland Data:

- Battarbee, R. W., R. G. Scaife, and S. j. Phetheon (1982), Paleoecological evidence for sea-level change in the Bann Estuary in early Mesolithic, in *Excavations at Mountsandel*, edited by Woodman, p. 8, HMSO.
- Burenhult, G. (1980), The archaeological excavation at Carrowmore, Co. Sligo, Ireland : excavation seasons 1977-79, *Theses and papers in North European Archaeology*, 9, 142.
- Buzer, J. S. (1980), POLLEN ANALYSES OF SEDIMENTS FROM LOUGH-INE AND BALLYALLY-LOUGH, CO CORK, SW IRELAND, *New Phytol.*, 86(1), 93-&.
- Carter, R. W. G., and P. Wilson (1980), Portstewart Strand and the Bann Estuary in *North Antrim and Londonderry: Irish Association for Quaternary Studies (IQUA) Field Guide no.13*, edited by P. Wilson, pp. 18-23.
- Carter, R. W. G. (1982), SEA LEVEL CHANGES IN NORTHERN IRELAND UK, *Proceedings of the Geologists' Association*, 93(1), 7-24.
- Carter, R. W. G., and J. D. Orford (1982), The south and east coasts of Co. Wexford, *Irish Association for Quaternary Studies (IQUA) Field Guide no.4*.
- Carter, R. W. G., R. J. N. Devoy, and J. Shaw (1989), Late Holocene sea levels in Ireland, *Journal of Quaternary Science*, 4(1), 7-24.
- Colhoun, E. A., A. T. Ryder, and N. Stephens (1973), <sup>14</sup>C age of an oak-hazel forest bed at Drumskillan, Co. Donegal and its relations to the Late-Midlandian and Littletonian raised beaches, *Irish Naturalists Journal*, 17, 321-327.
- Devoy, R. J. N., C. Delaney, R. W. G. Carter, and S. C. Jennings (1996), Coastal stratigraphies as indicators of environmental changes upon European Atlantic coasts in the Late Holocene, *J. Coast. Res.*, 12(3), 564-588.
- Dresser, P. Q., A. G. Smith, and G. W. Pearson (1973), Radiocarbon dating of the raised beach at Woodgrange Co. Down, *Proceedings of the Royal Irish Academy*, 73B, 53-56.
- Dresser, P. Q. (1980), DUBLIN RADIOCARBON-DATES, *Radiocarbon*, 22(4), 1028-1030.

Gaulin, C., G. Delibraïis, and M. Deneffe (1983), Analyse pollinique et datation par le  $^{14}\text{C}$  d'une tourbière submergée de l'âge de Bronze dans le Nord-Ouest d'Irlande (presqu'île de Termon Dungloe, Co. Donegal), *Comptes Rendus de l'Académie des Sciences Paris*, 296(II), 305-307.

Gehrels, R. (2004), Saltmarsh fieldwork, stratigraphy, micropalaeontology, transfer functions: Ireland, in *Late Holocene Shallow Marine Environments of Europe (HOLSMEER) Final Report*, edited by J. Scourse, pp. 107-120.

Harkness, D. D., and H. W. Wilson (1979), SCOTTISH-UNIVERSITIES RESEARCH AND REACTOR CENTER RADIOCARBON MEASUREMENTS - III, *Radiocarbon*, 21(2), 203-256.

Harmon, M. (2006), Saltmarsh archives of relative sea-level change during the late Holocene in the north of Ireland, Queens University, Belfast.

Hubbs, C. L., G. S. Bien, and H. E. Suess (1965), LA JOLLA NATURAL RADIOCARBON MEASUREMENTS .4, *Radiocarbon*, 7, 66-&.

Jessen, K. (1949), Studies of late Quaternary deposits and flora history of Ireland, *Proceedings of the Royal Irish Academy*, 52B, 85-290.

Kelley, J. T., J. A. G. Cooper, D. W. T. Jackson, D. F. Belknap, and R. J. Quinn (2006), Sea-level change and inner shelf stratigraphy off Northern Ireland, *Mar. Geol.*, 232(1-2), 1-15.

Maloney, B. K. (1985), A palaeoecological investigation of the Holocene back-barrier environment near Carnsore Point, Co. Wexford, *Proceedings of the Royal Irish Academy*, 85B, 73-89.

Manning, P. I., J. A. Robbie, and H. E. Wilson (1970), The geology of Belfast and the Lagan Valley, *Memoirs of the Geological Survey Northern Ireland*.

McCabe, A. M., J. R. Haynes, and N. F. MacMillan (1986), Late-Pleistocene tidewater glaciers and glaciomarine sequences from north County Mayo, Republic of Ireland, *Journal of Quaternary Science*, 1(1), 73-84.

McCabe, A. M., and J. R. Haynes (1996), A Late Pleistocene intertidal boulder pavement from an isostatically emergent coast, Dundalk Bay, eastern Ireland, *Earth Surf. Process. Landf.*, 21(6), 555-572.

McCabe, A. M., and P. U. Clark (1998), Ice-sheet variability around the north Atlantic Ocean during the last deglaciation, *Nature*, 392(6674), 373-377.

McCabe, A. M., and P. U. Clark (2003), Deglacial chronology from County Donegal, Ireland: implications for deglaciation of the British-Irish ice sheet, *J. Geol. Soc.*, 160, 847-855.

McCabe, A. M., P. U. Clark, and J. Clark (2005), AMS C-14 dating of deglacial events in the Irish Sea Basin and other sectors of the British-Irish ice sheet, *Quat. Sci. Rev.*, 24(14-15), 1673-1690.

Mitchell, G. F. (1971), LARNIAN CULTURE - MINIMAL VIEW, *Proceedings of the Prehistoric Society*, 37(DEC), 274-283.

Mitchell, G. F., and N. Stephens (1974), Is there evidence for a Holocene sea-level higher than that of today on the coasts of Ireland?, *Colloques Internationaux CNRS*, 219, 115-125.

Mitchell, G. F. (1976), *The Irish Landscape*, Collins, London.

Mitchell, G. F. (1977), Raised Beaches and sea levels, in *British Quaternary Studies-Recent Advances*, edited by F. w. Shotton, pp. 169-186, Clarendon Press.

Morrison, M. E., N. Stephens, M. Jope, F. W. Anderson, F. E. Round, H. Godwin, and E. H. Willis (1965), A SUBMERGED LATE-QUATERNARY DEPOSIT AT RODDANS PORT ON NORTH-EAST COAST OF IRELAND, *Philos. Trans. R. Soc. Lond. Ser. B-Biol. Sci.*, 249(758), 221-&.

Morrison, M. E. S., and N. Stephens (1961), Stratigraphy and pollen analysis of the raised beach deposits at Ballyhalbert, Co. Down, *New Phytol.*, 59, 153-162.

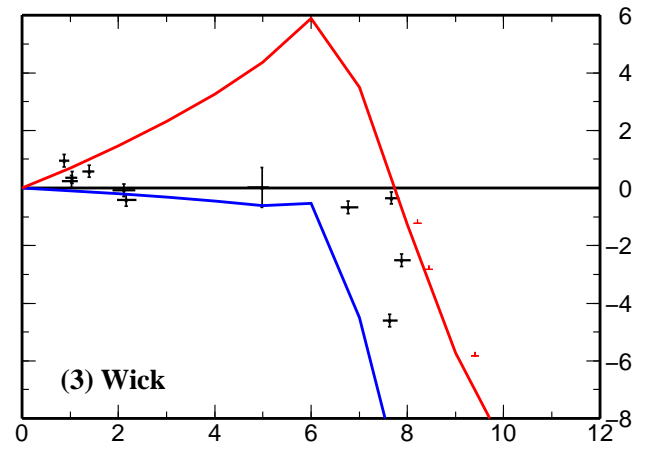
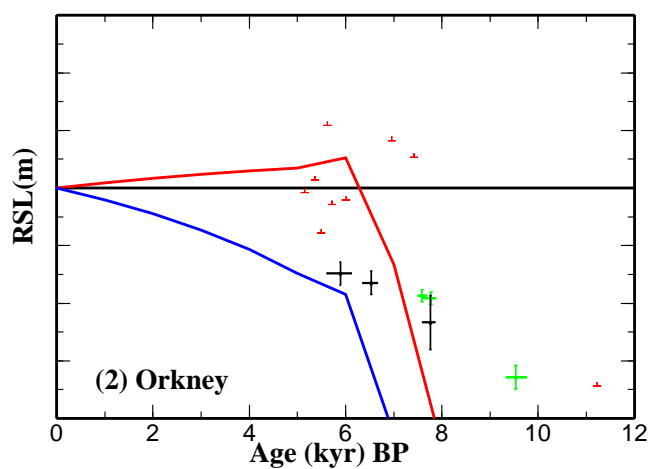
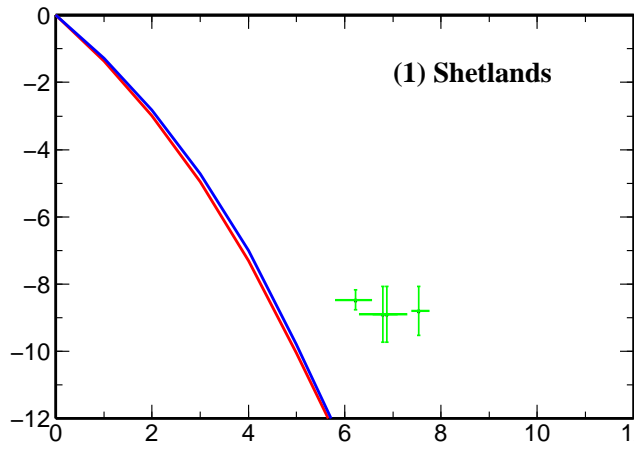
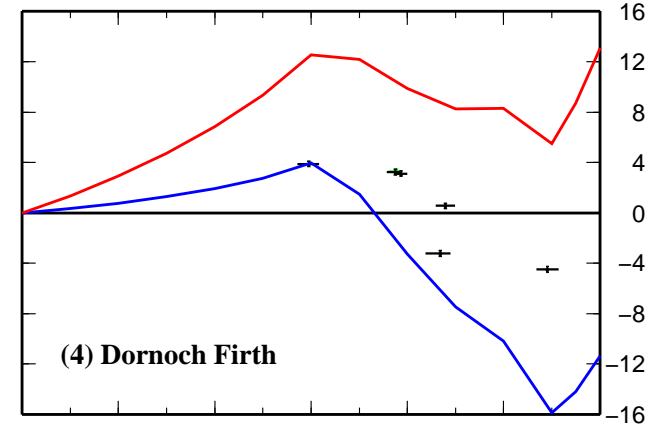
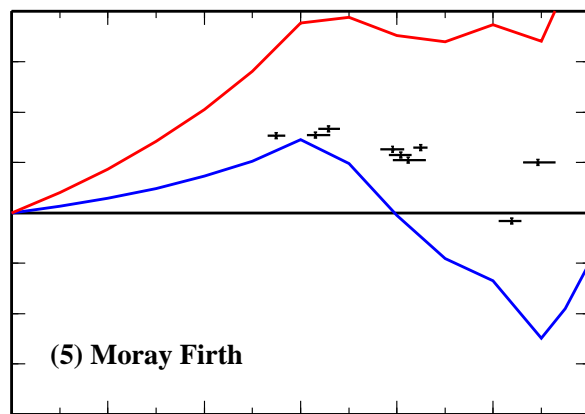
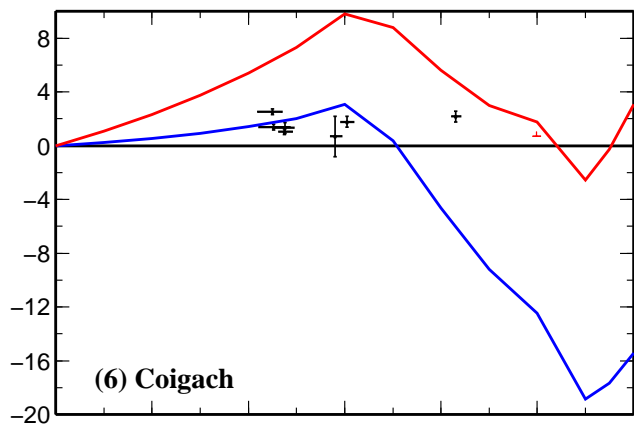
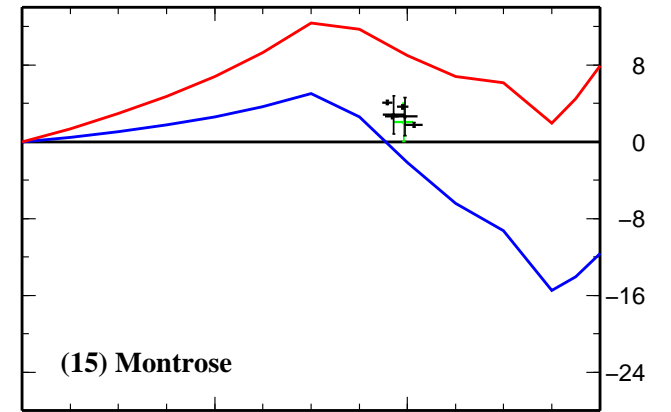
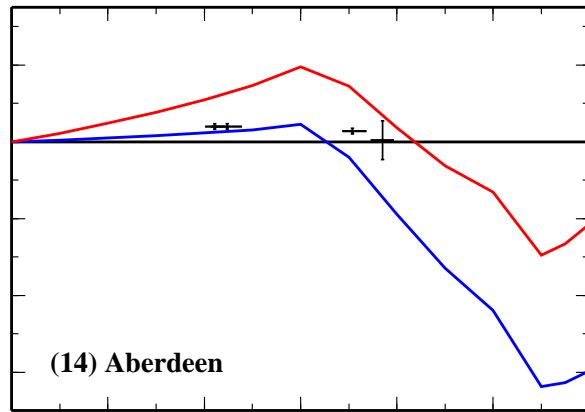
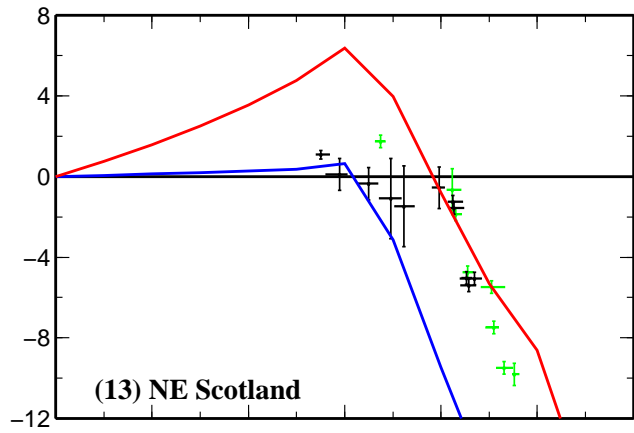
O'Sullivan, A. (2001), Foragers, Farmers and Fishers in a Coastal Landscape: An Intertidal Archaeological Survey of the Shannon Estuary, *Royal Irish Academy, Dublin*.

Orford, J. D., and R. W. G. Carter (1982), Geomorphological changes on the barrier coast of south Wexford, *Irish Geography*, 15, 70-84.

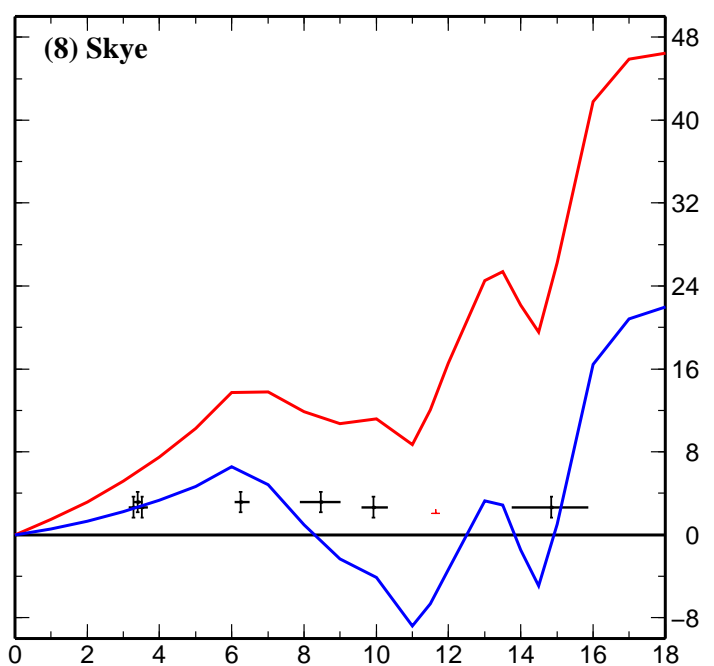
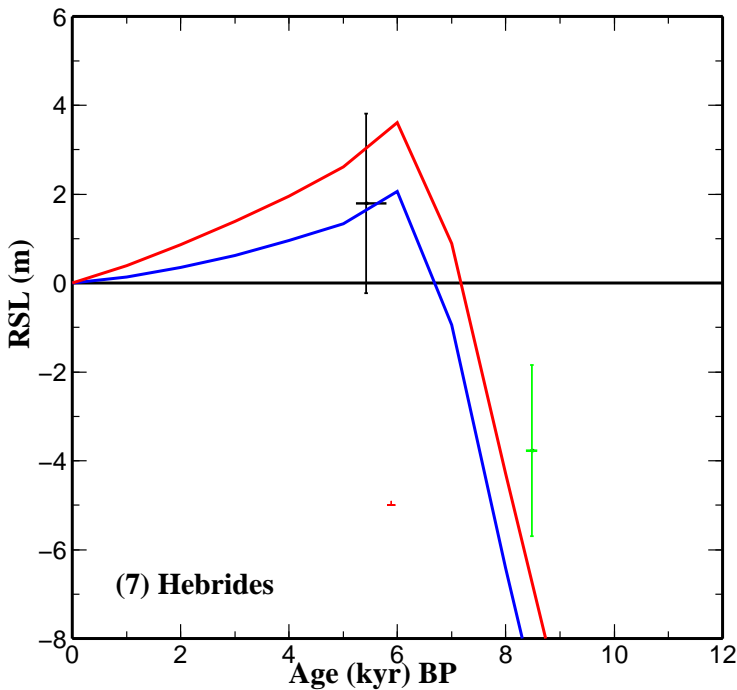
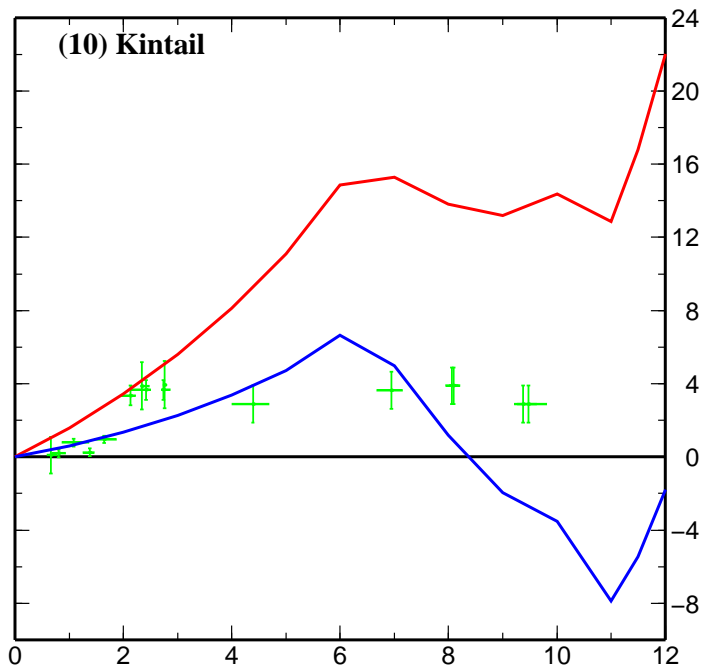
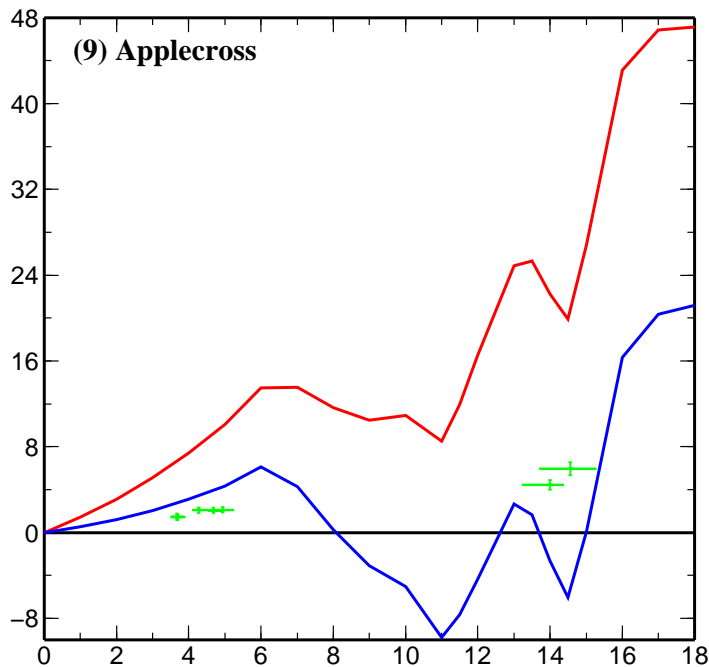
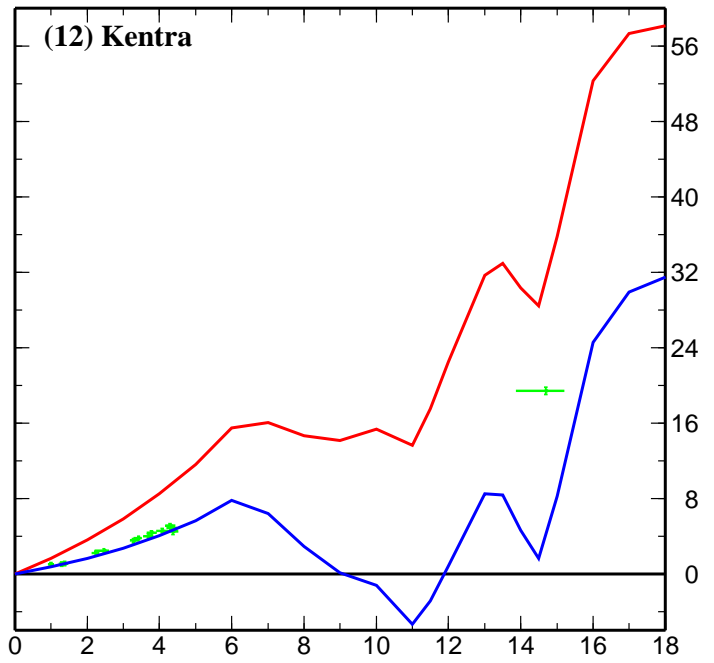
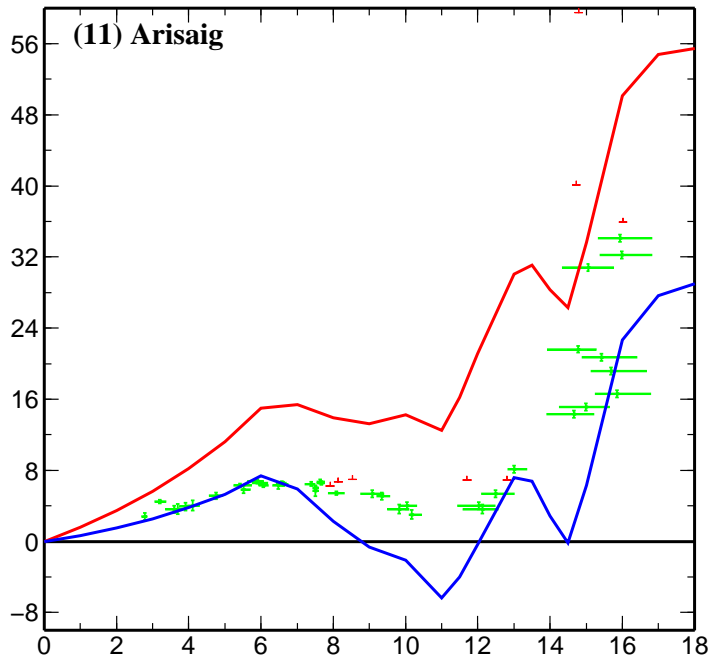
- Pearson, G. W., and J. R. Pilcher (1975), BELFAST RADIOCARBON-DATES VIII, *Radiocarbon*, 17(2), 226-238.
- Pearson, G. W. (1979), BELFAST RADIOCARBON DATES - IX, *Radiocarbon*, 21(2), 274-290.
- Penney, D. (1983), Post Glacial sediments and foraminifera at Dundalk, Ireland, University of Dublin (TCD).
- Prior, D. B., S. Holland, and M. M. Cruickshank (1981), A preliminary report on Late Devensian and early Flandrian deposits at Carnlough, Co. Antrim, *Irish Geography*, 14, 75-84.
- Shaw, J. (1985), Holocene coastal evolution, Co. Donegal, Ireland, The University of Ulster: Coleraine.
- Shaw, J., and R. W. G. Carter (1994), COASTAL PEATS FROM NORTHWEST IRELAND - IMPLICATIONS FOR LATE-HOLOCENE RELATIVE SEA-LEVEL CHANGE AND SHORELINE EVOLUTION, *Boreas*, 23(1), 74-91.
- Singh, G., and A. G. Smith (1973), Post Glacial vegetational history and relative land and sea level changes in Lecale, Co. Down, *Proceedings of the Royal Irish Academy*, 73B, 1-51.
- Sinnott, A. (1999), Holocene sea-level changes from the south and southeast coasts of Ireland, University College Cork
- Smith, A. G., and J. R. Pilcher (1973), RADIOCARBON-DATES AND VEGETATIONAL HISTORY OF BRITISH-ISLES, *New Phytol.*, 72(4), 903-&.
- Smith, A. G., G. W. Pearson, and J. R. Pilcher (1974), BELFAST RADIOCARBON DATES - VII, *Radiocarbon*, 16(2), 269-276.
- Stephens, N., and A. E. P. Collins (1960), The Quaternary deposits at Ringneill Quay and Ardmillan, Co. Down, *Proceedings of the Royal Irish Academy*, 61C, 41-77.
- Stillman, C. J. (1968), The post-glacial change in sea-level in southwest Ireland: new evidence from freshwater deposits on the floor of Bantry Bay, *Scientific Proceedings of the Royal Dublin Society* 3A, 125-127.
- Telford, M. B. (1978), Glenveagh Forest Park: the past and present vegetation, University of Dublin (TCD).

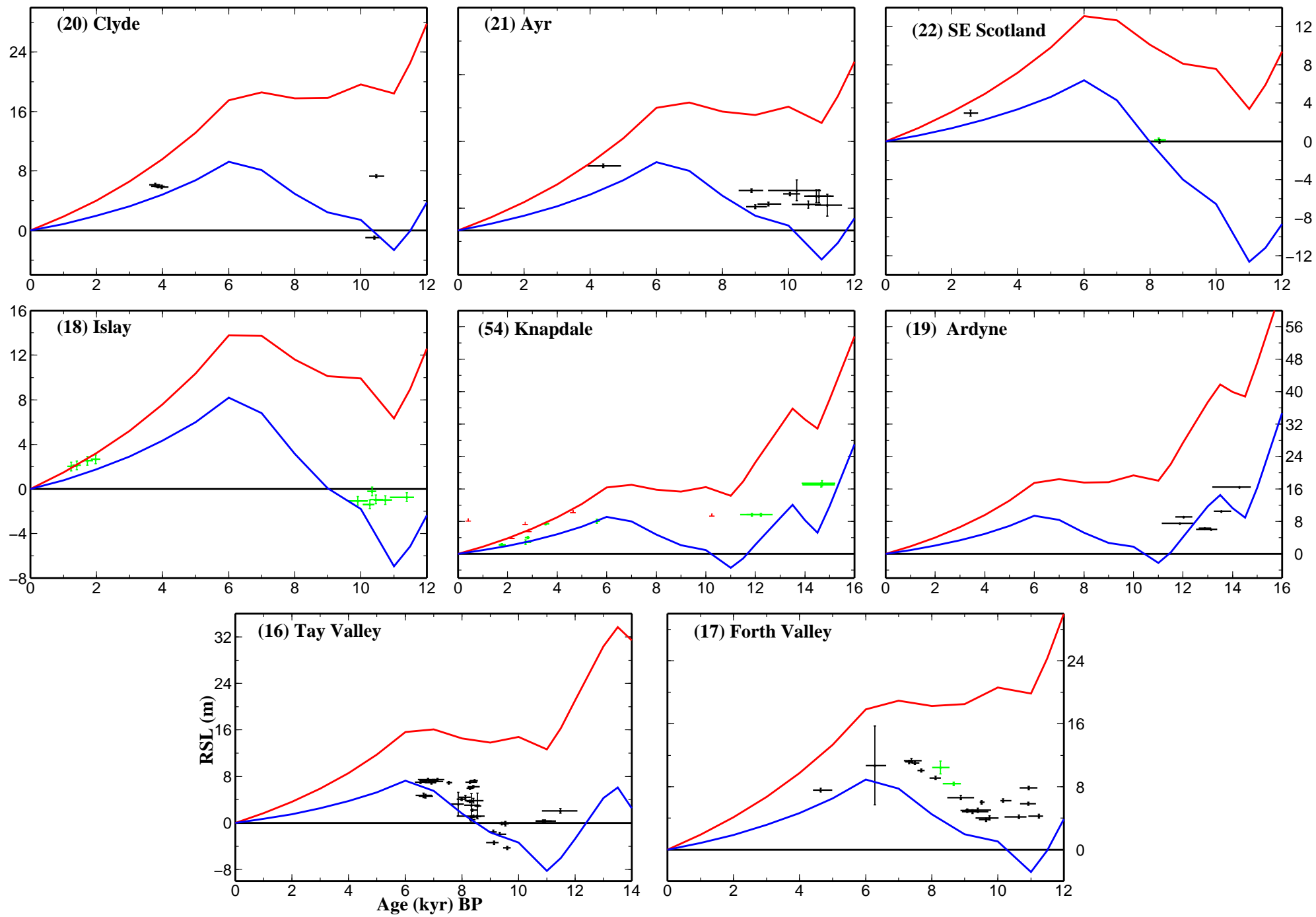
## **Appendix B: Predictions at all British Isles RSL data sites using the Shennan model**

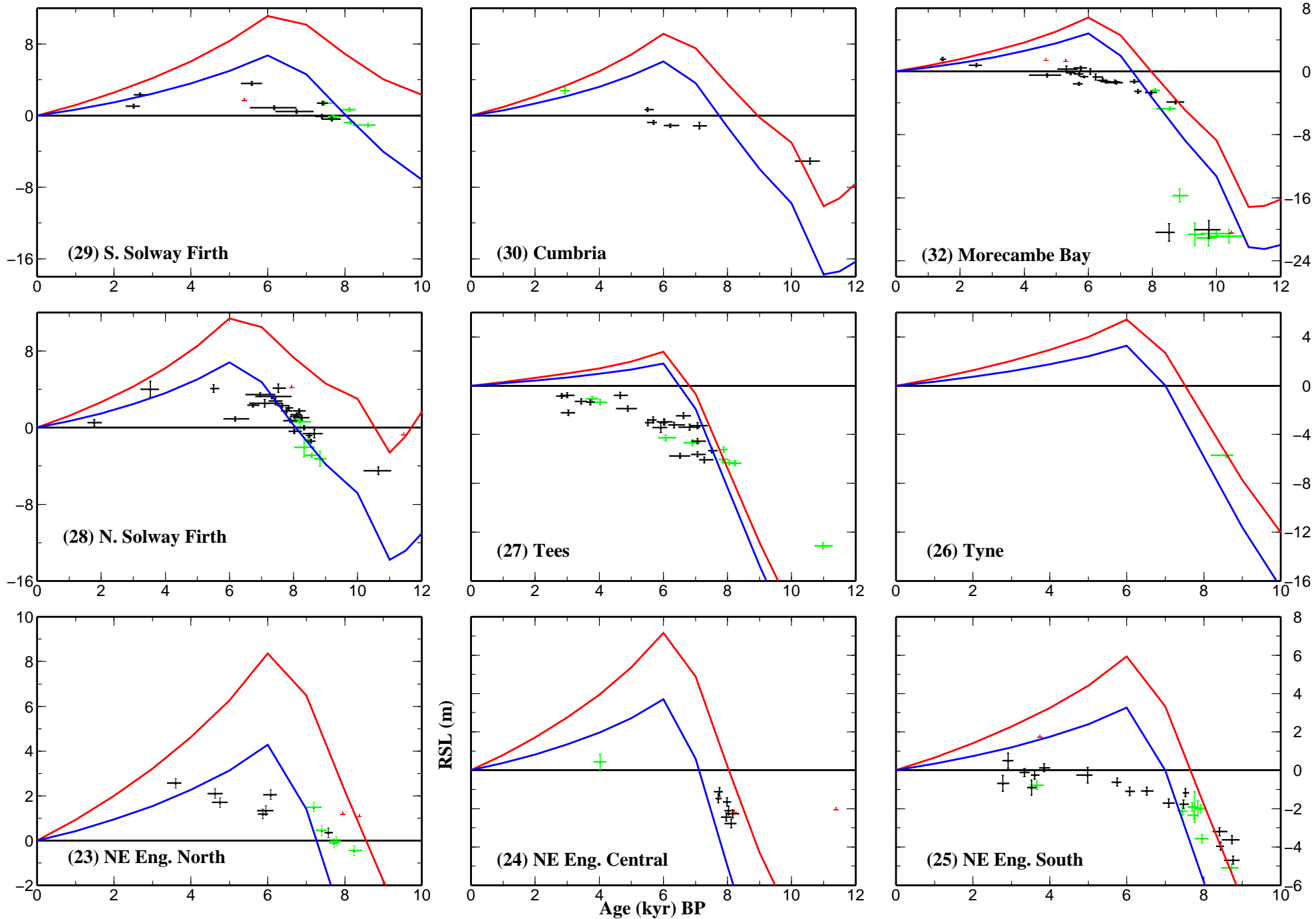
Comparison of predicted and observed sea level at all sites across Great Britain and Ireland. Symbols for the observed data are summarized in Appendix A. Predictions are shown for the Shennan model (shown in Fig. 2.5) for two earth models with different lithosphere thickness values: 71 km shown by solid red line and 96 km shown by the solid blue line; the upper and lower viscosity values are  $5 \times 10^{21}$  Pa s and  $4 \times 10^{22}$  Pa s, respectively. The data are separated into a series of plots numbered B1-B10 in relation to geographical location as follows: B1: North and NE Scotland; B2: NW Scotland; B3: Central Scotland; B4: NW and NE England; B5: NW England and Wales; B6: East England; B7: South England; B8: Southern Ireland; B9: West and North Ireland; B10: NE Ireland, Isle of Man and North Sea Basin



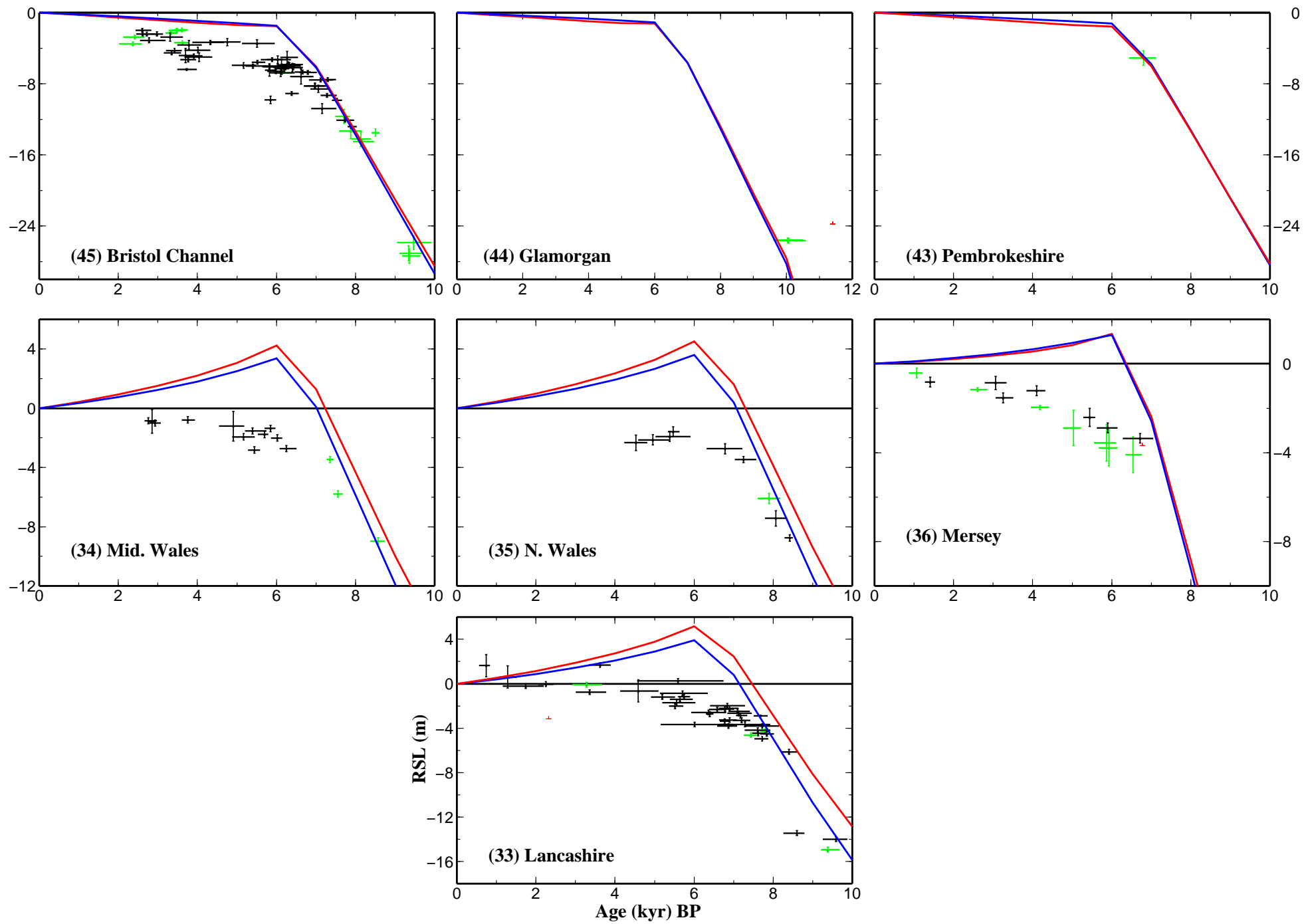
**B1**

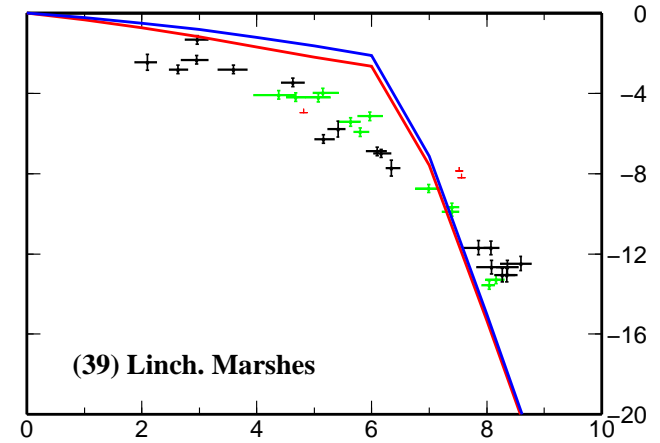
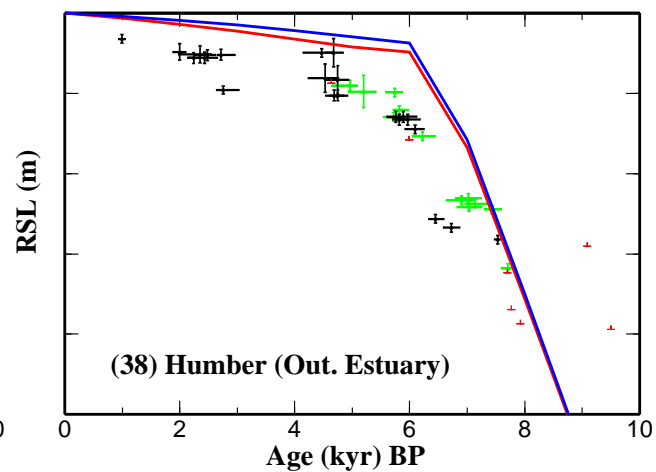
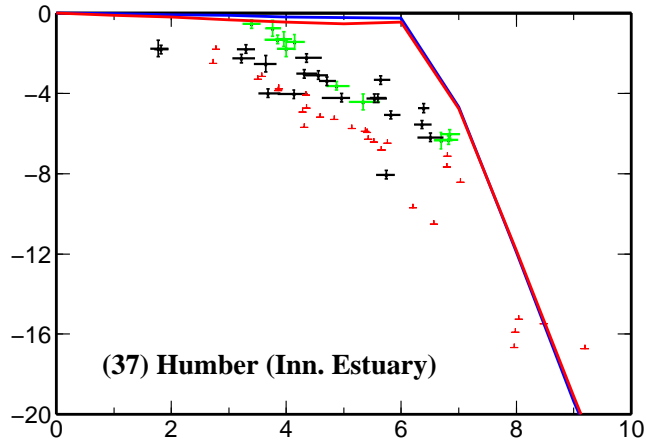
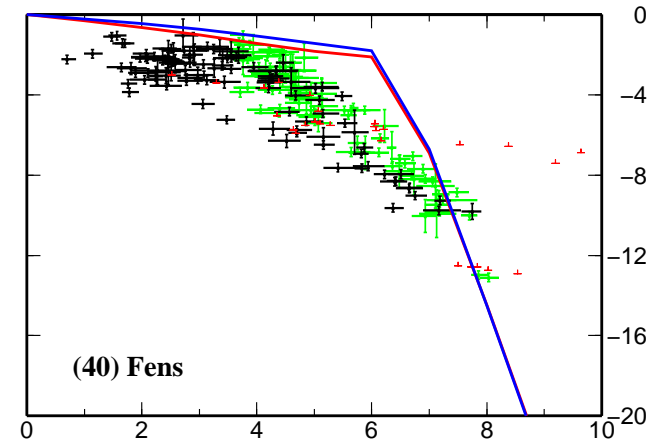
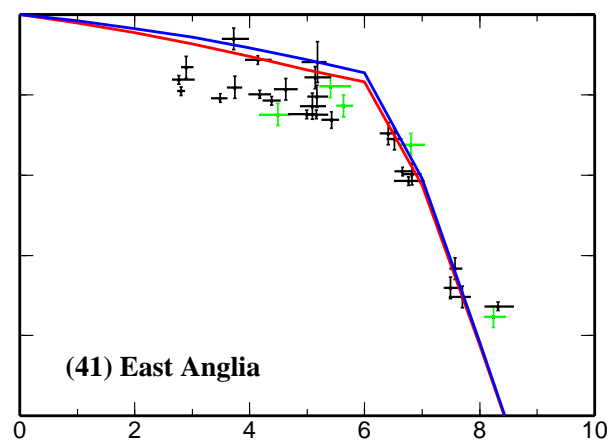
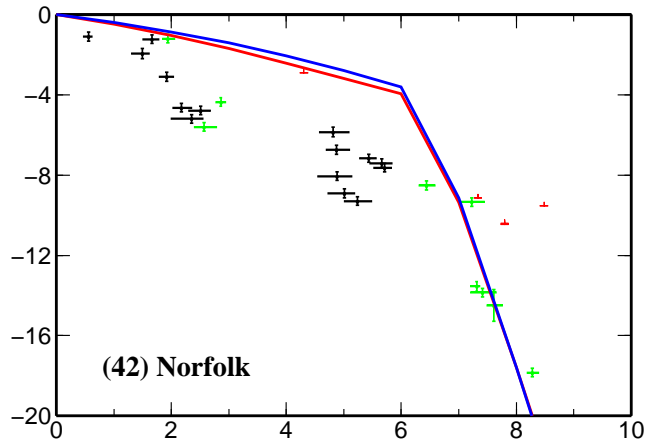
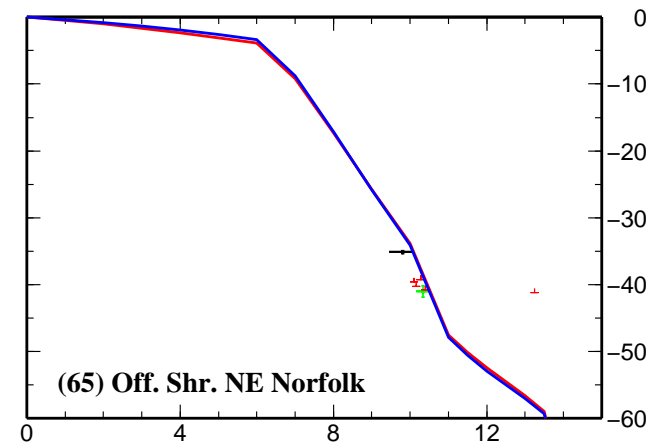
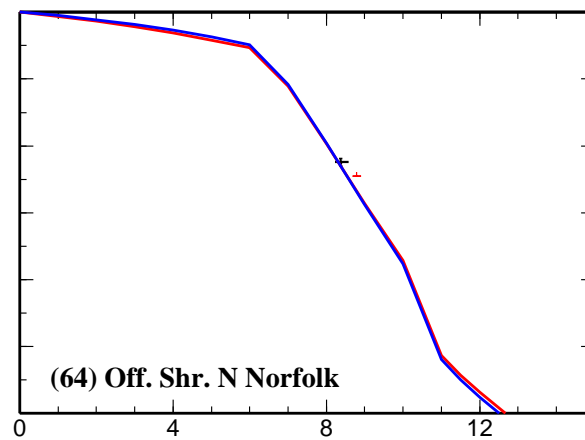
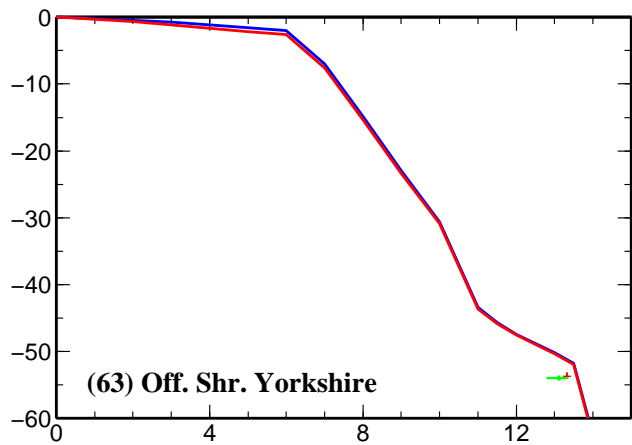


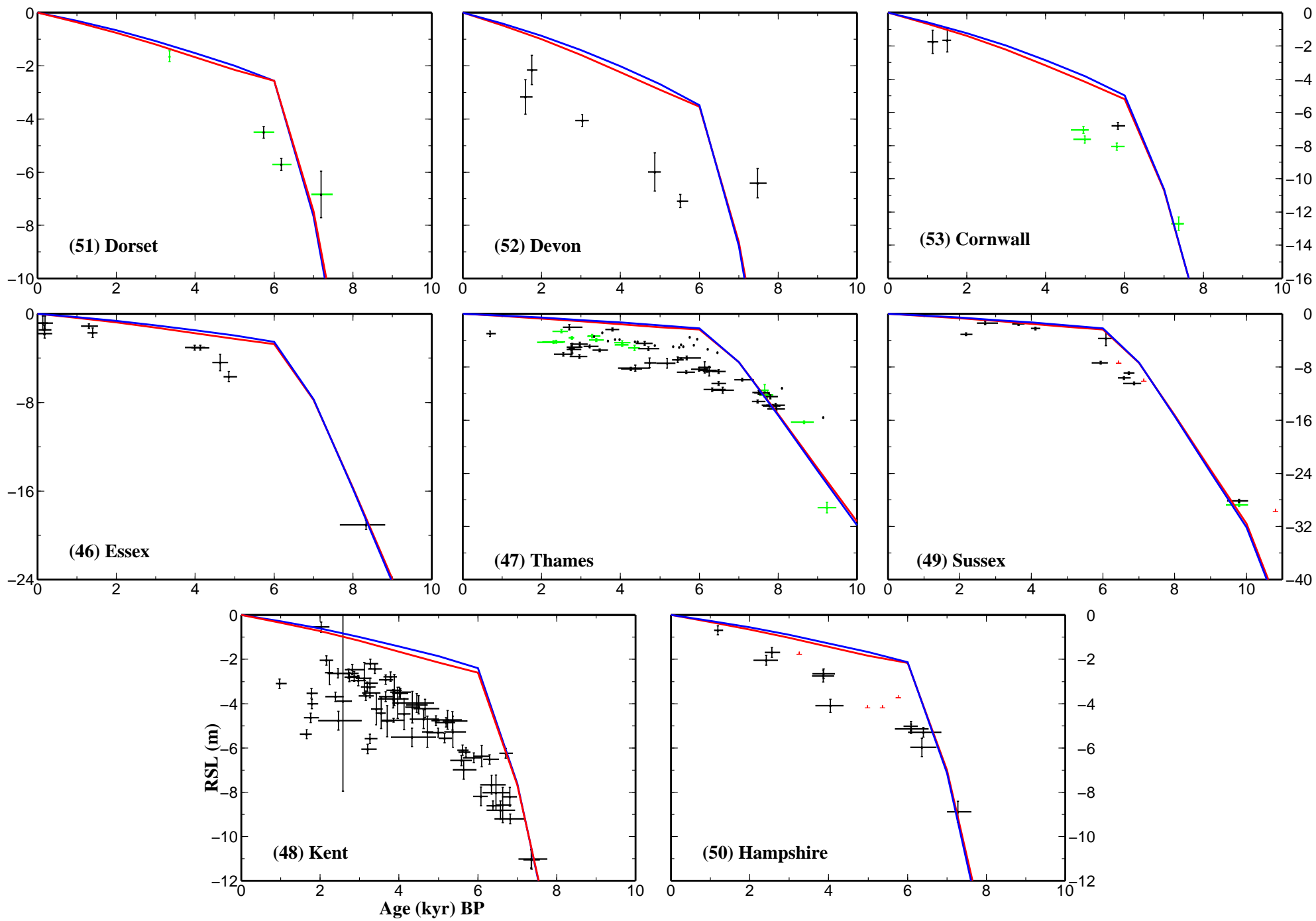


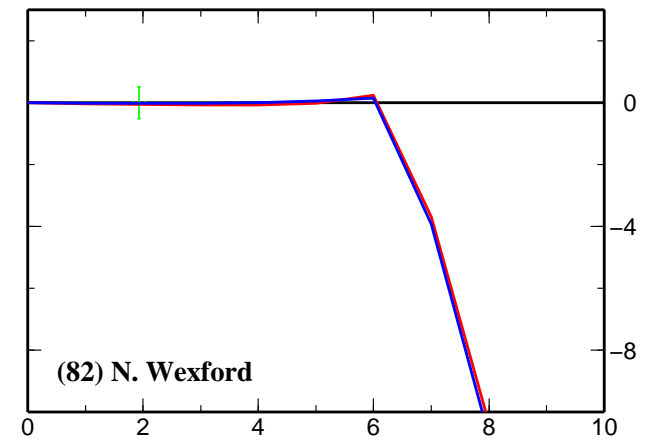
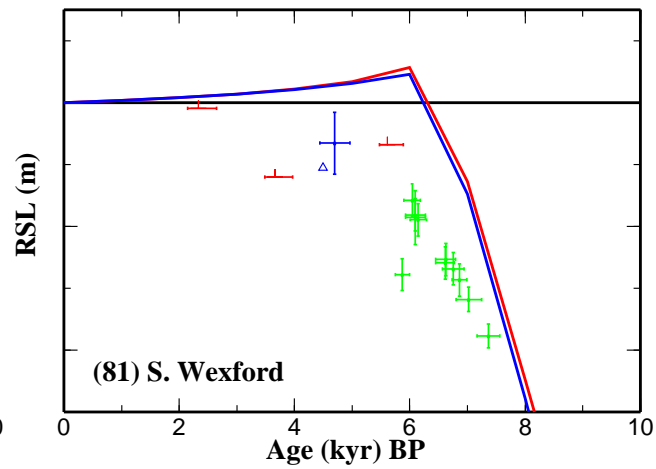
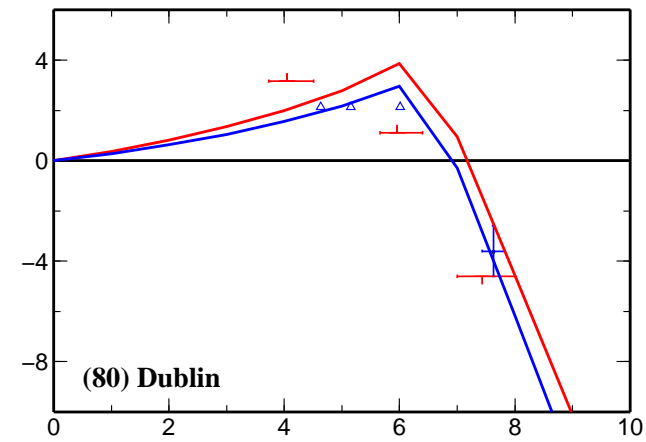
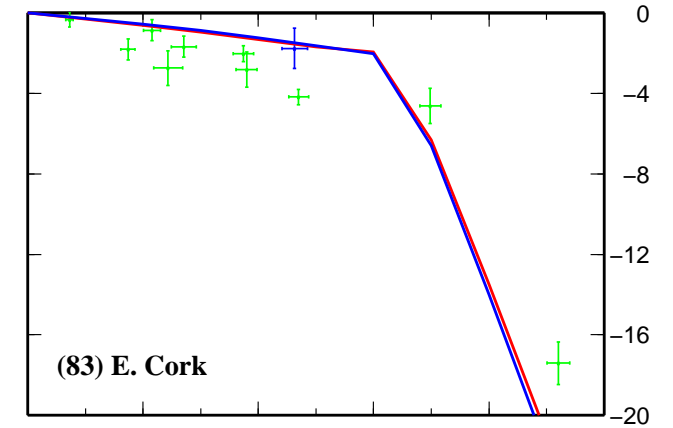
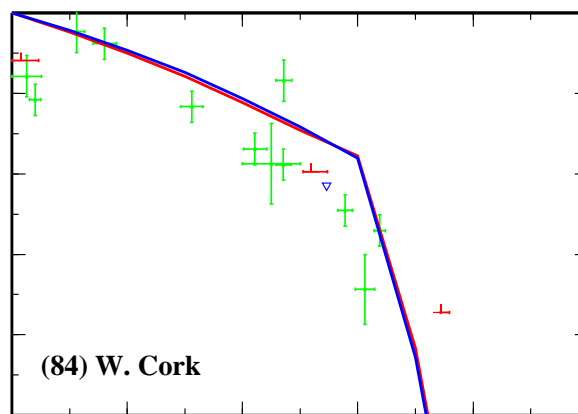
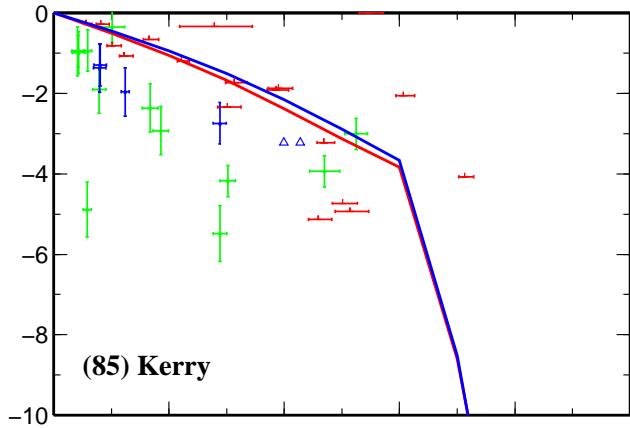
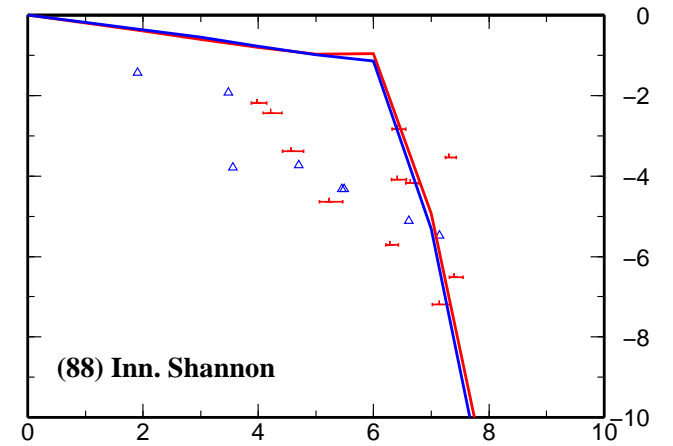
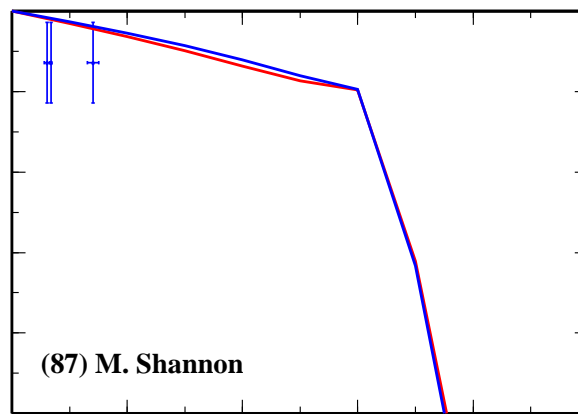
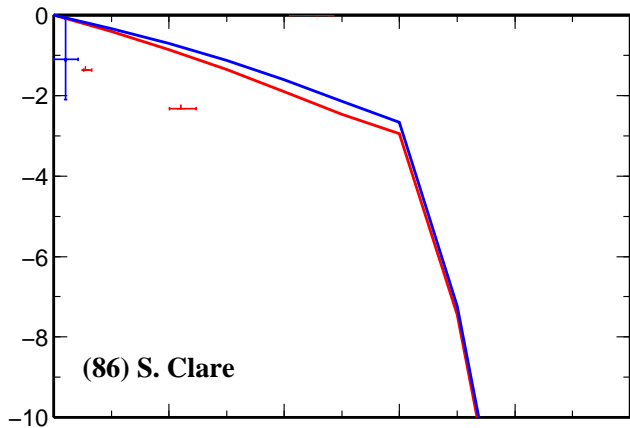


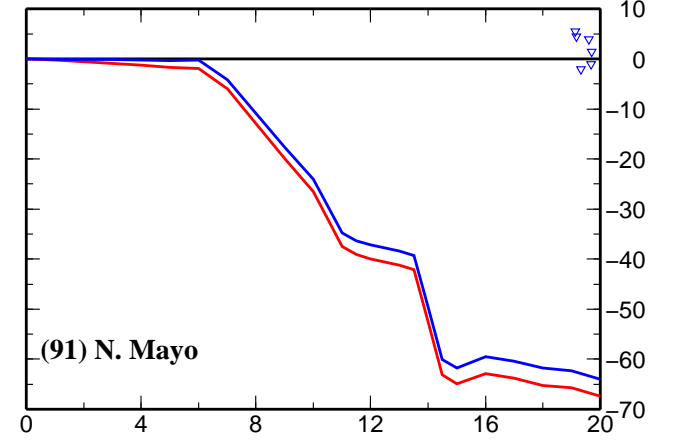
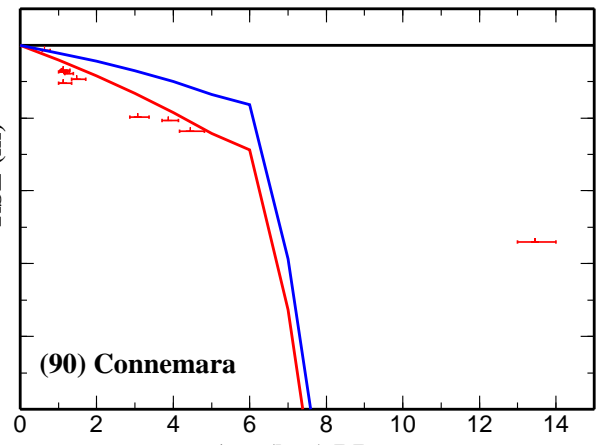
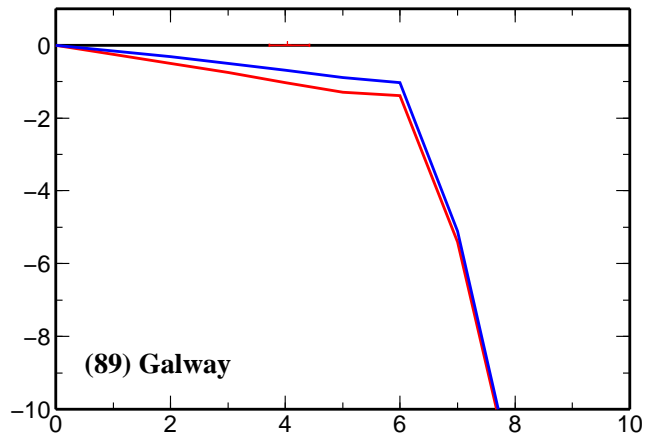
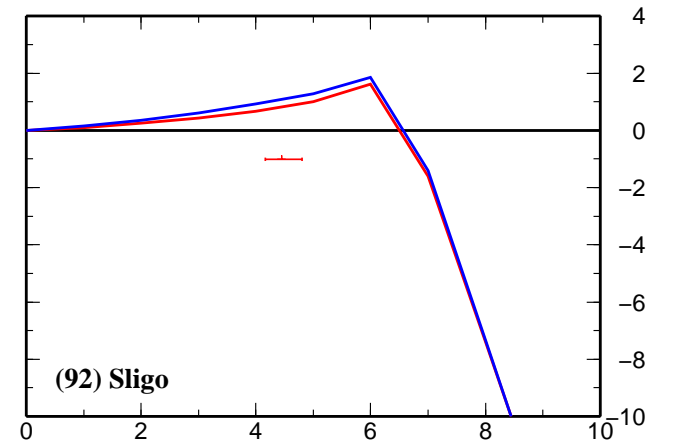
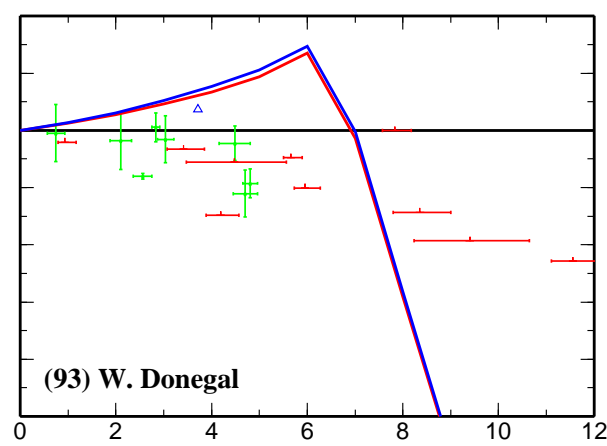
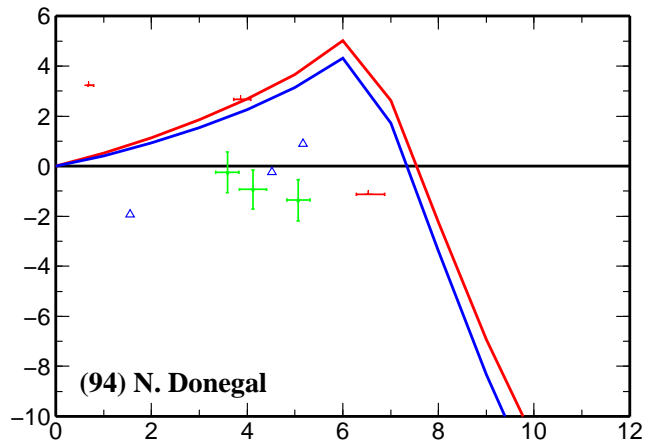
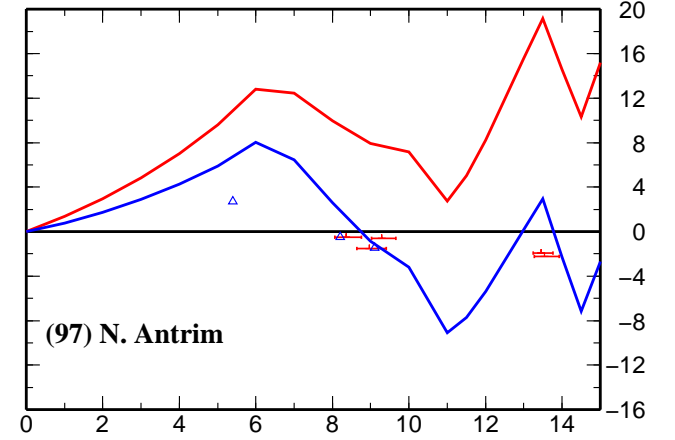
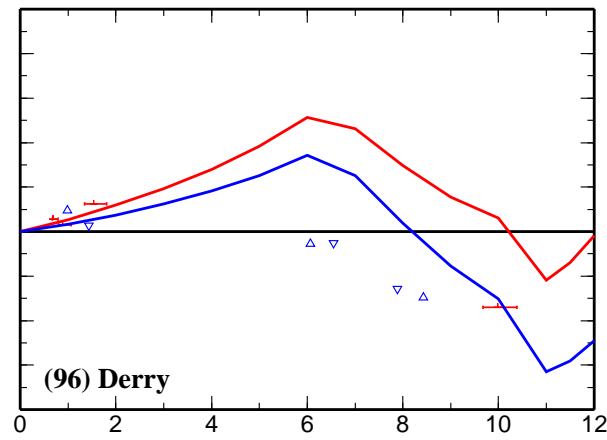
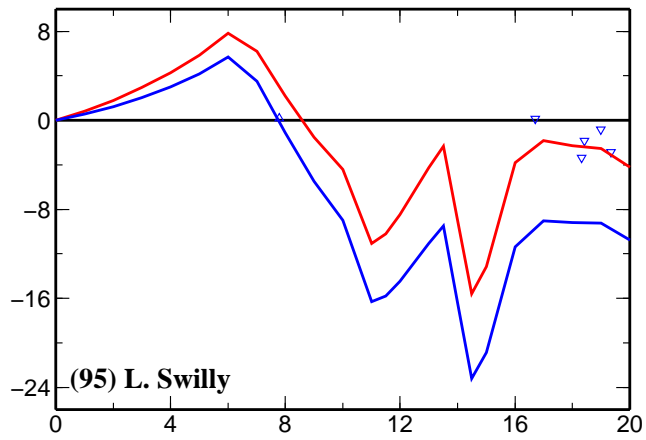
**B4**

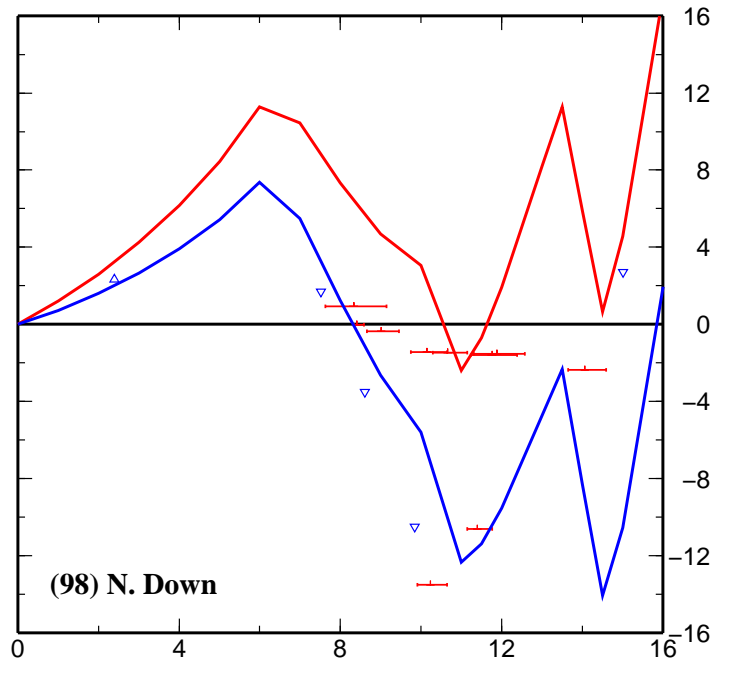
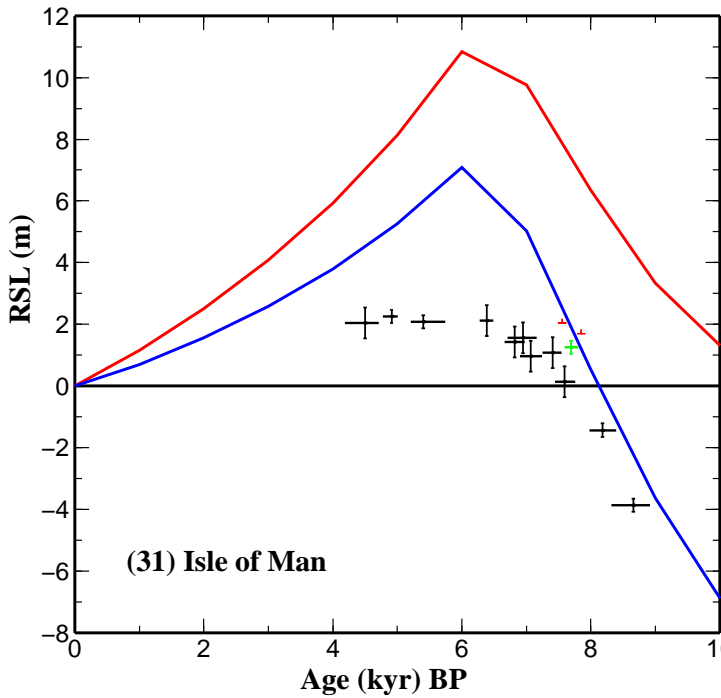
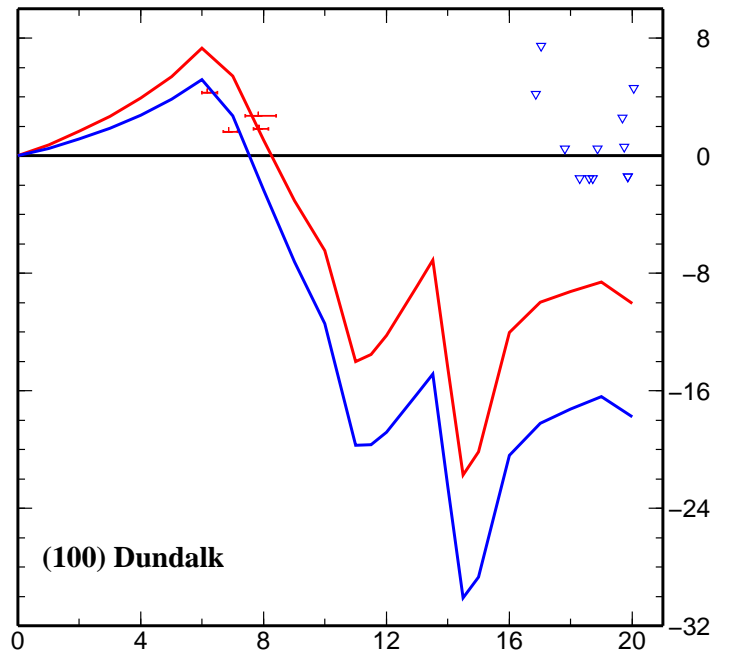
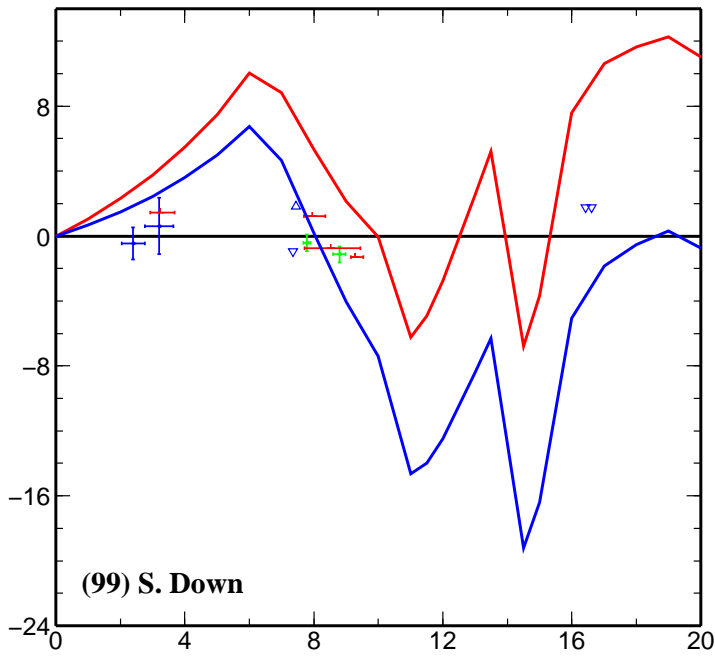
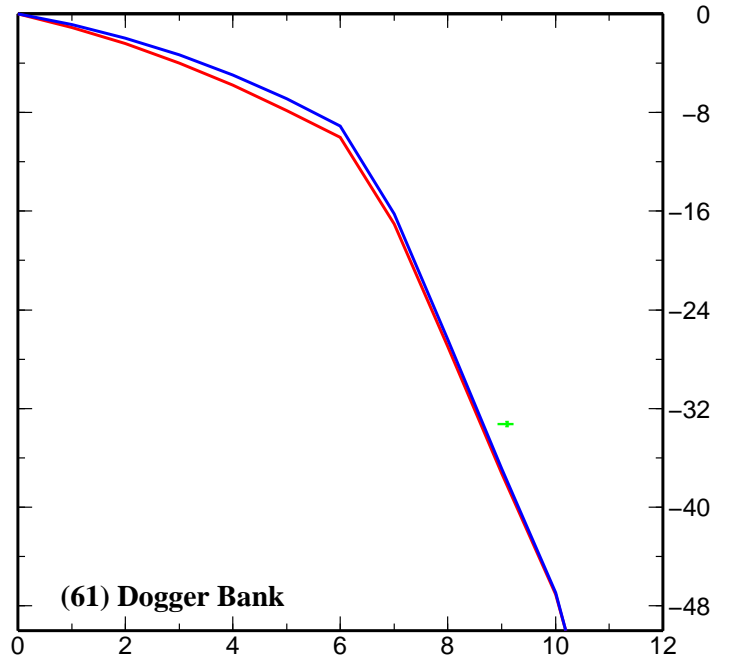
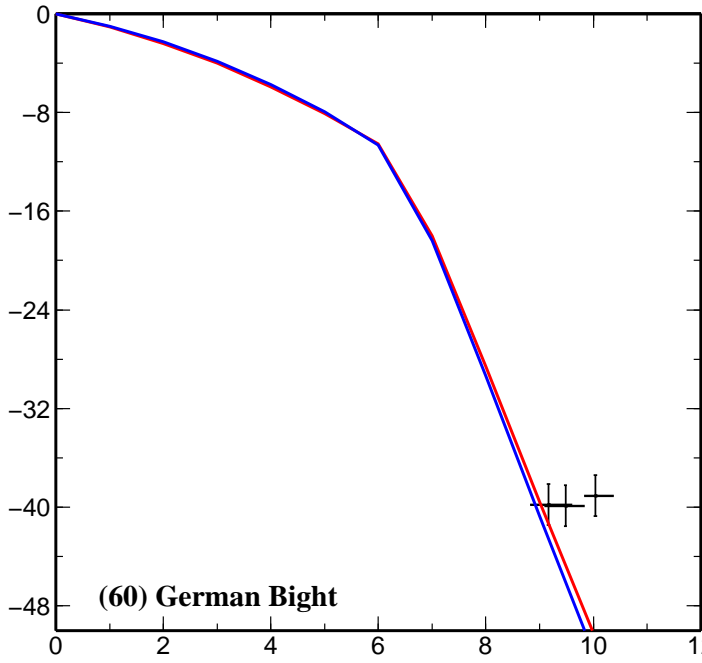






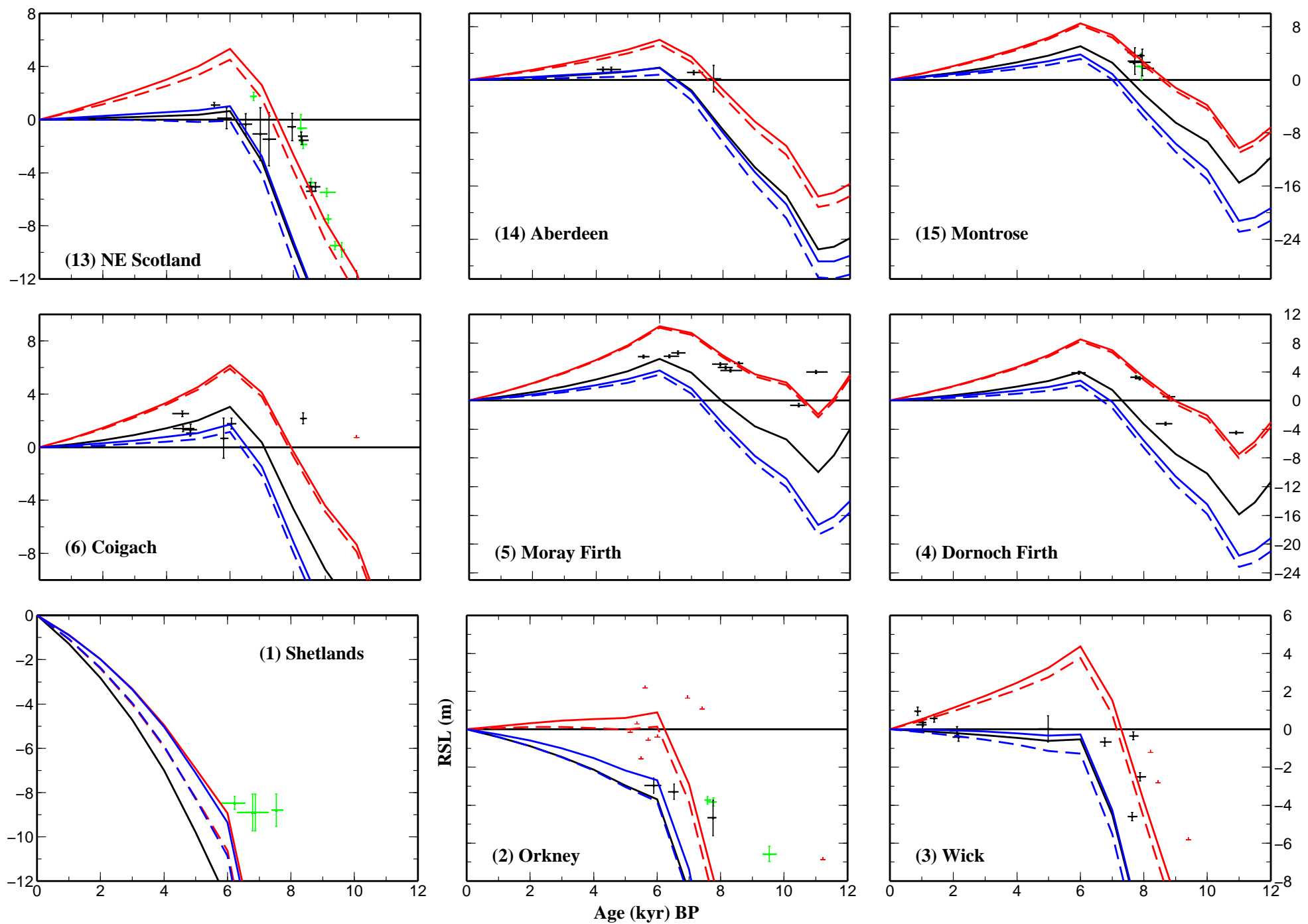




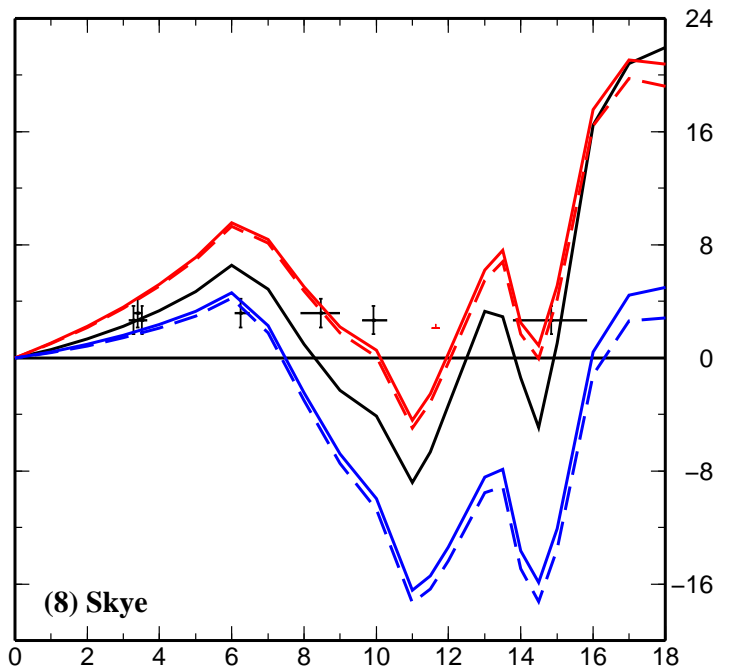
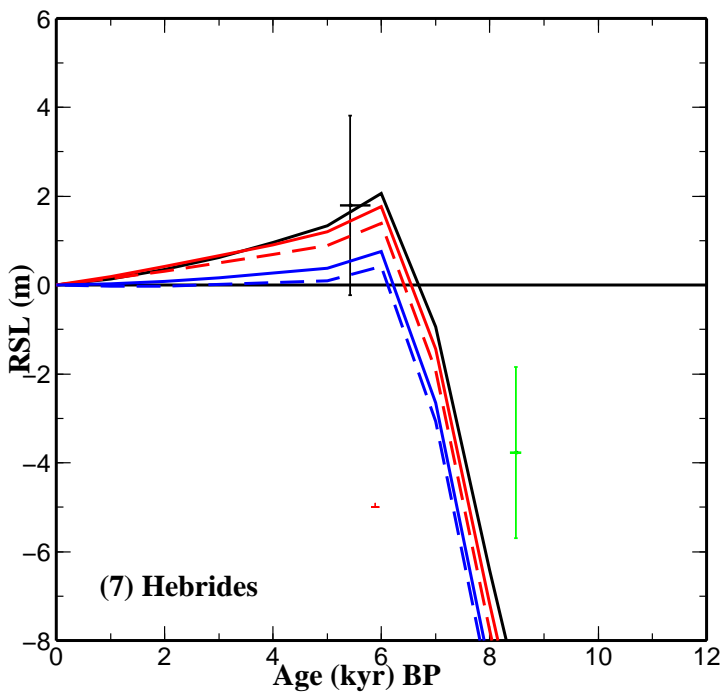
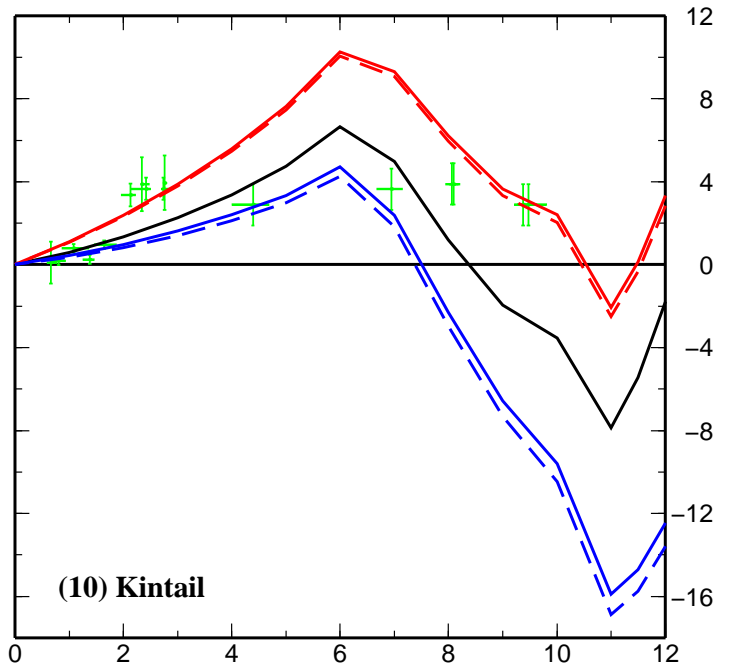
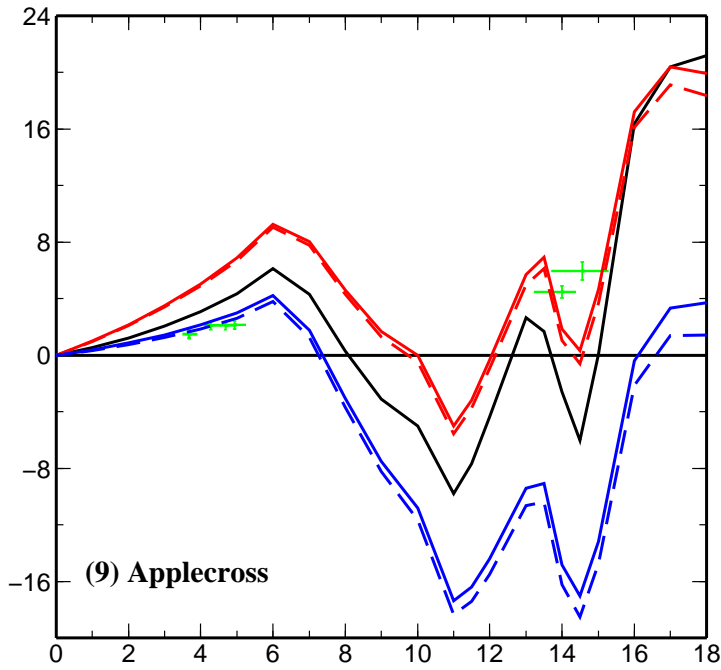
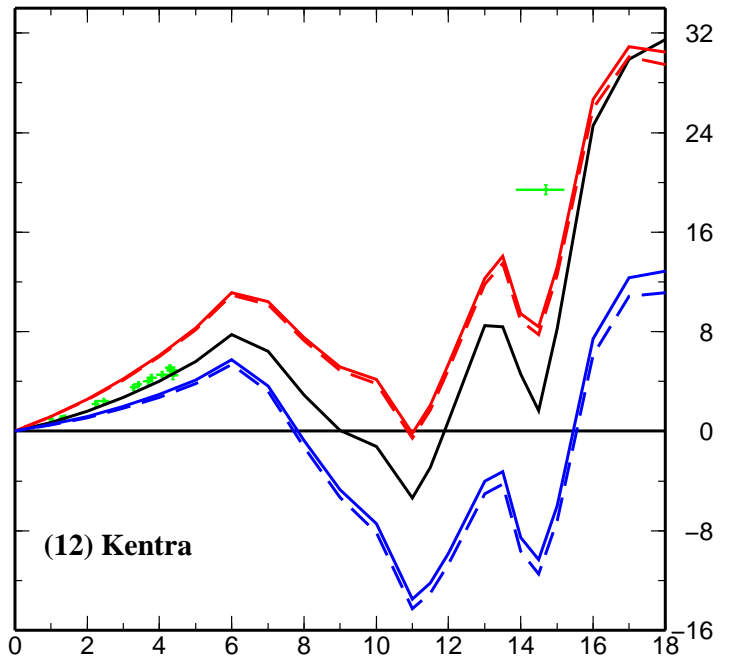
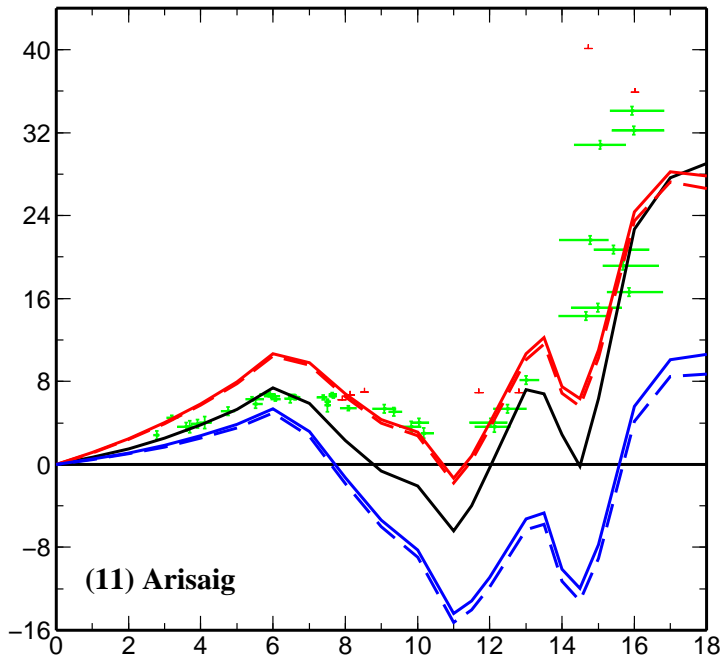


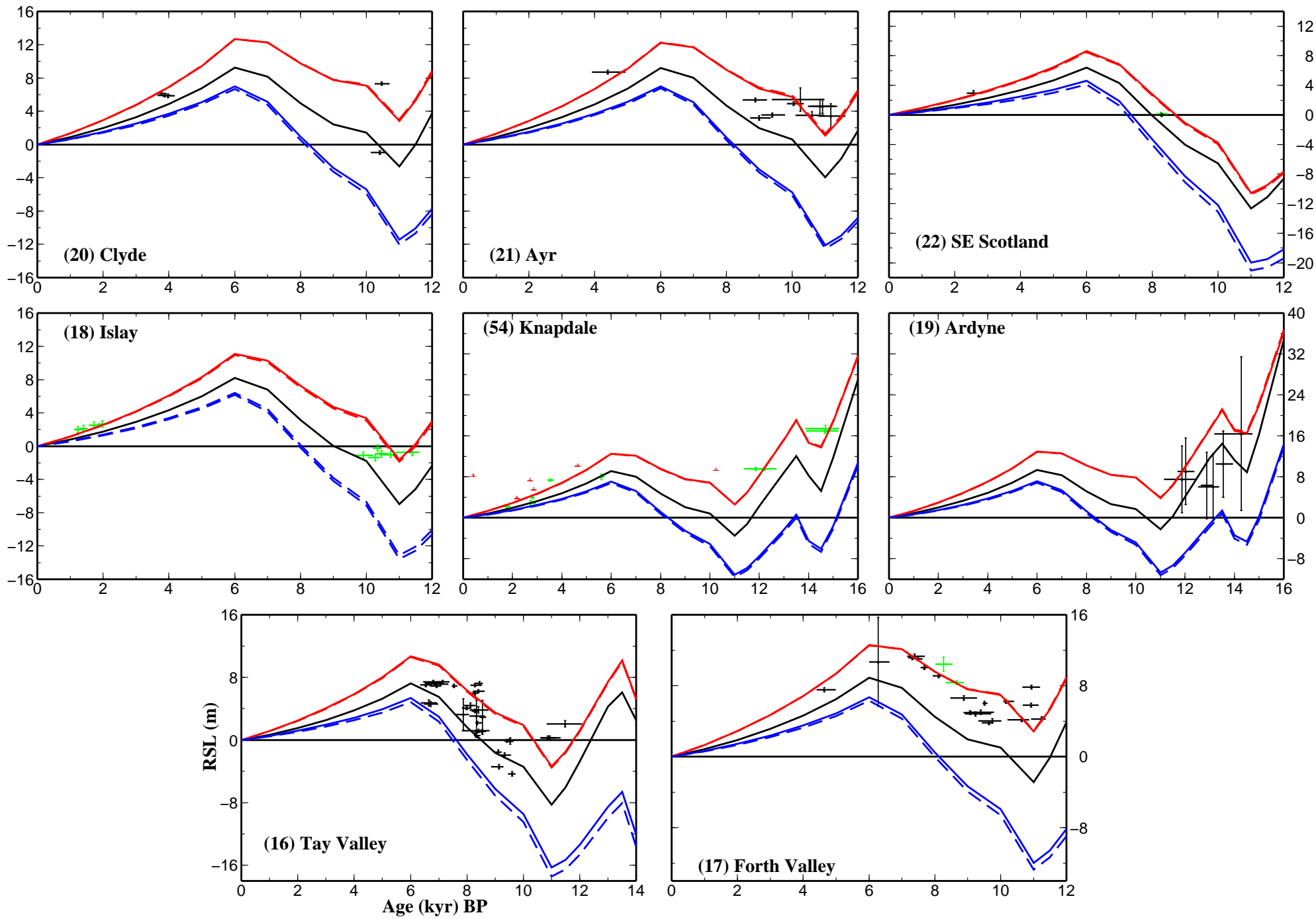
## **Appendix C: Predictions at all Great Britain RSL data sites for the Northsea ice models (NS-Thick and NS-Thin)**

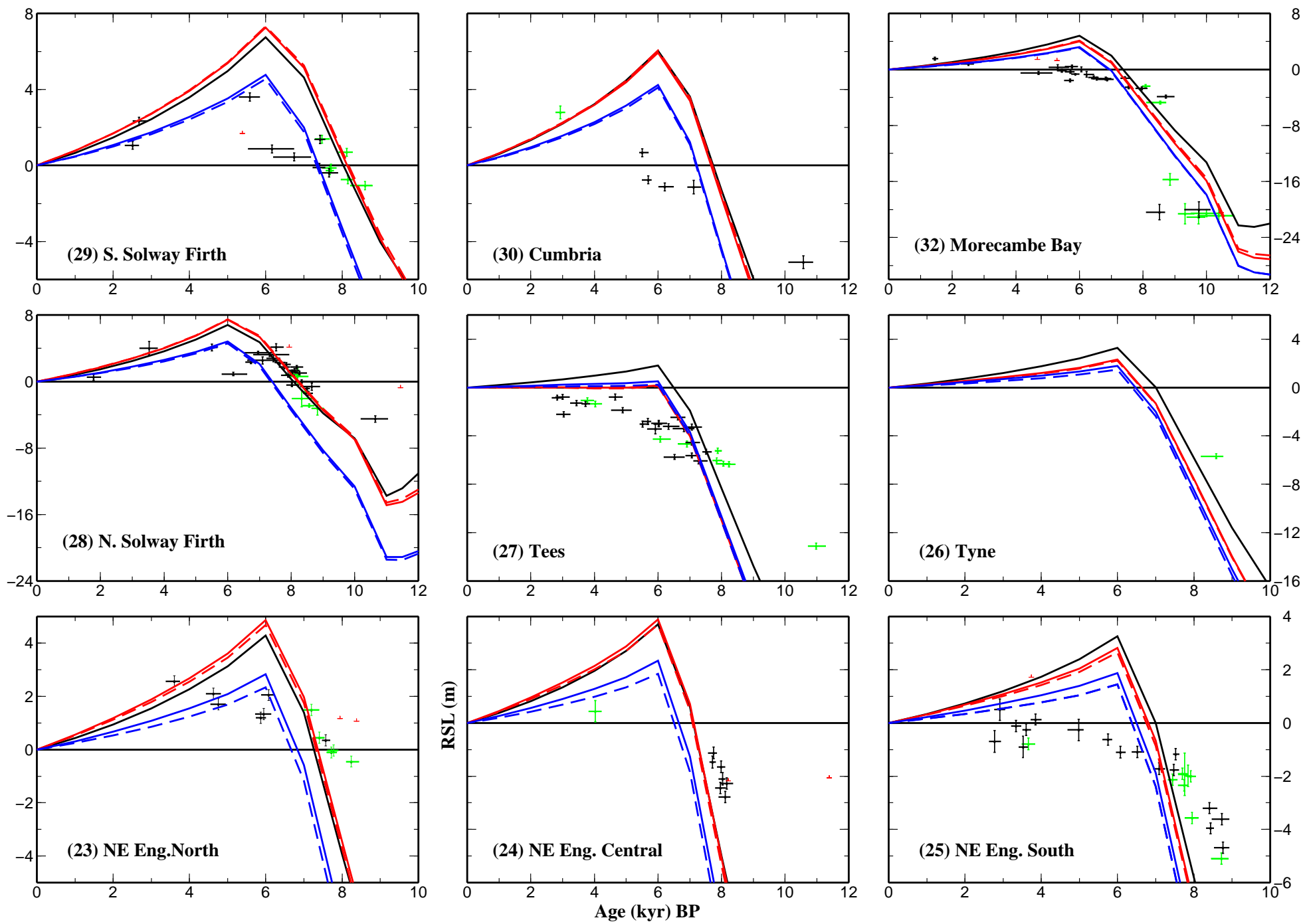
Comparison of predicted and observed sea level at all sites across Great Britain for the NS-Thick and NS-Thin ice models and the two reference earth models.. Symbols for the observed data are summarized in Appendix A. Predictions are shown using: the 71 km lithosphere earth model for the NS-Thick (solid red line) and NS-Thin (red-dashed line) models; the 96 km lithosphere earth model for the NS-Thick (blue solid line) and NS-Thin (blue dashed line). Additionally, predictions are shown using the 96 km lithosphere model for the Shennan model (solid black line). The data are separated into a series of plots numbered C1-C8 in relation to geographical location as follows: C1: North and NE Scotland; C2: NW Scotland; C3: Central Scotland; C4: NW and NE England; C5: Central England; C6: East England; C7: South England; C8: All offshore sites



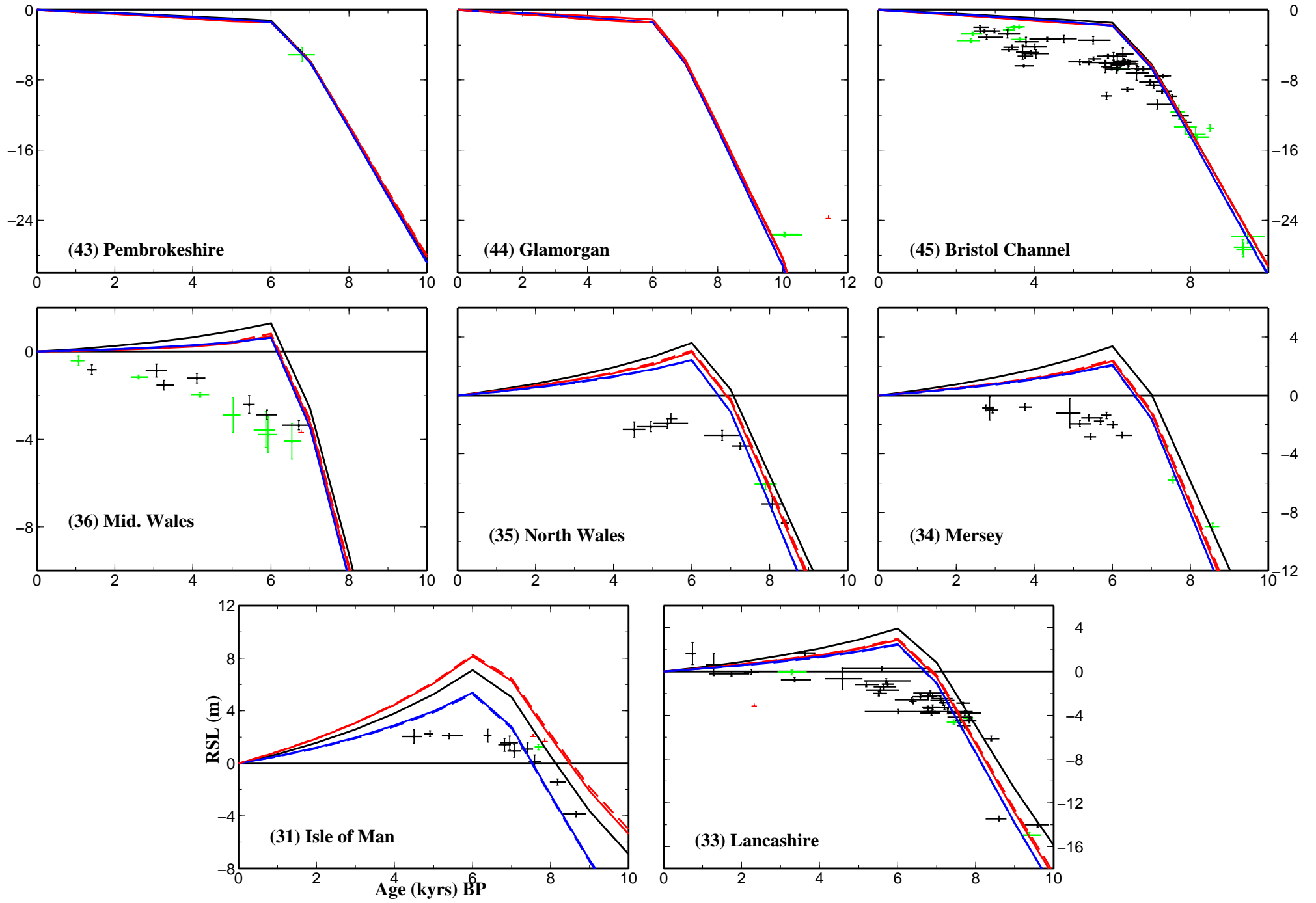
**C1**

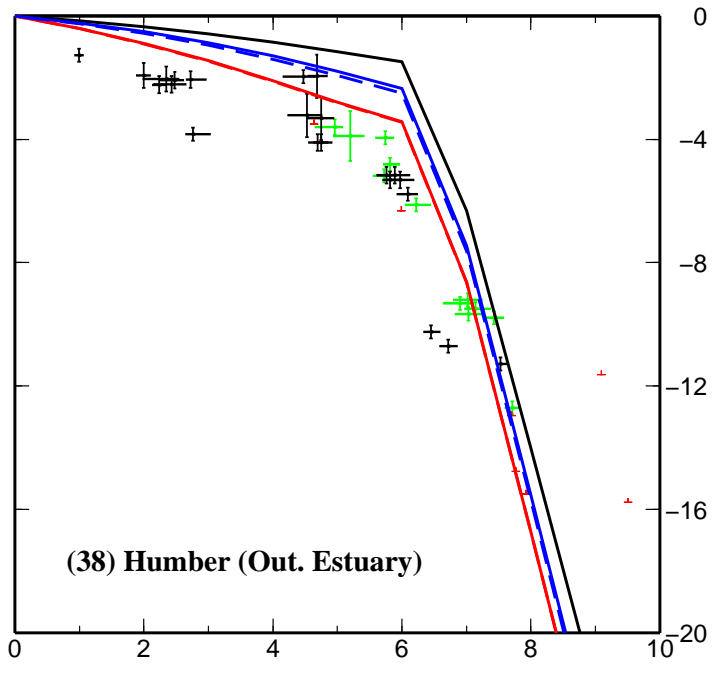
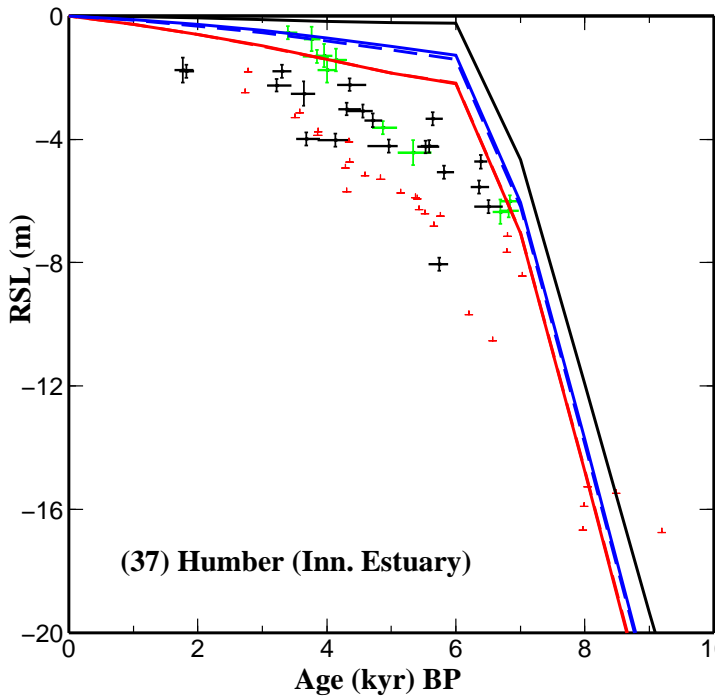
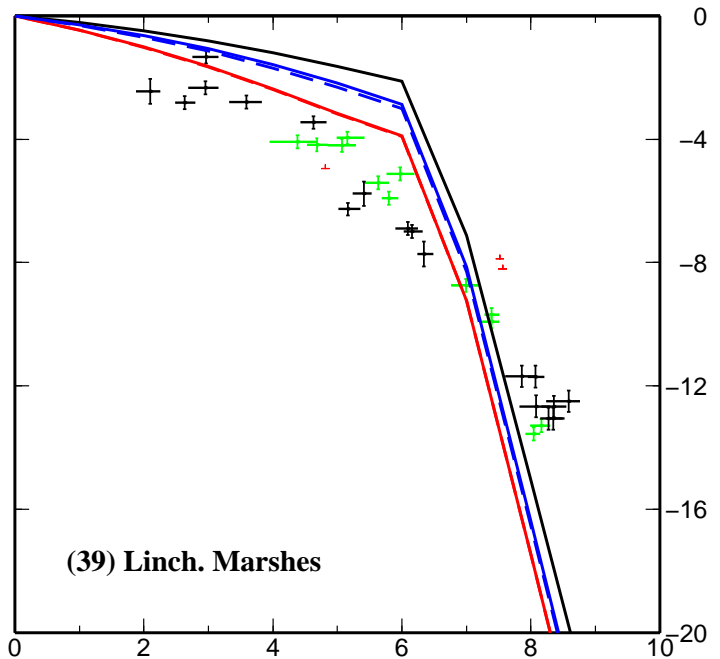
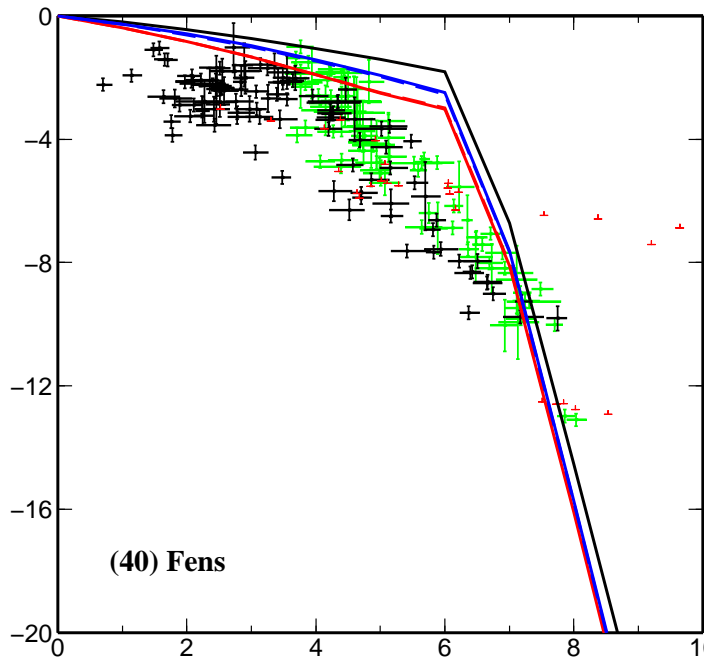
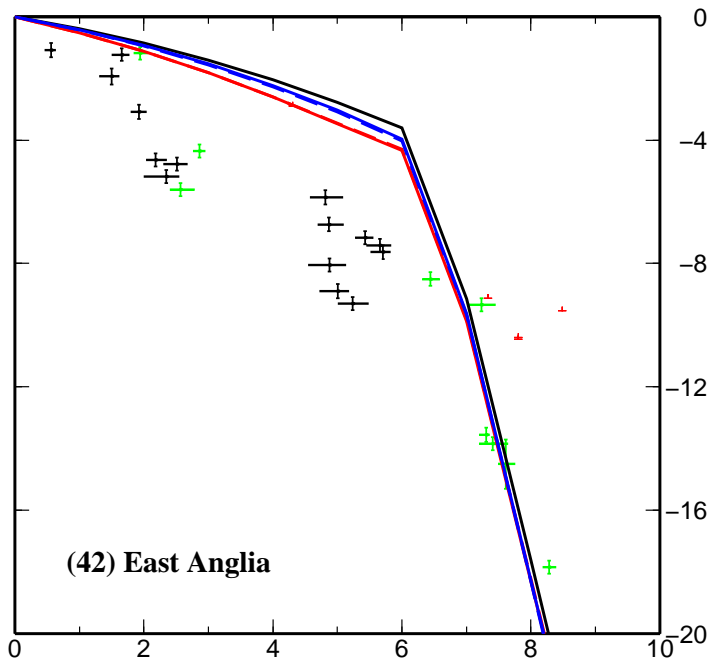
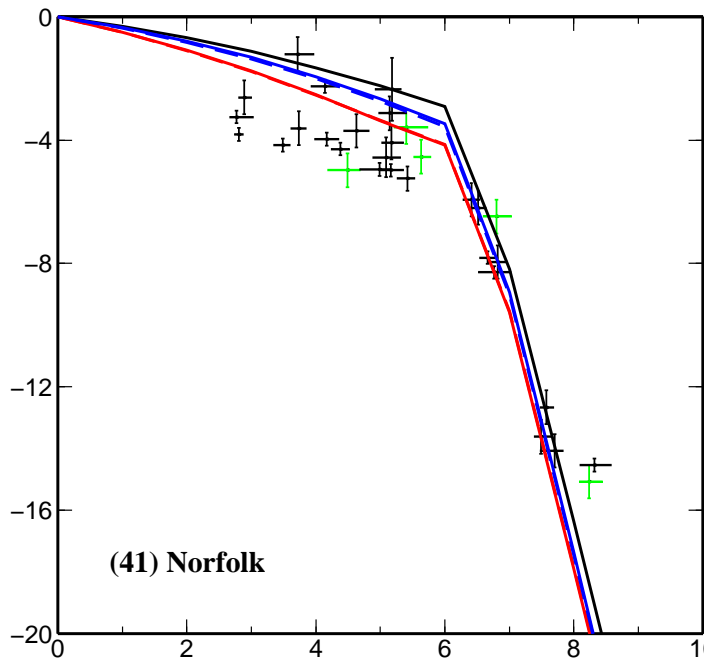


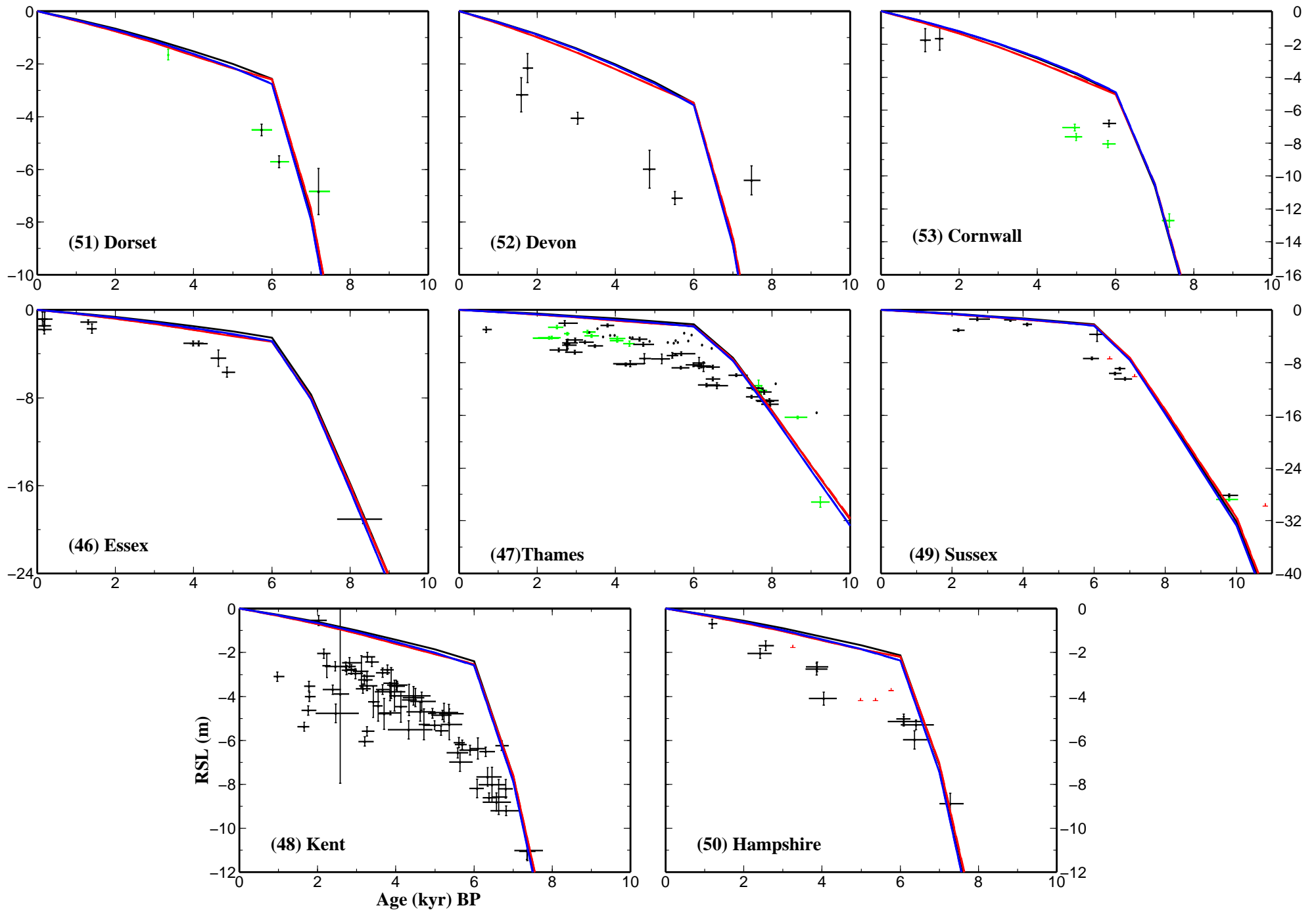


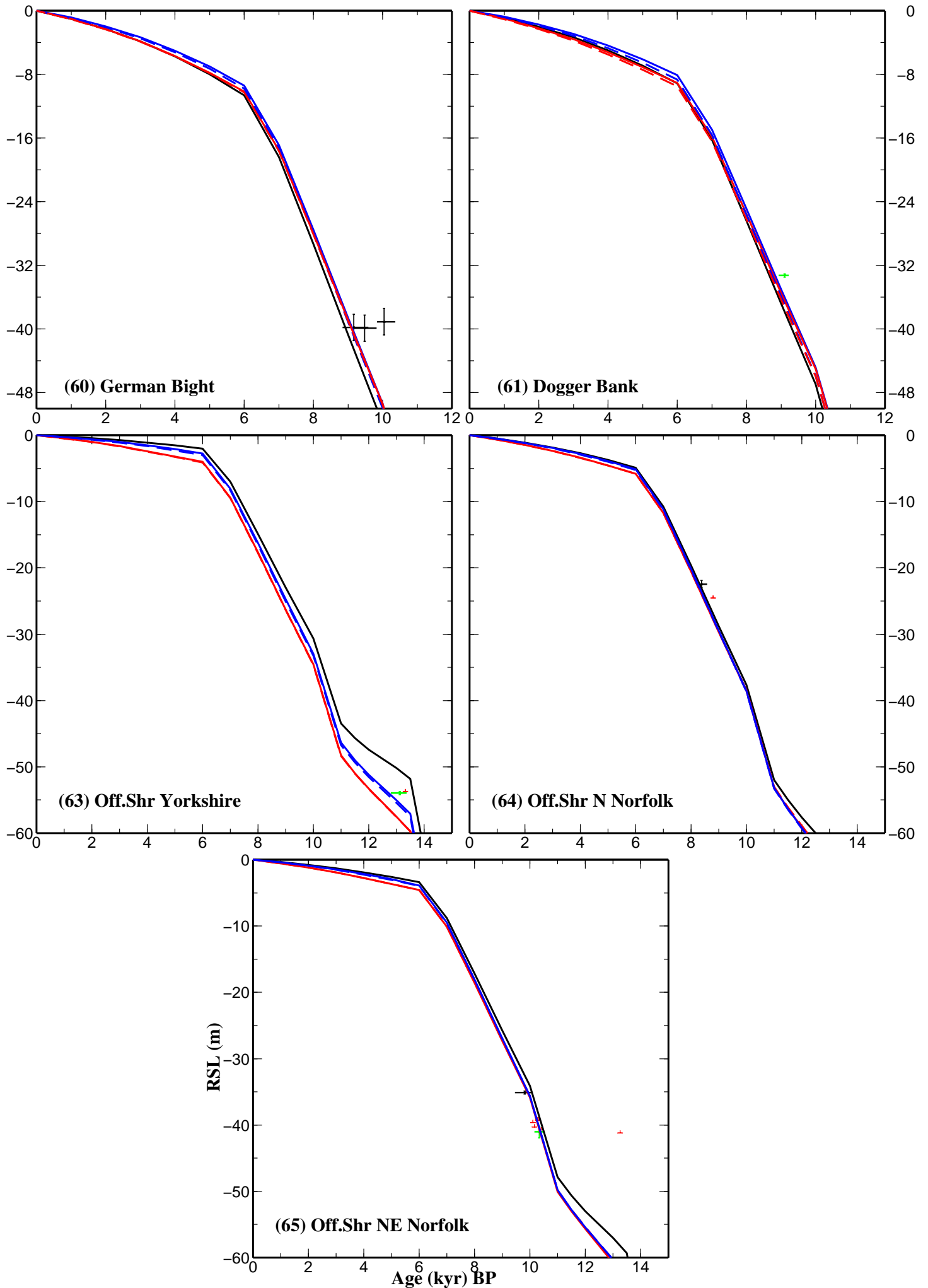


**C4**



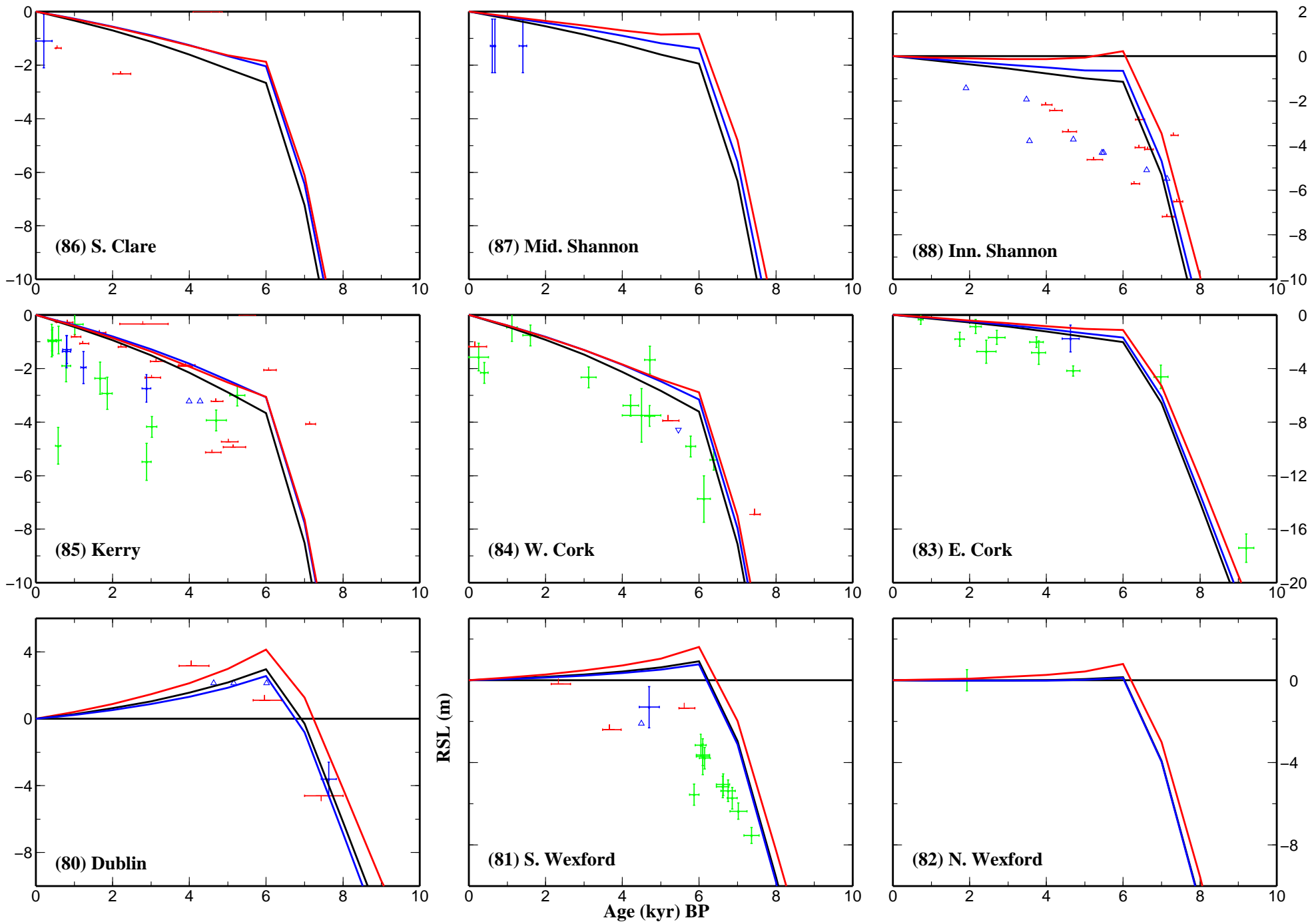




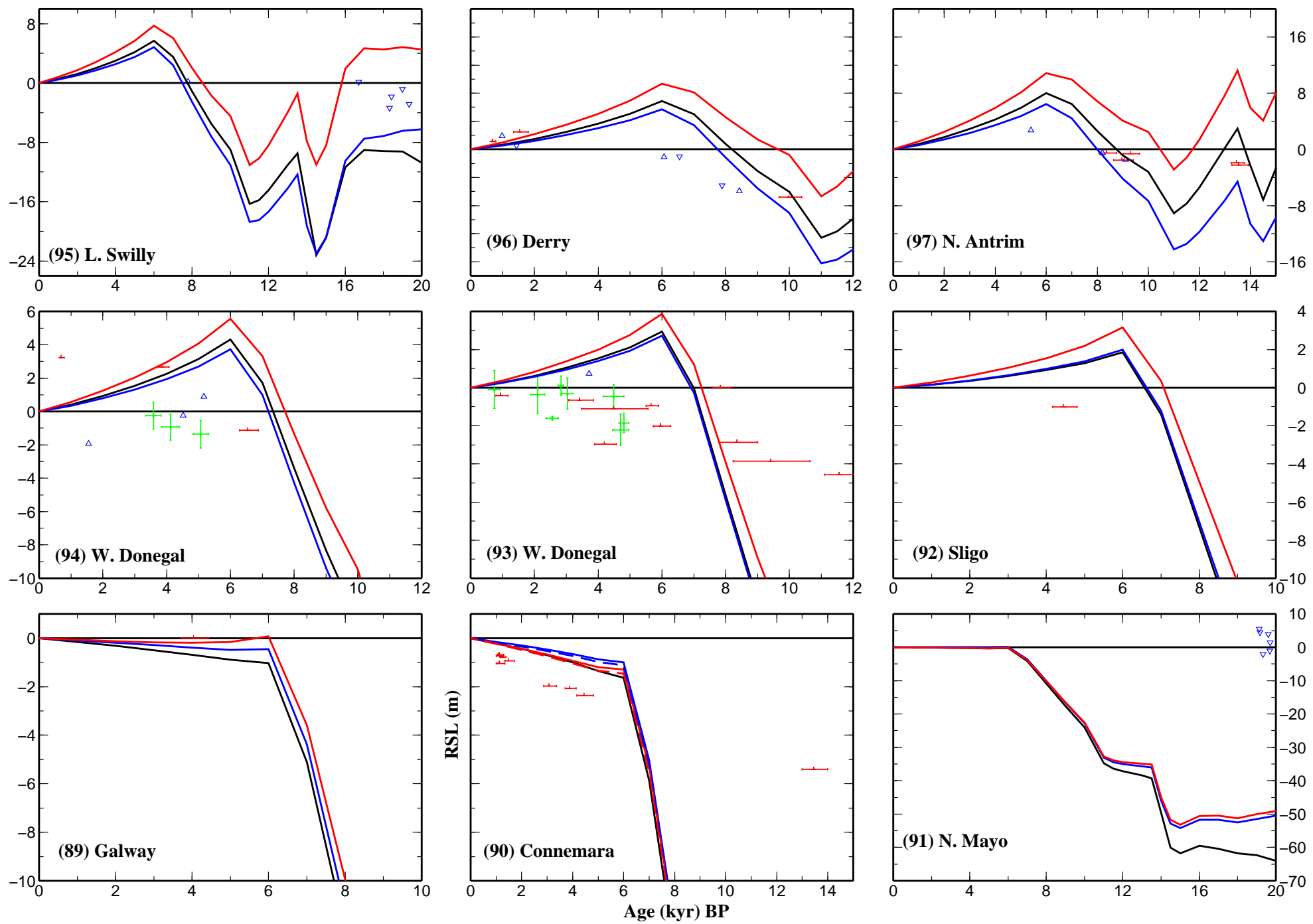


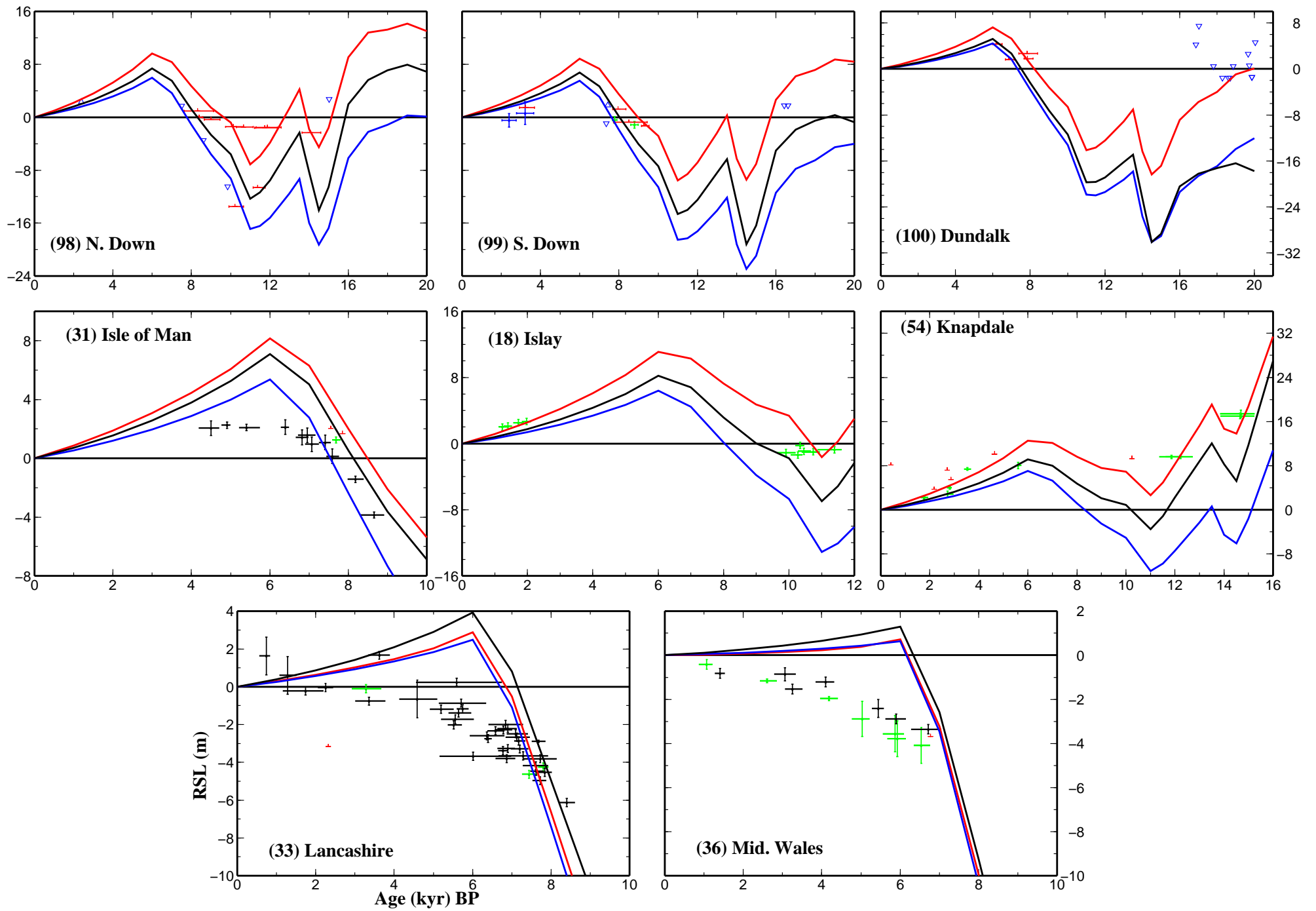
## **Appendix D: Predictions at all Irish and at a selection of Great Britain sites for the NS-Thick and Shennan model**

Comparison of predicted and observed sea levels at all sites across Ireland and a selection from across Great Britain. Predictions are shown using the 96 km lithosphere earth model for the Shennan model (solid black line) and for the NS-Thick model (solid blue line). Results are also shown using the 71 km lithosphere earth model for the NS-Thick model (solid red line). The data are separated into a series of numbered plots D1-D3 in relation to geographical location as follows: D1: Southern Ireland; D2: West and North Ireland; D3: NE Ireland, Isle of Man and sites from the NW coast of Great Britain.



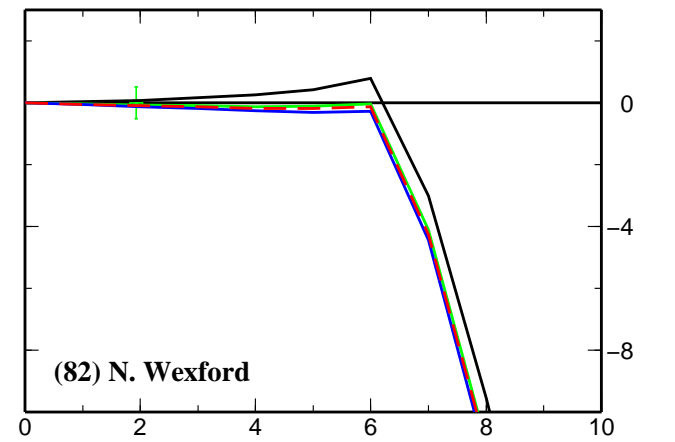
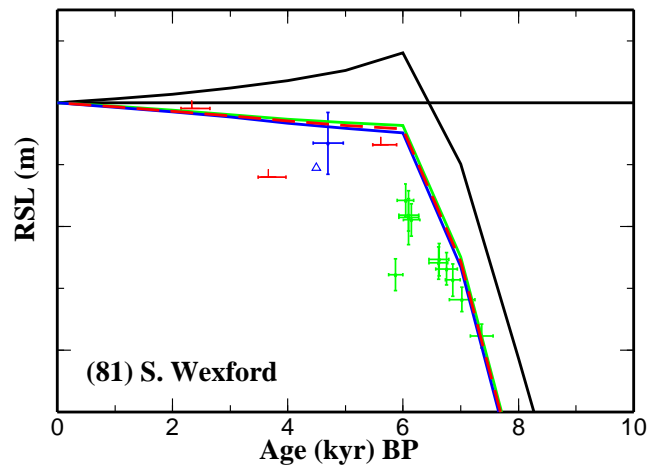
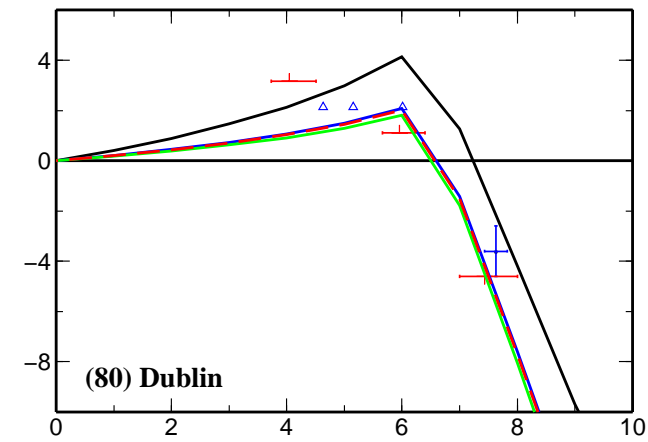
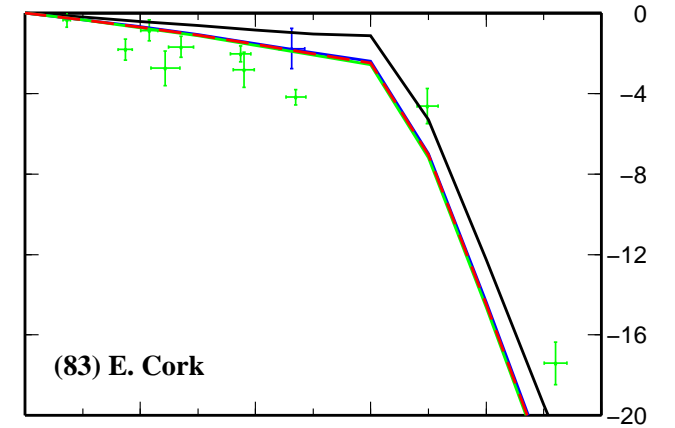
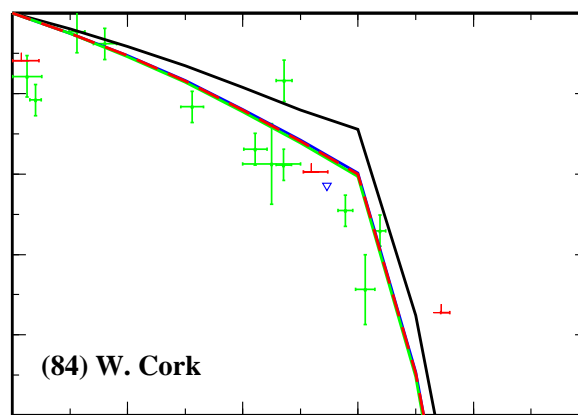
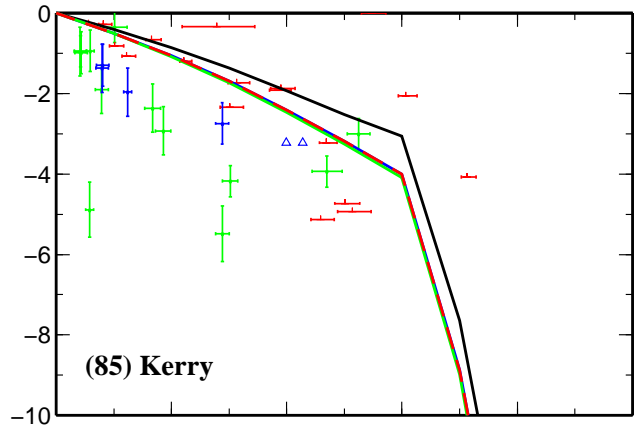
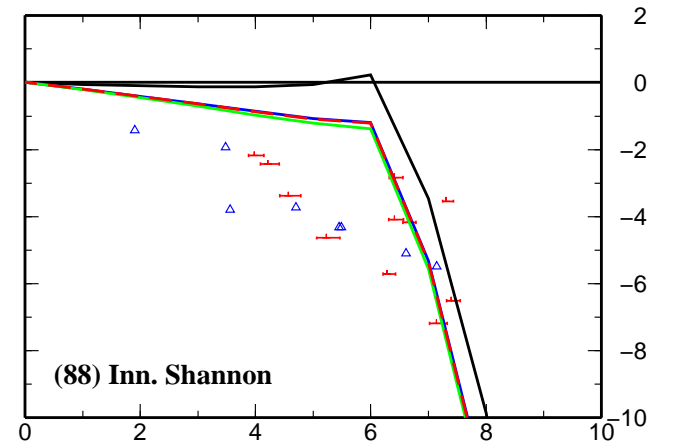
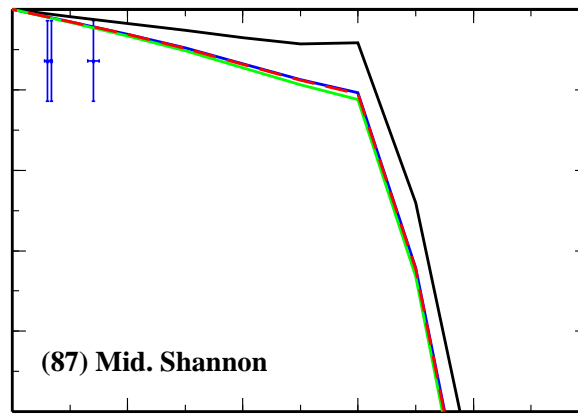
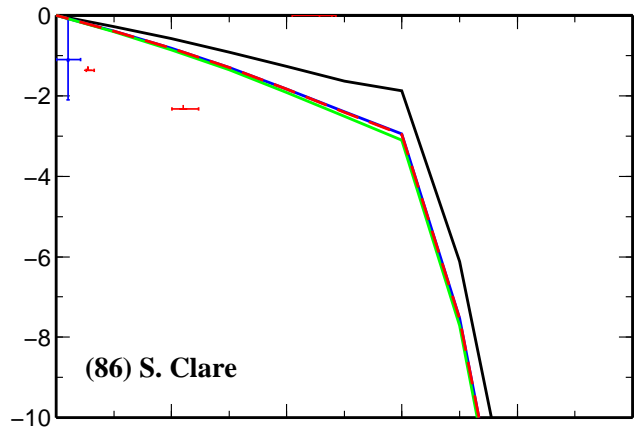
D1



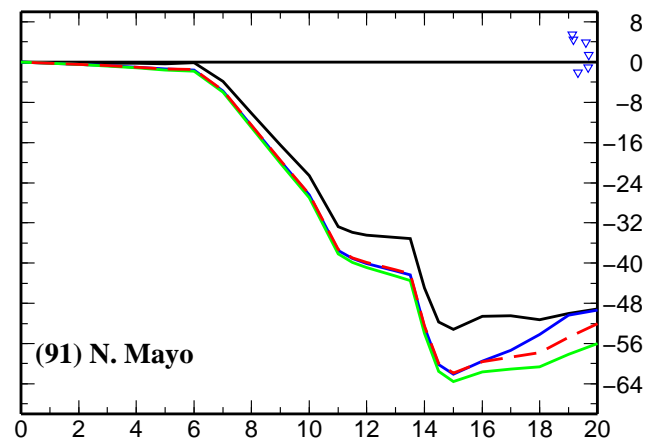
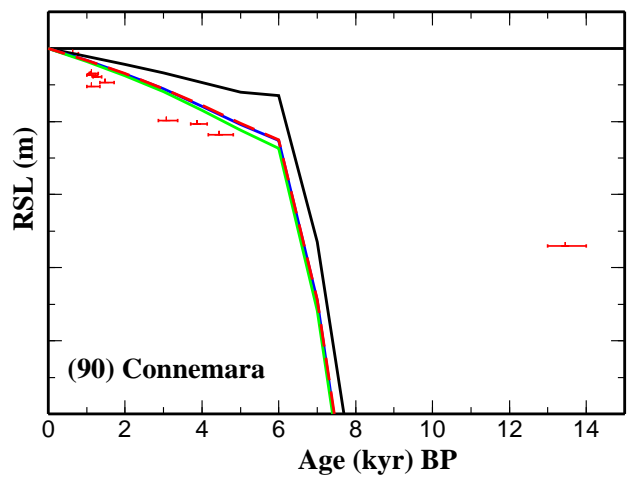
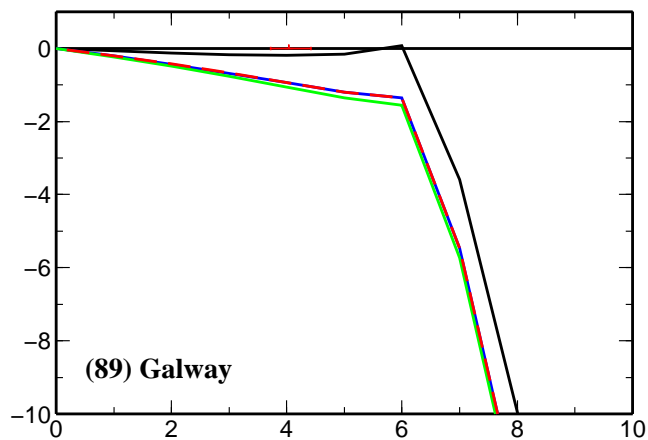
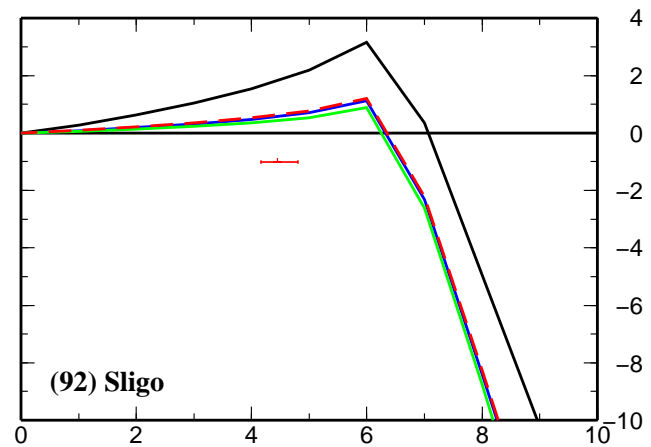
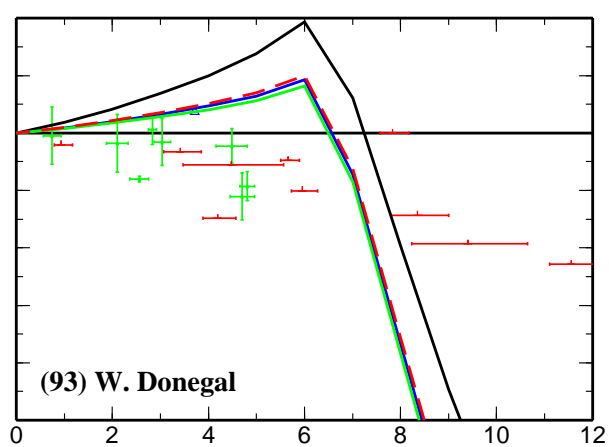
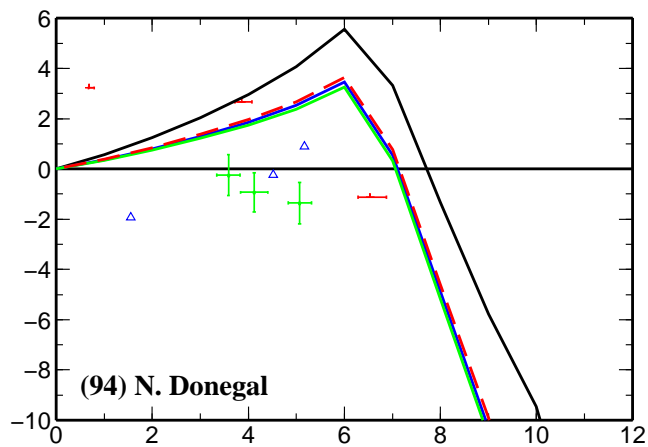
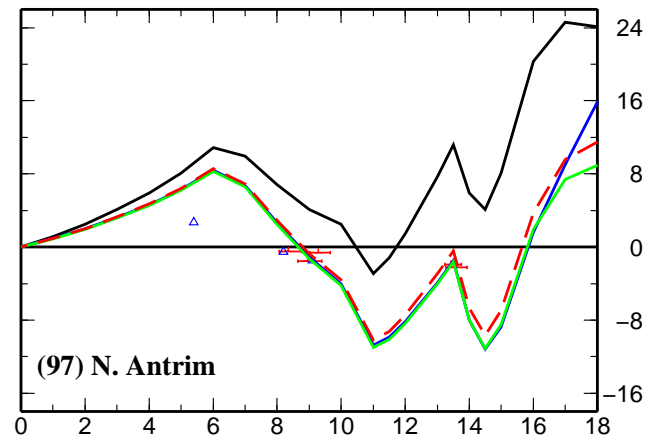
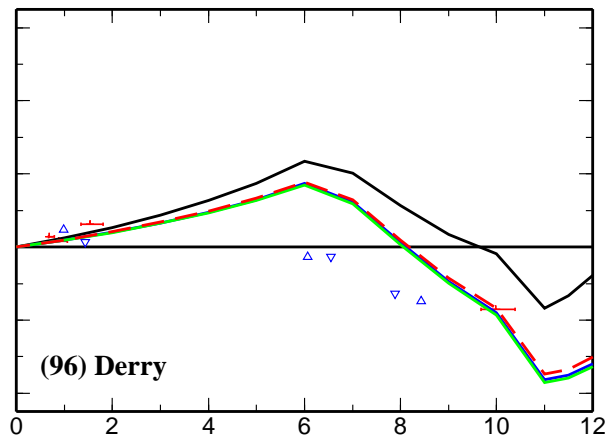
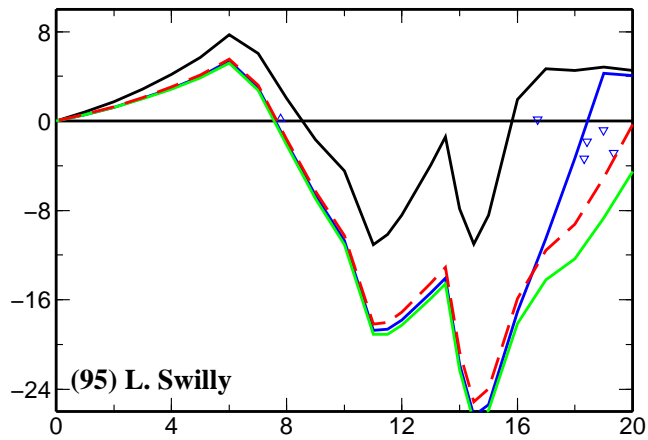


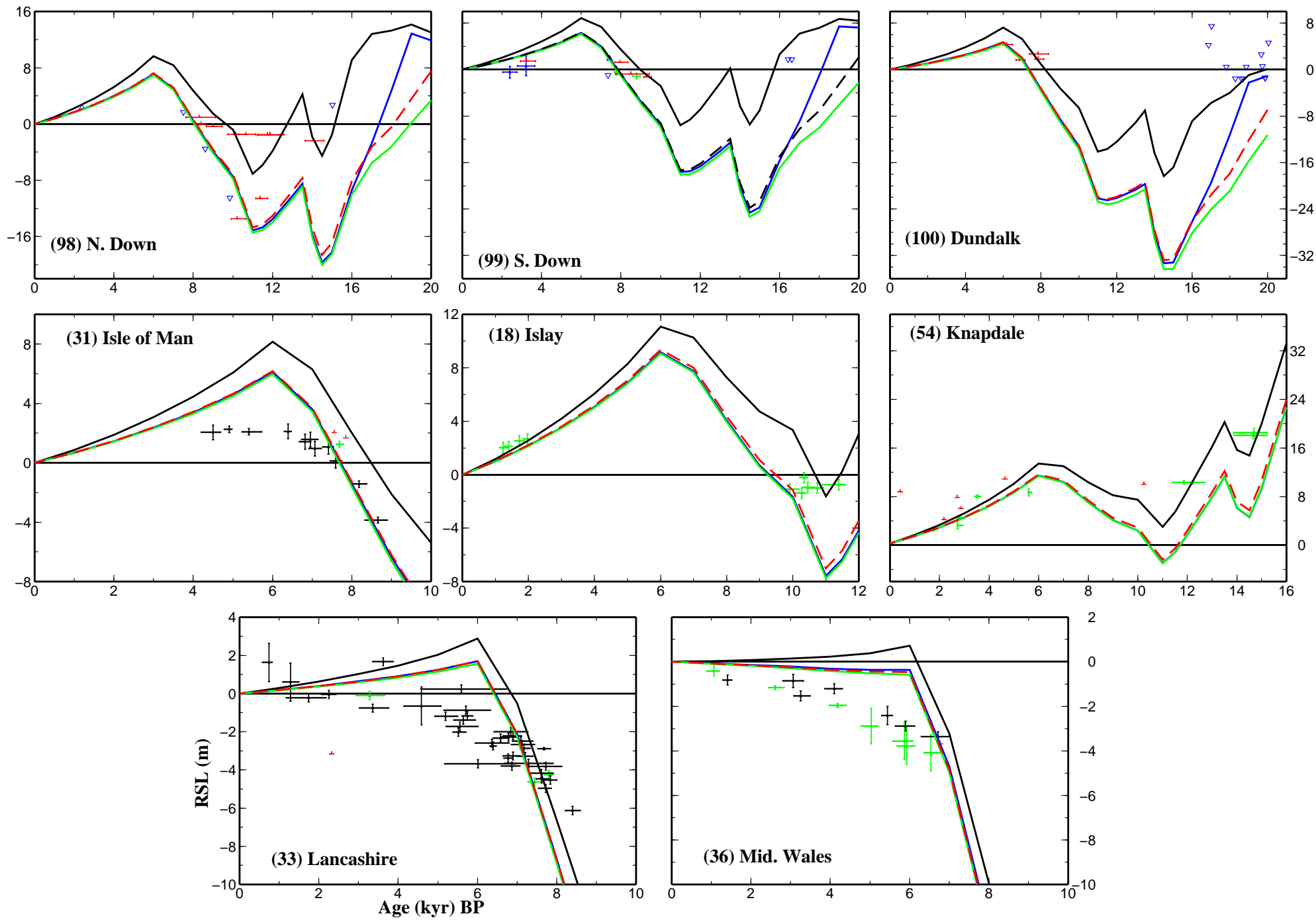
## **Appendix E: Predictions at all Irish and at a selection of Great Britain sites for the three revised Irish Ice models**

Comparison of predicted and observed sea levels at all sites across Ireland and a selection from across Great Britain for the three revised Irish Ice models. Predictions are shown using the 71 km lithosphere earth model for the NS-Thick model (solid black line); Model A (solid blue line); Model B (solid green line) and Model C (dashed red line). The data are separated into a series of numbered plots E1-E3 in relation to geographical location as follows: E1: Southern Ireland; E2: West and North Ireland; E3: NE Ireland, Isle of Man and sites from the NW coast of Great Britain.



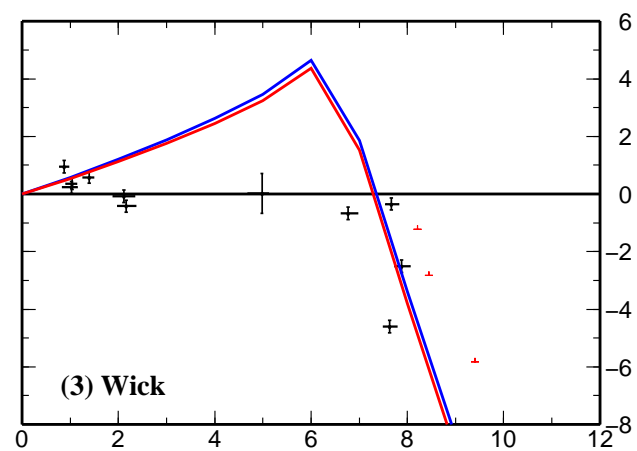
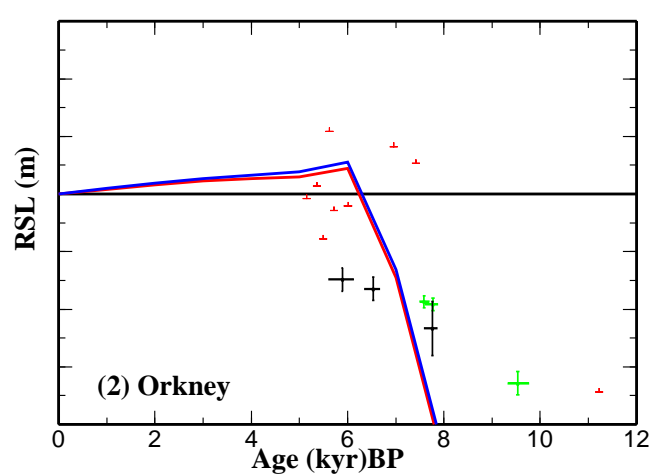
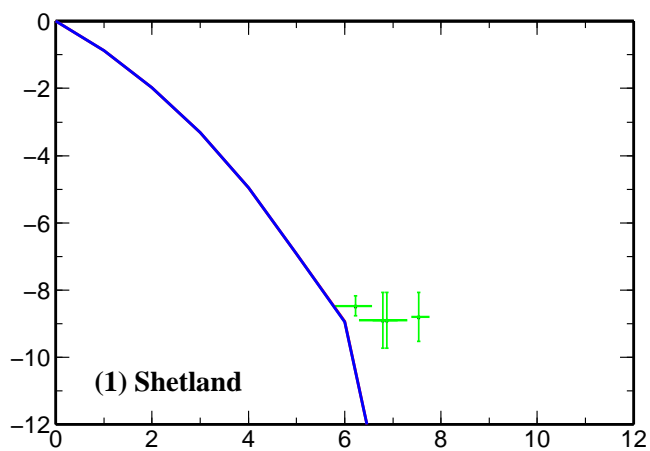
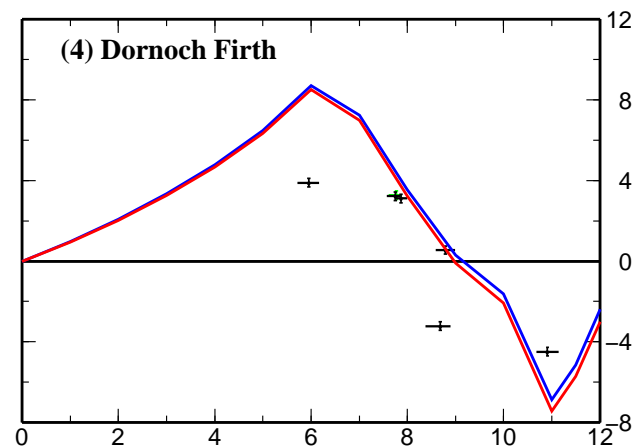
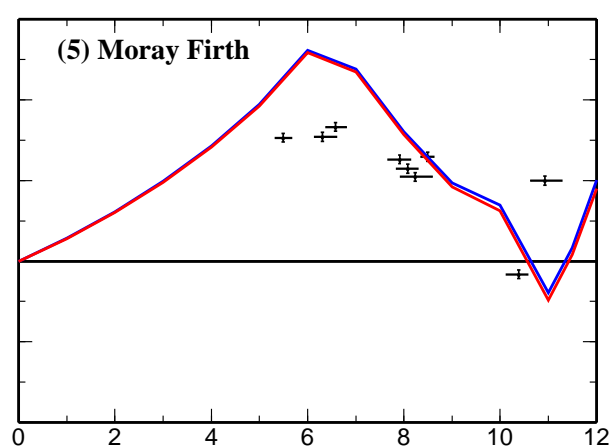
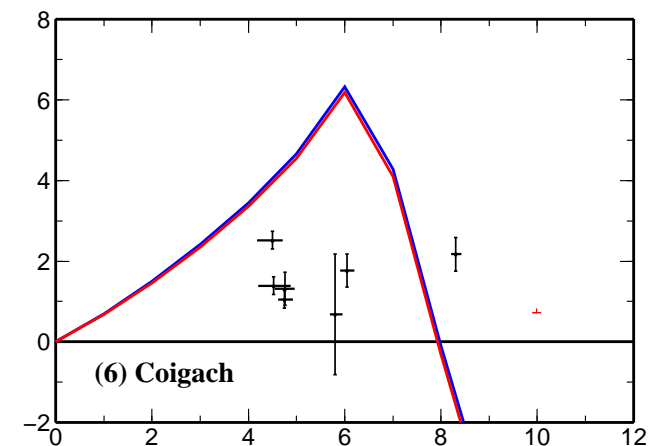
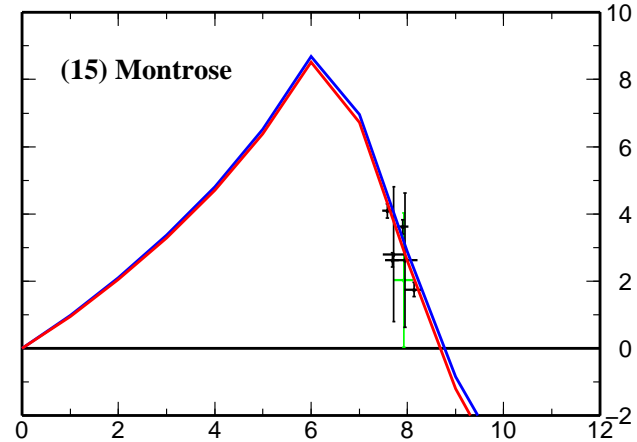
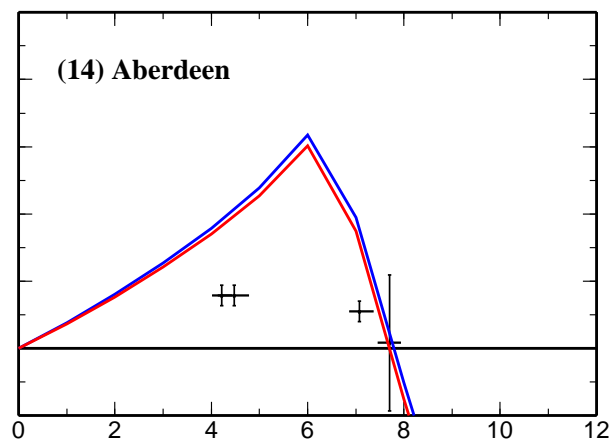
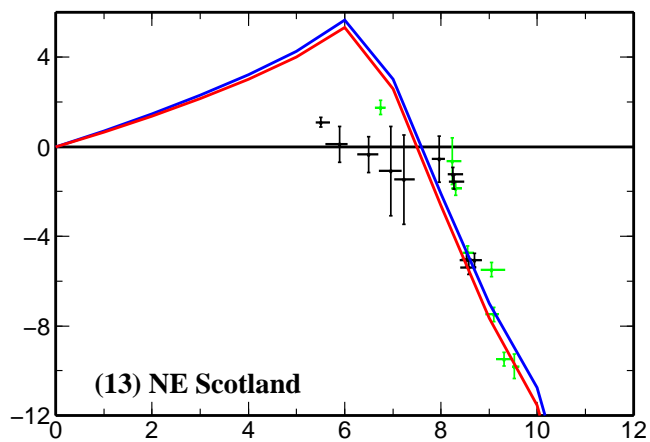
**E1**

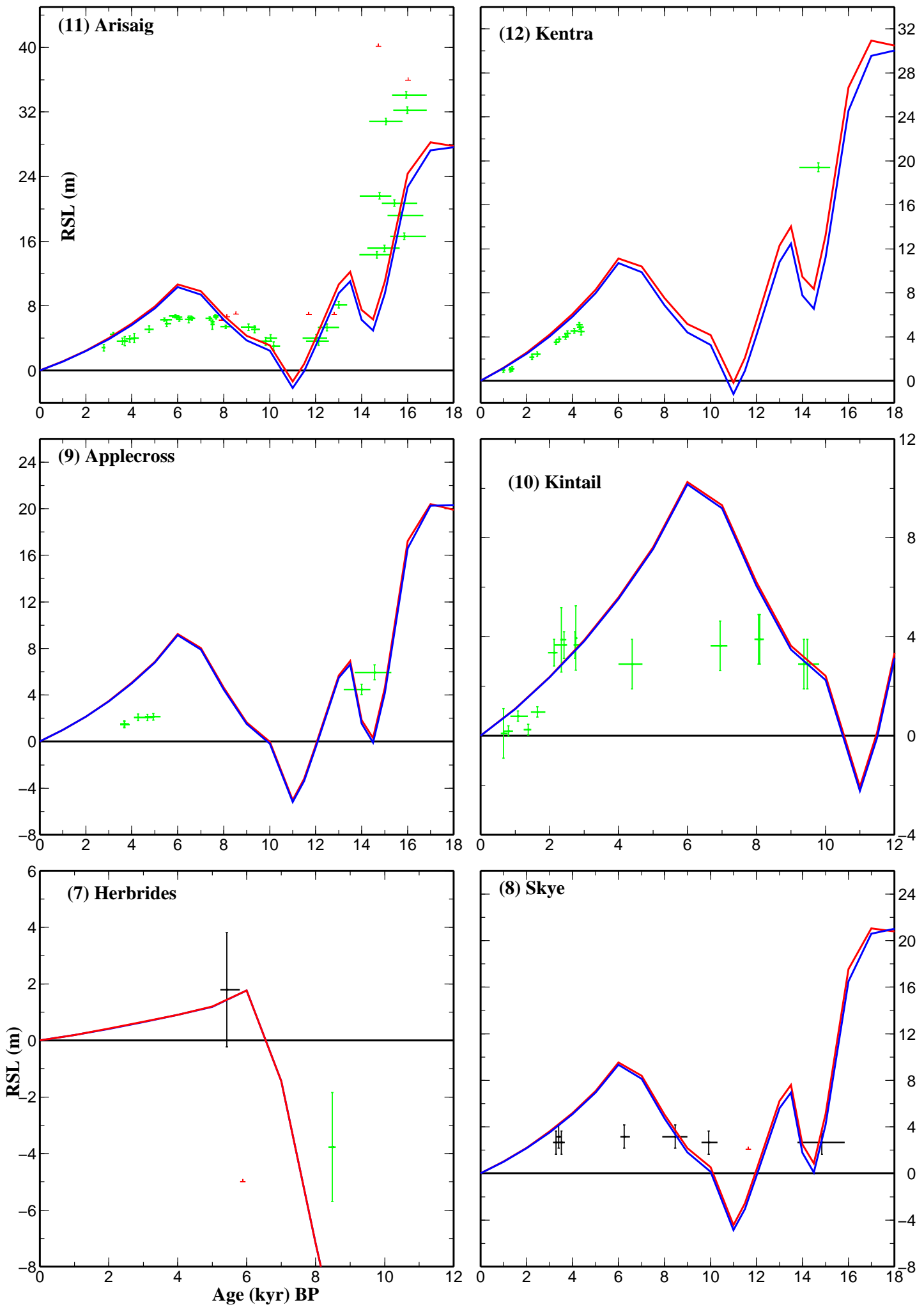


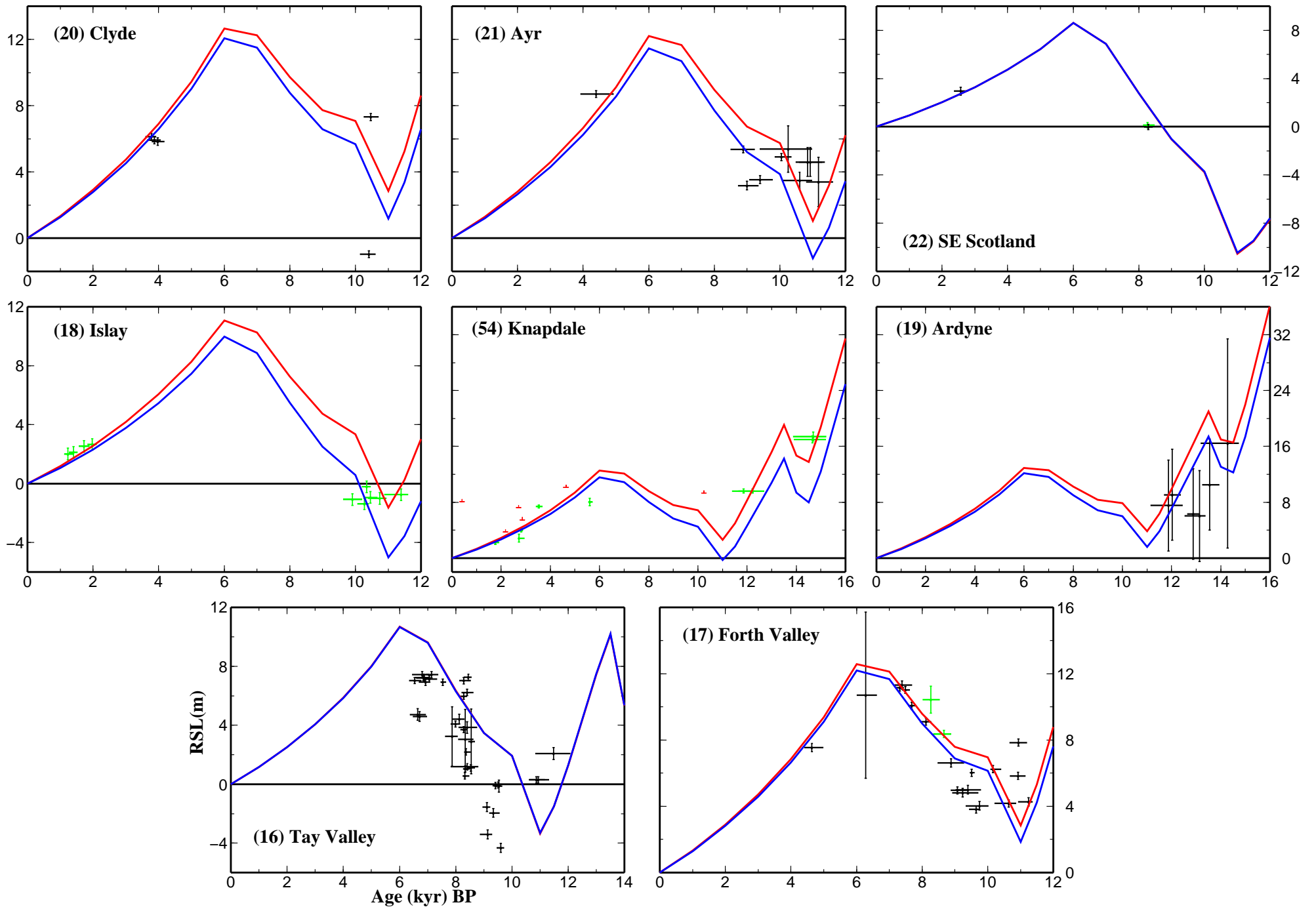


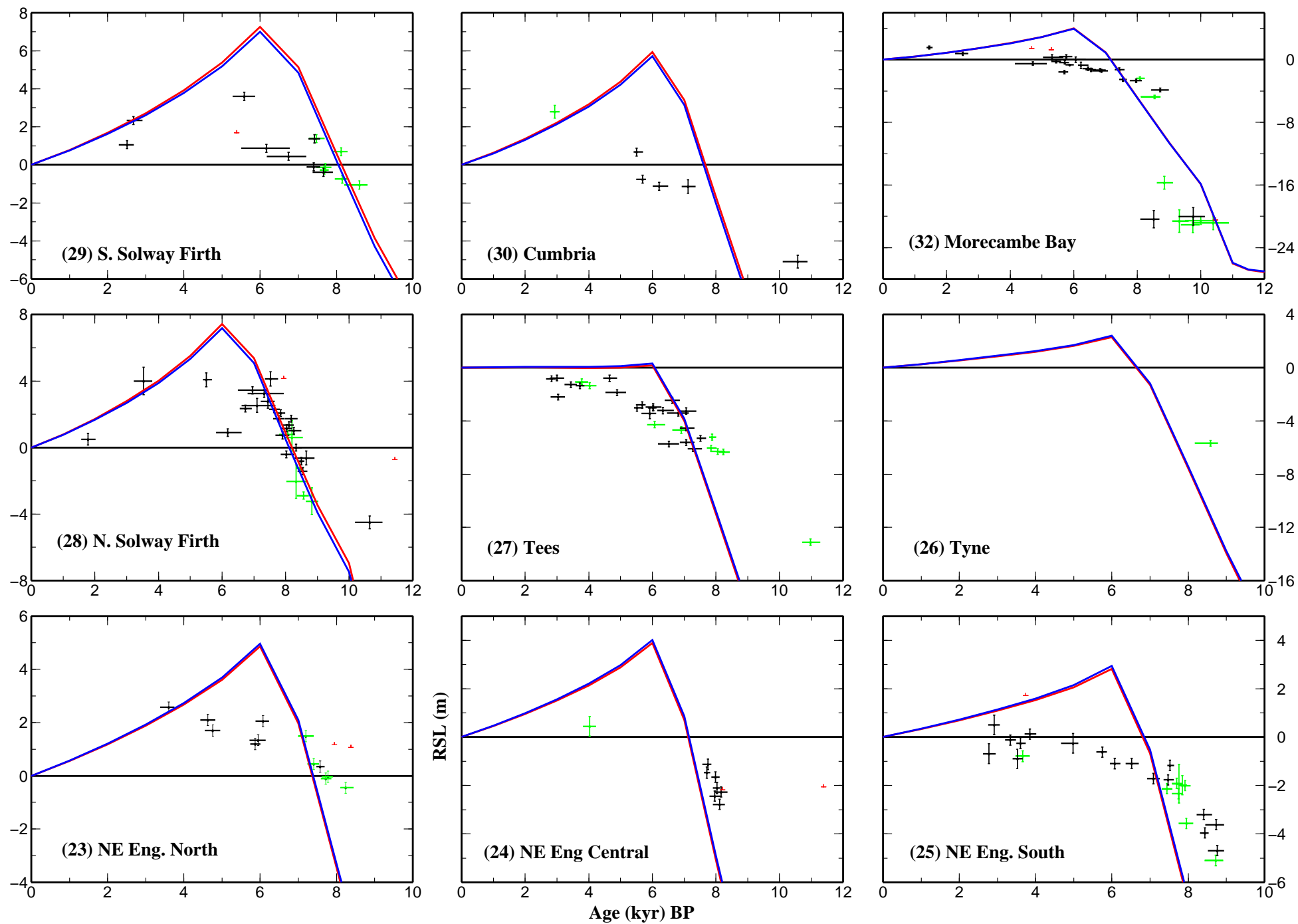
## **Appendix F: Predictions at all British Isles RSL data sites using the Brooks et al. model**

Comparison of predicted and observed sea level at all sites across Great Britain and Ireland. Predictions are shown using the 71 km lithosphere earth model for the Shennan model (solid red line) and the Brooks et al. model (see Fig. 2.13) (solid blue line). The data are separated into a series of plots numbered F1-F10 in relation to geographical location as follows: F1: North and NE Scotland; F2: NW Scotland; F3: Central Scotland; F4: NW and NE England; F5: NW England and Wales; F6: East England; F7: South England; F8: Southern Ireland; F9: West and North Ireland; F10: NE Ireland, Isle of Man and North Sea Basin

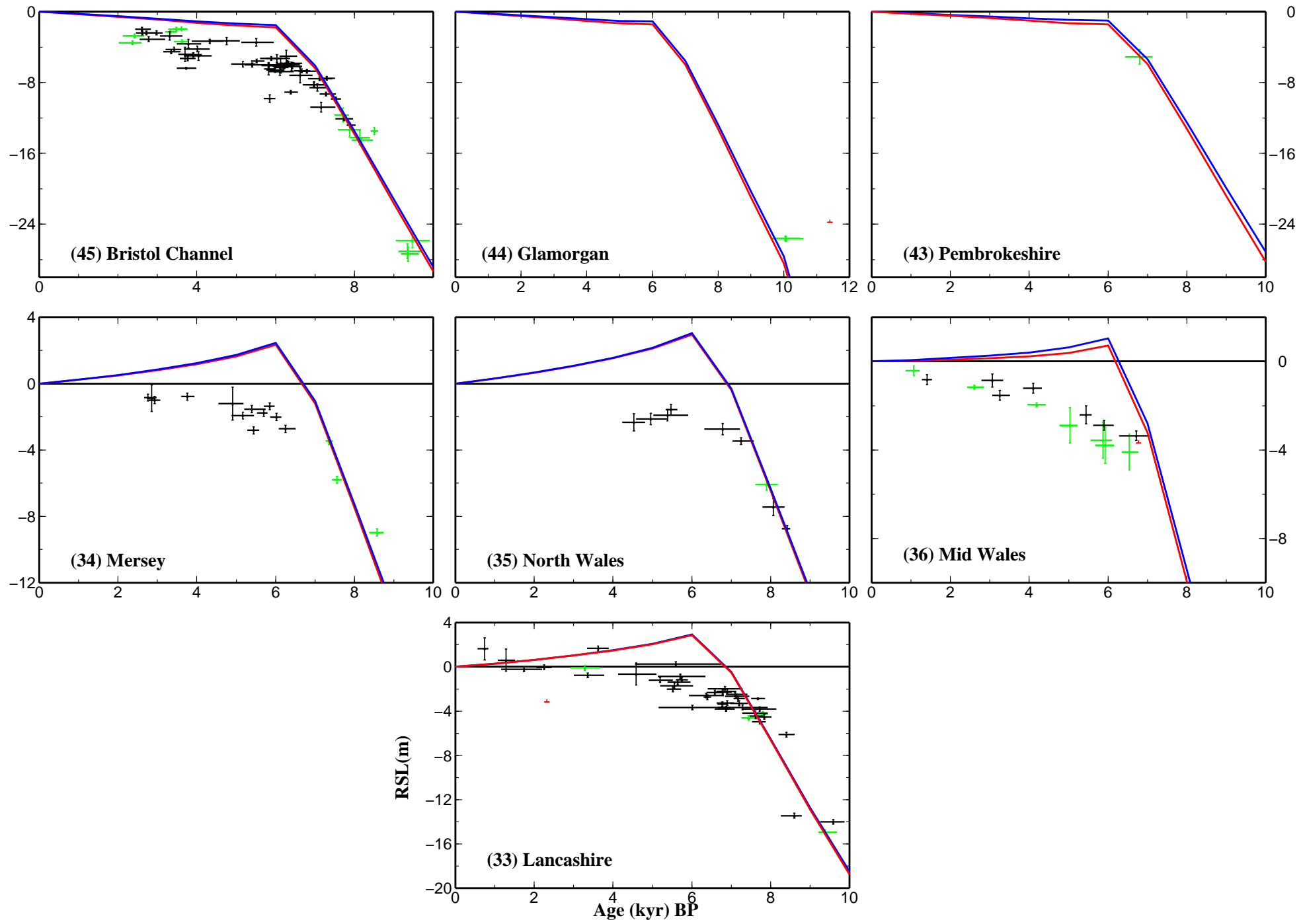


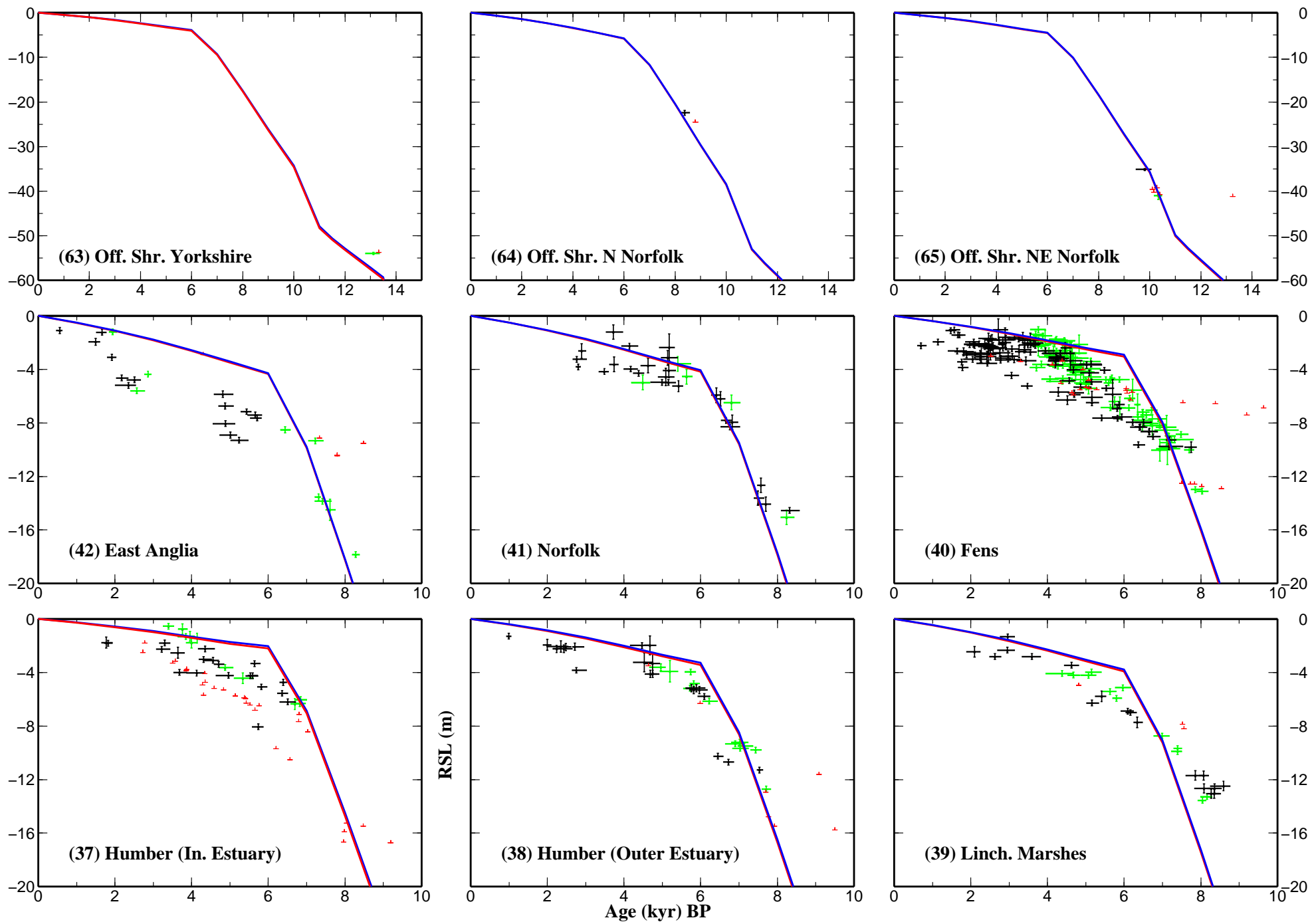


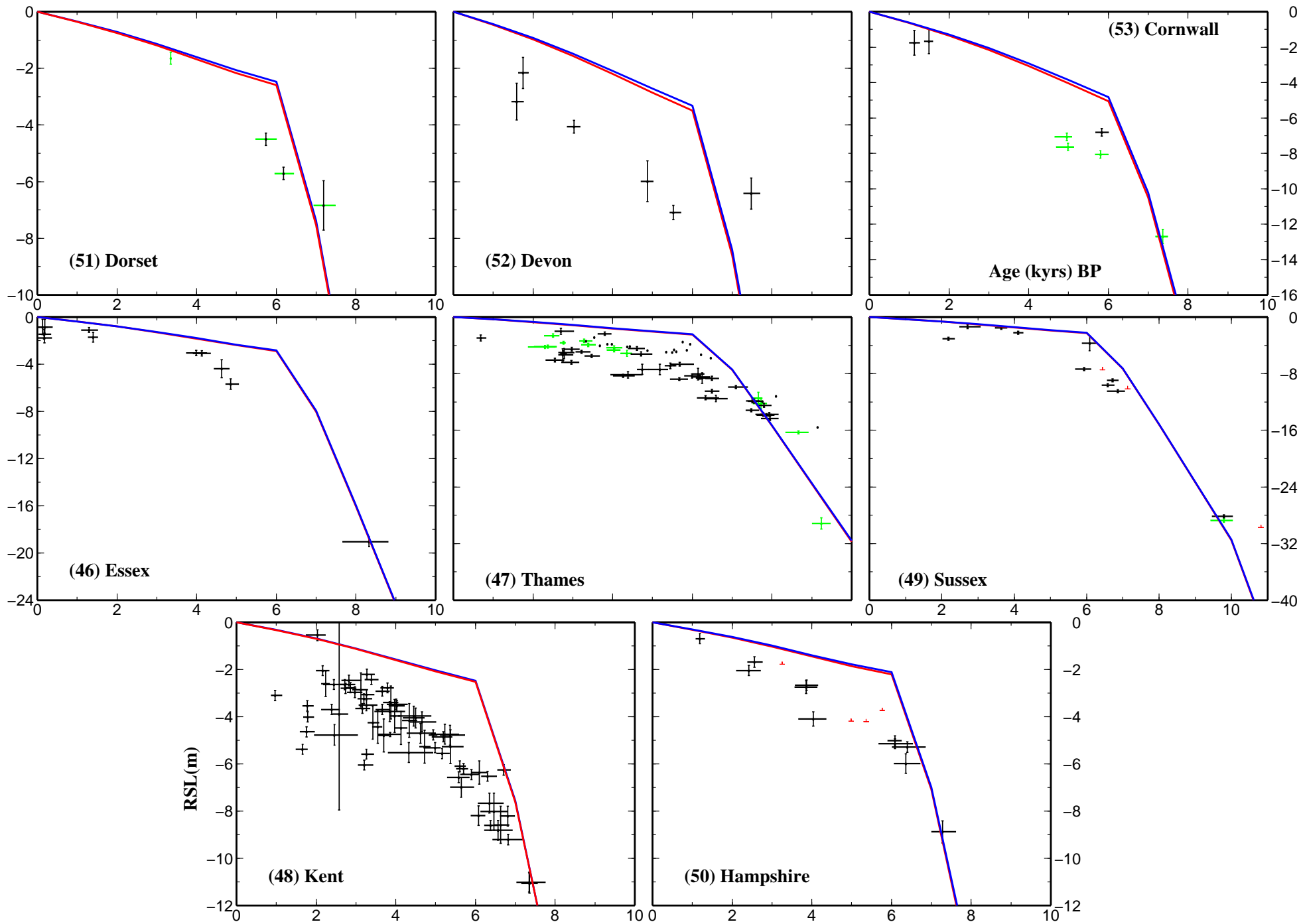


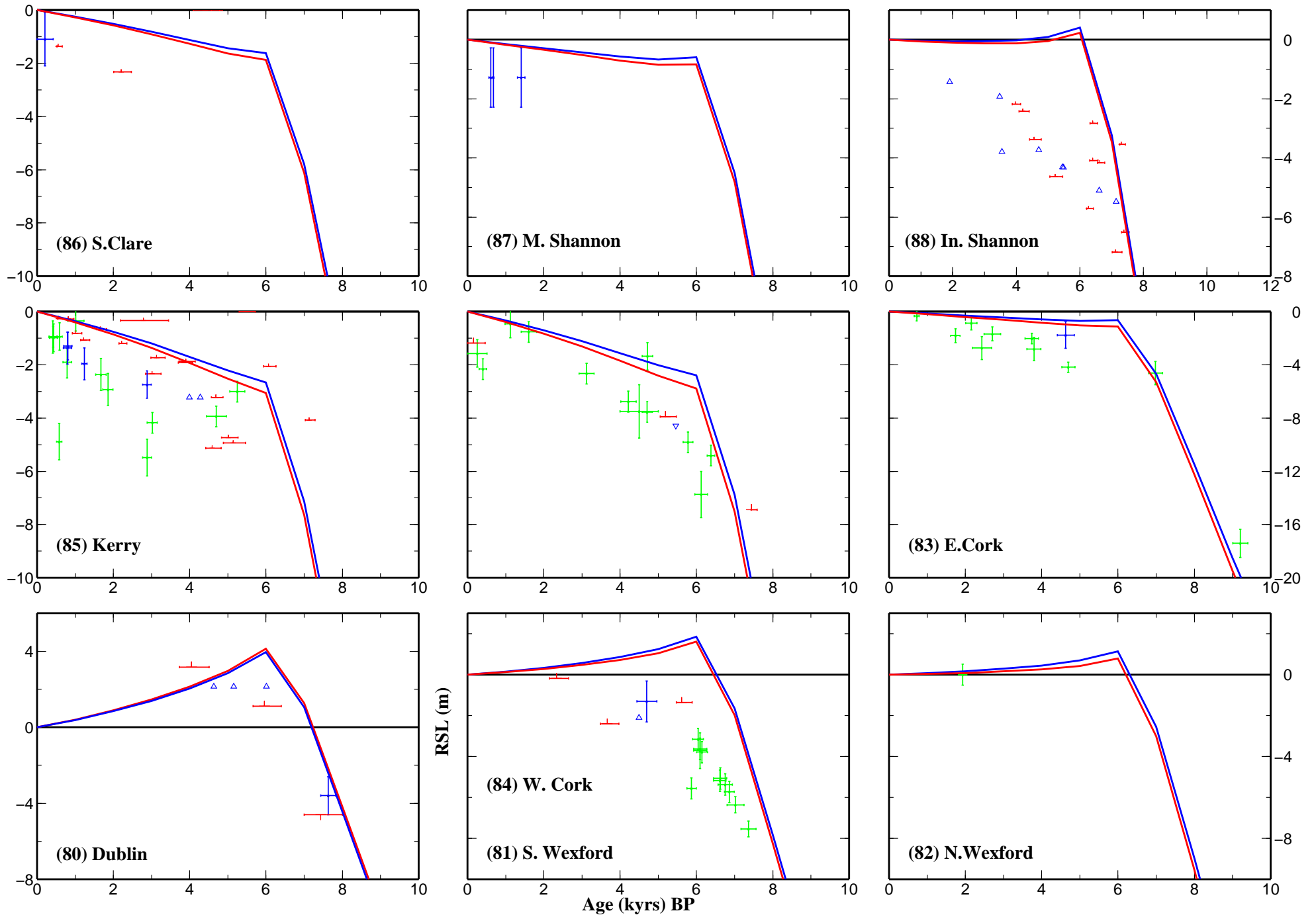


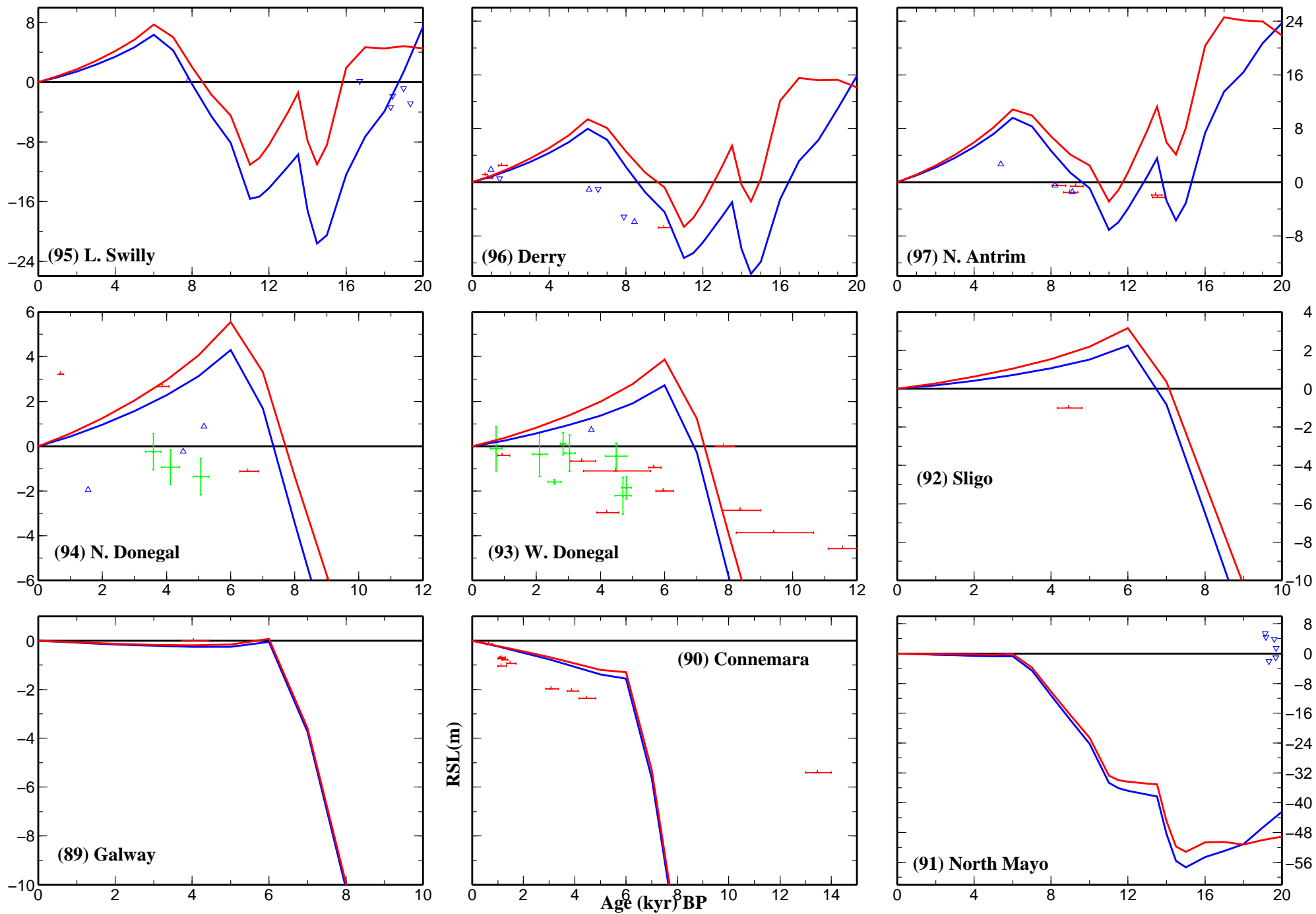
**F4**

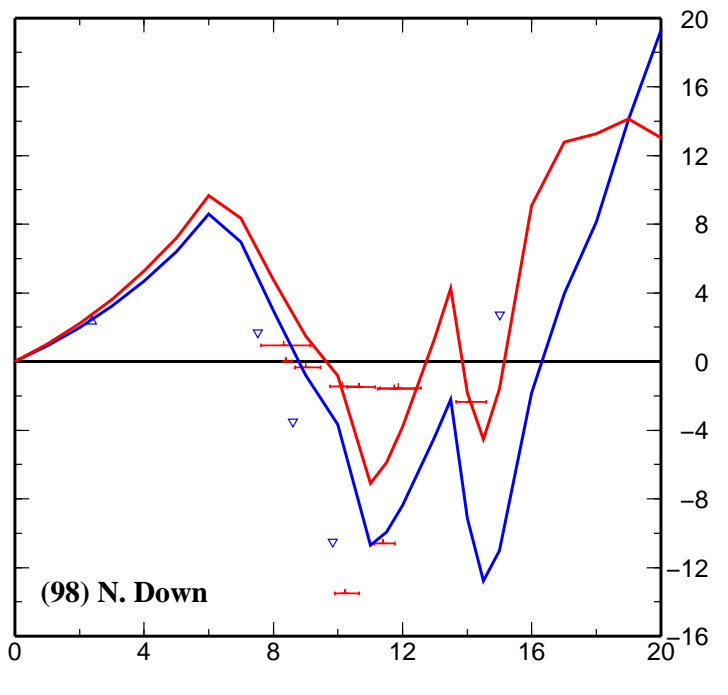
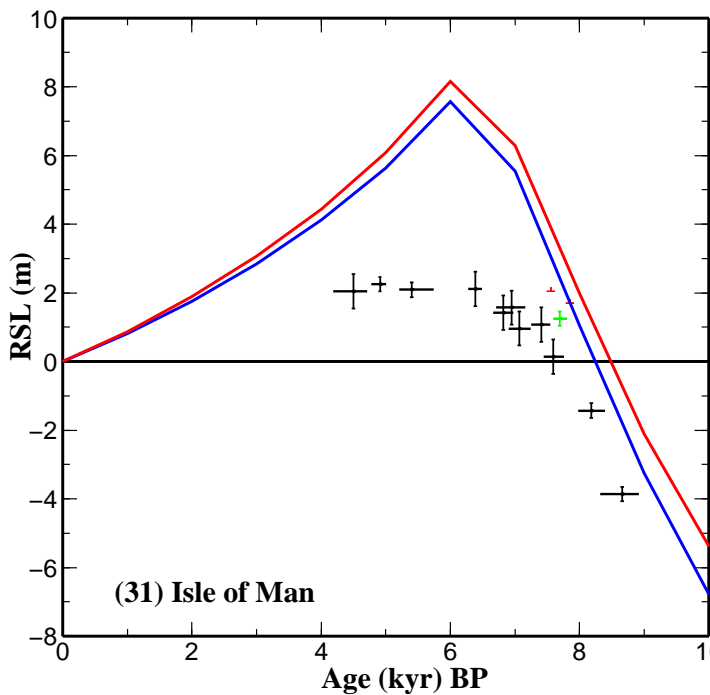
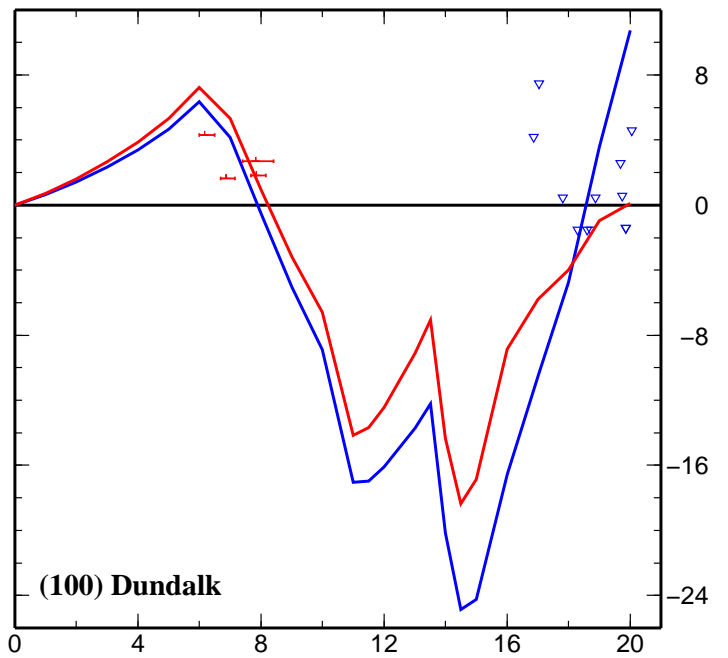
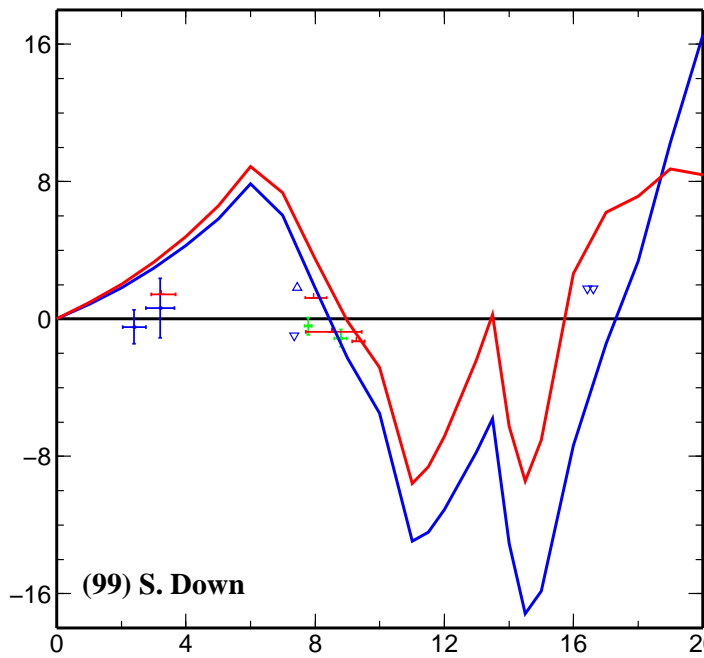
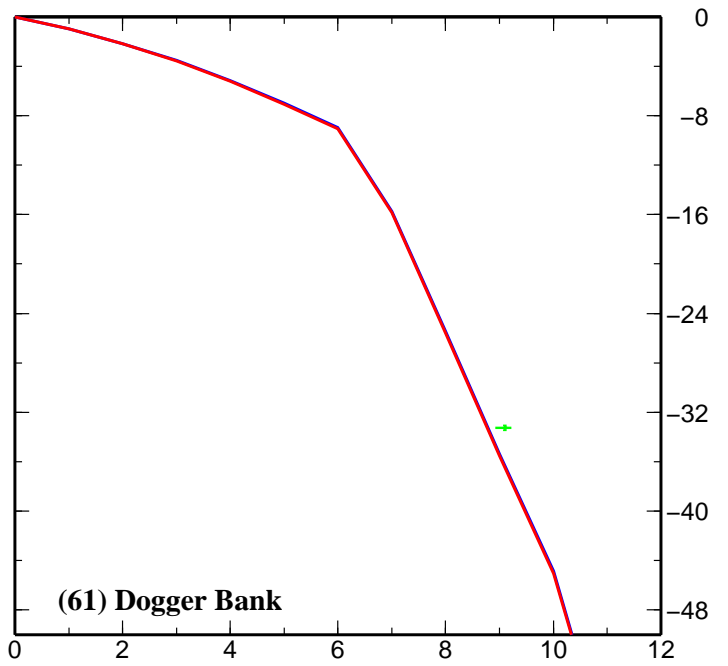
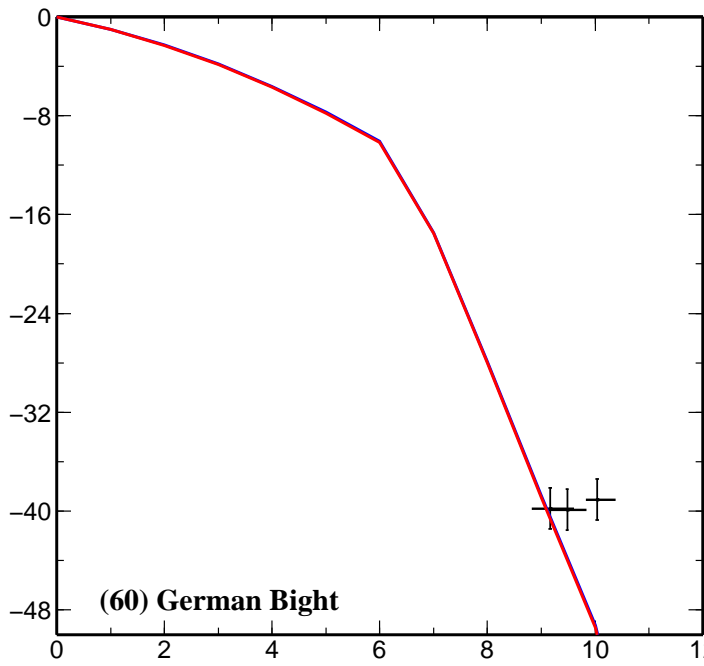






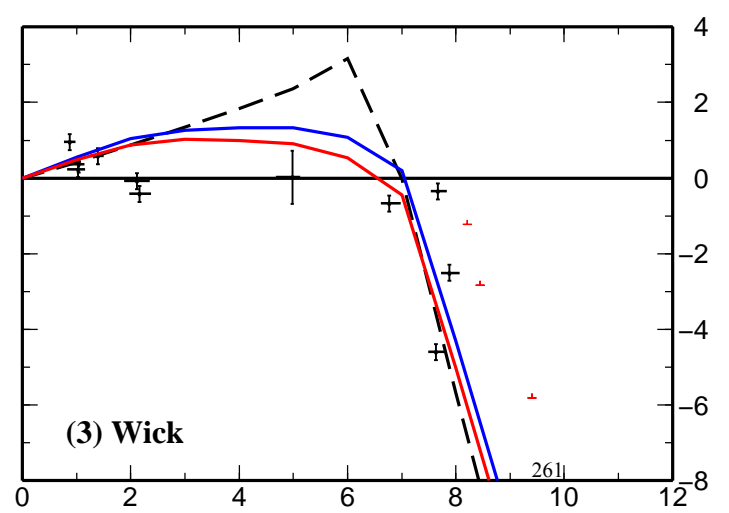
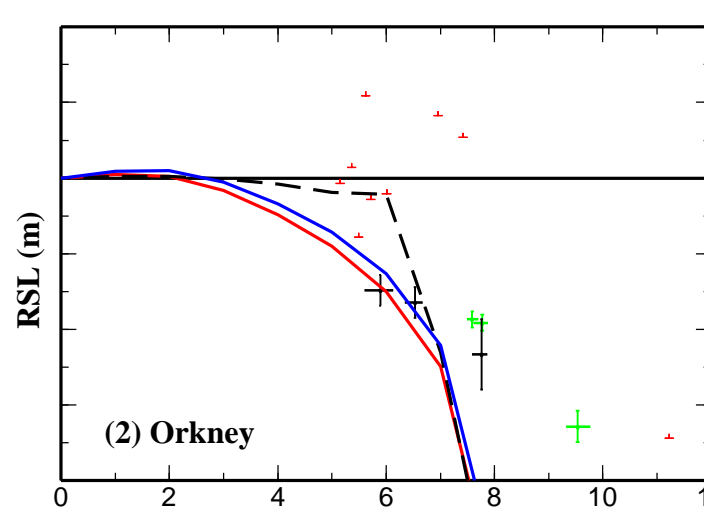
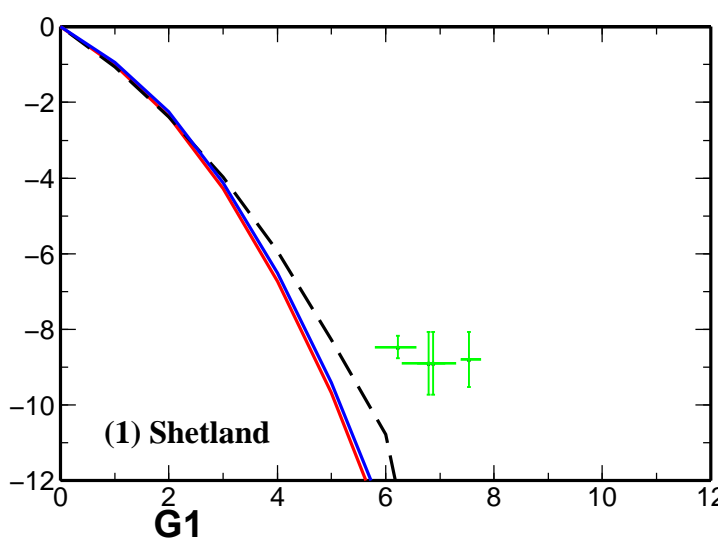
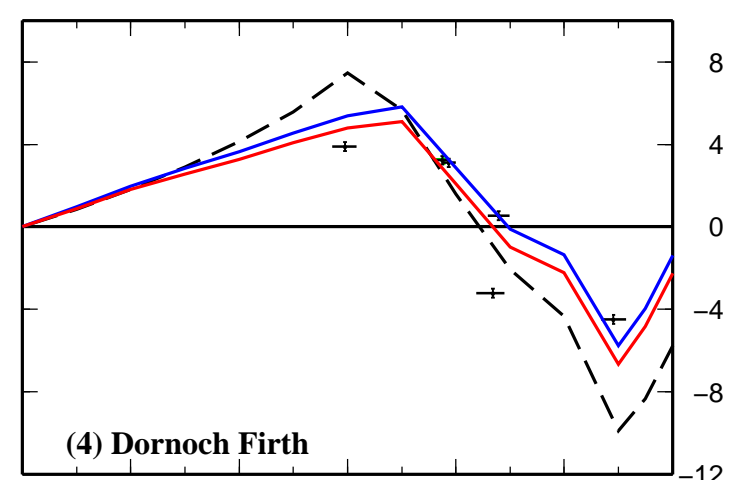
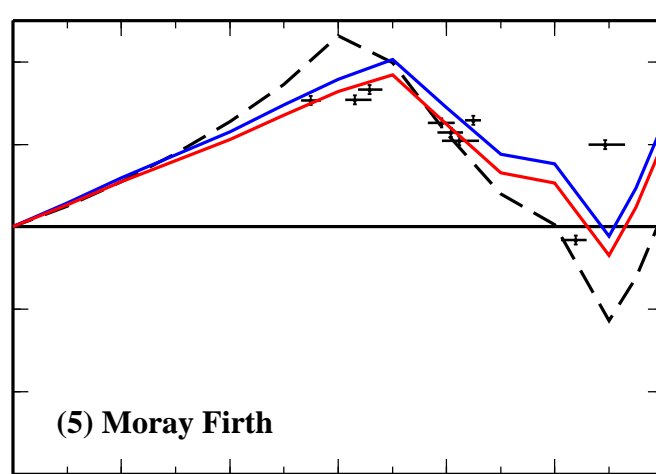
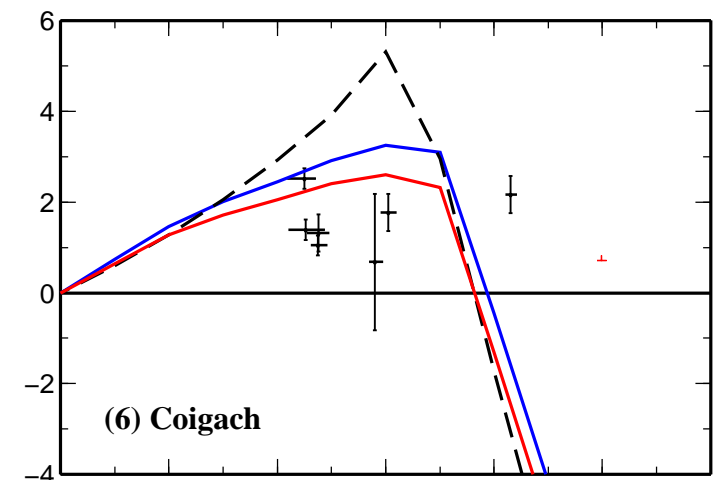
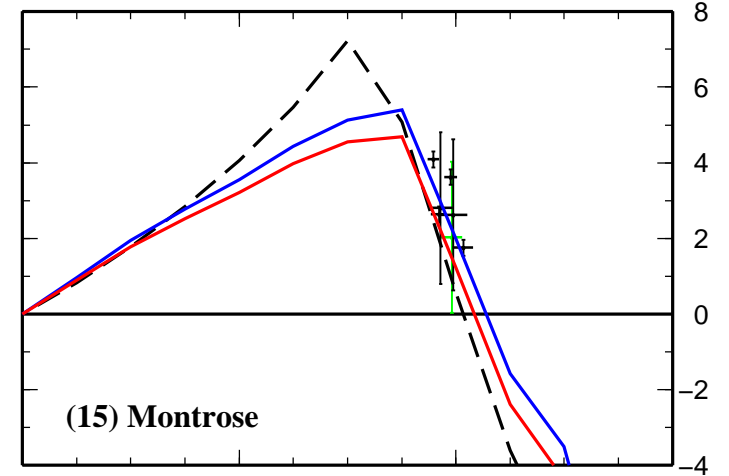
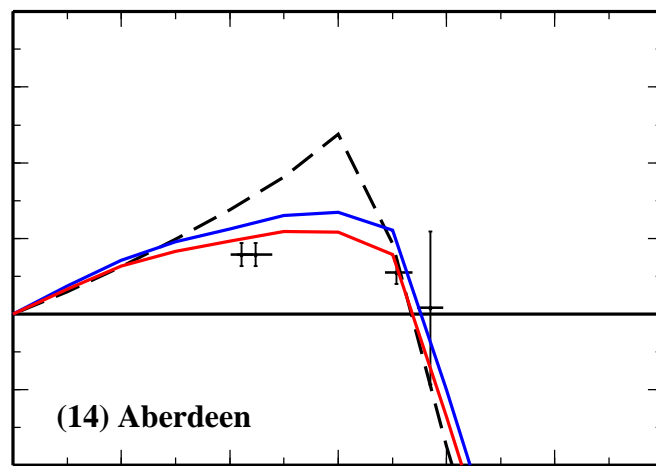
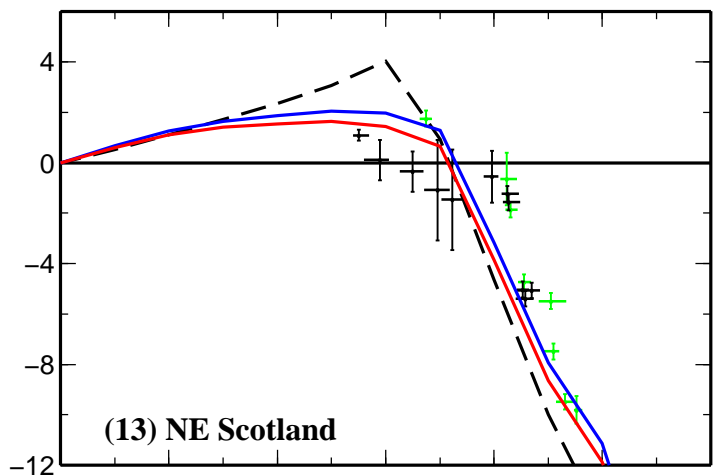






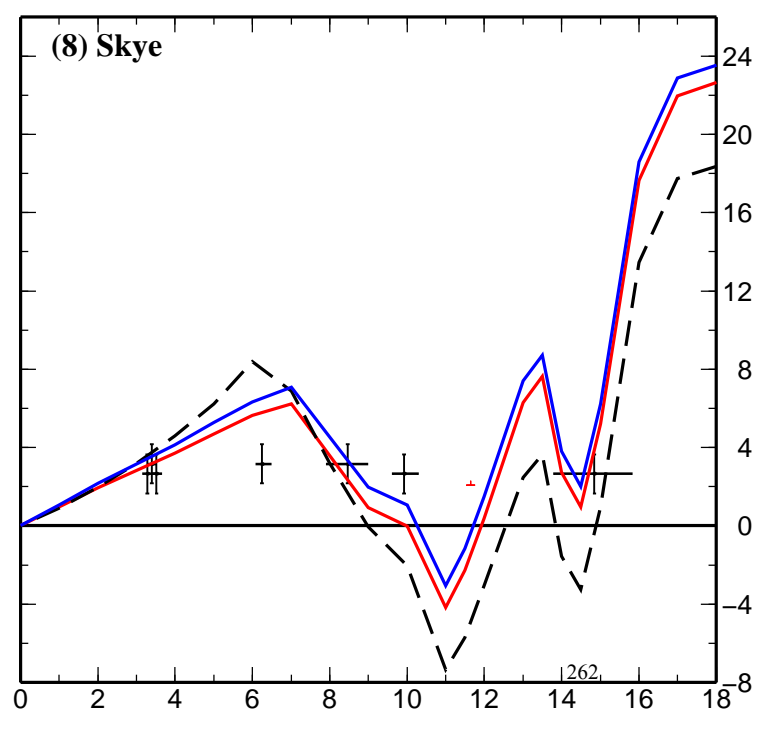
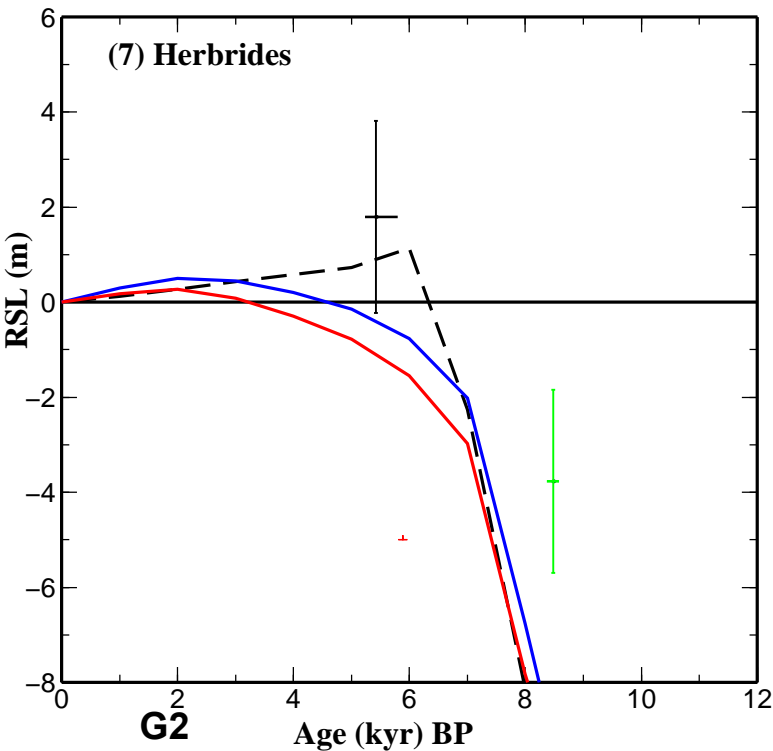
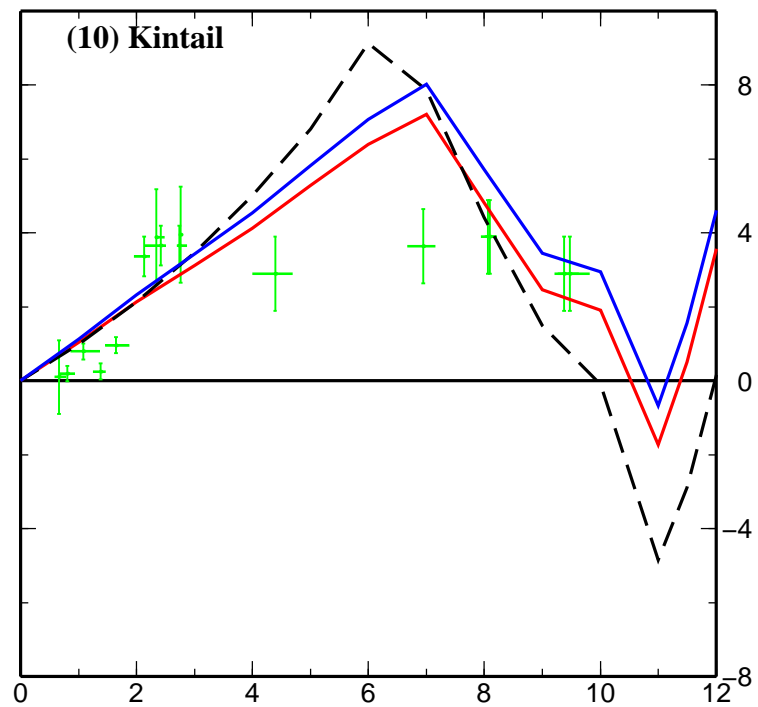
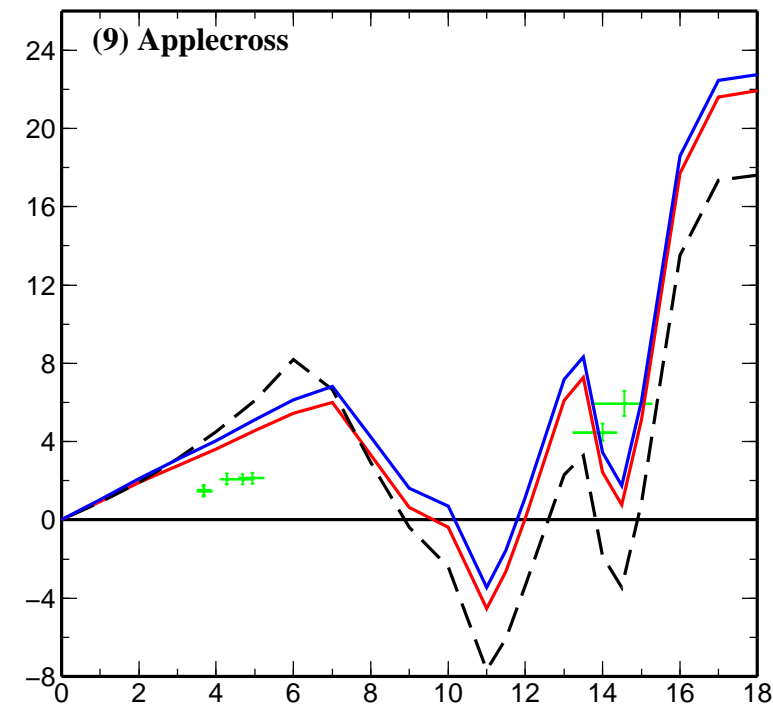
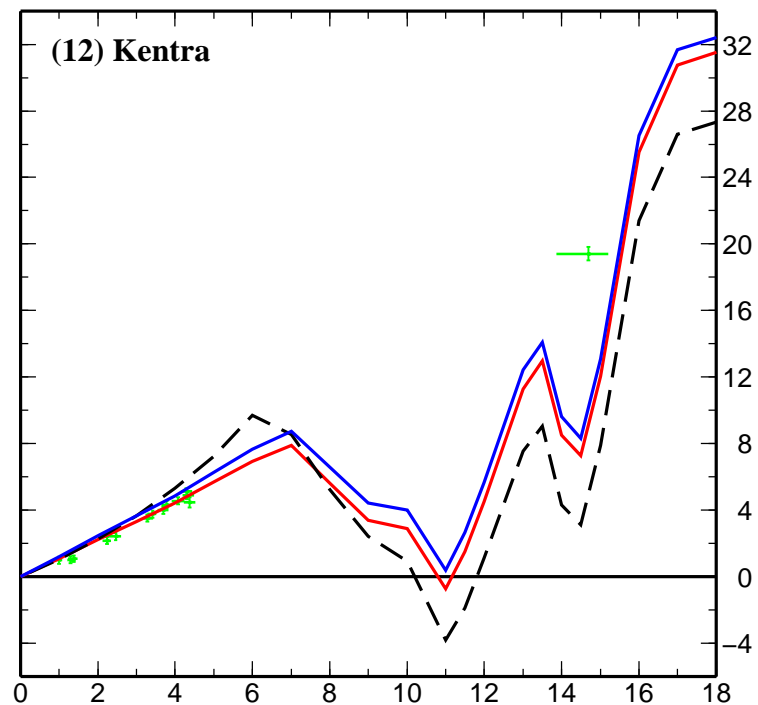
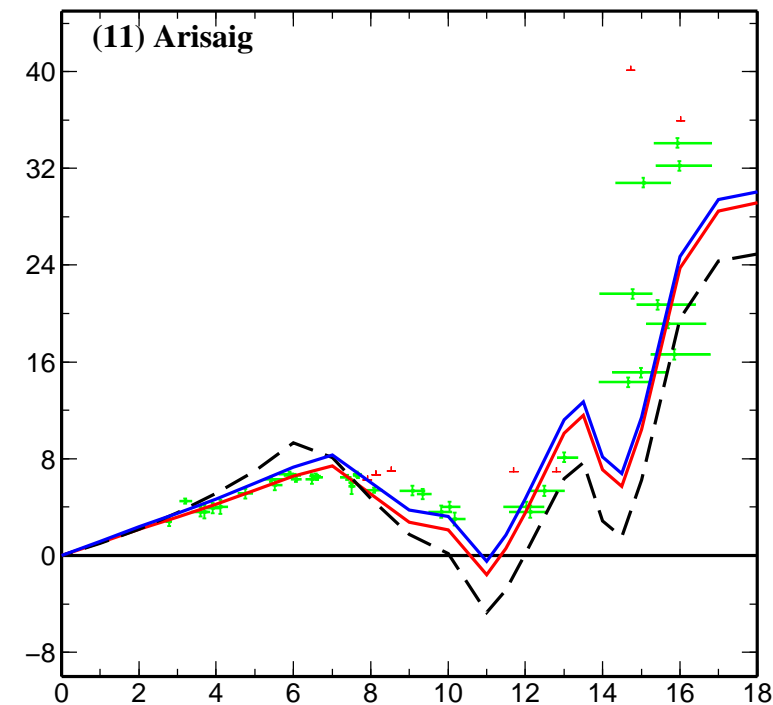
## **Appendix G: Predictions at all British Isles RSL data sites using the Brooks et al. model and the final BIIS GIA model**

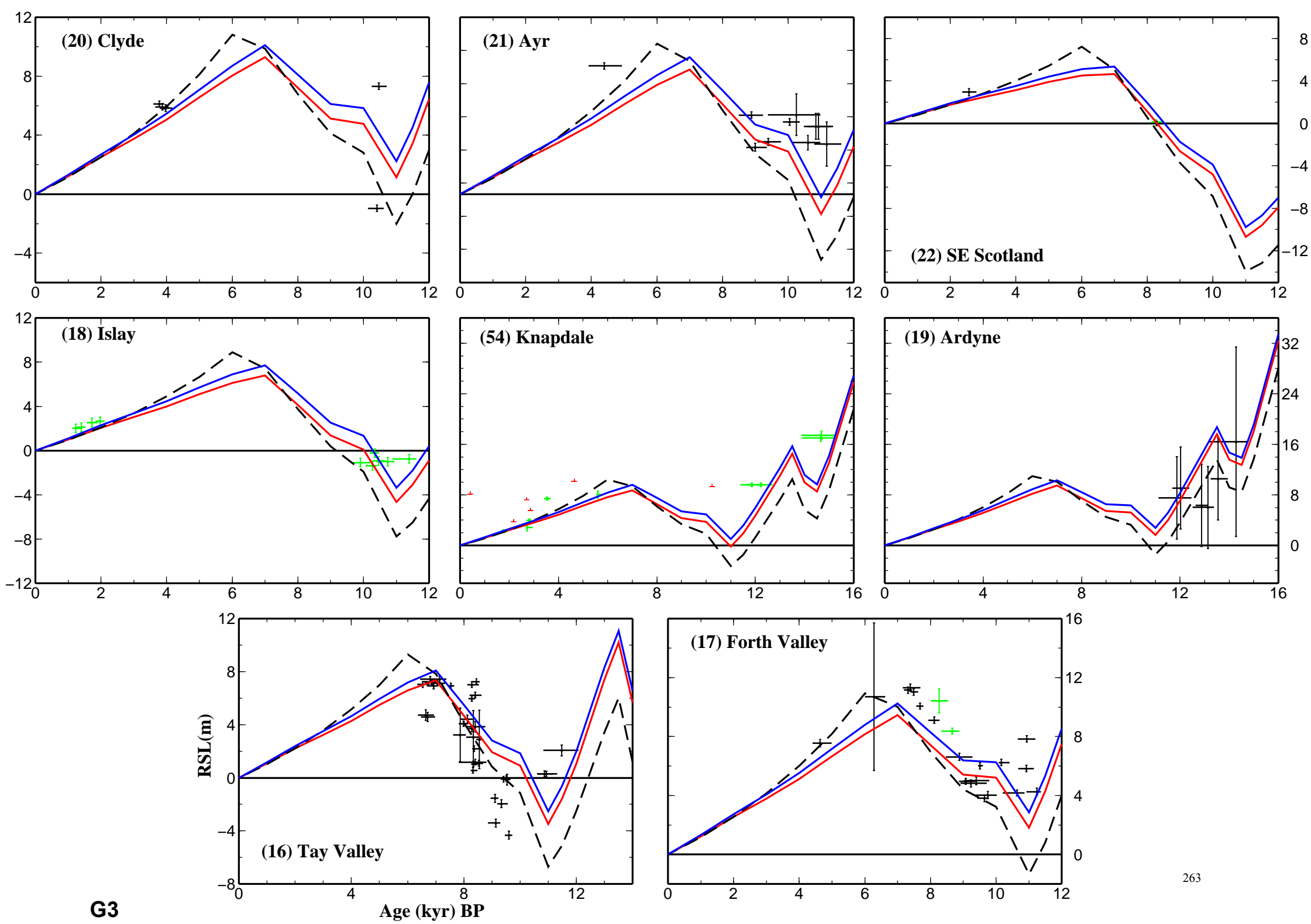
Comparison of predicted and observed sea level at all sites across Great Britain and Ireland. Predictions are shown using the optimum earth model inferred in Bradley et al. (2009) lithosphere thickness 71 km, upper mantle viscosity  $0.5 \times 10^{21}$  Pa s, and lower mantle viscosity  $3 \times 10^{22}$  Pa s for the Brooks et al. model (dashed black line) and the final BIIS GIA model (solid red line). Additionally, predictions are shown using the final BIIS GIA model using an earth model identical to the optimum earth model except that the viscosity in the lower mantle is higher, at  $6 \times 10^{22}$  Pa s (solid blue line). The data are separated into a series of plots numbered G1-G10 in relation to geographical location as follows: G1: North and NE Scotland; G2: NW Scotland; G3: Central Scotland; G4: NW and NE England; G5: NW England and Wales; G6: East England; G7: South England; G8: Southern Ireland; G9: West and North Ireland; G10: NE Ireland, Isle of Man and North Sea Basin

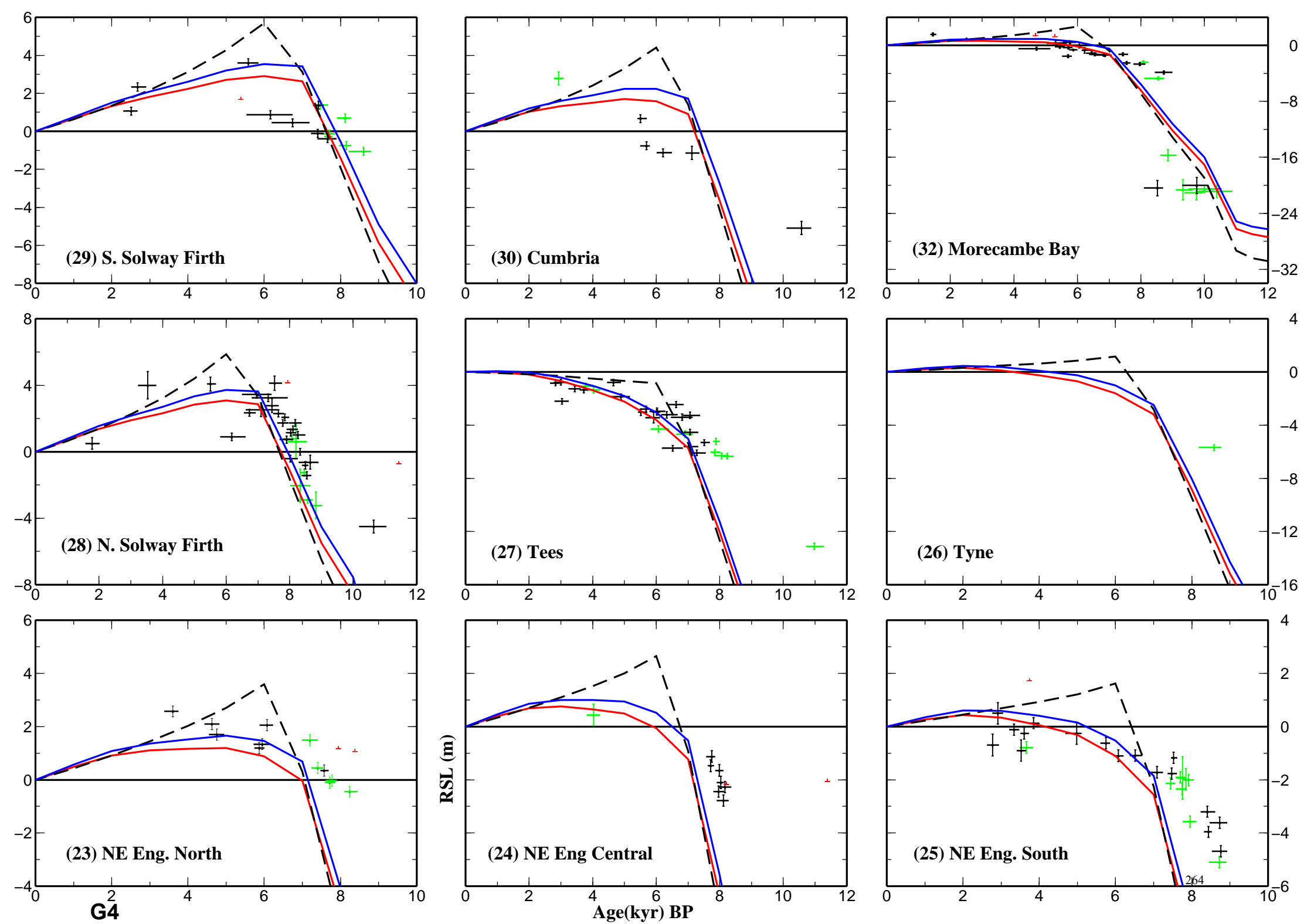


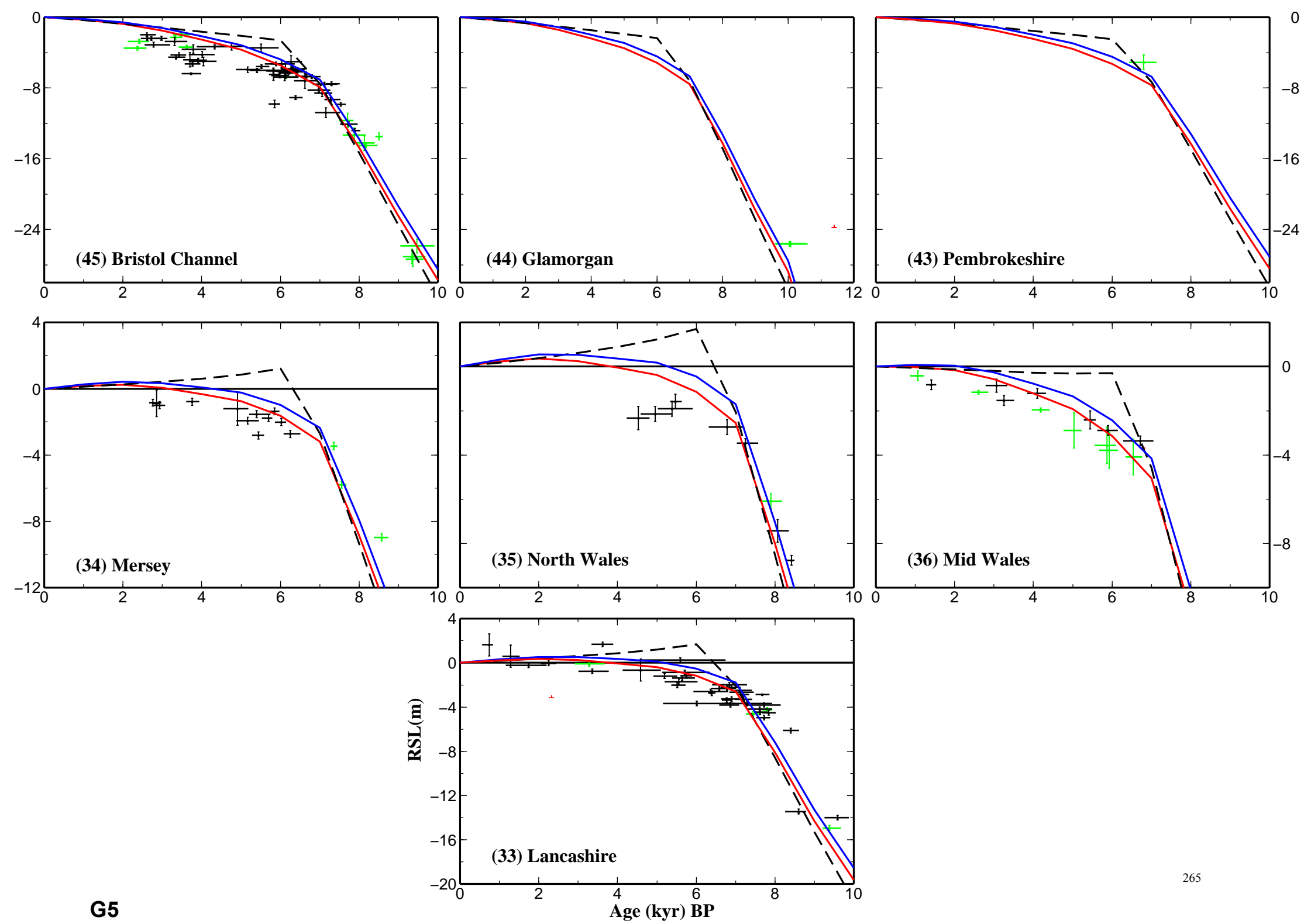
**G1**

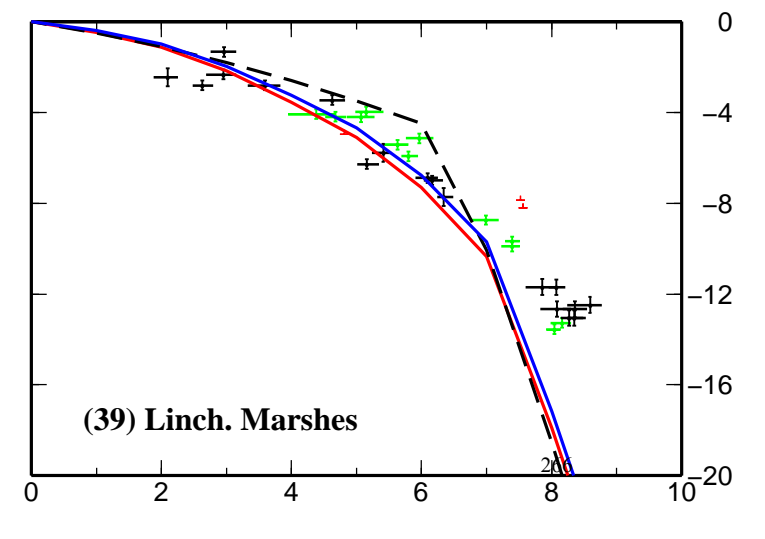
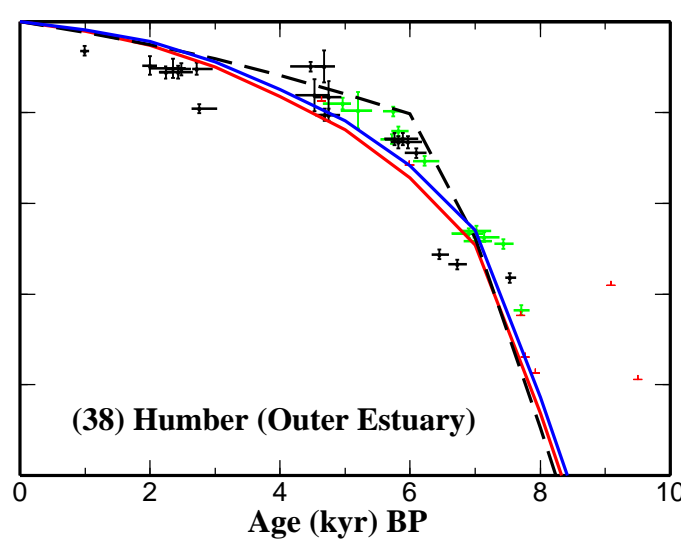
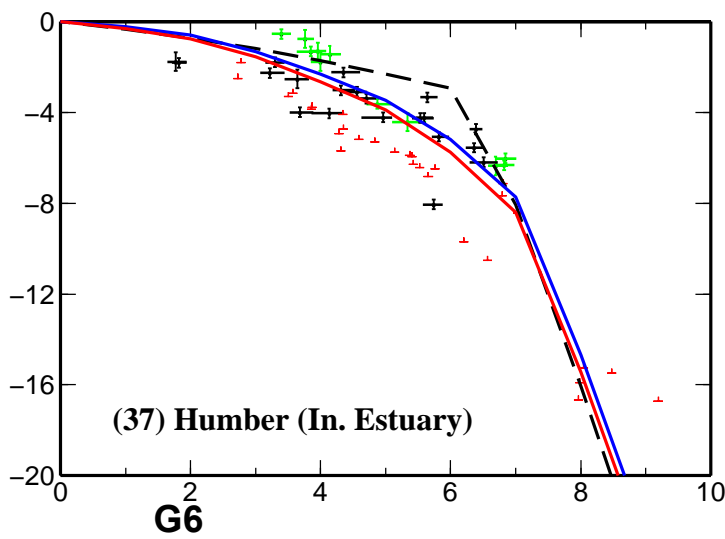
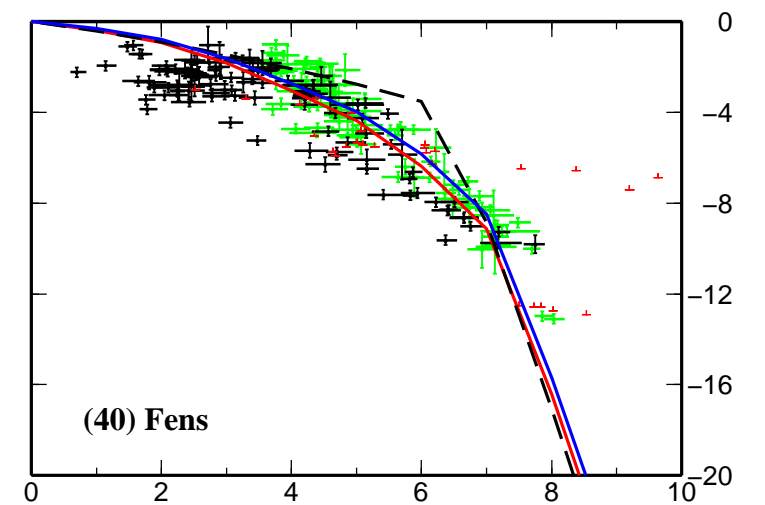
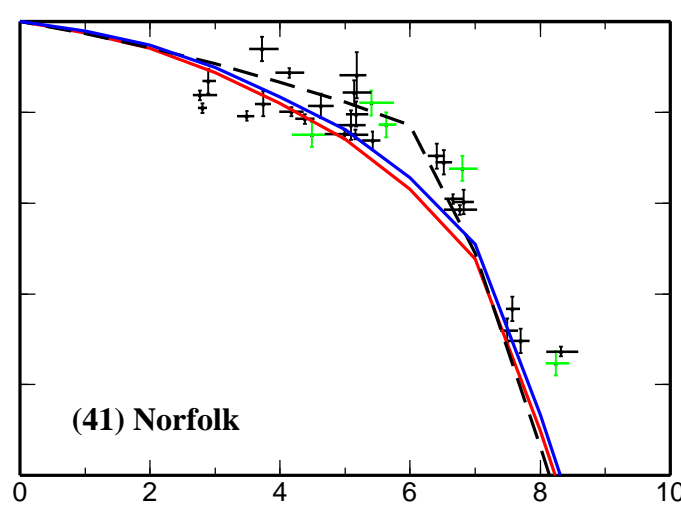
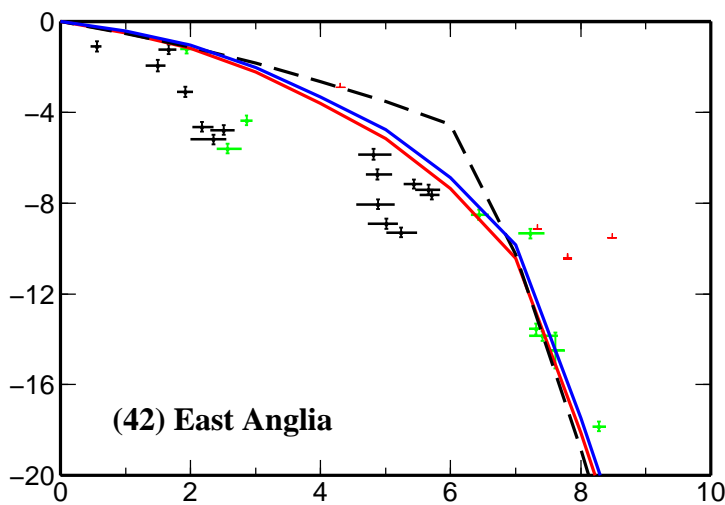
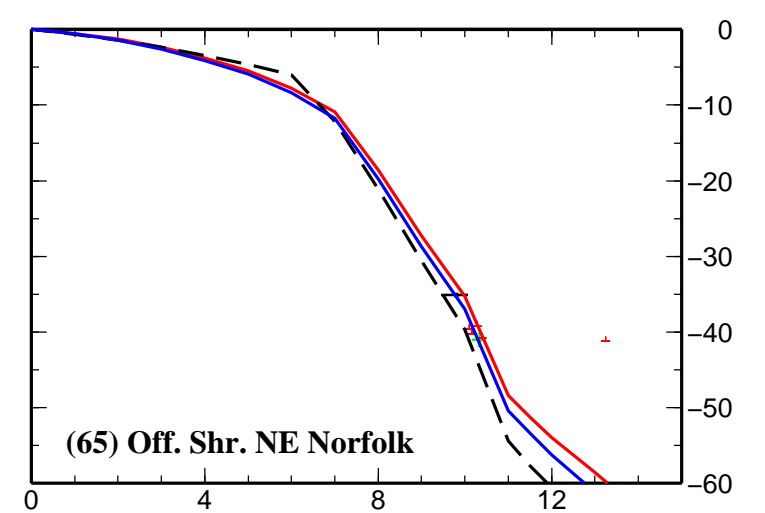
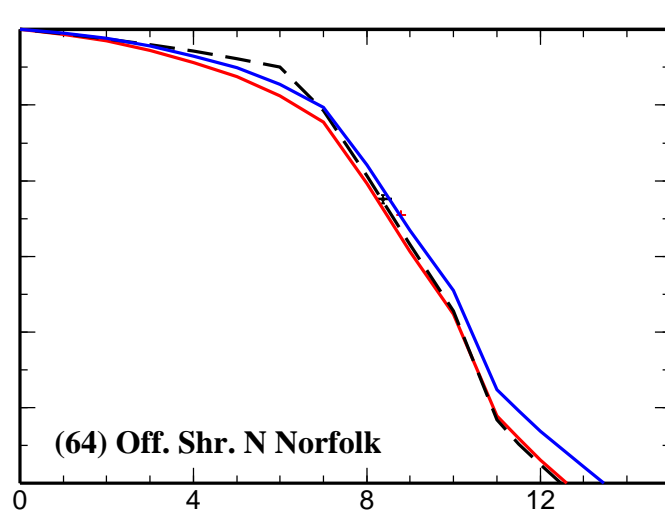
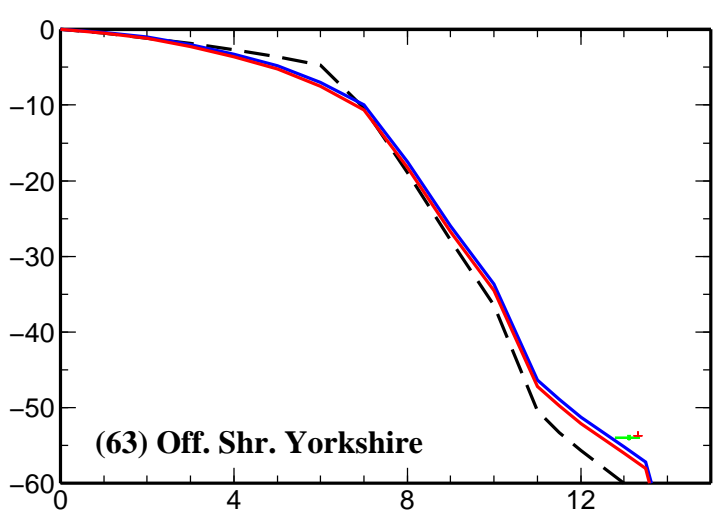
**RSL (m)**







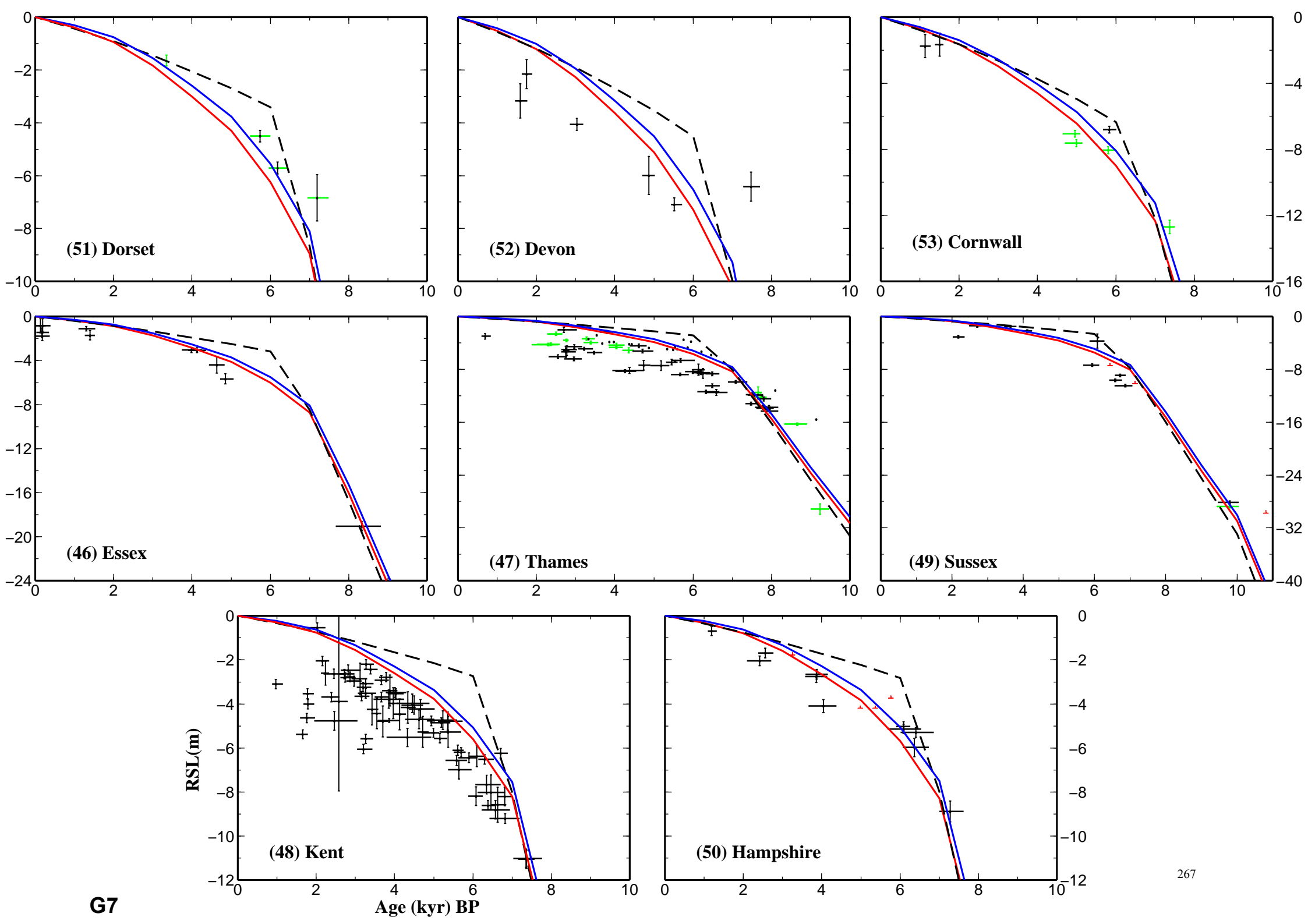


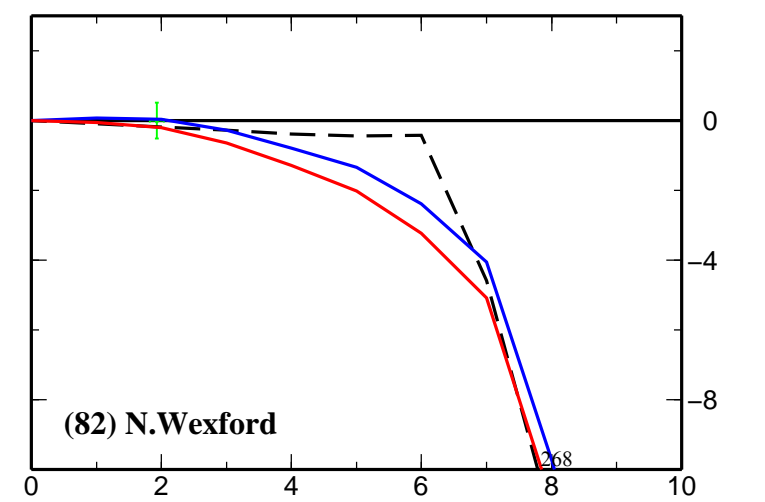
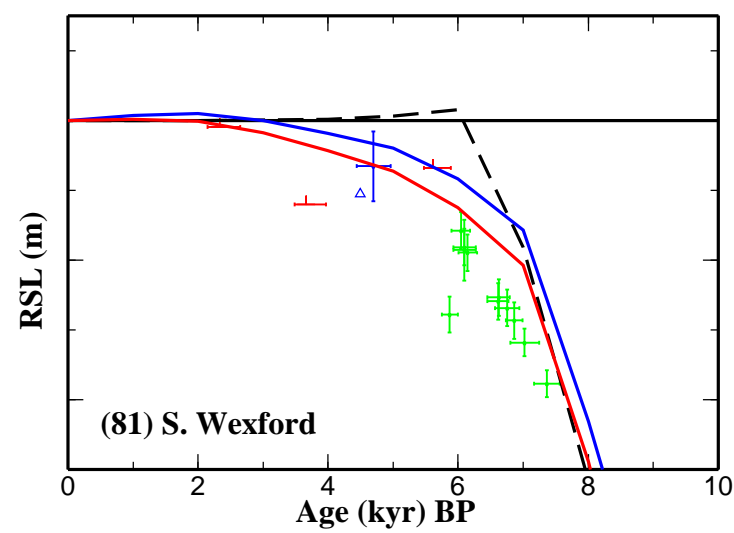
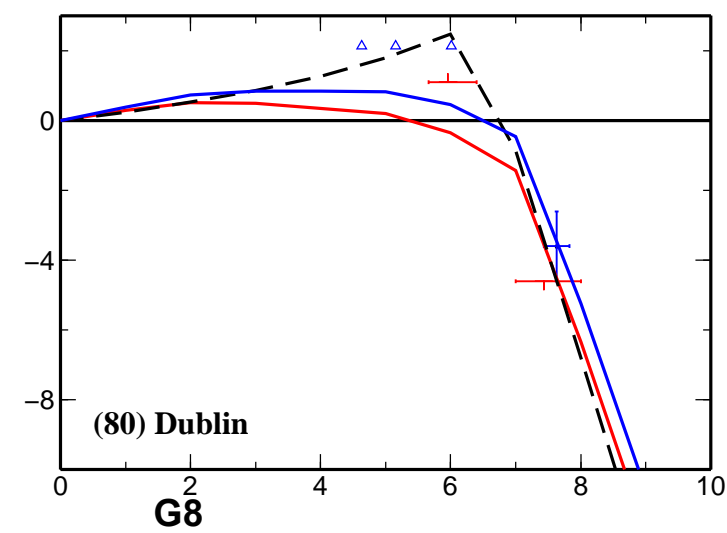
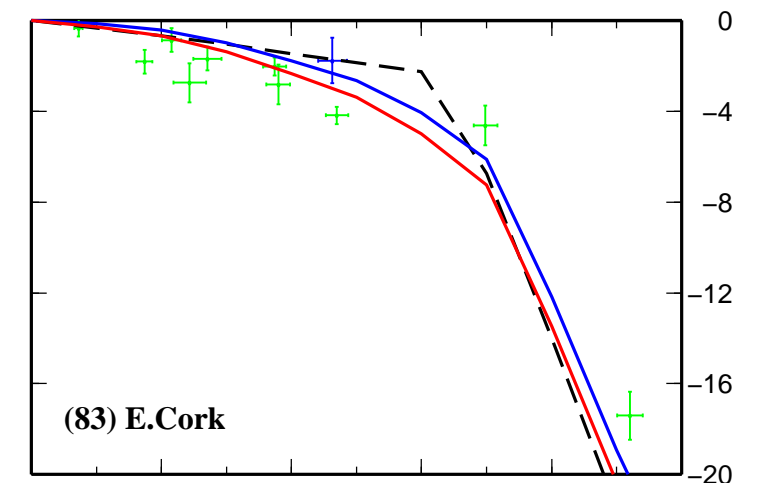
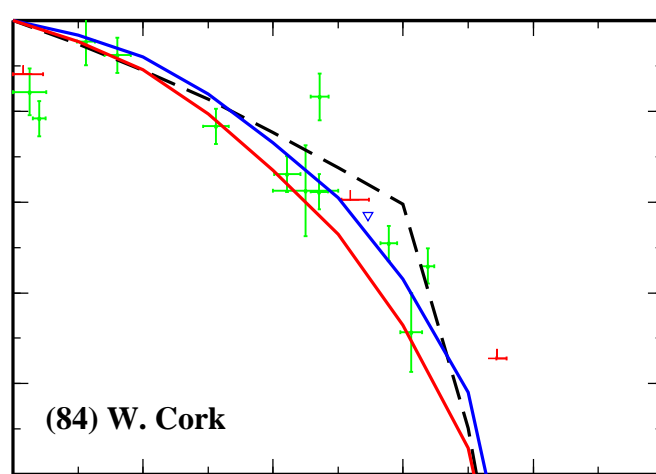
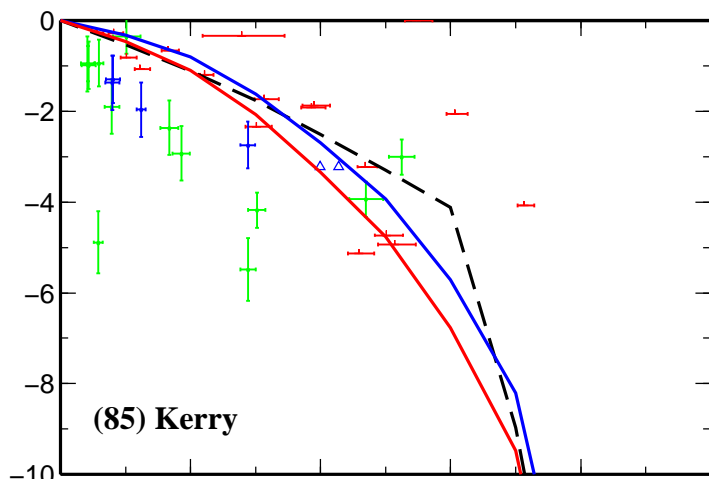
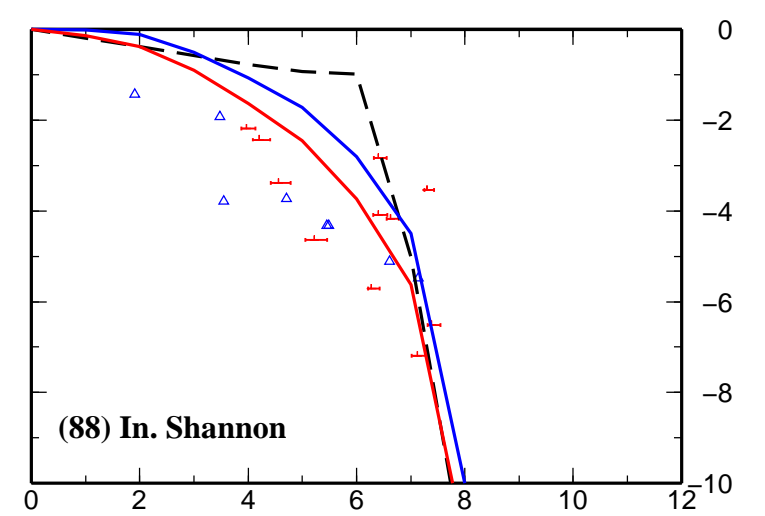
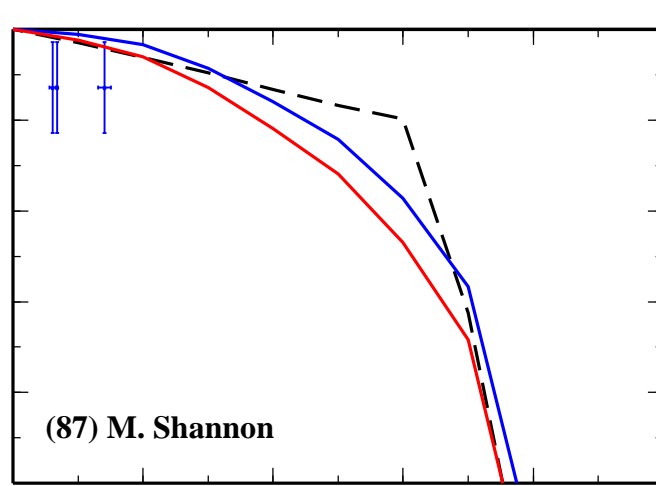
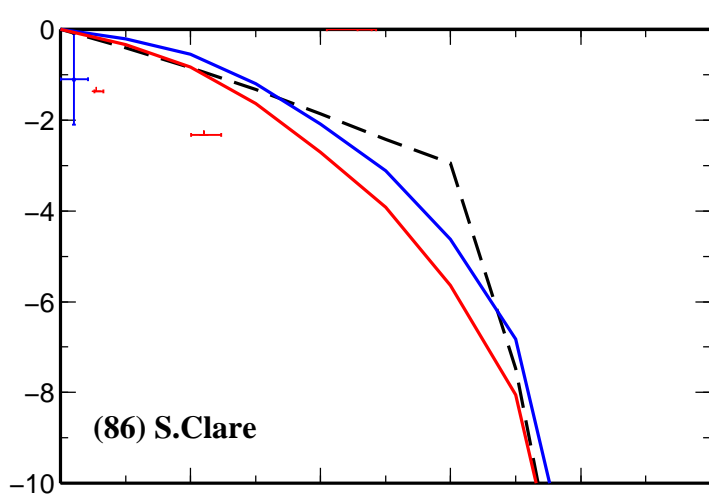


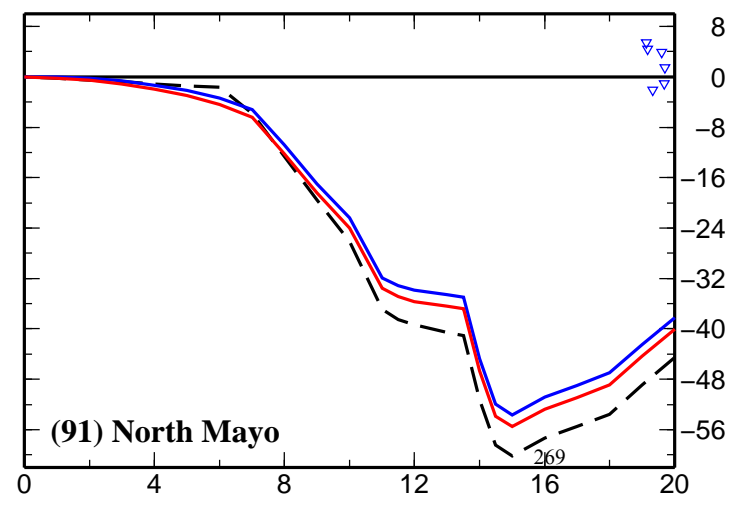
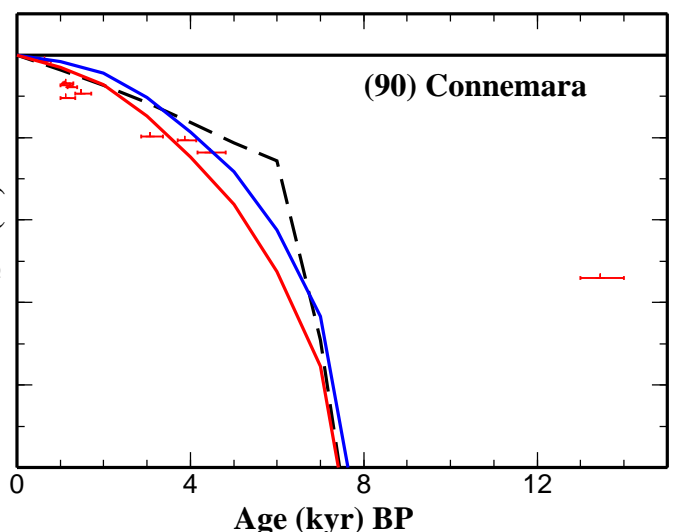
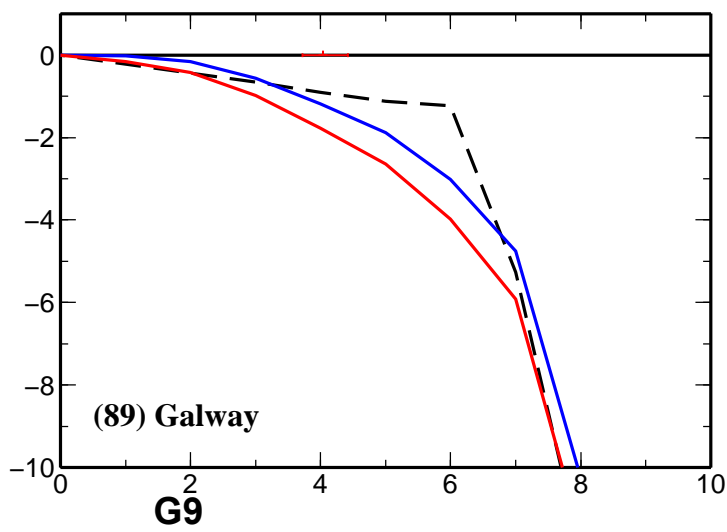
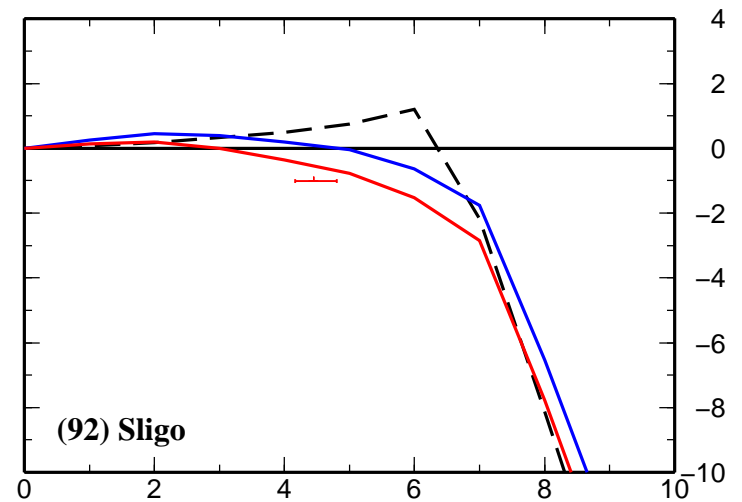
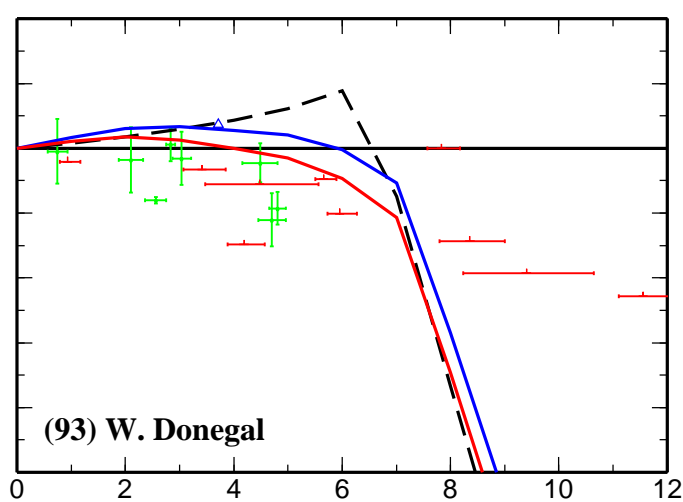
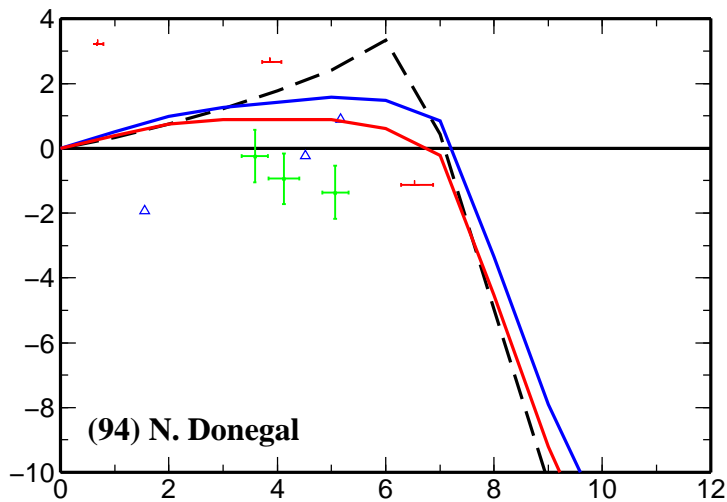
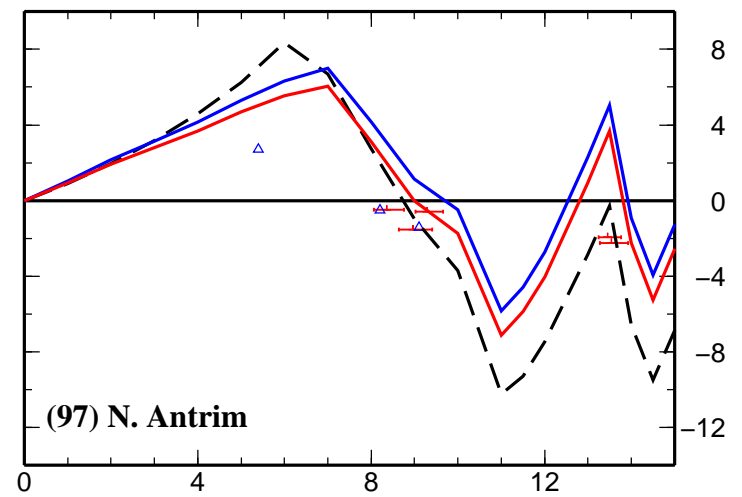
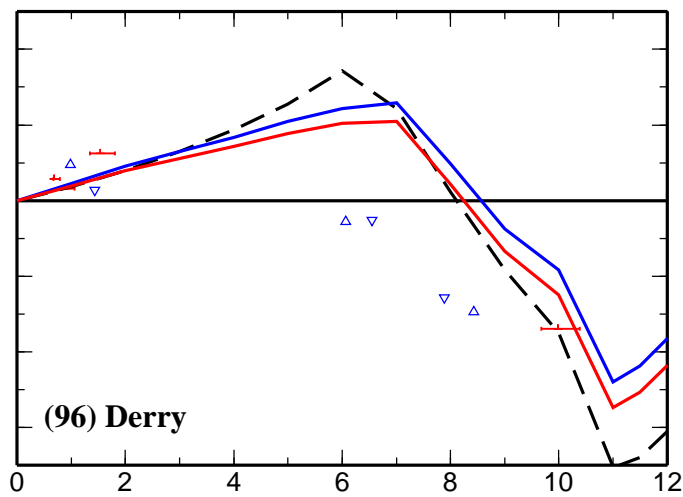
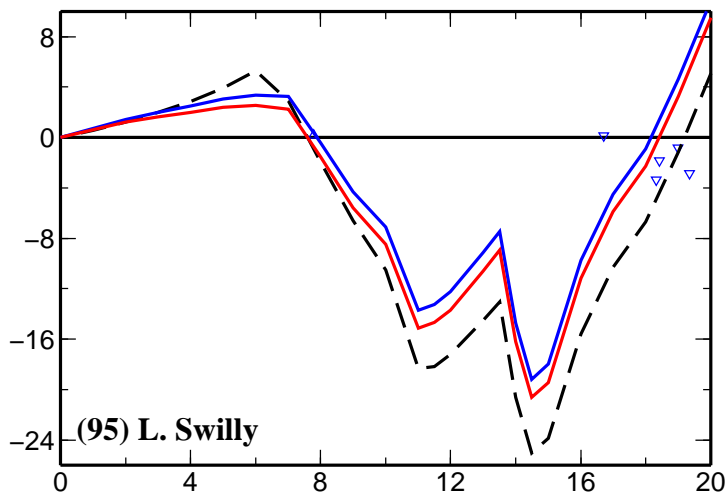
**G6**

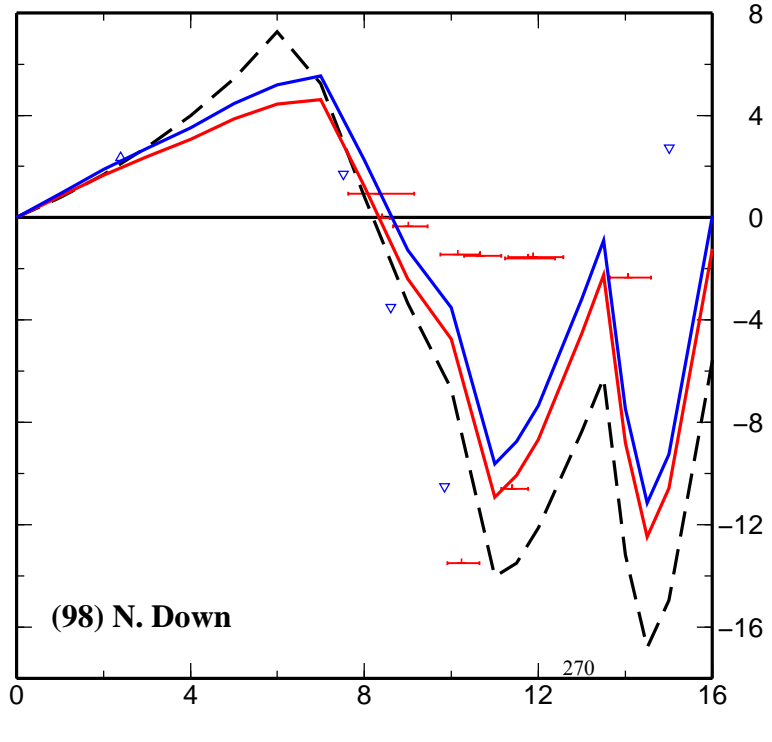
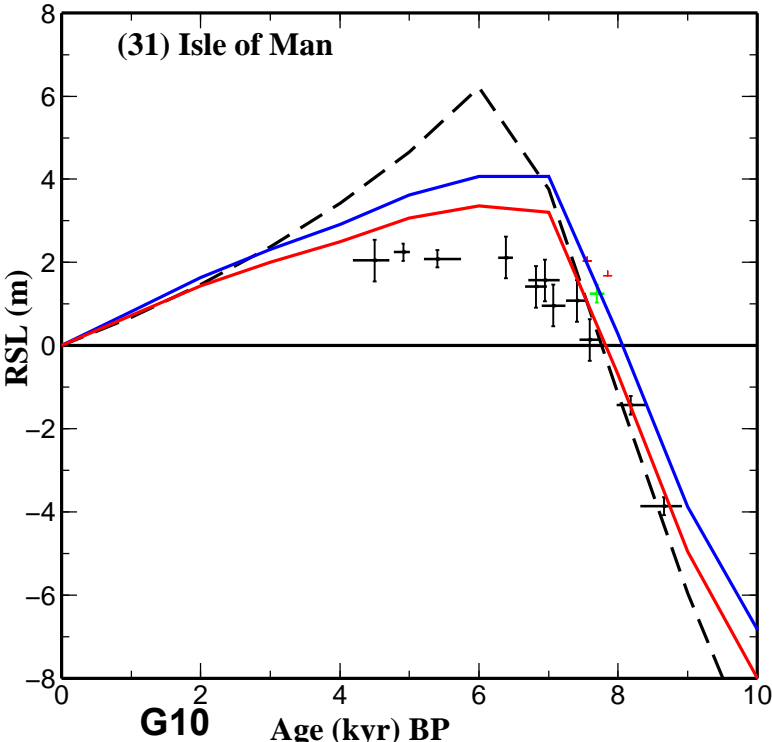
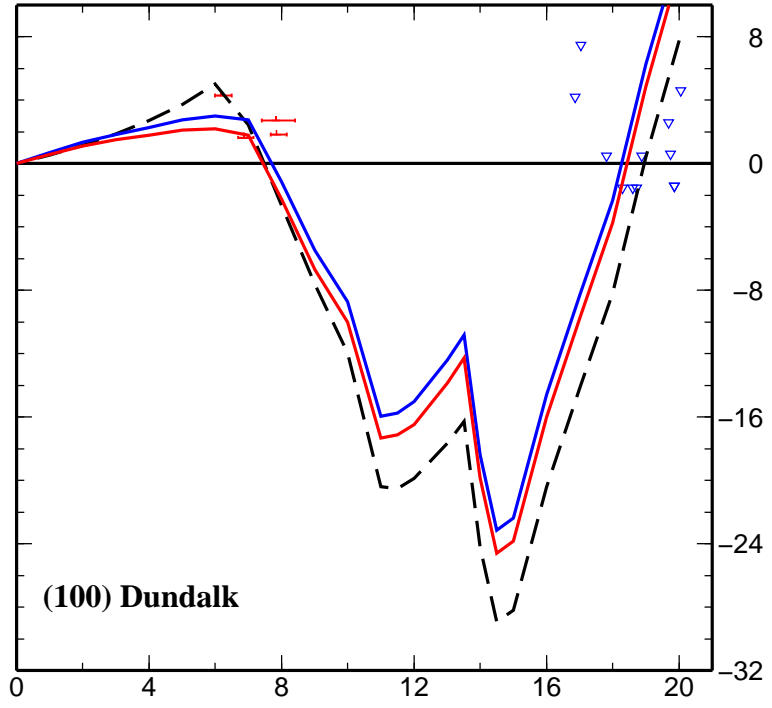
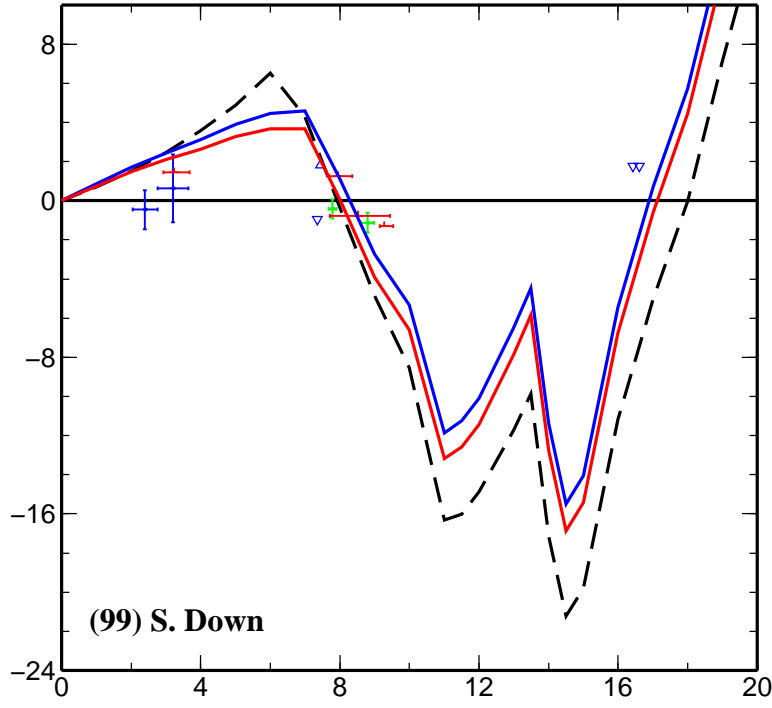
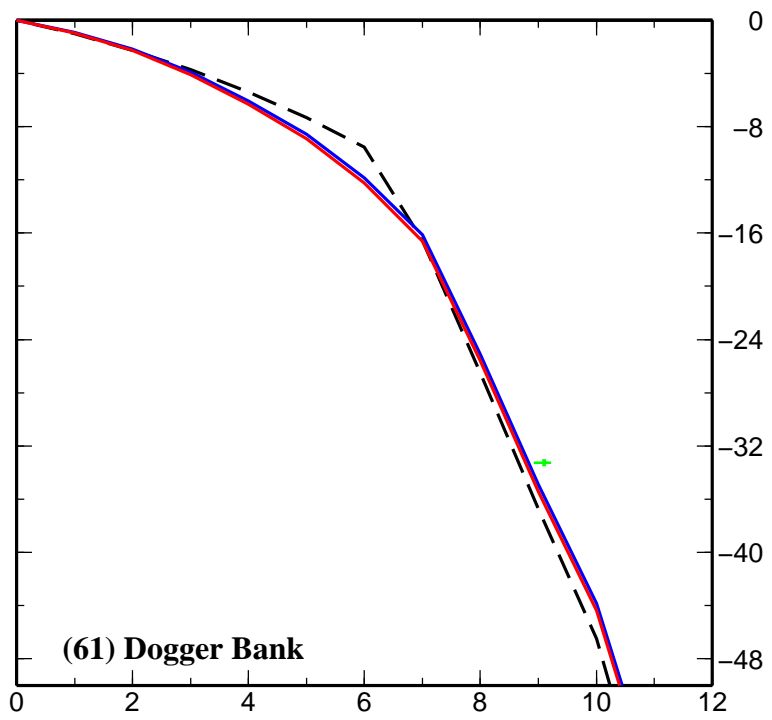
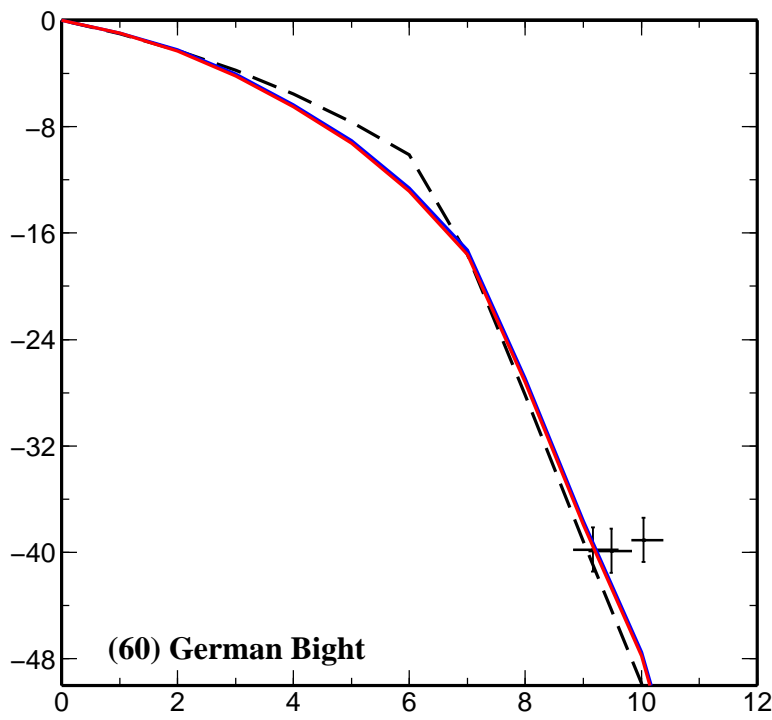
**Age (kyr) BP**

**RSL (m)**









**G10** Age (kyr BP)

## References

- Ai, Y.S. T.Y. Zheng W.W. Xu and Q. Li, (2008). Small scale hot upwelling near the North Yellow Sea of eastern China. *Geophysical Research Letters*, 35, -.
- Altamimi, Z. P. Sillard and C. Boucher, (2002). ITRF2000: A new release of the International Terrestrial Reference frame for earth science applications. *Journal of Geophysical Research-Solid Earth*, 107, -.
- Anderson, B.G., (1981). Late Weichselian ice sheets in Eurasia and Greenland. in *The Last Great Ice sheets*, eds. Denton, G. H. & Hughes, T. J. Wiley, New York.
- Anderson, J.B. S.S. Shipp A.L. Lowe J.S. Wellner and A.B. Mosola, (2002). The Antarctic Ice Sheet during the Last Glacial Maximum and its subsequent retreat history: a review. *Quaternary Science Reviews*, 21, 49-70.
- Argus, D.F. and W.R. Peltier, (2010). Constraining models of postglacial rebound using space geodesy: a detailed assessment of model ICE-5G (VM2) and its relatives. *Geophysical Journal International*, 181, 697-723.
- Ballantyne, C.K., (1997). Periglacial trimlines in the Scottish Highlands. *Quaternary International*, 38-9, 119-136.
- Ballantyne, C.K., (1999). Maximum altitude of Late Devensian glaciation on the Isle of Mull and Isle of Jura. *Scottish Journal of Geology*, 35, 97-106.
- Ballantyne, C.K., (2002). The Loch Lomond Readvance on the Isle of Mull, Scotland: glacier reconstruction and palaeoclimatic implications. *Journal of Quaternary Science*, 17, 759-771.
- Ballantyne, C.K., (2007). Glacial Landforms: Trimline and Palaeonunataks. in *Encyclopedia of Quaternary Science*, ed. Elias, S. A. Elsevier.
- Ballantyne, C.K., (2010). Extent and deglacial chronology of the last British-Irish Ice Sheet: implications of exposure dating using cosmogenic isotopes. *Journal of Quaternary Science*, 25, 515-534.
- Ballantyne, C.K. and A.M. Hall, (2008). The altitude of the last ice sheet in Caithness and east Sutherland, northern Scotland. *Scottish Journal of Geology*, 44, 169-181.
- Ballantyne, C.K. and G.E. Hallam, (2001). Maximum altitude of Late Devensian glaciation on South Uist, Outer Hebrides, Scotland. *Proceedings of the Geologists Association*, 112, 155-167.
- Ballantyne, C.K. and D. McCarroll, (1997). Maximum altitude of the Late Devensian ice sheet on the isle of Rum. *Scottish Journal of Geology*, 33, 183-186.
- Ballantyne, C.K. D. McCarroll A. Nesje S.O. Dahl and J.O. Stone, (1998). The last ice sheet in north-west Scotland: Reconstruction and implications. *Quaternary Science Reviews*, 17, 1149-1184.
- Ballantyne, C.K. D. McCarroll and J.O. Stone, (2006). Vertical dimensions and age of the Wicklow Mountains ice dome, Eastern Ireland, and implications for the extent of the last Irish Ice Sheet. *Quaternary Science Reviews*, 25, 2048-2058.
- Ballantyne, C.K. C. Schnabel and S. Xu, (2009). Readvance of the last British-Irish Ice Sheet during Greenland Interstade 1 (GI-1): the Wester Ross Readvance, NW Scotland. *Quaternary Science Reviews*, 28, 783-789.
- Ballantyne, C.K. J.O. Stone and L.K. Fifield, (2009). Glaciation and deglaciation of the SW Lake District, England: implications of cosmogenic Cl-36 exposure dating. *Proceedings of the Geologists Association*, 120, 139-144.
- Ballantyne, C.K. J.O. Stone and D. McCarroll, (2008). Dimensions and chronology of the last ice sheet in Western Ireland. *Quaternary Science Reviews*, 27, 185-200.

- Bard, E. B. Hamelin M. Arnold L. Montaggioni G. Cabioch G. Faure and F. Rougerie, (1996). Deglacial sea-level record from Tahiti corals and the timing of global meltwater discharge. *Nature*, 382, 241-244.
- Bard, E. B. Hamelin and D. Delanghe-Sabatier, (2010). Deglacial Meltwater Pulse 1B and Younger Dryas Sea Levels Revisited with Boreholes at Tahiti. *Science*, 327, 1235-1237.
- Bard, E. B. Hamelin and R.G. Fairbanks, (1990). U-Th Ages obtained by mass-spectrometry in corals from Barbados: Sea-level during the past 130,000 years. *Nature*, 346, 456-458.
- Bassett, S.E. G.A. Milne J.X. Mitrovica and P.U. Clark, (2005). Ice sheet and solid earth influences on far-field sea-level histories. *Science*, 309, 925-928.
- Benn, D.I., (1997). Glacier fluctuations in western Scotland. *Quaternary International*, 38-9, 137-147.
- Benn, D.I. and C.K. Ballantyne, (2005). Palaeoclimatic reconstruction from loch Lomond Readvance glaciers in the West Drumochter Hills, Scotland. *Journal of Quaternary Science*, 20, 577-592.
- Bentley, M.J., (1999). Volume of Antarctic Ice at the Last Glacial Maximum, and its impact on global sea level change. *Quaternary Science Reviews*, 18, 1569-1595.
- Bentley, M.J. C.J. Fogwill P.W. Kubik and D.E. Sugden, (2006). Geomorphological evidence and cosmogenic Be-10/Al-26 exposure ages for the Last Glacial Maximum and deglaciation of the Antarctic Peninsula Ice Sheet. *Geological Society of America Bulletin*, 118, 1149-1159.
- Bevis, M. E. Kendrick R. Smalley I. Dalziel D. Caccamise I. Sasgen M. Helsen F.W. Taylor H. Zhou A. Brown D. Raleigh M. Willis T. Wilson and S. Konfal, (2009). Geodetic measurements of vertical crustal velocity in West Antarctica and the implications for ice mass balance. *Geochemistry Geophysics Geosystems*, 10, -.
- Billen, M.I., (2008). Modeling the dynamics of subducting slabs. *Annual Review of Earth and Planetary Sciences*, 36, 325-356.
- Billen, M.I. and G. Hirth, (2005). Newtonian versus non-Newtonian upper mantle viscosity: Implications for subduction initiation. *Geophysical Research Letters*, 32, 4.
- Bird, M.I. L.K. Fifield T.S. Teh C.H. Chang N. Shirlaw and K. Lambeck, (2007). An inflection in the rate of early mid-Holocene eustatic sea-level rise: A new sea-level curve from Singapore. *Estuarine Coastal and Shelf Science*, 71, 523-536.
- Bos, J.A.A. J.H. Dickson G.R. Coope and W.G. Jardine, (2004). Flora, fauna and climate of Scotland during the Weichselian Middle Pleniglacial - palynological, macrofossil and coleopteran investigations. *Palaeogeography Palaeoclimatology Palaeoecology*, 204, 65-100.
- Boulton, G., (2010). Drainage pathways beneath ice sheets and their implications for ice sheet form and flow: the example of the British Ice Sheet during the Last Glacial Maximum. *Journal of Quaternary Science*, 25, 483-500.
- Boulton, G. and M. Hagdorn, (2006). Glaciology of the British Isles Ice Sheet during the last glacial cycle: form, flow, streams and lobes. *Quaternary Science Reviews*, 25, 3359-3390.
- Bowen, D.Q., (1999). A revised correlation of Quaternary deposits in the British Isles. *Geological Survey Special Report*, 23.
- Bowen, D.Q. F.M. Phillips A.M. McCabe P.C. Knutz and G.A. Sykes, (2002). New data for the Last Glacial Maximum in Great Britain and Ireland. *Quaternary Science Reviews*, 21, 89-101.
- Bowen, D.Q. J. Rose A.M. McCabe and D.G. Sutherland, (1986). Correlation of Quaternary Glaciation in Engand, Ireland, Scotland and Wales. *Quaternary Science Reviews*, 5, 299-340.

- Bradley, S.L. G.A. Milne F.N. Teferle R.M. Bingley and E.J. Orliac, (2009). Glacial isostatic adjustment of the British Isles: new constraints from GPS measurements of crustal motion. *Geophysical Journal International*, 178, 14-22.
- Bradley, S.L. G.A. Milne Y. Zong and B. Horton, (2010). Modelling sea-level data from China and Malay-Thai Peninsula to infer Holocene eustatic sea-level change. to be submitted.
- Bradley, S.L. R. Milne I. Shennan and R.J. Edwards, (2010). An improved glacial isostatic adjustment model for the British Isles. *Journal of Quaternary Science*, in press.
- Bradwell, T. M.S. Stoker N.R. Golledge C.K. Wilson J.W. Merritt D. Long J.D. Everest O.B. Hestvik A.G. Stevenson A.L. Hubbard A.G. Finlayson and H.E. Mathers, (2008). The northern sector of the last British Ice Sheet: Maximum extent and demise. *Earth-Science Reviews*, 88, 207-226.
- Brooks, A. and R.J. Edwards, (2006). The development of a sea-level database for Ireland. *Irish Journal of Earth Sciences*, 24, 13-27.
- Brooks, A.J., (2007). Late Devensian and Holocene relative sea-level change around Ireland. Unpublished PhD Thesis, Trinity College, Dublin.
- Brooks, A.J. S.L. Bradley R.J. Edwards G.A. Milne B. Horton and I. Shennan, (2008). Postglacial relative sea-level observations from Ireland and their role in glacial rebound modelling. *Journal of Quaternary Science*, 23, 175-192.
- Brooks, A.J. and R.J. Edwards, (2006). The development of a sea-level database for Ireland. *Irish Journal of Earth Sciences*, 24, 13-27.
- Brown, E.J. J. Rose R.G. Coope and J.J. Lowe, (2007). An MIS 3 age organic deposit from Balglass Burn, central Scotland: palaeoenvironmental significance and implications for the timing of the onset of the LGM ice sheet in the vicinity of the British Isles. *Journal of Quaternary Science*, 22, 295-308.
- Camoin, G.F. L.F. Montaggioni and C.J.R. Braithwaite, (2004). Late glacial to post glacial sea levels in the Western Indian Ocean. *Marine Geology*, 206, 119-146.
- Carr, S.J. H. Haflidason and H.P. Sejrup, (2000). Micromorphological evidence supporting Late Weichselian glaciation of the northern North Sea. *Boreas*, 29, 315-328.
- Carr, S.J. R. Holmes J.J.M. Van der Meer and J. Rose, (2006). The Last Glacial Maximum in the North Sea Basin: micromorphological evidence of extensive glaciation. *Journal of Quaternary Science*, 21, 131-153.
- Chiverrell, R.C. and G.S.P. Thomas, (2010). Extent and timing of the Last Glacial Maximum (LGM) in Britain and Ireland: a review. *Journal of Quaternary Science*, 25, 535-549.
- Clark, C.D., (1993). Mega-Scale Glacial Lineations and Cross-Cutting Ice-Flow Landforms. *Earth Surface Processes and Landforms*, 18, 1-29.
- Clark, C.D. D.J.A. Evans A. Khatwa T. Bradwell C.J. Jordan S.H. Marsh W.A. Mitchell and M.D. Bateman, (2004). Map and GIS database of glacial landforms and features related to the last British Ice Sheet. *Boreas*, 33, 359-375.
- Clark, C.D. and R.T. Meehan, (2001). Subglacial bedform geomorphology of the Irish Ice Sheet reveals major configuration changes during growth and decay. *Journal of Quaternary Science*, 16, 483-496.
- Clark, C.D. S.M. Tulaczyk C.R. Stokes and M. Canals, (2003). A groove-ploughing theory for the production of mega-scale glacial lineations, and implications for ice-stream mechanics. *Journal of Glaciology*, 49, 240-256.
- Clark, J.A. W.E. Farrell and W.R. Peltier, (1978). Global Changes in Post-Glacial Sea-Level - Numerical-Calculation. *Quaternary Research*, 9, 265-287.

- Clark, M.K. J.W.M. Bush and L.H. Royden, (2005). Dynamic topography produced by lower crustal flow against rheological strength heterogeneities bordering the Tibetan Plateau. *Geophysical Journal International*, 162, 575-590.
- Clark, P.U. J.X. Mitrovica G.A. Milne and M.E. Tamisiea, (2002). Sea-level fingerprinting as a direct test for the source of global meltwater pulse IA. *Science*, 295, 2438-2441.
- Clift, P. J. Lin and U. Barckhausen, (2002). Evidence of low flexural rigidity and low viscosity lower continental crust during continental break-up in the South China Sea. *Marine and Petroleum Geology*, 19, 951-970.
- Cofaigh, C.O. and D.J.A. Evans, (2007). Radiocarbon constraints on the age of the maximum advance of the British-Irish Ice Sheet in the Celtic Sea. *Quaternary Science Reviews*, 26, 1197-1203.
- Colgan, P.M., (2007). Glacial Landforms: Evidence of Glacier Recession. in *Encyclopedia of Quaternary Science*, ed. Elias, S. A. Elsevier.
- Colhoun, E.A. F.W. Shotton J.H. Dickson and A.M. McCabe, (1972). Middle Midlandian freshwater series at Derryvree, Maguiresbridge, County Fermanagh, Northern Ireland. *Proceedings of the Royal Society of London Series B*, 180, 273-292.
- Conway, H. B.L. Hall G.H. Denton A.M. Gades and E.D. Waddington, (1999). Past and future grounding-line retreat of the West Antarctic Ice Sheet. *Science*, 286, 280-283.
- Currie, C.A. and R.D. Hyndman, (2006). The thermal structure of subduction zone back arcs. *Journal of Geophysical Research-Solid Earth*, 111, 22.
- Dach, R. U. Hugentobler P. Fridez and M. Meindl, (2007). Bernese GPS software version 5.0 User Manual. 613.
- Davis, J.L. J.X. Mitrovica H.G. Scherneck and R. Fan, (1999). Investigations of Fennoscandian glacial isostatic adjustment using modern sea level records. *Journal of Geophysical Research-Solid Earth*, 104, 2733-2747.
- Dawson, A.G., (1984). Quaternary sea-Level changes in Western Scotand. *Quaternary Science Reviews*, 3, 345-368.
- Dawson, A.G. S. Hampton P. Fretwell S. Harrison and P. Greengrass, (2002). Defining the centre of glacio-isostatic uplift of the last Scottish ice-sheet: the Parallel Roads of Glen Roy, Scottish Highlands. *Journal of Quaternary Science*, 17, 527-533.
- Dickinson, W.R., (2001). Paleoshoreline record of relative Holocene sea levels on Pacific islands. *Earth-Science Reviews*, 55, 191-234.
- Dziewonski, A.M. and D.L. Anderson, (1981). Preliminary Reference Earth Model. *Physics of the Earth and Planetary Interiors*, 25, 297-356.
- Edwards, R., 2006. Sea Level Studies: Low energy coasts sedimentary indicators. in *Encyclopedia of Quaternary Science*, ed Elias, S. A. Elsevier.
- Evans, D.J.A. and D.I. Benn, (2007). Glacial Landforms: Introduction. in *Encyclopedia of Quaternary Science*, ed. Elias, S. A. Elsevier.
- Evans, D.J.A. C.D. Clark and W.A. Mitchell, (2005). The last British Ice Sheet: A review of the evidence utilised in the compilation of the Glacial Map of Britain. *Earth-Science Reviews*, 70, 253-312.
- Evans, D.J.A. S.J. Livingstone A. Vieli and C.O. Cofaigh, (2009). The palaeoglaciology of the central sector of the British and Irish Ice Sheet: reconciling glacial geomorphology and preliminary ice sheet modelling. *Quaternary Science Reviews*, 28, 739-757.

- Evans, J. C.J. Pudsey C. O'Coifagh P. Morris and E. Domack, (2005). Late Quaternary glacial history, flow dynamics and sedimentation along the eastern margin of the Antarctic Peninsula Ice Sheet. *Quaternary Science Reviews*, 24, 741-774.
- Fairbanks, R.G., (1989). A 17,000 year glacio-eustatic sea-level record: influence of glacial melting rates on the younger dryas event and deep-ocean circulation *Nature*, 342, 637-642.
- Farrell, W.E. and J.A. Clark, (1976). Postglacial Sea Level. *Geophysical Journal of the Royal Astronomical Society*, 46, 647-667.
- Finlayson, A. J. Merritt M. Browne J. Merritt A. McMillan and K. Whitbread, (2010). Ice sheet advance, dynamics, and decay configurations: evidence from west central Scotland. *Quaternary Science Reviews*, 29, 969-988.
- Fleming, K. P. Johnston D. Zwartz Y. Yokoyama K. Lambeck and J. Chappell, (1998). Refining the eustatic sea-level curve since the Last Glacial Maximum using far- and intermediate-field sites. *Earth and Planetary Science Letters*, 163, 327-342.
- Fleming, K. and K. Lambeck, (2004). Constraints on the Greenland Ice Sheet since the Last Glacial Maximum from sea-level observations and glacial-rebound models. *Quaternary Science Reviews*, 23, 1053-1077.
- Forte, A.M. and J.X. Mitrovica, (1996). New inferences of mantle viscosity from joint inversion of long-wavelength mantle convection and post-glacial rebound data. *Geophysical Research Letters*, 23, 1147-1150.
- Fretwell, P. I.R. Peterson and D.E. Smith, (2004). The use of Gaussian trend surfaces for modelling glacio-isostatic crustal rebound. *Scottish Journal of Geology*, 40, 175-179.
- Gehrels, R., (2010). Sea-level changes since the Last Glacial Maximum: an appraisal of the IPCC Fourth Assessment Report. *Journal of Quaternary Science*, 25, 26-38.
- Gehrels, W.R. D.F. Belknap B.R. Pearce and B. Gong, (1995). Modeling the Contribution of M(2) Tidal Amplification to the Holocene Rise of Mean High Water in the Gulf of Maine and the Bay of Fundy. *Marine Geology*, 124, 71-85.
- Glasser, N.F. and G.H.S. Smith, (1999). Glacial meltwater erosion of the Mid-Cheshire Ridge: implications for ice dynamics during the Late Devensian glaciation of northwest England. *Journal of Quaternary Science*, 14, 703-710.
- Golledge, N.R. A. Finlayson T. Bradwell and J.D. Everest, (2008). The last glaciation of Shetland, North Atlantic. *Geografiska Annaler Series a-Physical Geography*, 90A, 37-53.
- Golledge, N.R. and A. Hubbard, (2005). Evaluating Younger Dryas glacier reconstructions in part of the western Scottish Highlands: a combined empirical and theoretical approach. *Boreas*, 34, 274-286.
- Golledge, N.R. and M.S. Stoker, (2006). A palaeo-ice stream of the British ice sheet in eastern Scotland. *Boreas*, 35, 231-243.
- Graham, A.G.C. L. Lonergan and M.S. Stoker, (2007). Evidence for Late Pleistocene ice stream activity in the Witch Ground Basin, central North Sea, from 3D seismic reflection data. *Quaternary Science Reviews*, 26, 627-643.
- Graham, A.G.C. L. Lonergan and M.S. Stoker, (2009). Seafloor glacial features reveal the extent and decay of the last British Ice Sheet, east of Scotland. *Journal of Quaternary Science*, 24, 117-138.
- Graham, A.G.C. L. Lonergan and M.S. Stoker, (2010). Depositional environments and chronology of Late Weichselian glaciation and deglaciation in the central North Sea. *Boreas*, 39, 471-491.
- Greenwood, S.L. and C.D. Clark, (2009). Reconstructing the last Irish Ice Sheet 2: a geomorphologically-driven model of ice sheet growth, retreat and dynamics. *Quaternary Science Reviews*, 28, 3101-3123.

- Greenwood, S.L. and C.D. Clark, (2009). Reconstructing the last Irish Ice Sheet 1: changing flow geometries and ice flow dynamics deciphered from the glacial landform record. *Quaternary Science Reviews*, 28, 3085-3100.
- Gross, R.S. and J. Vondrak, (1999). Astrometric and space-geodetic observations of polar wander. *Geophysical Research Letters*, 26, 2085-2088.
- Hall, A.M. J.D. Peacock and E.R. Connell, (2003). New data for the Last Glacial Maximum in Great Britain and Ireland: a Scottish perspective on the paper by Bowen et al. (2002). *Quaternary Science Reviews*, 22, 1551-1554.
- Hall, A.M. and G. Whittington, (1989). Late Devensian Glaciation of Southern Caithness. *Scottish Journal of Geology*, 25, 307-324.
- Hall, B.L. C. Baroni and G.H. Denton, (2004). Holocene relative sea-level history of the Southern Victoria Land Coast, Antarctica. *Global and Planetary Change*, 42, 241-263.
- Hanebuth, T. K. Stattegger and P.M. Grootes, (2000). Rapid flooding of the Sunda Shelf: A late-glacial sea-level record. *Science*, 288, 1033-1035.
- Hegarty, S., (2004). Limits of Midlandian glaciation in south-eastern Ireland *Irish Geography*, 37, 60-76.
- Hibbert, F.D. W.E.N. Austin M.J. Lenc and R.W. Gatliff, (2010). British Ice Sheet dynamics inferred from North Atlantic ice-rafted debris records spanning the last 175 000 years. *Journal of Quaternary Science*, 25, 461-482.
- Hiemstra, J.F. D.J.A. Evans J.D. Scourse D. McCarroll M.F.A. Furze and E. Rhodes, (2006). New evidence for a grounded Irish Sea glaciation of the Isles of Scilly, UK. *Quaternary Science Reviews*, 25, 299-309.
- Hinton, A.C., (1995). Holocene Tides of the Wash, UK - the Influence of Water-Depth and Coastline-Shape Changes on the Record of Sea-Level Change. *Marine Geology*, 124, 87-111.
- Hirth, G. and D. Kohlstedt, (2003). Rheology of the upper mantle and the mantle wedge view from experimentalist. in *Inside the Subduction factory*, pp. 83-105, ed. Eiler, J. American Geophysical union.
- Horton, B.P. R.J. Edwards and J.M. Lloyd, (2000). Implications of a microfossil-based transfer function in Holocene sea-level studies. *Geological Society Special Publication*, 166, 41-54.
- Horton, B.P. P.L. Gibbard G.M. Milne R.J. Morley C. Purintavaragul and J.M. Stargardt, (2005). Holocene sea levels and palaeoenvironments, Malay-Thai Peninsula, southeast Asia. *Holocene*, 15, 1199-1213.
- Hubbard, A., (1999). High-resolution modeling of the advance of the younger dryas ice sheet and its climate in Scotland. *Quaternary Research*, 52, 27-43.
- Hubbard, A. T. Bradwell N. Golledge A. Hall H. Patton D. Sugden R. Cooper and M. Stoker, (2009). Dynamic cycles, ice streams and their impact on the extent, chronology and deglaciation of the British-Irish ice sheet. *Quaternary Science Reviews*, 28, 758-776.
- Huybrechts, P., (2002). Sea-level changes at the LGM from ice-dynamic reconstructions of the Greenland and Antarctic ice sheets during the glacial cycles. *Quaternary Science Reviews*, 21, 203-231.
- Ingolfsson, O. C. Hjort P.A. Berkman S. Björck E. Colhoun I.D. Goodwin B. Hall K. Hirakawa M. Melles P. Møller and M.L. Prentice, (1998). Antarctic glacial history since the Last Glacial Maximum: an overview of the record on land. *Antarctic Science*, 10, 326-344.
- Ivins, E.R. and T.S. James, (2005). Antarctic glacial isostatic adjustment: a new assessment. *Antarctic Science*, 17, 541-553.

- Jacobi, R.M. J. Rose A. MacLeod and T.F.G. Higham, (2009). Revised radiocarbon ages on woolly rhinoceros (*Coelodonta antiquitatis*) from western central Scotland: significance for timing the extinction of woolly rhinoceros in Britain and the onset of the LGM in central Scotland. *Quaternary Science Reviews*, 28, 2551-2556.
- James, T.S. J.J. Clague K.L. Wang and I. Hutchinson, (2000). Postglacial rebound at the northern Cascadia subduction zone. *Quaternary Science Reviews*, 19, 1527-1541.
- James, T.S. E.J. Gowan I. Wada and K.L. Wang, (2009). Viscosity of the asthenosphere from glacial isostatic adjustment and subduction dynamics at the northern Cascadia subduction zone, British Columbia, Canada. *Journal of Geophysical Research-Solid Earth*, 114, 13.
- Johansson, J.M. J.L. Davis H.G. Scherneck G.A. Milne M. Vermeer J.X. Mitrovica R.A. Bennett B. Jonsson G. Elgered P. Elosegui H. Koivula M. Poutanen B.O. Ronnang and I.I. Shapiro, (2002). Continuous GPS measurements of postglacial adjustment in Fennoscandia - 1. Geodetic results. *Journal of Geophysical Research-Solid Earth*, 107, -.
- Johnson, J.S. M.J. Bentley and K. Gohl, (2008). First exposure ages from the Amundsen Sea embayment, West Antarctica: The late quaternary context for recent thinning of Pine Island, Smith, and Pope Glaciers. *Geology*, 36, 223-226.
- Johnston, P. and K. Lambeck, (1999). Postglacial rebound and sea level contributions to changes in the geoid and the Earth's rotation axis. *Geophysical Journal International*, 136, 537-558.
- Johnston, P.J. and K. Lambeck, (2000). Automatic inference of ice models from postglacial sea level observations: Theory and application to the British Isles. *Journal of Geophysical Research-Solid Earth*, 105, 13179-13194.
- Kaufmann, G. and K. Lambeck, (2002). Glacial isostatic adjustment and the radial viscosity profile from inverse modeling. *Journal of Geophysical Research-Solid Earth*, 107, 15.
- Kaufmann, G. P. Wu and G.Y. Li, (2000). Glacial isostatic adjustment in Fennoscandia for a laterally heterogeneous earth. *Geophysical Journal International*, 143, 262-273.
- Kendall, R.A. and J.X. Mitrovica, (2007). Radial resolving power of far-field differential sea-level highstands in the inference of mantle viscosity. *Geophysical Journal International*, 171, 881-889.
- Kendall, R.A. J.X. Mitrovica and G.A. Milne, (2005). On post-glacial sea level - II. Numerical formulation and comparative results on spherically symmetric models. *Geophysical Journal International*, 161, 679-706.
- Knutz, P.C. W.E.N. Austin and E.J.W. Jones, (2001). Millennial-scale depositional cycles related to British Ice Sheet variability and North Atlantic paleocirculation since 45 kyr BP, Barra Fan, UK margin. *Paleoceanography*, 16, 53-64.
- Kopp, H. D. Klaeschen E.R. Flueh J. Bialas and C. Reichert, (2002). Crustal structure of the Java margin from seismic wide-angle and multichannel reflection data. *Journal of Geophysical Research-Solid Earth*, 107, -.
- Lamb, A.L. and C.K. Ballantyne, (1998). Palaeonunataks and the altitude of the last ice sheet in the SW Lake District, England. *Proceedings of the Geologists Association*, 109, 305-316.
- Lambeck, K., (1993). Glacial Rebound of the British-Isles .1. Preliminary Model Results. *Geophysical Journal International*, 115, 941-959.
- Lambeck, K., (1993). Glacial Rebound of the British-Isles .2. A High-Resolution, High-Precision Model. *Geophysical Journal International*, 115, 960-990.
- Lambeck, K., (1995). Late Devensian and holocene shorelines of the British Isles and North-Sea from models of glacio-hydro-isostatic rebound. *Journal of the Geological Society*, 152, 437-448.
- Lambeck, K., (1996). Glaciation and sea-level change for Ireland and the Irish Sea since Late Devensian/Midlandian time. *Journal of the Geological Society*, 153, 853-872.

- Lambeck, K., (1997). Sea-level change along the French Atlantic and channel coasts since the time of the last glacial maximum. *Palaeogeography Palaeoclimatology Palaeoecology*, 129, 1-22.
- Lambeck, K., (2002). Sea-Level change from mid-Holocene to recent time: An Australian example with global implications. in *Ice sheets, sea level and the dynamic earth* eds. Mitrovica, J. X. & Vermeersen, B. American Geophysical Union, Washington, D.C.
- Lambeck, K. P. Johnston C. Smither and M. Nakada, (1996). Glacial rebound of the British Isles .2. Constraints on mantle viscosity. *Geophysical Journal International*, 125, 340-354.
- Lambeck, K. P. Johnston C. Smither and M. Nakada, (1996). Glacial rebound of the British Isles .3. Constraints on mantle viscosity. *Geophysical Journal International*, 125, 340-354.
- Lambeck, K. and M. Nakada, (1990). Late Pleistocene and Holocene Sea-Level Change Along the Australian Coast. *Global and Planetary Change*, 89, 143-176.
- Lambeck, K. and A. Purcell, (2005). Sea-level change in the Mediterranean Sea since the LGM: model predictions for tectonically stable areas. *Quaternary Science Reviews*, 24, 1969-1988.
- Lambeck, K. A. Purcell J. Zhao and N.O. Svensson, (2010). The Scandinavian Ice Sheet: from MIS 4 to the end of the Last Glacial Maximum. *Boreas*, 39, 410-435.
- Lambeck, K. and A.P. Purcell, (2001). Sea-level change in the Irish Sea since the last glacial maximum: constraints from isostatic modelling. *Journal of Quaternary Science*, 16, 497-506.
- Lambeck, K. C. Smither and P. Johnston, (1998). Sea-level change, glacial rebound and mantle viscosity for northern Europe. *Geophysical Journal International*, 134, 102-144.
- Lebedev, S. and G. Nolet, (2003). Upper mantle beneath southeast Asia from S velocity tomography. *Journal of Geophysical Research-Solid Earth*, 108, 26.
- Lei, J.S. D.P. Zhao B. Steinberger B. Wu F.L. Shen and Z.X. Li, (2009). New seismic constraints on the upper mantle structure of the Hainan plume. *Physics of the Earth and Planetary Interiors*, 173, 33-50.
- Lidberg, M. J.M. Johansson H.G. Scherneck and J.L. Davis, (2007). An improved and extended GPS-derived 3D velocity field of the glacial isostatic adjustment (GIA) in Fennoscandia. *Journal of Geodesy*, 81, 213-230.
- Lidberg, M. J.M. Johansson H.G. Scherneck and G.A. Milne, (2010). Recent results based on continuous GPS observations of the GIA process in Fennoscandia from BIFROST. *Journal of Geodynamics*, 50, 8-18.
- Lloyd, J.M. and J.R. Evans, (2002). Contemporary and fossil foraminifera from isolation basins in northwest Scotland. *Journal of Quaternary Science*, 17, 431-443.
- Lowe, A.L. and J.B. Anderson, (2002). Reconstruction of the West Antarctic Ice Sheet in Pine Island Bay during the last glacial maximum and its subsequent retreat history. *Quaternary Science Reviews*, 21, 1879-1897.
- Lowe, J. T. Howard A. Pardaens J. Tinker S. Holt S. Wakelin G.A. Milne J. Leake J. Wolf K. Horsburgh T. Reeder G. Jenkins J. Ridley S. Dye and S.L. Bradley, 2009. UK Climate Projections science report: Marine and coastal projections Met Office Hadley Centre Exeter, UK.
- Lowe, J.J. H.H. Birks S.J. Brooks G.R. Coope D.D. Harkness F.E. Mayle C. Sheldrick C.S.M. Turney and M.J.C. Walker, (1999). The chronology of palaeoenvironmental changes during the last Glacial-Holocene transition: towards an event stratigraphy for the British Isles. *Journal of the Geological Society*, 156, 397-410.
- Lowe, J.J. and M.J.C. Walker, (1997). *Reconstructing Quaternary Environments*, 2nd edn, Vol., Addison-Welsey-Longman, London.

- Mackintosh, A. D. White D. Fink D.B. Gore J. Pickard and P.C. Fanning, (2007). Exposure ages from mountain dipsticks in Mac. Robertson Land, East Antarctica, indicate little change in ice-sheet thickness since the Last Glacial Maximum. *Geology*, 35, 551-554.
- McCabe, A.M., (1997). Geological constraints on geophysical models of relative sea-level change during deglaciation of the western Irish sea basin. *Journal of the Geological Society*, 154, 601-604.
- McCabe, A.M. and P.U. Clark, (2003). Deglacial chronology from County Donegal, Ireland: implications for deglaciation of the British-Irish ice sheet. *Journal of the Geological Society*, 160, 847-855.
- McCabe, A.M. P.U. Clark and J. Clark, (2005). AMS C-14 dating of deglacial events in the Irish Sea Basin and other sectors of the British-Irish ice sheet. *Quaternary Science Reviews*, 24, 1673-1690.
- McCarroll, D. and C.K. Ballantyne, (2000). The last ice sheet in Snowdonia. *Journal of Quaternary Science*, 15, 765-778.
- McCarthy, D.D. and B.J. Luzum, (1996). Path of the mean rotational pole from 1899 to 1994. *Geophysical Journal International*, 125, 623-629.
- Merritt, J.W. C.A. Auton E.R. Connell H.A. M. and P.J. D., (2003). *Cainozoic Geology and Landscape Evolution of North-East Scotland.*, edn, Vol., British Geological Survey, Edinburgh.
- Mickelson, D.M. and C. Winguth, (2007). Glacial Landforms: Evidence of Glacier and Ice Sheet Extent. in *Encyclopedia of Quaternary Science*, ed. Elias, S. A. Elsevier.
- Milne, G.A. J.L. Davis J.X. Mitrovica H.G. Scherneck J.M. Johansson M. Vermeer and H. Koivula, (2001). Space-geodetic constraints on glacial isostatic adjustment in Fennoscandia. *Science*, 291, 2381-2385.
- Milne, G.A. A.J. Long and S.E. Bassett, (2005). Modelling Holocene relative sea-level observations from the Caribbean and South America. *Quaternary Science Reviews*, 24, 1183-1202.
- Milne, G.A. and J.X. Mitrovica, (1998). Postglacial sea-level change on a rotating Earth. *Geophysical Journal International*, 133, 1-19.
- Milne, G.A. and J.X. Mitrovica, (1998). The influence of time-dependent ocean-continent geometry on predictions of post-glacial sea level change in Australia and New Zealand. *Geophysical Research Letters*, 25, 793-796.
- Milne, G.A. and J.X. Mitrovica, (2008). Searching for eustasy in deglacial sea-level histories. *Quaternary Science Reviews*, 27, 2292-2302.
- Milne, G.A. J.X. Mitrovica and J.L. Davis, (1999). Near-field hydro-isostasy: the implementation of a revised sea-level equation. *Geophysical Journal International*, 139, 464-482.
- Milne, G.A. J.X. Mitrovica H.G. Scherneck J.L. Davis J.M. Johansson H. Koivula and M. Vermeer, (2004). Continuous GPS measurements of postglacial adjustment in Fennoscandia: 2. Modeling results. *Journal of Geophysical Research-Solid Earth*, 109, -.
- Milne, G.A. I. Shennan B.A.R. Youngs A.I. Waugh F.N. Teferle R.M. Bingley S.E. Bassett C. Cuthbert-Brown and S.L. Bradley, (2006). Modelling the glacial isostatic adjustment of the UK region. *Philosophical Transactions of the Royal Society a-Mathematical Physical and Engineering Sciences*, 364, 931-948.
- Mitrovica, J.X., (1996). Haskell [1935] revisited. *Journal of Geophysical Research-Solid Earth*, 101, 555-569.
- Mitrovica, J.X. J.L. Davis and I.I. Shapiro, (1994). A Spectral Formalism for Computing 3-Dimensional Deformations Due to Surface Loads .1. Theory. *Journal of Geophysical Research-Solid Earth*, 99, 7057-7073.

- Mitrovica, J.X. J.L. Davis and I.I. Shapiro, (1994). A Spectral Formalism for Computing 3-Dimensional Deformations Due to Surface Loads .2. Present-Day Glacial Isostatic-Adjustment. *Journal of Geophysical Research-Solid Earth*, 99, 7075-7101.
- Mitrovica, J.X. and G.A. Milne, (1998). Glaciation-induced perturbations in the Earth's rotation: A new appraisal. *Journal of Geophysical Research-Solid Earth*, 103, 985-1005.
- Mitrovica, J.X. and G.A. Milne, (2002). On the origin of late Holocene sea-level highstands within equatorial ocean basins. *Quaternary Science Reviews*, 21, 2179-2190.
- Mitrovica, J.X. and G.A. Milne, (2003). On post-glacial sea level: I. General theory. *Geophysical Journal International*, 154, 253-267.
- Mitrovica, J.X. G.A. Milne and J.L. Davis, (2001). Glacial isostatic adjustment on a rotating earth. *Geophysical Journal International*, 147, 562-578.
- Mitrovica, J.X. J. Wahr I. Matsuyama A. Paulson and M.E. Tamisiea, (2006). Reanalysis of ancient eclipse, astronomic and geodetic data: A possible route to resolving the enigma of global sea-level rise. *Earth and Planetary Science Letters*, 243, 390-399.
- Munk, W.H. and G.J.F. MacDonald, (1960). *The Rotation of the Earth* edn, Vol., Cambridge University Press, Cambridge.
- Nakada, M. and K. Lambeck, (1989). Late Pleistocene and Holocene Sea-Level Change in the Australian Region and Mantle Rheology. *Geophysical Journal-Oxford*, 96, 497-517.
- Nakada, M. and J. Okuno, (2003). Perturbations of the Earth's rotation and their implications for the present-day mass balance of both polar ice caps. *Geophysical Journal International*, 152, 124-138.
- Nerem, R.S. and S.M. Klosko, (1996). Secular variations of the zonal harmonics and polar motion as geophysical constraints. in *Global Gravity Field and its Variations*, pp. 152-163, eds. Rapp, R., Cazenave, A. and Nerem, R. S. IAG Symp, Int. Assoc. of Geod.
- Nunn, P.D. and W.R. Peltier, (2001). Far-field test of the ICE-4G model of global isostatic response to deglaciation using empirical and theoretical Holocene sea-level reconstructions for the Fiji Islands, southwestern Pacific. *Quaternary Research*, 55, 203-214.
- O' Cofaigh, C. P. Dunlop and S. Benetti, (2010b). Marine geophysical evidence for Late Pleistocene ice sheet extent and recession off northwest Ireland. *Quaternary Science Reviews*, In press.
- O' Cofaigh, C. and D.J.A. Evans, (2001). Sedimentary evidence for deforming bed conditions associated with a grounded Irish Sea glacier, southern Ireland. *Journal of Quaternary Science*, 16, 435-454.
- O' Cofaigh, C. M. Telfer R. Bailey and D.J.A. Evans, (2010a). Late Pleistocene chronostratigraphy and ice sheet limits, southern Ireland. *Quaternary Science Reviews*, In press.
- O'Cofaigh, C. and D.J.A. Evans, (2007). Radiocarbon constraints on the age of the maximum advance of the British-Irish Ice Sheet in the Celtic Sea. *Quaternary Science Reviews*, 26, 1197-1203.
- Pedoja, K. J.W. Shen S. Kershaw and C. Tang, (2008). Coastal Quaternary morphologies on the northern coast of the South China Sea, China, and their implications for current tectonic models: A review and preliminary study. *Marine Geology*, 255, 103-117.
- Peltier, W.R., (1974). Impulse response of a Maxwell Earth. *Reviews of Geophysics*, 12, 649-669.
- Peltier, W.R., (1996). Mantle viscosity and ice-age ice sheet topography. *Science*, 273, 1359-1364.

- Peltier, W.R., (2002). On eustatic sea level history: Last Glacial Maximum to Holocene. *Quaternary Science Reviews*, 21, 377-396.
- Peltier, W.R., (2004). Global glacial isostasy and the surface of the ice-age earth: The ice-5G (VM2) model and grace. *Annual Review of Earth and Planetary Sciences*, 32, 111-149.
- Peltier, W.R. and R.G. Fairbanks, (2006). Global glacial ice volume and Last Glacial Maximum duration from an extended Barbados sea level record. *Quaternary Science Reviews*, 25, 3322-3337.
- Peltier, W.R. I. Shennan R. Drummond and B. Horton, (2002). On the postglacial isostatic adjustment of the British Isles and the shallow viscoelastic structure of the Earth. *Geophysical Journal International*, 148, 443-475.
- Phillips, W.M. A.M. Hall C.K. Ballantyne S. Binnie P.W. Ikubille and S. Freeman, (2008). Extent of the last ice sheet in northern Scotland tested with cosmogenic Be-10 exposure ages. *Journal of Quaternary Science*, 23, 101-107.
- Pollard, D. and R.M. DeConto, (2009). Modelling West Antarctic ice sheet growth and collapse through the past five million years. *Nature*, 458, 329-U389.
- Pudsey, C.J. and J. Evans, (2001). First survey of Antarctic sub-ice shelf sediments reveals mid-Holocene ice shelf retreat. *Geology*, 29, 787-790.
- Puspito, N.T. and K. Shimazaki, (1995). Mantle structure and seismotectonics of the Sunda and Banda arcs. *Tectonophysics*, 251, 215-228.
- Quinlan, G. and C. Beaumont, (1981). A comparison of observed and theoretical postglacial relative sea level in Atlantic Canada. *Canadian Journal of Earth Sciences*, 18, 1146-1163.
- Rae, A.C. S. Harrison T. Mighall and A.G. Dawson, (2004). Periglacial trimlines and nunataks of the Last Glacial Maximum: the Gap of Dunloe, southwest Ireland. *Journal of Quaternary Science*, 19, 87-97.
- Roberts, D.H. R.V. Dackombe and G.S.P. Thomas, (2007). Palaeo-ice streaming in the central sector of the British-Irish Ice Sheet during the Last Glacial Maximum: evidence from the northern Irish Sea Basin. *Boreas*, 36, 115-129.
- Rostami, K. W.R. Peltier and A. Mangini, (2000). Quaternary marine terraces, sea-level changes and uplift history of Patagonia, Argentina: comparisons with predictions of the ICE-4G (VM2) model of the global process of glacial isostatic adjustment. *Quaternary Science Reviews*, 19, 1495-1525.
- Scourse, J.D. and M.F.A. Furze, (2001). A critical review of the glaciomarine model for Irish sea deglaciation: evidence from southern Britain, the Celtic shelf and adjacent continental slope. *Journal of Quaternary Science*, 16, 419-434.
- Scourse, J.D. A.I. Haapaniemi E. Colmenero-Hidalgo V.L. Peck I.R. Hall W.E.N. Austin P.C. Knutz and R. Zahn, (2009). Growth, dynamics and deglaciation of the last British-Irish ice sheet: the deep-sea ice-rafted detritus record. *Quaternary Science Reviews*, 28, 3066-3084.
- Sejrup, H.P. H. Haflidason I. Aarseth E. King C.F. Forsberg D. Long and K. Rokoengen, (1994). Late Weichselian Glaciation History of the North North-Sea. *Boreas*, 23, 1-13.
- Sejrup, H.P. B.O. Hjelstuen K.I.T. Dahlgren H. Haflidason A. Kuijpers A. Nygard D. Praeg M.S. Stoker and T.O. Vorren, (2005). Pleistocene glacial history of the NW European continental margin. *Marine and Petroleum Geology*, 22, 1111-1129.
- Sejrup, H.P. E. Larsen J. Landvik E.L. King H. Haflidason and A. Nesje, (2000). Quaternary glaciations in southern Fennoscandia: evidence from southwestern Norway and the northern North Sea region. *Quaternary Science Reviews*, 19, 667-685.

- Sejrup, H.P. A. Nygard A.M. Hall and H. Hafliðason, (2009). Middle and Late Weichselian (Devensian) glaciation history of south-western Norway, North Sea and eastern UK. *Quaternary Science Reviews*, 28, 370-380.
- Selby, K.A. and D.E. Smith, (2007). Late Devensian and Holocene relative sea-level changes on the Isle of Skye, Scotland, UK. *Journal of Quaternary Science*, 22, 119-139.
- Sella, G.F. S. Stein T.H. Dixon M. Craymer T.S. James S. Mazzotti and R.K. Dokka, (2007). Observation of glacial isostatic adjustment in "stable" North America with GPS. *Geophysical Research Letters*, 34, -.
- Shennan, I., (1982). Interpretation of Flandrian sea-level data from the Fenland, England. *Proceeding of the Geologists' Association*, 93, 53-63.
- Shennan, I., (1986). Flandrian sea-level changes in the Fenland II. Tendencies of sea-level movement, altitudinal changes and local and regional factors. *Journal of Quaternary Science*, 1, 155-179.
- Shennan, I., (1999). Global meltwater discharge and the deglacial sea-level record from northwest Scotland. *Journal of Quaternary Science*, 14, 715-719.
- Shennan, I. S. Bradley G. Milne A. Brooks S. Bassett and S. Hamilton, (2006). Relative sea-level changes, glacial isostatic modelling and ice-sheet reconstructions from the British Isles since the Last Glacial Maximum. *Journal of Quaternary Science*, 21, 585-599.
- Shennan, I. T. Coulthard R. Flather B. Horton M. Macklin J. Rees and M. Wright, (2003). Integration of shelf evolution and river basin models to simulate Holocene sediment dynamics of the Humber Estuary during periods of sea-level change and variations in catchment sediment supply. *The Science of the Total Environment*, 314-316, 737-754.
- Shennan, I. S. Hamilton C. Hillier A. Hunter R. Woodall S. Bradley G. Milne A. Brooks and S. Bassett, (2006b). Relative sea-level observations in western Scotland since the Last Glacial Maximum for testing models of glacial isostatic land movements and ice-sheet reconstructions. *Journal of Quaternary Science*, 21, 601-613.
- Shennan, I. S. Hamilton C. Hillier A. Hunter R. Woodall S. Bradley G. Milne A. Brooks and S. Bassett, (2006). Relative sea-level observations in western Scotland since the Last Glacial Maximum for testing models of glacial isostatic land movements and ice-sheet reconstructions. *Journal of Quaternary Science*, 21, 601-613.
- Shennan, I. S. Hamilton C. Hillier and S. Woodroffe, (2005). A 16,000-year record of near-field relative sea-level changes, northwest Scotland, United Kingdom. *Quaternary International*, 133, 95-106.
- Shennan, I. and B. Horton, (2002). Holocene land- and sea-level changes in Great Britain. *Journal of Quaternary Science*, 17, 511-526.
- Shennan, I. J.B. Innes A.J. Long and Y.Q. Zong, (1995). Late Devensian and holocene relative sea-level changes in northwestern Scotland - New data to test existing models. *Quaternary International*, 26, 97-123.
- Shennan, I. K. Lambeck B. Horton J. Innes J. Lloyd J. McArthur T. Purcell and M. Rutherford, (2000). Late Devensian and Holocene records of relative sea-level changes in northwest Scotland and their implications for glacio-hydro-isostatic modelling. *Quaternary Science Reviews*, 19, 1103-1135.
- Shennan, I. G.A. Milne and S.L. Bradley, (2009). Late Holocene relative land- and sea-level changes: Providing information for stakeholders. *GSA today*, 19, 52-23.
- Shennan, I. W.R. Peltier R. Drummond and B. Horton, (2002). Global to local scale parameters determining relative sea-level changes and the post-glacial isostatic adjustment of Great Britain. *Quaternary Science Reviews*, 21, 397-408.
- Simpson, M.J.R. G.A. Milne P. Huybrechts and A.J. Long, (2009). Calibrating a glaciological model of the Greenland ice sheet from the Last Glacial Maximum to present-day using field observations of relative sea level and ice extent. *Quaternary Science Reviews*, 28, 1631-1657.

- Sissons, J.B., (1966). Relative sea-level changes between 10,300 and 8300 B.P in the carse of Stirling. *Trans Inst. Brit. Geogs.*, 39, 19-29.
- Sissons, J.B., (1967). *The Evolution of Scotland's Scenery.*, edn, Vol., Oliver and Boyd: Edinburgh.
- Sissons, J.B. and C.L. Brooks, (1971). Dating of early postglacial land and sea level changes in western Forth Valley. *Nature-Physical Science*, 234, 124-&.
- Smith, D.E. R.A. Cullingford and C.R. Firth, (2000). Patterns of isostatic land uplift during the Holocene: evidence from mainland Scotland. *Holocene*, 10, 489-501.
- Smith, D.E. P.T. Fretwell R.A. Cullingford and C.R. Firth, (2006). Towards improved empirical isobase models of Holocene land uplift for mainland Scotland, UK. *Philosophical Transactions of the Royal Society a-Mathematical Physical and Engineering Sciences*, 364, 949-972.
- Steigenberger, P. M. Rothacher R. Dietrich M. Fritsche A. Rulke and S. Vey, (2006). Reprocessing of a global GPS network. *Journal of Geophysical Research-Solid Earth*, 111, 13.
- Stirling, C.H. T.M. Esat K. Lambeck and M.T. McCulloch, (1998). Timing and duration of the Last Interglacial: evidence for a restricted interval of widespread coral reef growth. *Earth and Planetary Science Letters*, 160, 745-762.
- Stoker, M. and T. Bradwell, (2005). The Minch palaeo-ice stream, NW sector of the British-Irish Ice Sheet. *Journal of the Geological Society*, 162, 425-428.
- Stoker, M.S. K. Hitchen and C.C. Graham, 1993. The geology of the Hebrides and West Shetland shelves, and adjacent deep-water areas. in *British Geological Survey United Kingdom Offshore Regional Report HMSO, London*.
- Stone, J.O. G.A. Balco D.E. Sugden M.W. Caffee L.C. Sass S.G. Cowdery and C. Siddoway, (2003). Holocene deglaciation of Marie Byrd Land, West Antarctica. *Science*, 299, 99-102.
- Sugden, D.E. M.J. Bentley and C.O. Cofaigh, (2006). Geological and geomorphological insights into Antarctic ice sheet evolution. *Philosophical Transactions of the Royal Society a-Mathematical Physical and Engineering Sciences*, 364, 1607-1625.
- Sutherland, D.G., (1984). The Quaternary Deposits and Landforms of Scotland and the Neighboring Shelves - a Review. *Quaternary Science Reviews*, 3, 157-254.
- Tamisiea, M.E. J.X. Mitrovica and J.L. Davis, (2007). GRACE gravity data constrain ancient ice geometries and continental dynamics over Laurentia. *Science*, 316, 881-883.
- Tarasov, L. and W.R. Peltier, (2004). A geophysically constrained large ensemble analysis of the deglacial history of the North American ice-sheet complex. *Quaternary Science Reviews*, 23, 359-388.
- Teferle, F.N. R.M. Bingley E.J. Orliac S.D.P. Williams P.L. Woodworth D. McLaughlin T.F. Baker I. Shennan G.A. Milne S.L. Bradley and D.N. Hansen, (2009). Crustal motions in Great Britain: evidence from continuous GPS, absolute gravity and Holocene sea level data. *Geophysical Journal International*, 178, 23-46.
- Teferle, F.N. R.M. Bingley S.D.P. Williams T.F. Baker and A.H. Dodson, (2006). Using continuous GPS and absolute gravity to separate vertical land movements and changes in sea-level at tide-gauges in the UK. *Philosophical Transactions of the Royal Society a-Mathematical Physical and Engineering Sciences*, 364, 917-930.
- Teferle, F.N. E.J. Orliac and R.M. Bingley, (2007). An assessment of Bernese GPS software precise point positioning using IGS final products for global site velocities. *Gps Solutions*, 11, 205-213.
- Telfer, M.W. P. Wilson T.C. Lord and P.J. Vincent, (2009). New constraints on the age of the last ice sheet glaciation in NW England using optically stimulated luminescence dating. *Journal of Quaternary Science*, 24, 906-915.

- Thorp, P.W., (1986). A Mountain Icefield of Loch Lomond Stadial Age, Western Grampians, Scotland. *Boreas*, 15, 83-97.
- Tian, Y. D.P. Zhao R.M. Sun and J.W. Teng, (2009). Seismic imaging of the crust and upper mantle beneath the North China Craton. *Physics of the Earth and Planetary Interiors*, 172, 169-182.
- Tjia, H.D., (1996). Sea-level changes in the tectonically stable Malay-Thai Peninsula. *Quaternary International*, 31, 95-101.
- Tooley, M., (1982). Sea-level change in northern England. *Proceeding of the Geologists' Association*, 93, 43-51.
- Tooley, M.J., (1974). Sea-level changes during last 9000 years in northwest England. *Geographical Journal*, 140, 18-&.
- Tushingham, A.M. and W.R. Peltier, (1991). ICE-3G - A NEW GLOBAL-MODEL OF LATE PLEISTOCENE DEGLACIATION BASED UPON GEOPHYSICAL PREDICTIONS OF POSTGLACIAL RELATIVE SEA-LEVEL CHANGE. *Journal of Geophysical Research-Solid Earth and Planets*, 96, 4497-4523.
- Tushingham, A.M. and W.R. Peltier, (1992). Validation of the Ice-3g Model of Wurm-Wisconsin Deglaciation Using a Global Data-Base of Relative Sea-Level Histories. *Journal of Geophysical Research-Solid Earth*, 97, 3285-3304.
- Uehara, K. J.D. Scourse K.J. Horsburgh K. Lambeck and A.P. Purcell, (2006). Tidal evolution of the northwest European shelf seas from the Last Glacial Maximum to the present. *Journal of Geophysical Research-Oceans*, 111, -.
- Van de Plassche, O., (1986). *Sea Level research: A manual for the collection and evaluation of data.*, edn, Vol., Geobooks, Norwich.
- Vanderwerff, W., (1995). Structure and Morphotectonics of the Accretionary Prism Along the Eastern Sunda Western Banda Arc. *Journal of Southeast Asian Earth Sciences*, 11, 309-322.
- Verleyen, E. D.A. Hodgson G.A. Milne K. Sabbe and W. Vyverman, (2005). Relative sea-level history from the Lambert Glacier region, East Antarctica, and its relation to deglaciation and Holocene glacier readvance. *Quaternary Research*, 63, 45-52.
- Verleyen, E. D.A. Hodgson K. Sabbe and W. Vyverman, (2004). Late Quaternary deglaciation and climate history of the Larsemann Hills (East Antarctica). *Journal of Quaternary Science*, 19, 361-375.
- Wang, H. and M. VanStrydonck, (1997). Chronology of Holocene cheniers and oyster reefs on the coast of Bohai Bay, China. *Quaternary Research*, 47, 192-205.
- Wheller, G.E. R. Varne J.D. Foden and M.J. Abbott, (1987). Geochemistry of Quaternary Volcanism in the Sunda-Banda Arc, Indonesia, and 3-Component Genesis of Island-Arc Basaltic Magmas. *Journal of Volcanology and Geothermal Research*, 32, 137-160.
- Whittington, G. and A.M. Hall, (2002). The Tolsta Interstadial, Scotland: correlation with D-O cycles GI-8 to GI-5? , *Quaternary Science Reviews*, 21, 901-915.
- Widiyantoro, S. and R. van der Hilst, (1996). Structure and evolution of lithospheric slab beneath the Sunda arc, Indonesia. *Science*, 271, 1566-1570.
- Widiyantoro, S. and R. van der Hilst, (1997). Mantle structure beneath Indonesia inferred from high-resolution tomographic imaging. *Geophysical Journal International*, 130, 167-182.
- Williams, S.D.P., (2003). The effect of coloured noise on the uncertainties of rates estimated from geodetic time series. *Journal of Geodesy*, 76, 483-494.
- Williams, S.D.P., (2008). CATS: GPS coordinate time series analysis software. *Gps Solutions*, 12, 147-153.

- Williams, S.D.P. Y. Bock P. Fang P. Jamason R.M. Nikolaidis L. Prawirodirdjo M. Miller and D.J. Johnson, (2004). Error analysis of continuous GPS position time series. *Journal of Geophysical Research-Solid Earth*, 109, -.
- Winder, R.O. and S.M. Peacock, (2001). Viscous forces acting on subducting lithosphere. *Journal of Geophysical Research-Solid Earth*, 106, 21937-21951.
- Woodroffe, C.D., (2005). Late Quaternary sea-level highstands in the central and eastern Indian Ocean: A review. *Global and Planetary Change*, 49, 121-138.
- Woodroffe, S.A. and B.P. Horton, (2005). Holocene sea-level changes in the Indo-Pacific. *Journal of Asian Earth Sciences*, 25, 29-43.
- Woodworth, P.L. F.N. Teferle R.M. Bingley I. Shennan and S.D.P. Williams, (2009). Trends in UK mean sea level revisited. *Geophysical Journal International*, 176, 19-30.
- Yim, W.W.S., (1999). Radiocarbon dating and the reconstruction of late Quaternary sea-level changes in Hong Kong. *Quaternary International*, 55, 77-91.
- Yokoyama, Y. K. Lambeck P. De Deckker P. Johnston and L.K. Fifield, (2000). Timing of the Last Glacial Maximum from observed sea-level minima. *Nature*, 406, 713-716.
- Yokoyama, Y. A. Purcell J.F. Marshall and K. Lambeck, (2006). Sea-level during the early deglaciation period in the Great Barrier Reef, Australia. *Global and Planetary Change*, 53, 147-153.
- Yu, K.F. D.S. Liu C.D. Shen J.X. Zhao T.G. Chen J.L. Zhong H.T. Zhao and C.J. Song, (2002). High-frequency climatic oscillations recorded in a Holocene coral reef at Leizhou Peninsula, South China sea. *Science in China Series D-Earth Sciences*, 45, 1057-+.
- Yu, S.Y. B.E. Berglund P. Sandgren and K. Lambeck, (2007). Evidence for a rapid sea-level rise 7600 yr ago. *Geology*, 35, 891-894.
- Zang, S. H. Zhou and R. Wei, (2008). Progress in studies on the structure and physical properties of the mantle in China. *Acta Seismologica Sinica*, 21, 526-534.
- Zong, Y.Q., (2004). Mid-holocene sea-level highstand along the southeast coast of China. *Quaternary International*, 117, 55-67.